Organophosphorous borane complexes : from frustration to inspiration

Jonathan Dupré

Normandie Université

THESE

Pour obtenir le diplôme de doctorat

Spécialité : Chimie

Préparée au sein de l'ENSICAEN et de l'UNICAEN

Organophosphorus Borane Complexes : From Frustration to Inspiration

Présentée et soutenue par
Jonathan DUPRÉ

Thèse soutenue publiquement le 19 Octobre 2017 devant le jury composé de		
M. Thibault Cantat	Ingénieur de Recherche / CEA Saclay / Paris-Saclay	Rapporteur
M. Joseph Moran	Maître de Conférences HDR / Université de Strasbourg / Strasbourg	Rapporteur
M. Jacques Rouden	Professeur des Universités / Université de Caen Normandie / Caen	Examinateur
Mme. Hélène Gérard	Professeur des Universités / Université Pierre et Marie Curie / Paris	Examinateur
M. Sami Lakhdar	Chargé de Recherche CNRS / Université de Caen Normandie / Caen	Co-encadrant de thèse
Mme. Annie-Claude Gaumont	Professeur des Universités / Université de Caen Normandie / Caen	Directrice de thèse

Thèse dirigée par Annie-Claude Gaumont, Laboratoire de Chimie Moléculaire et Thio-Organique.

UNIVERSITÉ CAEN NORMANDIE

ENSICAEN
ÉCOLE PUBLIQUE D'INGÉNIEURS
CENTRE DE RECHERCHE

ED 508 NC
Normande de Chimie

lcmt

Remerciements

“Il n’existe pas de meilleur exercice pour le cœur que de se pencher pour aider quelqu’un à se relever" John A. Holmes (poète Américain).

Je voudrais remercier sincèrement Monsieur Thibaut Cantat (Ingénieur de Recherche au CEA) et Monsieur Joseph Moran (Maître de Conférences à L’université de Strasbourg) pour avoir accepté de juger mon travail de thèse en tant que rapporteurs. De plus, j’aimerais tout particulièrement remercier Madame Hélène Gérard (Professeur à l’Université Pierre et Marie Curie de Paris) d’avoir accepté de faire partie de mon jury de thèse et de m’avoir accordé autant de pédagogie, de temps et d’intérêt lors de mon initiation aux calculs de chimie théorique. Enfin, je remercie Monsieur Keith A. Woerpel (Professeur à L’université de New-York) et Mr. Jacques Rouden (professeur à l’université de Caen) pour sa participation au jury de thèse.

Je souhaiterais exprimer toute ma gratitude au professeur Annie Claude Gaumont pour m’avoir accepté dans son groupe de recherche et pour m’avoir donné l’opportunité de mener cette thèse. Par ailleurs, j’aimerais également la remercier pour les conseils justes et raisonnés qu’elle me donnait déjà il y 6 ans lors de mes études en licence de chimie à l’université de Caen.

Cette thèse m’a aussi permis de travailler avec mon « Daddy » de la chimie, le docteur Sami Lakhdar. Mille merci de m’avoir tant ouvert les yeux sur la chimie « Aies toujours un regard neuf sur les choses ! ». Travailler avec toi a été une ***magnifique*** expérience intellectuelle et humaine. Je te remercie de m’avoir fait grandir et murir, de m’avoir fait confiance en me donnant de la liberté, de m’avoir toujours aidé à me débloquer lors de mes problèmes de chimie. Enfin, et j’insiste sur cette qualité : Merci de m’avoir toujours aidé à me relever dans les innombrables échecs de la thèse, sans discrédit et sans jugement.

D’autres part, j’aimerais remercier tous les doctorants, post-doctorants, IE, ingénieur recherche, techniciens, Lydia et tout le secrétariat… peu importe le poste, merci à toutes et tous pour votre amitié, votre aide et votre bonne humeur pendant ces trois années. Etant ancien étudiant de Caen, je veux remercier particulièrement Monsieur Stéphane Perrio, qui dès la deuxième année de licence m’a permis de trouver ma passion pour la chimie organique. J’espère que tu resteras proche des étudiants comme tu l’as été avec moi. Tu fais partis de ces rares enseignants, investit et à l’écoute, que les étudiants auront la chance de croiser.

Avant de terminer, il n'y aura jamais assez de mots pour exprimer mon éternelle reconnaissance à mes parents qui m'ont permis de réaliser ce rêve difficile de carrière sans jamais vraiment comprendre ou cela aboutira. Votre confiance, votre investissement humain, matériel et financier sont autant de sacrifices que j'espère pouvoir un jour vous rendre au centuple. Et donc une dernière fois, non maman je ne fais ni de la physique ni des maths et non papa, je n'ai pas été prof à la fac de Caen pendant 3 ans. Alors qu'est-ce que je faisais ? Je dirais que j'essayais de comprendre une infime partie de la ***chimie*** dans le monde qui nous entoure. Expliquer ce qu'on fait pendant une thèse de chimie, c'est comme expliquer à un enfant comme on fait les bébés : on ne se sait jamais par où commencer et on finit toujours par déformer la réalité pour simplifier ! Malheureusement, les chimistes ont beaucoup de mal à déformer la réalité…

Enfin, la thèse c'est un marathon d'une éphémère longévité ! Les 14 premiers kilomètres sont stimulants voir euphorisants mais fatiguant sur la fin. Les 14 suivants sont passionnants mais beaucoup trop courts, frustrants et très éprouvants. Quant aux 14 derniers kilomètres, ils sont carrément lapidaires, stressants et tellement énergivore. Heureusement, j'ai toujours trouvé le réconfort, l'énergie et le soutien infaillible de ma co-équipière, elle-même courant le marathon de ses études de médecine. Les vacances, les soirées, les publis, les RDV, les Week-end sont autant de mots auxquels j'aimerais juxtaposer désolé et merci. Merci de partager ma vie, de m'aider à me relever quand je tombe mais aussi et surtout, d'accepter.

"*Tout échec ouvre la voie du dépassement, tout succès limite*"
Robert Sabatier (Poète Français) dans Le livre de la déraison souriante, 1991.

List of Abbreviations

A
Abs: Absorbance
Ac: Acetyl
Alk: Alkyl
Ar: Aryl

B
Bn: Benzyl
Boc: *tert*-Butoxycarbonyl
Bu: Butyl

C
Cat.: Catalyst

D
DABCO: 1,4-Diazabicyclo[2.2.2]octane
DBU: 1,8-Diazabicyclo[5.4.0]undec-7-ene
DCE: Dichloroethane
DMF: *N,N*-dimethylformamide
DMSO: Dimethylsulfoxide
d.r.: diastereoisomeric ratio

E
E : Electrophilicity
ε: Molar extinction coefficient
ee: Enantiomeric excess
EI: Electronic impact
Eq. = Equiv: Equivalent
ESI: Electrospray ionisation
Et: Ethyl
EWG: Electron withdrawing group

F
FLP(s): Frustrated Lewis Pair(s)

H
HPLC: High Performance Liquid Chromatography
HRMS: High Resolution Mass Spectroscopy

H
HSAB: Hard and Soft Acids and Bases

I
IR: Infrared

K
KIE: Kinetic Isotop Effect

L
LA: Lewis acid
LB: Lewis base
LG: Leaving group

M
MBH: Morita-Baylis-Hillman
Me: Methyl
MO: Molecular orbital
Mp: Melting point

N
N: Nucleophilicity
n.d.: Not determined
NHC: *N*-heterocyclic carbene
NMR: Nuclear Magnetic resonance

P
PBs: Phosphine borane complexes
Ph: Phenyl
Ppm: Parts per million
Pr: Propyl

R
RDS: Rate determining step
r.t.: Room temperature

S
s_N: Specific sensitivity nucleophilicity

T
THF : Tetrahydrofuran
TLC: Thin layer chromatography
TTMS : Trimethylsilylsilane
Tol: Tolyl
Ts: Tosyl

Table of Contents

Remerciements..... 3

List of Abbreviations..... 5

Table of Contents..... 6

Summary.....10

Chapter I: Reactivity of Organophosphorus-Organoborane Compounds....15

1. Organic reactions catalysed by Lewis acids and bases.....16

1.1. The concepts of Lewis acids and bases.....16

1.2. Phosphines in catalysis.....17

1.3. Boranes as Lewis acid catalysts 24

1.4. Lewis acid Lewis base dual catalysis by phosphine borane 30

2. From Lewis acid Lewis base complexes to Frustrated Lewis Pairs. 31

2.1. Phosphorous-borane (P-B) Lewis-acid Lewis-base complexes.....31

2.2. Formation of Frustrated Lewis Pairs (FLPs).....37

3. On the investigation of a reaction mechanism.....46

3.1. Kinetic methods to investigate reaction mechanisms 47

3.2. Density functional theory to investigate reaction mechanisms.....50

Chapter II: Metal-Free Hydrogenation of Electron-Poor Olefins Catalysed by P/B Frustrated Lewis Pairs 53

1. State of the art on the mechanistic investigations of FLPs-catalyzed hydrogenation of unsaturated compounds 54

1.1. Hydrogenation of unpolarised alkenes and electron rich olefins with P/B FLPs...55

1.2. Hydrogenation of polycyclic aromatic hydrocarbons and heterocycles with P/B FLPs 59

1.3. Hydrogenation of carbonyl derivatives with P/B FLPs 60

1.4. Hydrogenation of α,β-unsaturated carbonyl derivatives with P/B FLPs 61

2. Reduction of Michael acceptors by P/B FLPs 64

2.1. Synthesis of FLPs and catalytic reduction of methylvinyl ketone under H_2. 64

2.2. Stoechiometric reaction of FLPs with Michael acceptors.....66

3. Study of the reaction mechanism.....68

3.1. Reactions of 33 and 34 with diarylcarbenium cations under pseudo-first order conditions 69

3.2. Determination of the nucleophilicity and the Lewis basicity parameters 69

3.3. Determination of the intrinsic barriers for the reactions of 33,34 with 41a-c 71

3.4. Proposition of a reaction mechanism 72

4. Exploration of the hydrophosphination of Michael acceptors with phosphonium salts in C-P bond formation 73

4.1. C-P bond formation utilizing phosphonium salts HPR_3^+ 74

4.2. Expected reactivity of H-PS in the hydrophosphination of Michael acceptors 75

4.3. Hydrophosphination of Michael acceptors with $[Ar_3PH]^+[X]^-$ 75

4.5. Application of the hydrophosphination of olefins to cross-coupling metathesis as protecting groups of phosphines 80

5. Conclusion and perspectives 80

5.1. Conclusion 80

5.2. Outlooks 81

Chapter III: Quantification of the Hydride Donor Ability of Phosphine Borane Complexes 83

1. Hydride transfers in organic synthesis 84

1.1. Main organic hydride donors in organic synthesis 84

1.2 Borane complexes as hydride donors 92

2. Hydricity of phosphine boranes and comparison with other hydride donors 97

2.1 Toward a unified scale to compare the hydricity of hydride donors? 97

2.2 Hydricity of phosphine borane complexes 29a-g 98

2.3 Increasing the hydricity of PBs 103

2.4 Comparison of the hydricity of PBs with those of other hydride donors 109

3. Conclusion and perspectives 110

3.1 Conclusions 110

3.2 Perspectives 112

Chapter IV: Borenium cations derived from LB-BH_3 as reactive intermediates in borylation reaction 115

1. Literature survey of advances in the borylation reactions 116

1.1. Development of transition metal catalysed borylation reaction 116

1.2. Intermolecular borylation reaction with LB-BH_3 (LB = phosphine, amine, carbene). 118

1.3. Intramolecular borylation reaction with LB-BH_3 (LB = phosphine, amine, carbene). 120

1.4. Cross-dehydrocoupling reactions catalysed by Lewis acids 122
2. Development of a catalytic version of the electrophilic borylation of phosphinite boranes complexes. 124
2.1. Study of transition metals and Lewis acid or Lewis base catalyzed borylation. .124
2.2. Unravelling the origin of the failure of the catalyzed borylations 126
3. Development of a method for the migration of C_6F_5 to phosphorus-borane derivatives. 127
3.1. Migration of C_6F_5 from $B(C_6F_5)_3$ to PB in the literature.....127
3.2. Optimization of the reactions conditions.....128
3.3. Scope of the phosphorus borane complexes for the mono-migration of C_6F_5.....129
3.4. Example of the double migration of C_6F_5.....132
4. Kinetic study of the mechanism of the migration of C_6F_5 134
4.1. Proposed mechanism and determination of the relevant parameters to study ..134
4.2. Study of the formation of B_2H_6. 135
4.3. Measurement of the effect of C_6F_5 on the hydricity of $R_3P\text{-}BH_{3-n}(C_6F_5)_n$, $0 \leq n \leq 2$. 136
5. Computational study of the migrations of C_6F_5 138
5.1. Description of the system and tools 138
5.2. Thermodynamic study of the successive migrations. 141
5.3. Designing a simple model to describe both the hydride and the C_6F_5 migrations. 145
5.4. Investigation in the experimental selectivity 147
6. Conclusion and perspectives 154
6.1. Conclusion.....154
6.2. Perspectives.....155

Chapter V: Lewis acid catalyzed Regioselective Markovnikov hydrophosphination of styrene. 157
1. Survey of the Markovnikov regioselective hydrophosphination in the literature 158
1.1. Metal free-mediated Markovnikov regioselective hydrophosphination of styrene 159
1.2. Transition metal-mediated Markovnikov hydrophosphination of styrenes.....160
2. Toward an organocatalyzed alkene Markovnikov regioselective hydrophosphination 162
2.1. Identification of the problem and proposed approach.....162
2.2. Tritylium salts as organic Lewis acids 163
2.3. Characterization of tritylium salts and use in organocatalysis.....164
3. Organocatalyzed Markovnikov hydrophosphination of alkenes. 168

3.1. Development of the reaction conditions for the organo-catalyzed Markovnikov hydrophosphination of aryl alkenes. 168

3.2. Insights in the reactions mechanisms of the organocatalyzed hydrophosphination. 173

4. Conclusion and perspectives 178

4.1. Conclusion 178

4.2. Perspectives 179

6. General Conclusion 181

7. Experimental part 185

8. **Appendix**..... 274

Summary

This thesis has been carried out in the Laboratoire de Chimie Moléculaire et Thio-Organique in the group of Prof. Annie-Claude Gaumont under the supervision of Dr. Sami Lakhdar. It focuses on explorating the reactivity of a wide range of organophosphorus borane complexes going from frustrating P-B bond to organophosphorus borane complexes possessing strong P-B interaction. Indeed, while phosphorus and boron chemistry are widely taught to graduate students but also studied in research due to the rich chemistry they offer, chemistry involving the study of the interactions of the two latter atoms is less familiar.

PhD guideline

A general picture of the guiding principle of this PhD project is drawn in Figure 1. It illustrates the four different cases that have been studied during this work. Those cases depend on the nature of the Lewis acid and the Lewis bases on one side, and on the strength of the interaction between each other on the other side.

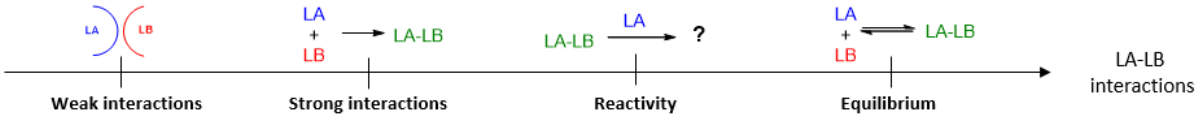

Figure 1 Qualitative scale of the interaction strength between Lewis acid and Lewis base: Guiding principle of the PhD, LA: Lewis acid, LB: Lewis base.

In all the cases, the reactivity was investigated using physical-organic tools such as linear free energy relationship and also computational methods in order to collect data allowing us to unravel reactions mechanisms. Mechanistic studies permitted us not only to understand factors controlling reaction mechanism but also to design new reactions.

Contents

In a first part, we focus our attention to the situation where a bulky LA (BR_3) and LB (PR'_3) are prevented to form a complex due to steric repulsions. Those systems are now well known as Frustrated Lewis Pairs (P/B FLPs). Such systems have found valuable applications in the activation of small inert molecules such as H_2, CO_2, CO or SO_2, to quote a few. Consequently, P/B FLPs have been used in the metal-free hydrogenation reactions of unsaturated compounds such as alkenes, heterocycles, carbonyls and α,β-unsaturated compounds. While he synthetic use of P/B FLPs has largely been explored during the last decade, mechanistic investigations are rare and have only been focused on understanding cases where FLPs are

extremely efficient. In our study, we focused on understanding the failure of P/B FLPs to catalyse hydrogenation of Michael acceptors.

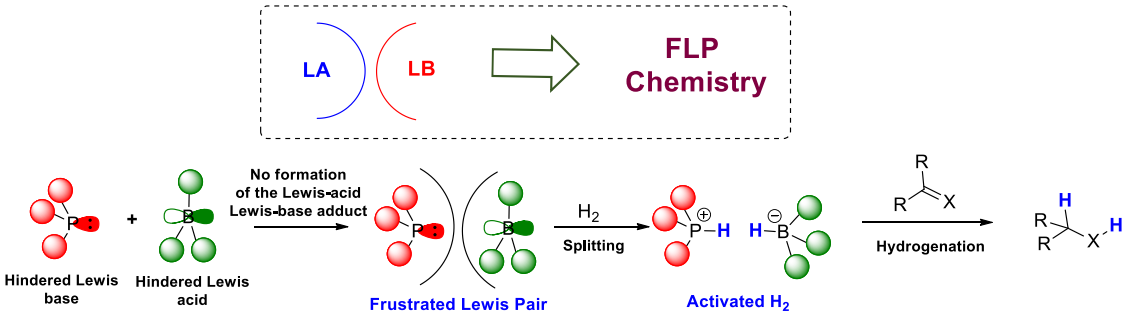

Figure 2 General figure of the first part: FLP chemistry.

In a second part, we investigated the nucleophilic reactivity of phosphine borane complexes (PBs) and relates structures, which are known to exhibit hydride donor properties. In this context, kinetics of their reaction with reference electrophiles have been measured, allowing the evaluation of the effects of several parameters (substituents, structure, solvent, etc…) on the hydricity of P-BH_3. In the light of these data, we investigated the potential of phosphine borane complexes (PBs) to behave as hydride donors in organic synthesis as reducing agents.

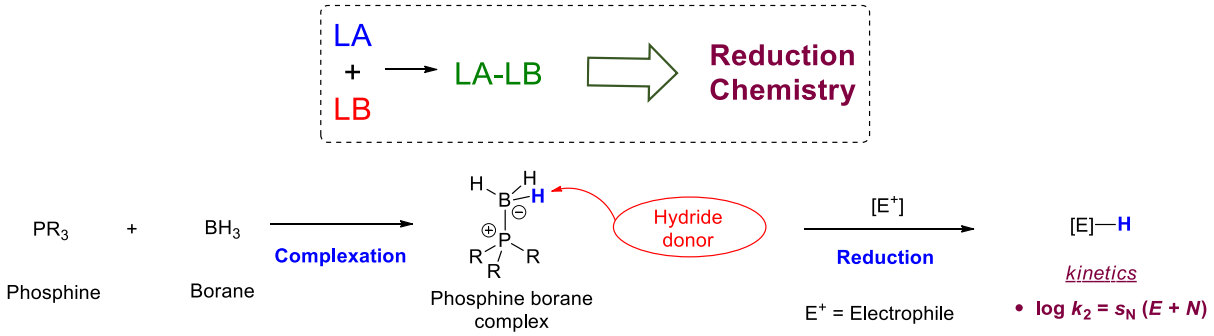

Figure 3 General figure of the second part: Reduction chemistry

The third part of this thesis is dedicated to reactions of Lewis acid Lewis base complex in the presence of another Lewis acid. This approach is largely used in Lewis acid catalysis to perform silylation, borylation or dehydrocoupling reactions and represent an important synthetic method. The case of dehydrocoupling reactions is particularly interesting as H_2 is obtained as a sole side product. In this methodology, the Lewis acid (LA) is expected to act as an hydride abstractor to generate a Bronsted base ([LA-H]$^-$) which can deprotonate a substrate to release H_2 and regenerate LA. Based on this methodology, reactions of R_3P-BH_3 with a strong Lewis acid have been attempted to lead to serendipitous results, which have been rationalized based on a combination of kinetics and DFT calculations.

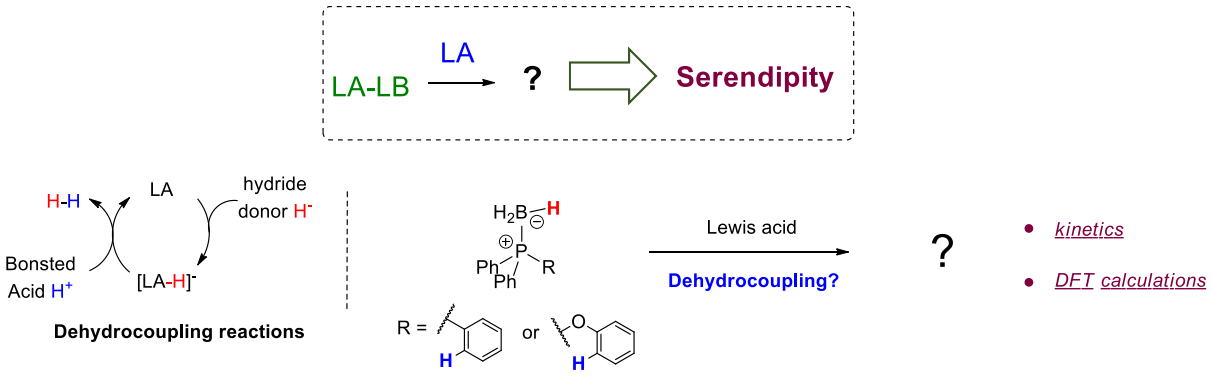

Figure 4 General figure of the third part: Serendipity.

The last chapter of this thesis describes the first organocatalyzed Markovnikov hydrophosphination of alkenes. We specifically showed that tritylium cations can act as efficient Lewis acids to catalyse this transformation. Scope and limitations of this process are discussed on the basis of mechanistic investigations. The implication of these works on understanding previous results reported in the lab are also discussed.

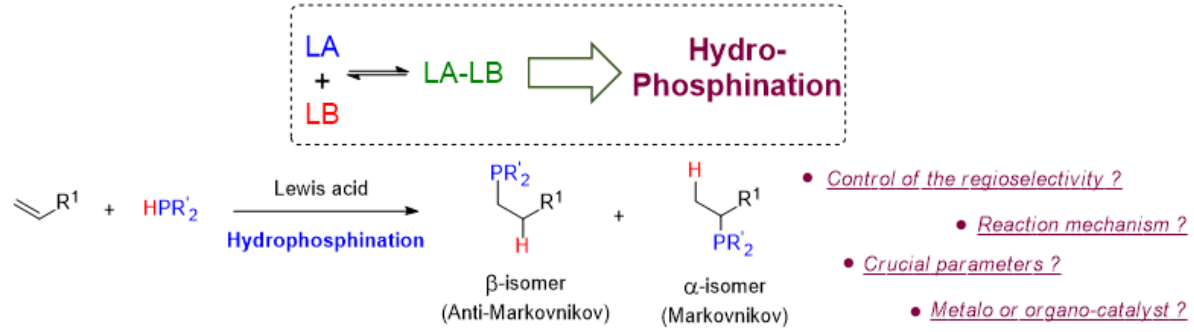

Figure 5 General figure of the fifth part: Markovnikov hydrophosphination

Scientific productions

Up to now, the first part of this thesis has been published as a communication in Organic letters (Dupré, J.; Gaumont, A.-C.; Lakhdar, S. *Org. Lett.* **2017**, *19*, 694) from ACS publications. A copy of the publication has been reproduced at the end of the manuscript. A second article about the hydricity of PBs and their reaction with $B(C_6F_5)_3$ will be submitted soon

The scientific results of the thesis have also been presented during symposium and conferences.

- National symposium: 5 oral communications and 3 posters
- International symposium: 2 oral communications and 2 posters.

Besides, with a group of PhD students from the University of Caen and in the framework of the scientific day of our doctoral school, we organized a symposium in chemistry for PhD students from the University of Rouen, Caen and Le Havre.

- 100 attendants, 40 posters, 16 oral communications, 2 invited speakers (Dr. Damien Bonne, assistant professor, Aix-Marseille/FR and Dr. Steve Van Zutphen, MagPie Polymers CEO, Nemours/FR)

1. Chapter I: Reactivity of Organophosphorus-Organoborane Compounds

1. Organic reactions catalysed by Lewis acids and bases

Introduced about two centuries ago by Berzelium (1836), catalysis is undoubetly one of the most important concept in chemistry, which continues to occupy a pivotal role in academia as well as in industry. Because of the spectacular evolution that the field has experienced through the years, the definition of the term “catalysis” has seen many changes and adjustement that one can recognize when going through textbooks and reviews. Perhaps, one of the most reliable definition is that introduced by the IUPAC which stated: “Catalyst: a *substance that increases the rate of a reaction without modifying the overall standard Gibbs energy change in the reaction; the process is called catalysis. The catalyst is both a reactant and product of the reaction. The words catalyst and catalysis should not be used when the added substance reduces the rate of reaction*.”[1] The action of a catalyst from an energetic point of view will be developed in the section 4.1.2.

1.1. The concepts of Lewis acids and bases

In 1923, G. N. Lewis proposed a theory to distinguish the nature of molecules from their electronic differences.[2] Hence, Lewis acids are defined as electron-pair acceptors while Lewis bases corresponds to electron pair donors.

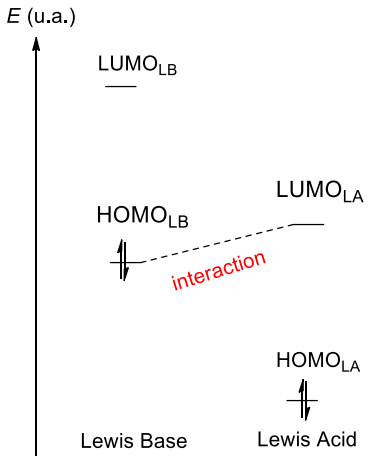

Figure 1.1 Energetic representation of Lewis acid (LA) and Lewis base (LB) interaction according to the frontier orbital theory.

More precisely according to the frontier orbital theory,[3] Lewis acids are characterized by a low-lying “lowest-unoccupied molecular orbital” which can interact with a lone electron-pair in the

[1] https://goldbook.iupac.org/C00876.html
[2] a) Lewis, G.N. **1923** *Valence and the Structure of Atoms and Molecules*, Chemical Catalog Co., Inc., New York, p. 142.
[3] a) Fukui, K.; Yonezawa, T.; Shingu, H. *J. Chem. Phys.* **1952**, *20*, 722. b) Fukui, K. *Science,* **1982**, *218*, 747.

high-lying “highest occupied molecular orbital” of a Lewis base (*Figure 1.1*).The nature of the HOMO of the Lewis base and the LUMO of the Lewis acid have been classified by Jensen in 1980 depending on the nature of the molecular orbitals.[4] He proposed nine types of interactions involving nonbonding electron pairs (n), σ bonding electron pairs, π bonding electron pairs and their corresponding antibonding orbitals, n*, σ* and π* respectively. In most cases, the interaction between Lewis acids and bases can be explained by n→n*, n→ σ* and n→ π* interactions which imply that, in several cases, the Lewis basic character of a molecule is due to its lone pair electron, as initially proposed by Lewis. This classification forms the conceptual interactions which are evoked to understand the modes of interactions between molecules.

1.2. Phosphines in catalysis

1.2.1. Electronic description of the phosphorous atom

Organophosphorous compounds are ubiquitous molecules which are widely employed in chemistry, industry and pharmacology due to the versatile behaviour of the phosphorous atom. The phosphorous atom is present at the row 15 in the periodic table with the following electronic structure P (Z = 15): $[_{10}Ne]\ 3s^2\ 3p^3$. Consequently, as commonly known for the nitrogen atom, it exits at the oxidation state (+III). However, due to the possibility of the phosphorous to extend its electronic structure, it is also stable at the oxidation state (+V). In this context, the hybridization theory predicts that, in molecules, phosphorous atom will adopt either an sp^3-hybridization with a tetrahedral molecular geometry or an sp^3d-hydridization with a trigonal bipyramidal molecular geometry (*Figure 1.2*).

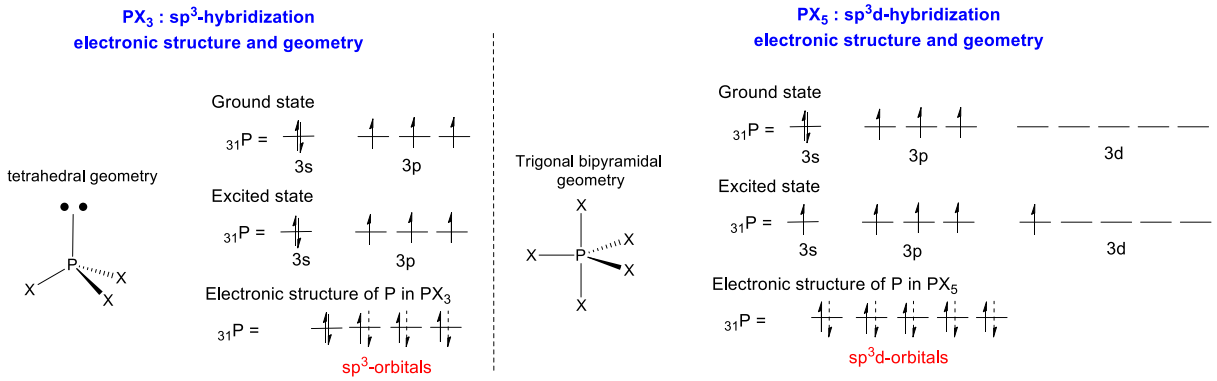

Figure 1.2 Electronic structures and geometries of P-atom depending on its hybridization state.

Moreover, it is noteworthy to mention that several other geometries can be adopted depending on the bond order between the phosphorous and its substituents. As an example,

[4] Jensen, W.B. **1980** *The Lewis Acid-Base Concepts*, Wiley-Interscience, New York.

triphenylphosphine oxide (Ph_3PO) and triphenylphosphonium salt ($[HPPh_3]^+$) have tetrahedral geometries around the P-atom.

A completely different concept has been reviewed by Gilheany to define the nature of the bonding in phosphines, phosphine oxides, and phosphonium ylides.[5] Based on calculations, the authors provided strong evidences of *the non-involvment of d-orbital* to explain the bonding of R_3PY compounds (R = H, alkyl, aryl and Y = electron lone pair, O or S). Theoretical and experimental data suggest that the bonding and non-bonding MOs can be explained by Walsh diagrams (*Figure 1.3*).

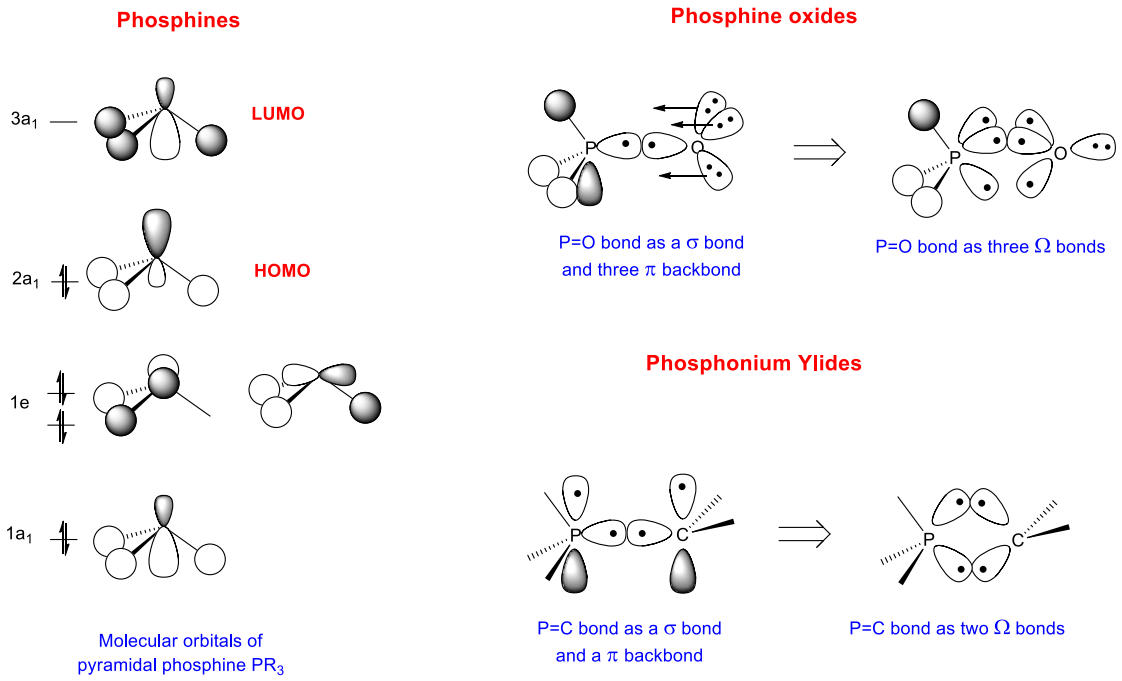

Figure 1.3 Molecular Orbitals of PR_3 using Walsh diagrams and representation of P=O and P=C bonds according to the concept of "banana bonds".

In the case of phosphines, the representation shows that $1a_1$ and 1e orbitals are the three bonding orbitals. However, $2a_1$ is non-bonding because the bonding of the p orbital is exactly balanced by the antibonding of the s orbital. Finally, the LUMO is $3a_1$ type molecular orbital. In this way, the s electrons do not contribute to bonding, and yet the nonbonding electrons are not in the s orbital. According to this description, it is proposed that, in phosphine oxide compounds, the PO bond is a formal triple bond with the three curved regions of electron density disposed between P and O in a symmetrical fashion at 120° to each other in Newman projection along the PO coordinate as shown in bond orbital form from *Figure 1.3*, right side. These curve shapes of molecular orbitals are called "banana bonds" symbolized by Ω. Finally,

[5] For a review on the nature of bondings in P-derivatives, see: Gilheany. D. *Chem. Rev.* **1994**, *94*, 1339. For seminal publications, see a) Kuhhigg, W. *Angew. Chem. Int. Ed.* **1984**, *23*, 272 b) Reed. A. E.; Schlever. P. v. R. *J. Am. Chem. Soc.* **1990**, *112*, 1434 c) Reed, A. E.; Weinhold, F. *J. Am. Chem. Soc.* **1986**, *108*, 3586

in the case of phosphonium ylides, this is analogous to PO as the chemical bonding can be described as two Ω bonds. These descriptions should be much more accurate than those of the hydridization theory as it rationalizes experimental observations.

Another electronic specificity of the phosphorous atom is its electronegativity (χ = 2.19), according to Pauling scale. It is significantly lower than nitrogen (χ = 3.04), explaining why the latter forms weaker bonds with highly electronegative atoms (Cl, O) and stronger bonds with poorly electronegative ones (C, H). An obvious thermodynamic consequence of this property is that phosphines (PR_3) exhibit lower Bronsted basicity compared to amines (NR_3) (*Figure 1.4*).

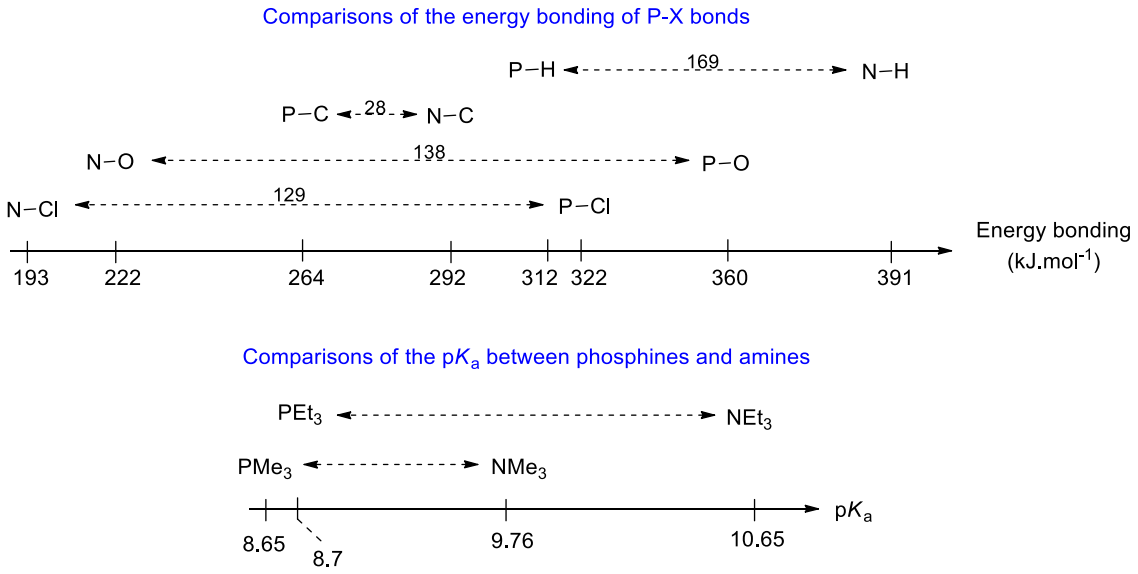

Figure 1.4 Comparison of the bonding energy of P-X and N-X bonds (top) and pK_a (in water) of phosphines and amines (bottom).[6]

Another remarkable electronic property of organophosphorous molecules containing a P-atom at the oxidation state (III) is due to the presence of the electron lone pair. In the same way than amines, phosphines exhibit a σ-donor character, meaning that they are able to interact with an electron-deficient partner by forming a σ-bond. But unlike amines, phosphines are also capable to develop a π-type interaction with electron rich partners leading to a recovery of electron density by backdonation in the d orbitals or in the σ* orbital of the P-R bond (*Figure 1.5*). A scale of σ-donor and π-acceptor character of phosphines has been established by Rahman et al. by studying the shift of the carbonyl wavelengths in phosphine-nickel-tricarbonyl complexes $[(R_3P)Ni(CO)_3]$.[7] The more electron density the phosphine ligand donated to the metal, the

[6] For energy bonding, see Editor, Hartley, F.R. **1990** *The Chemistry of Organophosphorus Compounds,* Vol 1., J. Wiley & Sons Ltd., New York. For pK_a values, see Hall, H. K. *J. Am. Chem. Soc.* **1957**, 79, 5441.

[7] Rahman, M. M.; Liu, H.-Y.; Eriks, K.; Prock, A.; Giering, W. P. *Organometallics* **1989**, *8*, 1.

more π-backbonding occurred to the carbonyl ligands, weakening the C≡O triple bond, thus lowering the ν_{CO} IR stretching frequency.

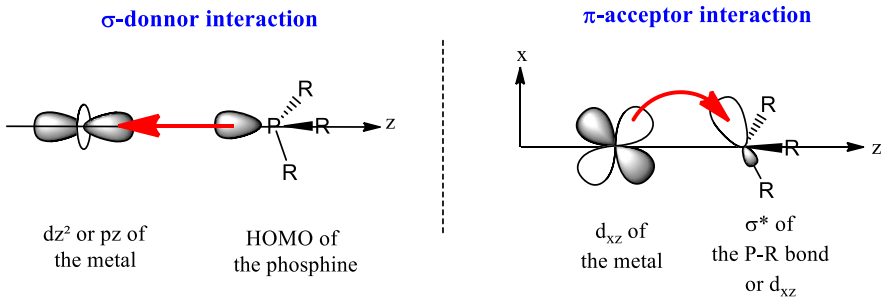

Figure 1.5 Orbital interactions of phosphines with a metal: σ-donor and π-acceptor characters.

The last important parameter of organophosphines is the steric hindrance of phosphorous containing ligands. The size or steric bulk of phosphines, also known as cone angle (θ), was introduced by Tolman in 1977 reflects the approximate amount of space that the ligand consumed about the metal center. In this regard, a detailed list of σ-donating ability of phosphines and their cone angles (θ) or Tolman angles (*Table 1.1*) is now available.[8] Based on this, we can see that the tolman angle increases with the decrease of the σ-donor character of phosphines.

Table 1.1 P-(III) ligands ranked by Tolman's electronic parameter (v) and Tolman's angle (θ).

PR_3	v (cm^{-1})	θ (°)	PR_3	v (cm^{-1})	θ (°)
P(*t*-Bu)$_3$	2056	212	PPh_3	2069	145
P(*i*-Pr)$_3$	2059	160	PPh_2OEt	2072	133
PMe_3	2064	118	PPh_2H	2073	128
P(*p*-anisol)$_3$	2066	146	P(OEt)$_3$	2076	109
P(*o*-Tol)$_3$	2067	194	$PPhH_2$	2077	101
P(*p*-Tol)$_3$	2067	146	PH_3	2083	87

Those purely electronic and steric considerations give a solid background to anticipate and more importantly explain the rich reactivity of the phosphorous atom in chemical reactions.

[8] a) Tolman, C. A. *J. Am. Chem. Soc.* **1970**, *92*, 2956. b) Tolman, C. a. *Chem. Rev.* **1977**, *77*, 313.

1.2.2. Nomenclature of organophosphorus compounds

An exhaustive presentation of organophosphorus derivatives includes their singular nomenclature which is extracted from the IUPAC nomenclature rules of organophosphorus compounds (*Figure 1.6*).[9]

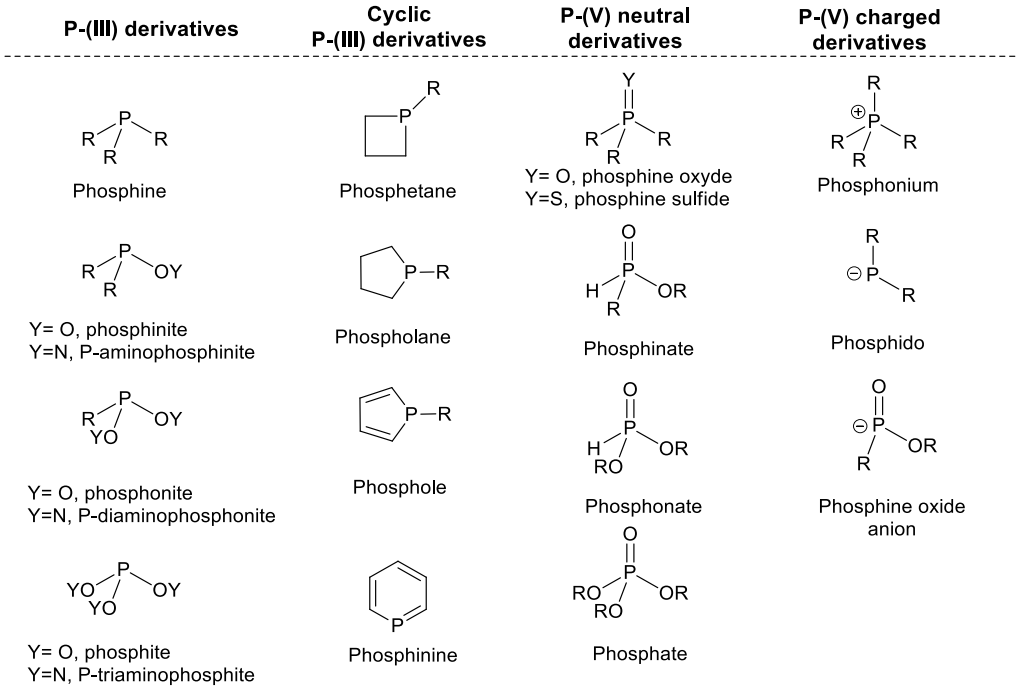

Figure 1.6 Nomenclature of organophosphorus compounds according to the IUPAC rules of nomenclature.

1.2.3. Phosphines as Lewis base catalysts

Apart from their use as ligands for transition metal catalysis, Lewis bases such as carbenes, amines and phosphines have been used as lewis base organocatalysts in various chemical reactions. Chiral derivatives of these catalysts have been shown to be highly efficient in various enantioselective transformations. All of them promote the activation of a reagent by either n→n*, n→ σ* and n→ π* interactions, decreasing the activation energy of the transition state and thus, increasing the rate of the reaction.[10] For our concern, we will focus here on phosphine-catalysed reactions only.

An outstanding illustration of phosphines as organocatalysts is certainly the Morita-Baylis-Hillman (MBH) reaction.[11] Formally, this reaction promotes the condensation of an electron-poor double bond with a carbonyl compound in the presence of a Lewis base. *Scheme 1.1* shows

[9] http://goldbook.iupac.org
[10] Vedejs, E.; Denmark. S. 2016, Lewis Base Catalysis in Organic Synthesis, Editor: Wiley. ISBN: 978-3-527-33618-0.
[11] a) Baylis, A. B.; Hillman, M. E. D. **1972** German Patent 2155113. b) Morita, K., Suzuki, Z., and H. Hirose. **1968**. *Bull. Chem. Soc. Jpn*. 41, 2815.

a BINOL-derived phosphine catalysed enantioselective addition of an imine to an unsaturated ketone with yields up to 94% and ees up to 95%.[12]

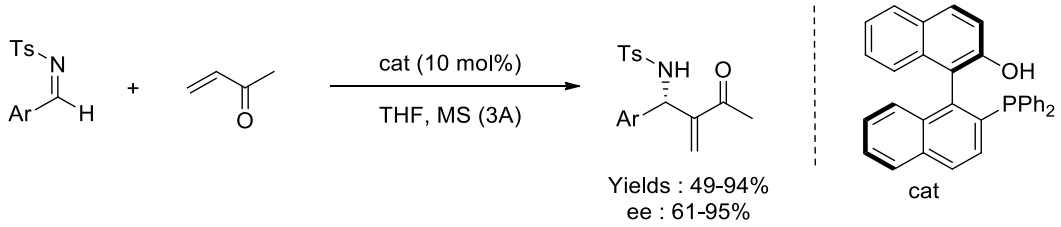

Scheme 1.1 Asymmetric aza-MBH catalysed by chiral phosphine as Lewis base.

In this reaction, a dual catalysis takes place. First, a n→π* interaction between the lone electron-pair of the phosphine and the enone leads to the formation of the enolate **1**. This event is assisted by a Bronsted catalysed stabilization of this intermediate **2** by a hydrogen bonding. In addition, due to these specific interactions, a very efficient chirality transfer takes place during the addition of the enolate **2** to the imine yielding the intermediate **3,** to form **4** after prototropic equilibrium. The proton delivery is either performed by the catalyst or the proton of the substrate (*Scheme 1.2*).

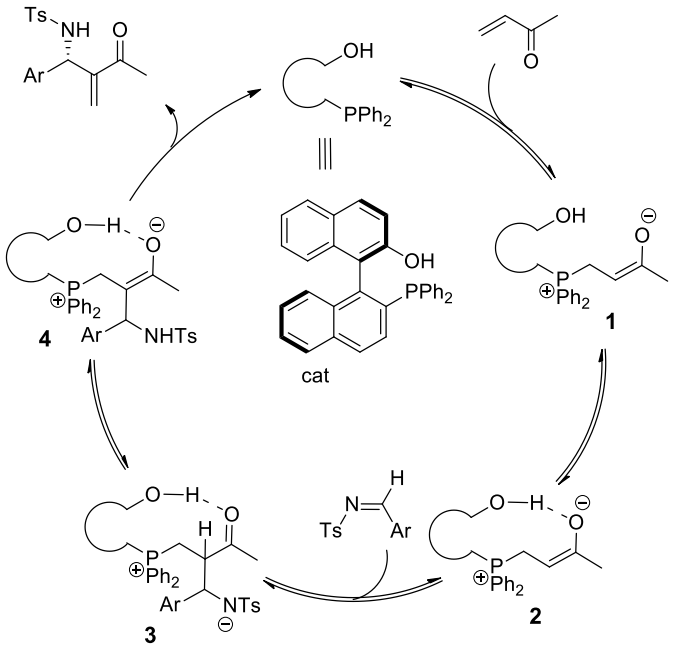

Scheme 1.2 Proposed reaction mechanism of the aza-MBH reaction.

Another nice illustration of the potential of phosphines as Lewis base catalysts is the three-component condensation of aldehydes, siloxyalkynes and amines, reported by Mrksich and Kozmin in 2013 (*Scheme 1.3*).[13] By exploiting a n→ σ* interaction between phosphine and

[12] Shi, M.; Li, C. Q. *J. Am. Chem. Soc.* **2005**, *127*, 3790.
[13] Montavon, T. J.; Li, J.; Cabrera-Pardo, J. R.; Mrksich, M.; Kozmin, S. A. *Nat. Chem.* **2011**, *4*, 45.

siloxane, the authors suggested the generation of a reactive ketene intermediate, which reacts with amine and aldehyde to furnish a β-hydroxyamide backbone with a high diastereomeric ratio. Regarding the mechanism, $(4\text{-anisol})_3P$ adds at the siloxane to yield a pentavalent silicon intermediate **5** which eliminates the ynolate **6**. The latter is protonated by the alcohol to furnish the ynol which rapidly tautomerizes into ketene **7**. Then a condensation, whose transition state can be formalized by a Zimmerman-Traxler model, yields the β-hydroxyamide.

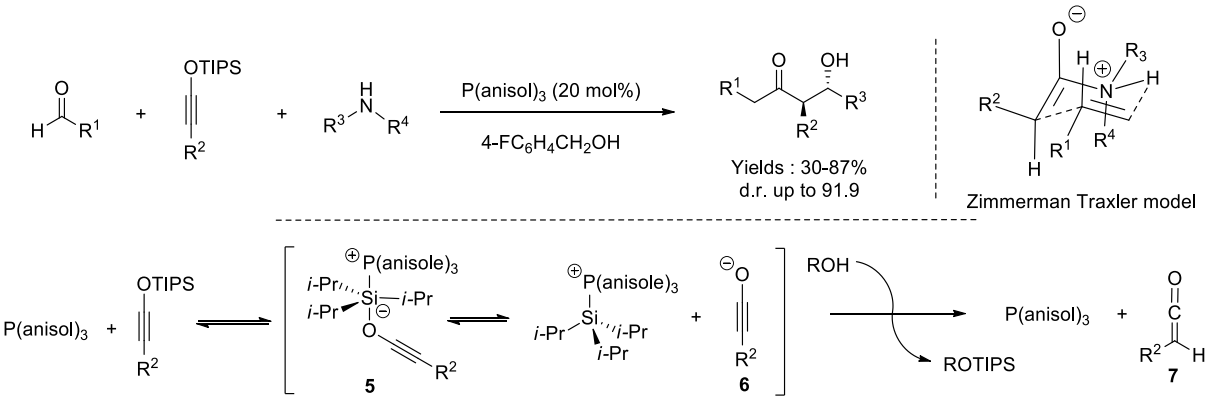

Scheme 1.3 Three components condensation reaction, proposed mechanism and transition state

A last example concerns the activation of B-B bonds and the catalytic C-B bond formation with a n→n* interaction between the electron lone-pair of phosphines and n* orbital of $B_2(pin)_2$. This strategy has been employed by Gulays et al. who developped the first metal-free asymmetric boron-addition reaction with achiral boron reagents. [14] The authors showed that PPh_3 or the chiral phosphine Josiphos (4 mol%) are able to promote the reaction with an excess of Cs_2CO_3 (15 mol%) in the presence of methanol (2.5 eq) at 70°C in THF (*Scheme 1.4*).

[14] Bonet, A.; Gulyás, H.; Fernández, E. *Angew. Chem. - Int. Ed.* **2010**, *49* (30), 5130.

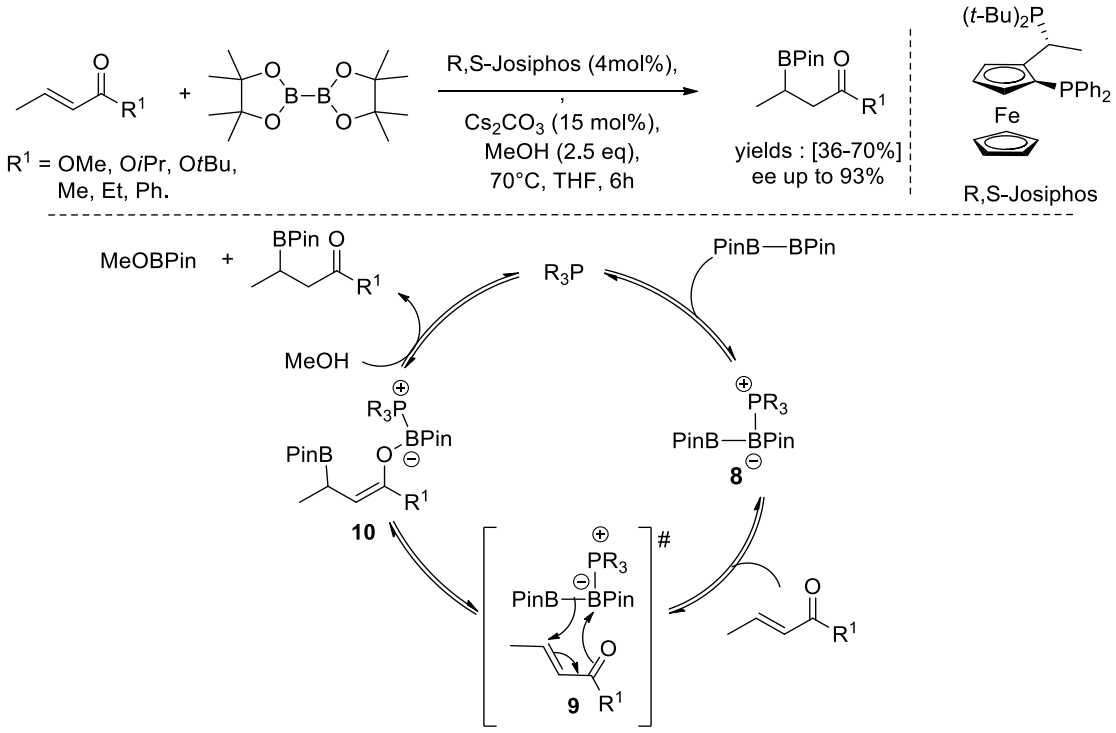

Scheme 1.4 Asymmetric boron addition at enones catalysed by chiral phosphines.

The proposed reaction mechanism starts with the formation of the phosphine-borane complex **8** upon the reaction of the phosphine with the Lewis acid B_2pin_2. This ate complex reacts then with the enone though the formation of the adduct **9**, in which the heterolytic cleavage of the B-B bond occurs **9**, as highlighted by Hoveyda et al.[15b] It gives rise to the boron enolate **10**, which yields the 1,4-boryl adduct upon hydrolysis with methanol. It is proposed that the base assists the B-B bond cleavage while the methanol hydrolyses the B-O bond of **10**, yielding the product.

The three previous examples clearly evidence the great potential of phosphines to activate pro-nucleophiles by various key interactions. More importantly, it highlights that the understanding of the reactivity of P-atom is a key to anticipate unprecedented reactions.

1.3. Boranes as Lewis acid catalysts

1.3.1. Electronic structure of the boron atom and properties of organoboron compounds

Boron chemistry is traditionally associated with the concept of Lewis acidity. Indeed, according to the electronic structure of boron [$_5$B]: [He] $2s^2$ $2p^1$ and after hybridization, it remains an empty p orbital along with three sp^2 orbitals (*Figure 1.7*). Consequently, neutral organoboron compounds will adopt a unique trigonal planar molecular geometry and behave as electron

[15] a) Dang, L.; Lin, Z.; Marder, T. B. *Chem. Commun.* **2009**, 3987 b) Lee, K. S.; Zhugralin, A. R.; Hoveyda, A. H. *J. Am. Chem. Soc.* **2009**, *131*, 7253.

lone pair acceptors. Those unique properties led to use them in organocatalysis, designing fluoride and cyanide anion sensors and optoelectronics due to their non-linear optical properties.[16]

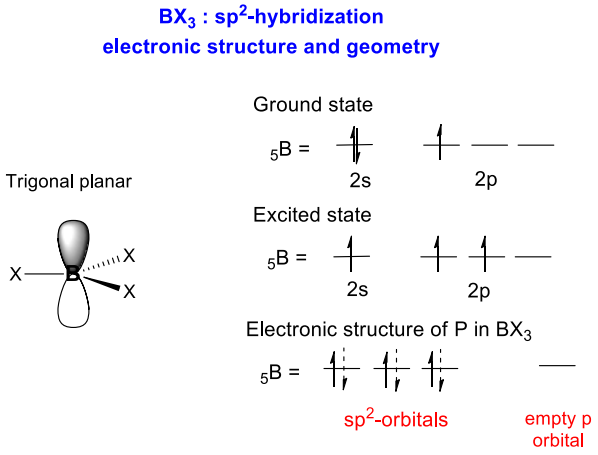

Figure 1.7 Electronic structure and geometry of B-atom in BX_3.

During the last years, several methods have been developed to quantify the Lewis acidity of these compounds. Nowadays, three different scales for the estimation of Lewis acidity of boron compounds exist. The first one is based on the fluoride ion affinity (FIA) of Lewis acids as a quantitative measure of their acidity, but rarely used in the literature.[17] The two others, more popular, are based on NMR spectroscopy. The Gutmann-Beckett method, initially introduced to describe the acidic character of solvents, is based on the change in the ^{31}P NMR chemical shift of Et_3PO upon complexation with a Lewis acid.[18] This method was extended by Beckett et al. to a wide range of Lewis acids.[19] The second popular method has been introduced by Childs et al. and is based on the ^{1}H NMR changes of the γ-proton of crotonaldehyde upon complexation with Lewis acids compared to the chemical shift of the γ-proton in crotonaldehyde-BBr_3 complexes.[20] Hence, an acidity scale can be built up based on these methods (*Figure 1.8*).

[16] a) G. Kaur, N. Lin, H. Fang, B. Wang, in: C.D. Geddes, J.R. Lakowicz (Eds.), Glucose Sensing. Topics in Fluorescence Spectroscopy, vol. 11, Springer, **2006**, pp. 377–397 b) Z. Guo, I. Shin, J. Yoon, *Chem. Commun*. **2012**, *48*, 5956–5967 c) E. Galbraith, T.D. James, *Chem. Soc. Rev*. **2010** ,*39*, 3831–3842

[17] Sivaev, I. B.; Bregadze, V. I. *Coord. Chem. Rev.* **2014**, *270–271*, 75.

[18] Gutmann, V. *Coord. Chem. Rev.* **1976**, *18* (2), 225.

[19] Beckett, M. A.; Strickland, G. C.; Holland, J. R.; Varma, K. S. *Polymer*, **1996**, 37, 4629–4631.

[20] a) Childs, R. F.; Mulholland, D. L.; Nixon, A. *Can. J. Chem.* **1982**, *60*, 801. For extended values with perfluoroaryl boranes see b) L. Luo, T.J. Marks, in: *Topics in Catalysis*, Vol. 7, Baltzer AG, Amsterdam, **1999**, pp.97.

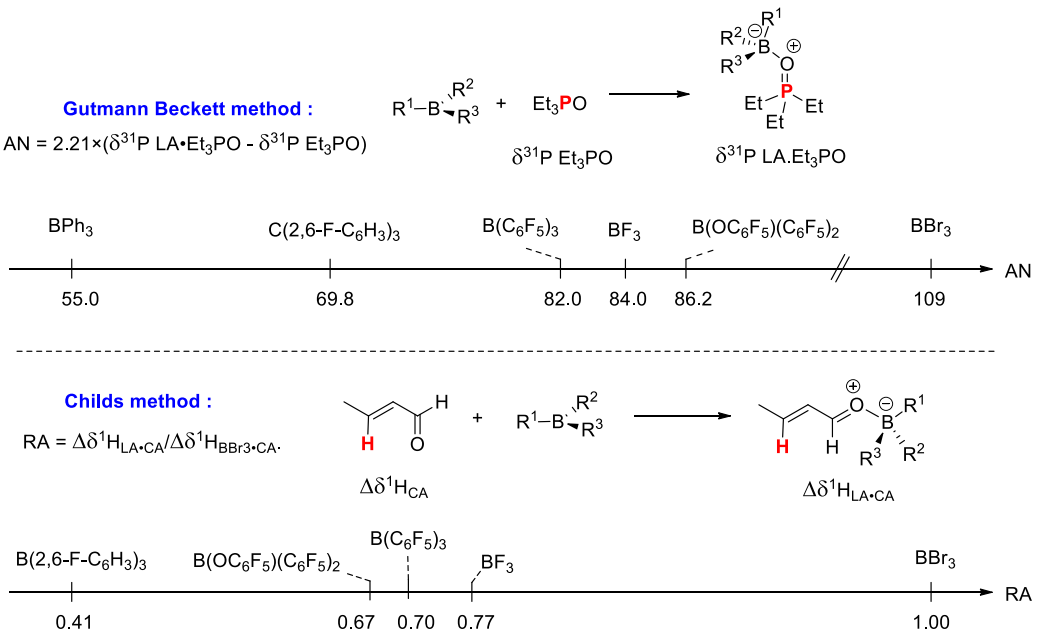

Figure 1.8 classification of the Lewis acidity of selected organoboron compounds according to two methods. AN = Acceptor Numbers, RA = Relative Acidity, CA = Crotonaldehyde.

Those experimental measurements clearly highlight the great potential of perfluorinated boron compounds such as $B(C_6F_5)_3$ and $B(OC_6F_5)(C_6F_5)_2$ as strong Lewis acids, which have a similar Lewis acidity as BF_3. However, an appreciable difference exists between BF_3 and perfluorinated boranes. Indeed, the steric hindrance of the bulky ligands renders hardly accessible the empty p orbital. It confers unique properties to sterically encumbered boranes such as stability to air and water ($B(C_6F_5)_2(C_6Cl_5)$)[21]. A major application of this property in Frustrated Lewis Pairs will be developed later on.

1.3.2. Nomenclature of organoboron compounds

Owing to their unique geometry, organoboron compounds have a relatively simple nomenclature which is drawn according to the IUPAC rules of nomenclature.[9]

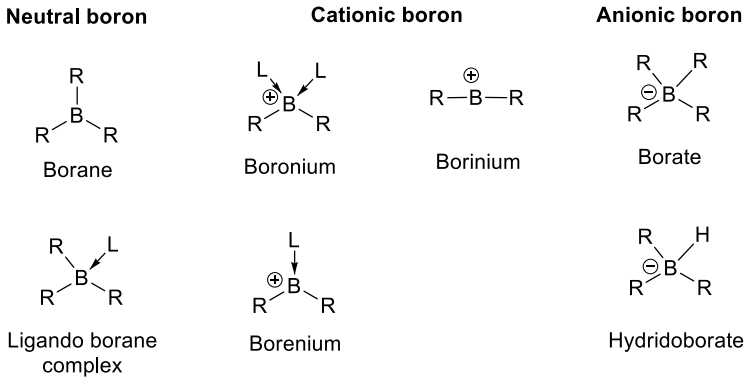

Figure 1.9 Nomenclature of organoboron compounds

[21] Scott, D. J.; Fuchter, M. J.; Ashley, A. E. *Angew. Chem. Int. Ed.* **2014**, *53*, 10218.

It is extended to the charged boron atoms which are often involved in reaction mechanisms.

1.3.3. Boranes as Lewis acid catalysts

The emergence of borane-catalysed reactions was a milestone in the field of Lewis-acid catalysis which has long been restricted to the use of metal-based Lewis acids such as $AlCl_3$, $TiCl_4$ or $SnCl_4$. The attractiveness for those new metal-free catalysts is not only due to the absence of metal but more importantly to the high Lewis acidity of electron-deficient boranes (low LUMO) and their stability. In this context, $B(C_6F_5)_3$ is a staple Lewis acid catalyst due to its steric bulk coupled with the electron-withdrawing nature of the three C_6F_5 groups.[22]

A nice example of the efficiency of $B(C_6F_5)_3$ as a Lewis acid has been reported by Gevorguyan et al. in 2002 who suggested that this Lewis acid can generate a reactive silylium cation in the hydrosilylation of alkenes (*Scheme 1.5*).[23] This concept has previously been reported by Lambert et al. who employed the triarylcarbenium cation $[Ph_3C]^+[B(C_6F_5)_4]^-$ as an organic Lewis acid.[24]

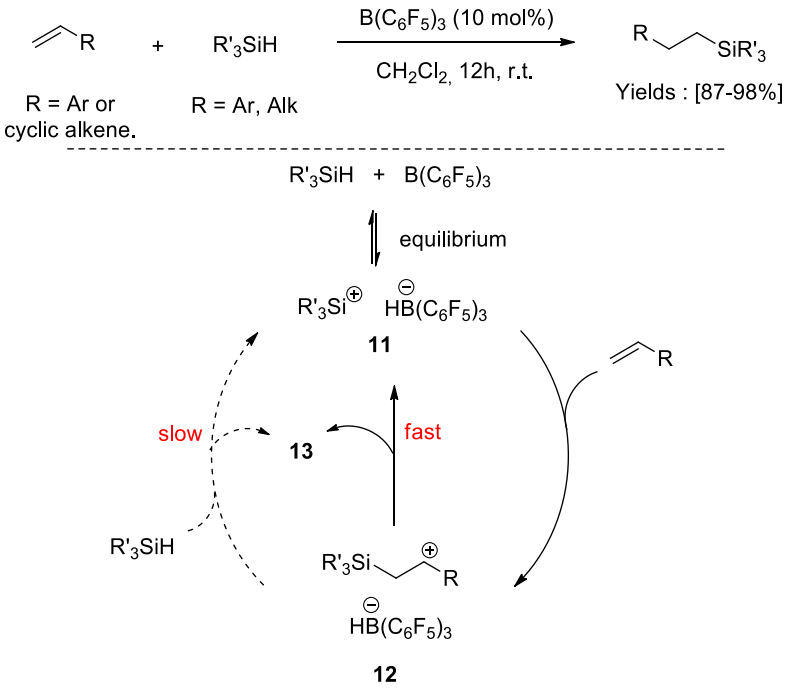

Scheme 1.5 Hydrosilylation of alkenes catalysed by a silylium cation and proposed mechanism.

This hydrosilylation consists in the generation of the reactive silylium cation **11**. This strong Lewis acid is then trapped by the poorly nucleophilic aryl alkene to generate a stabilized carbocation **12**. Finally, a hydride transfer by $H[B(C_6F_5)_3]^-$ takes place to yield the

[22] Lawson, J. R.; Melen, R. L. *Inorg. Chem.* **2016**.
[23] Rubin, M.; Schwier, T.; Gevorgyan, V. *J. Org. Chem.* **2002**, *67*, 1936.
[24] a) Lambert, J. B.; Zhao, Y. *J. Am. Chem. Soc.* **1996**, *118*, 7867. b) Lambert, J. B.; Zhao, Y.; Wu, H. *J. Org. Chem.* **1999**, *64*, 2729.

hydrosilylation product **13**. The asset of this reaction holds on the generation of a highly Lewis acid silylium cation with $B(C_6F_5)_3$.

Recently, another example reflecting the capacity of $B(C_6F_5)_3$ to activate hydroborane through a catalytic electrophilic C-H borylation of aniline has been reported by Oestriech and al (*Scheme 1.6*).[25]

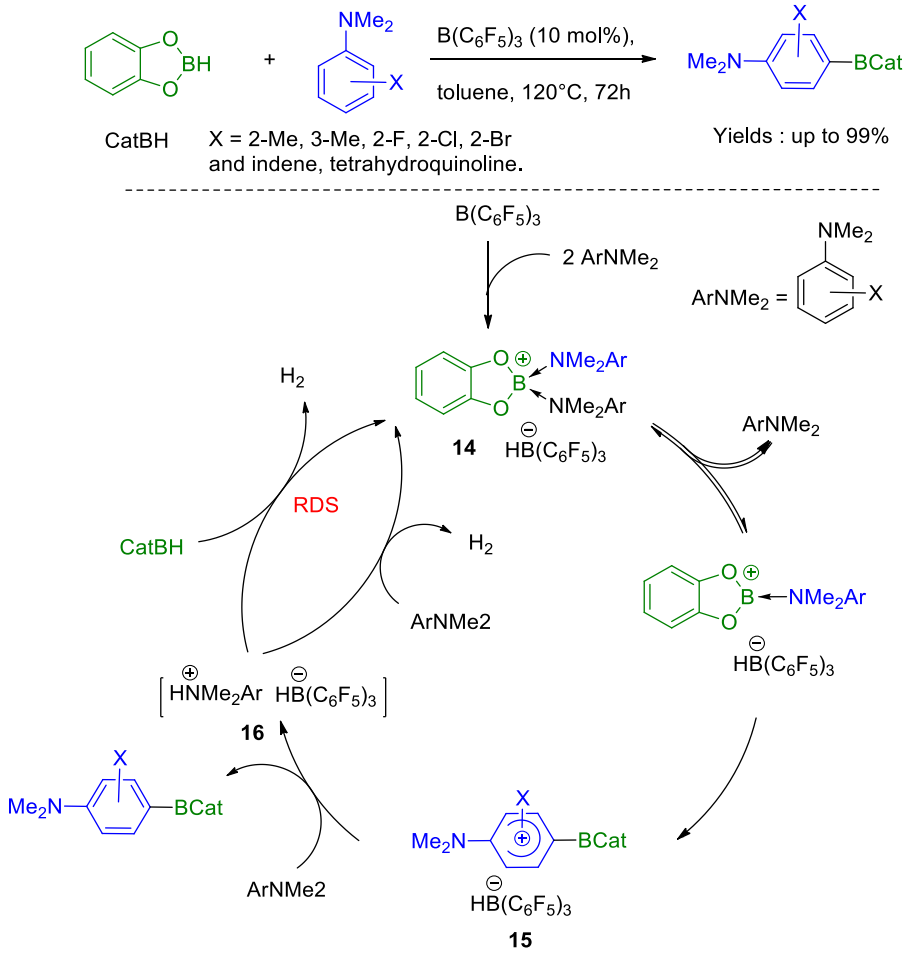

Scheme 1.6 : Borylation of aniline with catecholborane initiated by $B(C_6F_5)_3$.

The formation of a highly reactive borenium cation **14** stabilized by the coordination of aniline was initiated via a hydride transfer from the catechol borane catBH to $B(C_6F_5)_3$ ($\sigma \rightarrow n^*$ interaction). After decoodination of a ligand, an electrophilic aromatic substitution of aniline to the borenium led to the Whealand intermediate analogue **15** which is rapidly deprotonated by the aniline. The activated complex ammonium hydridoborate **16** released H_2 in a final step which has been identified as the rate-determining step (RDS). Here again, the presence of $B(C_6F_5)_3$ as initiation source allows the formation of a more reactive Lewis acid.

[25] Yin, Q.; Klare, H. F. T.; Oestreich, M. *Angew. Chemie Int. Ed.* **2017**, *56*, 1.

Another kind of reactivity is the activation of acid-sensitive electrophiles with the use of $H_2O.B(C_6F_5)_3$. In this field, Moran et al. have developed an efficient methodology to perform the S_N1 substitution of numerous acid-sensitive allylic alohols using only 1 mol% of $B(C_6F_5)_3$ with yields ranging from 55 to 99% in nitrobenzene at either 22 or 80°C (*Scheme 1.7*).[26] More importantly, they showed that the Lewis acidity of $H_2O.B(C_6F_5)_3$ is strong enough to activate the substitution of allylic alcohol but is also able to release H_2O (no product inhibition).

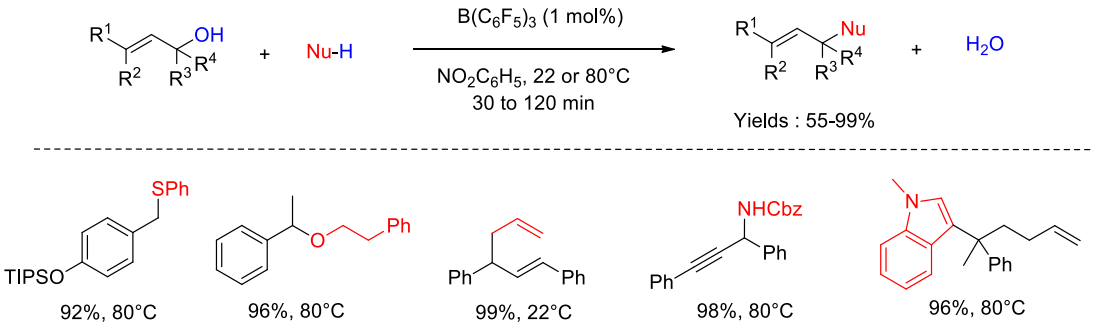

Scheme 1.7 Intermolecular $B(C_6F_5)_3$-catalyzed alcohol substitution in the presence of acid-labile protecting groups or acid-sensitive functionalities

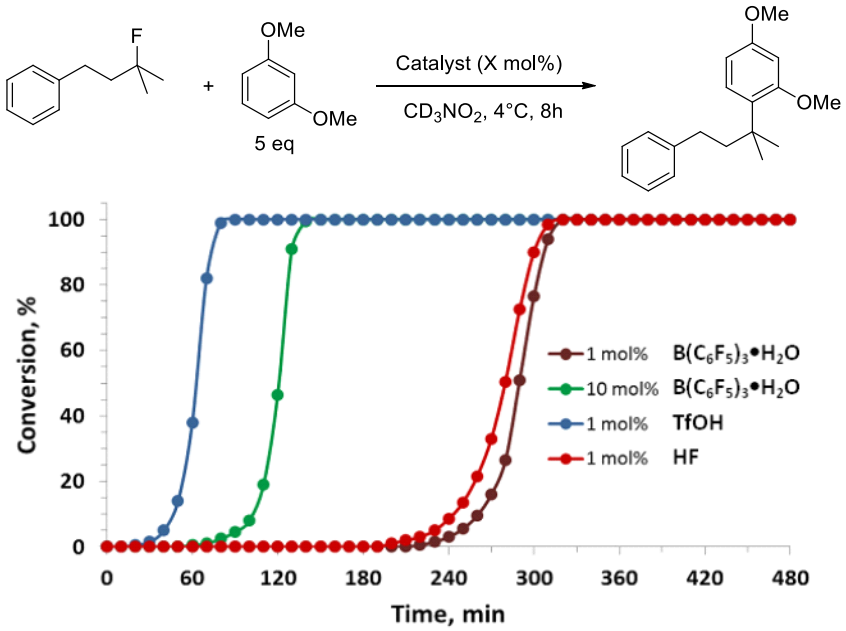

Figure 1.10 Time-dependent NMR study at 4 °C revealing an autocatalytic kinetic profile (taken from ref 26c).

The same group has extended the concept to the development of a mediated $H_2O.B(C_6F_5)_3$ Friedel-Craft reactions of tertiary aliphatic fluorides. The method has been showed to be

[26] a) Hellal, M.; Falk, F. C.; Wolf, E. ; Dryzhakov, M.; Moran, J. *Org. Biomol. Chem.*,**2014**, *12*, 5990 b) Dryzhakov, M.; Richmond, E.; Moran, J. *Synthesis* **2016**, *48*, 935 c) Dryzhakov, M.; Moran, J. *ACS Catal.* **2016**, *6*, 3670.

completely selective for F- over other leaving groups and displays an autocatalytic kinetic profile (*Figure 1.10*).

1.4. Lewis acid Lewis base dual catalysis by phosphine borane

Owing to their high activity in Lewis base catalysis from one side and Lewis acid catalysis from the other side, phosphine borane compounds have been used in a dual Lewis acid Lewis base catalysis. Based on this strategy, Bourissou et al. have shown that the PB ligands **17** are able to cleave the dimeric [Pd(μ-Cl)(allyl)]$_2$ to form a complex **18** with a strong P-Pd interaction but also, and more surprisingly, a B-Pd interaction.[27] The same ligand was also able to displace the labile dimethyl sulphide ligand from (Me_2S)AuCl yielding the complex **19** with a short Au-B bond (*Scheme 1.8*). Those two examples highlighted that monophosphine-borane ligands behave as bidentate ambiphilic ligands.

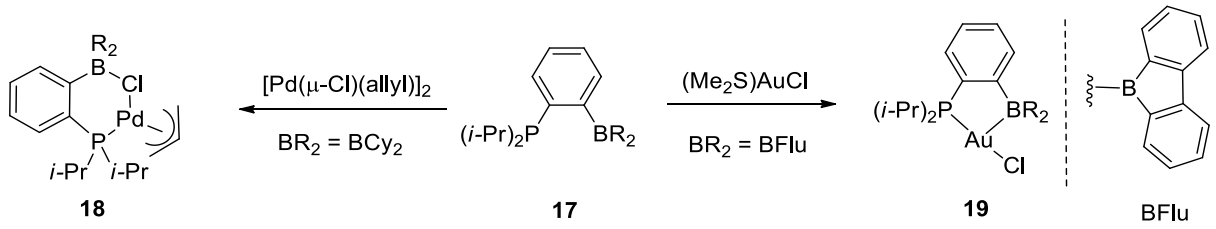

18 **17** **19** BFlu

Scheme 1.8 Phosphine borane amphiphilic ligand in the complexation of Pd and Au metals.

Aware of these properties, Fontaine et al. used PB ligands as organocatalysts for the challenging reduction of CO_2 to methanol using hydroboranes.[28] This methodology combines the nucleophilic activation of CO_2 by a n→π* interaction with the phosphine which is immediately quenched by a n→n* interaction with the borane to reversibly yield **20**. The latter is first reduced by the external hydride donor HBcat to yield the formaldehyde-catalyst adduct **21**. Finally, a second reduction step with HBcat yielded the reduced form **22** which is subsequently reduced with a third equivalent of hydride to furnish **23** (*Scheme 1.9*). Computational studies showed that, as soon as the coordination of CO_2 takes place, the reduction pathway is thermodynamically highly favourable highlighting the importance of the Lewis acid character of the borane and the Lewis basic character of the phosphine in the catalyst.

[27] Bontemps, S.; Bouhadir, G.; Miqueu, K.; Bourissou, D. *J. Am. Chem. Soc.* **2006**, *128*, 12056.
[28] Courtemanche, M.-A.; Légaré, M.-A.; Maron, L.; Fontaine, F.-G. *J. Am. Chem. Soc.* **2013**, *135*, 9326.

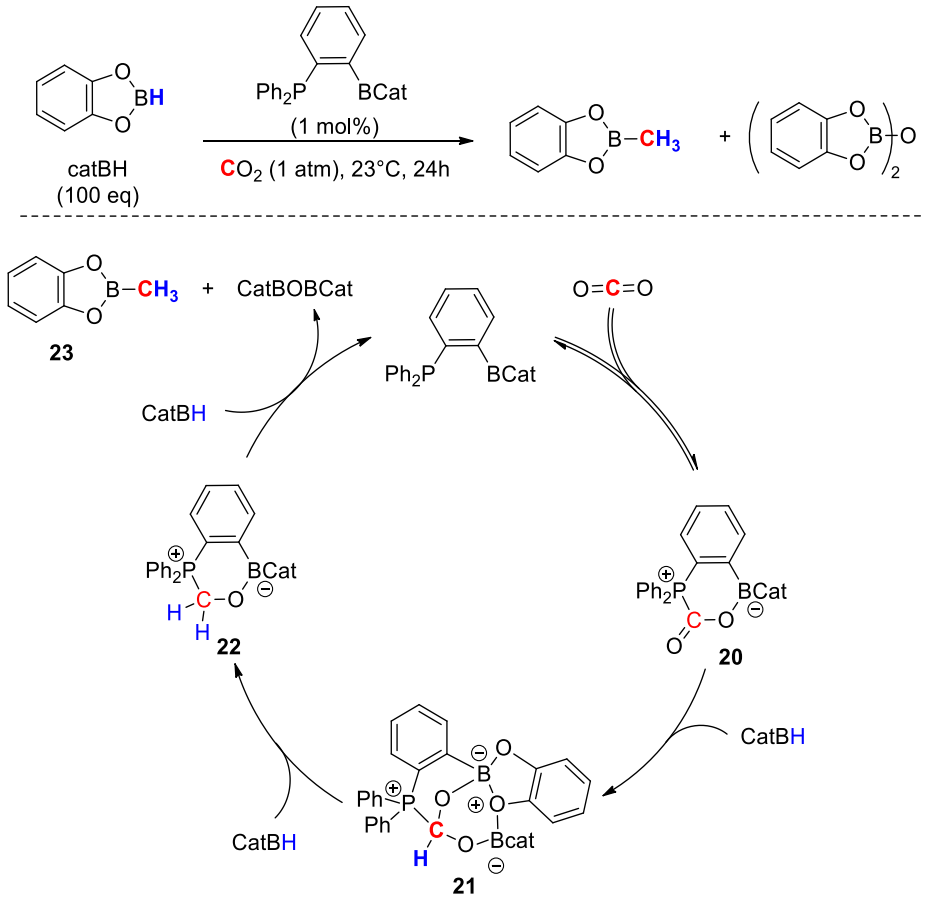

Scheme 1.9 Catalytic four electrons reduction of CO_2 in methanol analogues using a dual Lewis acid Lewis base catalyst.

2. From Lewis acid Lewis base complexes to Frustrated Lewis Pairs.

When a Lewis acid is directly in the presence of a Lewis base, they quench each other. The resulting so-called Lewis-acid Lewis-base complex is characterized by novel properties which are completely different from those of the free components.

2.1. Phosphorous-borane (P-B) Lewis-acid Lewis-base complexes

2.1.1. Electronic and structural description of P-B complexes.

The nature of the chemical bond between a Lewis-acid and a Lewis-base in the complex is tricky. In 1976, Damasco et al. reported an extensive study on the nature of P-B bond based on ^{31}P and ^{11}B NMR measurements.[29] The results were consistent with a σ-bond model between P and B. However, based on ^{11}B-^{1}H coupling constants, they were not able to discriminate between the σ-bonding and borane hyperconjugative models (*Figure 1.11*). The latter one is less frequently quoted in the literature although it explains high thermal and oxidative stability of the phosphinoborine trimers and tetramers, $(R_2PBH_2)_{3,4}$. It also

[29] Cowley, A. H.; Damasco, M. C. *J. Am. Chem. Soc.* **1970**, *93*, 6815.

rationalizes the existence of $COBH_3$ and PF_3BH_3 and the nonexistence of species such as $COBF_3$, PF_3BF_3, and NF_3BF_3.[30] More precisely, it corresponds to a π-interaction between the σ-BH bond and the d orbitals of the phosphorous which can be seen as a hyperconjugation (*Figure 1.11*).

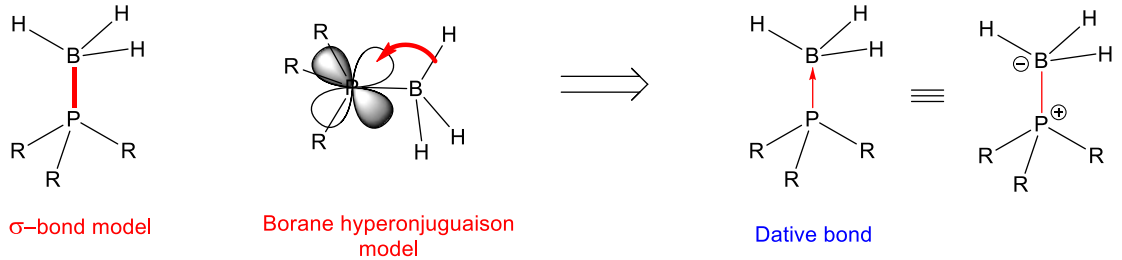

Figure 1.11 σ-bond and borane hyperconjugation models to describe the dative P-B bond between phosphine and borane.

As a consequence of the predominance of the σ-bond, the term "dative bond", referring to the P-B bond, is commonly used in the literature. It is also supported by the sp^3 hybridized of P and B as witnessed by the tetrahedral geometries of the two atoms.

A second important type of parameters which strongly influences the nature of the P-B bond is the polarity and the polarizability of the bond. Indeed, depending on the substituents at the phosphorus atom, the strength of the P-B bond can significantly be affected. Parry and Snow suggested that the unusual stability of HF_2PBH_3 compared to F_3PBH_3 is due to the fact that the two fluorines on HF_2P do not pull the electron pair back as far as the three fluorines on F_3P.[31] As a result, stronger overlap occurs at the bonding distance (1.83 Å). When H_3P is the Lewis base instead of F_3P, the electron cloud is so diffuse and the distance is so large that the bond is weak.

2.1.2. Consequences of the coordination to the B-H and P-H bonds.

Another consequence of the quenching of the electron lone pair of phosphines with boranes is the increase of the acidity of the P-H bond. Indeed, the P-B σ-bond decreases the electron density on the phosphorous, weakening the adjacent P-H bond. In 2009, Guillemin et al. investigated the effect of boron on the acidity of phosphine boranes complexes.[32] Their experimental and theoretical studies on a series of phosphines and their resulting phosphine borane complexes showed that BH_3 attachment leads to a substantial increase (from 80 to 110

[30] W. A. G. Graham and F. G. A. Stone, **1956** *J. Inorg. Nucl. Chem.*, 3, 164.
[31] a) Parry, R.W.; Edwards, L.J. J. Am. Chem. Soc. **1959**, 81, 3554. 21. b) Snow, S.A. Studies of Boranes and Metalla Boranes: I. Metal Complexes of Bis(trimethylphosphine)-Diborane(4). II. Synthesis and Characterization of 2-(Dichloroboryl)pentaborane(9); Ph.D. Dissertation, University of Utah: Salt Lake City, UT, 1985; see Abstract.
[32] Hurtado, M.; Yanez, M.; Herrero, R.; Guerrero, A.; Juan, Z. D.; José-Luis, M. A.; Khater, B.; Guillemin, J. C. *Chem. - A Eur. J.* **2009**, *15*, 4622.

kJ/mol) in the intrinsic acidity of the phosphine borane complex. Moreover, the acidity-enhancement was evaluated to be between 13 and 18 orders of magnitude in terms of ionization constants (*Table 1.2*).

Table 1.2 Experimental and calculated gas-phase acidities (GA) values. All values in kJ/mol. Calculated values, obtained at the B3LYP/6-311++ G(3df,2p) level, are given in italics

$$HA\ (g) \xrightarrow{\Delta_r G^0_m} H^+\ (g) + A^-\ (g)$$

Phosphine	GA (RPH_2)	GA ($RPH_2.BH_3$)	–δGA
$PhPH_2$	1457.3 (±0.8)	1375.0 (±2.5)	82.3
	1455.1	*1379.1*	*76.00*
$PhCH_2PH_2$	1493.8 (±0.9)	1380.4 (±2.5)	*113.4*
	1495.3	*1382.8*	*115.1*
$c\text{-}C_3H_5PH_2$	1510.0 (±3.0)	1408.9 (±2.8)	101.1
	1507.8	*1402.0*	*105.8*
CH_3PH_2	1530.0 (±3.0)	1411.9 (±2.3)	118.1
	1530.7	*1410.2*	*120.5*

On the other hand, the B-H bond is also significantly affected. In a seminal work dedicated to understanding the reactivity of N-heterocyclic carbene boryl radicals, Curran et al. have demonstrated that the Bond Dissociation Energy (DBE) of the B-H bond of carbene-borane complexes is significantly lower than those of other hydrogen donors.[33] While it is comparable to that of TTMS (tris(trimethylsilyl)silane), it is less labile than the Sn-H bond of Bu_3SnH (*Figure 1.12*).[34] In the case of NHC-BH_3, the resulting radical is delocalized over the whole NHC moiety while in the case of Bu_3P-BH_3, only d orbitals are able to stabilize, to some extent, the radical.

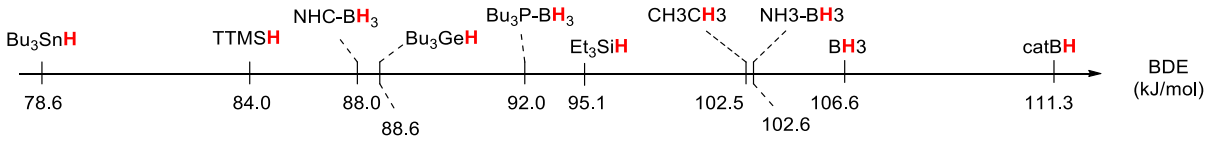

NHC-BH3 = 1,3-bis-(2,6-diisopropylphenyl)imidazol-2-ylidene borane

Figure 1.12 BDE of several hydride donors based on CBS-4 energy. Basis set: (6- 311+G(3d2f,2df,p)) and HF/3-21G.*

[33] Ueng, S. H.; Solovyev, A.; Yuan, X.; Geib, S. J.; Fensterbank, L.; Lacôte, E.; Malacria, M.; Newcomb, M.; Walton, J. C.; Curran, D. P. *J. Am. Chem. Soc.* **2009**, *131* (31), 11256.
[34] a) Ueng, S. H.; Solovyev, A.; Yuan, X.; Geib, S. J.; Fensterbank, L.; Lacôte, E.; Malacria, M.; Newcomb, M.; Walton, J. C.; Curran, D. P. *J. Am. Chem. Soc.* **2009**, *131*, 11256. b) Rablen, P. R. *J. Am. Chem. Soc.* **1997**, *119* (35), 8350. c) Rablen, P. R.; Hartwig, J. F. *J. Am. Chem. Soc.* **1996**, *118*, 4648.

Alongside from a decrease of the BDE of the B-H bond, the coordination of BH_3 has also an influence on the hydricity of the hydride. Mayr et al. measured kinetics of the reaction of NHC-borane with various electrophiles and showed that they are better hydride donors than the well-known Hantzsch esters (*Figure 1.13*).[35] Furthermore, they were able to reduce imines or molononitriles and perform a one-pot reductive amination. The reactivity of these hydride donors has been attributed to the stability of the resulting borenium cation exerted by the substituents of the boron atom. Surprizingly, the hydricity of phosphine borane complexes has been omitted, even though it has been shown that they react with strong Bronsted acids, providing an insight of their potential as neutral hydride donors.[36]

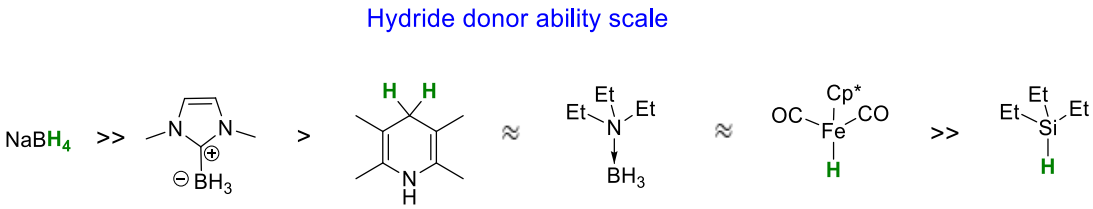

Figure 1.13 Plot of a qualitative hydride donor ability of several hydride donors.

2.1.3. Phosphine boranes complexes in organic synthesis

A challenging type of reactions, which continues to abstract the attention of researchers is perhaps the dehydrogenation of organic compounds such as amine, phosphine and carbene borane complexes.[37] Phosphine-borane complexes were found to undergo thermal dehydrocoupling in the 1950s when monomers were heated to 150 °C and released hydrogen to form a mixture of cyclic trimer and tetramers.[38] In this regard, Manners et al. who showed that he dehydrocoupling of secondary and primary phosphine borane complexes can be achieved by using a Rh-based catalyst $[Rh(1,5\text{-cod})(\mu\text{-Cl})]_2$ or the salt $[Rh(1,5\text{-cod})2][O_3SCF_3]$. However, a thermal activation, about 90°C, is necessary to observe the formation of H_2 along with the linear diboraphosphine (*Scheme 1.10*).[39]

[35] a) Horn, M.; Schappele, L. H.; Lang-Wittkowski, G.; Mayr, H.; Ofial, A. R. *Chem. - A Eur. J.* **2013**, *19*, 249. b) Horn, M.; Mayr, H.; Lacôte, E.; Merling, E.; Deaner, J.; Wells, S.; McFadden, T.; Curran, D. P. *Org. Lett.* **2012**, *14*, 82.
[36] a) Cazorla, C.; De Vries, T. S.; Vedejs, E. *Org. Lett.* **2013**, *15*, 984. b) Denmark, S. E.; Werner, N. S. *Org. Lett.* **2011**, *13*, 4596.
[37] a) Staubitz, A.; Robertson, A. P. M.; Sloan, M. E.; Manners, I. *Chem. Rev.* **2010**, *110* (7), 4023. b) Johnson, H. C.; Hooper, T. N.; Weller, A. S. *Top. Organomet. Chem.* **2015**, *49*, 153.
[38] Burg, A. B.; Wagner, R. I. *J. Am. Chem. Soc.* **1952**, *75*, 3872.
[39] Dorn, H.; Singh, R; A.; Massey, J. A.; Lough, A. J., Manners, I. *Angew. Chem. Int. Ed.* **1999**, *38*, 3321.

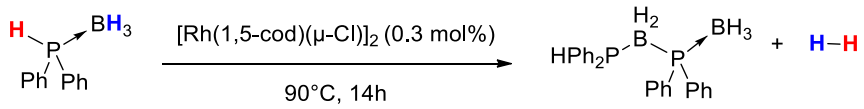

Scheme 1.10 Catalytic dehydrocoupling of H_3B-P(H)Ph_2 with Rh(I)

In 2003, an organocatalytic approach has been developed by Gaumont et al. who employed $B(C_6F_5)_3$ as a catalyst for the dehydrocoupling of the primary phosphine borane PhH_2P-BH_3 at 90°C.[40] Interestingly, only 5 mol% of the catalyst was necessary to completely release H_2 from PhH_2P-BH_3 yielding polyphosphinoboranes (*Scheme 1.11*). The authors proposed the formation of the intermediate **24** by ligand exchange. In addition, the acceptor strength of Lewis-acidic perfluororinated triarylborane should contribute to activate the P–H bond by withdrawing electron density from the phosphorus.

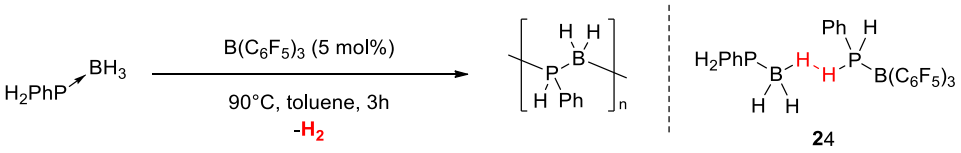

Scheme 1.11 : Dehydrocoupling of H_2PhP-BH_3 catalysed by $B(C_6F_5)_3$

These two examples highlight the potential of phosphine-borane complexes in the hydrogen storage challenge. Another application of P-B complexes is the C-P bond formation through a hydrophosphination pathway. The addition of a P-H bond across an unsymmetrical unsaturated carbon-carbon bond can give rise to two different isomers depending if it adds following a Markovnikov (α-addition) or anti-Markovnikov (β-addition) regioselectivity. The outcome of the reaction is usually dependent on the reaction conditions and challenges exist in controlling i) the regioselectivity and ii) the number of P-H additions (*Scheme 1.12*).

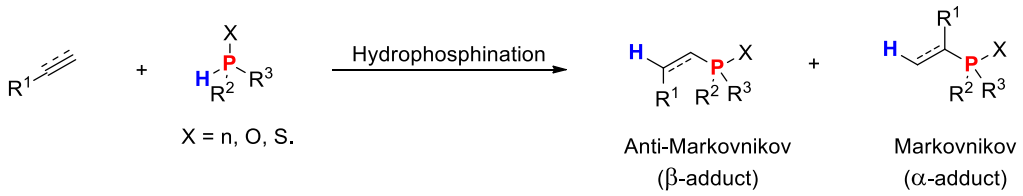

Scheme 1.12 Hydrophosphination of a multiple C-C bond and related regioisomers resulting from a Markovnikov addition or anti-Markovnikov addition.

The last two decades have witnessed an impressive number of publications related with these challenges.[41] For our concern, we will present two examples of hydrophosphination with

[40] Denis, J.-M.; Forintos, H.; Szelke, H.; Toupet, L.; Pham, T.-N.; Madec, P.-J.; Gaumont, A.-C. *Chem. Commun.* **2003**, No. 1, 54.
[41] a) Bange, C. A.; Waterman, R. *Chem. - A Eur. J.* **2016**, *22*, 1.

HPh_2P-BH_3 under either basic or metal catalysed conditions. First, Imamoto et al. reported the hydrophosphination of enones with HPh_2P-BH_3 catalysed by KOH. (*Scheme 1.13*).[42]

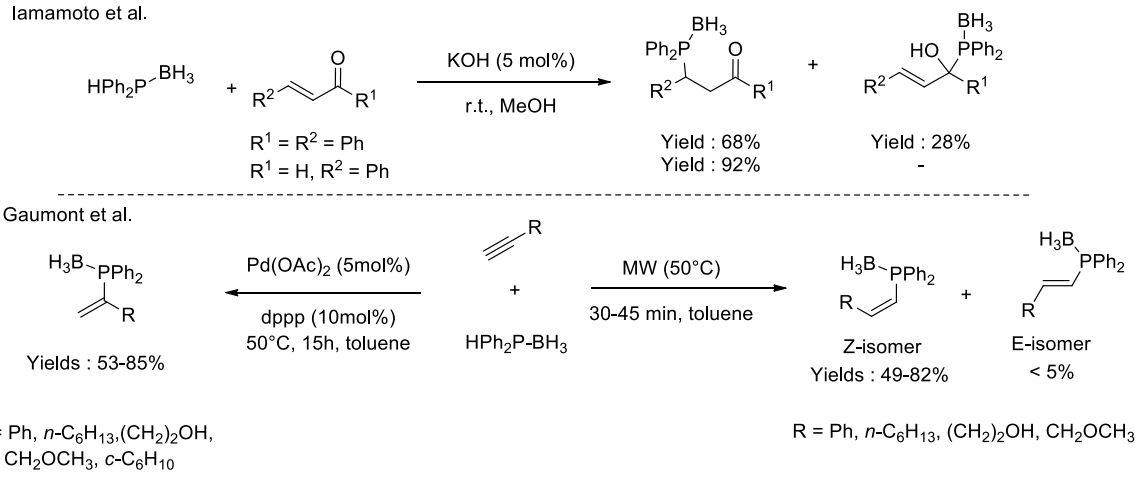

Scheme 1.13 Regioselective anti-Markovnikov hydrophosphination of enones and enal with KOH (top) and dual Anti-Markovnikov and Markovnikov hydrophosphination of alkynes either micro-wave assisted or Palladium catalyzed.

The reaction proceeds smoothly at r.t. and with a good selectivity for the 1,4-adduct. However, in the case of enals, the authors observed the formation of the 1,2 hydrophosphination adduct as a sole compound. As expected, no α-adduct was detected. Gaumont et al. reported a microwave assisted hydrophosphination of aliphatic and aromatic acetylene derivatives.[43] Within half an hour under irradiation at 50°C , the anti-Markovnikov addition takes place yielding vinylphosphine boranes in modest to good yields (from 49 to 82%). Interestingly, the addition of palladium catalyst reverses the regioselectivity in favour of the α-adduct with yields ranging from 53 to 85%.

Recently, Bourissou et al. used the strength of the P-B bond to isolate reactive borenium cations, which have a singular reactivity with Lewis base due to their strong Lewis acid character. They used a naphtyl bridge which exhibit unique properties to enforce the P-B interaction despite the steric shielding.[44]

[42] a) Imamoto, T.; Kusumoto, T.; Suzuki, N.; Sato, K. *J. Am. Chem. Soc.* **1985**, *107*, 5301. b) Imamoto, T.; Oshiki, T.; Onozawa, T.; Kusumoto, T. *J. Am. Chem. Soc.* **1990**, *112*, 5244.
[43] Mimeau, D.; Gaumont, A. C. *J. Org. Chem.* **2003**, *68*, 7016.
[44] a) Devillard, M.; Brousses, R.; Miqueu, K.; Bouhadir, G.; Bourissou, D. *Angew. Chem. Int. Ed.* **2015**, *54*, 5722. b) Devillard, M.; Mallet-Ladeira, S.; Bouhadir, G.; Bourissou, D. *Chem. Commun.* **2016**, *52*, 8877. c) Devillard, M.; Bouhadir, G.; Mallet-Ladeira, S.; Miqueu, K.; Bourissou, D. *Organometallics* **2016**, *35*, 3788.

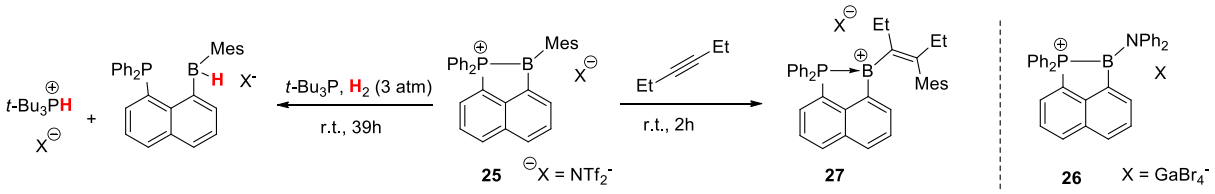

Scheme 1.14 Reactivity of P-(naphtyl) stabilized borenium cations with H_2 and 3-hexyne

Based on this strategy, they synthesized borenium **25**, and later on, they set up a new strategy to form **26** by involving an external NH compound. The strong interest in these new molecules is their ability to react with weak Lewis base such as H_2 or alkyne. Hence, the authors were able to cleave H_2 upon Lewis base assistance or to add **25** onto alkyne to yield the carboboration adduct **27** via the formation of a vinyl cation.

2.2. Formation of Frustrated Lewis Pairs (FLPs)

In all previous examples, we described systems possessing strong interaction between the electron lone pair of the phosphorous and the empty orbital of the boron. If now this interaction is prohibited due to the steric hindrance of both Lewis acid and base, the system behaves as if the free doublet of the Lewis base was “frustrated” and both Lewis acid and Lewis base will exist in solution without reacting with each other.

2.2.1. Brief history of the discovery of FLPs

The FLPs’ tale begins in the middle of the XXth century with the work of Brown et al. who noticed that the reaction between lutidine and trifluoroborane lead to the formation of the Lewis-acid Lewis-base complex **28** while the reaction with the same Lewis base with trimethylborane was unproductive.[45] By examining different models, they proposed that the steric interferences were responsible for these observations. In 1959, Wittig and Benz published a paper on the synthesis of benzyne using 2-fluorophenylmagnesium chloride. With the aim to bring more functionalization, the authors were surprised to observe that a mixture of triphenylphosphine and triphenylborane with the benzyne intermediate lead to the 1,2-phosphinoboration adduct **29** and not to the formation of the expected Lewis-acid Lewis base adducts Ph_3P-BPh_3 (*Figure 1.14*).[46]

[45] Brown, H. B.; Schlesinger, H. I.; Cardo, S. Z. *J. Am. Chem. Soc.* **1942**, *1743*, 325.
[46] Wittig, G.; Benz, E. *Chem. Ber.* **1959**, *92*, 1999.

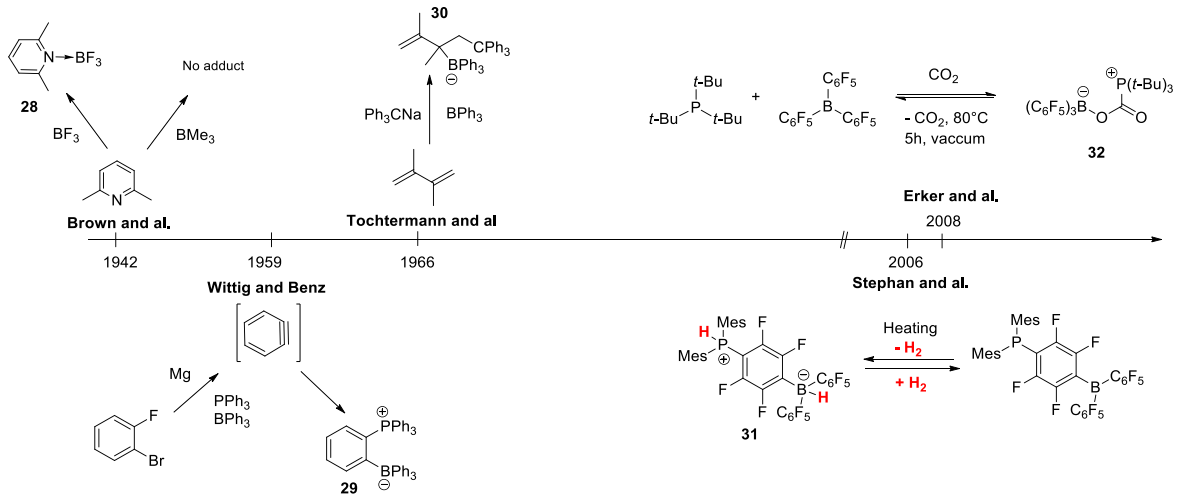

Figure 1.14 Brief history of the discovery of FLPs

The absence of interaction between sterically encumbered Lewis acids and Lewis bases was brought by Tochtermann in 1966. The authors found that 2,3-dimethylbutadiene was not attacked by tritylsodium salt alone, but forms a carbo-boration adduct **30** when triphenylborane was present. They proposed that the double bond was activated through the formation of a π-complex with BPh_3 followed by the nucleophilic addition of the stabilized carbanion. It is only in 2006 that the term "Frustrated Lewis Pairs" was proposed by Stephan et al. who found that H_2 could be reversibly cleaved by the phosphino-borane **31** possessing both a Lewis acid site and a Lewis base one.[47] In the same period, the group of Erker published a work dealing with the reversible activation of CO_2 with the frustrated Lewis pair t-$Bu_3P/B(C_6F_5)_3$ to yield the adduct **32**.[48]

2.2.2. Mechanistic investigations in the activation of H_2.

Since the discovery of FLPs, the activation of many other molecules such as CO, SO_2, N_2O etc. have been studied and several Lewis acids and bases have been designed in this way.[49] Several groups have also questioned mechanistic considerations in order to understand the activation mode of small molecules by FLPs.

Due to the steric hindrance of both Lewis acid and Lewis base, it is reasonable to assume that the FLP is not covalently bonded but forms an aggregate through Van der Walls interactions (Coulomb and dispersion) which is called an "encounter complex". This hypothesis has not been validated experimentally, presumably due to the dynamic of these complexes in

[47] Welch, G. C.; San Juan, R. R.; Masuda, J. D.; Stephan, D. W. *Science* **2006**, *314*, 1124.
[48] Mömming, C. M.; Otten, E.; Kehr, G.; Fröhlich, R.; Grimme, S.; Stephan, D. W.; Erker, G. *Angew. Chem., Int. Ed.* **2009**, *48*, 6643.
[49] For a review, see: Stephan, D. W.; Erker, G. *Angew. Chem., Int. Ed.* **2015**, *54*, 6400.

solution.[50] However, the association of $P(Mes)_3$ and $B(C_6F_5)_3$ has been investigated by NMR and has confirmed the presence of interactions with an equilibrium constant of K = 0.3-0.7 M^{-1} (*Figure 1.15*).

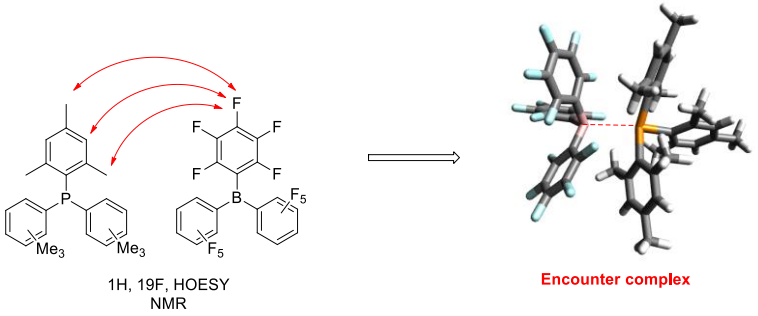

Figure 1.15 Encounter complex resulting from the association between $P(Mes)_3$ and $B(C_6F_5)_3$. Simulation by molecular mechanics with Avogadro®, force field: UFF, algorithm: steepest descent.

Based on this value, the Gibbs free energy of the formation of the encounter complex was calculated to be slightly endergonic by +0.4(±0.2) kcal/mol. This complex is able to polarize the molecule of H_2 via orbital interactions. Hence, an interaction between the HOMO of the Lewis base and the σ* of H_2 destabilizes the σ bond between the two hydrogens. This leads to an increase of the electron density on one hydrogen, allowing an interaction between the σ orbital and the LUMO of the Lewis acid (*Figure 1.16*).

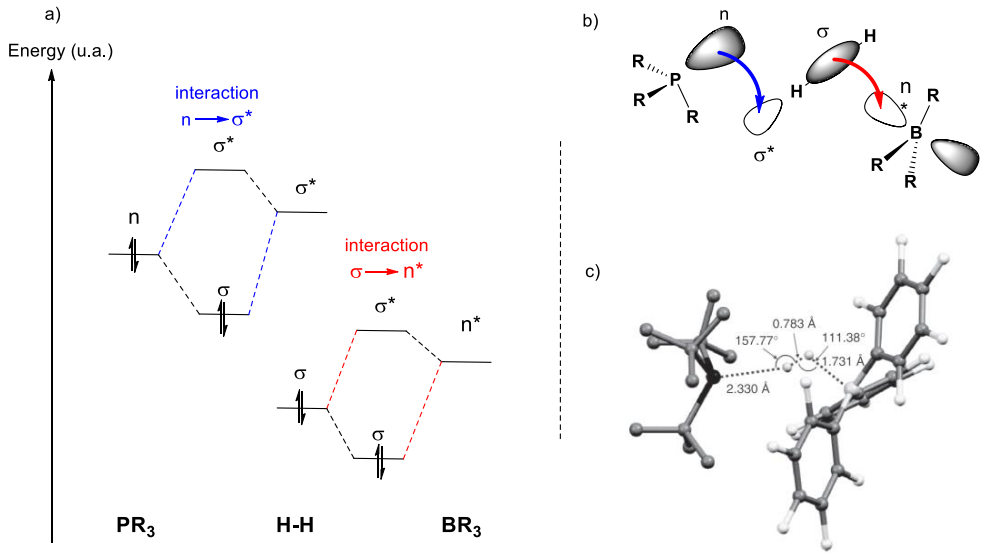

Figure 1.16 a) Orbital interactions in the FLPs activation of H_2 b) Representation of the transition state c) Calculated transition state of the activation of H_2 with t-$Bu_3P/B(C_6F_5)_3$ (representation with mercury).

These two interactions led Papai and later on Grimme to propose a transition state in which both P-H and B-H σ bonds are formed concomitantly with the destruction of the H-H σ bond

[50] Rocchigiani, L.; Ciancaleoni, G.; Zuccaccia, C.; MacChioni, A. *J. Am. Chem. Soc.* **2014**, *136*, 112.

as suggested by DFT-calculations.[51] Both authors found that the transition state of the H_2 activation by the FLP consisting of tBu$_3$P/B(C_6F_5)$_3$ adopts a geometry, which highlights a strong interaction between tBu$_3$P's lone pair and H_2 in an "end-on" (P–H–H angle 157.8°) and interactions of the empty orbital of B(C_6F_5)$_3$ in a "side-on" (B–H–H angle 111.4°) manner.

2.2.3. Applications of Frustrated Lewis pairs chemistry

The ability of many inter- and intramolecular FLPs to heterolytically cleave small molecules has resulted in the development of a variety of methods for metal-free catalytic functionalization. In this paragraph, we will limit the discussion to hydrogenation reaction resulting from the activation of H_2.

- General mechanism of the hydrogenation of unsaturated compounds

Complexes resulting from the heterolytic cleavage of H_2, are characterized by a Bronsted acid phosphonium cation and nucleophilic hydridoborate anion. Their performances in the hydrogenation of unsaturated compounds hinge on the acidity of the phosphonium ion to promote the protonation of the multiple bond and the hydricity of the hydridoborate to add on the resulting carbocation.

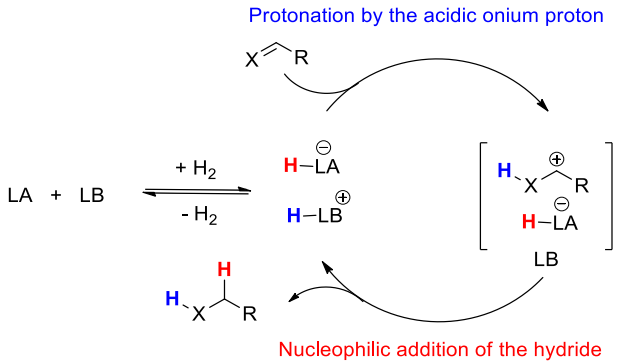

Figure 1.17 General mechanism of the hydrogenation of unsaturated compounds by FLPs

As a consequence, the choice of the Lewis acid (LA) and the Lewis base (LB) is crucial to modulate the reactivity of FLPs in hydrogenation reactions.

2.2.3.1. Catalytic hydrogenation by P/B FLPs

FLPs composed by a phosphine as a Lewis base and a borane as Lewis acid have been the first category to be developed. They represent good candidates to perform hydrogenation reaction because phosphonium salts are acidic protons, as reported by Goel et al., pK_a ($[HPh_3]^+[BF_4]^-$ = 2.7 and $[HP(Mes)_2]^+[BF_4]^-$ = 3.08.[52] As a consequence, with his initial catalyst, Stephan et al. shown that sterically demanding aldimines, protected nitriles, and an aziridine

[51] a) Rokob, T. A.; Hamza, A.; Stirling, A.; Pápai, I. *J. Am. Chem. Soc.* **2009**, *131*, 2029. b) Schirmer, B.; Grimme, S. *Chem. Commun.* **2010**, *46*, 7942.
[52] Allman, T.; Goel, R. G. *Can. J. Chem.* **1982**, *60*, 716.

were effectively hydrogenated in the presence of 5 mol % $(R_2PH)(C_6F_4)BH(C_6F_5)_2$ (R = Mes, tBu) at 80−120 °C under 1−5 atm H_2 in reaction times ranging from 1 to 48 h.[53]

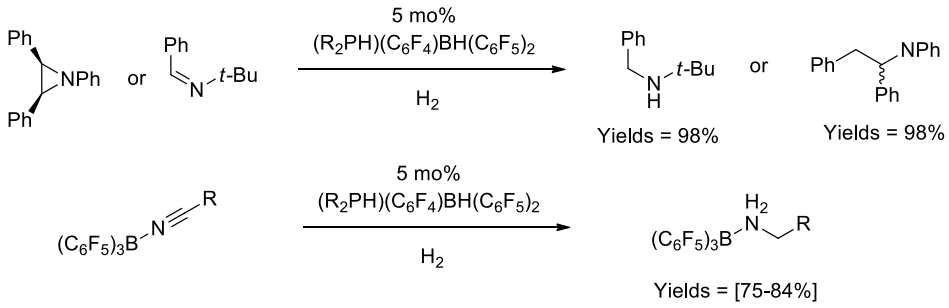

Scheme 1.15 Hydrogenation of aldimines, aziridines and nitrile with P/B

One of the oldest and most important application of the hydrogenation technology is the conversion of unsaturated hydrocarbons to alkanes or alkenes. This challenge has been overcome by Paradies et al. who used P/Bs under H_2 pressure to reduce a wide variety of unpolarised alkenes. It is however necessary to use weakly electron-releasing phosphines in order to form a highly acidic proton. The reactions preceeded smoothly in CH_2Cl_2 with 20 mol% of $B(C_6F_5)_3$ and either $(2,6\text{-}C_6H_3Cl_2)_3P$, $(C_{10}H_7)_3P$ or the less acidic bisphosphine GemPhos. The reactions were completed within 24 to 48h at 50°C and under 5 bar H_2 with yields ranging from 85 to 99%.

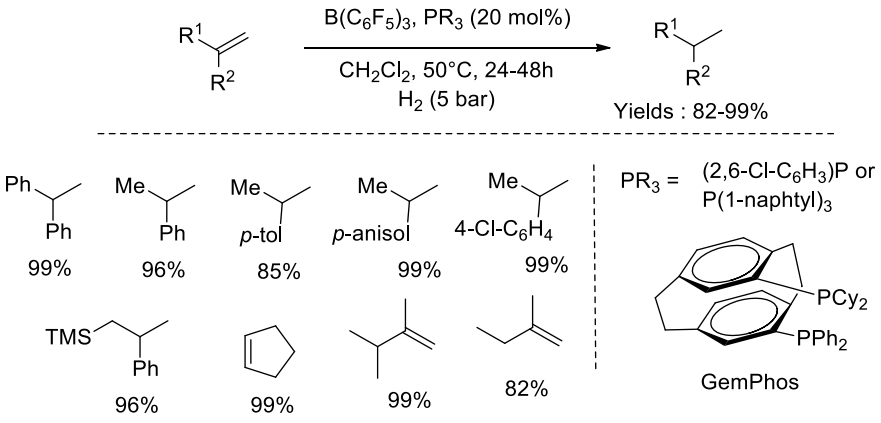

Scheme 1.16 Hydrogenation of alkenes with P/Bs

Seeking for extending the scope of the substrates, alkynes were involved in reduction methodology by P/B FLPs. However, depending on the nature of the phosphine, two adducts can be obtained. Reactions of $B(C_6F_5)_3$, tBu_3P, and PhC≡CH resulted in deprotonation of the alkyne, while the use of the less basic phosphine $(o\text{-}C_6H_4Me)_3P$ gave the 1,2-addition product

[53] Chase, P. A.; Welch, G. C.; Jurca, T.; Stephan, D. W. *Angew. Chem., Int. Ed.* **2007**, *46*, 8050.

(*Scheme 1.17*).[54] The use of intramolecular FLPs provided macrocyclic and chain-like species $[(H)C=C(Ph)Mes_2PC_6F_4B(C_6F_5)_2]_2$.

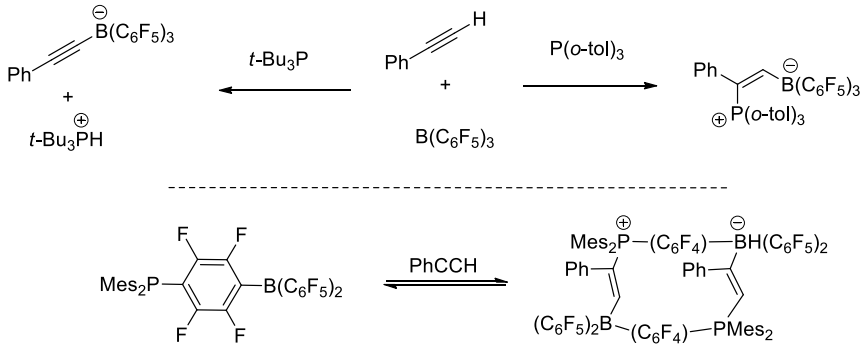

Scheme 1.17 Reaction of alkynes with P/B depending on the nature of the phosphine.

The case of carbonyl and carboxyl compounds is still problematic due to the competitive Lewis base character of the carbon-oxygen bond (catalyst inhibition). Even though FLP-based methodologies have been developed to perform the hydrogenation of aldehydes or ketones, there often consist on a tandem hydrosylilation/hydrogenation reaction.[55] More precisely, in a first step, the carbonyl is converted into a silyl enol ether which is easier to reduce due to the vanishing of the Lewis base character of the oxygen.

2.2.3.2. Catalytic hydrogenation by N/B FLPs

The limited range of substrates reduced by P/Bs FLP have encouraged researchers to seek for new catalysts with higher functional tolerance especially versus enone, enamine and imines. To reach this goal, the nature of the Lewis base has been changed. In this way, nitrogen containing Lewis bases have been found to be better candidates than phosphines due to the acidity of the proton in the corresponding ammonium salt. Because the electrophilicity of carbonyl compounds is lower than that of carbocations resulting from the activation of electron-rich alkenes,[56] the hydricity of the hydridoborate needed also to be enhanced. This could be done by decreasing the strength of the electron withdrawing groups of the Lewis acid. By combining those two criteria, Soós et al. performed the hydrogenation of carbonyl compounds with either TMP, DABCO or quinuclidine and $B(C_6F_5)_2(Mes)$. With this catalytic system, they were able to reduce imines, enamines and enones at room temperature

[54] a) Dureen, M. A.; Stephan, D. W. *J. Am. Chem. Soc.* **2009**, *131*, 8396. b) Dureen, M. A.; Brown, C. C.; Stephan, D. W. *Organometallics* **2010**, *29*, 6594.
[55] Paradies, J. *Synpacts* **2013**, *24*, 777.
[56] Allgäuer D. R.; *PhD dissertation*, **2013**, Ludwig-Maximilians- University of Munich.

in benzene within 2 to 6 days under 4 bars H_2 with yields ranging from 49 to 99% (*Scheme 1.18*).[57] Malonates and allenes have also been reduced using this strategy.[58]

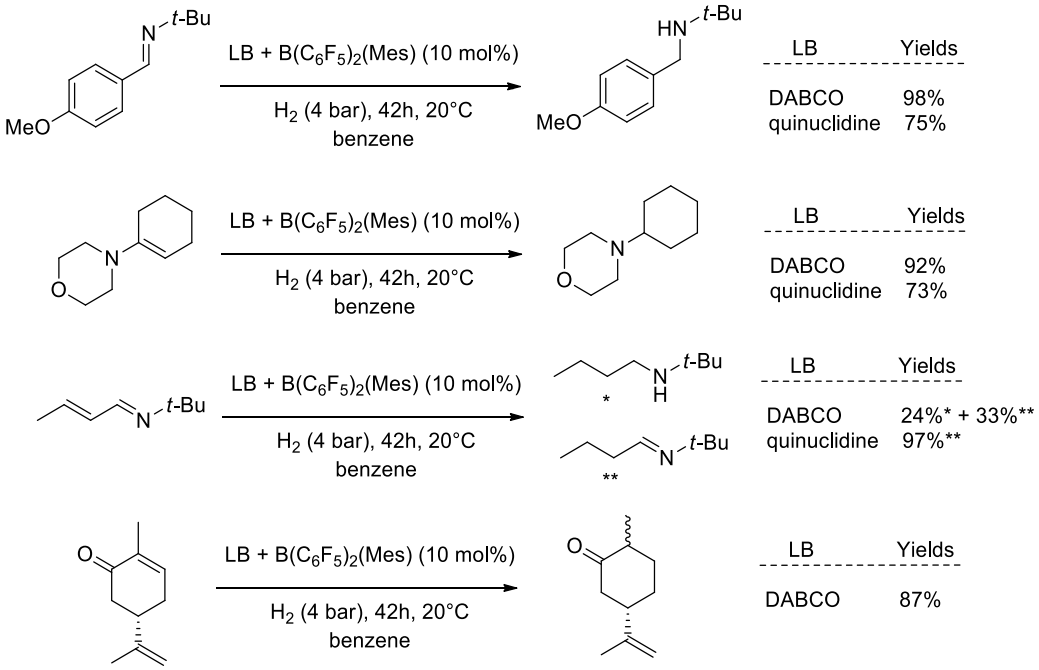

Scheme 1.18 Hydrogenation of imines, enamines and enones with quinuclidine or DABCO + B(C6F5)(Mes)

In order to solve the monoreduction of alkynes issue, Repo et al. designed a new ansa-aminoborane which corresponds to a N/B catalyst.[59] The authors reduced a wide variety of disubstituted alkynes in the corresponding cis-alkene using 5 to 10 mol% of the catalyst under 2 bars of H_2 within 3h at 80°C with yields ranging from 80-95% (*Scheme 1.19*). Mechanistic investigations highlighted that the catalytic system is formed by cleavage of the B-C_6F_5 bond under H_2 atmosphere resulting in the formation of the aminoborane **33**. After hydroboration of the alkyne, the latter complex **34** is then able to cleave a molecule of H_2 leading to the formation of the cis-alkenes through a protodeboration reaction.

[57] a) Erős, G.; Mehdi, H.; Pápai, I.; Rokob, T. A.; Király, P.; Tárkányi, G.; Soós, T. *Angew. Chem., Int. Ed.* **2010**, *49*, 6559. b) Erős, G.; Nagy, K.; Mehdi, H.; Pápai, I.; Nagy, P.; Király, P.; Tárkányi, G.; Soós, T. *Chem. - A Eur. J.* **2012**, *18*, 574.

[58] Inés, B.; Palomas, D.; Holle, S.; Steinberg, S.; Nicasio, J. a.; Alcarazo, M. *Angew. Chem. Int. Ed.* **2012**, *51* (49), 12367.

[59] Chernichenko, K.; Madarász, Á.; Pápai, I.; Nieger, M.; Leskelä, M.; Repo, T. *Nat. Chem.* **2013**, *5*, 718.

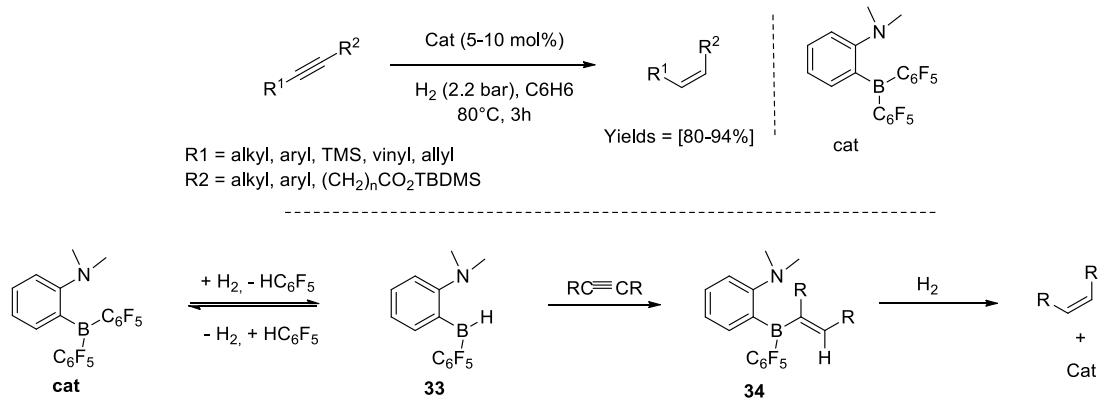

Scheme 1.19 Hydrogenation of alkynes with an aminoborane catalyst under H_2

It has to be noticed that the reduction of terminal alkynes or alkenes lead to the hydroboration adduct, which didn't undergo the protodeboration.

Recently, it has been demonstrated that aldimines, ketones and malonates could be reduced by FLPs under H_2 without the presence of a sterically hindered Lewis base. Indeed, the substrate itself behaves as a Lewis base in the reduction reaction.[60] Enantioselective versions of the hydrogenation of substrates have also been done by FLPs based on the use of either a chiral Lewis acid, chiral Lewis base or substrate.[61] A remarkable example has been reported by Du et al. who used a chiral diene as ligand for borane-catalysed metal free hydrogenation of imines.[62] A broad scope of ketimines have been hydrogenated using 10 mol% $HB(C_6F_5)_2$ and 5 mol% of chiral diene in mesitylene at r.t. under 20 bars H_2 within 15h. The isolated yields range from 63 to 99% with ee up to 89% (*Scheme 1.20*).

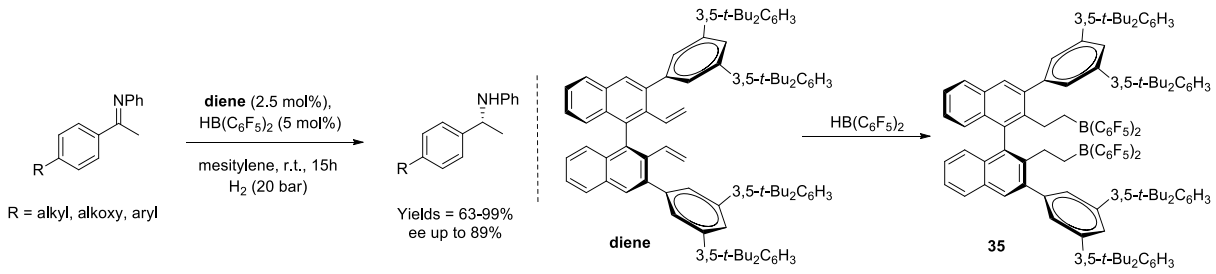

Scheme 1.20 Hydrogenation of ketimines with a chiral diene and $HB(C_6F_5)_2$.

[60] a) Longobardi, L. E.; Tang, T.; Stephan, D. W. *Dalt. Trans.* **2014**, *43*, 15723−15726. b) Mahdi, T.; Stephan, D. W. *J. Am. Chem. Soc.* **2014**, *136*, 15809. c) Greb, L.; Daniliuc, C. G.; Bergander, K.; Paradies, J. *Angew. Chemie - Int. Ed.* **2013**, *52*, 5876.

[61] For a review see: a) Ren, X.; Du, H. *J. Am. Chem. Soc.* **2016**, 810. b) Shi, L.; Zhou, Y.-G. *ChemCatChem* **2015**, *7*, 54.

[62] Liu, Y.; Du, H. *J. Am. Chem. Soc.* **2013**, *135*, 6810.

The efficient chiral catalyst was form by the hydroboration of the chiral alkene yielding the highly hindered borane **35**. The latter, in association with ketimines, was able to cleave the molecule of H_2 yielding the amine.

2.2.3.3. Unusual catalytic hydrogenation reactions by FLP.

While the scope of substrates has been expanded to carbonyl, carboxyl, nitro-olefins, ethers and nitriles, the reaction conditions are still limited. Only a few explicit reports of H_2 activation by FLPs in donor-solvent media exists and all of which are based on stoichiometric phosphine or amine bases. Furthermore, none of them described any subsequent catalytic hydrogenation reactivity. By modifying the nature of the Lewis base, Ashley et al. were able to use diethyl ether and THF[63] as Lewis base in association with the air stable $B(C_6Cl_5)(C_6F_5)_2$ to perform the cleavage of H_2 and hydrogenate tosyl imines, a challenging electron-poor substrates to reduce (*Scheme 1.21*).[64] This work has been considered as a breakthrough in the field of FLP chemistry as it allowed the generation of strong Bronsted acids (**36**, **37**)* capable to activate a broader range of organic functions.[65]

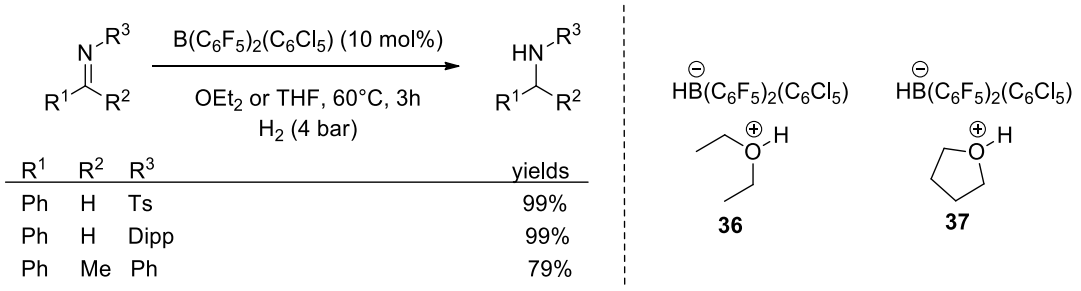

Scheme 1.21 Hydrogenation of aldimines and ketimines (selected examples) with ethers and $B(C_6Cl_5)(C_6F_5)_2$ under H_2 atmosphere.

A last example of the unusual use of FLPs was reported by Du et al.[66] Upon mixing Piers' borane and chiral tert-butylsulfinamide, they isolated a dimeric chiral sulphonamide borane **38** capable to catalyse the hydride and the proton transfer of the ammonia borane complexes **39** to imines. Based on both experimental and theoretical studies, the authors suggested the involvement of a 8-membered ring hydrogen transfer transition state (*Scheme 1.22*).

[63] The pKa of protonated THF has been measured to be -2.05 and those of diethyl ether to be -3.59 in aqueous H_2SO_4. See ref 62 and related articles.
[64] Scott, D. J.; Fuchter, M. J.; Ashley, A. E. *Angew. Chem. Int. Ed.* **2014**, *53*, 10218.
[65] Arnett, E.; Wu, C. Y. *J. Am. Chem. Soc*. **1960**, *82*, 4999.
[66] Li, S.; Li, G.; Meng, W.; Du, H. *J. Am. Chem. Soc.* **2016**, *138*, 12956.

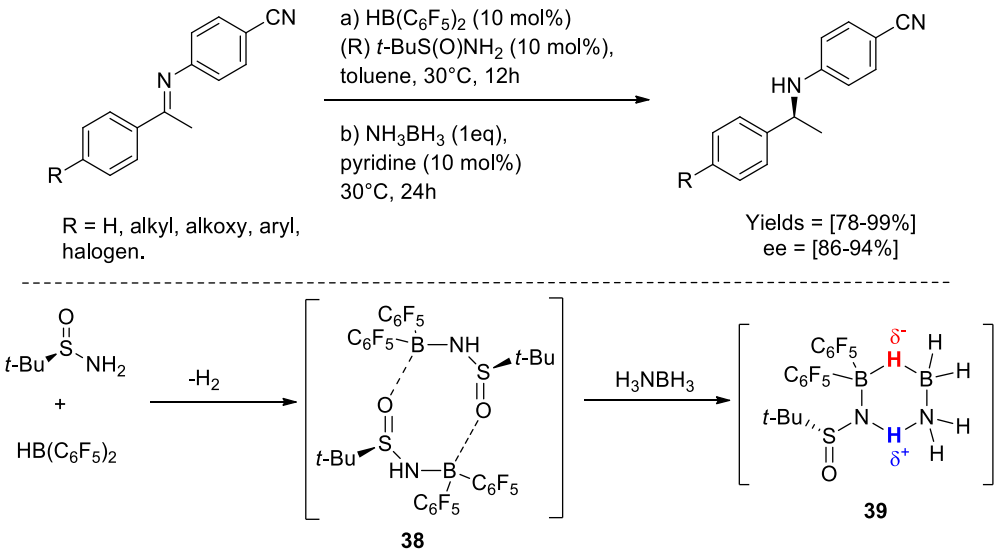

Scheme 1.22 Hydrogenation of imines with a sulphonamide-borane complex and ammonia-borane as H_2 source.

The previous examples have shown how the prevention of the electron lone pair quenching by a Lewis base can provide a rich source of reactivity. FLPs catalysed hydrogenation reactions have been particularly studied, including chiral versions, and a broad range of unsaturated compounds have been reduced.

3. On the investigation of a reaction mechanism

The goal of organic synthesis is mainly to provide efficient methods to access a wide panel of organic molecules which have attractive activities. However, if one designs a new reaction, plans to extend a methodology or improve the robustness of a catalyst, it becomes vital to understand how the reaction proceeds. To do so, chemists need tools and concepts to draw upon. In the late 1920s, the pioneering works of Sir Christopher Ingold (mechanistic study of S_N1 and S_N2 reactions) and Louis Hammett (author of the famous book *Physical Organic Chemistry*, 1940), rocked the beginning of the so-called Physical Organic Chemistry. This branch of chemistry could be defined as “The study of reactions from the point of view of their mechanism and the relationship between structure and reactivity”. This includes not only the formation of intermediates and transition structures, the mapping out of reaction trajectories and the free energy changes that occur along a reaction path, but selectivity. In the context, Georges Withsides coined physical organic chemistry as “A Swiss Army Knife”.[67]

[67] Whitesides. G. *Isr. J. Chem*. **2016**, *56*, 66 – 82

3.1. Kinetic methods to investigate reaction mechanisms

3.1.1. Rate expression of a chemical reaction

From a general point of view, measuring the kinetic of a reaction allow to access several information:

- The rate constant of the reaction allows to determine the activation barrier of the reaction. However, in general, if the reaction proceeds via more than one elementary step, only the rate constant associated to the rate determining step can be accessed.
- In some cases, the expression of the rate constant of the reaction allow to know which reactants are involved in the rate determining step and, by extrapolation, identify reactants which are not involved.
- Understand the origin of selectivity problems in the outcome of some reactions (see Curtin-Hammett principle).

If we consider the general reaction aA + bB = cC, where a, b and c are the stoichiometric coefficients, k_1 the rate constant for the formation of C and k_{-1} for the formation of A + B, the general rate of the reaction is as written in equation (1), with [X] the molar concentration of X and α, β and γ the partial orders of A, B and C.

$$r = \frac{1}{c}\frac{d[C]}{dt} = k_1[A]^{\alpha}[B]^{\beta} - k_{-1}[C]^{\gamma} \qquad (1)$$

In general, and more especially regarding organic reactions, we can assume that k_1 is greater than k_{-1} because if it was not the case, the expected reaction would never occur. As a consequence, second term can be neglected. Moreover, in the case of an elementary step, according to Van't Hoff law, we can assume that the partial orders of A, B and C are equal to their stoichiometric coefficients, respectively. It means that the equation (1) can be rewritten as equation (2) where k_2 is the second order rate constant (α = β = 1).

$$r = \frac{d[C]}{dt} = k_2[A][B] \qquad (2)$$

3.1.2. Kinetic treatment of the nucleophiles

In 1994, Mayr and Patz have developed a linear free energy relationship equation (3), based on the reaction rates of benzhydrilium ions, cationic metal π-complexes, and diazonium ions with n, π and σ nucleophiles.[68]

$$\log k_{20°C} = s_N(N + E) \qquad (3)$$

In the three-parameter equation (3), $k_{20°C}$ is the second order rate constant ($M^{-1}s^{-1}$), s_N is the nucleophilie-specific slope parameter, *N* is the nucleophilicity parameter and *E* is the

[68] Mayr, H.; Patz, M. *Angew. Chem., Int. Ed.* **1994**, *33*, 938.

electrophilicity parameter. Practically, Mayr used blue coloured benzhydrilium cations and followed their consumption spectrophotometrically during their reaction with nucleophiles and measured the rate constant (Beer-Lambert law). Based on this correlation equation, the reactivity of many classes of nucleophiles and electrophiles can be determined. Hence, the reaction of a nucleophile (N, s_N parameters) and an electrophile (E parameter) can occur at r.t. if the following rule of thumb is verified: $E + N > -5$. It has to be noticed that this rule is only valid if i) the reaction is an elementary step and ii) the rate low can be written as in equation (2).

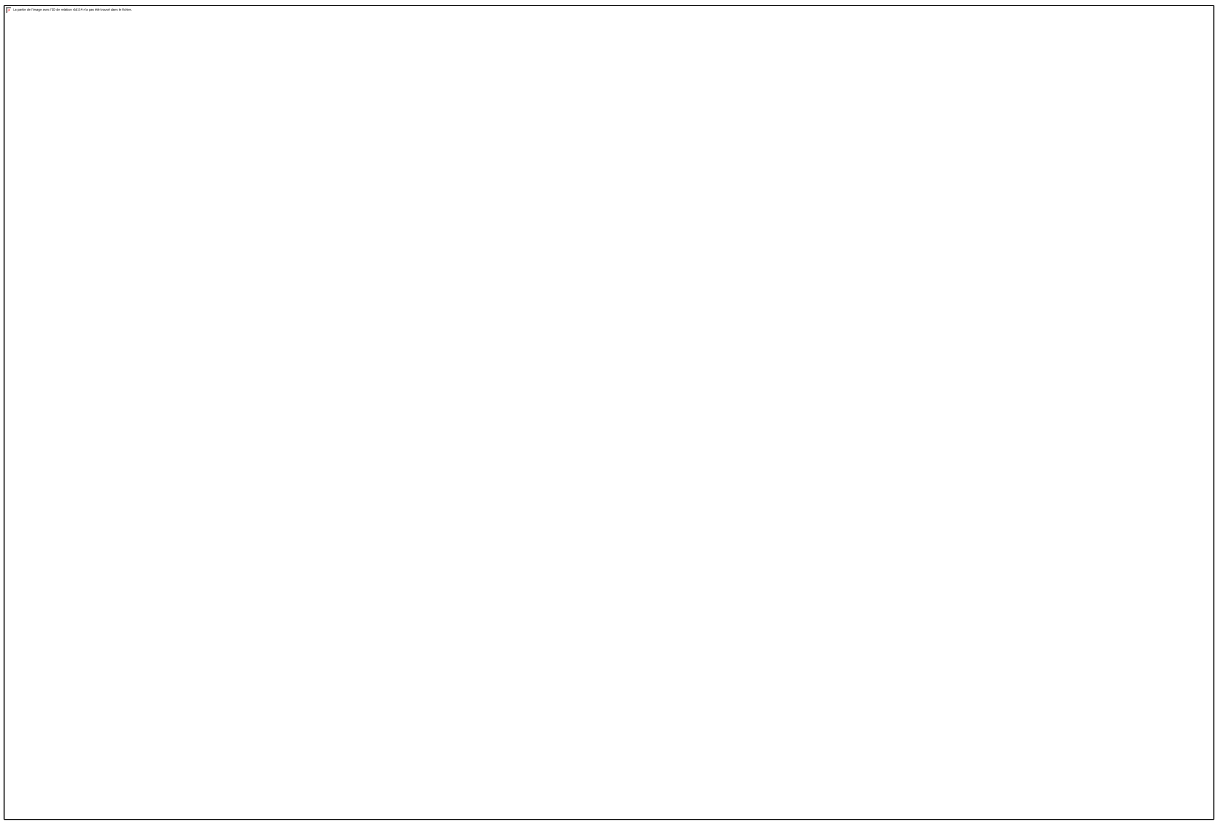

Figure 1.18 Plot of log k(20 °C) vs E for the reactions of benzhydrylium cations with π-nucleophiles.[69]

Thank to this correlation, the parameters for a wide variety of electrophiles and nucleophiles have been measured in various solvents.[70] *Figure 1.18* shows how one can determine the nucleophilicity parameters (N, s_N) for a given nucleophile.

As required by equation (3) plots of log k values against the E parameters of the electrophile provides a linear correlation. Slopes of these linear correlations yield the nucleophile-specific

[69] Mayr, H.; Bug, T.; Gotta, M. F.; Hering, N.; Irrgang, B.; Janker, B.; Kempf, B.; Loos, R.; Ofial, A. R.; Remennikov, G.; Schimmel, H. *J. Am. Chem. Soc.* **2001**, *123*, 9500.
[70] For the database see http://www.cup.lmu.de/oc/mayr/reaktionsdatenbank/

slope parameter (s_N) while the nucleophilicity parameter (*N*) is derived from the negative intercepts on the abscissa.

With these kinetic data in hands, it is easier to discuss a reaction mechanism depending on the nucleophile and the electrophile, which are involved. For instance, DABCO (s_N = 0.70, *N* = 18.80) reacts two thousand times faster than tri-*n*-butylphosphine (s_N = 0.69, *N* = 15.49) with a given electrophile. As a second example, it shows that carbene borane complexes are better H-nucleophiles than amine borane complexes. More especially, it becomes possible to investigate the rate-determining step of a reaction in more details.

3.1.3. Thermodynamic treatment of Lewis bases

While Mayr developed the linear free energy relationship for the quantitative treatment of nucleophiles, he also developed a thermodynamic approach to quantify Lewis basicity toward C-centered electrophiles which uses benzhydrylium ions (Ar_2CH^+) as reference Lewis acids.[71] When the reaction between the blue coloured benzhydrilium cations (Lewis acid, LA) and a Lewis base (LB) was not governed by an equilibrium constant greater than 10^4, an appreciable equilibrium could be observed as reflected by the non-zero final absorbance when the plateau is reached. Assuming the linearity of Beer-Lambert law (equation 4), it is possible to determine the equilibrium constant *K* (equation 5).

$$Abs = \varepsilon l c \qquad (4)$$

$$K = \frac{[LA-LB]}{[LA][LB]} = \frac{(Abs_0 - Abs)}{Abs\{[LB]_0 - \frac{(Abs_0 - Abs)}{\varepsilon l}\}} \qquad (5)$$

In equations (4) and (5), Abs is the absorbance of the blue coloured LA, ε is the molar absorption coefficient of LA, l the length path and LA-LB the adduct formed by the reaction between LB and LA. Using the *K* value of the studied elementary step, it is possible to access the Gibbs free energy ΔG° and thus have more information about the reaction mechanism.

In order to quantify the Lewis basicity parameters and Lewis acidity parameters, Mayr and al introduced the following equation (6),

$$log\ K_{20°C} = LA + LB \qquad (6)$$

Based on this equation, the authors built an impressive database of LA/LB values as shown in the *Figure 1.19*.

[71] Mayr, H.; Ammer, J.; Baidya, M.; Maji, B.; Nigst, T. A.; Ofial, A. R.; Singer, T. *J. Am. Chem. Soc.* **2015**, *137* (7), 2580.

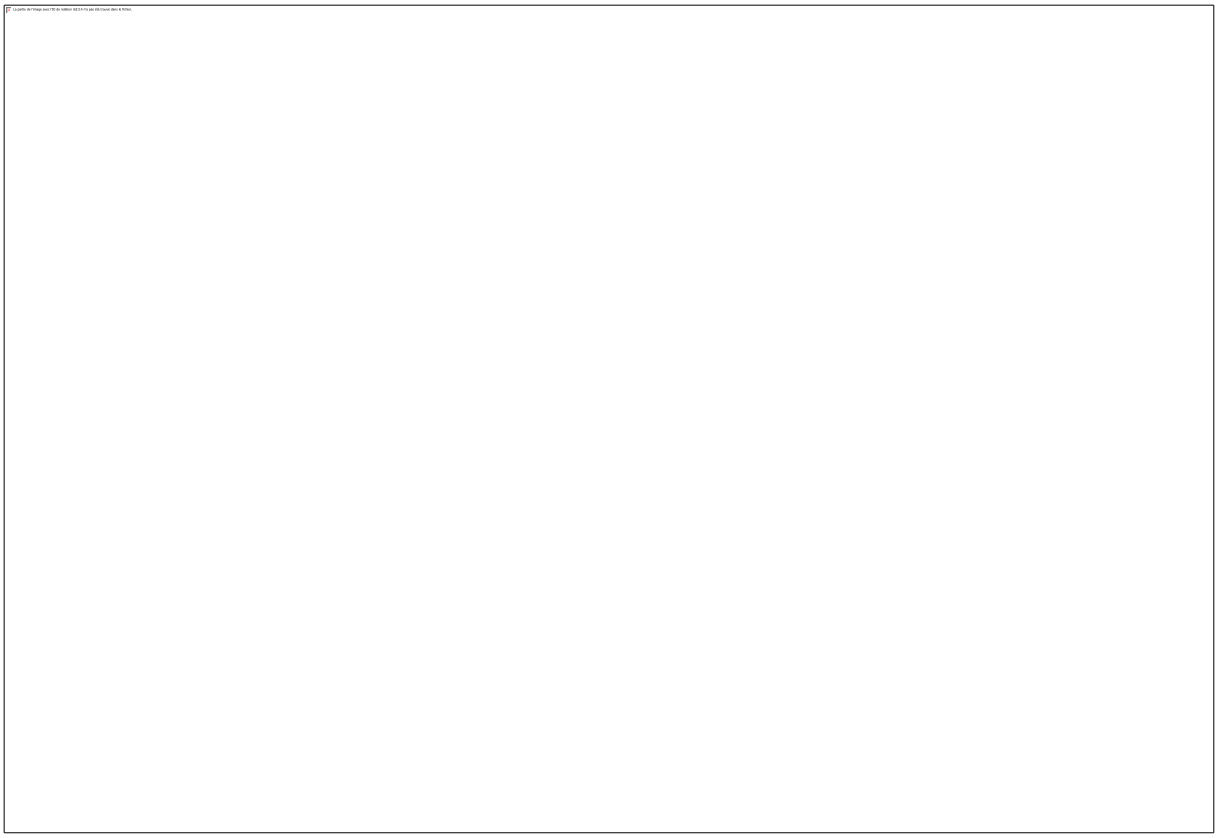

Figure 1.19 Plot of log K for reactions of benzhydrylium ions E^+ with Lewis bases in CH_2Cl_2 against the Lewis acidity parameters LA_{CH2Cl2} of the benzhydrilium ions.[71]

3.2. Density functional theory to investigate reaction mechanisms

3.2.1. Presentation of the concept

The late century has witnessed the beginning of a new way of thinking chemistry by means of computational chemistry. In this shifting, chemists have tried to predict the behaviour of molecules and more especially electrons using different models. Begun in 1927 with Thomas-Fermi model, it is only in 1964 that the real DFT emerges with the work of Hohenberg and Kohn.[72]

The electronic of a system composed by N electrons can be described adequately by means of the non-relativistic Schrödinger equation (7) in Born-Oppenheimer approximation as in equation (8),

$$\hat{H}\Psi = E\Psi \qquad (7)$$

Where *E* is the electronic energy, $\Psi = \Psi(x_1, x_2,\ldots,x_N)$ is the *N*-electrons wave-function and $\hat{H}$ is the Hamiltonian operator (in atomic units).

[72] Hohenberg, P.; Kohn, W. *Phys. Rev.* **1964**, *136*, B864.

$$\hat{H} = \sum_{i=1}^{N}\left(-\frac{1}{2}\nabla^2{}_i\right) + \sum_{i=1}^{N} v(r_i) + \sum_{i=1}^{N}\sum_{i<j}^{N}\frac{1}{r_{ij}} \qquad (8)$$

In the equation (8) of the Hamiltonian operator, $v(r_i)$ denotes the external potential acting on electron *i*.

The first theorem of Hoenberg and Kohn stated that "For any system of electrons in an external potential $v_{ext}(r_i)$, that potential is determined, except for a constant, by the ground state density $\rho(r_i)$. In other words, $\rho(r_i)$ define the external potential $v_{ext}(r_i)$ and thus all properties. We remind that electron density is an observable which shows how the electrons are distributed.

Then in order to link the electron density of the system to its energy, these authors have postulated a second theorem: "A universal functional for the energy $E[\rho(r_i)]$ of the density $\rho(r_i)$ can be defined for all electron systems. The exact ground state energy is the global minimum for a given $V_{ext}(r_i)$ and the density $\rho(r_i)$ which minimizes this functional is the exact ground state density". In other words, the functional $E[\rho(r_i)]$ alone is sufficient to determine the exact ground state energy and density.

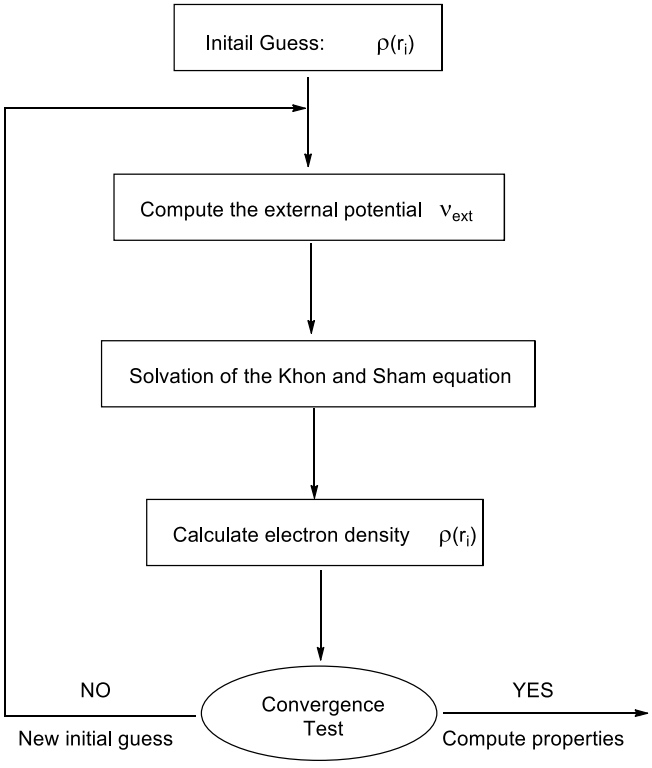

Figure 1.20 Simplified iterative process occurring in a DFT computation of any system.

Based on these two theorems, the exact energy of any system can be known only on condition that the mathematical form of the functional is also known. This last point leads theoretical chemists to design several functionals depending on the studied system (B3LYP is the most used to represent organic molecules).

As depicted in *Figure 1.20*, the simplified general procedure of system computation begins with an initial guess of the system and as a consequence of $\rho(r_i)$. Then, thanks to the two theorems of Hohenberg and kohn, the external potential can be computed. The third step is the solvation of the Kohn and Sham equation, which lead to a new external potential. The latter allows the determination of a new set of $\rho(r_i)$ which is compared with a convergence criterion to start again the process or compute the properties.

Because the electronic of the system is known, a broad range of properties can be computed such as IR frequencies, NMR properties, molecular orbitals or free Gibbs energy. For our concern in organic chemistry, we will limit the exploitation of the results to these four properties. Consequently, based on these properties it is possible to study a reaction mechanism and access both kinetic (activation barrier) and thermodynamic (free Gibbs energy of the reaction)

2. Chapter II: Metal-Free Hydrogenation of Electron-Poor Olefins Catalysed by P/B Frustrated Lewis Pairs

P/B based Frustrated Lewis Pairs (FLPs) are formed when sterically demanding substituents are present on P and B atoms precluding association and formation of a classical Lewis acid-Lewis-base complex. FLPs able to cleave small molecules of high binding energies such as H_2, CO or CO_2 to quote a few and the resulting adducts find applications in hydrogenation or carbonylation reactions, traditionally performed under transition metal catalysis. While the mechanism of the cleavage of H_2 has been deeply investigated by NMR spectroscopy, DFT-calculations and kinetics,[1] the hydrogenation mechanism of unsaturated compounds has scarcely been explored. In particular, P/B FLPs, which are used to hydrogenate unsaturated compounds under H_2, have never been employed to catalyse the reduction of electron poor olefins. Achieving this kind of transformation is of interest as the reduction of Michael acceptors is usually not properly realized under organic or organometallic conditions due to the presence of electrophilic and coordinating fragments such as carbonyl of carboxyl ones.

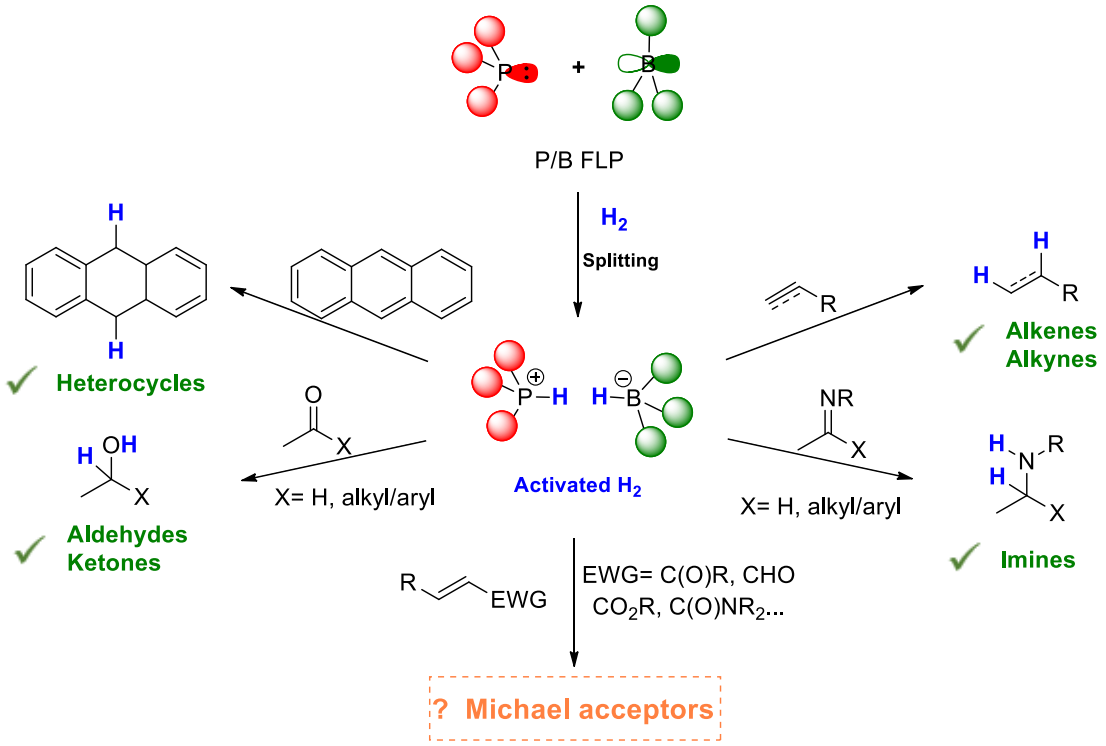

Scheme 2.1 Context of the study of the use of P/B FLPs for the hydrogenation of unsaturated compounds

1. State of the art on the mechanistic investigations of FLPs-catalyzed hydrogenation of unsaturated compounds

[1] For reviews, see a) Stephan, D. W. *Acc. Chem. Res.* **2015**, *48*, 306 b) Stephan, D. W.; Erker, G. *Angew. Chem. Int. Ed.* **2015**, *54*, 6400.

In this first part, we survey reports from the literature dealing with mechanistic studies on the hydrogenation of alkenes using several types of FLPs in order to evaluate the influences of several parameters on the hydrogenation of unsaturated compounds (nature of the Lewis acid/base, solvent, pressure of H_2 etc…). In these paragraph, the combination of a Lewis acid (LA) with a Lewis base (LB) forming a FLP will be denoted LA/LB.

1.1. Hydrogenation of unpolarised alkenes and electron rich olefins with P/B FLPs

In 2012, Paradies and Grimme reported on an FLP system capable of hydrogen activation at temperatures below -80°C.[2] Indeed, in situ-NMR studies of a combination of $B(C_6F_5)_3$ **1** with **2a-e** under 5 bars of H_2 in temperatures ranging from -80°C to -60°C were consistent with the formation of phosphonium borate salt $[R_3PH]^+[(C_6F_5)_3BH]^-$ **3** (*Scheme 2.2*).

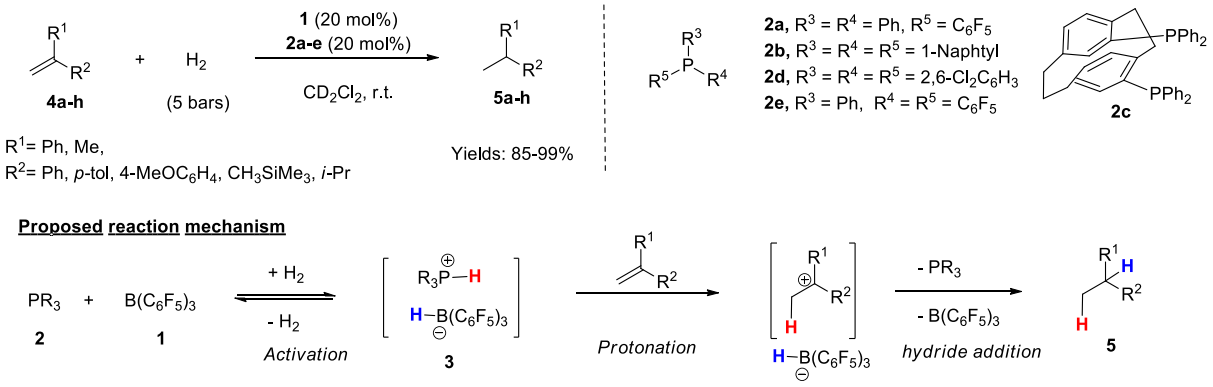

Scheme 2.2 General scheme of the hydrogenation of olefins with P/Bs under H_2. Yields were determined by ^1H NMR spectroscopy with the residual solvent signal as an internal standard.

Complex **3** has been shown to be active in hydrogenation of olefins **4a-h** at room temperature to form the saturated adducts **5a-h** (*Scheme 2.2*). The proposed mechanism involves a protonation of the olefin followed by a subsequent hydride transfer. While various phosphorous-based Lewis bases **2a-e** were tested, the authors found that a balance between the protonation and efficient hydride addition was critical, explaining the lack of reactivity of $PPh(C_6F_5)_2$ **2e**. The protonation step of the olefin has been discussed along with the nucleophilicity parameters by Mayr et al. Indeed, Paradies and Grimme found that olefin possessing $1.10 < N < 4.40$ were quantitatively reduced, highlighting the involvement of the protonation of olefins. More importantly, they have been able to intercept the carbocation resulting from this protonation with Ph_2NPh. Additional DFT-calculations highlighted that the formation of the Lewis pair adduct and the cleavage of H_2 are endergonic for phosphines at r.t.

[2] Greb, L.; Oña-Burgos, P.; Schirmer, B.; Grimme, S.; Stephan, D. W.; Paradies, J. *Angew. Chem. Int. Ed.* **2012**, *51*, 10164

However, it becomes exergonic at -60°C. In addition, the reduction of double bonds is computed to be highly exergonic.

In another study, the Paradies group reported on the impact of electronic effects of triarylphosphines on the hydrogen activation and hydrogenation of olefins.[3] In particular, by means of NMR spectroscopy, they measured the pK_a of phosphonium salts **6a-g** in CH_3CN and showed that the acidity of the corresponding phosphoniums salts [**6**-H]$^+$ increases with increasing the number of fluorine substituents as electron withdrawing groups (*Figure 2.1*).

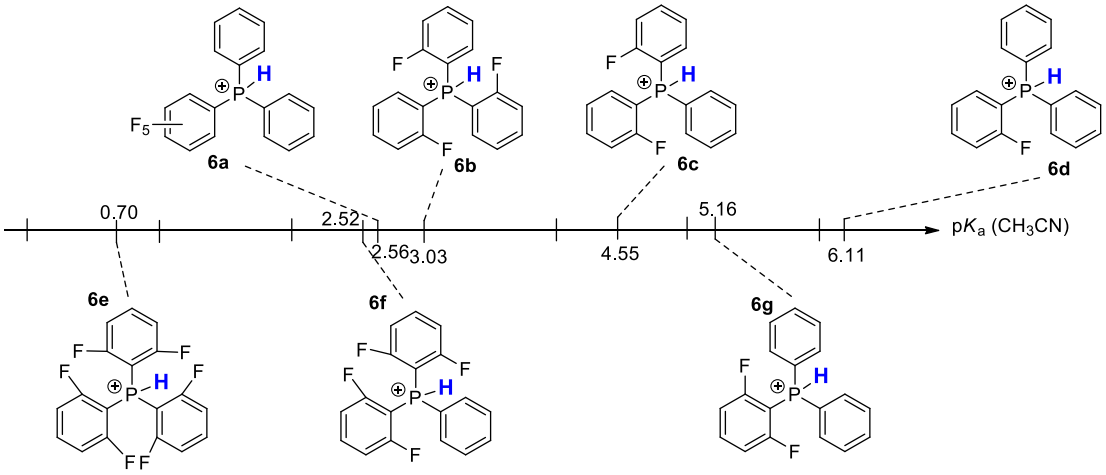

Figure 2.1 pK_a *of the conjugate acids (in MeCN) of the phosphines* ***6a-g***

Based on these thermodynamic data, the authors proposed the general reaction mechanism depicted in *Scheme 2.3*, consisting of the heterolytic cleavage of H_2 (step 1), the protonation of the olefin (step 2) and the reduction of the carbocation by the hydridoborate species (step 3). The last two events (2 and 3), have been discussed with the support of computational and kinetic studies. Indeed, for electron-rich olefins, the hydrogenation step follows a zero-order dependence on alkene, showing no influence of the structure of the olefin in the rate determining step while it becomes first-order in the case of electron-poor ones. The same trend was observed when changing the nature of the phosphine from low to high pK_a of the conjugate phosphonium salt respectively. This clearly indicates that the rate determining step is the protonation of the olefin (event 2). This was confirmed by computational study as the cleavage of H_2 by the FLP **6d**/**1** is exergonic by 3.7 kcal/mol and the protonation of 1,1-diphenylethylene by the later complex was endergonic by 12.9 kcal/mol (B2PLYP-D3, CH_2Cl_2, 25°C).

[3] Greb, L.; Tussing, S.; Schirmer, B.; Oña-Burgos, P.; Kaupmees, K.; Lõkov, M.; Leito, I.; Grimme, S.; Paradies, J. *Chem. Sci.* **2013**, *4* , 2788

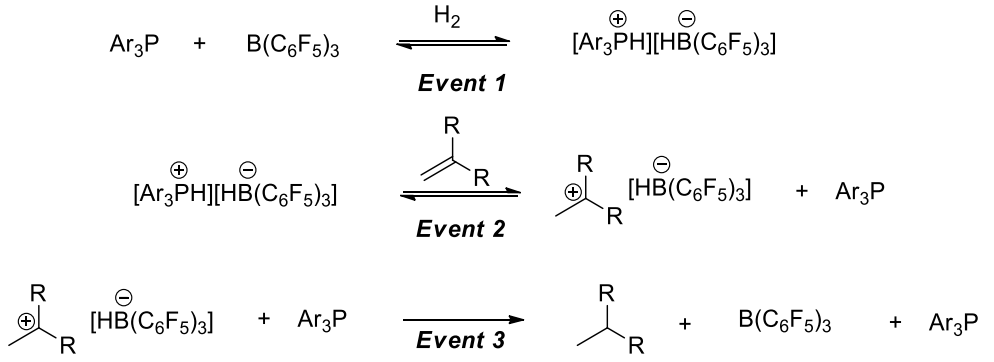

Scheme 2.3 Proposed reaction mechanism for the hydrogenation of olefins.

A study based on the development of a domino hydrosilylation/hydrogenation process of enones with FLP showed that [2.2]paracyclophane-derived bisphosphines **9a-c** can be used as Lewis bases.[4] In this regard, enones **7** can be transformed into the hydrosilylation adducts **8** even in the presence of 10 mol% of **1** and **9** in toluene (*Scheme 2.4*). Then, exposure of the crude mixture to 5 bars of H_2 resulted in the formation of the silyl ethers **10** with a *syn*-diastereoselectivity.

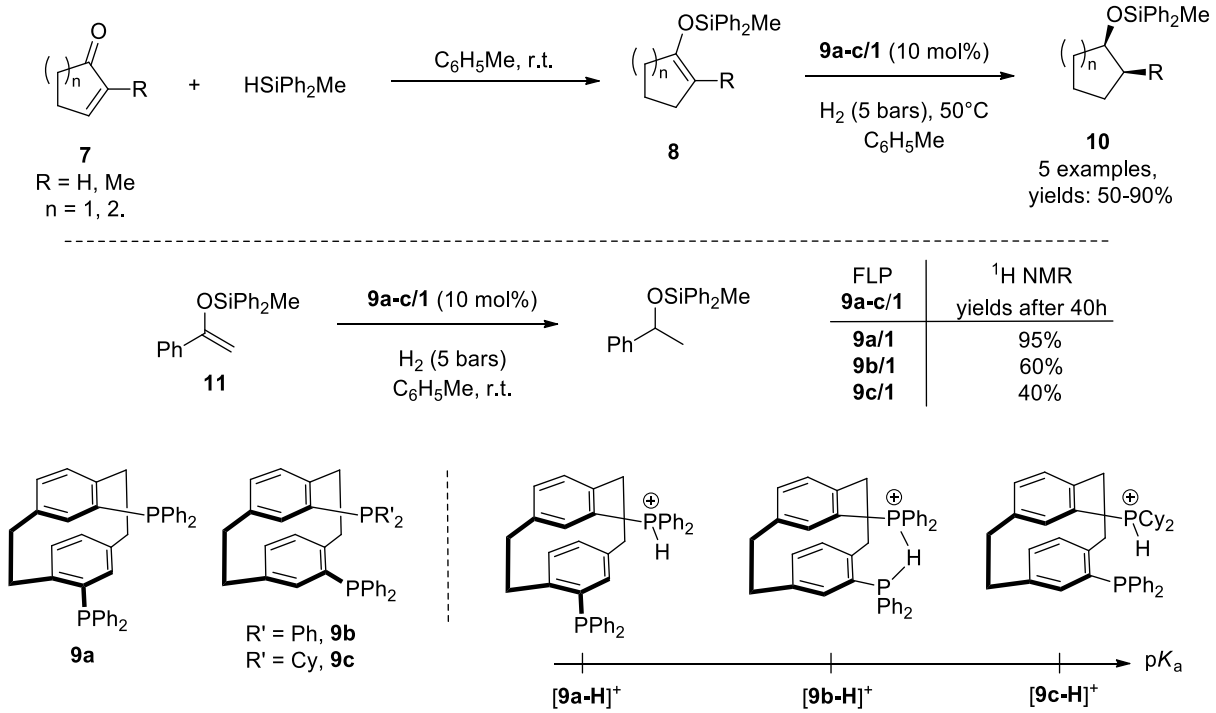

*Scheme 2.4 Domino hydrosilylation/hydrogenation of **8** under H_2 catalysed by **9a** or **9c**/**1** (top) and study of the influence of the Lewis base on the hydrogenation, structures of **9a-c** and of the corresponding Bronsted acids (bottom)*

[4] Greb, L.; Oña-Burgos, P.; Kubas, A.; Falk, F. C.; Breher, F.; Fink, K.; Paradies, J. *Dalt. Trans.* **2012**, *41*, 9056

In particular, the authors found that the highest yields in the reduction of **11** were obtained with the system **9a-c**/**1** where **9a** showed higher performances than **9b** and **9c**. The pK_a of the proton of [**9a-c**-H]$^+$[H-B(C_6F_5)$_3$]$^-$ resulting from the splitting of H_2 by **9a-c**/**1** explains this trend as it evolves in this order PPh_2-H^+ < PPh_2-H^+-PPh_2 < PCy_2-H^+.It shows again that, in the case of electron rich olefins stabilizing the transient carbocation, the rate determining step of the hydrogenation is the protonation of the olefin.

Silyl enol ether have also been reduced by Erker et al. with the pair 1,8-bis(diphenylphosphino)-naphthalene and **1**.[5] Importantly, by crystalizing the encounter complex resulting from the cleavage of H_2, the authors found a weak P^+-H---H-B^- interaction between the phosphonium cation and the hydridoborate anion, as the distance between the two hydrogen is 2.08 Å. It shows a reversible H_2-activation process at r.t, thus reflecting the formation of an acidic phosphonium cation.

In 2015, Stephan et al. reported the use of an FLP composed by the electrophilic fluorophosphonium salt **12** as a Lewis acid and an amine, to reduce alkenes.[6] First, a study of the HOMO and LUMO of **12**/$HNPh_2$ showed a π-stacking-stabilized structure of the encounter complex **14**. Moreover, quantum calculations of the cleavage of H_2 by **12** and $HNPh_2$ leading to **13** showed an exergonic reaction (ΔG = - 22.6 kcal/mol) and associated to a relatively low activation barrier, $\Delta G^{\#}$ = 12.9 kcal/mol.

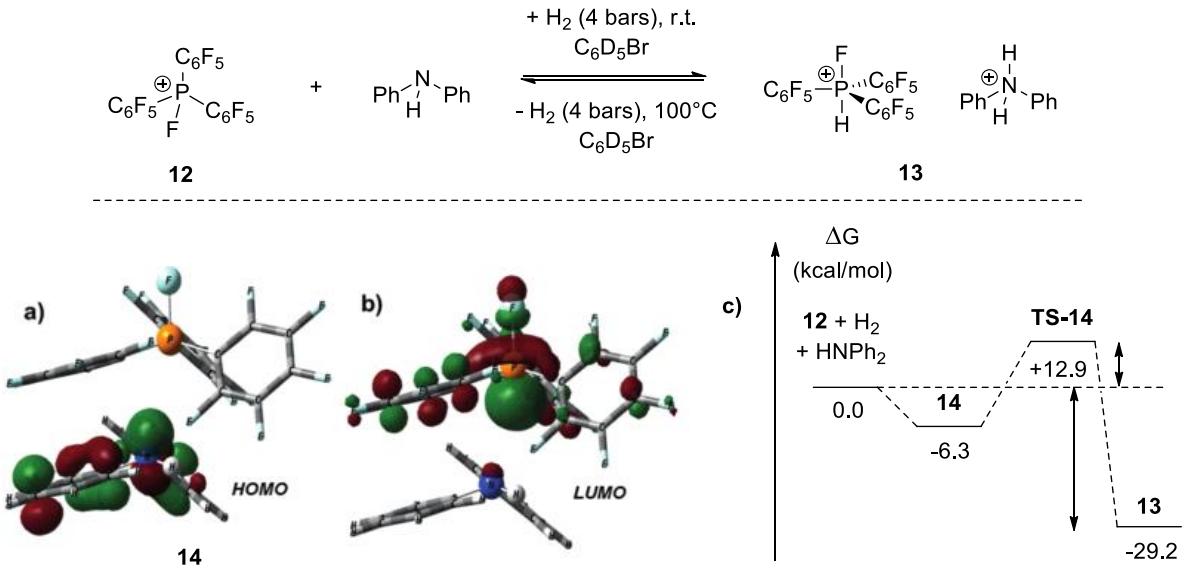

*Scheme 2.5 Reversible H_2 spitting using **12**/$HNPh_2$ at either r.t. or 100°C (top) and a) HOMO of **14**, b) LUMO of **14** obtained by DFT calculations at WB97XD/def2TZV level of theory and c) reaction coordinate of the activation of H_2 by $[(C_6F_5)_3PF]^+$/Ph_2NH.*

[5] Wang, H.; Fröhlich, R.; Kehr, G.; Erker, G. *Chem. Commun.* **2008**, 5966
[6] vom Stein, T.; Peréz, M.; Dobrovetsky, R.; Winkelhaus, D.; Caputo, C. B.; Stephan, D. W. *Angew. Chemie Int. Ed.* **2015**, *54*, 10178

The hydrogenation of the 1,1-diphenylethylene **4a** has been used as a reaction model to survey the catalytic activity of **13**. However, almost no reduction was observed at 100°C under 4 bars of H_2. The use of Tol_2NSiEt_3 allowed to reach full conversion leading the authors to find that **12**/tol_2NH (1 mol%) + Et_3SiH (20 mol%) is a suitable system to perform the reduction of 12 examples of 1,1-diubstituted olefins in yields ranging from 14 to 99%.

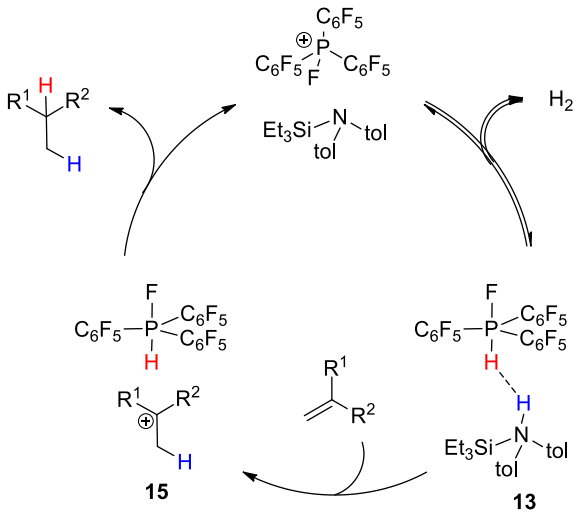

*Scheme 2.6 Proposed reaction mechanism for the hydrogenation of alkenes with **24**/Tol_2NH (1mol%) + Et_3SiH (20 mol%), H_2 (4 bars), C_6D_5Br.*

In the proposed reaction mechanism, the authors evoked the formation of the carbocation **15** and the reduction of the later by $HP(C_6F_5)_3F$. The addition of $HSiEt_3$ is expected to allow the formation of Tol_2NSiEt_3 which is more acidic than tol_2NH.

1.2. Hydrogenation of polycyclic aromatic hydrocarbons and heterocycles with P/B FLPs

In this section, the mechanistic studies dealing with the reduction of polycyclic aromatic hydrocarbons and heterocycles will be briefly reviewed.

The reduction of anthracene derivatives, tetracene and tetraphene **16a-e** have been achieved with **1**/$PhP(C_6F_5)_2$ **2e** or $P(C_6F_5)_3$ **2f** (10 mol%) under 102 bars H_2 at 80°C for 48h. The resulting adduct has been isolated in yields ranging from 30 to 97% (*Scheme 2.7*).[7a] Interestingly, the use of the phosphines Ph_3P, tBu_3P or 1,8-bis(PPh_2)(C_10H_6) **2g** showed no catalytic reduction and the reduction of naphthalene has not been reached under the above-mentioned conditions.

[7] a) Segawa, Y.; Stephan, D. W. *Chem. Commun.* **2012**, *48*, 11963 b) M. C. Courtney, A. C. MacCormack and R. M. More-O'Ferrall, *J. Phys. Org. Chem.*, **2002**, *15*, 529.

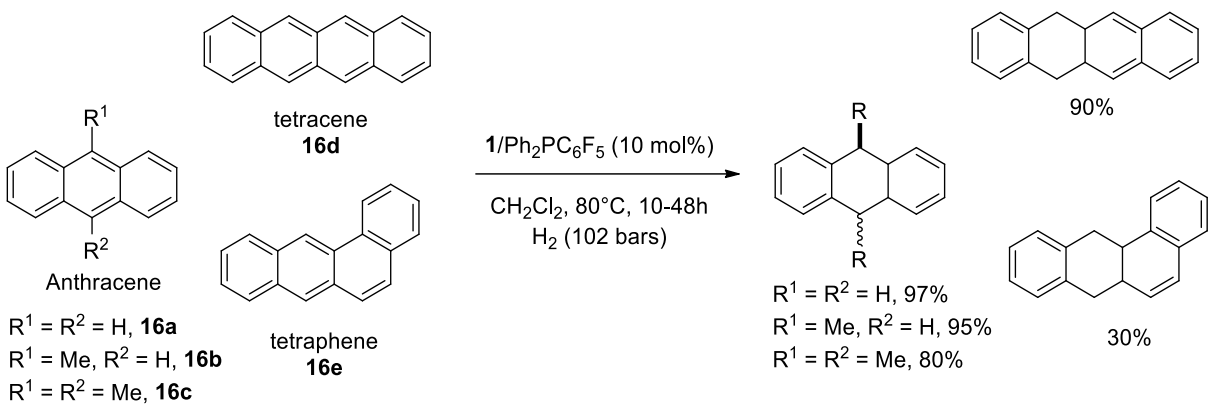

*Scheme 2.7 hydrogenation of polycyclic aromatic hydrocarbons **16a-e** with **1/2e** under H_2.*

This successful reduction suggests that **2e** provides the optimum balance between steric bulk and Lewis basicity for FLP hydrogenation catalysis. Based on this hypothesis, the apparent selectivity for anthracene fragments and no reactivity with naphthalene is consistent with the lower computed p*K*a value (in 50:50 aqueous/trifluoroethanol) of protonated anthracene (-13.3) compared to that of protonated naphthalene (-20.4). [7b] Lastly, the authors investigated the origin of the preference for the formation of the cis-isomer by means of theoretical calculations and showed that the hydride delivery, in the last step of the mechanism, is not reversible. This example illustrates that the reduction of heterocycles is clearly more difficult than that of electron-rich alkenes due to the low pK_a of the olefin. This requires forming highly acidic protons through the use of very weak Bronsted bases. The consequence of this drawback is that the cleavage of H_2 is much more difficult because, in many cases, decreasing the Bronsted basicity also decreases the nucleophilicity of phosphine. Thus, high hydrogen pressure is necessary.

1.3. Hydrogenation of carbonyl derivatives with P/B FLPs

Among the diversity of unsaturated compounds which are reducible by FLP under H_2, the main examples concern the reduction of carbonyl derivatives and more specifically imines.

In this field, P/B FLPs have been widely used to reduce imines, aziridines, enamines and many related compounds.[8] After the discovery of the activity of the intramolecular FLP **17** in H_2 splitting,[9] Stephan et al. used the latter in the reduction of imines **18** (*Scheme 2.8*).[10] The use 5 mol% of **17** under 4 bars of H_2 at 120°C affords the corresponding ammonium salts **19** in excellent yields (79 to 98%). It is noteworthy to precise that different types of intramolecular FLP, such as **20**, has been developed by Erker to perform the reduction of imines.[11] In these

[8] For a reviw, see Shi, L.; Zhou, Y.-G. *ChemCatChem* **2015**, *7*, 54
[9] Welch, G. C.; San Juan, R. R.; Masuda, J. D.; Stephan, D. W *Science* **2006**, 314, 1124.
[10] Chase, P. A.; Welch, G. C.; Jurca, T.; Stephan, D. W. *Angew. Chem. Int. Ed.* **2007**, *46*, 8050
[11] Spies, P.; Schwendemann, S.; Lange, S.; Kehr, G.; Fröhlich, R.; Erker, G. *Angew. Chem. Int. Ed.* **2008**, *47*, 7543

two studies, the authors showed that the substituents at the phosphorous atom were crucial. Indeed, the Lewis base part, R-PCy_2, cleaves H_2 but didn't led to any hydrogenation owing to the high pK_a of the phosphonium salt.

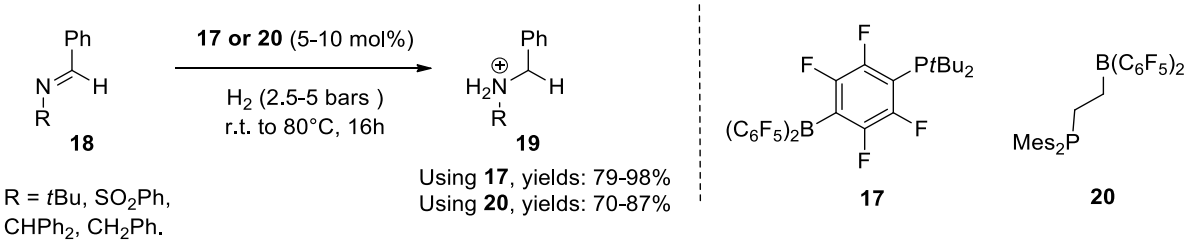

*Scheme 2.8 Hydrogenation of imines with the two intramolecular FLPs **17** and **20**.*

Recently, an original FLP system has been designed by Krempner et al.[12] which involves the use of Verkade's organosuperbases **21** as a Lewis base (pK_a = 33.6). This allowed them to use weak to moderate Lewis acid such as BPh_3 **22a** or 9-BBN **22b** which are less moisture sensitive than **1**.[13] After demonstrating the efficiency of **22**/**21** in H_2 activation by means of NMR spectroscopy, they showed that the use of 5 mol% of the catalyst under 50 to 100 bars of H_2 in THF at 25 to 80°C (depending on the nature of the Lewis acid) were able to catalyse the reduction of N-benzylidene aldimine **23** to the saturated aniline **24**.

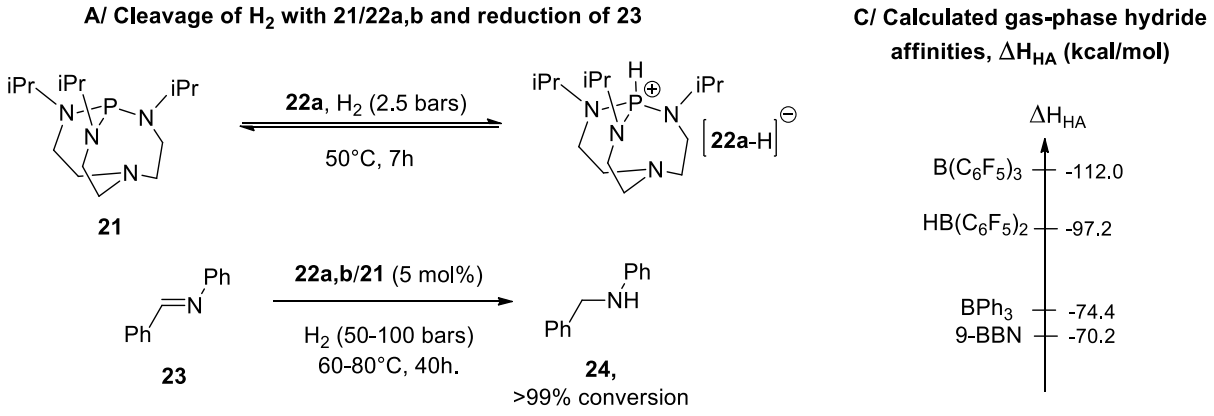

*Figure 2.2 Utilisation of organo-superbases **22a-b** for the cleavage of H_2 and the hydrogenation of aldimine **23** (left) and scale of the Lewis acidity of Lewis acids compared to $B(C_6F_5)_3$ (density functional theory with the B3LYP functional and the split valence polarization (SVP) basis set).*

1.4. Hydrogenation of α,β-unsaturated carbonyl derivatives with P/B FLPs

As a last part of this literature survey, we will focus the use of FLPs in the reduction of α,β-unsaturated carbonyl derivatives.

[12] Mummadi, S.; Unruh, D. K.; Zhao, J.; Li, S.; Krempner, C. *J. Am. Chem. Soc.* **2016**, *138*, 3286
[13] Chin- tareddy, V. R.; Ellern, A.; Verkade, J. G., *J. Org. Chem.* **2010**, *75*, 7166 b) Chintareddy, V. R.; Wadhwa, K.; Verkade, J. G., *J. Org. Chem.* **2009**, *74*, 8118 c) Reddy, Chinta Reddy V.; Urgaonkar, S.; Verkade, J. G., *Org. Lett.* **2005**, *7*, 4427.

In 2013, Paradies et al. studied the reaction of nitroolefins **25a** with **1** or similar Lewis acids such as B(2,6-F_2-C_6H_3) **26** and P(*t*-Bu)$_3$ or TMP as a Lewis base under H_2.[14] Interestingly, they showed that **25a** was not reduced using the FLP **1**/P(*t*-Bu)$_3$ while the use of **26**/TMP allowed the reaction to occur. This was attributed to the reduced Lewis acidity of **26** with respect to **1**, suggesting an increased nucleophilic character of the hydride in [H-**26**]$^-$ anion.[15] In the case of the FLP **1**/P(*t*-Bu)$_3$, the authors observed the formation of an oxime **25b**, resulting from the conjugate addition of P(*t*-Bu)$_3$ to the β-position of **25a** followed and the reduction of the generated nitronate by another P(*t*-Bu)$_3$.

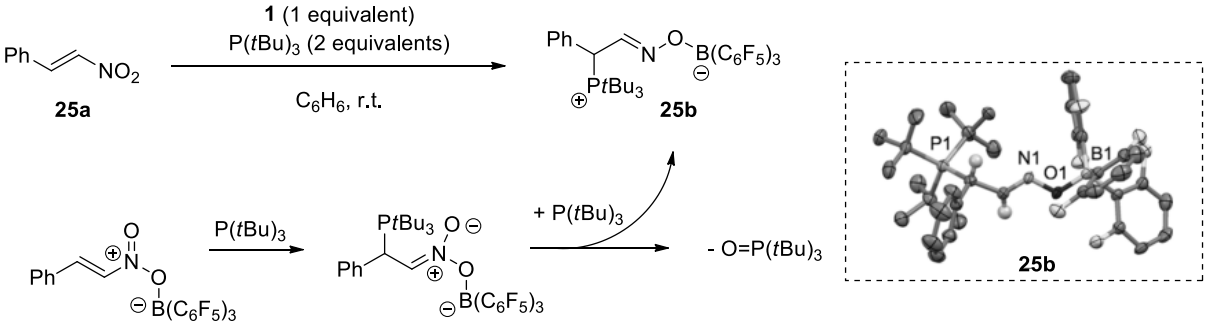

*Scheme 2.9 Reactivity of the pair **1**/P(t-Bu)$_3$ with **25a** and key steps of the proposed reaction mechanism.*

Using the same approach, Alcarazo et al. reported the reduction of allenes **27** with P/B and N/B FLPs.[16] The authors showed that the use of 20 mol% of **1**/PMes$_3$ or P(*t*Bu)$_3$ under 60 bars H_2 for 3 days at 60°C catalysed the reduction of **27** to form the ester **28** with 66 and 64% yields, respectively (*Scheme 2.10*). It shows that the FLP **1**/PAr$_3$ is able to cleave H_2 and reduce unsaturated bond even in the presence of ester as functional groups.

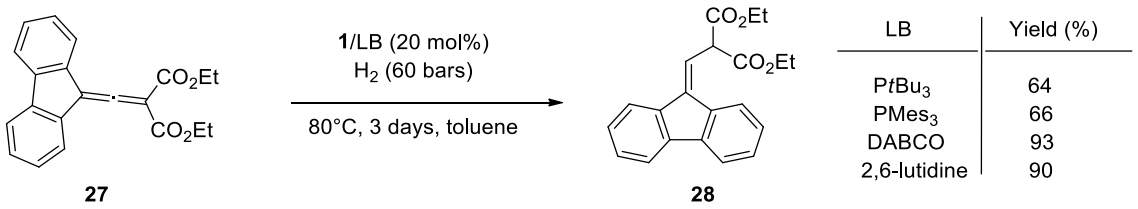

*Scheme 2.10 Catalytic hydrogenation of **27** using P/B and N/B FLPs. In the case of DABCO and 2,6-lutidine, the catalyst loading was reduced to 15 mol%.*

More recently, Berionni et al. measured the nucleophilicity of an array of hydridoborate salts **29a-c** according to Mayr equation in order to establish a reactivity scale.[17] As expected, the

[14] Greb, L.; Daniliuc, C. G.; Bergander, K.; Paradies, J. *Angew. Chem. Int. Ed.* **2013**, *52*, 5876.
[15] The relative Lewis acidity of **53** compared to **1** (set to 100%) was determined to be 58%and 82% according to the methods of Childs and Gutmann-Beckett, respectively. Morgan, M. M.; Marwitz, A. J. V.; Piers, W. E.; Parvez, M. *Organometallics* **2013**, *32*, 317 b) Beckett, M.A.; Brassington, D. S.; Coles, S. J.; Hursthouse, M. B. *Inorg. Chem. Commun.* **2000**, *3*, 530
[16] Inés, B.; Palomas, D.; Holle, S.; Steinberg, S.; Nicasio, J. a.; Alcarazo, M. *Angew. Chem. Int. Ed.* **2012**, *51*, 12367.
[17] Morozova, V.; Mayer, P.; Berionni, G. *Angew. Chem. Int. Ed.* **2015**, *54*, 14058.

hydricity of hydridoborates salts **29a-c** increases with the decrease of the Lewis acidity. These salts have then been used for the reduction of various quinone methides **30a**, in good to excellent yields (70-94%). In these cases, the reaction mechanism seems to be different. Indeed, it was proposed that the hydride transfer to the quinone methides **30a** takes place in a first place to yield the corresponding stable phenolate **30b**. The latter is then expected to protonate on the Bronsted acid, resulting from the cleavage of H_2 by the phosphine, to form the saturated adduct **30c**.

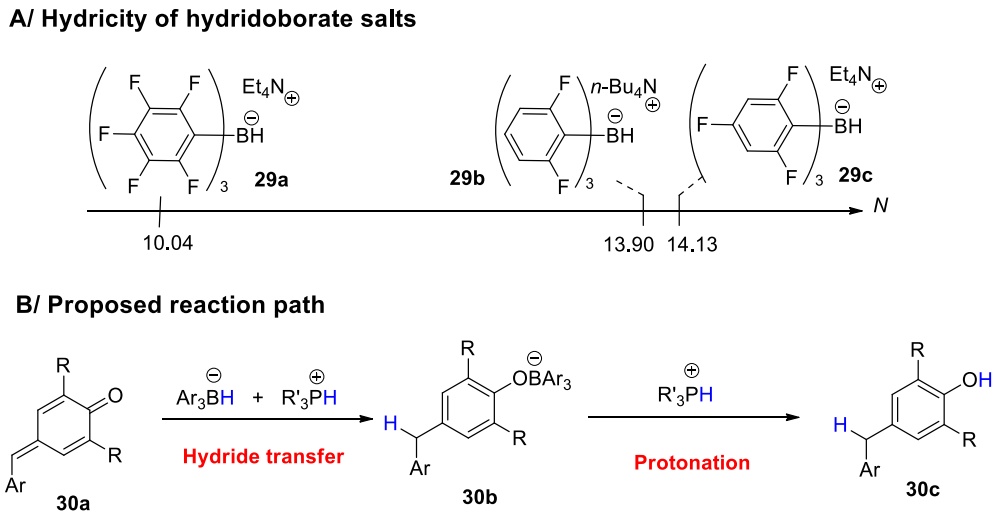

*Scheme 2.11 Hydricity scale of selected hydridoborate salts (A/) and proposed reaction mechanism or the reduction of quinone methides **30a** into **30c** (B/)*

Along with the reduction of allenes with P/B and N/B FLPs, Alcarazo et al. investigated the catalytic hydrogenation of alkylidene malonates **31**.[16] The authors showed that **31** was reduced by **1**/DABCO into **32** under 60 bars H_2 at 80°C for 24h in yields ranging from 79 to 96%. Mechanistic studies, based on D-labelling experiments, have been performed, highlighting the occurrence of an activation of the electrophile by the formation of a hydrogen-bond concomitantly to the hydride transfer, as drawn in the *Scheme 2.12* with the transition state TS-**32.**

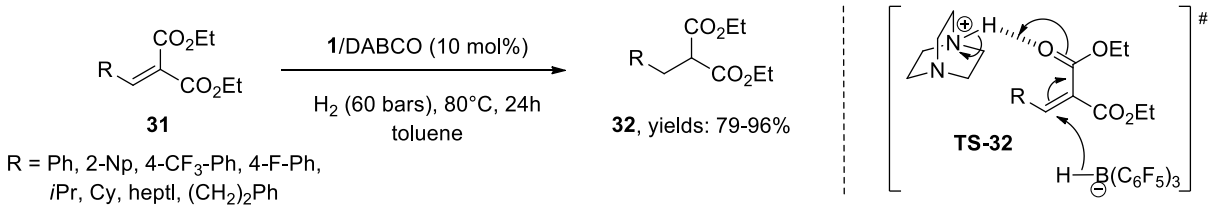

*Scheme 2.12 Hydrogenation of alkylidene malonates **31** with **1**/DABCO and postulated transition state.*

The same group modified the nature of the Lewis-acid by reducing the Lewis acidity to increase the strength of the hydride and found that, in line with the work of Berionni, $[(2,4,6\text{-}F_3\text{-}C_6H_2)_3BH]^-$ **29d** was a good candidate as strong hydride donor.[18] Based on this methodology, they were able to hydrogenate a broad range of electron-poor alkenes such as α,β-unsaturated- esters, sulfones, malonates and nitro using $(2,4,6\text{-}F_3\text{-}C_6H_2)_3B$/DABCO (5 mol%, 5 bars H_2, 50°, 24h).

Partial conclusions: This state of the art on the FLP catalysed reduction of olefins allowed us to draw several conclusions. First of all, in the case of electron-rich olefins, one can assume that the formation of a carbocation resulting from the protonation of the olefin by the phosphonium salt is crucial. In this case, perfluorinated phosphines, exhibiting low pK_a *must be used along with weak Lewis acids under* H_2*. However, regarding the phosphine catalyzed hydrogenation of electron-poor double bonds, it seems to be much more difficult. Indeed, while intramolecular P/B FLP are able to catalyse the reduction of imines, it exists no examples using a simple FLP composed by a phosphine and a Lewis acid exhibiting the same activity. It is intriguing as we evidenced that phosphonium salts are strong Bronsted acids, capable to enhance the electrophilicity of carbonyl derivatives. In addition, while even weak hydridoborate salts have been shown to be able to reduce quinone methides, P/B should be relevant candidates to catalyse the reduction of carbonyl derivatives and even α,β-unsaturated compounds under* H_2*.*

2. Reduction of Michael acceptors by P/B FLPs

As mentioned in the previous part, the catalytic reduction of α,β-unsaturated carbonyl compounds have never been realized under FLP conditions including phosphines as Lewis base. Intrigued by these observations, we embarked on designing a P/B system to perform such a reaction.

2.1. Synthesis of FLPs and catalytic reduction of methylvinyl ketone under H_2.

To initiate this work, we selected the commonly used $B(C_6F_5)_3$ **1** as Lewis acid and two sterically encumbered phosphines as Lewis bases, tri(1-naphthyl)phosphine **33** and tris(*o*-tolyl)phosphine **34**, $P(C_{10}H_7)_3$ and P(*o*-tol)$_3$ respectively (Scheme 2.13). Due to the high Brønsted acidity of its phosphonium salt (pK_a ($C_2H_4Cl_2$) = 6.7)[3], $P(C_{10}H_7)_3$ has proved to be an efficient Lewis base in the FLP catalysed hydrogenation of unpolarised olefins. Besides, P(*o*-

[18] Nicasio, J. A.; Steinberg, S.; Inés, B.; Alcarazo, M. *Chem. - A Eur. J.* **2013,** *19*, 11016.

tol)$_3$ **34** is known to be effective in cleaving H_2 in the presence of $B(C_6F_5)_3$ to yield the resulting phosphonium hydridoborate **34b** (pK_a (CH_2Cl_2) = 3.2)[19,20].

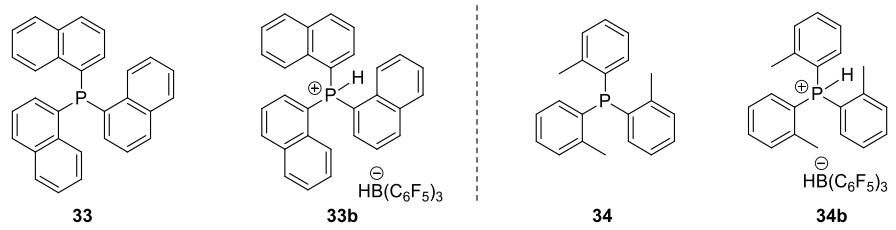

*Scheme 2.13 Structures of tri(1-naphthyl)phosphine **33** and tris(o-tolyl)phosphine **34**, and related phosphonium hydridoborate salts resulting from the cleavage of H_2.*

In the presence of $B(C_6F_5)_3$ **1**, both phosphines were able to cleave the dihydrogen molecule under a pressure of 4 bars of H_2 within 12 hours in CH_2Cl_2. This has been evidenced by the decolouration of the solution during the cleavage, yielding **33b** and **34b** in good yields. The catalytic reduction of the methylvinylketone **35a** with **33** or **34** in the presence of **1** (10 mol %) was selected as a benchmark reaction. As shown in Scheme 2.14, both reactions did not proceed under 4 atmospheres of H_2 at r.t. and only traces of the reduction adduct **36a** could be detected within 12h. Indeed, ^{31}P NMR spectrum of the crude mixture showed in both cases the appearance of new peaks at 28.6 ppm and 27.7 ppm with **33** and **34**, respectively, which have been assigned to the phosphination adducts **37** and **38**.

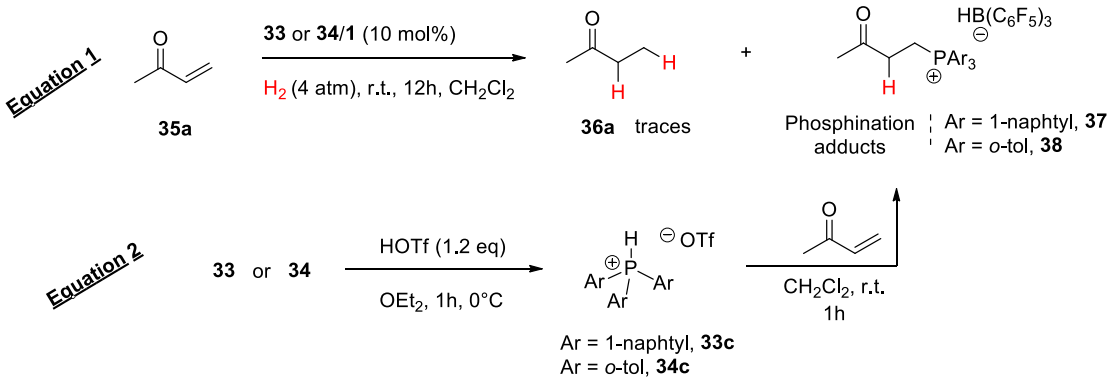

*Scheme 2.14 Catalytic reduction methylvinyl ketone **35a** with **33**,**34**/**1** (10 mol %) under H_2 atmosphere (top). Reaction of phosphonium ions **33,34-c** with methylvinyl ketone **35a** in CH_2Cl_2 at room temperature (bottom).*

These first experiments highlighted that, under catalytic conditions (equation 1), instead of observing the expected hydrogenation product of **35a** with **33b** or **34b**, the hydrophosphination pathway took place leading to the formation of the phosphoniums adducts (confirmed by equation 2).

[19] F. E. Herkes in *CATALYSIS OF ORGANIC REACTIONS*, Marcel Dekker, Inc., New-York, **1998**, pp. 475

[20] Ullrich, M.; Lough, A. J.; Stephan, D. W. *J. Am. Chem. Soc.* **2009**, *131*, 52.

In order to confirm these structures, phosphines **33** and **34** have been treated with triflic acid to yield the corresponding phosphonium triflate **33c** and **34c** which have been reacted with a stoichiometric amount of **35a**. As expected, we observed the formation of the anti-Markovnikov adducts resulting from the hydrophosphination reaction of **35a**. These results also indicate that the reaction outcome is counterion independent in both cases.

2.2. Stoechiometric reaction of FLPs with Michael acceptors

With the aim to better understand the reactivity of **33,34-b**, we prepared these salts following a protocol previously described by Berionni et al.[17] In this context, phosphonium salt **33c** or **34c** were mixed with **1**, followed by the addition of triethylsilane to the mixture to yield **33b** or **34b** with 84 and 80% yields respectively (*Scheme 2.15*).

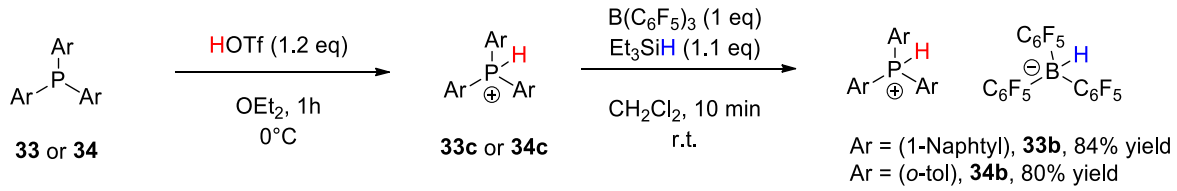

*Scheme 2.15 Two steps synthesis of complexes **33**b and **34**b.*

The two complexes were characterized in solution by NMR spectroscopy (^{1}H, ^{31}P and ^{11}B) as shown in the *Figure 2.3*.

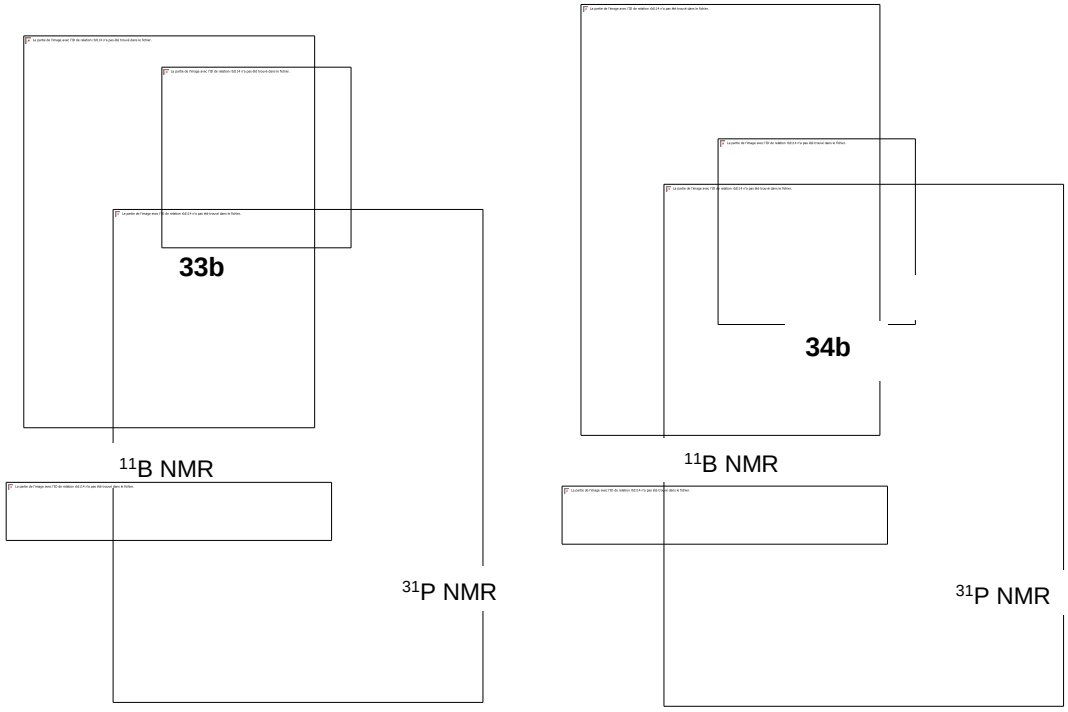

*Figure 2.3 Characterization of **33b** and **34b** both in solutions (CD_2Cl_2) by ^{31}P and ^{11}B NMR spectroscopy.*

The compound **34b** was recrystallized from a saturated solution of CH_2Cl_2 in *n*-pentane to yield colourless crystals of **34b** suitable for X-ray analysis (*Figure 2.4*). Thee X-ray structure highlighted the proximity between the acid proton and the hydrogen of the hydridoborate (d = 1.901 Å).

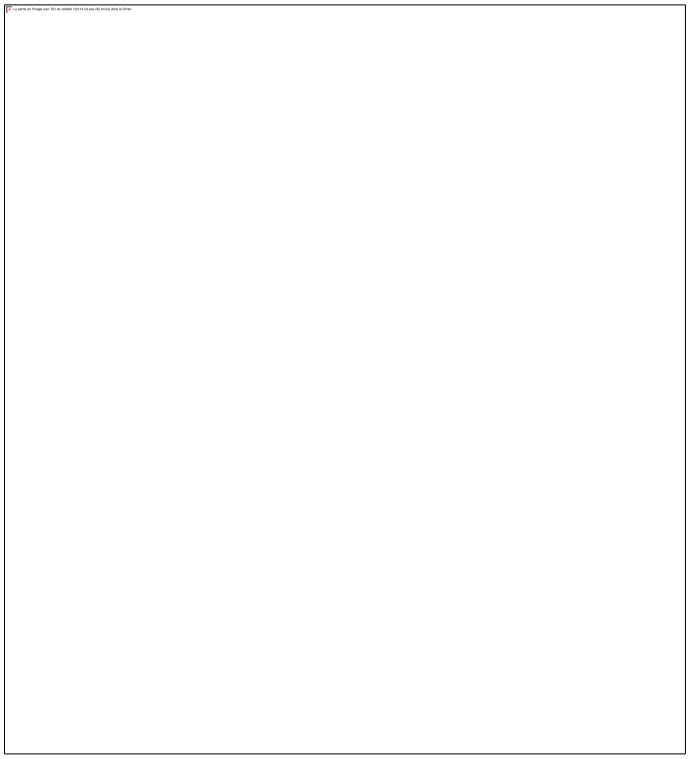

*Figure 2.4 X-ray structure of **34b**, ORTEP representation. Colours: Boron (pink), phosphorous (purple) and fluorine (yellow).*

We then investigated the stoichiometric reactions between **33,34-b** and several Michael acceptors by controlling the hydrogenation/hydrophosphination outcomes. For this study, five electron poor alkenes **35a-e** were used as depicted *Scheme 2.16*. The electrophilicity parameters of each alkenes **35a-e** have already been quantified by Mayr et al., allowing a direct comparison between the reaction outcomes and the electrophilicity of the alkene.

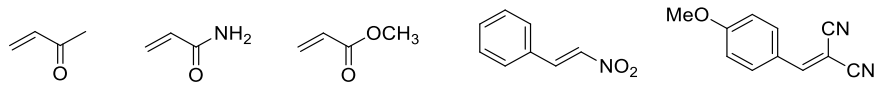

35a	**35b**	**35c**	**35d**	**35e**
E = -16.48	*E* = -23.54	*E* = -18.92	*E* = -13.85	*E* = -10.80

*Scheme 2.16 Structures and electrophilicity parameters of Michael acceptors **35a-e** employed in this study.*

The five olefins have been placed in a Schlenk at r.t. with **33b** or **34b** in solution in dichloromethane for 12h, respectively. At the term of the reaction time, the crude mixture was analysed by NMR spectroscopy and the conversions were determined according to the ^{1}H

NMR spectra. Hence, a mixture or the reduction adduct **39a-e** and the hydrophosphination adducts **40a-j** were obtained in each case (*Table 2.1*).

*Table 2.1 Reaction outcome of the reactions of **33,34-b** with **35a-e** and their electrophilicity parameters*

FLP	Alkene	*E*	Reduction, (%)	Hydrophosphination, (%)
33b	**35a**	-16.48[21]	**39a,** (39%)	**40a,** (61%)
	35b	-23.54[21]	**39b,** (54%)	**40b,** (46%)
	35c	-18.92[21]	**39c,** (28%)	**40c,** (72%)
	35d	-13.85[22]	**39d,** (100%)	**40d,** (0%)
	35e	-10.80[23]	**39e,** (100%)	**40e,** (0%)
34b	**35a**	-16.48[21]	**39a,** (47%)	**40f,** (53%)
	35b	-23.54[21]	**39b,** (69%)	**40g,** (31%)
	35c	-18.92[21]	**39c,** (47%)	**40h,** (53%)
	35d	-13.85[22]	**39d,** (100%)	**40i,** (0%)
	35e	-10.80[23]	**39e,** (100%)	**40j,** (0%)

While a mixture of hydrophosphination and reduction adducts was detected for the reactions of **33,34-b** with Michael acceptors **35a-c**, only reduction adducts **39d,e** were obtained when **33,34-b** were combined with **35d,e**. Moreover, it clearly seems that **34b** was able to promote more hydrogenation than **33b**, showing that the electronic or the steric properties of the phosphine plays an important role. In addition, the electrophilicity of the Michael acceptor is also a guideline to understand the observed reactivity. Indeed, for a given FLP, the less electrophilic Michael acceptors led to the more hydrogenation and the highest electrophilic ones to the more hydrophosphination.

While the reduction/hydrophosphination outcomes should be linked to i) the electrophilicity of the Michael acceptor, ii) the Bronsted basicity of the carbonyl groups and iii) the nature of the phosphine, the previous elements didn't allow us to understand the regioselectivity and thus to propose a mechanism. To get more insights in the reactivity of these FLPs, we thus embarked in a study of the reaction mechanism.

3. Study of the reaction mechanism

We decided to investigate in more details the reaction mechanism by using kinetics to measure both the nucleophilicity and the Lewis basicity of phosphines responsible for the anti-

[21] Allgäuer, D. Dissertation, Faculty of Chemistry and Pharmacy, LMU München, **2014**.
[22] Zenz, I.; Mayr, H. *J. Org. Chem.* **2011**, *76*, 9370.
[23] Lemek, T.; Mayr, H. *J. Org. Chem.* **2003**, *68*, 6880.

Markovnikov hydrophosphination. For that purpose, the two nucleophiles **33,34** were studied according to Mayr nucleophilicity scale (based on equation 1) and Mayr Lewis-basicity scale (based on equation 2).

$$\log(k_{20°C}) = s_N(E + N) \qquad (1)$$

$$\log(K_{20°C}) = LA + LB \qquad (2)$$

3.1. Reactions of **33** and **34** with diarylcarbenium cations under pseudo-first order conditions

Due to the structures of the sterically hindered phosphines **33,34,** low nucleophilicity parameters were expected. Consequently, blue coloured diarylcarbenium cations **41a-c** (*Scheme 2.17*) possessing relatively high electrophilicity have been found to be suitable electrophiles to perform kinetics.

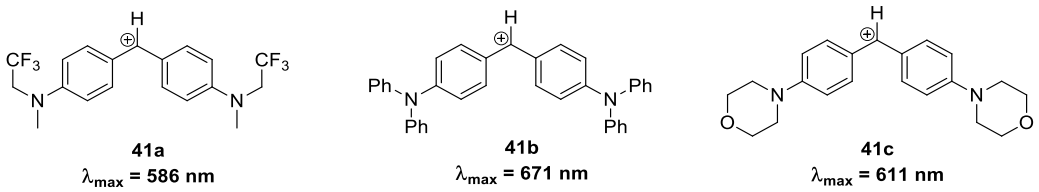

*Scheme 2.17 Structure of diarylcarbenium cations **41a-c***

Hence, reactions of phosphines **33,34** with benzhydrilium salts **41a-c** were investigated with a care to the second order rate constants k_2 (*Scheme 2.18*). In order to determine k_2, reactions were performed under pseudo-first order approximations. In these conditions, [Nu] > 10×[E], allowing us to assume that [Nu] is constant during the whole reaction and defining a first order observable constant k_{obs}. Based on these assumptions, both k_{obs} and k_2 could be determined as shown in the *Scheme 2.18*.

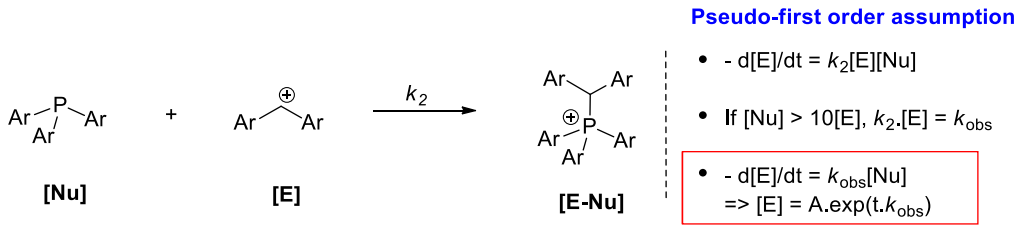

Scheme 2.18 General scheme of the reaction of phosphines with benzhydrilium salts under pseudo-first order conditions.

3.2. Determination of the nucleophilicity and the Lewis basicity parameters

When a large excess of phosphines **33,34** was combined with benzhydrilium ions **41a−c**, mono-exponential decays of the absorbance of **41a−c** were observed according to the pseudo-

first order reaction conditions (*Figure 2.5*). In line with previous studies by Mayr et al. on the reactivity of tertiary phosphines, reversible processes have also been observed when phosphines were combined with **41a−c**.[24] Plotting rate constants k_{obs}, derived from mono-exponential decays against concentrations of nucleophiles **33,34** gives linear correlations where the slopes yielded second-order rate constants for the reaction of **33,34** with **41a−c**. Lastly, as required by equation (1), the logarithms of the second order rate constants (log k_2) and the E parameters of the benzhydrylium ions **41a−c** correlate linearly (*Figure 2.5*). The slopes give the nucleophile-specific sensitivity parameters s_N while the intercepts on the abscissa yield the nucleophilicity parameters *N*, which are gathered in the *Table 2.2*.

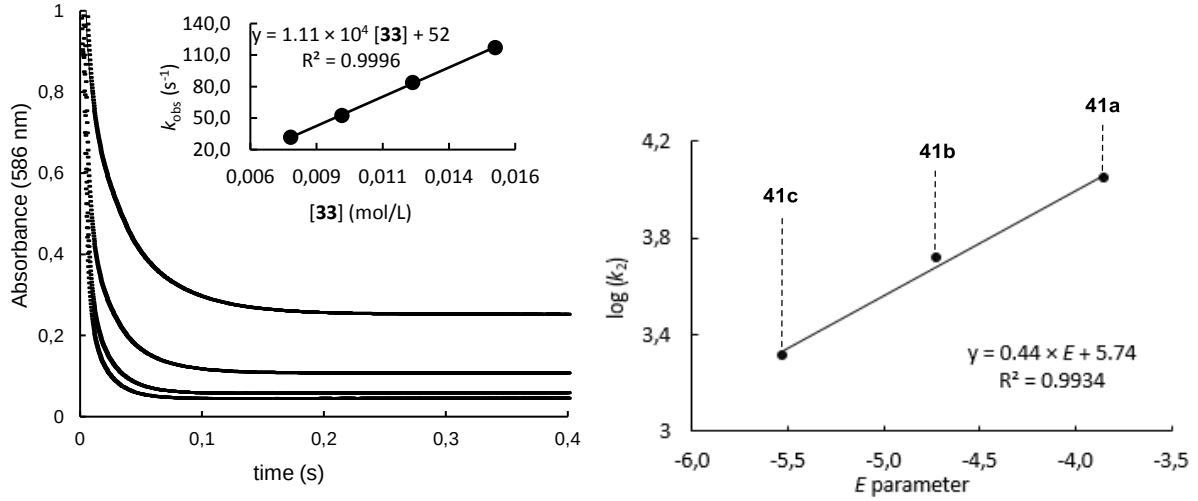

*Figure 2.5 (Left) Plot of the absorbance at 586 nm against time for the reactions of **41a** (1.35 × 10⁻⁴ mol/L) with **33** at different initial concentrations. (Right) Plot of log k_2 vs E for reactions of phosphines **33** (triangles) and **34** (circles) with benzhydrilium ions **41a,c***

Table 2.2 Second-order rate constants, nucleophilicity N, and Lewis basicity LB *for reactions of **33,34** with benzhydrilium ions **41a−c** in MeCN or CH_2Cl_2 at 20 °C.*In acetonitrile and **in dichloromethane.*

Phosphines	Electrophiles	k_2 ($M^{-1}s^{-1}$)	*N*, s_N	*LB*
33*	**41a**	1.11×10^4	13.17, 0.44	8.62
	41b	5.23×10^3		
	41c	2.05×10^3		
34**	**41a**	1.31×10^3	8.40, 0.68	7.77
	41b	2.87×10^2		
	41c	9.48×10^1		

As the reactions of phosphines **33** and **34** with benzhydrylium ions proceeded incompletely, we also studied the corresponding equilibrium constants (*K*) by UV−vis spectroscopy. The

[24] Kempf, B.; Mayr, H. *Chem. - A Eur. J.* **2005**, *11*, 917.

Lewis basicity of **33** and **34** was quantified by using an approach recently introduced by Mayr, who found that the *K* values for reaction of benzhydrylium ions with various Lewis bases can be expressed as the sum of a Lewis acidity parameter LA and a Lewis basicity parameter LB (equation 2). By using the previously determined Lewis acidity (LA) of benzhydrilium ions and the measured equilibrium constants (*K*), the Lewis basicity of **33,34** were determined (*Table 2.2*).

Table 1 shows that **33** is about 18 times more reactive than **34**. This can presumably be due to the steric hindrance of the tolyl group due to its high Tolman angle (θ[**34**] = 194°).[25] On the other hands, it also shows that the Lewis basicity of **33** was determined to be 10 times higher than that of **34**, highlighting less reversible addition of **33** with electrophiles than **34**.

3.3. Determination of the intrinsic barriers for the reactions of **33,34** with **41a-c.**

Having the rate constants of the reactions of **33,34** with benzhydrilium ions and the related equilibrium constants in hand, we then employed the Marcus equation (equation 3, working terms neglected) to calculate barriers $\Delta G_0^{\ddagger}$ for these reactions. First, we calculated the Gibbs energy of activation when the effect of the thermodynamic driving force is eliminated (ΔG_0 = 0).[26] Thus, by substituting $\Delta G^{\ddagger}$ and ΔG_0 into the Marcus eq 3, the intrinsic barriers $\Delta G_0^{\ddagger}$ for the reactions of **33,34** with **41a−c** were calculated.

$$\Delta G^{\ddagger} = \Delta G_0^{\ddagger} + \frac{\Delta G_0}{2} + \frac{(\Delta G_0)^2}{16.\Delta G_0^{\ddagger}} \qquad (3)$$

*Table 2.3 Activation Energies $\Delta G^{\ddagger}$, Reaction Free Energies ΔG_0, and Intrinsic Barriers $\Delta G_0^{\ddagger}$ (in kJ/mol) for the reactions of Benzhydrylium Ions **41a−c** with Phosphines **33,34**.*

Phosphines	Electrophiles	$\Delta G^{\ddagger}$	ΔG_0	$\Delta G_0^{\ddagger}$
33	**41c**	49.1	-18.4	57.9
	41b	50.9	-15.5	58.4
	41a	53.2	-10.7	58.4
34	**41c**	54.3	-12.8	60.5
	41b	58.0	-10.9	63.3
	41a	60.7	-6.66	63.9

As shown in Table 2, the intrinsic barriers of the reactions of **34** with **41a−c** are ~3−5 kJ/mol greater than those for **33**. This indicates that more reorganizing energy is needed for the reaction of **34** than for the reactions with **33**, most probably due to the steric hindrance.

[25] Tolman, C. A. *J. Am. Chem. Soc.* **1970**, *92*, 2956.
[26] Mayr, H.; Ammer, J.; Baidya, M.; Maji, B.; Nigst, T. A.; Ofial, A. R.; Singer, T. *J. Am. Chem. Soc.* **2015**, *137* (7), 2580.

3.4. Proposed reaction mechanism

Based on the hydricity of phosphonium and ammonium borohydride determined by Berionni in one hand ($N_{[NEt4][HB(C6F5)3]}$ = 10.01),[17] and the nucleophilicity, carbon Lewis basicity, and intrinsic reactivity of phosphines **33,34**, on the other hand, the following reaction mechanism can be proposed (*Scheme 2.19*). When the phosphonium borohydride **42a**, formed upon heterolytic cleavage of H_2 by the FLPs, reacts with Michael acceptors **35**, two pathways are possible:

- (a) If the phosphonium ion is not acidic enough ($pK_a \geq 6$), typically in the case of trialkylphosphines, the borohydride is the only nucleophilic species present in the media which reacts with the Michael acceptor to give the carbanion **42b**, which is subsequently protonated to yield **42c**.

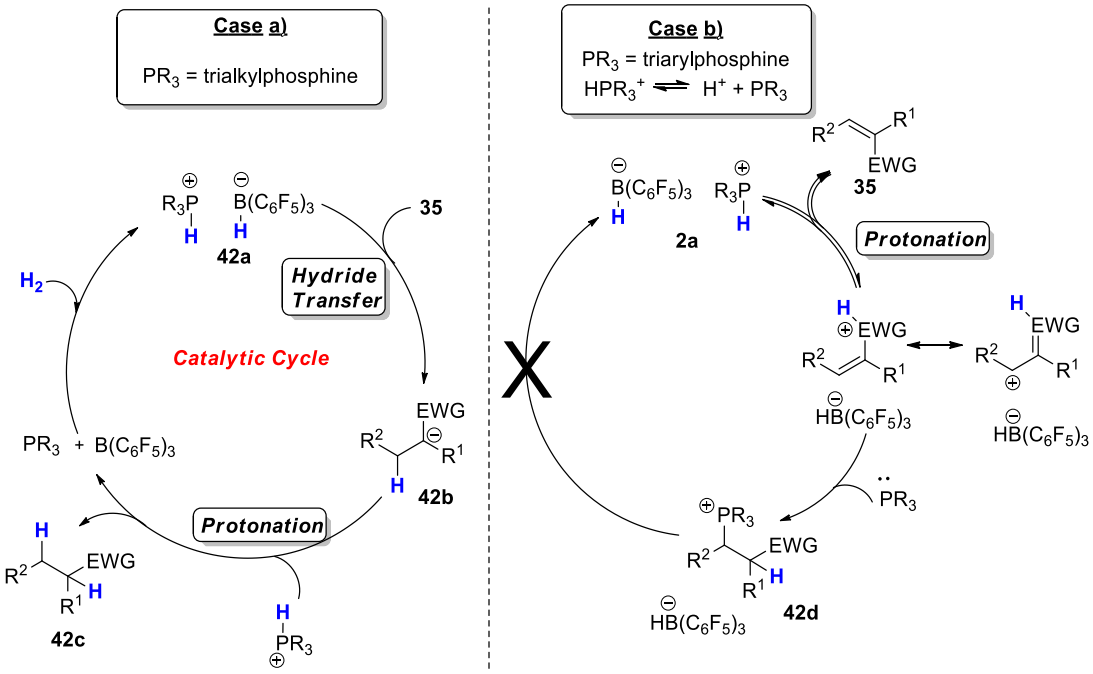

Scheme 2.19 Proposed reaction mechanism for phosphine−($B(C_6F_5)_3$) hydrogenation of Michael acceptors

In this case, the nucleophilicity of the borohydrides is crucial for the feasibility of the reduction. This explanation also holds for ammonium borohydrides,[27] which have low Brønsted acidities and thus can efficiently reduce Michael acceptors.

- (b) If now the generated phosphonium borohydride is acidic, for instance, triarylphosphonium salts, then two nucleophiles are present in the media: the free phosphine and the borohydride. On one hand, if the nucleophilicity of the borohydride is significantly greater than that of the phosphine, the hydrogenation pathway is predominant and only the saturated product **42c** is formed. On the other hand, if the phosphine is more nucleophilic than the borohydride, such

[27] Inés, B.; Palomas, D.; Holle, S.; Steinberg, S.; Nicasio, J. a.; Alcarazo, M. *Angew. Chem., Int. Ed.* **2012**, *51* (49), 12367.

as in the case of tri(1-naphthyl)phosphine **33** (*N* = 13.17 vs *N* = 10.04), the phosphorus addition at the terminal methylene group is kinetically favourable and the hydrophosphination adduct **42d** can be formed. This may rationalize the failure of those phosphines in reducing activated alkenes in the presence of $B(C_6F_5)_3$ under H_2 atmosphere. However, if the phosphine has a lower nucleophilicity than the borohydride, as in the case of **33** (N = 10.04 vs 8.40), the hydride transfer step can take place faster than the addition of the phosphine, leading to the formation of **42c**. The kinetic and thermodynamic data also rationalize the reaction outcomes for the addition of **33,34** to **35a-e**. The predominance of the hydrophosphination over the reduction adduct in the case of the reaction of **34** with **35a-e** (*Figure 2.6*) is a consequence of the low Lewis basicity of **34** and the high intrinsic reactivity $\Delta G_0^{\ddagger}$.

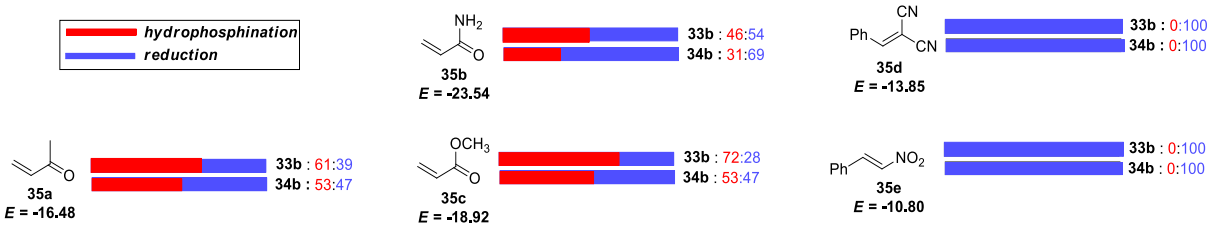

*Figure 2.6 Product distributions of the reactions of **33,34b**−$HB(C_6F_5)_3$ with Michael acceptors **35a−e***

Because the Mayr's rule of thumb predicts that reactions of **35b** (E = −23.54)[21] and **35c** (E = −18.92)[21] with phosphines **33,34** and borohydrides are not kinetically possible at room temperature, the observed reaction outcome given in *Figure 2.6* is presumably the result of a proton induction at the carbonyl oxygen that enhances the electrophilicities of the enones **35b,c**. In the case of the reactions of **33,34-b** with the Michael acceptors **35d,e**, phosphine and hydride transfer events are possible because of the high reactivity of both electrophiles. However, as proton activation is less favourable, the phosphine attacks are highly reversible and reduction pathway predominates.

4. Exploration of the hydrophosphination of Michael acceptors with phosphonium salts in C-P bond formation

As an extension of the unexpected results obtained in the FLP-catalytic reduction of electron-poor olefins with phosphines as Lewis bases, we decided to investigate the potential of phosphoniums salts in the C-P-bond formation.

4.1. C-P bond formation utilizing phosphonium salts HPR_3^+

Phosphoniums salts R_4P^+ are versatile and robust compounds widely used in organocatalysis as phase transfer catalysts[28] and Lewis acid catalysis[29], in the field of ionic liquids,[30] or as useful buildings blocks in organic synthesis. Moreover, phosphoniums salts (**PS**) present the advantages to be thermally stable and have a low toxicity.[31] Despite the important broad of applications of **PS**, their diversity is generally limited due to the lack of methodologies dealing with their synthesis. Indeed, they are usually obtained by alkylation reactions with alkyl halides or by arylation reactions with organometallic reagents which often lead to complex mixtures and purification issues. In the case of α-functionalized phosphonium salts, their synthesis requires the use of hazardous reagents or high thermal activation.[32]

Recently, tertiary phosphonium salts $[R_3PH]^+[X]^-$ (named H-**PS** later on) have been used as precursors for the synthesis of **PS**. Those salts are given scant attention although they present the advantages to be highly air and moisture stable and are easily accessible by a simple protonation of the free phosphine with a strong Brönsted acid. Exploiting the low BDE of the P-H bond of those salts, Grubbs et al have involved triphenylphosphonium tetrafluoroborate $[Ph_3PH]^+[BF_4]^-$ **43b** in a radical mediated addition to olefins (*Scheme 2.20*).[33] While a broad scope of tetra-alkylphosphonium salts were accessed with excellent yields, the methodology suffers from a limited functional toleranceass only alkyl, aryl, alkoxy or carbamoyl groups were reported. To the best of our knowledge, it is the sole example utilizing H-**PS** in C-P bond formation.

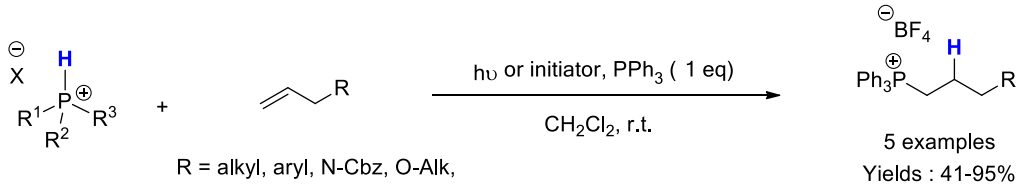

Scheme 2.20 Radical mediated hydrophosphination of terminal olefins with phosphonium salts.

[28] a) Wang, H.; Wang, K.; Ren, Y.; Li, N.; Tang, B.; Zhao, G. *Adv. Synth. Catal*. **2017**, *359*, 1.b) Fan, A.; Chuah, G. K.; Jaenicke, S. *Catal. Today* **2012**, *198*, 300. c) Maruoka, K. **2008** Asymmetric Phase Transfer Catalysis, Editor: Wiley-VCH.
[29]Denmark, S. E.; Werner, N. S. *Org. Lett.* **2011**, *13*, 4596.
[30] a) Del Sesto, R. E.; Corley, C.; Robertson, A.; Wilkes, J. S. *J. Organomet. Chem.* **2005**, *690*, 2536. b) McNulty, J.; Cheekoori, S.; Nair, J. J.; Larichev, V.; Capretta, A.; Robertson, A. J. *Tetrahedron Lett.* **2005**, *46*, 3641. c) McNulty, J.; Nair, J. J.; Cheekoori, S.; Larichev, V.; Capretta, A.; Robertson, A. J. *Chem. - A Eur. J.* **2006**, *12*, 9314.
[31] Hartmann, D. O.; Pereira, C. S. *New J. Chem.* **2013**, *37*, 1569.
[32] H. J. Cristau.; F. Plénat in Preparation, properties and reactions of phosphonium salts, chapter 2; Edited by Frank R. Hartley. © 1994 John Wiley & Sons, Ltd. ISBN: 0-471-93057-1
[33] Daeffler, C. S.; Grubbs, R. H. *Org. Lett.* **2011**, *13*, 6429.

4.2. Expected reactivity of H-**PS** in the hydrophosphination of Michael acceptors

Based on Grubbs' work from one side and on our previous work on P/B FLPs from the other side, we wondered if we could benefit from the acidity of the proton of $[R_3PH^+].[X]^-$ to functionalize olefins via an ionic hydrophosphination pathway. Indeed, Morris et al have measured pK_a of phosphonium salts in CH_2Cl_2 using a methodology based on the determination of equilibrium constants with iron complexes and showed that it ranges from 1.6 to 8.6 for $[HPPh_3]^+.[BF_4]^-$ and $[HPCy_3]^+.[BF_4]^-$, respectively.[34] Consequently, H-**PS** should be good candidates for the ionic hydrophosphination of olefins due to the acidic character of the proton. This parameter would be of great importance as it explain the release of the phosphine which should be in equilibrium with the corresponding phosphonium salt (step 1). On the other side, H-**PS** can be expected to activate Michael acceptors via a Bronsted acid activation as shown by the step 2 of *Scheme 2.21* (hydrogen bonding). In the last step, the phosphine would add on the electrophilic system to yield the hydrophosphination adduct after protonation (step 3).

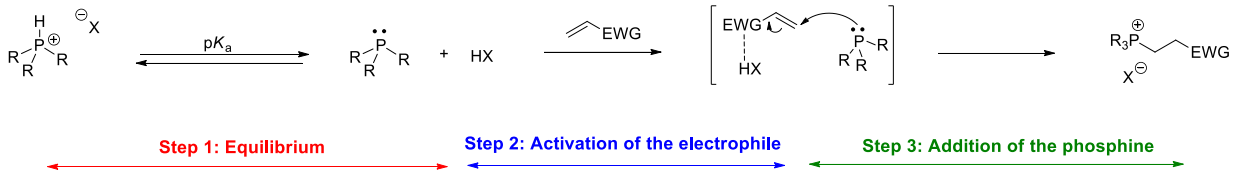

Scheme 2.21 Proposed reaction mechanism for the hydrophosphination of polarized olefins

4.3. Hydrophosphination of Michael acceptors with $[Ar_3PH]^+[X]^-$

To verify our proposed reaction mechanism, we commenced by preparing the triphenylphosphonium salt $[HPPh_3]^+.[OTf]^-$ **43b** containing the non-coordinating triflate anion. To illustrate the reactivity of this salt with Michael acceptors, methyl vinyl ketone **35a** has been chosen as a surrogate substrate as it contains a carbonyl group which can be activated via a hydrogen bonding.

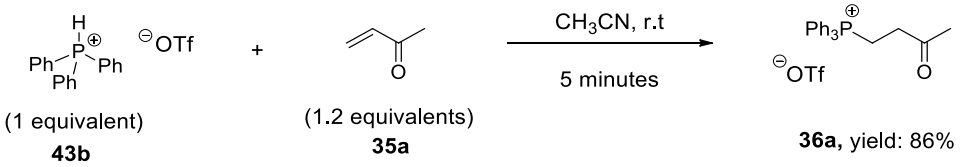

(1 equivalent) **43b** (1.2 equivalents) **35a** **36a,** yield: 86%

*Scheme 2.22 Optimized conditions of the reaction of **43b** with **35a** leading to the formation of **36a** which precipitated in ethyl acetate*

[34] Li, T.; Lough, A. J.; Morris, R. H. *Chem. - A Eur. J.* **2007**, *13*, 3796.

In line with our working hypothesis, we were pleased to observe the complete conversion of the starting phosphonium salts and the formation of a unique product which appears as a singlet in ^{31}P NMR spectroscopy. The isolation of the product by a simple precipitation in ethyl acetate yielded the hydrophosphination adduct **36a** resulting from the addition of the P-H bond to the C=C double bond. After optimization, we found that the reaction was completed within only 5 minutes in acetonitrile. It's noteworthy to mention that the reaction proceeds well in either CH_2Cl_2 or CH_3CN but is limited by the solubility of **43b**. With the optimized conditions in hand, we applied our procedure for the synthesis of a variety of functionalized **PS** (*Scheme 2.23*).

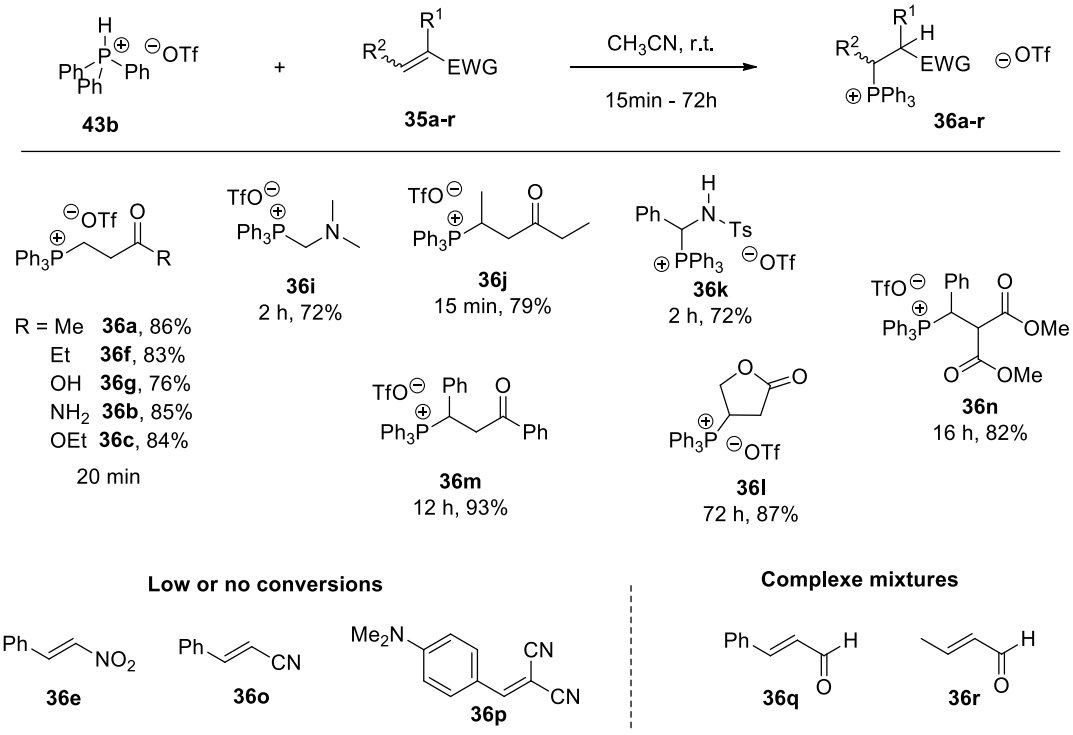

*Scheme 2.23 Scope and limitations of the reaction of **43b** with various Michael acceptors **35a-r**. Conditions: (**43b**, 0.36 mmol, 1 eq), olefin (**35a-r**, 1.05 eq), CH_3CN, c = 0.2 mol/L, r.t.*

As depicted in *Scheme 2.23*, **43b** reacts smoothly with a large scope of electrophiles **35a-l,** to furnish the hydrophosphination adducts **36a-p** in good to excellent yields. It is noteworthy to mention the broad functional tolerance of the reaction as ketones, ester, amide, carboxylic acids and even imines were tolerant to the used conditions and gave the desired adducts with excellent yields (from 72 to 93%). To extend our study to other Michael acceptors, reactions of **43b** with nitrostyrene **35d**, cinnamonitrile **35o**, α-(4-(dimethylamino)benzylidene) malononitrile **35p**, cinnamaldehyde **35q** and crotonaldehyde **35r** were performed. While the reaction of **43b** with nitrostyrene **35e** led to only 25% of the hydrophosphination adduct after 12h, only starting material were recovered when the phosphonium salt was reacted with the malononitriles **35o-p**. In the case of unsaturated aldehydes **35q-r**, complex reaction mixtures were detected by ^{31}P NMR spectroscopy when they were mixed with **43b** in CH_3CN.

4.4. Investigation in the parameters governing the hydrophosphination reaction

4.4.1. Effect of the pK_a on the rate of the hydrophosphination reaction

Intrigued by this lack of reactivity with nitro and cyano -electrophiles **35e** and **35o-p**, we wondered which parameters would be crucial to explain the absence of hydrophosphination. Indeed, based on Mayr electrophilicity, methylvinylketone **35a** (E = -16.48) is less electrophilic than malononitrile **35p** (E = -13.30). Consequently, one would expect faster hydrophosphination with malononitrile than methylvinylketone. In order to shed light into this puzzling observations, we investigated the effects of i) the pK_a of the proton of phosphonium salts **43-46b** and ii) the nucleophilicity of phosphines **43-46** in a solution of the phosphonium salt **43-46b.**

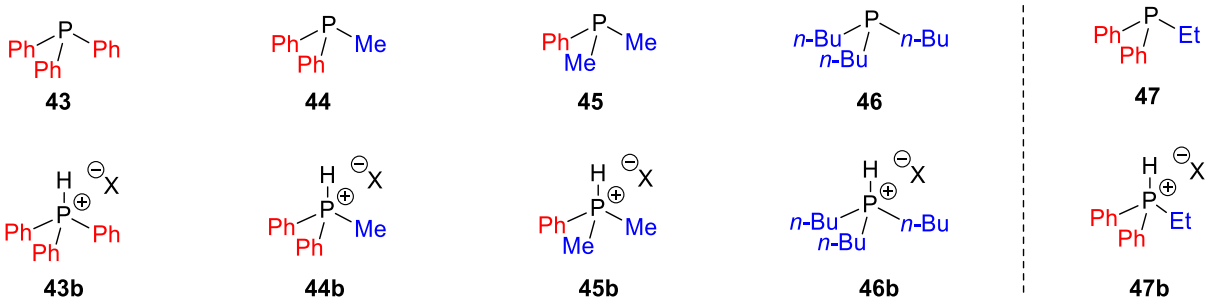

*Scheme 2.24 Structure of phosphines **43-47** and their corresponding phosphonium salts **43-47b** used for the study of the* pK_a *effect.*

To investigate the influence of the pK_a of the phosphine **43-46** in this reaction, four phosphonium salts **43-46b** were synthesized. The pK_a of each phosphonium salt **43-46b** have already been measured in CH_3CN, allowing a direct assessment of the importance of the pK_a on the reactivity with Michael acceptors.[34] The reactions of **43-46b** with **35f** were selected as model reaction and the conversion of the hydrophosphination adduct **48a-d** was followed by ^{31}P NMR spectroscopy (*Table 2.4*).

*Table 2.4 Kinetic study of the hydrophosphination of **35f** with **43-46b**. The reaction was monitored by ^{31}P NMR. *pK_a determined by Morris et al. in CH_2Cl_2. Conditions: (**43-46b**, 0.36 mmol, 1 eq), **35f** (1.2 eq), CH_3CN c = 0.2 mol/L, r.t*

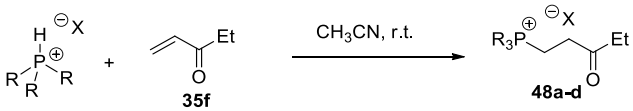

Phosphonium salts	pK_a	Reaction time	Product, Yield (%)
43b	1.6	< 5min	**48a**, 83
44b	3.3	20 min	**48b,** 87
45b	5.7	36h	**48c,** 93
46b	8.2	No reaction	**48d,** 0

Importantly, this study reveals that the rate of the hydrophosphination reaction dramatically decreases when the acidity of the proton increases. In the case of tri-*n*-butylphosphonium salt (pK_a = 8.2), the low acidity of the proton suppresses the formation of the desired product **48d**. This conclusion indicates that the pK_a of the proton is a relevant parameter which explain this reactivity (see step 1, *Scheme 2.21*). However, while the nature of the phosphine **43-46** changes the pK_a of the proton, the nucleophilicity parameter of the free phosphine is also strongly affected.

4.4.2. Effect of the solvent, counter ion and protonation state on the nucleophilicity of phosphines.

To gain further insights in the reaction mechanism, kinetics of the reactions of free phosphines and phosphines in equilibrium with their phosphonium salts have been recorded with benzhydrylium electrophiles.[26] For that purpose, three diarylcarbenium **41d-f** (*Scheme 2.25*) cations were selected to measure kinetics of the reactions with phosphines according to the previous equation (1).

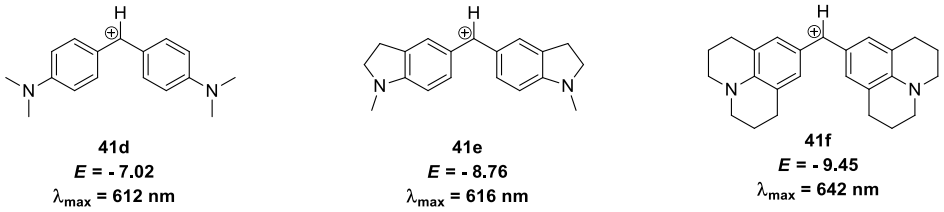

*Scheme 2.25 Structure, electrophilicity parameters and maximum wavelengths absorption of the diarylcarbenium cations **41d-f** used in this study. Counter ion: BF_4^-.*

Based on this approach, second order rate constants, nucleophilicity parameters and specific sensitivity nucleophilicity parameters were determined (*Table 2.5*). We first measured kinetics of the reaction of **43b** with benzhydrilium ions **41d-f** in acetonitrile at 20°C and compared its nucleophilicity parameter with that of triphenylphosphine **43**. Interestingly, we found that **43** and **43b** (pK_a = 1.6) have nucleophilicity values in the same order of magnitude regardless of its protonation state (*N* = 15.50 *vs* 14.91). However, when the less acidic ethyldiphenylphosphonium salt **47b** (pK_a = 3.6) was combined with **41d-f**, the nucleophilicity parameter *N* decreases from 17.88 for the free phosphine to 11.93. Decreasing further the Brönsted acidity of the phosphonium salt (pK_a (n-Bu)$_3$P = 8.4), resulted in no reaction with Benzhydrilium salts, even after a long reaction time. We then studied effect of the phosphonium counterion. As shown in the *Table 2.5*, tetrafluoroborate **43b[BF_4]** and trifluoromethanulfonate **43b[OTf]** triphenylphosphonium ions react with **41d-f** at almost the same second order rate constants, thus showing that the counterion is not involved in the rate-determining step of the reaction.

*Table 2.5 Second order rate constants for the reactions of the phosphines **43-47** and the phosphonium salts **43b,47b** with reference electrophiles **41d-f** in CH_3CN or CH_2Cl_2 at 20°C. [a] KIE: Kinetic Isotope effect.*

Nucleophile (solvent)	Electrophile	k_2 ($M^{-1}s^{-1}$)	N, s_N	KIE[a]
43	**41d**	2.86×10^4	15.50, 0.52	
(CH_3CN)	**41e**	2.87×10^3		
	41f	1.64×10^3		
43b[OTf]	**41d**	1.13×10^4	14.91, 0.51	
(CH_3CN)	**41e**	1.37×10^3		
	41f	6.49×10^2		
47	**41d**	7.74×10^4	17.88, 0.45	
(CH_3CN)	**41e**	1.07×10^4		
	41f	6.69×10^3		
47b[OTf]	**41d**	5.74×10^2	11.93, 0.56	
(CH_3CN)	**41e**	5.98×10^1		
	41f	2.48×10^1		
D-43b[OTf]	**41d**	1.22×10^4	14.80, 0.51	1.01
(CH_3CN)	**41e**	1.48×10^3		0.92
	41f	6.62×10^2		1.00
43b[OTf]	**41d**	2.22×10^4	14.32, 0.58	
(CH_2Cl_2)	**41e**	1.68×10^3		
	41f	8.66×10^2		
43b[BF_4]	**41d**	1.03×10^4	14.80, 0.51	
(CH_3CN)	**41e**	1.12×10^3		
	41f	6.13×10^2		

Lastly, the Kinetic Isotope Effect (KIE) was also studied and reveals that the proton is not involved in the rate determining step as KIE values are closed to 1 for three benzhydrilium salts.

This study confirms the reaction mechanism proposed in the *Scheme 2.21* and shows that both the pK_a and the nucleophilicity parameters of phosphines explains the reactivity of H-**PS** in the hydrophosphination of Michael acceptors.

4.5. Application of the hydrophosphination of olefins to cross-coupling metathesis as protecting groups of phosphines.

As our group has a background in cross-coupling metathesis, we decided to apply the hydrophosphination reaction to this domain as a continuation of the PhD thesis of Dr. Alexandra Fillippi.[35] Ring-closing metathesis reactions are known to be robust and functional tolerant strategies to promote the cyclization of compounds. However, when compounds possess coordinating ligands, the cyclization becomes much more challenging. In this context, diallylphosphines represent a class of molecules which are able to deactivate the metathesis catalyst through coordination and are thus difficult to cyclize under these conditions.

With the aim to synthesize phosphine possessing an original structure, we envisaged to use our hydrophosphination conditions to phenyldiallylphosphonium salt **49** which has been chosen as a model phosphonium salt, to yield the quaternary phosphonium salt **50**. Then, the ring-closing metathesis method was applied to **50**, affording the functionalized phosphonium salt **51**.

As expected, the hydrophosphination reaction proceeded well under the previously optimized conditions leading to the quantitative formation of **50**. Then, the addition of only 5 mol% of Grubbs II catalyst in CH_2Cl_2 at 40°C lead to quantitative conversions of **50** affording the desired product **51**.

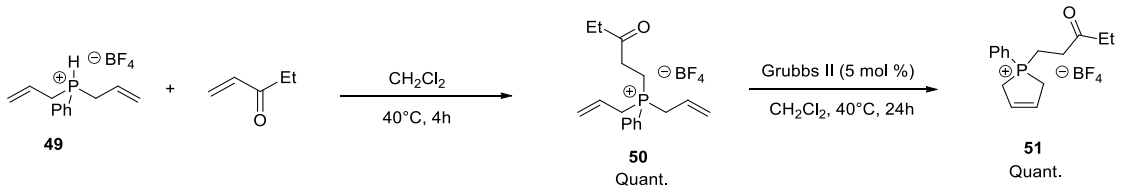

Scheme 2.26 Development of a tandem procedure for the functionalization of phosphonium salt.

This application is the first example of a metathesis reaction, involving a phosphonium salt backbone, and allows the formation of highly functionalized phosphonium salts. From a synthetic point of view, it also provides a new alternative to protect phosphines from oxidation or water during sensitive procedures.

5. Conclusion and perspectives

5.1. Conclusion

This first part of my PhD described a detailed investigation of the FLPs catalyzed hydrogenation of electron-poor olefins under hydrogen atmosphere. It was shown, based on

[35] Fillippi, A. Dissertation, Laboratoire de Chimie Moléculaire et Thio-Organique, University of Caen – ENSICAEN, France, **2015**.

recent literature survey, that P/B based FLPs are commonly used for the reduction of various unsaturated compounds such as alkenes, alkynes, imines, enamine, heterocycles, ketones but scarcely enones. Our stoichiometric study of the reaction of Michael acceptors with $[Ar_3PH][HB(C_6F_5)_3]$ revealed the formation of a phosphination adduct, resulting from a hydrophosphination pathways instead of the expected reduction compounds.

To unravel the mechanism of the reaction, kinetic studies allowed us to measure the nucleophilicity of phosphines used in the P/B FLP. By coupling these kinetic data with pK_a of phosphines, we were able to propose a reaction mechanism. In this mechanism, the acidic proton of the phosphonium part is expected to activate the carbonyl function, releasing the free phosphine which compete with $HB(C_6F_5)_3$ as nucleophile. Depending on the nucleophilicity of phosphine, either the reduction ($N_{HB(C6F5)3} > N_{PR3}$) or the hydrophosphination adducts ($N_{HB(C6F5)3} < N_{PR3}$) is obtained. These data, correlated with the electrophilicity parameters of Michael acceptors, provided a guideline to anticipate their reactivity.

Based on these results, the hydrophosphination pathways was explored to access various functionalized phosphonium salts using the scarcely reported $[HPR_3][X]$. A deep mechanistic study was realized to understand the reaction mechanism and the limitations of the methods. Indeed, while triaryl, alkyldiaryl and aryldialkylphosphonium salts reacted with Michael acceptors to yield the corresponding phosphoniums salts, trialkylphosphonium salts did not react. Our survey revealed that both the pK_a and the nucleophilicity of phosphines were the relevant parameters to understand the reactivity. More importantly, we confirmed the reaction postulated mechanism for the hydrophosphination of electron-poor alkenes with P/B based FLP.

Finally, the hydrophosphination reaction was used as a protection method of phosphines electron lone pairs in ring-closing metathesis reactions which remains challenging with free phosphines. Hence, we developed a tandem procedure to access cyclic phosphonium salts under smooth conditions and more importantly, requiring a simple Grubbs II catalyst.

5.2. Outlooks

In light of this work, several interesting perspectives can be drawn.

First of all, our study on P/B based FLP showed that we now have the important parameters which control the feasibility of FLP catalyzed reduction of alkenes. Indeed, to get the reduction adduct, the Lewis base must fill the following requirements:

- Lower nucleophilicity of the Lewis base than the hydridoborate anion.
- High Tolman angle or low Lewis basicity of the Lewis base
- Moderate to low pK_a of the onium salt (< 6).

These requirements must be coupled with the experimental conditions which are the pressure of H_2 for the heterolytic cleavage and the temperature. Based on these aspects, we can anticipate that 1,3,5-trimesitylphosphine or tris(3-methoxy-1,5-dimethylphenyl)phosphine would be suitable candidates. Indeed, they have very low nucleophilicity parameters (no reaction with diarylcarbenium cations)[36] and high tolman angle. However, due to the low nucleophilicity parameters, it would be expected to impose high pressure of dihydrogen. This drawback could be overcome by using an even more acidic Lewis acid than $B(C_6F_5)_3$. As evidenced by our literature survey about Guttman Beckett and child Lewis acidity scale, $B(OC_6F_5)_3$ would be suitable for this study. As a consequence, 1,3,5-trimesitylphosphine in association with $B(OC_6F_5)_3$ or tris(3-methoxy-1,5-dimethylphenyl)phosphine in association with $B(C_6F_5)_3$ would be suitable P/B systems to perform hydrogenation of a wide variety of substrates including Michael acceptors (Scheme 2.27).

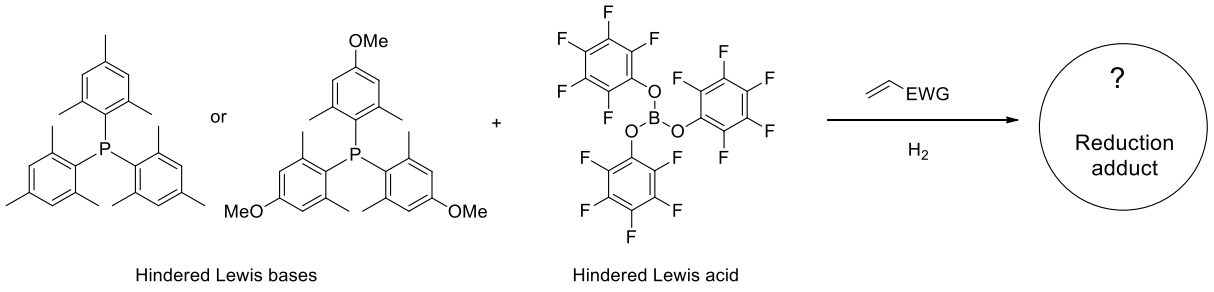

Scheme 2.27 Proposed strategy for the reduction of Michael acceptors

[36] Follet, E.; Mayer, P.; Stephenson, D. S.; Ofial, A. R.; Berionni, G. *Chem. - A Eur. J.* **2017**. DOI : 10.1002/chem.201701080

3. Chapter III: Quantification of the Hydride Donor Ability of Phosphine Borane Complexes.

Hydride transfers play a pivotal role in organic synthesis as they give access to key intermediates in many reactions such as Cannizzaro and Meerwein-Ponndorf-Verley reactions. They are also widely employed in the reduction of the carbon atom from oxidation states +IV (CO_2) to -IV (CH_4). While reduction reactions have been historically achieved by the use of organometallic reagents, the last decades have witnessed the emergence of fine-tuned metal free hydride donors allowing smooth reduction and sometimes increase the functional tolerance. In that context, Lewis base-borane complexes have been found to be good candidates to take up this challenge as their reactivity can be modulated by modifying the nature of the Lewis base.

This chapter is dedicated to the study of phosphine borane complexes (PBs) as reductants in ionic reduction of electrophiles. In a first place, a brief overview of reduction reactions allowed us to estimate the potential of PBs in reduction reactions in terms of hydricity of the B-H bond, functional tolerance of substrates and selectivity of the addition. By means of kinetics, the hydricity of PBs have been measured and the nucleophilicity parameters of PBs have been compared with those of their analogues amine and carbene borane. This allowed us to build a predictive scale of the reduction of electrophiles with PBs.

1. Hydride transfers in organic synthesis
    1.1. Main organic hydride donors in organic synthesis
        1.1.1. The biological system NADP/NADP(H)

Before screening the use of transition metal free hydride donors in synthesis, it is important to remind that reduction steps take place in the core of the cells. A nice example of this phenomenon is the enzymatic complexes NADPH oxidase.[1] This enzyme is involved in several biological activities and is mainly responsible for fighting against the Reactive Oxygen species (ROS) which are highly toxic for living. They correspond to oxygen centred radicals such as $O_2^{\cdot -}, HOO^{\cdot}$ or $HO^{\cdot}$. Under acidic conditions, superoxide radical anions can undergo a dismutation reaction to yield hydrogen peroxide (H_2O_2) which forms hypochlorous acid under another enzymatic reaction with myeloperoxidase enzyme (*Figure 3.1*).

[1] Christine Deffert, Bernard Lardy, Francoise Morel. Rôles des NADPH oxydases lors de pathologies humaines à l'aide de modèles murins transgéniques. Biologie cellulaire. Université de Grenoble, **2009**. HAL Id: tel-00862905

Figure 3.1 Enzyme-catalysed neutralization of ROS through the action of NADPH/NADP+ enzymes. NOX is an isoform of NADPH oxidase, MOP: myeloperoxidase.

From a chemical point of view, $NADP^+$ (Nicotinamide adenine dinucleotide phosphate) corresponds to the oxidized form of NADPH and both provide the reducing equivalents for biosynthetic reactions in living cells. In the structures of these enzymatic complexes, it can be noticed that $NADP^+$ results from a hydride donation from the pyridinyl ring of NADPH to P47. This hydride transfer is the key step of the regulation of ROS in the body.

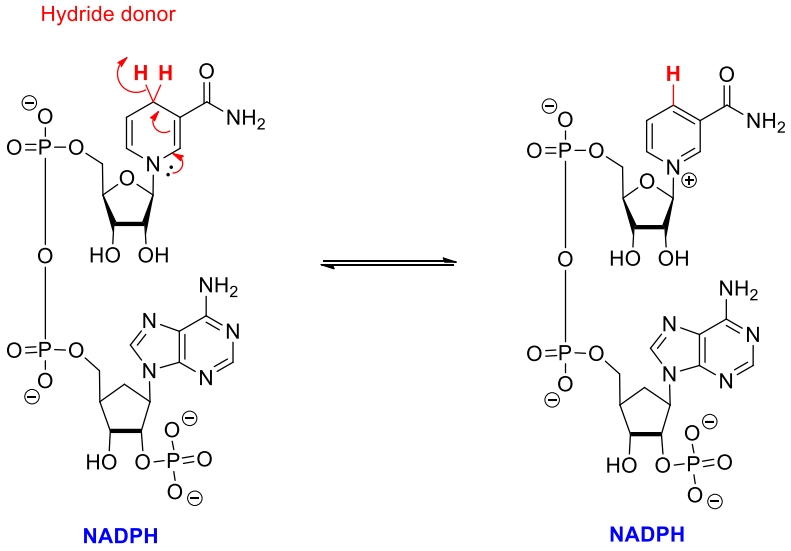

Scheme 3.1 Structures of NADPH and $NADP^+$.

NADPH/NADP have recently been used by Trost et al. in the synthesis of a diol fragment, involved in the total synthesis of (-)-Lasonolide A (*Scheme 3.2*).[2] Indeed, in the presence of NADP and isopropanol, the β-ketoester **1** was converted into the β-hydroxyester **2.** The diastereoselectivity was significantly enhanced by the use of CDX-O24, a chiral enzyme, allowing the formation of the *syn* diastereoisomer.

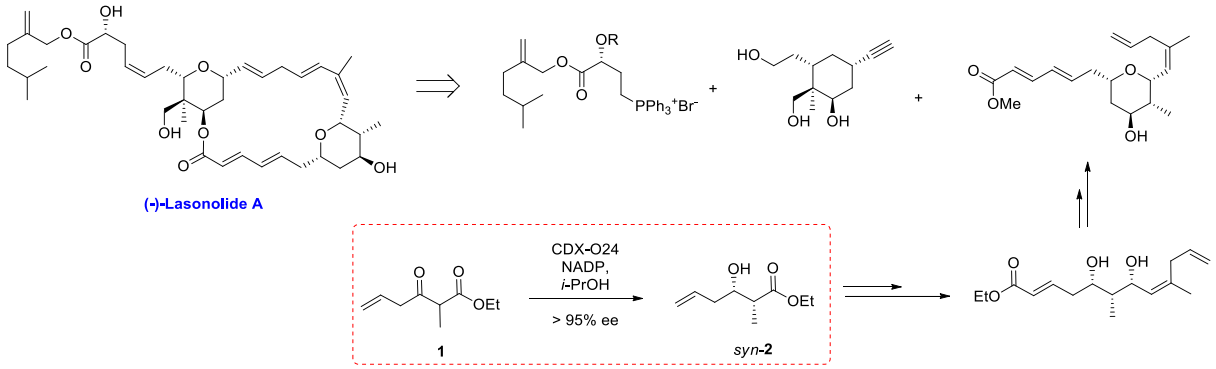

Scheme 3.2 Utilization of NADP in a diastereoselective reduction step involved in the total synthesis of (-)-Lasonolide A

1.1.2 Boron and aluminium based hydride donors

Organic reduction of unsaturated compounds has long been performed by using boron and aluminium hydrides.

Among the strongest boron or aluminium based hydride donors, $LiAlH_4$ allows the complete reduction of a plethora of functional groups such as acyl chlorides, amides, esters, ketones, aldehydes, imines and activated C-X bonds (X = halogen, OTs, etc..). Similarly, AlH_3 is also used as reducing agent and is even stronger than $LiAlH_4$. However, this reagent is very sensitive to water as the formation of Al_2O_3 is very exothermic. Based on these drawbacks and seeking for more chemoselectivity and more easily handled hydride donors, boron derivatives have been used as they have HOMO orbitals lower in energy than aluminium based hydride donors. This difference makes BH_3 less reactive than AlH_3; and $NaBH_4$ less reactive than $NaAlH_4$. Therefore, $NaBH_4$ in only able to reduce imines, ketones and aldehydes in most cases. In order to decrease further the HOMO of the hydride, electron withdrawing substituents, such as cyano group, can be introduced on the boron atom center. In this approach, the electron density is delocalized on the cyano group, decreasing the HOMO of the hydride and thus it's hydricity. Consequently, $NaBH_3CN$ can exclusively be used to reduce imines because the energy of its LUMO is lower than that of ketones.

[2] Stivala, C. E.; Frandrick, D. R.; Hull, K. L; Huang, A.; Poock, C.; Kalkofen, R.; Trost, B. M. *J. Am. Chem. Soc.* **2016**, *138*, 11690

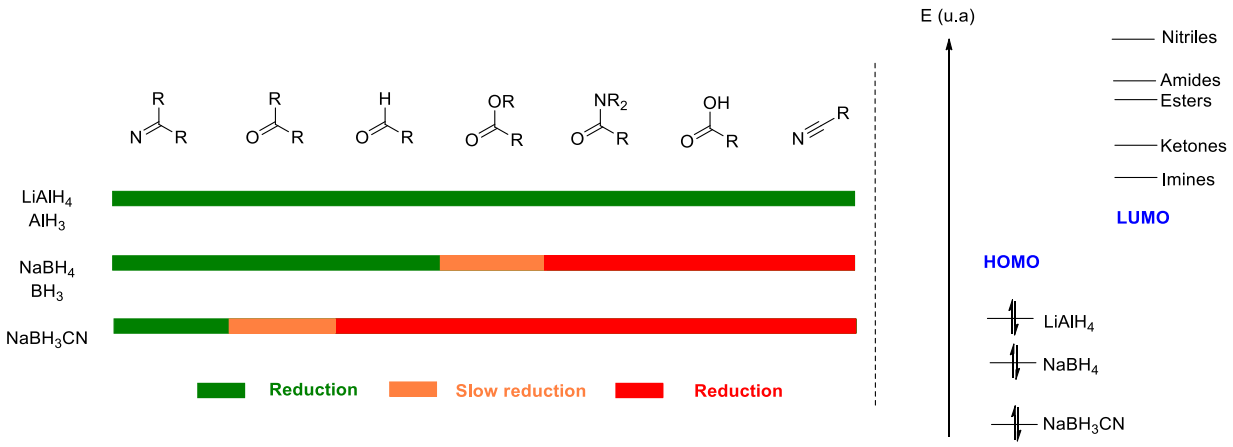

Scheme 3.3 Representation of the carbonyl reductions using Al and B-based hydride donors. Molecular orbitals drawing of the HOMO and LUMO (qualitative).

As depicted in the *Scheme 3.3*, it is complex to control the reduction steps of carbon atoms present at oxidation states from (+III) to (-I). Indeed, in most cases, the reduction product is more reactive than the starting molecule.

The chemoselectivity is also a critical drawback for the use of lithium and aluminium hydrides. For instance, there are very few reagents capable to reduce ketones and not aldehydes or imines and not sulfonic esters. In some cases, carbonyl groups can be reduced with a good chemoselectivity as in the case of carboxylic acids with BH_3 or Weinred amides with DIBAL. In the case of activated C-X bonds, they are usually reduced under various conditions such as $LiAlH_4$, $NaBH_4$ or Li/naphthalene.

A last problem with the use of the above-mentioned hydride donors is the regioselectivity of the reduction. Indeed, the reduction of α,β-unsaturated compounds with $LiAlH_4$ or $NaBH_4$ leads to the reduction of both the C=C and C=X doubles bonds. To overcome this problem, Luche et al. have developed reaction conditions requiring the use of cerium salts, able to enhance the electrophilicity of the carbonyl group yielding the allylic alcohol with high regioselectivity.[3]

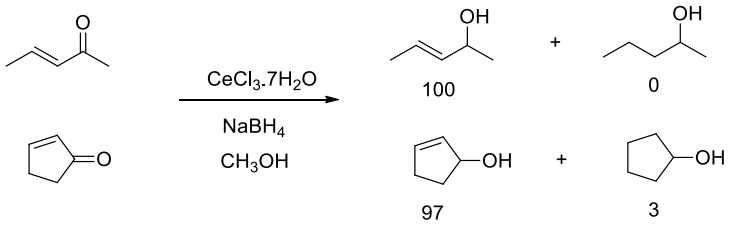

Scheme 3.4 Reduction of α,β-unsaturated carbonyl compounds with Luche conditions.

[3] Luche, J.-L. *J. Am. Chem. Soc.* **1978**, *100*, 2226.

The main transition-metal free hydride donors can reduce a broad variety of C=X and C-X bonds. However, they present several disadvantages such as chemo and/or regioselectivity issues, justifying the need to develop a new range of ionic hydride donors.

1.1.3 Hantzsch esters as hydride donors

Another class of hydride donors have been developed by Arthur Hantzsch in 1882 and are known as Hantzsch esters.[4]

These reagents which belong to the family of Di-HydroPyridines (DHP) exhibit important pharmacological properties such as antihypertensive, antibiotic, anti-inflammatory, and antifungal activity.[5] From a structural point of view, 5 forms of DHP can exist (*Scheme 3.5*). However, only the A and B forms are expected to be stable as they contain five conjugated sp^2 carbon atoms while only 4 in the case of C, D and E.

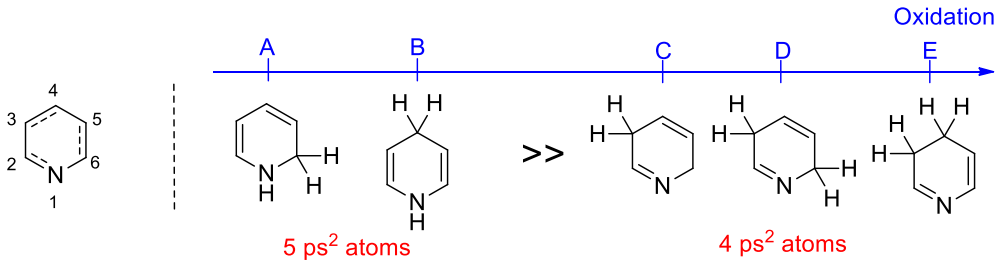

Scheme 3.5 The five forms of DHP and their relative stability toward oxidation.

In order to increase their hydricity, DHP have been substituted in the 3,5 positions by π-acceptor substituents such as esters, amides, nitrile or nitro groups, extending the conjugated system and thus the resonance. In addition, the substitution of the nitrogen atom has been found to destabilize the molecule. Based on these structural effects, a panel of DHP have been synthesized. The mostly used Hantzsch ester **3**, as well as DHP **4**,**5** have been drawn in the *Scheme 3.6*.[6]

[4] Hantzsch, A. *Justus Liebigs Ann. Chemie* **1882,** *215,* 1.
[5] a) Wang, A. L.; Iadecola, C.; Wang, G. *Journal of Geriatric Cardiology*, **2017**, *14*, 67. b) Marchalin, S.; Svorc, L.; Olsovska, D.; Panakova, A.; Vihonska, Z.; Kovaryova, K.; Olejnikova, P. *Sci Pharm*. **2014**, *82*, 221. c) Adhikari, A. V.; Shabaraya, R.; Kumar, S.; Ulloora, S. *Med. Chem. Res*, **2013**, *22*, 1549, d) Node, K.; Inoue, T.; Komoda, H.*Clin. Exp. Hypertension*, **2010**, *32*, 121, e) Abu-Melha, H. *Spectrochim. Acta, Part A: Mol. Biomol. Spectrosc*. **2013**, *113*, 115.
[6] a) Meyers, A. I. Stout, D. M. *Chem. Rev.* **1982**, *82*, 223 b) Kuthan, J.; Kurfurst, A. *Ind. Eng. Chem. Prod. Res. Dev.* **1982**, *21*, 191.

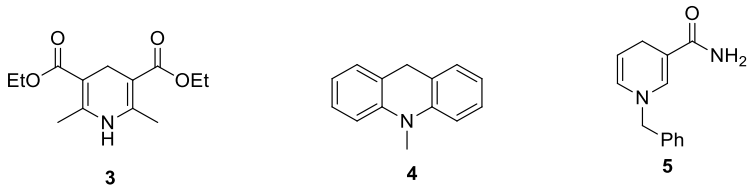

Scheme 3.6 Mainly used Hantzsch ester and DHP as hydride donors.

From a synthetic point of view, Hantzsch esters are used in organic synthesis as soft hydride donors (according to HSAB theory) to perform the reduction of functional groups. Due to this electronic property, the reduction proceeds under orbital control making the reduction selective for α,β-unsaturated compounds such as enone **6a**, enamine **6b,** nitroalkene **6c** or iminium salt **6d** to quote a few, with good functional tolerance (*Scheme 3.7*).[7]

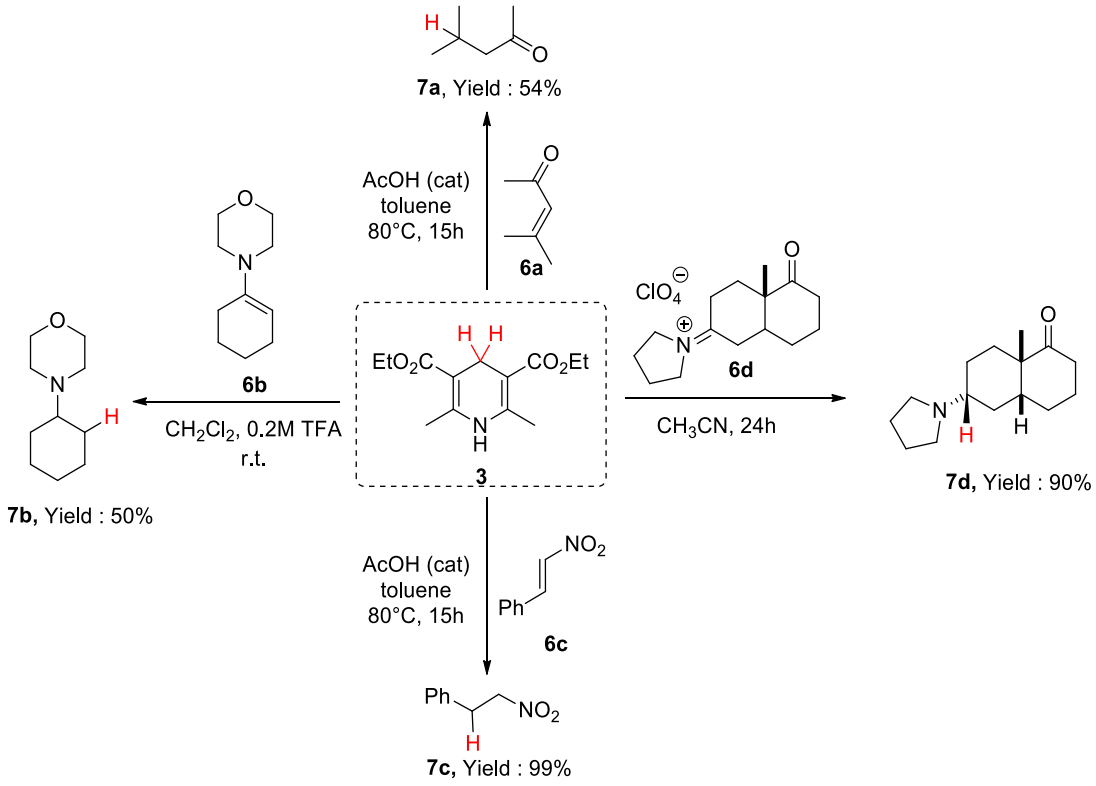

*Scheme 3.7 Selected examples of the reduction potential of α,β-unsaturated compounds, enamine or iminium salts **6a-d** with Hantzsch ester **3**.*

[7] a) Inoue, Y.; Imaizumi, S.; Itoh, H.; Shinya, T.; Hashimoto, H.; Miyano, S. *Bull. Chem. Soc. Jpn.* **1988**, *61*, 3020. b) Pandit, U. K.; Gase, R. A.; Mas Cabré, F. R.; De Nie-Sarink, M. J. *J. Chem. Soc. Chem. Commun.* **1975**, 211. c) Singh, S.; Sharma, V. K.; Gill, S.; Sahota, R. I. K. *J. Chem. Soc. Perkin Trans. 1* **1985**, 437.

1.1.4 Silicon based hydride donors

Silicon-based hydride donors are soft reductive agents compared to their boron and aluminium-based analogues. In addition to their abilities to serve as ionic hydride donors, their reaction by-products are safer and more easily handled than those of other reagents.

Organosilane have relatively closed structures to hydrocarbon in that they are not water and oxygen sensitive. However, precautions must be taken with low molecular weight silanes which are pyrophoric (CH_3SiH_3, Cl_2SiH_2 or $EtSiH_3$). Considering the electronegativity of silicon (χ = 1.8)[8] and hydrogen atoms (χ = 2.1)[8], the chemical bond is weakly metallic. This provides a weaker hydridic reducing character compared to DHP or boron and aluminium based hydride donors. The comparison of the bond strengths of several silanes provide a scale to classify their ability to release their hydride (*Table 3.1*).

Table 3.1 Bond strengths of selected organosilane.[9]

Silane	F_3SiH	Et_3SiH	SiH_4	Cl_3SiH	$PhMeSiH_2$	$PhSiH_3$	$(MeS)_3SiH$	TTMS
Bond strength (kJ/mol)	419	398	384	382	382	377	366	351

Due to their low hydricity, organosilanes present the tremendous advantage to be compatible with highly acidic conditions. This is in the core of the reduction strategy of several functional groups such as alcohols, ketones, esters or polarized C-X bonds, where X depict a leaving group. For instance, the reduction of the benzyl halide **8** or the ketone **10** have been performed under the above-mentioned conditions (*Scheme 3.8*).[10]

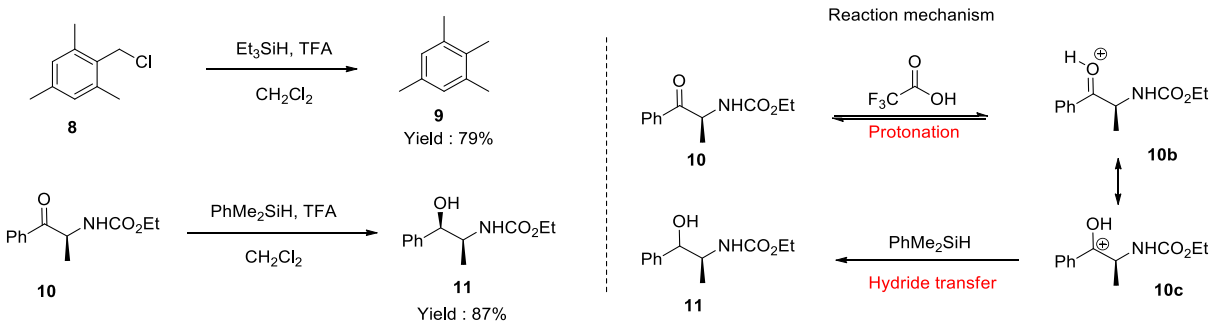

*Scheme 3.8 Reduction of benzyl halide **8** and keto-amine **10** with silanes under acidic conditions.*

[8] Electronegativity values are given according Pauling scale.
[9] a) Walsh, R. *Acc. Chem. Res.*, **1981**, *14*, 246. b) Chatgilialoglu, C. *Chem. Rev.* **1995**, *95*, 1229. c) Ding, L.; Marshall, P. *J. Am. Chem. Soc.* **1992**, *114*, 5754.
[10] a) Barclay, L. R. C.; Sonawane, H. R.; MacDonald, M. C. *Can. J. Chem.* **1972**, *50*, 281. b) Fujita, M.; Hiyama, T. *J. Org. Chem.* **1988**, *53*, 5415.

In the proposed mechanism, the highly acidic conditions allow the formation of a short life-time carbocation **10c** which is then rapidly reduced by the hydride of the organosilane to yield **11**. This reduction method is frequently used in total synthesis as for example the synthesis of the (+)-estrone (*Scheme 3.9*).[11]

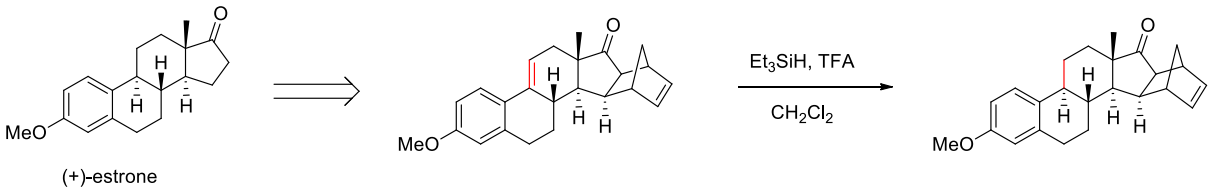

Scheme 3.9 Silane reduction step of C=C double bonds using silane in acidic conditions.

While tetravalent silanes present a weak reactivity and require the use of an external activator, the hydricity of silanes can be strongly increased under their hypervalent form.[12]

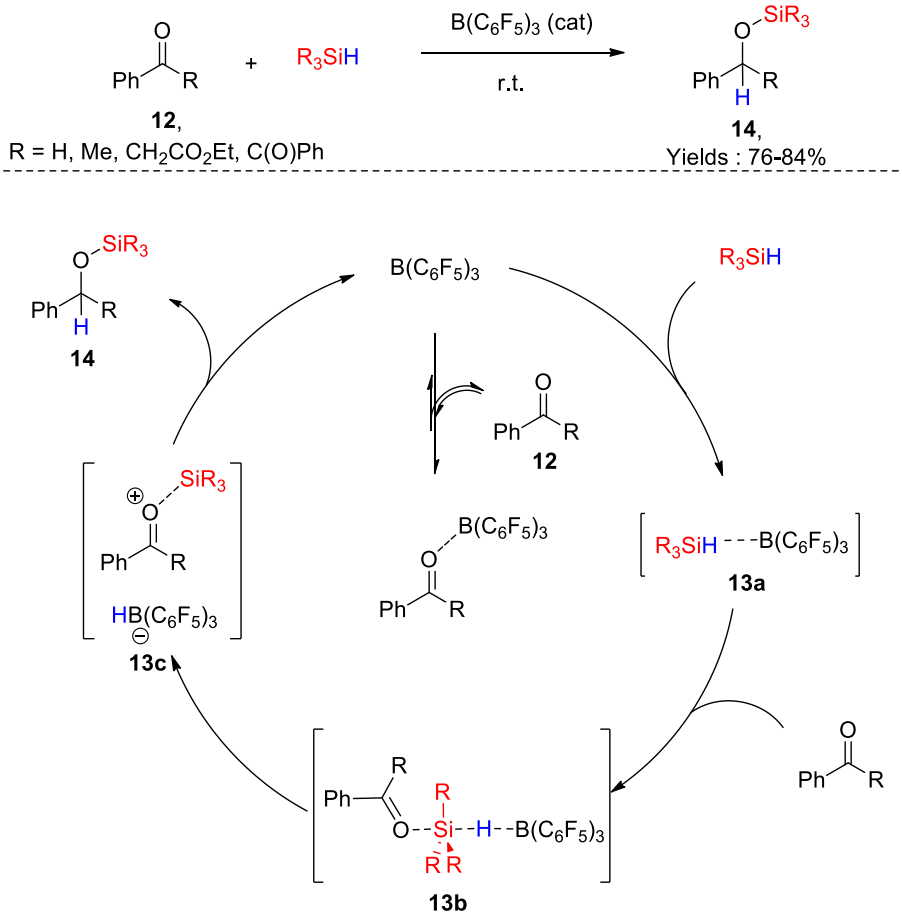

Scheme 3.10 Reduction of ketones using silane and $B(C_6F_5)_3$ and proposed reaction mechanism.

[11] Takano, S.; Moriya, M.; Ogasawara, K. *Tetrahedron Lett.* **1992**, *33*, 1909.
[12] For a comprehensive review of hypervalent silicon, see Rendler, S., Oestreich, M., *Synthesis* **2005**, *11*, 1727.

Based on this strategy, Oestriech et al. used $B(C_6F_5)_3$ and a silane to perfom the reduction of a wide variety of carbonyl and carboxyl groups **12**.[13] In that case, the Lewis acid strongly interact with the hydride of R_3SiH **13a** to generate a limit form in which the silicon atom behaves as a Lewis acid silylium ion (limit model) as shown in *Scheme 3.10*. The carbonyl group will then coordinate to the silane, yielding the pentavalent silicon compound **13b**. At this stage, the hydride transfer to the carbonyl takes place to release **14** either in an intramolecular manner or via the formation on the ion pair **13c**. Hence, imine, ketones, aldehydes or esters can be reduced employing this strategy.

1.2 Borane complexes as hydride donors

As mentioned in chapter 1, the complexation of a Lewis base with BH_3 confer new properties to the resulting Lewis-base borane adduct such as an hydridic character of the hydrogen atoms. Phosphines, carbenes and amines are able to form such complexes and have thus a potential use in reduction reactions.

1.2.1 Carbene boranes as hydride donors

N-Heterocyclic carbenes (NHC)[14] have a divalent six-electron carbon, stabilized by the lone pairs on the adjacent nitrogen atoms. They are considered as essential Lewis bases due to their strong σ-donors and weak π-acceptors properties. Besides, they are important compounds in transition metal chemistry,[15] in organocatalysis[16] and as stabilizing ligands of unstable species such as B=B bonds.[17]

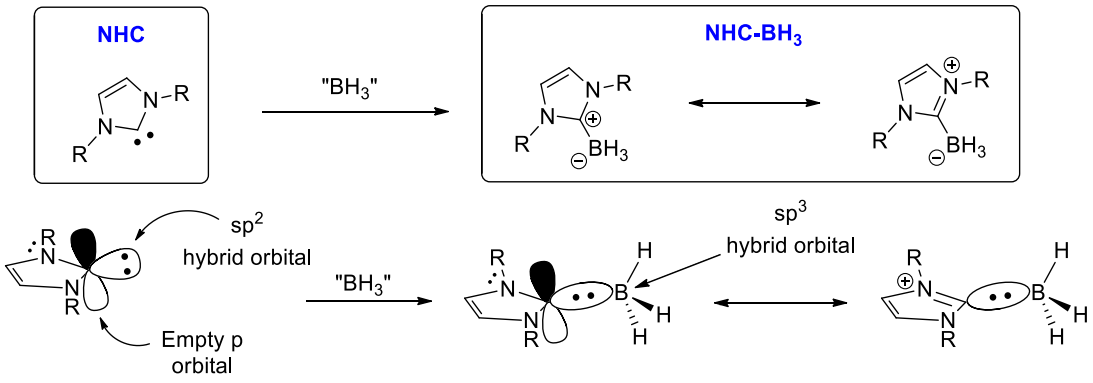

Scheme 3.11 Structure of NHC and NHC-BH3 and drawing of the resonance structures.

[13] Oestreich, M. Hermeke, J. Mohr, J. *Chem. Soc. Rev.* **2015**, ***44***, 2202.
[14] a) Ofele, K. *J. Organomet. Chem.* **1968**, 42. b) Wanzlick, H. -W.; Schonherr, H. -J. *Angew. Chem. Int. Ed.* **1968**, *7*, 141
[15] a) Glorius, F. *Top. Organomet. Chem.* **2007**, *21*,1. b) Díez-González, G.; Marion, N.; Nolan, S. P. *Chem. Rev.* **2009**, *109*, 3612.
[16] a) Enders, D.; Niemeier, O.; Henseler, A. *Chem. Rev.* **2007**, *107,* 5606. b) Marion, N.; Díez-González, S.; Nolan, S. P. *Angew. Chem. Int. Ed.* **2007**, *46*, 2988.
[17] Wang, Y.; Quillian, B.; Wei, P.; Wannere, C. S.; Xie, Y.; King, R. B.; Schaefer, H. F.; Schleyer, P. V. R.; Robinson, G. H. *J. Am. Chem. Soc.* **2007**, *129*, 12412.

NHC-trihydridoborate, resulting from the coordination of NHC to BH_3, are solids that are easy to make and handle (*Scheme 3.11*).[18] This stability is due to the eight electrons, tetravalent boron atom. Owing to the strong σ-donors character of NHC, the B-H bonds of NHC-boranes are known to be good hydride donors as well as hydrogen donors in radical reactions.[19]

Since the last centuries, chemists have designed a plethora of chemical structures for carbene-boranes in order to i) increase their thermal and chemical stability and ii) enhance their σ-donor character (*Scheme 3.12*).

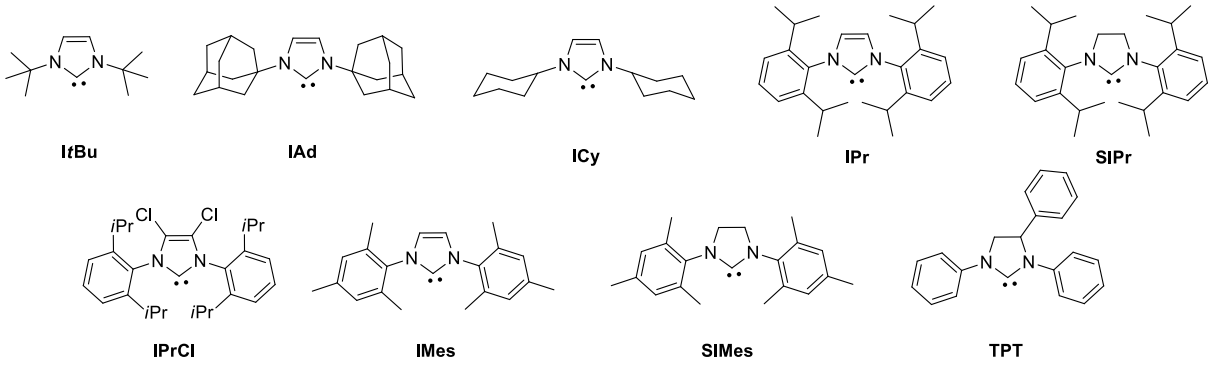

Scheme 3.12 Chemical structures of commonly used NHC in organic synthesis.

However, the effect of the σ-donor character is directly related to the hydricity of NHC-BH_3 making the comparison of the electronics of NHC a relevant parameter to anticipate the hydricity. As a consequence, by measuring the carbonyl stretching frequencies of a series of NHC, it is possible to investigate the effect of the chemical structure of NHC to the hydricity of the corresponding NHC-BH_3. In this context, Nolan et al. reported the carbonyl stretching frequencies of a series of [NHC-Ir$(CO)_2$Cl].[20]

Table 3.2 Carbonyl stretching frequencies of [NHC-Ir$(CO)_2$Cl] compounds. NHC refers to the structures presented in the Scheme 3.12.

NHC	TPT	IPrCl	SIPr	SIMEs	IPr	IMes	I*t*Bu	ICy	IAd
ν_{CO} **(cm^{-1})**	2072	2071	2068	2068	2067	2066	2065	2065	2063

In one hand, they have shown that NHCs are much more strongly donating ligands than the strongest donating tertiary phosphine. On the other hand, they demonstrated that, while there

[18] For a review, see Curran, D. P.; Solovyev, A.; Makhlouf Brahmi, M.; Fensterbank, L.; Malacria, M.; Lacôte, E. *Angew. Chem., Int. Ed.* **2011**, *50*, 10294.
[19] Ueng, S. H.; Brahmi, M. M.; Derat, E.; Fensterbank, L.; Lacôte, E.; Malacria, M.; Curran, D. P. *J. Am. Chem. Soc.* **2008**, *130*, 10082.
[20] Kelly III, R. a.; Clavier, H.; Giudice, S.; Scott, N. M.; Stevens, E. D.; Bordner, J.; Samardjiev, I.; Hoff, C. D.; Cavallo, L.; Nolan, S. P. *Organometallics* **2008**, *27*, 202.

is little difference between NHC themselves, modifications on the imidazole ring seems to have a crucial effect on the electronics.

The reactivity with diverse array of electrophiles such as NBS, NIS, Br_2, I_2 or alkyl halides has also been screened by Fensterbank, Malacria, Lacôte, Curran et al.[22] In most cases, NHC-BH_3 have been able to either promote the hydride abstraction or the nucleophilic substitution yielding **15**-**17** in excellent yields (*Scheme 3.13*).

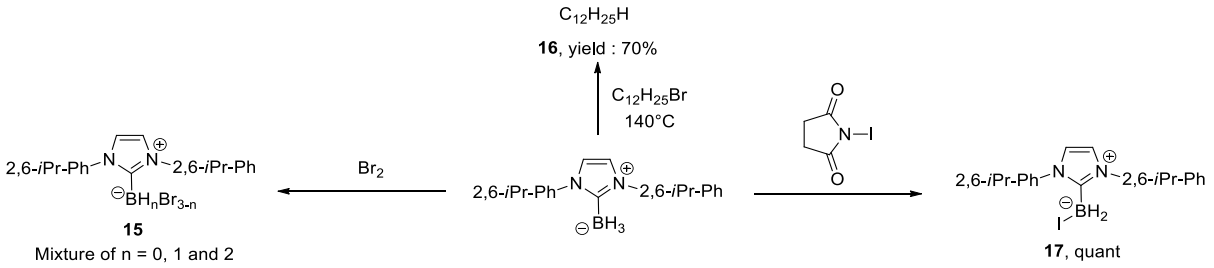

Scheme 3.13 Hydride abstraction of NHC-BH_3 by several electrophiles.

A last example of the use of NHC-BH_3 in organic synthesis is the reduction of carbonyl functions through Lewis acidic activation as in the case of the chemo- and enantioselective reduction of acetophenone **18** with the chiral hydridoborate **19** to yield the alcohol **20** with 80% yield and 84% ee (*Scheme 3.14*).[21] As reported by Fensterbank, Malacria, Lacôte, Curran et al., aryl halides are not reduced directly by NHC-boranes, but such reductions can be promoted by employing palladium catalysts.[22] Another nice illustration is the quantitative reduction of the iodine of the aryliodide **21** using the trihydridoborate **22** to yield **23** with a perfect chemoselectivity.

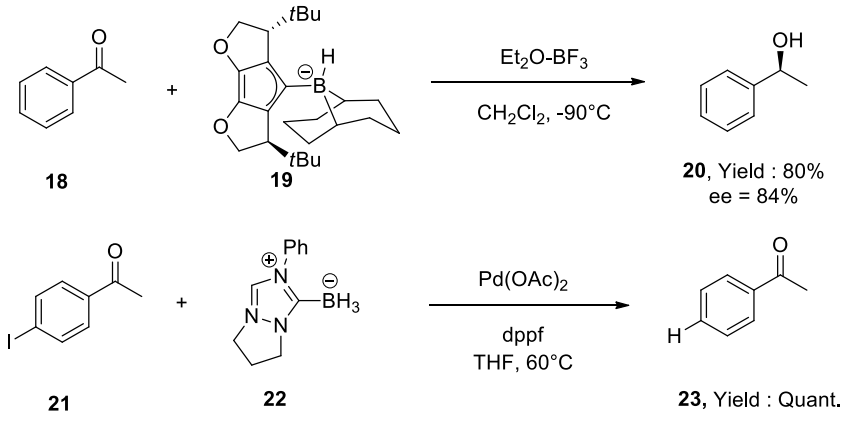

Scheme 3.14 Chiral reduction of ketones by IPr assisted by $BF_3.OEt_2$ and reduction of aryliodine bond.

[21] Lindsay, D. M.; McArthur, D. *Chem. Commun.* **2010**, *46*, 2474.
[22] Monot, J.; Makhlouf Brahmi, M.; Ueng, S.-H.; Robert, C.; Desage-El Murr, M.; Curran, D. P.; Malacria, M.; Fensterbank, L.; Lacôte, E. *Org. Lett.* **2009**, *11*, 4914.

1.2.3 Amine and phosphine borane as hydride donors

Like carbenes, amines and phosphines boranes are convenient σ-donor ligands capable to form Lewis-acid Lewis-base adducts with BH_3. However, unlike carbene boranes complexes, phosphine- and amine- boranes have scarcely been used in organic synthesis. Indeed, the corresponding adducts are thermically less stable than NHC-boranes. In addition, as highlighted by the *Table 3.3* gathering carbonyl stretching frequencies of several ligands, phosphines and amines are weaker σ-donors than carbenes.[23]

*Table 3.3 Carbonyl stretching frequencies of $[LMo(CO)_6]$ in different media. **See Scheme 3.12 ** Determined in Hexane.*

Ligand	$P(OMe)_3$	PPh_3	NMe_3	PMe_3	PCy_3	IPr*	CO
Media	Hexane	Hexane	KBr	C_5H_{10}	KBr	KBr	KBr
ν_{CO}	2082	2075	2074	2071	2065	2061	1982
(cm^{-1})			2072**		2064**		

From a synthetic point of view, phosphine and amine-borane complexes have been shown to react with strong Bronsted acids such as bistriflimidic or tetrafluoroboric acids.[24] However, except under very specific conditions,[25] phosphine-boranes have not found use as reducing reagents in organic synthesis. One of these scarce examples is the reduction of the conjugated C=C double bond of the chiral N-vinyl sulfoximine **24** using Ph_2PH-BH_3 at 80°C to form **25** in 84% yield (*Scheme 3.15*).[26]

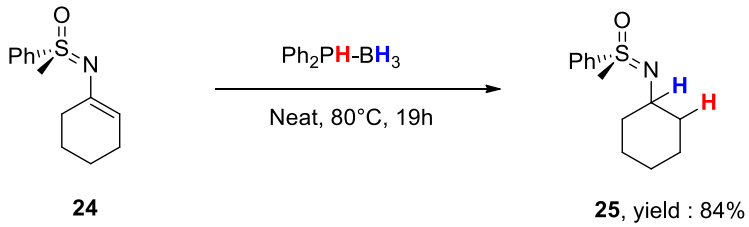

24 **25**, yield : 84%

Scheme 3.15 Reduction of a chiral N-Vinylsulfoximines with Ph_2PH-BH_3.

There are substantial works concerning the use of amine-borane adducts in reduction reactions. For instance, trityl tetrafluoroborate salt is reduced to tripheylmethane **26** by either pyridine or trimethylamine-borane complexes in acetonitrile at -55°C in 52 and 96% yield

[23] a) Darensbourg, D. J.; Brown, T. L. *Inorg. Chem.* **1968**, *7*, 959 b) Koelle, U. *J. Organomet. Chem.* **1977**, *133*, 53 c) Davies, M. S.; Pierens, R. K.; Aroney, M. J. *J. Organomet. Chem.* **1993**, *458*, 141 d) Gao, Y.-C.; Shi, Q.-Z.; Kershner, D. L.; Basolo, F. *Inorg. Chem.* **1988**, *27*, 188.
[24] De Vries, T. S.; Prokofjevs, A.; Vedejs, E. *Chem. Rev.* **2012**, *112*, 4246.
[25] Schlieve, C. R.; Tam, A.; Nilsson, B. L.; Lieven, C. J.; Raines, R. T.; Levin, L. A. *Exp. Eye Res.* **2006**, *83*, 1252
[26] Hetzer, R. H.; Gais, H.-J.; Raabe, G. *Synthesis* **2008,** 1126.

respectively.[27] Including transition metal catalysis, phenylpropargyl alcohol **27a**, quinoleine **27b** , halide **27c,** triflate ester **27d** and ester **27e** have been reduced using *t*BuNH$_2$-BH$_3$ and in the presence of 10% Pd-C/methanol at r.t. to give the desired products in yields ranging from 82 to 97% (*Scheme 3.16*).[28,29]

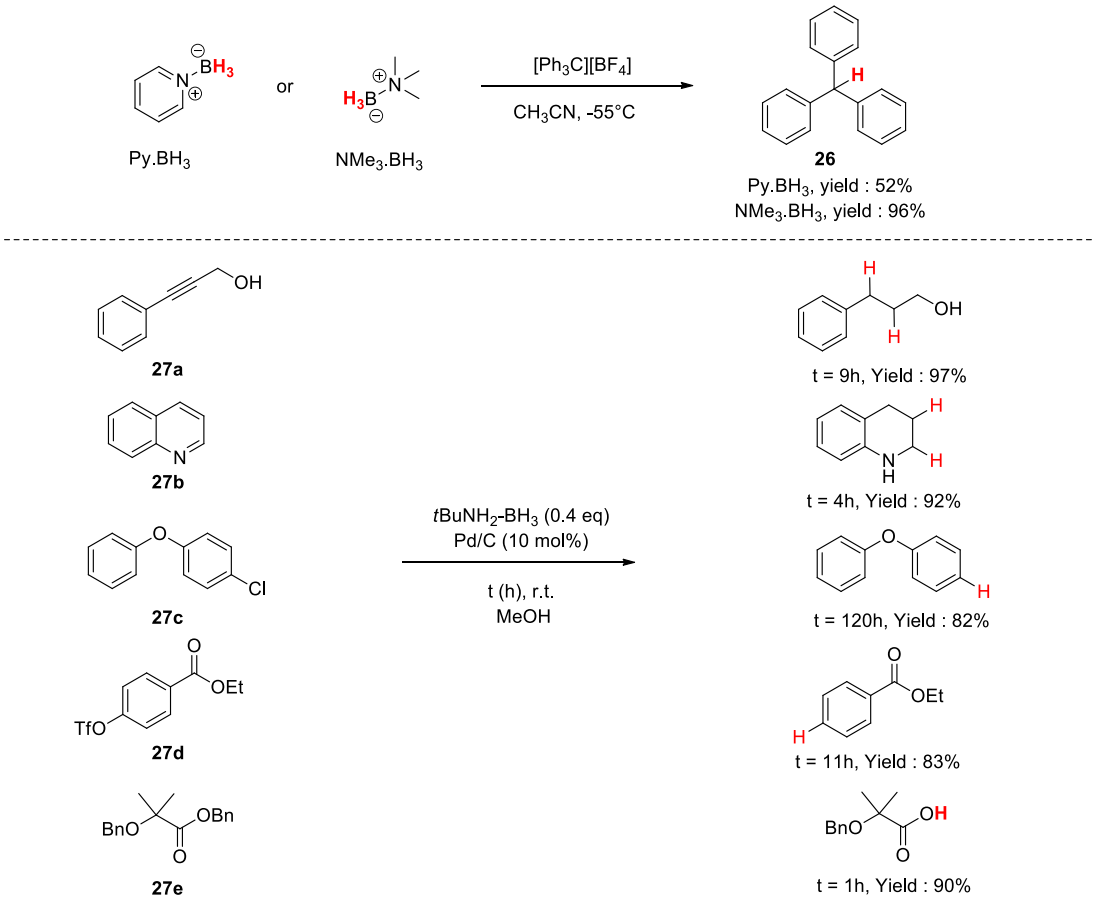

*Scheme 3.16 (top) Oxidation of amine borane with trityl tetrafluoroborate salt and (bottom) Palladium catalysed reduction of functional groups using t-*BuNH$_2$-BH$_3$.

The reducing ability of amine-borane complexes was found to be highly dependent upon the amine moiety. In the case of aliphatic-substituted amine-boranes, reducing ability generally decreased with increasing alkyl substitution: $H_3N{\cdot}BH_3 > RNH_2 \cdot BH_3 > R_2NH{\cdot}BH_3 > R_3N{\cdot}BH_3$.[30]

At present, the main interest of these compounds remains in the central global socioeconomic challenges of the next decades: the sustainable supply of energy and its appropriate storage.

[27] Benjamin, L. E.; Carvalho, D. A.; Stafiej, S. F.; Takacs, E. A. *Inorg. Chem.* **1970**, *9*, 1844.
[28] a) Couturier, M.; Andresen, B. M.; Tucker, J. L.; Dube ´, P.; Brenek, S. J.; Negri, J. T. *Tetrahedron Lett.* **2001**, *42*, 2763. b) Couturier, M.; Tucker, J. L.; Andresen, B. M.; Dubé, P.; Brenek, S. J.; Negri, J. T. *Tetrahedron Lett.* **2001**, *42*, 2285. c) Couturier, M.; Tucker, J. L.; Andresen, B. M.; Dubé, P.; Negri, J. T. *Org. Lett.* **2001**, *3*, 465.
[29] For an extensive review, see Staubitz, A.; Robertson, A. P. M.; Sloan, M. E.; Manners, I. *Chem. Rev.* **2010**, *110*, 4023.
[30] Hutchins, R. O.; Learn, K.; Nazer, B.; Pytlewski, D.; Pelter, A. *Org. Prep. Proced. Int.* **1984**, *16*, 335

Indeed, $H_3B{\cdot}NH_3$ is an air-stable solid containing a high weight percentage of hydrogen (19.6 wt%), and thus has been explored extensively as a potential candidate for chemical hydrogen storage media. In the case of H_3P-BH_3, the potential in the hydrogen storage is obviously less important but is still attractive (12.6 wt%). As a consequence, numerous transition metal catalysed dehydrocoupling of amine-boranes and, to a lesser extent, phosphine-boranes have been reported recently and continue to stimulate the scientists involved in this field.[31]

2. Hydricity of phosphine boranes and comparison with other hydride donors

2.1 Toward a unified scale to compare the hydricity of hydride donors?

Except the direct comparison of the scope of substrates reduced by all hydride donors, it doesn't exist a unified scale to classify their hydricity. Since the reduction reactions are among the main reaction types in organic synthesis, these data would represent a great advantage to better understand the problems of chemoselectivity and functional tolerance in complex molecules as PBs are smooth hydride donors.

Based on this context, Mayr used the previously mentioned nucleophilicity scale to quantify the hydricity of several hydride donors and thus predict the feasibility of the reduction of various electrophiles (*Scheme 3.17*).[32]

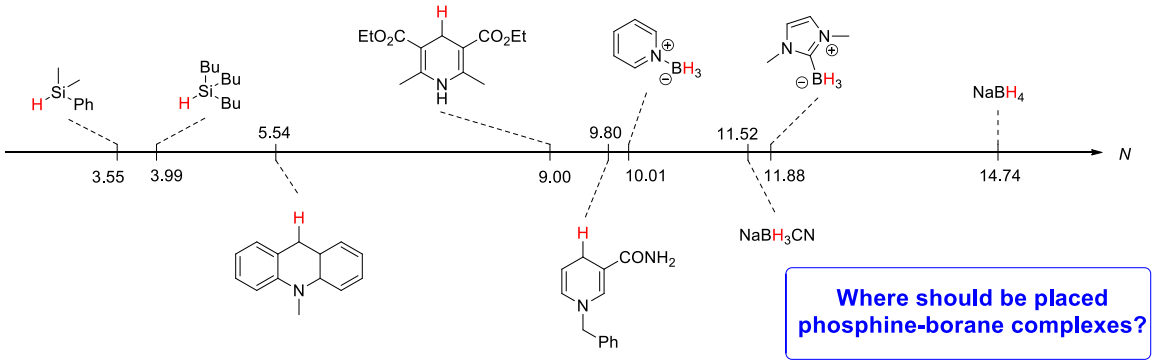

Scheme 3.17 Nucleophilicity scale of several hydride donors according to Mayr relationship.

In agreement with the strength of hydride donors found in the literature, $NaBH_4$ is the best hydride donor of this series. Its hydricity can be decreased by substituting H by CN. Then, from the stronger to the weaker hydride donor, we find carbene borane > pyridine borane ≈ Hantzsch esters > silanes. However, among smooth hydride donors, phosphine boranes complexes have never been investigated in term of hydricity. This lack is of great significance as it's still not clear in the literature if the electronic and steric nature of phosphine have a

[31] For some reviews, see a) Bhunya, S.; Malakar, T.; Ganguly, G.; Paul, A. *ACS Catal.* **2016**, *6*, 7907 b) Rossin, A.; Peruzzini, M. *Chem. Rev.* **2016,** *116*, 8848.
[32] Horn, M.; Schappele, L. H.; Lang-Wittkowski, G.; Mayr, H; Ofial, A. R. *Chem. Eur. J.* **2013**, *19*, 249.

significant impact on the strength of the hydride. As it could be expected that it behaves in the same way than amine-borane, Curran et al. have shown that they react differently (*Scheme 3.18*).[33]

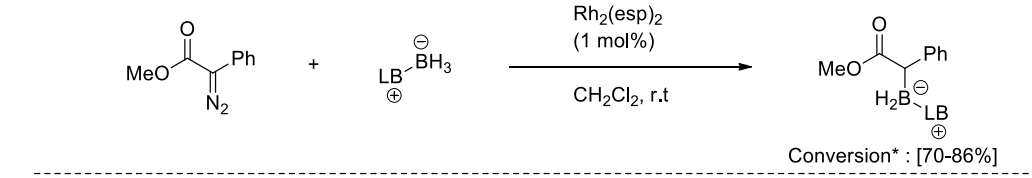

LB-BH$_3$	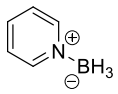	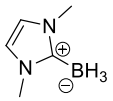		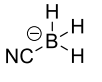 Bu$_4$N$^+$	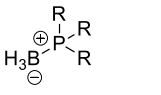 R = Ph, or R = Bu
$k_{relative}$ (L/mol/s)	2.5	1	0.33	0.18	0.06

*Scheme 3.18 Relative rate constants in the rhodium catalysed insertion reactions of LB-BH$_3$ in diazocompounds. *Conversions determined by ^{11}B NMR spectroscopy.*

Indeed, these authors studied the reactivity of a series of LB–BH$_3$ (LB=NHCs, pyridines, phosphines…) in Rh(II)-catalyzed B−H insertion reactions with methyl 2-phenyl-2-diazoacetate and showed that amine–boranes react with different rates according to the sigma donor character of the amine ligand. However, in the case of phosphine boranes, the authors showed that Ph$_3$P-BH$_3$ reacts at the same rate than Bu$_3$P-BH$_3$ while it is well known that PBu$_3$ ligand are more σ-donors than PPh$_3$.

With the aim to better understand the relationship between the structure of phosphines and the reactivity of the resulting phosphine-borane complexes in reduction reactions, we embarked on a kinetic study of these complexes using Mayr methodology, based on the equation 1.

$$\log k_{20°C} = s_N(N + E) \qquad (1)$$

2.2 Hydricity of phosphine borane complexes **29a-g**

2.2.1 Reactions between PBs **29a-g** and Benzhydrylium salts **28a-f**

In a first step, we needed to select suitable electrophiles to quantify the nucleophilicity of PBs. As in the case of sterically hindered phosphines, we planned to measure the second-order-rate constants of the reactions of PBs with reference electrophiles using the stopped flow spectrophotometry technique under pseudo-first order conditions. In this regard, we selected

[33] Allen, T. H.; Curran, D. P. *J. Org. Chem*. **2016**, *81*, 2094.

Benzhydryliums salts **28a-f** as reference electrophiles as they react with PBs with acceptable reaction rates ($10^{-2} < k < 10^{4}$).

*Table 3.4 Benzhydrylium salts **28a-f**, chemical structures, maximum wavelength absorbance in dichloromethane and related electrophilicity parameters.*

Benzhydrylium ion	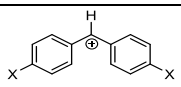	λ_{max} (nm)	E^{*}
28a	X = $NPh(CH_2CF_3)$	601	–3.14
28b	X = $NMe(CH_2CF_3)$	593	–3.85
28c	X = NPh_2	667	–4.72
28d	X = $N(CH_2CH_2)_2O$	610	–5.53
28e	X = N(Ph)(Me)	615	–5.89
28f	X = NMe_2	605	–7.02

*Taken from ref [34]

In a second step, we needed to select phosphines which would allow us to understand the relationship between their structure and the reactivity of their hydride in the corresponding PBs. For that purpose, we synthesized mono, bis and tri-alkylphosphine or arylphosphine as Lewis bases for **29a-d**. Secondary and primary phosphines in **29e-g** were also selected to understand the consequences of the class of phosphines (*Scheme 3.19*).

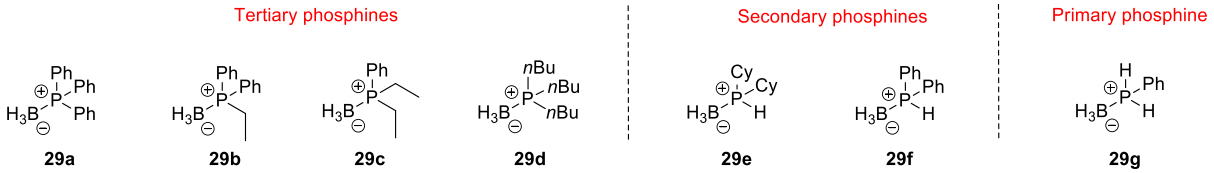

Scheme 3.19 Structures of phosphine boranes selected for the measurement of the hydricity

First, we studied the reactions of **29a** with benzhydrylium ions **28b-d** (*Table 3.4*) in acetonitrile at 20 °C. As depicted in the *Scheme 3.20*, treatment of one equivalent of electrophiles **28b-d** with **29a** in deuterated acetonitrile at 20 °C led to the quantitative formation of the diarylmethane **30a-c** as confirmed by ^{1}H NMR spectroscopy (*Figure 3.2*).

[34] Mayr, H.; Ofial, A. R. *Acc. Chem. Res.* **2016**, *49*, 952.

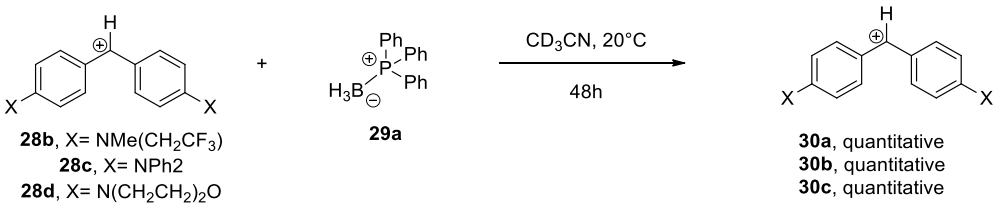

*Scheme 3.20 Reactions of benzhydrylium ions **28b-d** with triphenylphosphine–borane **29a** in CD_3CN at 20 °C.*

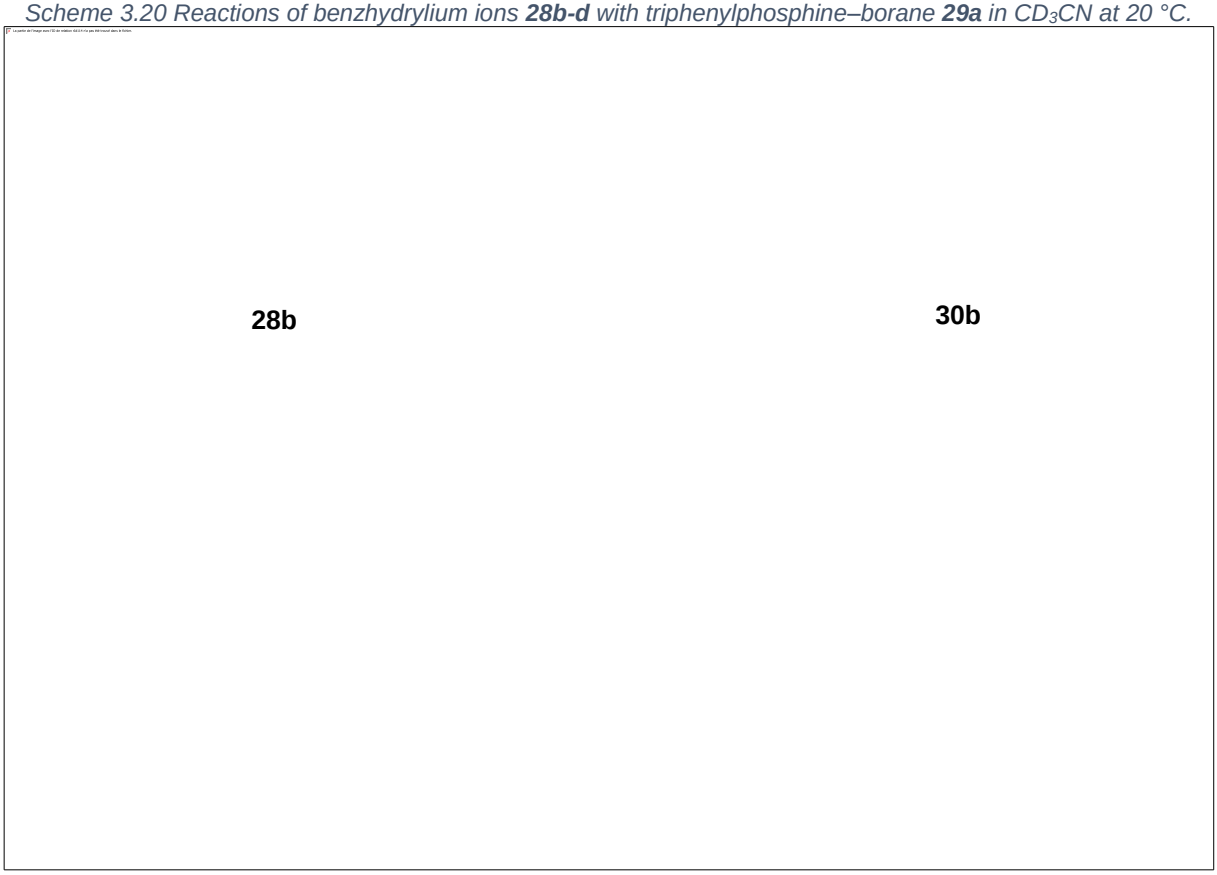

*Figure 3.2 ^1H NMR spectra of the stoichiometric reaction between **28b** and **29a** in CD_3CN at 20°C in 48h.*

2.2.2 Kinetic investigations

Kinetics of the reactions of **29a-g** and benzhydrylium salts **28a-f** in dichloromethane at 20°C were monitored spectrophotometrically at the maximum wavelengths of Ar_2CH^+ **28** (*Table 3.4*), by following the disappearance of the electrophile. To simplify the kinetics, **29a-g** were introduced in large excess (> 10 equivalents), which resulted in monoexponetioal decays of the UV-vis absorbances. The first order rate constant k_{obs} (s^{-1}) was derived from fitting of the exponential function $A(t) = A(0)\exp(-k_{obs}t)$ to the time-dependant absorbances A(t) of the electrophile (*Figure 3.3*). Sloped of the linear plots of k_{obs} against the concentrations of the excess nucleophile allowed the determination of the second-order rate constant k_2 for the studied reactions.

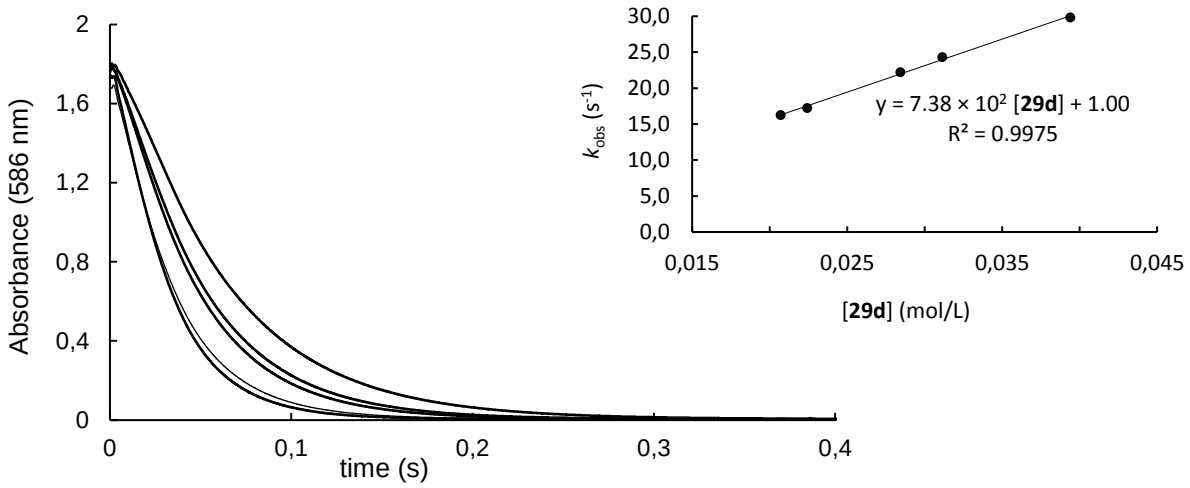

*Figure 3.3 Decay of the absorbance of **28b** (1.26 × 10^{-4} mol/L) at 586 nm during its reaction with **29d** (five concentrations: [2.07, 2.24, 2.84, 3.11, 3.94] × 10^{-2} mol/L) in CH_2Cl_2 at 20°C. Linear correlations of k_{obs} with increasing concentrations of **29d**.*

As shown in the *Figure 3.3*, all the reactions are quantitative showing that no reversible processes take place.

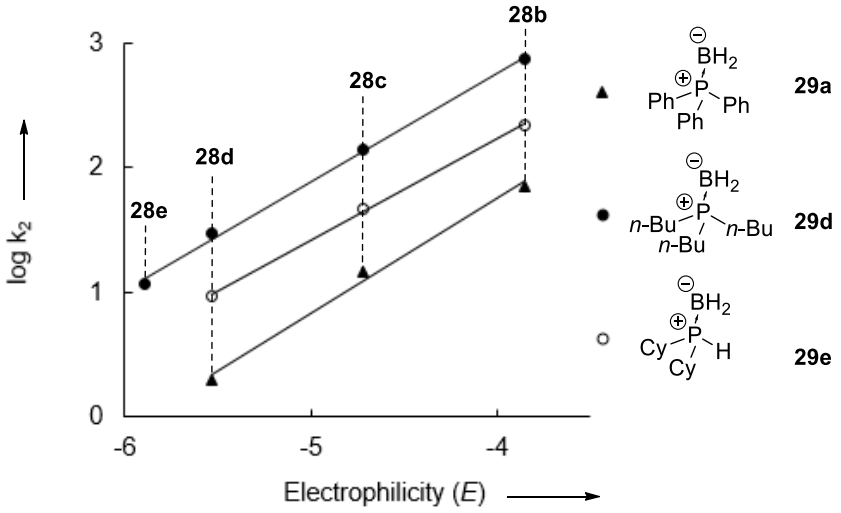

Figure 3.4 Plots of log(k_2) for the reactions of PBs **29a,d,e** with reference electrophile **28b-e** against the electrophilicity parameters *E*.

Then, based on the equation (1), plots of log(k_2) for the reactions of PBs with reference electrophiles against the corresponding electrophilicity parameters *E* are linear as depicted in the *Figure 3.4*. From the linearity of these correlations, one can deduce the nucleophilicity parameters *N* and s_N. The results are gathered in the *Table 3.5*.

*Table 3.5 Second order rate constants for the reactions of PBs **29a-g** with benzhydrylium cations **28a-g** in dichloromethane at 20°C, nucleophilicity (N) and specific sensitivity nucleophilicity parameters (s_N).*

R_3PBH_3	Ar_2CH^+	E(Ar_2CH+)	k_2 (L/mol/s)	s_N	*N*
PPh_3BH_3	**28b**	-3.85	70.8		
29a	**28c**	-4.72	14.8		
	28d	-5.53	2.01	0.92	5.91
$EtPPh_2BH_3$	**28b**	-3.85	732		
29b	**28c**	-4.72	192		
	28d	-5.53	34.5		
	28e	-5.89	14.8	0.83	7.36
Et_2PPhBH_3	**28b**	-3.85	159		
29c	**28c**	-4.72	28.9		
	28d	-5.53	4.74	0.91	6.29
Bu_3PBH_3	**28b**	-3.85	738		
29d	**28c**	-4.72	142		
	28d	-5.53	29.4		
	28e	-5.89	11.9	0.87	7.18
Ph_2PHBH_3	**28b**	-3.85	19.9		
29f	**28c**	-4.72	3.94		
	28d	-5.53	0.79	0.83	5.42
Cy_2PHBH_3	**28b**	-3.85	218		
29e	**28c**	-4.72	47.1		
	28d	-5.53	9.24	0.82	6.73
$PhPH_2BH_3$	**28b**	-3.85	272		
29g	**28c**	-4.72	65.6		
	28d	-5.53	21.4	0.66	7.53

While a direct comparison of k_2 values is no easy from the *Table 3.5*, we selected the electrophile **28b** (used in the kinetics with all PBs) and drawn the *Scheme 3.21*, showing the comparison of the k_2 with the same reference electrophile.

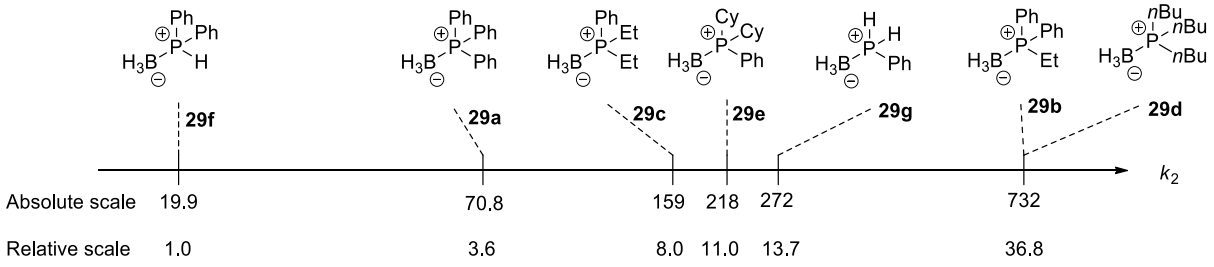

*Scheme 3.21 Reactivities (log k_2 toward **28b**) for the reactions of PBs **29a-g** with **28b** in CH_2Cl_2 at 20°C.*

As shown in the *Scheme 3.21*, the nature of the substituents influences the reaction rate with **28b** by almost a factor of 37. More precisely, substituting phenyl by ethyl substituents on the

phosphorous atom center increases the reaction rate by 10. In addition, the class of the phosphine modify the reaction rate. Regarding the specific nucleophilicity parameter s_N, it shows that the nucleophilic centers are significantly affected by the class of phosphines especially in the case of primary phosphines (s_N(tertiary or secondary) = [0.82-0.92], and s_N(primary) = 0.66).

Table 3.5 shows that the nucleophilicity of **29a-g** vary from 5.91 to 7.36 when excluding $PhPH_2BH_3$ **29g** due to its low specific sensitivity nucleophilicity parameter. This range of nucleophilicity values indicates a difference of reactivity by almost a factor of 28. Hence, the effect of the substituents and the class of the phosphine (tertiary or secondary) on the nucleophilicity is relatively low. These data are in line with the experimental observations by Curran an al. that PPh_3BH_3 and PBu_3BH_3 react at the same rates in Rh(II)-catalyzed B−H insertion reactions with methyl 2-phenyl-2-diazoacetate.[33]

2.3 Increasing the hydricity of PBs

The above-presented results show the low hydricity of PBs **29a-g** and thus their limited use in organic synthesis as hydride donors. With the aim to increase the hydricity of PBs we wondered the nature of the physical and structural parameters governing the ability of hydride to migrate.

2.3.1 Design of new borane Lewis acids to stabilize the borenium cations

A first strategy to enhance the hydricity of PBs would be to modify the substituents on the boron atom as it is expected to stabilize the borenium cation. As highlighted in the *Scheme 3.22*, the general reaction between R_3PBH_3 and Ar_2CH^+ yields the reduced adduct Ar_2CH_2 along with the formation of a borenium cation.

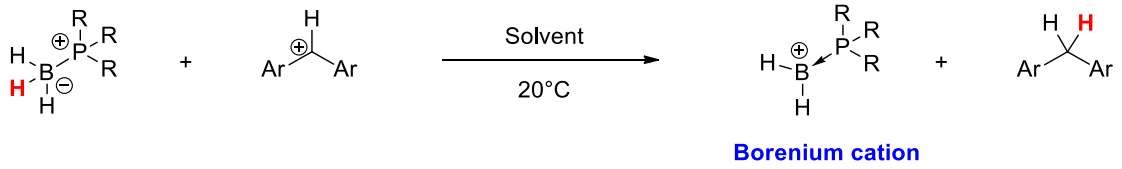

Scheme 3.22 General reaction between R_3PBH_3 and a diarylcarbenium cation yielding the reduced diarylmethane adduct and a borenium cation. The counter ion of $[HCAr_2]^+$ is $[BF_4]^-$

Based on *Scheme 3.22*, we hypothesized that the existence of the borenium cation and consequently its stabilization would represent a relevant parameter to modulate the reactivity of PBs. In this way, we investigated the use of pinacol **31a** and catechol **31b** boranes in the presence of a Lewis base, instead of BH_3. Moreover, because Ph_2PEt have shown to form one of the stronger hydride in association with BH_3, we have selected this phosphine as Lewis base.

First of all, we have tried to synthesize the phosphine borane complexes resulting from the association between **31a,b** and Ph_2PEt. Hence, R_2BH was added dropwise to a solution of Ph_2PEt in dichloromethane and the resulting solution was stirred at room temperature for hours. However, based on ^{31}P and ^{11}B NMR records of the crude, no phosphine borane complexes were formed. It shows that **31a,b** are significantly less acidic than BH_3. In spite of this observation, we wondered if a Lewis-acid Lewis-base adduct would be formed in solution with a very low equilibrium constant. Indeed, we had in mind that, even though the Lewis acidity is expected to be low, as soon as the Lewis base would coordinate the boron center, the hydride would become highly nucleophilic (*Scheme 3.23*).

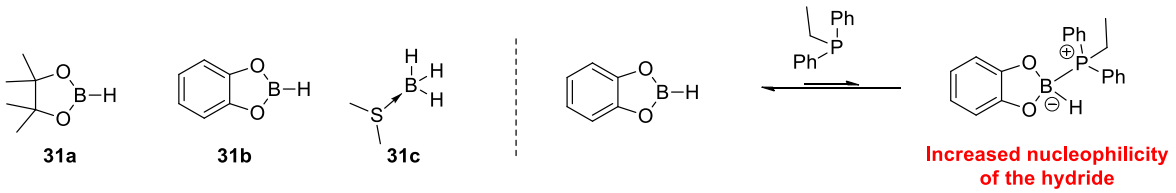

*Scheme 3.23 Chemical structures of boranes **31a-c** and coordination of $EtPPh_2$ to catechol **31b** borane for the enhancement of the nucleophilicity of the hydride.*

To verify this hypothesis, we decided to investigate the reduction of the 1-phenylpropan-1-one **32** with **31a,c** in the presence and the absence of 10 mol% of $EtPPh_2$. For that purpose, solutions of boranes, **32** and $EtPPh_2$ (in relevant cases) were mixed in CH_2Cl_2 under argon for 24h. The crude mixtures were treated with HCl (1.0 mol/L). After extraction, the crude products were analysed by ^1H NMR to determine the conversion into alcohol **33** (*Table 3.6*).

*Table 3.6 Reduction of 1-phenylpropan-1-one **32** with **31a-c** in the presence or the absence of $EtPPh_2$.*

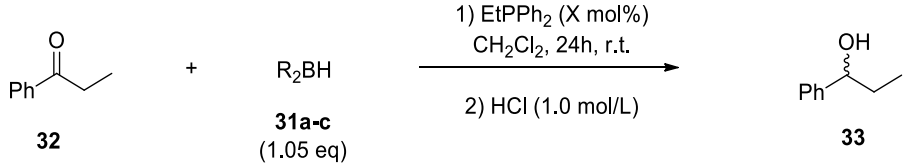

Entry	R_2BH	$EtPPh_2$	CH_2Cl_2	C=O (%) ^1H NMR	OH (%) ^1H NMR
1	**31c**	0	0.4 M	17	83
2	**31c**	10 mol %	0.4 M	25	75
3	**31c**	100 mol %	0.4 M	90	10
4	**31b**	0	0.4 M	100	0
5	**31b**	10 mol %	0.4 M	100	0
6	**31a**	0	0.4 M	100	0
7	**31a**	10 mol %	0.4 M	100	0

As it can be observed in the *Table 3.6*, the use of $EtPPh_2$ proved to be detrimental to the reduction of the carbonyl function. Indeed, $EtPPh_2$ significantly decreased the rate of the

hydride transfer. In addition, it shows that hydride transfer is strongly dependant on the nature of the borane **31a-c**. It proves that, unlike silicon, boron atom is not able to bond a ligand in a 4-electrons 3-centers manner. Regarding **31a-b**, the Lewis acidity is importantly decreased. Therefore, neither the coordination of boron to $EtPPh_2$ nor to the carbonyl group is possible, precluding the occurrence of the hydride transfer.

This study shed light on the importance of the Lewis acidity of the boron atom to envisage a hydride transfer. A subtle balance must be found between the Lewis acidity of the borane and the stabilization of the borenium cation.

2.3.2 Influence of the Lewis base on the hydricity of PBs

Due to our unfruitful attempts to increase the hydricity of PBS by modifying the nature of the Lewis acid, we focused our attention on the nature of the Lewis base.

- Borenium cations: properties, stability and isolation.

Borenium correspond to a planar three coordinate borocation, which is in turn formally isoelectronic with free borane (*Scheme 3.24*).[35]

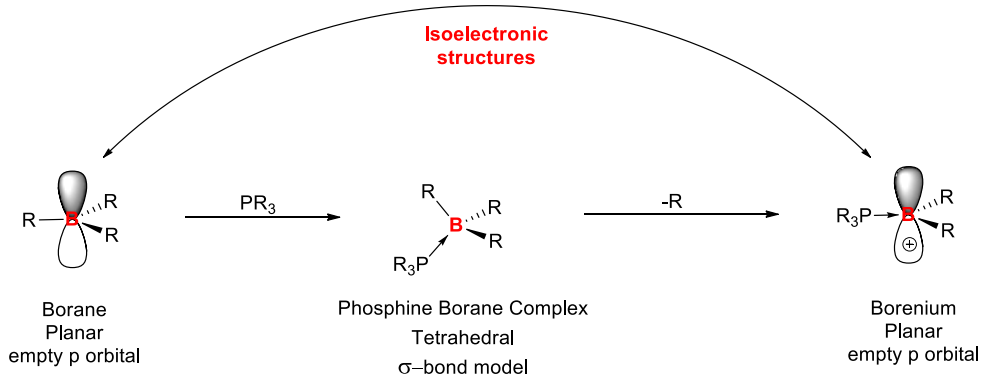

Scheme 3.24 Comparison between the electronic structures and geometries of borane, phosphine borane complexes and borenium cation.

Among the plethora of works in the field of borenium chemistry, Stephan et al. reported a study on the nature of the boron atom in the complex resulting from the association of $P(t\text{Bu})_3$ and **31b** in the presence of $B(C_6F_5)_3$ as hydride quencher.[36] The authors aimed at determining if the boron is best described as a borenium cation or a boryl-phosphonium cation in the product **34** (*Scheme 3.25*).

[35] For a recent review, see: a) Eisenberger, P.; Crudden, C. *Dalt. Trans.* **2017**, *46*, 4874. For other reviews, see: b) Piers, W. E.; Bourke, S. C.; Conroy, K. D. *Angew. Chem., Int. Ed.* **2005**, *44*, 5016 and reference 33

[36] Dureen, M. A.; Lough, A.; Gilbert, T. M.; Stephan, D. W. *Chem. Commun.* **2008,** *913*, 4303.

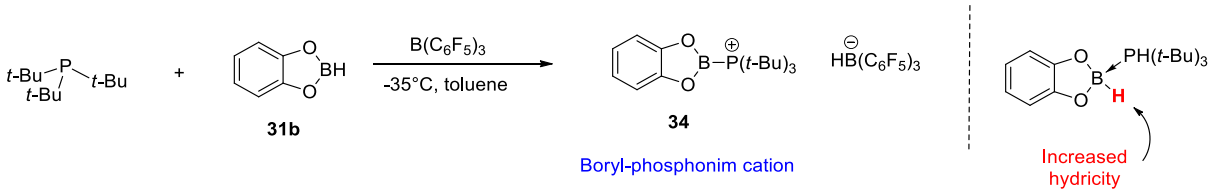

Scheme 3.25 Synthesis and characterization of a boryl-phosphonium cation.

The results were consistent with a significant π-donation from O to B while no $[B(OR)_2]^+$ cation has been isolated to date. However, a deep NBO study performed by DFT suggested that $[(C_6H_4O_2)BPMe_3]^+$ **34** is essentially a phosphonium cation with one unusual, very slightly electron-donating $(C_6H_4O_2)B$ substituent, where the B atom is about as Lewis acidic as a proton. It shows that the stability of the borenium is a relevant guideline in this reactivity.

Bourissou et al. have also investigated borenium chemistry by designing a phosphino-naphtyl backbone able to promote a P→B interaction, responsible for the stabilization of the borenium cations **36** and **37** (*Scheme 3.26*).[37] In addition, they have shown that if the boron atom was substituted by an amino group such as in compound **35**, the P→B interaction was precluded, likely due to the strong π-donation resulting in a significantly reduced Lewis acidity of the boron center. Regarding the structure of borenium cation in solution, it is important to precise that they often form dimers or cyclic trimers through hydride bridges.[38]

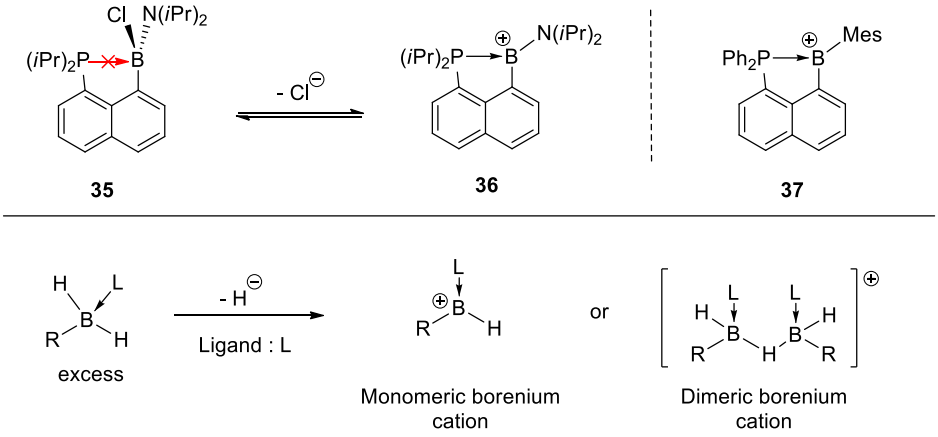

*Scheme 3.26 (top) Phosphino-naphtyl borenium cations **36,37** isolated by Bourissou et al. (bottom) Aggregation states of borenium cations in solution.*

[37] a) Devillard, M.; Mallet-Ladeira, S.; Bouhadir, G.; Bourissou, D. *Chem. Commun.* **2016**, *52*, 8877 b) Devillard, M.; Bouhadir, G.; Mallet-Ladeira, S.; Miqueu, K.; Bourissou, D. *Organometallics* **2016**, *35*, 3788.

[38] Prokofjevs, A.; Kampf, J. W.; Solovyev, A.; Curran, D. P.; Vedejs, E. *J. Am. Chem. Soc.* **2013**, *135*, 15686.

On the light of these studies, it become clear that the expected borenium cation can be stabilized by either σ or π-donating groups. In any case, it was shown that phosphine ligand are able to stabilize borenium cations even if it can't be clearly detected in solution.

2.3.3 Design of new phosphine ligands to stabilize borenium cations.

Based on this literature survey, we thought to stabilize the borenium cation by designing the substituents on the phosphorous atom in order to induce stabilizing interactions. With this objective in mind, we designed PBs resulting from three strategies (*Figure 3.5*). The first strategy is a direct π-interaction (DPI) shown by molecules **38a** and **29h** able to share electron density with the borenium using Buchwald type ligands. The second strategy hinge on the use of two effects: a bend effect targeting to bring "perpendicularly" to the empty p orbital an aryl substituent and a π-interaction between P and a heteroatom in order to help the formation of a boryl-phosphonium cation **29i**. The third strategy aims at destabilizing the borenium to see if the hydricity decreases. To do so, we selected an electron rich π-planar backbone unable to interact with the borenium cation as shown by the molecules **29j** and **38b.**

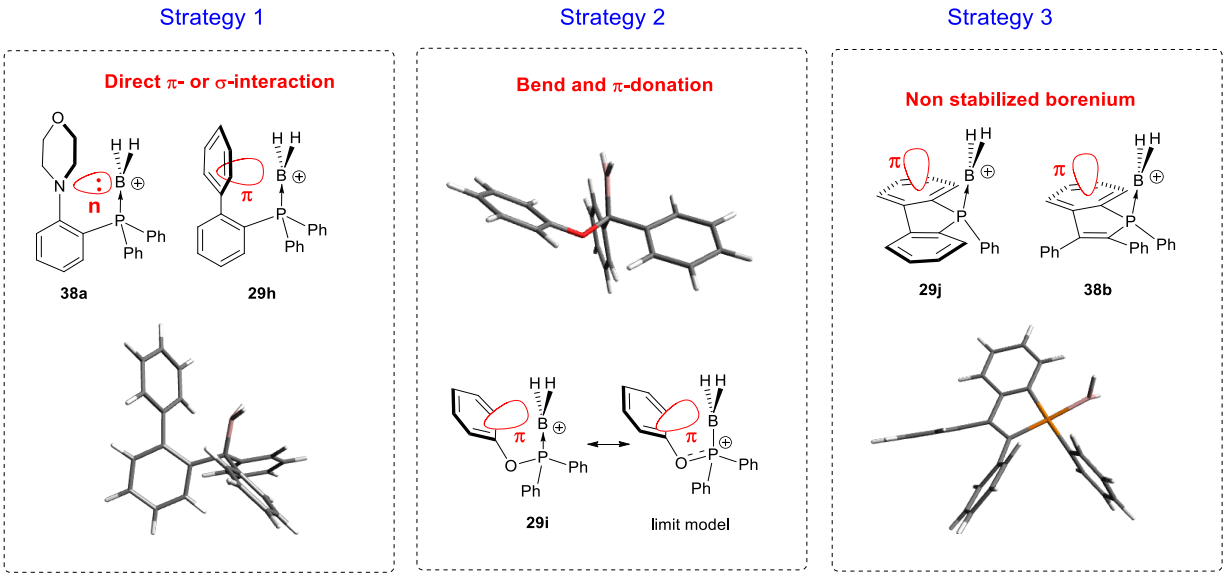

*Figure 3.5 Presentation of the three strategies with the corresponding targeted molecules **29h-j** and **38a-b** and their modelization (Avogadro®, force field: UFF, conjugate gradient).*

Phosphines boranes complexes **29h-j** were synthesized in excellent yields ranging from 78 to 93% using classical methods of the literature (*Scheme 3.27*). Unfortunately, we were not able to synthesize the adduct **38a** containing a morpholino substituent as well as the benzophosphole borane complexe **38b** due to deboration occurring at r.t.

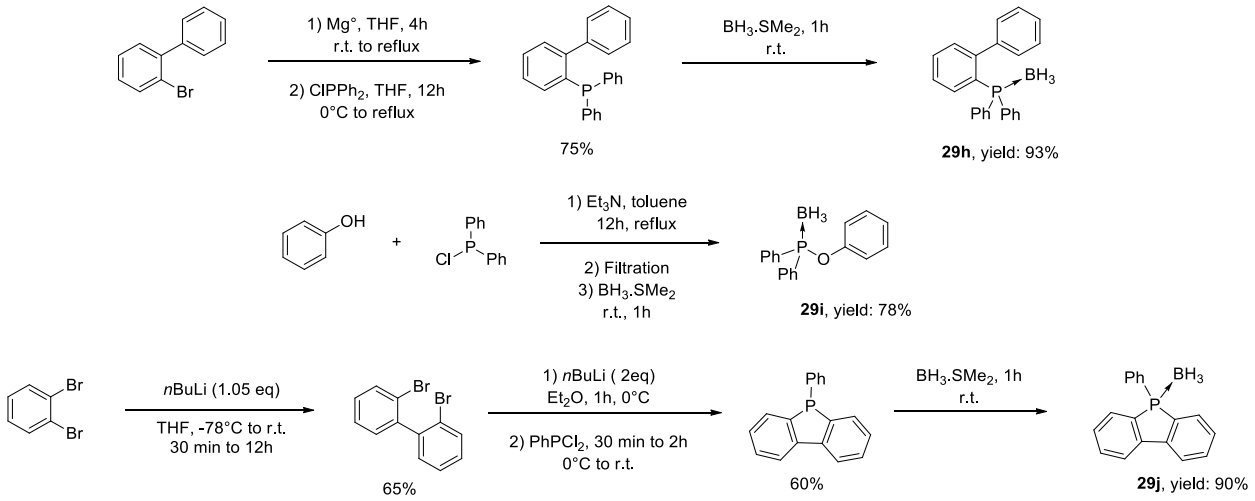

*Scheme 3.27 Synthesis of phosphine borane complexes **29h-j** for the study of the hydricity.*

With the aim to confirm the proximity between the boron moiety and the π-system of **29h**, a crystallographic structure of a crystal grown after slow evaporation of a solution of CH_2Cl_2 was obtained. As shown in the *Figure 3.6*, an overlap is possible between the empty p orbital of the borenium cation and the aromatic π system. Indeed, an average B-C_6H_5 distance of 3.591 Å is a little bit shorter than expected.

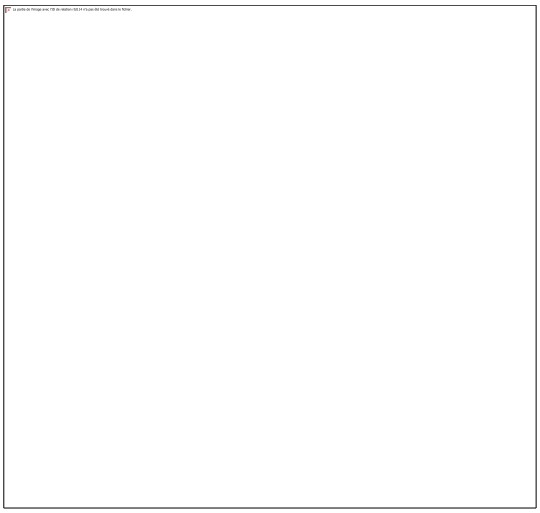

*Figure 3.6 Crystallographic structure of **29h**, Boron in pink and phosphorous in orange. ORTEP representation.*

With PBs **29h-j** in hand, we investigated their reactions with diarylcarbenium cations **28a-g** and measured kinetics (*Table 3.7*).

*Table 3.7 Second order rate constants for the reactions of PBs **29h-j** with benzhydrylium cations **28a-f** in dichloromethane at 20°C, nucleophilicity (N) and specific sensitivity nucleophilicity parameters (s_N).*

R_3PBH_3	Ar_2CH^+	E(Ar_2CH+)	k_2 (L/mol/s)	s_N	*N*
(BiPh)PPh_2BH_3	**28a**	-3.14	4695		
29h	**28b**	-3.85	1695		

	28d	-5.53	30.7		
	28f	-7.02	1.34	0.94	7.16
$PhOPPh_2BH_3$	**28b**	-3.85	931		
29i	**28c**	-4.72	245		
	28d	-5.53	43.9		
	28e	-5.89	18.8	0.83	7.48
Dibenzo-BH_3	**28a**	-3.14	162		
29j	**28b**	-3.85	22.7		
	28d	-5.53	0.76	0.96	5.37

First of all, if we compare each results with those of PPh_3BH_3 **29a** (N = 5.91 and s_N = 0.92), we can see that all of the three strategies worked well. Regarding, the installation of a biphenyl ring in **29h**, capable to interact with the empty p orbital of the borenium cation, the nucleophilicity increased and thus, the rate of the hydride transfer by almost a factor of 18 with comparable s_N. This also indicates that the nature of the nucleophilic center is the same and allow us to attribute the enhanced nucleophilicity to the structural change. In the case of $(PhO)PPh_2BH_3$ **29i**, the hydricity is even higher than that of **29h**. By comparison with **29a**, the second order rate constants increased by a factor of 37. This may be attributed to the inductive effect of the oxygen atom on the phosphorous center. However, while it should only exert an attractive inductive effect decreasing the σ-donor character of the phosphorous center (Tolman electronic parameter PPh_3 = 2069 and Ph_2POPh = 2075), it becomes reasonable to also attribute the better hydricity to a π-stabilized boryl-phosphonium cation, as mentioned by Stephan et al.[36] Finally, the low hydricity found in the case of **29j** is the consequence of a non-stabilized borenium cation. Indeed, the π-system of the planar benzophosphole is not able to develop a stabilizing interaction because both the π-system and the p orbital of the borenium are collinear but not within the same axis.

This study, dedicated to the design of the phosphines, confirmed that the hydricity of PBs is linked to the stabilization of the borenium cation. In addition, it also highlights that, contrary to conventional wisdom, σ-donor substituents on the phosphorous atom don't increase significantly the hydricity, probably due to the fact that phosphonium cations are stable adduct regardless the substitution of the P atom center. However, π-donor ligands allow an even better conjugation of the positive charge on three atoms instead of only two.

2.4 Comparison of the hydricity of PBs with those of other hydride donors

The first part of this chapter exemplified the use of the main transition metal free hydride donors in organic reductions. As we have measured the nucleophilicity of several PBs, a comparison of the hydricity can be done according to Mayr nucleophilicity scale.

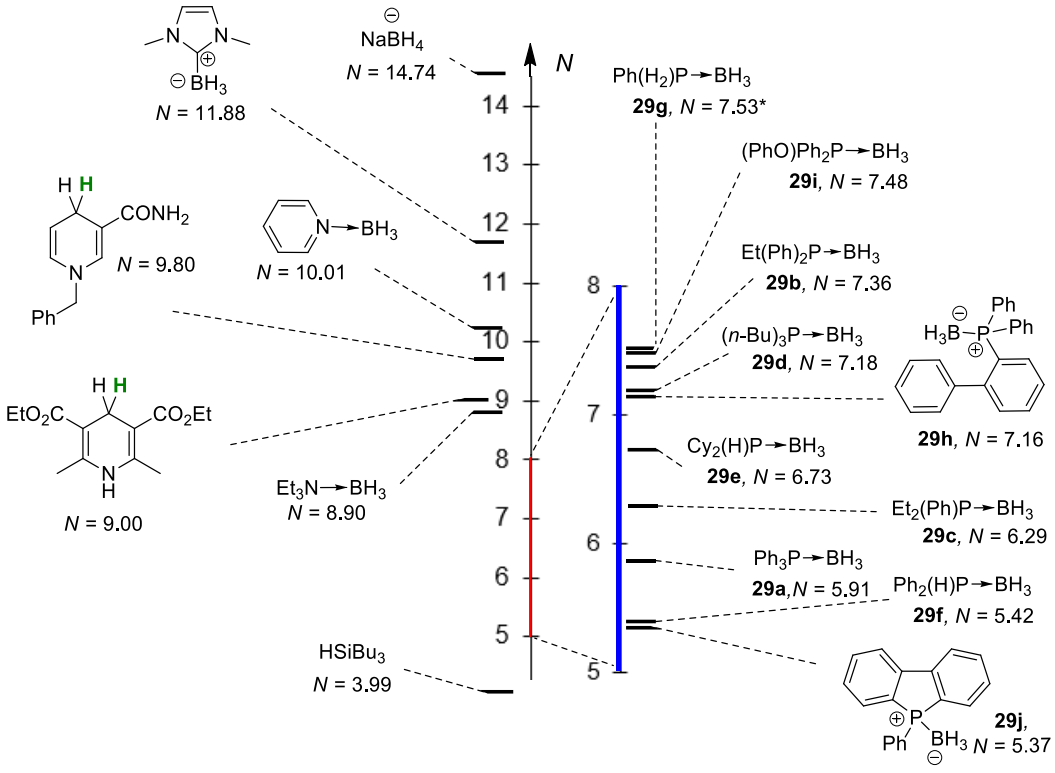

*Figure 3.7 Comparison of the hydricity of PBs **29a-j** with common hydride donors in ionic organic reductions.*

As shown in the *Figure 3.7*, the nucleophilicity of PBs is placed between those of the less reactive Hantzsch esters or amine boranes and silanes, confirming that they are weak hydride donors. In addition, their nucleophilicity parameters varies by a factor of 145 from the less to the more reactive of them.

3. Conclusion and perspectives

3.1 Conclusions

In conclusion, we have performed a deep structural and mechanistic study of the hydride transfer reactions involving transition-metal-free ionic hydride donors. A brief survey of the most commonly used hydride donors has been realized showing that phosphine borane complexes had never been investigated as hydride donors to quantify their hydricity.

We have shown that PBs are suitable hydride donors to reduce benzhydrylium salts which are blue colored reference electrophiles. Based on this observation, we used Mayr linear free energy relationship to quantify the nucleophilicity parameters of phosphine borane complexes (*N* and s_N). To perform this study, eight phosphine borane complexes have been synthesized in order to cover the different kind of substituents on the phosphorous atom (aryl, alkyl) and each classes of phosphines (tertiary, secondary and primary). According to our kinetic data, we found that the nucleophilicity of phosphines, ranging from *N* = 5.91 to 7.36, is not strongly influenced by the nature of the phosphine.

Seeking for methods to increase the hydricity of PBs, we hypothesized that the stabilization of the borenium cation resulting from the hydride transfer would be a relevant parameter to increase this hydricity. As a consequence, we synthesized three new fine-tuned PBs' capable to induce stabilizing π- or σ- interactions with the empty p orbital of the borenium cation. As expected, our kinetic data showed that the nucleophilicity could be increased by a factor of 37 in the best cases. On the other hand, we investigated the influence of the boron substituents and shown that the Lewis acidity of the borane is also a crucial parameter. Indeed, alkoxyborane are not Lewis acidic enough to be complexes by phosphine or other Lewis bases and are thus inactive in reduction reactions without any activation source.

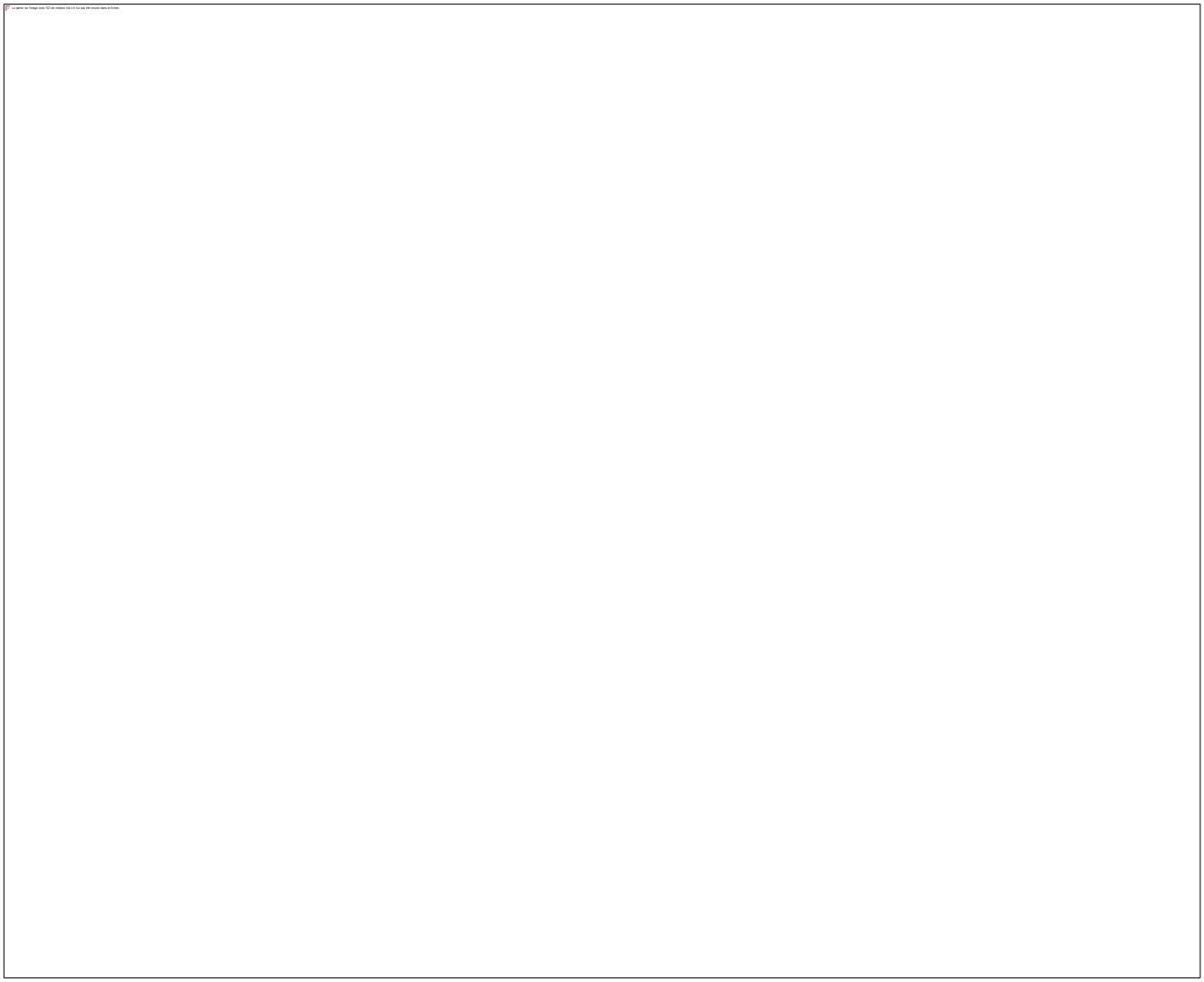

Figure 3.8 Plot of the nucleophilicity of several hydride donors against the electrophilicity of various electrophiles

Finally, by combining our kinetic results with those already reported by Mayr et al., we were able to furnish a guideline to anticipate the feasibility of the reduction of several electrophiles, as shown in *Figure 3.8*. Indeed, according to Mayr rule of thumb, a chemical reaction between a nucleophile characterized by a nucleophilicity parameter *N* and an electrophile with an

electrophilicity parameter *E* is feasible at 20°C if $E + N > -5$. *Figure 3.8* is a useful tool to see if the reduction of the main functional groups is possible. To use it, one must select the type of electrophiles to reduce on the abscissa and read vertically the intercept corresponding to the green surface, which indicates that the reduction is possible at r.t. Thus, the use of phosphine borane complexes as reducing agents can be relevant in the case of functionalized molecules as their use doesn't require strict conditions. More precisely, they can be used to reduce the most reactive α,β-unsaturated compounds, iminium salts or diarylcarbenium cations. Indeed, we verified that benzylidene malononitrile (Ph-CH=C(CN)$_2$, *E* = -9.42) Eschenmoser salt ([Cl][H$_2$C=N(CH$_3$)$_2$], *E* = -6.69) and several diarylcarbenium cations are reduced with *n*Bu$_3$P-BH$_3$.

3.2 Perspectives

As evidenced by the previous conclusion and a part of this chapter, PBs are weak reducing agents. Many efforts have been dedicated to the enhancement of the hydricity with moderate success. Nonetheless, there is another way to increase the hydricity, requiring the use of phosphido-borane R$_2$P-BH$_3$. Indeed, this kind of anionic reagents are known to be strong hydride donors due to the negative hyperconjugation of the n orbital of the phosphorous with the anti-bonding σ* orbital of the boron center (*Scheme 3.28*). This strong interaction is expected to weaken the boron-hydrogen σ bond and thus facilitate the hydride transfer.

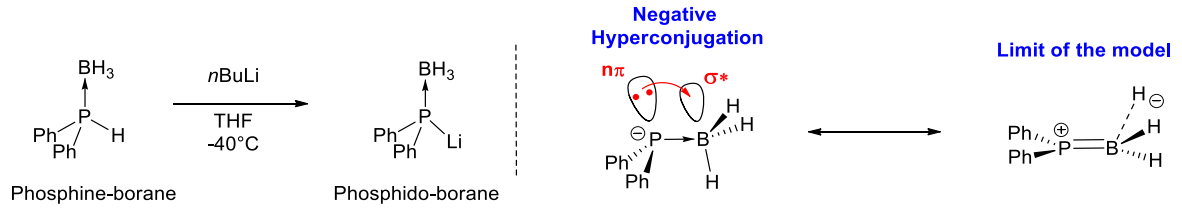

Scheme 3.28 Synthesis of phosphido-borane by deprotonation of diphenylphosphine borane complex. Negative hyperconjugation model rending account for the increased hydricity of phosphido-borane complexes.

In our lab, phosphido-borane complexes have been already used reduction of carbonyl groups such as aldehydes.[39] With this aim to use these anionic compounds as hydride donors, we have synthesized the diphenylphosphido-borane by a deprotonation of Ph$_2$HP-BH$_3$ with *n*-BuLi. The product is yellow making it suitable to perform UV-Vis kinetics. However, the major drawback of this reagent is the ambident character. Indeed, it is nucleophilic via the phosphorous atom leading to the kinetic product and via the hydride to yield the thermodynamic product (*Scheme 3.29*). We have measured the nucleophilicity of the P-attack with benzylidene malonate derivatives to show that the nucleophilicity of [Ph$_2$P-BH$_3$][Li] is 29.29

[39] Queval, R. Dissertation. Laboratoire de Chimie Moléculaire et Thio-Organique, Université de Caen, ENSICAEN, France. **2010**

.To access the nucleophilicity of the hydride, we thought that the use of sterically encumbered electrophiles would impose a high reversibility to the equilibrium between P- and H- attacks.

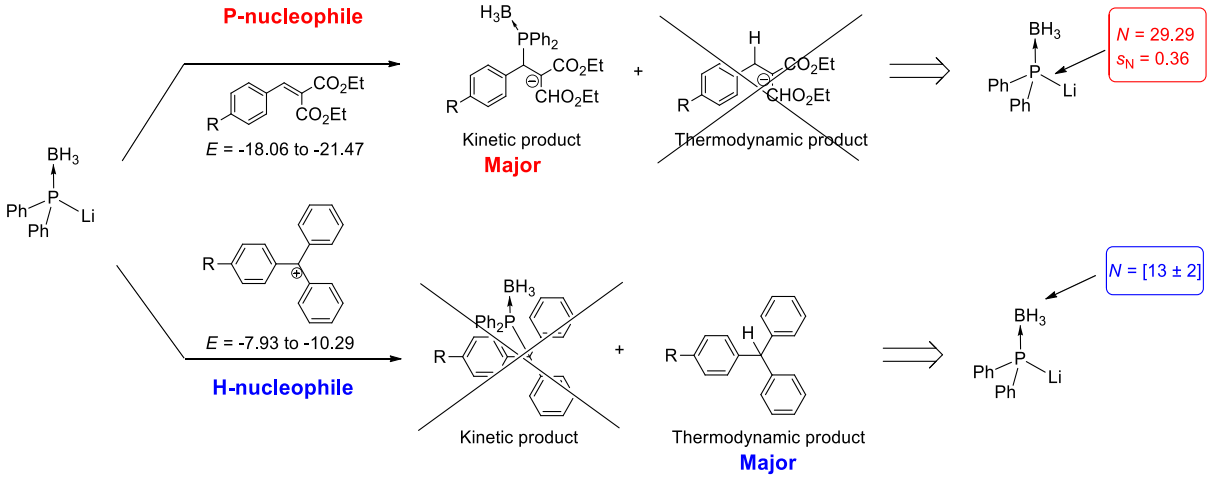

Scheme 3.29 Study of the ambivalent nucleophile [Ph_2P-BH_3][Li]: P- versus H-nucleophilicity

Thus we selected sterically encumbered trityliums cations to perform the reactions. In spite of the formation of the reduced adduct (according to ^{1}H NMR), we were not able to record reliable kinetics due to the overlap between the red-orange coloured tritylium salts and the yellow colored [Ph_2P-BH_3][Li]. In addition, owing to the sensitivity of [Ph_2P-BH_3][Li], the reaction conditions must be extremely strict making the reagent hard to handle. Even though we did not get suitable kinetics, our observations that [Ph_2P-BH_3][Li] react with trityliums salt to yield the reduced triarylmethane adduct allow us to estimate the hydricity of [Ph_2P-BH_3][Li] to roughly 13.

This conclusion is important as the ambident behaviour of phosphido-borane is well known in phosphorous chemistry but had never been measured yet. As a perspective, it would be important to quantify the hydricity of several phosphide-borane adducts and investigate the effect of both the borane and the phosphorous substituents.

4. Chapter IV: Borenium cations derived from LB-BH_3 as reactive intermediates in borylation reaction.

During the last few decades, Lewis base (LB = amine, phosphine, carbene…) borane complexes have attracted attention as starting materials in borylation reactions. These complexes present the unequivocal advantage to be air and moisture stable. Moreover, as shown in the last chapter, they can be precursors of reactive trivalent borenium cation which are poorly explored yet. In this part, we focused on exploring the reactivity of the BH_3 group of phosphine borane complexes and use them as a source of boron in borylation reactions. Thus, we embarked on a literature survey of the methods to make C-B bonds with boranes.

1. Literature survey of advances in the borylation reactions
   1.1. Development of transition metal catalysed borylation reaction

In 1995, Hartwig et al. reported the first "Hydrocarbon Functionalization by Transition Metal Boryls".[1] By using a ferrocenylcatechol reagent **1** with arene and alkene substrates **2a-c** under H_2 atmosphere and UV irradiation, the authors observed the formation of the borylation adducts **3a-e** (*Scheme 4.1*).

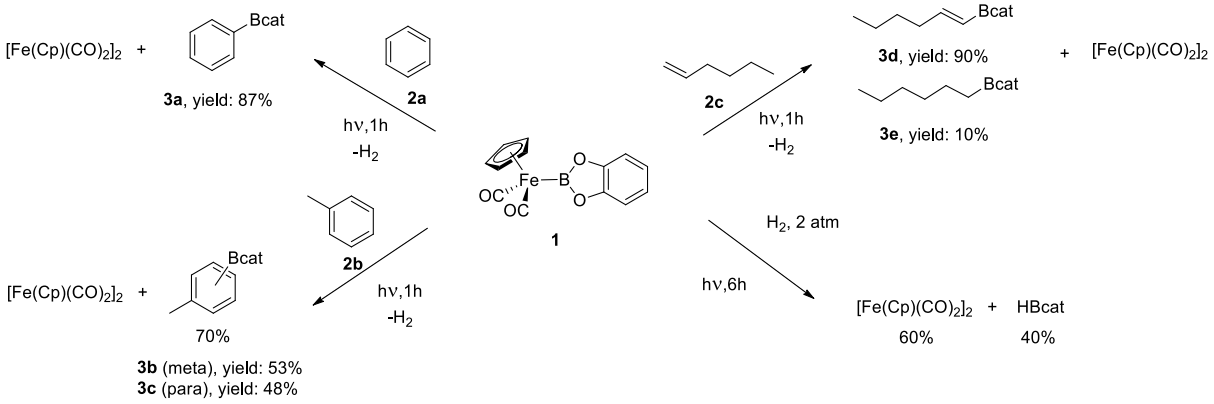

Scheme 4.1 Ferrocene borylation of arene and alkenes

Few years later, the same group reported the borylation of alkanes using third-row metals such as the tungsten-based catalyst **4**.[2] Interestingly, the sole product of this reaction was the linear alkylboronate esters **5a-b**. From a mechanistic point of view, the authors proposed either a direct alkane activation by the photochemically excited state of the complex or the initial decoordination of a carbonyl ligand to yield a 16-electrons intermediate able to better interact with the alkane (*Scheme 4.2*).

[1] Waltz, K. M.; He, X.; Muhoro, C.; Hartwig, J. F. *J. Am. Chem. Soc.* **1995**, *117*, 11357.
[2] Waltz, K. M. Hartwig, J. F. *Science* **1997**, *277*, 211.

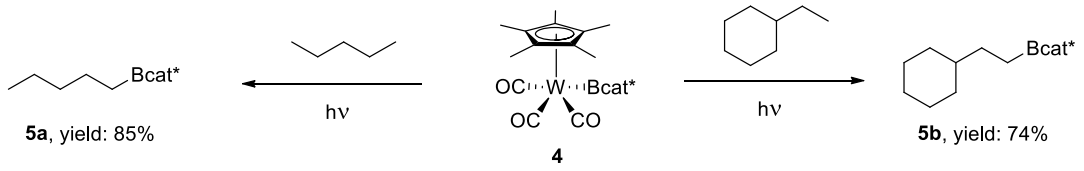

Scheme 4.2 Selective functionalization of alkanes transition metal boryl complexes. Bcat correspond to 4,6-dimethylphenyl boronic ester.*

Seeking for a catalytic version of the reaction, Smith reported the borylation of benzene with HBpin catalysed by 17 mol % of an Iridium catalyst [Cp*Ir-(PMe_3)(Ph)(H)] in neat benzene at 150°C for 5 days, yielding C_6H_5Bpin in 53% yield.[3] Interestingly, they found that the reactivity was borane-source dependent. The authors showed that this reaction occurred with only three turnovers, possibly due to the insufficient labile character of the dative ligand. Based on these results, Hartwig et al. developed a new rhodium based catalyst containing a hexamethylbenzene ligand supposed to dissociate more readily, and thus allowing the addition of the diboron reagent to generate an intermediate that could functionalize alkanes and arenes in a catalytic process (*Scheme 4.3*). As a consequence, the reaction of a linear alkane **6** with $B_2(pin)_2$ (bis(pinolato)diboron) catalysed by 2.5 mol% [Cp*Rh(η4-C_6Me_6)] **7** led to alkylboronate esters in high yields ranging from 70 to 88% with perfect selectivity of the primary C-H bond sites (*Scheme 4.3*).[4]

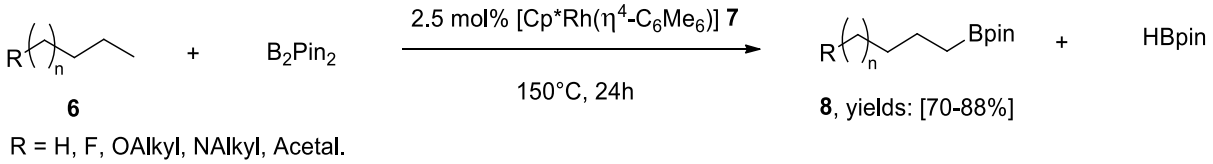

Scheme 4.3 Borylation of linear alkanes catalysed by a rhodium complex.

Collaborations between Ishiyama, Miyaura and Hartwig led to designing the highly active iridium catalyst [Ir(OMe)(COD)]$_2$ **9** in the presence of sterically hindered additives (4,4'-di-tert-butyl-2,2'-bipyridine (dtbpy) or 3,4,7,8- tetramethyl-1,10-phenanthroline (Me_4phen)), as shown in *Scheme 4.4*.[5] The latter system turned out to be highly efficient to catalyse the borylation of various heteroarenes such as pyrazoles **10a**, pyrimidines **10b**, benzimidazole **10c**, benzoxazole **10d** or azaindoles with B_2pin_2 as boron source to yield **11a-d** in good to excellent yields (*Scheme 4.4*).[6]

[3] Iverson, C. N.; Smith, III, M. R. *J. Am. Chem. Soc.* **1999**, *121*, 7696.
[4] a) Chen, H.; Schlecht, S.; Semple, T. C.; Hartwig, J. F. *Science* **2000**, *287*, 1995. b) Lawrence, J. D.; Takahashi, M.; Bae, C.; Hartwig, J. F. *J. Am. Chem. Soc.* **2004**, *126*, 15334. c) Shimada, S.; Batsanov, A. S.; Howard, J. A. K.; Marder, T. B. *Angew. Chem. Int. Ed.* **2001**, *40*, 2168.
[5] a) Ishiyama, T.; Takagi, J.; Yonekawa, Y.; Hartwig, J. F.; Miyaura, N. *Adv. Synth. Catal.* **2003**, *345*, 1103 b) Ishiyama, T.; Nobuta, Y.; Hartwig, J. F.; Miyaura, N. *Chem. Commun.* **2003**, 2924.c) Ishiyama, T.; Miyaura, N. *Pure Appl. Chem.* **2006**, *78*, 1369.
[6] For a review, see Larsen, M. A. Hartwig, J. F. *J. Am. Chem. Soc.* **2014**, *136*, 4287−4299

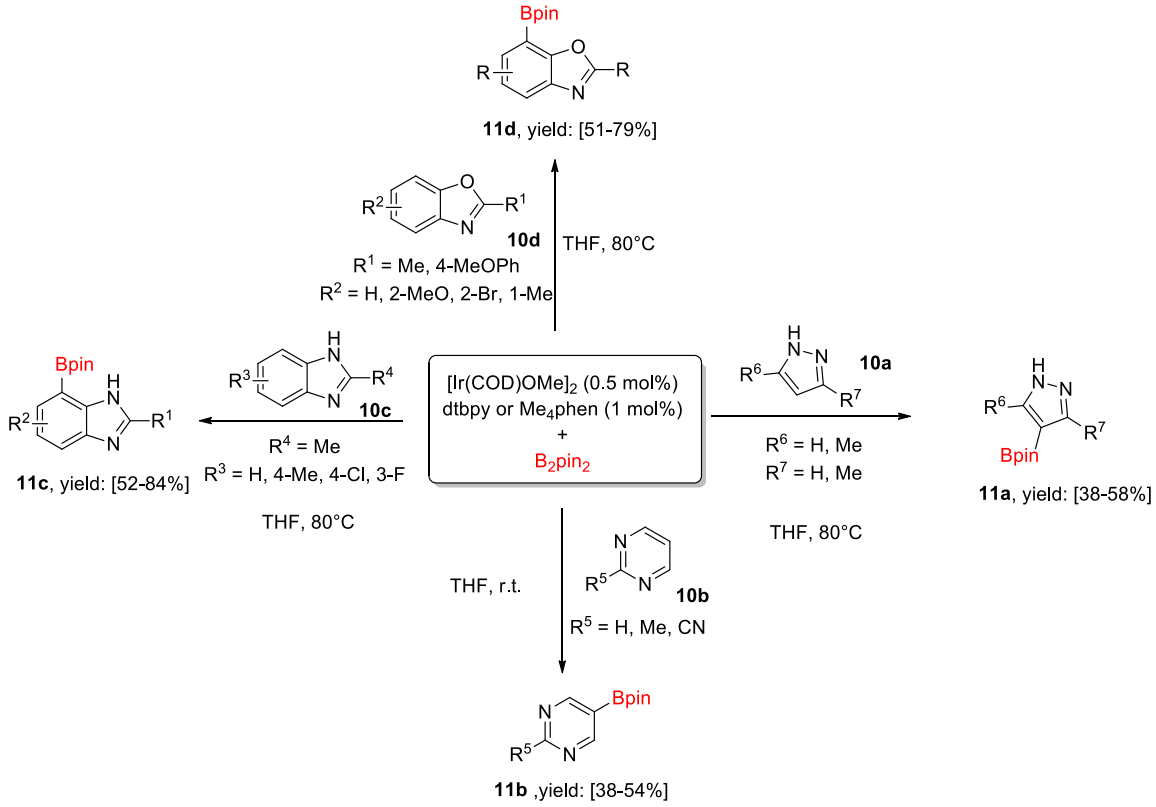

Scheme 4.4 Catalytic borylation of pyrazoles, pyrimidines, benzimidazole, benzoxazole or azaindoles with [Ir(OMe)(COD)]$_2$/Me_4Phen and B_2pin_2 as boron source.

The latter catalyst is still used in organic synthesis especially in tandem reactions as borylation adducts are frequently used in transition metal cross coupling reactions.

1.2. Intermolecular borylation reaction with LB-BH_3 (LB = phosphine, amine, carbene).

Borylation reaction has largely profited from the remarkable development of the field of C-H activation. While less than 1 mol% of the catalyst/ligand systems are able to promote the reaction, a significant part of the boron source is systematically lost during the reaction. Seeking for a more atom economical version of this reaction, Vedejs et al. used LB-BR_3 as a new boron source instead of B_2pin_2.

From a conceptual perspective, this new approach completely changed the expected reactivity of the boron atom. Indeed, as we have shown in the previous chapter, Lewis-acid Lewis-base complexes are hydride donors. This electronic property implies that borylation reactions will occur via the formation of a borenium cation. As shown in the *Scheme 4.5*, two cases must be distinguished: a) the borenium cation will be formed via the heterolytic abstraction of a leaving group LG (in the case of LB-BR_2(LG)), or b) the borenium cation will be formed via an heterolytic abstraction of an hydride in the case of LB-BH_3 (if we exclude oxido-reduction reactions).

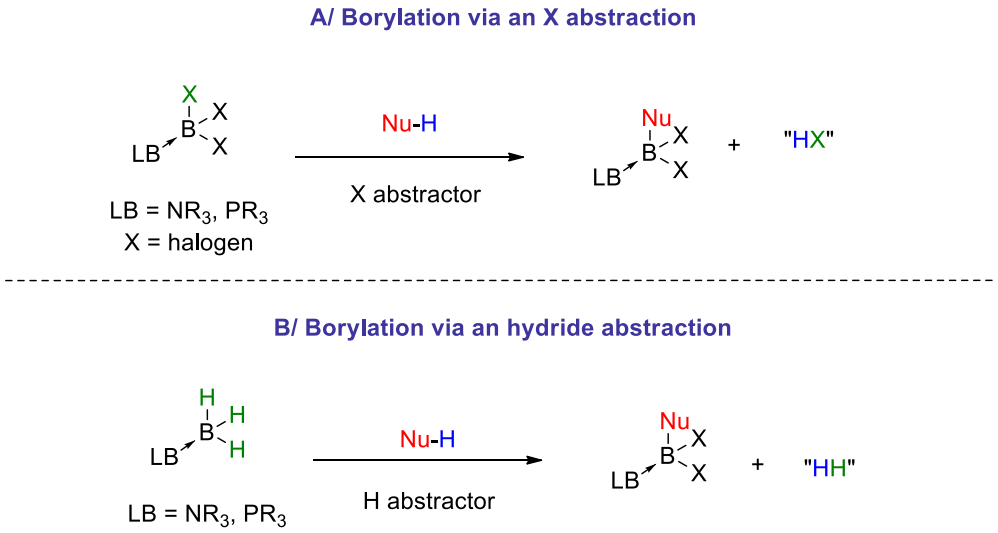

Scheme 4.5 Borylation of LB-BR_3 via either an X abstraction or an hydride abstraction.

The case of electrophilic borylation of electron-rich aromatic and heteroaromatic substrates with LB-BH_2(LG) (LG = leaving group) have been studied by several groups.[7] However, intermolecular borylations of LB-BH_3 compounds are much more challenging and only scarce examples have been reported so far. Among these reports, Vedejs et al. studied the activation of triethylamine borane for intermolecular borylation.[8] While treatment of triethylamine borane **12** with 50 mol% of Tf_2NH led to the formation of the dimer **13** (*Scheme 4.6*). The latter treated with one equivalent of the strong acid afforded exclusively the amine borane complex **14**, as confirmed by ^{11}B NMR (two maxima, δ = 0.6 and −7.4 ppm in CD_2Cl_2, assigned to O-bound and N-bound covalent bistriflimidate).

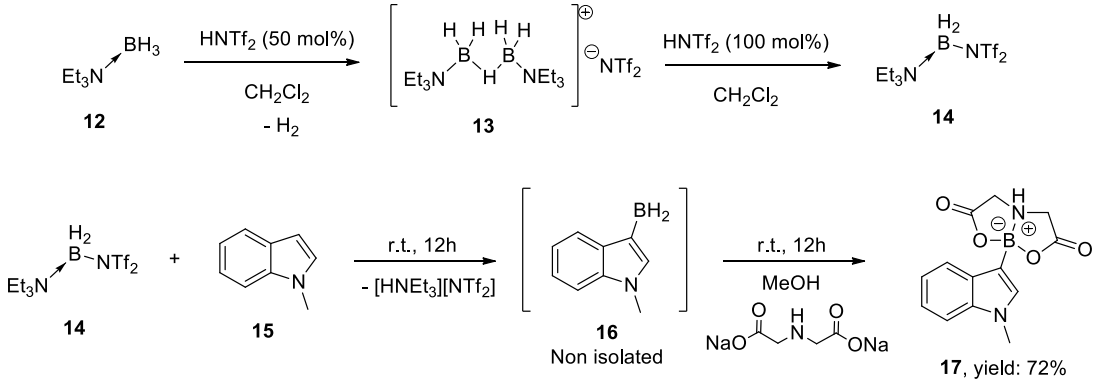

Scheme 4.6 Activation of triethylamine borane for intermolecular borylation with N-methyl indole.

The borenium analogue **14** probed to be able to promote the borylation of N-methylindole **15** over 12 hours at room temperature to furnish **16**. Due to difficulties to isolate **16**, the authors

[7] For a review, see Chem. Rev. **2012**, *112*, 4246.
[8] Prokofjevs, A. Ph. D. Dissertation, University of Michigan, **2012**.

treated the mixture with disodium iminodiacetate in methanol and isolate **17** in 72% yield. Regarding the mechanism of the reaction, they proposed an electrophilic borylation of **15**, followed by internal proton transfer to form directly the ammonium salt $HNEt_3^+$ Tf_2N^-, without releasing Tf_2NH.

1.3. Intramolecular borylation reaction with LB-BH_3 (LB = phosphine, amine, carbene).

Based on the same approach, intramolecular borylation of LB-BH_3 has been achieved using several types of Lewis bases. In this context, the highly electrophilic H-bridge dimer **21** has been generated by treating *N*,*N*-dimethylbenzylamine **19** derivatives with 50 mol% of the tritylium salt $[Ph_3C]^+[B(C_6F_5)_4]^-$ **20** in bromobenzene (*Scheme 4.7*).[9] While no cyclization occurred at r.t., increasing the charge of **20** to 90 mol% led to the formation of cyclic products **22** within 4h at 20 °C. Reductive treatment of the crude mixture with $[Bu_4N]^+[BH_4]^-$, gave cyclic adducts **23** in yields ranging from 55 to 76%. Careful investigations have shown that the main product was the labile borenium salt **22**.

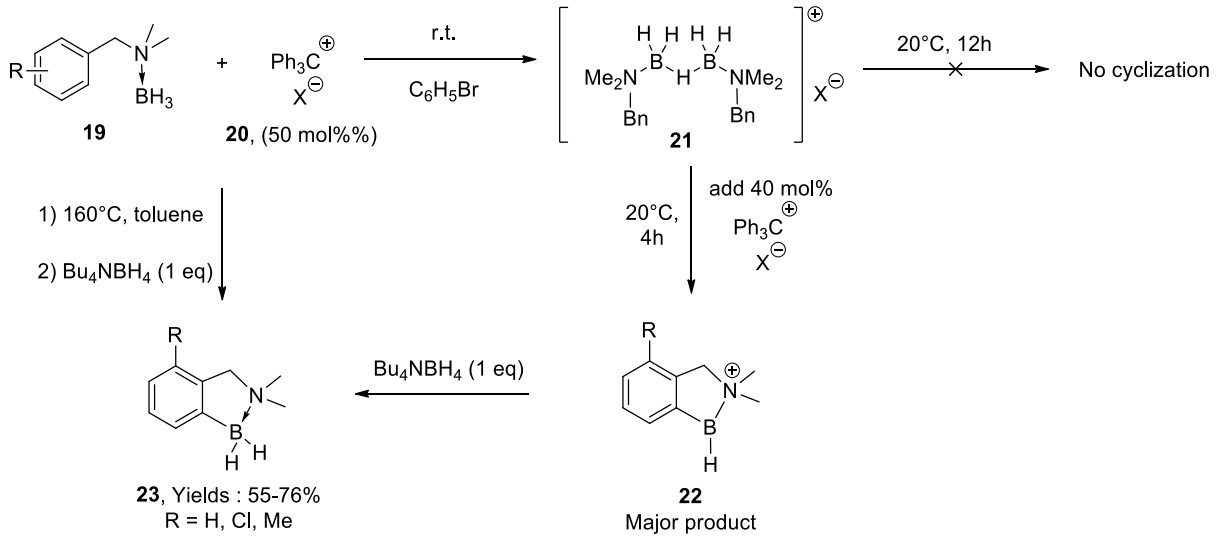

Scheme 4.7 Intramolecular nitrogen-directed aromatic borylation of N,N-benzylamine-borane derivatives. X^-: $[B(C_6F_5)_4]^-$

A catalytic version of this reaction was developed by employing 5 mol% of $[Ph_3C]^+[B(C_6F_5)_4]^-$ **20** under high temperature conditions (160°C, in toluene). The mechanism was studied but remains unclear.[10] Kinetic Isotop Effect (KIE) study of the borylation of **24** showed a k_H/k_D = 2.8, indicating that the C-H(D) bond at which boron substitution occurs is broken during or before the regioselectivite-determining step (*Scheme 4.8*). DFT-calculations showed that the borenium π-complex **25** and the Wheland intermediate **26** have similar energies (ΔE = 0.43

[9] Vedejs, E.; Nguyen, T.; Powell, D. R.; Schrimpf, M. R. *Chem. Commun.* **1996**, 2721.
[10] Vries, T. S. De; Prokofjevs, A.; Harvey, J. N.; Vedejs, E. *J. Am. Chem. Soc.* **2009**, *131*, 14679.

kcal/mol). Furthermore, it is unclear wether **22** results from the direct cyclization of **25** or if it forms upon the deprotonation of **26** followed by a hydride transfer.

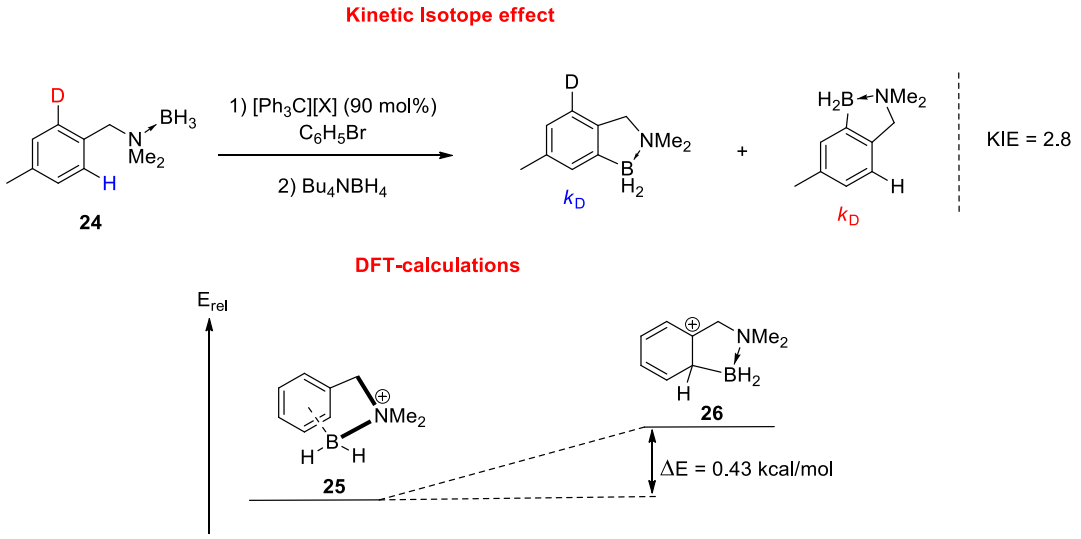

*Scheme 4.8 KIE study with N,N-(4-methyl)benzylamine-borane **24** and tritylium salt **20** (top) and DFT calculations of boron cations **25** and **26** (B3LYP/6-31G*) (bottom).*

Carbon or heteroatom-tethered phosphorous analogues have also been considered for the intramolecular borylation. In this context, phosphinite borane complexes **27** ($R_2P(OAr)BH_3$) have been shown to cyclize in the presence of 90 mol% of $[Ph_3C]^+[B(C_6F_5)_4]^-$ **20** in bromobenzene at room temperature.[11] After reduction with Bu_4NBH_4, bicyclic adducts **28** are obtained in very low yields together with a side product which has not been identified. While the activation with $[Ph_3C]^+[B(C_6F_5)_4]^-$ led to low conversions, $HNTf_2$ can also promote the reaction with a significant improvement of the yields (from 41 to 84%). For the above-mentioned activation, the benzylamine analogue suggested that typical hydride acceptors might generate transient borenium cations **29** or equivalent electrophilic species which undergo electrophilic cyclization to yield **30a,b** and **28a-i** after reductive treatment (*Scheme 4.9*).

[11] Carzola, C.; De Vries, T. S.; Vedejs, E. *Org. Lett.*, **2013**,*15*, 984.

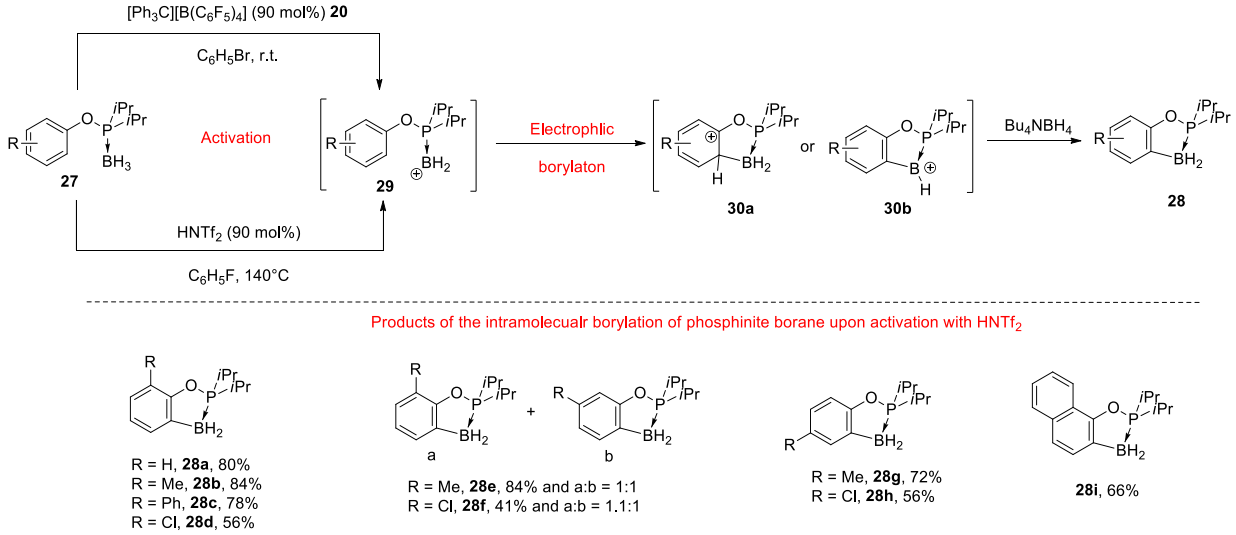

*Scheme 4.9 Electrophilic borylation of phosphinite borane complexes **27** (top) and scope of the borylation mediated by $HNTf_2$. Conditions: **27** (0.2 mmol), Tf_2NH (0.18 mmol), PhF (1 mL), 140 °C, 16 h, sealed tube, quenched with Bu_4NBH_4.*

Besides these cases, to the best of our knowledge, there are no examples of organocatalyzed borylation reactions. In view of this situation, we report in the following section a survey of the nature of the organocatalysts used in the functionalization of arenes and involving a dehydrocoupling step.

1.4. Cross-dehydrocoupling reactions catalysed by Lewis acids

Cross-dehydrocoupling reactions correspond to the connection of two different molecules entities with a formal loss of a molecule of dihydrogene.[12] In 2016, Hou et al. reported the metal-free, catalytic C–H silylation of a series of aromatic compounds such as *N*,*N*-disubstituted anilines **31** with various hydrosilanes **33** by using $B(C_6F_5)_3$ as a catalyst.[13] The authors showed that the use of 1-2.5 mol% of $B(C_6F_5)_3$ along with 3 equivalents of **33** and 1 equivalent of **31** in chlorobenzene at 120°C for 6-24h led to the formation of the para-silylated derivatives **32a-l** in yields ranging from 41 to 84% (*Scheme 4.10*). The scope of arenes includes indole and piperazine substrates.

[12] For reviews on cross-dehydrocoupling reactions, see X. M. Jie, Y. P. Shang, P. Hu and W. P. Su, *Angew. Chem., Int. Ed.,* **2013**, *52*, 3630; Kuhl, M. N. Hopkinson and F. Glorius, *Angew. Chem., Int. Ed.*, **2012**, *51*, 8230

[13] Ma, Y.; Wang, B.; Zhang, L.; Hou, Z. *J. Am. Chem. Soc.* **2016**, *138*, 3663.

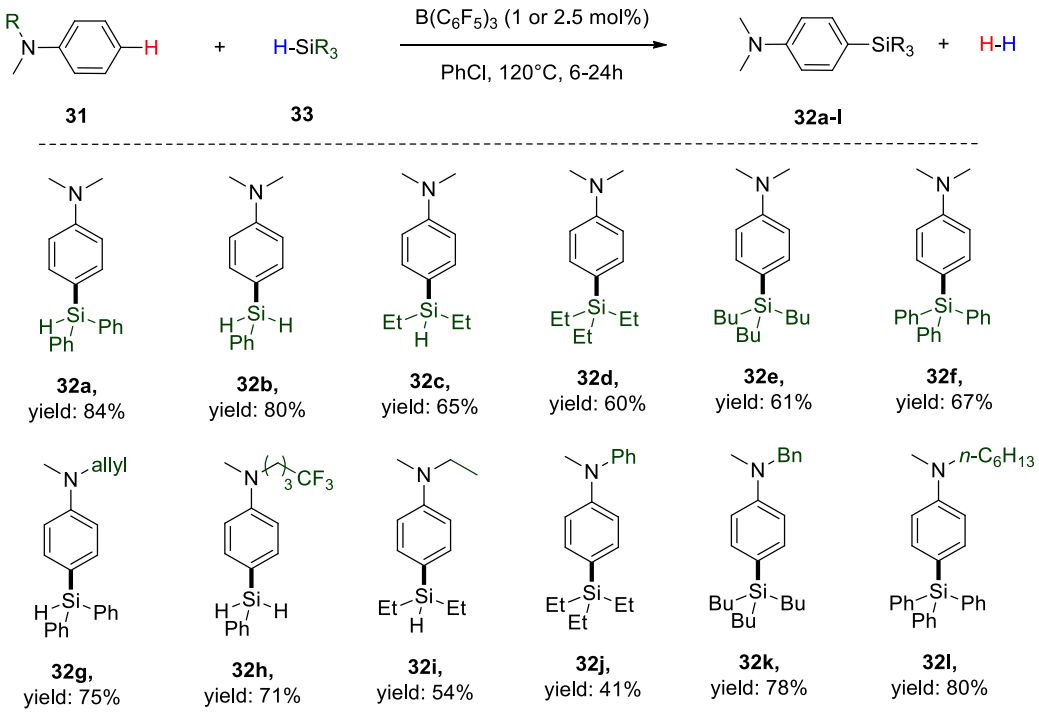

*Scheme 4.10 C–H silylation of various substituted aniline derivatives with hydrosilanes. **31** (0.25 mmol), **33** (0.75 mmol), $B(C_6F_5)_3$ (1-2.5 mol%) and chlorobenzene (0.5 mL) under N_2 at 120 °C for 6-24 h.*

According to the authors, the reaction starts with a weak activation of hydrosilane **33** by $B(C_6F_5)_3$ to generate the transient intermediate **34**, as shown in *Scheme 4.11*. The next step consists of a back-side nucleophilic attack of the para-carbon of **31** electron-demanding silicon center and would generate the ion-pair intermediate **35**. Then the formed $[HB(C_6F_5)_3]^-$ would deprotonate the later intermediate to release H_2 and regenerate the catalyst.

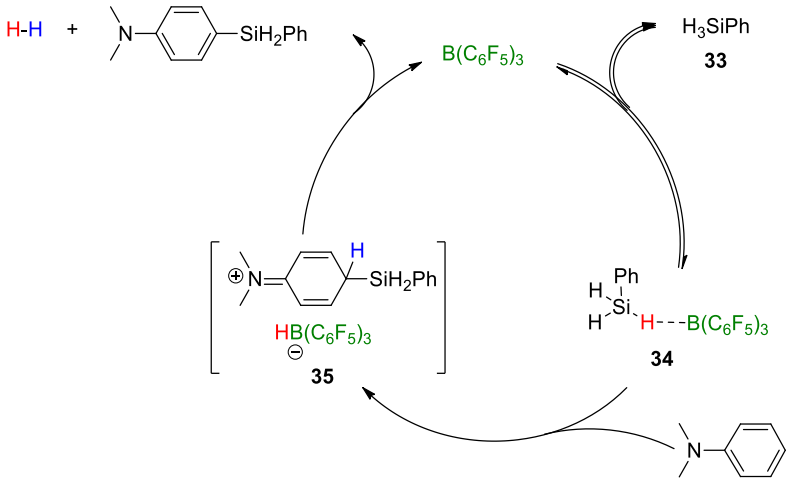

Scheme 4.11 Proposed mechanism for boron-catalyzed C–H silylation of N,N-dimethylaniline.

This example shed light on the dual role of $B(C_6F_5)_3$ which: i) behaves as a Lewis acid to generate **35** and ii) to rearomatize the latter upon loss of H_2. This example highlights a unique reactivity which would be very useful to develop new C-H activation via dehydrocoupling pathways.

2. Development of a catalytic version of the electrophilic borylation of phosphinite boranes complexes.

The abovementioned example prompted us to consider employing $B(C_6F_5)_3$ as a catalyst for the electrophilic borylation of phosphinite boranes previously reported by Vedjes with the use of stoichiometric amount of trityl cation or catalytic strong acid conditions (*Scheme 4.12*).

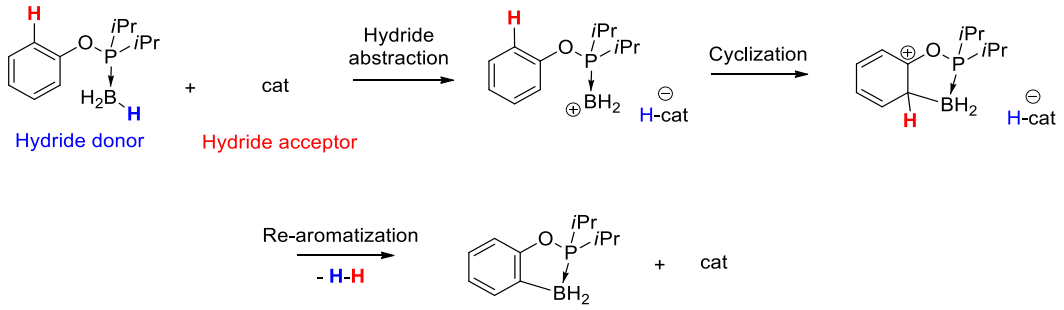

Scheme 4.12 Working hypothesis for a catalytic version of the intra-molecular borylation of phosphinite-borane complexes.

2.1. Study of transition metals and Lewis acid or Lewis base catalyzed borylation.

First of all, we targeted metal-based Lewis acids such as $FeCl_2$, $FeCl_3$, $CuCl_2.H_2O$ and $AlEt_3$. Hence, 20 mol% of each complex was mixed with phenyl di-isopropylphosphinite borane **27a** in fluorobenzene at r.t. and 100°C for 24h. However, no borylation adduct was detected in solution, and according to the chemical shift of **27a** (δ = -43.4 ppm in NMR spectroscopy), only the starting material was recovered. In another approach based on our experiences on FLP chemistry, we envisaged to involve a sterically hindered Lewis acid (for the hydride abstraction) and a sterically hindered base (for the deprotonation). The formed LA-H.LB-H complex was expected to release H_2 upon heating. Based on this strategy, we used $B(C_6F_5)_3$ as the Lewis acid and N- or P-based Lewis bases already reported in FLP chemistry (*Table 4.1*). In all the cases, no borylation adduct **28a** was detected. However, we noticed the formation of an unidentified side-product with a chemical shift of δ = -35.2 ppm in ^{11}B NMR spectroscopy (40% with respect to **27a**).

*Table 4.1 intramolecular borylation tests of **27a** by FLPs. Conditions: **27a** (0.18 mmol), B(C6F5)3 (0.04 mmol) C_6H_5F (1.0 mL). *the catalyst loading of DABCO as well as $B(C_6F_5)_3$ have been both increased to 100%.*

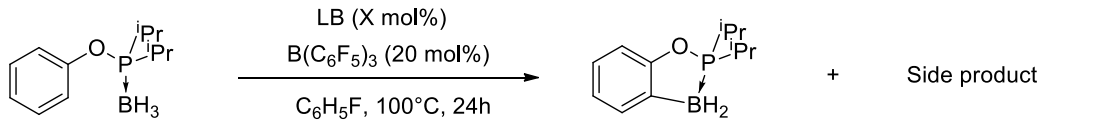

27a
^{11}B NMP, δ= -43.4 ppm

28a
^{11}B NMP, δ= -31.0 ppm

31
^{11}B NMP, δ= -35.2 ppm

Entry	Lewis base	LB loading (mol %)	**27a** (%)	Side product (%)
1	Et_3N	20	62	38
2	DABCO	20	95	5
2b*	DABCO	100	72	18
3	$^{i}Pr_2NH$	20	90	10
4	TMP	20	79	21
5	Quinuclidine	20	92	8
6	P(1-Np)$_3$	20	60	40
7	P(*o*-tol)$_3$	20	65	35

In the light of the above results, we were interested in understanding the failure of this reaction. We hypothesized that, because $B(C_6F_5)_3$ have been shown to abstract hydrides of PBs, the problem should originate from the deprotonation of the Wheland intermediate. In addition, the release of H_2 sould be more difficult than expected. To test this, we reproduced the reaction with P(1-Np)$_3$ and P(*o*-tol)$_3$ as Lewis bases and $B(C_6F_5)_3$, and we added furan as a dihydrogen scavenger[14] in order to help the regeneration of the FLP (*Scheme 4.13*).

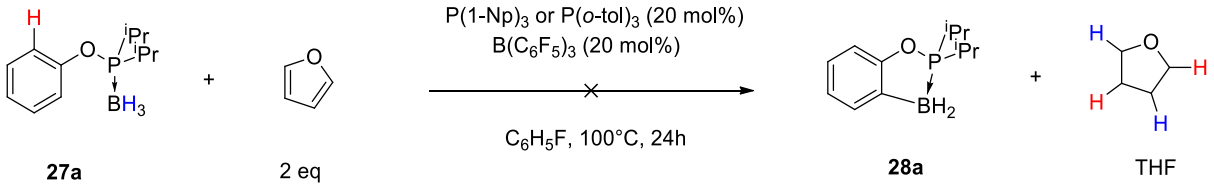

27a 2 eq **28a** THF

*Scheme 4.13 FLP catalysed test of the borylation of **27a** with furan as dihydrogen scavenger. Conditions: **27a** (0.18 mmol), furan (0.36 mmol), C_6H_5F (1.0 mL).*

While this methodology didn't allow us to observe the formation of the borylation adduct **28a**, it showed similar reaction outcomes to those reported in *Table 4.1*. This result indicates that, either the deprotonation of the Wheland intermediate does not take place or that H-bridged aggregates are formed in solution preventing the cyclization. In all cases, the addition of a Lewis bases seems unproductive.

[14] Scott, D. J.; Fuchter, M. J.; Ashley, A. E. *Angew. Chem. Int. Ed*. **2014**, *53*, 10218.

Based on Vedejs' works showing that tritylium salts are able to promote the borylation of benzylamine borane complexes.[7] A last approach was attempted using an organic Lewis acid. We employed $HSiEt_3$, $B(C_6F_5)_3$, tritylium salts and borinic acid $(2\text{-ClPh})_2BOH$ to promote the reaction. However, as shown in *Scheme 4.14*, reactions of **27a** with 20 mol% of the latter catalysts in C_6H_5F at r.t. or even at 140°C for 24h didn't led to the formation of the expected borylation adduct **28a**.

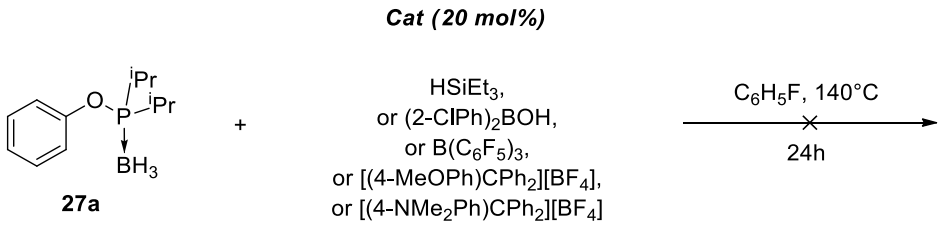

*Scheme 4.14 Unsuccessful tests of the borylation of **27a** with organic Lewis acids. Conditions: **27a** (0.18 mmol), C_6H_5F (1.0 mL).*

In the cases of $HSiEt_3$ and $(2\text{-ClPh})_2BOH$, no reaction occurred and only **27a** was detected in the final crude mixture. The use of even more stable tritylium salts, supposed to form stronger hydride donors was also inefficient.

2.2. Unravelling the origin of the failure of the catalyzed borylations

While the use of $B(C_6F_5)_3$ didn't led to the desired product, we noticed again the formation of the side product up to 52 mol% with respect to **27a** (*Scheme 4.14*). Intrigued by its recurrent formation when $B(C_6F_5)_3$ is employed as a Lewis acid, we decided to elucidate its structure. It was purified by flash column chromatography affording a stable white powder which was analysed. **27a** is characterized a 1:1:1:1 quadruplet-like at δ = 143.8 ppm in ^{31}P NMR spectroscopy corresponding to P-BH_3 (J = 89.0 Hz), and a doublet at δ = -43.4 ppm in $\{^1H\}$-^{11}B NMR spectroscopy (J = 89.0 Hz, P-BH_3). Comparatively, the new product was characterized by a broad singlet at δ = 127.1 ppm in ^{31}P NMR spectroscopy and a doublet, J = 89.0 Hz, at δ = -35.7 ppm. More interestingly, this compound revealed three peaks in ^{19}F NMR spectroscopy at δ = -128.2, -159.8 and -164.5, very similar to the C_6F_5 moiety. Finally, ^1H and ^2D NMR correlations coupled with fragmentation and high-resolution mass spectroscopy confirmed the structure of the new product as the migration of a C_6F_5 moiety to the boron atom (*Scheme 4.15*). According to the weight found after the purification of **31**, a yield of 49% was determined.

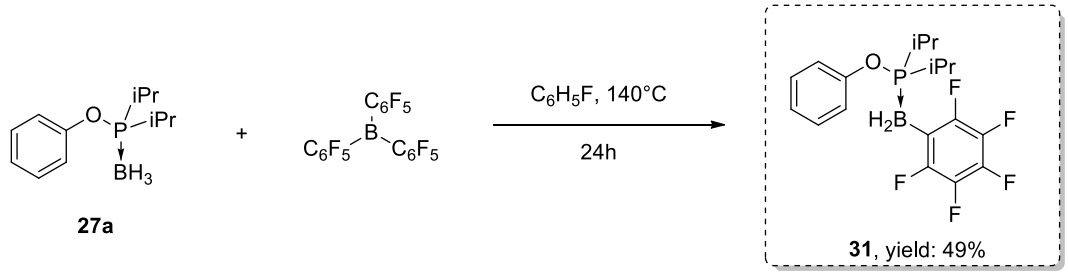

*Scheme 4.15 Identification of the structure of **31**. Conditions: **27a** (0.18 mmol), $B(C_6F_5)_3$ (20 mol%), C_6H_5F (1.0 mL).*

In the structure of **31**, the migration of only one fragment C_6F_5 is observed. Based on the yield of 49%, and on the initial loading of $B(C_6F_5)_3$ (20 mol%), it indicated that the three fragments of $B(C_6F_5)_3$ migrated. In this case, a maximum yield of 60% would have been expected. Thus it seemed crucial to us to understand the formation of this mono-migration adduct as it should provide valuable mechanistic information in explaining the failure of the expected borylation. In addition, from a synthetic point of view, R_3P-$BH_2(C_6F_5)$ complexes are almost unknown compounds in the literature despite the fact that the presence of the electron withdrawing aryl group would confer original properties to the boron atom.

3. Development of a method for the migration of C_6F_5 to phosphorus-borane derivatives

3.1. Migration of C_6F_5 from $B(C_6F_5)_3$ to PB in the literature

To the best of our knowledge, only two reports dealing with the migration of C_6F_5 have been reported so far. In 2010, Lancaster et al. have highlighted that borane dimethyl sulfide complex H_3B-SMe_2 and tris(pentafluorophenyl)borane complexed to diethylether $(C_6F_5)_3B.OEt_2$ **32**, undergo facile exchange of hydride and pentafluorophenyl ligands, yielding $(C_6F_5)_2HB.SMe_2$ **33** and $(C_6F_5)H_2B.SMe_2$ **34** depending on the ratio of reagents used (*Scheme 4.16*).[15]

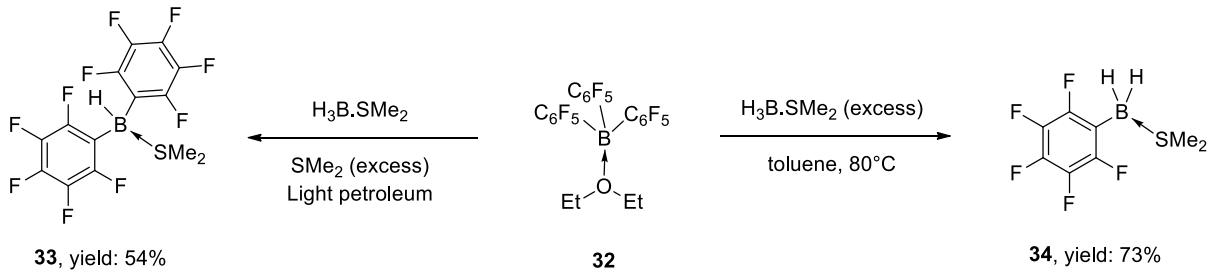

Scheme 4.16 Selective mono and double migration of C_6F_5 from $B(C_6F_5)_3$ with H_3B-SMe_2 complexes. Conditions: double-migration: $(C_6F_5)_3B_3OEt_2$ (11.0 mmol), $H_3B.SMe_2$ (5.5 mmol), 0°C, reaction time (unspecified); Mono-migration: $(C_6F_5)_3B.OEt_2$ (7.4 mmol), $H_3B.SMe_2$ (25.3 mmol), 0°C, reaction time 2h.

While the formation of **34** was accomplished with 73% yield, it decreases slightly regarding those of **33** to 54%. The authors showed that $B(C_6F_5)_3$ and H_3B-SMe_2 in petroleum ether with an excess of SMe_2 yielded **33** while **34** was obtained in the presence of an excess of H_3B-

[15] Fuller, A. M.; Hughes, D. L.; Lancaster, S. J.; White, C. M. *Organometallics* **2010,** *29*, 2194.

SMe_2 in toluene warmed at 80 °C.The other work was reported by Prokofjevs who studied the use of a base-stabilized $B_2H_5^+$ complex for borylation reactions.[16] In the course of the study, the author employed $B(C_6F_5)_3$ to generate the H-bridge **35** from Et_3N-BH_3 and promote an intermolecular borylation with nucleophiles. However, it was observed that **35** evolved at 50°C leading to adduct **36**, which results from the mono-migration of C_6F_5 (*Table 4.2*). The author suggested that **36** is the result of a disproportionation reaction involving $[HB(C_6F_5)_3]^-$ derivative. This singular reactivity was exemplified with other LB-BH_3 complexes including Ph_3P-BH_3 in 71% yield.

*Table 4.2 Synthesis of $C_6F_5BH_2$ complexes with $B(C_6F_5)_3$. Conditions: 0.36:1 $B(C_6F_5)_3$/LB-BH_3, 50°C, 1h. * reaction time 1h.* Yield are indicated with respect to Et_3N-BH_3.*

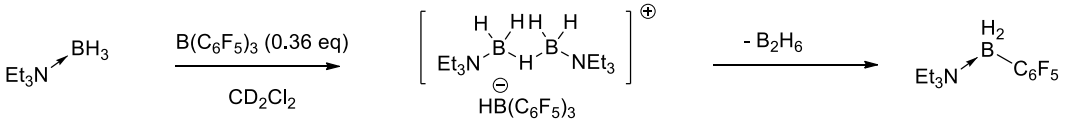

35 **36**

Entry	LB-BH_3	Solvent	Product	Yield* (%)
1*	Et_3N-BH_3	C_6H_5F	Et_3N-$BH_2(C_6F_5)$	> 99
2	Me_3N-BH_3	CH_2Cl_2	Me_3N-$BH_2(C_6F_5)$	97
3	$BnMe_2N$-BH_3	C_6H_5F	$BnMe_2N$-$BH_2(C_6F_5)$	> 99
4	Ph_3P-BH_3	CH_2Cl_2	Ph_3P-$BH_2(C_6F_5)$	71

Importantly, this study confirms that $B(C_6F_5)_3$ is an efficient hydride abstractor of phosphine borane complexes and that "$[C_6F_5]^-$" can migrate to borenium cations. Nevertheless, we were intrigued by the fact that the migration of C_6F_5 takes place faster than the rearomatization of the Wheland intermediate. With the aim to shed light on these puzzling experimental observations and focused at understanding i) the origin of the three migrations of C_6F_5, ii) the influence of the Lewis base and iii) the reaction mechanism, we embarked on a study on the migration of C_6F_5 from both a synthetic and mechanistic points of view.

3.2. Optimization of the reactions conditions

In the first place, we conducted classical optimization of the reaction parameters such as the loading and the purity of the reagents, the nature of the solvent, the temperature and the reaction time. We selected **27a** (phenyl diisopropylphosphinite borane complex) as the reference phosphinite-borane complex for this study and used commercially $B(C_6F_5)_3$, 97% purity. A summary of the results is presented in the *Table 4.3*.

[16] Prokofjevs, A. *Angew. Chem., Int. Ed.* **2015**, *54*, 13401.

*Table 4.3 Optimization of the reaction parameters for the mono-migration of C_6F_5. Conditions: **27a** (0.18 mmol, 1 eq), solvent (1.0 mL). In red: studied parameters.*

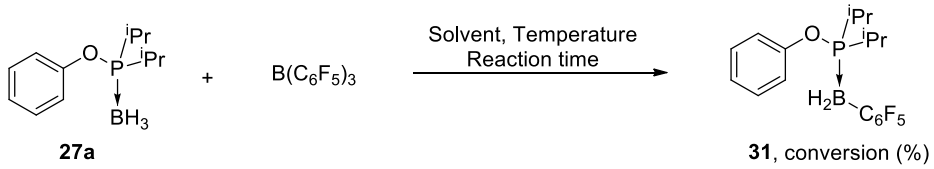

27a **31**, conversion (%)

Entry	$B(C_6F_5)_3$ (eq)	Solvent	Temperature (°C)	Reaction time (h)	Conversion 11B NMR (%)
1	0.40	C_6H_5F	140	24	>99
2	0.33	C_6H_5F	140	24	95
3	0.36	C_6H_5F	140	24	>99
4	0.36	C_6H_5Br,	140	24	66
5	0.36	$C_2H_4Cl_2$	140	24	78
6	0.36	C_6H_5F	80	24	0
7	0.36	C_6H_5F	100	24	0
8	0.36	C_6H_5F	120	24	15
9	0.36	C_6H_5F	140	1	>99

This optimization study shows that the loading in $B(C_6F_5)_3$ can be decreased to 36 mol% (theoretical 0.33 eq) to reach full conversion. In addition, we selected non-nucleophilic solvent to prevent side-reactions with the borenium cations and due to the high temperature imposed by the reaction, it was necessary to select solvents with T_{evap} > 80°C. Due to these constrains, we showed that fluorobenzene was a suitable solvent.[17] In our concern, only 15% conversion was noticed at 120°C after 24h, but a full conversion was observed at 140°C. At this temperature, the reaction time could be dropped to 1h to observe a full conversion. This point importantly differs from the results reported by Prokofjevs in the study with H_3B-PPh_3 where a temperature of 50°C was sufficient.[16]

3.3. Scope of the phosphorus borane complexes for the mono-migration of C_6F_5.

With the optimized conditions in hands, we then turned our attention on exploring the robustness of the reaction conditions and the variety of PBs susceptible to yield the mono migration adduct.

[17] Later, we found that benzene, toluene and acetonitrile are also suitable solvent even if they are also weak nucleophiles.

To reach this goal, we have synthesized 11 phosphinite-borane complexes[18] and 4 phosphine-borane complexes by modifying i) the nature of the substituents of both phosphinite and phosphines and ii) the class of phosphines. We were pleased to see that the reactions between 0.36 equivalent of $B(C_6F_5)_3$ and phosphorus-boranes adducts **37a-o** proceeded well in C_6H_5F at 140°C within 1h with isolated yields in **38a-o** ranging from 75 to 93% (*Scheme 4.17*).

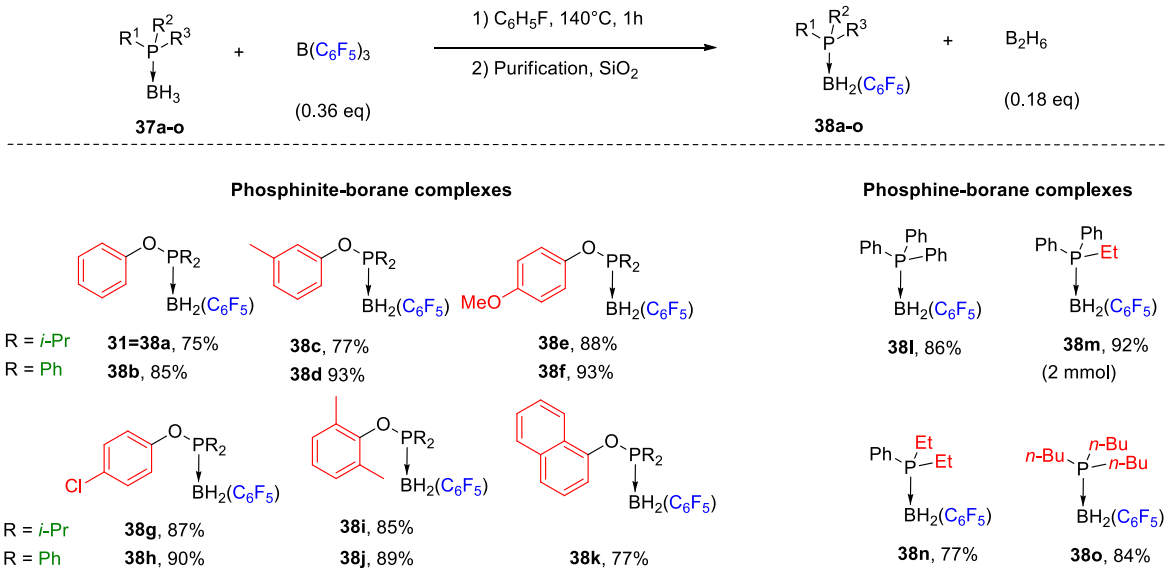

*Scheme 4.17 Scope of the migration of C_6F_5 from $B(C_6F_5)_3$ to phosphine and phosphinite-borane complexes **37a-o**. Conditions: **37a-o** (0.25 mmol, 1 eq), $B(C_6F_5)_3$ (0.09 mmol, 036 eq), solvent (c = 0.5 mol/L), 140°C, 1h. Yields were calculated after purification and isolation of **38a-o**.*

Besides, as the three C_6F_5 groups migrate, we postulated the formation of B_2H_6 at the end of the reaction. As it can be seen, in the series of phosphinite borane complexes, the nature of the aryl group tethered to the oxygen doesn't influence the yields whatever its electron donating or attracting properties. Similarly, substituting diisopropyl-P by diphenyl-P didn't modify the reaction outcomes and allowed even to slightly increase the yields. In addition, in the case of the sterically hindered (2,6-dimethylphenyl)di-isopropylphopshinite borane **37i**, we were surprised to notice that the migration proceeded well in high yields. The structure was confirmed by growing crystals from a saturated solution of **38i** in *n*-pentane and diethyl ether at -18°C for a week, suitable for X-ray crystallography (*Figure 4.1*).

[18] A scheme describing the synthesis of phosphine and phosphinite borane have been presented in the chapter 3.

*Figure 4.1 X-Ray structure of **38i**. Orange: P, Yellow: F, pink: B and red O.*

As it can be seen in the *Figure 4.1*, **38i** is characterized at the solid state by a π-stacking[19] type structure with distances of 3.306 and 3.246 between the C_6F_5 and 2,6-Me_2Ph motifs. These motifs interact one with another through π-π interactions.

While the migration takes place with phosphinite and tertiary phosphine-borane complexes in high yields, it is not the case when using secondary or primary phosphines borane complexes **37q-s**. Not only the reactions were not selective but the full conversion was not reached. Furthermore, we were not able to purify the expected products **38q-s** as they decompose on silica gel. We attributed their structures by comparison of the ^{11}B NMR spectrum with that of analogous compounds (*Figure 4.2*).

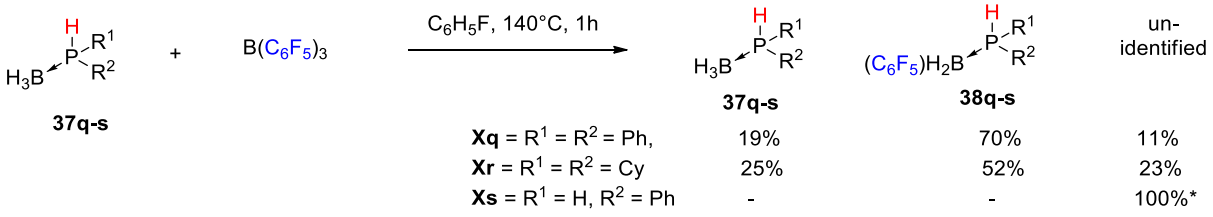

*Figure 4.2 Test of the migration of C_6F_5 to secondary and primary phosphine borane complexes **37q-s**. Conditions: **37q-s** (0.25 mmol, 1 eq), $B(C_6F_5)_3$ (0.09 mmol, 036 eq), solvent (c = 0.5 mol/L), 140°C, 1h.*In this case, several peaks were detected on the ^{11}B NMR spectra.*

As these compounds are susceptible to undergo dehydration reaction as it has been shown previously,[20] we did not investigate this reactivity in more details.

[19] Martinez, C. R.; Iverson, B. L. *Chem. Sci.* **2012**, *3*, 2191.
[20] Staubitz, A.; Robertson, A. P. M.; Sloan, M. E.; Manners, I. *Chem. Rev.* **2010**, *110*, 4023.

3.4. Example of the double migration of C_6F_5.

Because the mono-migration of C_6F_5 proceeded well under our conditions, we wondered whether we could use the same methodology to access the more challenging double migration adduct (*Scheme 4.18*). As a proof of concept, we treated **37m** with 0.69 equivalents of $B(C_6F_5)_3$.

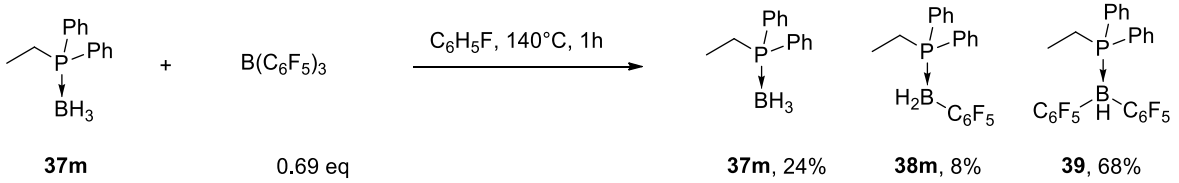

*Scheme 4.18 Investigations in the double migration of C_6F_5 with **37m**. Conditions: **37m** (0.18 mmol, 1 eq), $B(C_6F_5)_3$ (0.69 eq), solvent (c = 0.5 mol/L), 140°C, 1h. Conversion determined by ^{11}B NMR of the crude.*

The hetero-NMR (^{11}B and ^{31}P) study of the reaction mixture confirmed the formation of a new product **39** along with the known mono-adduct **38m** and the starting compound **37m**. $\{^1H\}$-^{11}B NMR spectrum showed the appearance of a broad signal with a characteristic P-B coupling constant *J* = 89.0 Hz at δ = -25.3 ppm (^{11}B NMR) and the ^{31}P NMR spectrum a broad singlet at δ = 10.6 ppm (*Figure 4.3*).

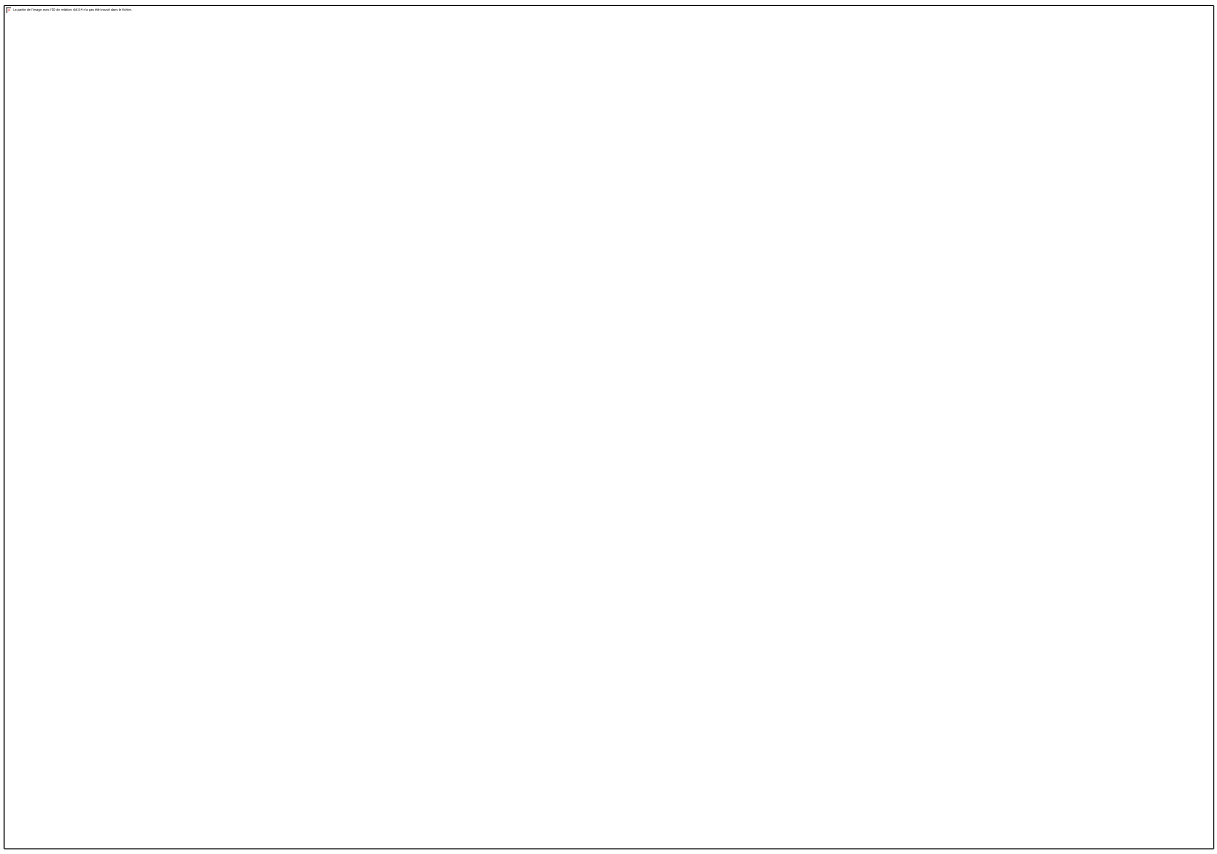

*Figure 4.3 ^1H NMR spectra of **39** in CD_3Cl_3 recorded on a 400MHz spectrometer.*

The compound **39** was purified by a quick flash column chromatography to yield a white solid. Recording ^1H NMR in $CDCl_3$ of **39** confirmed the occurrence of a double migration adduct as

the characteristic proton beared by the boron atom was attributed to the broad singlet at δ = [3.59-4.02] ppm (*Figure 4.3*). Finally, crystals suitable for X-ray diffraction of **39** were grown from a saturated solution in hexane/dichloromethane at r.t. for 3 days definitely confirming the structure of the double migration adduct. The expected compound was formed in 53% yield according to our reactions conditions (*Figure 4.4*)

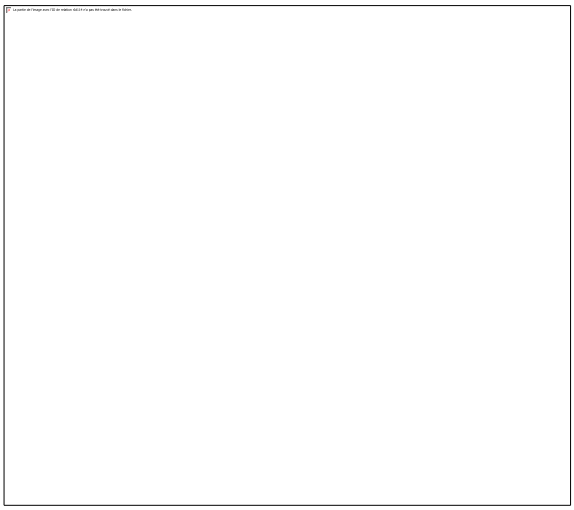

*Figure 4.4 X-Ray structure of **39**. Displacement ellipsoids are drawn at the 50% probability level. Orange: P, Yellow: F, pink: B.*

Despite our success in isolating the expected adduct, we wondered why the yield was so low (53%). Indeed, if we assume that the three fragments can migrate, we should expect a significant higher yield (theoretically, 100% with 0.69 eq $B(C_6F_5)_3$). It seems fair to postulate that the second migration equilibrates and/or is less rapid than the first one as the three C_6F_5 migrates to **37a** to yield 100% of the mono adduct. Therefore, two difficulties can occur, either i) the formed B_2H_6 in solution interact with $B(C_6F_5)_3$ to form the complex **40,** inactive toward the hydride abstraction of R_3PBH_3 or ii) because the second migration is obviously more demanding in energy than the first one, the three fragments are not able to migrate. To elucidate this question, we used our conditions with 1 equivalent of the mono-adduct and 0.36 eq of $B(C_6F_5)_3$. After 1h, analysis of the crude mixture indicated a full conversion in **38m** which was purified to yield 75% of **39**. This conclusion clearly indicates that, similarly with R_3P-BH_3, the three C_6F_5 moieties can migrate on R_3P-$BH_2(C_6F_5)$ to yield R_3P-$BH_2(C_6F_5)_2$. Moreover, it shows that it must exist interactions between B_2H_6 and $B(C_6F_5)_3$ in solution which prevent the hydride abstraction (*Scheme 4.19*).

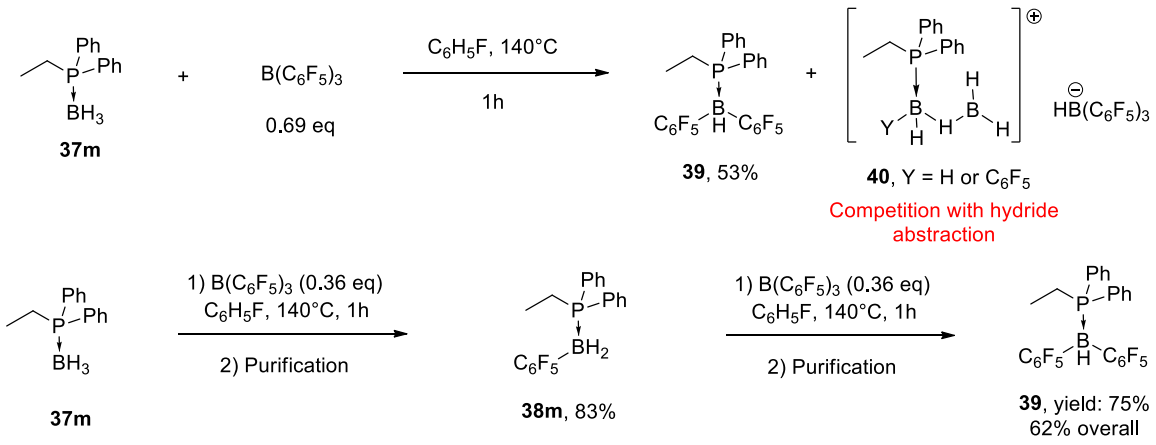

*Scheme 4.19 Summary of the double migration of C_6F_5 with **37m** or **38m**. Conditions: **37m** or **38m** (0.18 mmol, 1 eq), $B(C_6F_5)_3$ (0.36 or 0.69 eq), solvent (c = 0.5 mol/L), 140°C, 1h (isolated yields).*

4. Kinetic study of the mechanism of the migration of C_6F_5

Our study of the mono and double migration of C_6F_5 provided important structural information about the products. However, regarding the products distribution as well as the reaction mechanism, many points remain unclear. First of all, the origin of the migration of the three C_6F_5 in the cases of both the mono- and bis-C_6F_5 adducts must be investigated. We need furthermore to clarify the reaction outcomes and especially the reasons why we have never observed a mixture of mono- and bis-C_6F_5 adducts. Finally, the requirement of elevated temperature needed also to be clarified as similar reaction takes place at 50°C with benzylamine and PPh_3BH_3.

4.1. Proposed mechanism and determination of the relevant parameters to study

On the light of the above results, the following reaction mechanism can be proposed for the three consecutive migrations (*Scheme 4.20*).

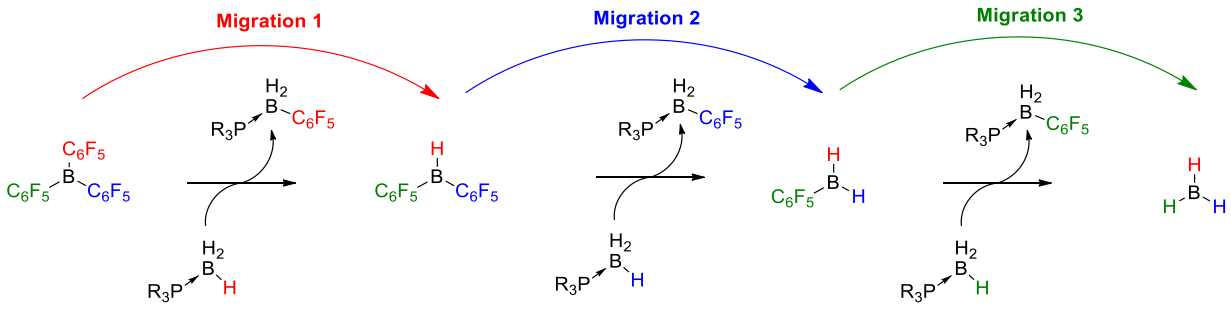

Scheme 4.20 Proposed reaction mechanism on the light of the results

In a first step, a hydride transfer takes place between the phosphorus borane complex R_3P-BH_3 and $B(C_6F_5)_3$ to form the ion pair $[R_3PBH_2]^+[HB(C_6F_5)_3]^-$. In a second step, the migration of C_6F_5 occurs to yield the mono-migration R_3P-$BH_2(C_6F_5)$ adduct and $HB(C_6F_5)_2$. At this stage, another hydride transfer takes place involving the formed $HB(C_6F_5)_2$ and R_3P-BH_3 instead of

R_3P-$BH_2(C_6F_5)$. This hypothesis must be verified by comparing the hydricity of R_3P-BH_3 and R_3P-$BH_2(C_6F_5)$. After a second migration of C_6F_5, $H_2B(C_6F_5)$ and the mono-migration product are released. The same process happens a last time to finally yield a third equivalent of R_3P-$BH_2(C_6F_5)$ (with respect to $B(C_6F_5)_3$).

To get insight into the proposal, we investigate the following parameters:

- Hydricity of R_3P-$BH_{3-n}(C_6F_5)_n$, with $0 \leq n \leq 2$.
- Energy barriers and reaction energies corresponding to the elementary steps of each migrations (Ea_1, Ea_2 and Ea_3).
- Energy barriers and reaction energies corresponding to the elementary steps of a second migration to rationalize the selectivity for the mono-migration (Ea_1', Ea_2' and Ea_3').
- Dimerization of B_2H_6.

4.2. Study of the formation of B_2H_6.

As shown in *Scheme 4.20*, BH_3 and more probably B_2H_6 must be released in the reaction mixture to rationalize the migration of the three C_6F_5 fragments. With the aim to verify this, we have designed an experimental set-up (*Figure 4.5*). In a sealed flask, $B(C_6F_5)_3$ and **37o** (Bu_3PBH_3) were stirred in C_6H_5F at 140°C for 1h. At the end of the reaction and by maintaining the temperature at 140°C, the produced gas of the flask was bubbled in a solution of concentrated PPh_3 in CH_2Cl_2 (1.0 mol/L), by opening the connector A. Then the solution of B was concentrated under reduced pressure to remove all volatiles and analysed by NMR spectroscopy.

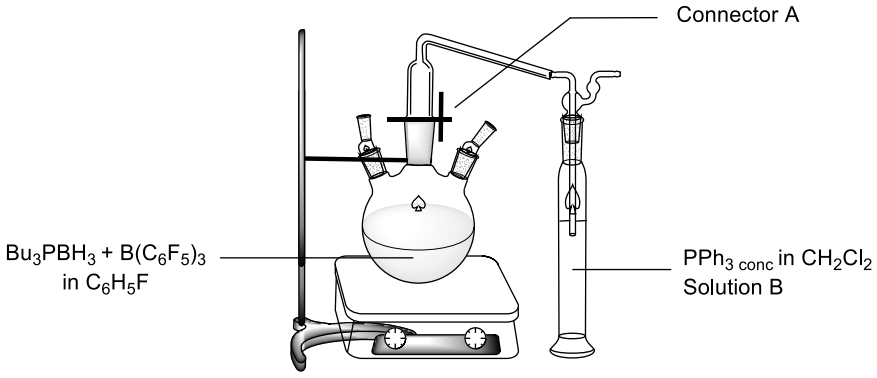

Figure 4.5 Experimental set-up for the quenching of BH_3.

As shown in *Figure 4.6*, we observe the presence of a broad singlet at δ = 21.2 along with two singlets at δ = -5.5 and δ = 29.1 in the ^{31}P NMR spectrum, corresponding to PPh_3 and $(O)PPh_3$, respectively. In addition, ^{11}B NMR spectroscopy revealed the appearance of a broad singlet at δ = -37.4 ppm which correlated with the later signal at δ = 21.2 ppm, confirming the formation

of Ph_3P-BH_3 and thus the formation of either BH_3 or B_2H_6 (more probably). Finally, we verified that B_2H_6 does not come from Bu_3PBH_3 which could decompose into PBu_3 and BH_3 upon warming by reproducing the test without $B(C_6F_5)_3$.

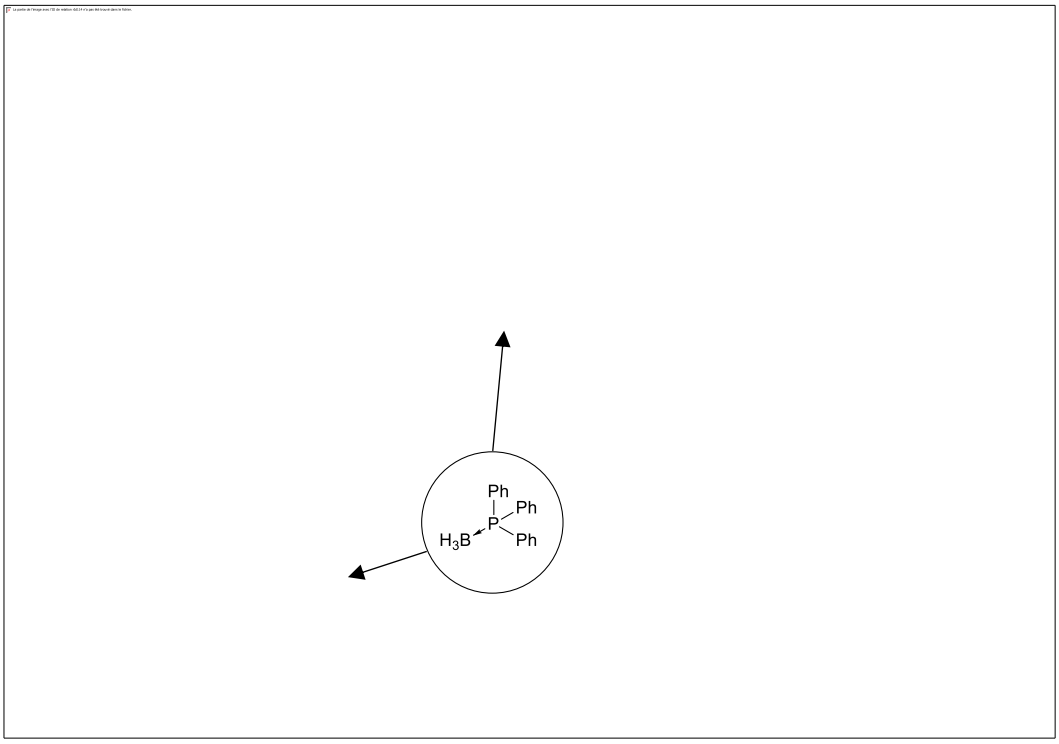

Figure 4.6 ^{11}B (dark-red) and ^{31}P (black) NMR spectra of the solution B in $CDCl_3$.

This BH_3-quenching trapping study confirms the formation of B_2H_6 in the mixture and in the gaseous form at the end of the reaction.

4.3. Measurement of the effect of C_6F_5 on the hydricity of R_3P-$BH_{3-n}(C_6F_5)_n$, $0 \leq n \leq 2$.

Another goal of this study was to understand the origin of the selective formation of the mono-adducts (**38a-s**, see *Scheme 4.17*) with 0.36 equivalents of $B(C_6F_5)_3$, which could be due to lower hydricity of R_3P-$BH_{3-n}(C_6F_5)_n$ when $_n$ increases.

As a model of the effect of C_6F_5, we measured the hydricity of $Et(Ph)_2P$-BH_3 **37m**, $Et(Ph)_2P$-$BH_2(C_6F_5)$ **38m** and $Et(Ph)_2P$-$BH(C_6F_5)_2$ **39** by using Mayr linear free energy relationship which has been largely discussed in chapter 3.

$$\log k_{20°C} = s_N(E + N) \qquad (1)$$

We used benzhydrylium salts **41a-d**[21] as reference electrophiles and studied their reaction under pseudo-first order conditions for the determination of k_2. The results are gathered in *Table 4.4*. Because the formation of **39** requires a significant amount of $B(C_6F_5)_3$, we measured

[21] The chemical structure of diarylcarbenium cations **41a-d** can be found in the chapter 3 by looking at the electrophilicity parameter provided in the *Table 4.4*.

kinetics of its reaction with **41a** to compare the second order rate constant of the three nucleophiles with the same electrophile **41a**.

*Table 4.4 Measurement of the nucleophilicity parameters of $Et(Ph)_2P\text{-}BH_{3-n}(C_6F_5)_n$ **37m**, **38m** and **39** at 20°C in CH_2Cl_2.*

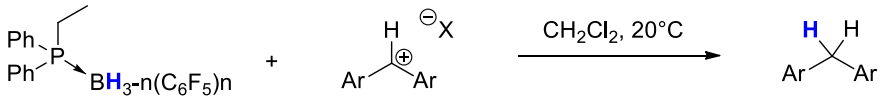

37m, n = 0
38m, n = 1
39, n = 2

41a-d

$Et(Ph)_2P\text{-}BH_{3-n}(C_6F_5)_n$	Ar_2CH^+	*E*	k_2 ($L.mol^{-1}.s^{-1}$)	*N* / s_N
37m, n=0	**41a**	-3.85	7.32×10^2	7.36 / 0.83
	41b	-4.72	1.92×10^2	
	41c	-5.53	3.45×10^1	
	41d	-5.89	1.48×10^1	
38m, n=1	**41a**	-3.85	1.02×10^1	5.20 / 0.74
	41b	-4.72	2.32	
	41c	-5.53	5.32×10^{-1}	
	41d	-5.89	3.24×10^{-1}	
39, n=2	**41a**	-3.85	5.42×10^{-1}	n.d.

The measured nucleophilicity values of the hydride from **37m** and **38m** show that substituting a hydrogen with a C_6F_5 resulted in decreasing significantly *N* from 7.36 to 5.20. This can obviously be attributed to the electron-withdrawing effect of the perfluorinated substituent. Interestingly, we observe a slight diminution of the specific sensitivity nucleophilicity parameter s_N (0.83 to 0.74), highlighting that the nature of the nucleophilic center is almost unchanged. These data provide strong kinetic insights to explain the exclusive formation of the mono-adduct $R_3P\text{-}BH_2(C_6F_5)$ and confirm that the hydride transfer is a key-step of the mechanism.

To further evaluate the effects of C_6F_5 on the hydricity of $R_3P\text{-}BH_{3-n}(C_6F_5)_n$, we also measured the second order rate constant of the reaction of **39** with **41a** and compare it with those found when employing **37m** and **38m** (*Scheme 4.21*). This study revealed that while the first migration leads to the formation of **38m** that is about 72 times less reactive than the parent one, the second migration does not affect tremendously the hydricity of **39**.

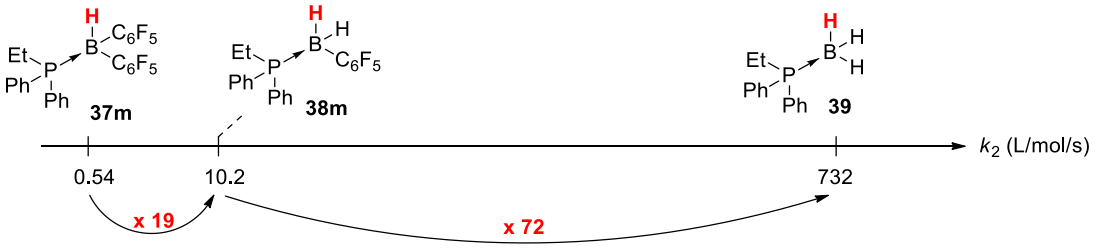

*Scheme 4.21 Plot of the second order rate constant of the reactions of **37m**, **38m** and **39** with **41a** at 20°C in CH_2Cl_2.*

5. Computational study of the migrations of C_6F_5

Because the access to reaction intermediates $HB(C_6F_5)_2$ and $H_2B(C_6F_5)$ resulting from the first and the second migration of C_6F_5 have not been isolated, we decided to undertake a computational study of the mechanism of the reaction. This was carried out at the laboratoire de Chimie Théorique (LCT) in Paris under the supervision of Prof. Hélène Gérard.

In this part, the C_6F_5 group will be sometimes abbreviated Y.

5.1. Description of the system and tools

A mathematical and quantum description is required to calculate any chemical system. It includes i) the basis set to express the molecular orbitals, ii) the functional to calculate the energy of the system and iii) a model to describe the solvent.

5.1.1. Choice of the basis set

An atomic orbitals derived basis set is used and we have chosen the 6-31++G(d,p). In this description, 6 primitive gaussian represent each core atomic orbital basis function. Regarding the valence orbitals, they are described by two basis functions: (*double-zeta*), i) a linear combination of 3 primitive Gaussian functions and ii) another one Gaussian function. To better represent the atoms and improve the modelling of core electrons, we added d-polarization to all atoms (and p on hydrogen atoms). Finally, because the molecules involved in our study are highly polar and thus carry out negatively charges centers, it is necessary to add diffuse functions on all atoms (++) which allow some radical flexibility of the wave function.

No test on the effect of the basis set was carried out. Indeed, due to the size of the system, we used the basis set 6-31++G(d,p) which is a good compromise to get acceptable calculation time.

5.1.2. Choice of the functional

As DFT-calculations strongly depend on the nature of the functional, it is important to verify the deviations of the reaction energies with respect of the functional. For that purpose, we studied the simple system presented in the *Scheme 4.22* undergoing a hydride exchange between **42a** and BH_3 yielding either a separate ion pair **43** or a H-bridge **44**. Calculations were done with

five different functionals. Solvent effects were included using a PCM approach as these transformations result in charged intermediates.

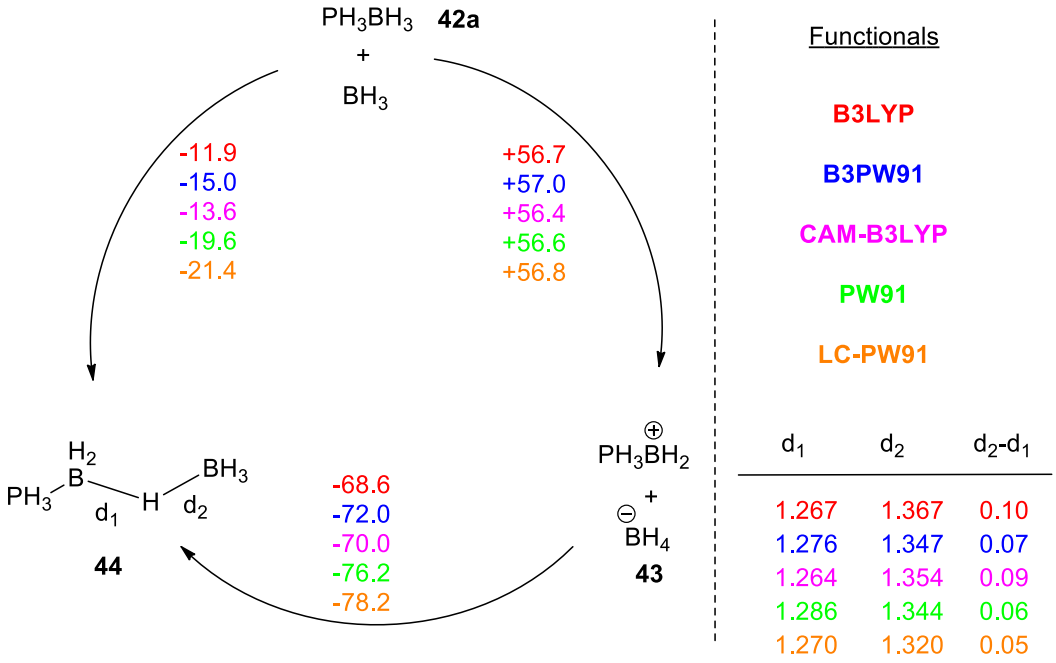

*Scheme 4.22 Effect of the functional on the energies of neutral **44** and charged intermediates **43** involved in the hydride migration between **42a** and BH_3. Conditions: 6-31++G(d,p), solvent : PCM. Energies are given in kcal/mol and distances in Å*

First, we can notice that all functionals furnish the same results for the direct hydride transfer yielding **43** with less than 0.6 kcal/mol difference. However, regarding the calculation of the hydride bridge **44**, we can observe significant differences. In particular, the formation of the hydride bridge **44** is 9.5 kcal/mol more favourable with LC-PW91 than with B3LYP. Bond distances act in a same way as the d_2 distance is also found to be the longer for B3LYP and the shorter for LC-PW91. As a consequence, H-bridges are significantly differently described with LC-PW91 and B3LYP. Consequently, we have chosen to compute all reaction pathways with both LC-PW91 and B3LYP.

5.1.3. Modelling the solvent

A last important point is the description of the solvation of molecules. Both explicit and implicit solvations were considered.

We used the Polarizable Continuum Model (PCM) which consist in approximating the solvent as a structureless, dielectric medium whose interaction with the solute is mediated by its permittivity, ε. The solute is accommodated inside a molecular cavity, built as a set of interlocking spheres centered on the atoms constituting the molecule under investigation. The surface of this cavity is covered by charges as a consequence of the polarization of the dielectric medium. These charges interact with the electronic density of the molecules in the

cavity, thus resulting in a response of the molecule electronic structure to the polarization of the solvent.

We also evaluated the coordination potential of the solvent to borane and thus the necessity to add also an explicit representation. Coordination of fluorobenzene to BH_3 was found to be exothermic by 1.9 kcal/mol with B3LYP and by 5.4 kcal/mol with LC-PW91, and is thus thermodynamically impossible when entropic contributions are taken into account. Consequently, we calculated structures by involving a molecule of fluorobenzene in the calculation (explicit) only for borenium cations and by considering implicit (PCM) C_6H_5F for all systems. Indeed, the coordination of C_6H_5F to the borenium $[H_3PBH_2]^+$ is exothermic by 10.7 kcal/mol with B3LYP and by 16.7 kcal/mol with LC-PW91.

The effect of the solvent has been studied on the three migrations of C_6F_5 from $B(C_6F_5)_3$, $HB(C_6F_5)_2$, $H_2B(C_6F_5)$ to H_3PBH_3 **42a** by supposing the formation (*Table 4.5*) (i) of a separated ion pair between borohydride and a borenium cation[22] coordinated to C_6H_5F **45** or (ii) the formation of a hydride-bridged dimer **46**.

Table 4.5 Effect of the solvent and the method to take it into account.

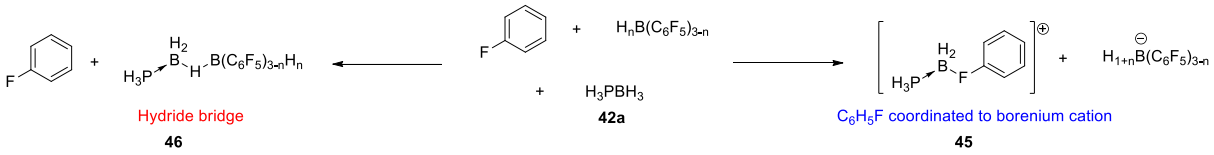

ΔE (kcal/mol)	n = 0, first migration		n = 1, second migration		n = 2, third migration	
Model	H-bridge	Ion pair	H-bridge	Ion pair	H-bridge	Ion pair
Explicit	+0.3	+87.6	-7.0	+94.2	-6.8	+111.3
PCM explicit-implicit	+0.5	+31.9	-4.3	+36.1	-7.3	+42.2

Regarding the formation of **46**, the use of PCM does not hardly influences the energy of the system as no charged intermediates are involved. However, the use of PCM decreases the endothermicity of the borohydride-borenium ion pair **45** formation by a large increasing value as the substitution of the latter decreases (from 55.7 kcal/mol for the first migration to 69.1 kcal/mol in the case of the third migration). In line with a larger delocalization of the minus charge by the C_6F_5 moiety, the more C_6F_5 are present, the lesser the PCM correction.

[22] According to our kinetic study, the formation of the borenium cation would be the less favourable steps of the reaction mechanism.

5.2. Thermodynamic study of the successive migrations.

5.2.1. Calculations of the reaction energies

We initiated this study by calculating the reaction energies of the three migrations in order to verify their exergonicity. To do so, we used H_3PBH_3 **42a**, Ph_3PBH_3 **37l**, Me_3PBH_3 **42b** and $PhOP(Me)_2BH_3$ **42c** in order to evaluate the effects of the substituents on the phosphorous (*Table 4.6*). In addition, two cases have been distinguished, depending on the dimerization of BH_3 to B_2H_6 at the end of the reaction.

*Table 4.6 Calculations of the energies reactions between PH_3BH_3 **42a**, Ph_3PBH_3 **37l**, Me_3PBH_3 **42b,** $MeOPMe_2BH_3$ **42c** and $B(C_6F_5)_3$ in the gas phase. Conditions: B3LYP, 6-31++G(d,p), PCM. Values in parentheses have been computed with the functional LC-PW91.*

No dimerization of BH_3

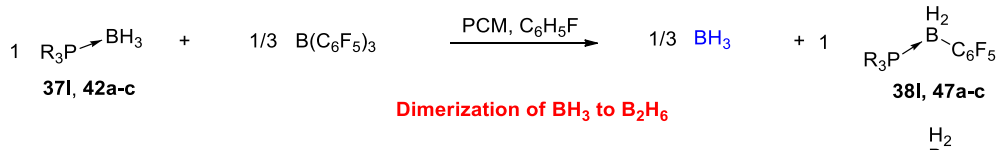

Dimerization of BH_3 to B_2H_6

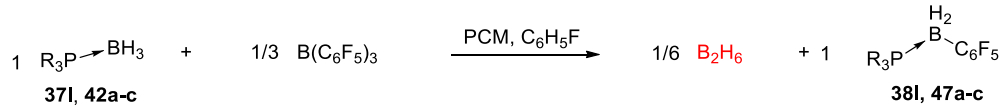

R_3PBH_3	No dimerization of BH_3		Dimerization of BH_3	
	ΔE (kcal/mol)	ΔG (kcal/mol)	ΔE (kcal/mol)	ΔG (kcal/mol)
H_3PBH_3 **42a**	+1.3 (-0.2)	+2.5 (-0.6)	-5.3 (-9.1)	-1.3 (-6.7)
Ph_3PBH_3 **37l**	+1.3	+2.6	-5.2	-1.3
Me_3PBH_3 **42b**	-0.8	+0.5	-7.3	-3.4
$MeOPMe_2BH_3$ **42c**	-0.2 (-0.4)	+0.6 (-0.3)	-6.7 (-9.3)	-3.2 (-6.5)

It can be seen that substitution of the phosphine stabilizes the products, in particular in the case of tri-alkylphosphine borane complexes **42b** for which the reaction energy is decreased by about 2 kcal/mol with respect to H_3PBH_3 or Ph_3PBH_3. Replacing one methyl by a methoxy only slightly decreases this effect. On the other side, dimerization of BH_3 is exothermic by 19.8 kcal/mol (B3LYP) and this exothermicity is large enough not to be totally counterbalanced by the entropic cost of dimerization. The exothermicity of the dimerization is even increased to 26.7 kcal/mol when using LC-PW91 showing the high stabilization of H-bridges with this functional. When included in the ligand exchange reaction described above with a 1/3 stoichiometric coefficient, this dimerization appears as a driving force of the reaction which becomes exothermic and exergonic whatever the substitution of the phosphine. Because the calculations are significantly shorter with H_3PBH_3, we will perform the calculations with this phosphine-borane complex as a surrogate of triarylphosphine boranes.

5.2.2. Calculations of the reaction energies for successive steps

We have shown that the overall migrations reactions between BY_3 and **42a** or **42c** are exothermic and exergonic regardless the nature of the functional. However, we noticed a better stabilization of the H-bridges intermediates using LC-PW91. With the aim to better understand the effect of the functional on the reaction energies, we calculated each successive migrations of Y from BY_3 to **42a** and **42c** with both B3LYP and LC-PW91 when a H-bridge is involved via the dimeric boranes intermediates (*Figure 4.7*).

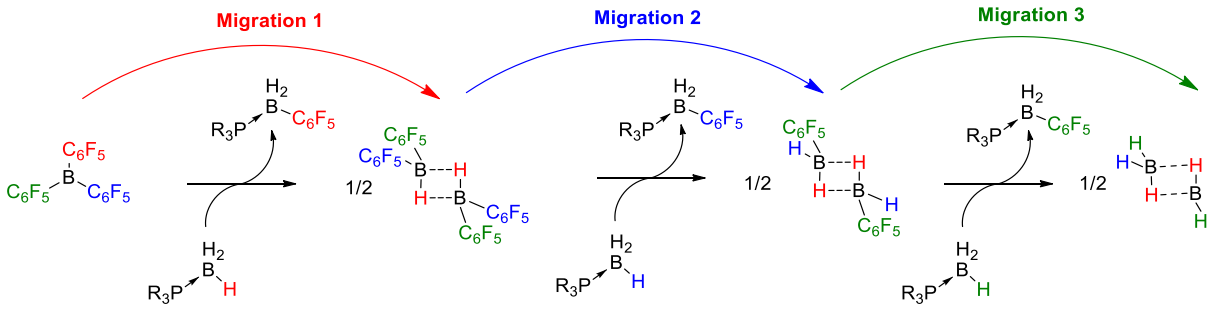

*Figure 4.7 Study of the 3 successive migrations of Y from BY_3 to **42a** and **42c**.*

In the *Table 4.7* are gathered the reaction energies corresponding to each migrations of Y to **42a** or **42c** with B3LYP and LC-PW91. It can be seen that each migration is thermodynamically favourable as the Gibbs free energies is negative and thus, the three migrations are clearly exergonic as well as the overall reaction.

*Table 4.7 Calculations of the energies reactions of each migration between PH_3BH_3 **42a**, $MeOPMe_2BH_3$ **42c** and $B(C_6F_5)_3$ in the gas phase. Conditions: B3LYP, 6-31++G(d,p), PCM. Values in parentheses have been computed with the functional LC-PW91*

R_3PBH_3	E or G (kcal/mol)	First migration	Second migration	Third migration
42a	ΔE	-8.9 (-19.2)	-4.9 (-4.5)	-2.0 (-3.3)
	ΔG	+0.2 (-12.2)	-4.1 (-5.0)	-0.2 (-2.9)
42c	ΔE	-10.4 (-19.7)	-6.4 (-4.8)	-3.4 (-3.5)
	ΔG	-1.7 (-11.9)	-6.0 (-4.8)	-2.0 (-2.7)

This trend is valid for both computational level with a significalty greater stabilization at the LC-PW91 level (≈ 10 kcal/mol). For instance, in the case of the first migration, we can see that the reaction energies are significantly different with B3LYP and LC-PW91. Indeed, $\Delta G_{H3PBH3}^{B3LYP} = +0.2$ kcal/mol while $\Delta G_{H3PBH3}^{LCPW91} = -12.2$ kcal/mol and $\Delta G_{MeOPMe2BH3}^{B3LYP} = -1.7$ kcal/mol while $\Delta G_{MeOPMe2BH3}^{LCPW91} = -11.9$ kcal/mol. This clearly supports that H-bridges are much more stabilized by LC-PW91 than B3LYP. That's why, because in the first migration, a H-bridge is formed, a significant difference is observed in the reaction energies between the two functionals.

5.2.3. Interactions between reactants or intermediates

We next examined the structure resulting from the interaction of the phosphine borane with H_nBY_{3-n}. These results were already presented in the *Table 4.5* but a more extensive study is still needed. We observe that the formation of a hydride-bridge **46** between **42a** and the three boranes leads to an energetically unfavoured adduct (ΔE > 0) when starting from the dimeric form of the boranes.

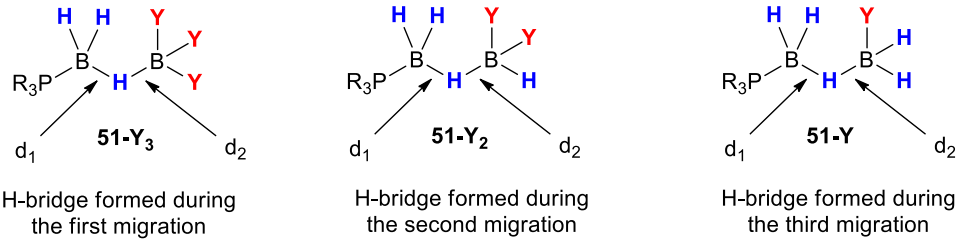

Scheme 4.23 Structure of H-bridges postulated during each migration.

The evolution of the distance of the H-bonding as well as the B-H-B angle has been revealed to be a good marker of its stability (*Scheme 4.23*). For instance, in the case of H-bridges between **42a** and H_nBY_{3-n}, the distance of the H-bonding is decreased from 1.403 Å (n = 1), 1.362 Å (n = 2) and 1.387 Å (n = 3) and the B-H-B angle from 136.3, 125.6 and 126.9°, respectively. Nevertheless, the binding energy is small in all cases except for the first migration computed with LC-PW91 (less than 10 kcal/mol in absolute value) and these species are thus not thermodynamically stable when entropic effects are taken into account (*Table 4.8*). This is especially the case for the formation of the hydride bridge as **51-Y_3** doesn't occur at r.t. as the Gibbs free energy associated to its formation is high: ΔG = 15.3 and 18.3 kcal/mol with H_3PBH_3 **42a** and $MeOPMe_2BH_3$ **42c**, respectively. *This result is in line with the fact that we were not able to detect the formation of any intermediates* ***51-Y_n*** *(n = 1-3).*

Table 4.8 Calculations of the energies reactions for the formation of H-bridges between ***42a*** *or* ***42c*** *and H_nBY_{3-n} in the gas phase. Conditions: B3LYP, 6-31++G(d,p), PCM. Values in parentheses have been computed with the functional LC-PW91.*

R_3PBH_3	E/G in kcal/mol and d in Å	First migration	Second migration	Third migration
42a	$\Delta E_{H\text{-bridge}}$	+1.0 (-13.1)	+0.8 (-1.0)	+3.2 (+1.5)
	$\Delta G_{H\text{-bridge}}$	+15.3 (+ 2.2)	+5.4 (+5.6)	+7.9 (+7.2)
	d_1	1.2907 (1.2697)	1.2767 (1.2698)	1.2664 (1.2702)
	d_2	1.4033 (1.3373)	1.3624 (1.3216)	1.3868 (1.3244)
42c	$\Delta E_{H\text{-bridge}}$	+2.1 (-12.5)	+0.7 (-1.4)	+2.5 (+0.7)
	$\Delta G_{H\text{-bridge}}$	+18.3 (+4.1)	+6.8 (+6.4)	+9.3 (+7.4)
	d_1	1.3042 (1.2733)	1.2864 (1.2774)	1.2723 (1.2758)
	d_2	1.4026 (1.3492)	1.3500 (1.3150)	1.3841 (1.3175)

Decomposition of these species to an ion pair (borenium and borohydride) is highly disfavoured, even when including coordination of C_6H_5F to the borenium cation. It can be excluded that **45** would be formed as an intermediate in the reaction mechanism. It can never be proposed that the transition state may have some kind of ion-pair character.

5.2.4. Double migration to the same phosphine borane complex.

With the aim to evaluate the competitive formation of adducts resulting from the double migration of C_6F_5 from $B(C_6F_5)_3$ to **42a** and **42c**, we calculated the thermodynamics of the formation of **48a,c** with and without considering the dimerization of BH_3 (*Table 4.9*).

*Table 4.9 Calculations of the reaction energies of the double migration between PH_3BH_3 **42a**, Ph_3PBH_3 **37l**, Me_3PBH_3 **42b,** $MeOPMe_2BH_3$ **42c** and $B(C_6F_5)_3$ in the gas phase. Conditions: B3LYP, 6-31++G(d,p), PCM. Values in parentheses have been computed with the functional LC-PW91.*

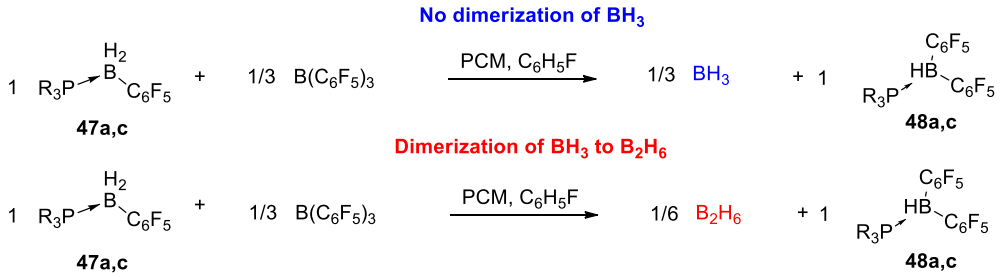

R_3PBH_3	No dimerization of BH_3		Dimerization of BH_3	
(Product)	ΔE (kcal/mol)	ΔG (kcal/mol)	ΔE (kcal/mol)	ΔG (kcal/mol)
H_3PBH_2Y **47a**	+1.3 (-0.2)	+2.5 (-0.6)	-5.3 (-9.1)	-1.3 (-6.7)
H_3PBHY_2 **48a**	+3.6 (+2.0)	+2.7 (+2.2)	-2.9 (-7.0)	-1.2 (-4.0)
$MeOPMe_2BH_3$ **47c**	-0.2 (-0.4)	+0.6 (-0.3)	-6.7 (-9.3)	-3.2 (-6.5)
$MeOPMe_2BH_3$ **48c**	+6.5 (+3.1)	+8.0 (+4.5)	0.0 (-5.9)	+4.1 (-1.7)

In this case, it can be seen that the substitution of the phosphine destabilizes the products as the formation of **48c** is less favourable than that of **48a** by about 2.9 kcal/mol by considering the dimerization of BH_3 with the functional B3LYP. This tendency is confirmed when the calculations are reproduced with LC-PW91 but the difference ranges from 1.1 to 2.3 kcal/mol in the case of the dimerization for the energy and the energy free Gibbs respectively. Importantly, even by considering the dimerization of BH_3 to B_2H_6, the formation of **48c** becomes endothermic and endergonic while the reverse case is observed for the formation of **48a** with B3LYP. Indeed, by comparing these data with those gathered in the *Table 4.6*, the formation of **47c** is thermodynamically favoured compared to **48c** by about 7 kcal/mol with B3LYP and 5 kcal/mol with LCPW91. *On the light of these results, formation of the double migration of C_6F_5*

*from $B(C_6F_5)_3$ to the same phosphine borane complex will be disfavoured compared to two simple migration to two phosphine borane complexes **42a-c**.*

5.3. Designing a simple model to describe both the hydride and the C_6F_5 migrations.

5.3.1. A simple model of the hydride exchange

Before investigating in detail, the reaction mechanism, we needed to understand how both the hydride transfer and the aryl migration take place. For that purpose, we built a simple system composed by H_3P-BH_3 **42a** (surrogate of phosphine and phosphinite borane complexes) and BH_3 in order to investigate the hydride exchange occurring in the H-bridge adduct. Based on this system, two structures TS-**49-I** and TS-**49-N** have been located as transition states (TS) which differ by *the number of hydrogen beared on boron atoms* (*Figure 4.8*). Then, it was shown that both transition states connect on both sides of the reaction paths to the hydride-bridged structures.

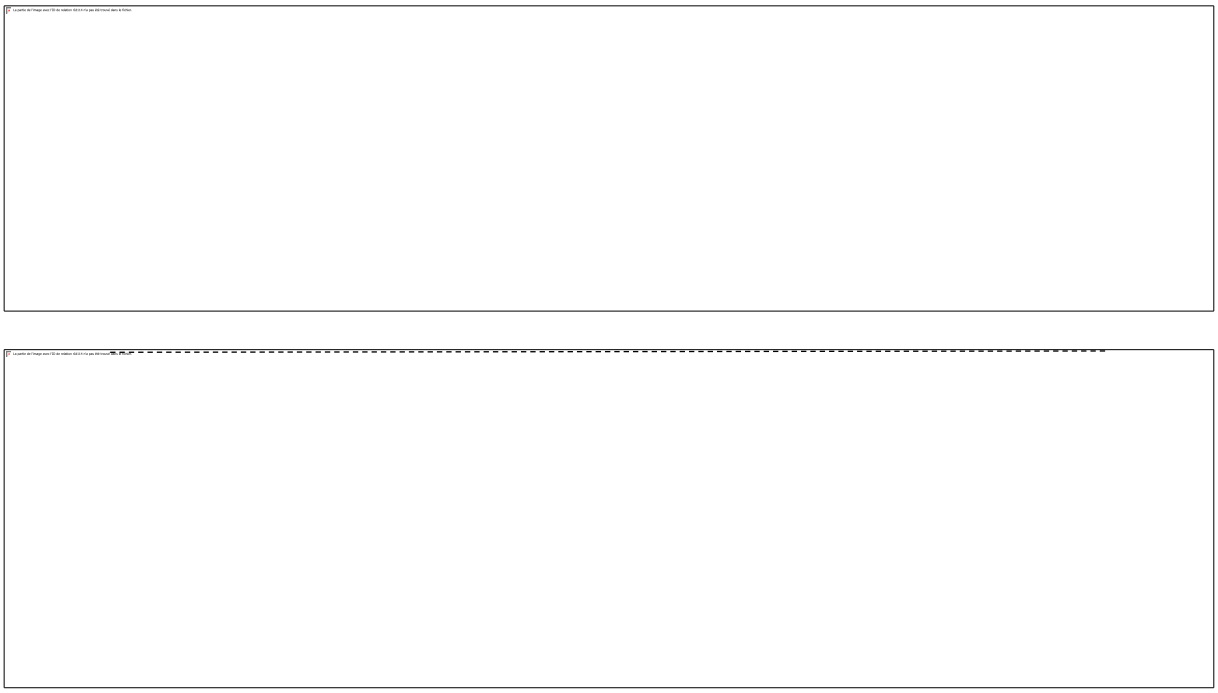

*Figure 4.8 (top) Ionic transition state TS-**49-I** of the exchange of hydrogen (in red and blue) and connected structures **42a**. (bottom) Neutral transition state TS-**49-N** of the exchange of hydrogen (in red and blue) and connected structures **42a**. Conditions: B3LYP, 6-31++G(d,p), solvent : C_6H_5F, PCM.*

Interestingly, the two different transition states TS-**49-I,N** can also be differentiated by the "charge" separation in their formal description: TS-**49-I** can indeed be described as ionic, with four short B-H bonds on the same boron atom whereas TS-**49-N** is neutral. Regarding energies of the TS, it can be seen that the "ionic" one TS-**49-I** is 9.4 kcal/mol higher in energy than TS-**49-N** with B3LYP but only 2.9 kcal/mol with LC-PW91. This is in line with the high energy of the borenium-borohydride ion pair found in the previous part. Besides, a closer look at the

"neutral" transition state TS-**49-N** shows that it implies the exchange of hydrogens beared by the P-B adduct and not the borane. *However, in our synthetic cases, C_6F_5 which are involved in the migration must originate from the borane. It shows that, probably, the neutral transition state TS-**49-N** is not relevant in our case because it cannot be transferred to a mechanism leading to the desired product*.

5.3.2. Simple model of the hydride exchange in the presence of C_6F_5.

Because the last migration of C_6F_5 from $H_2B(C_6F_5)$ to **42a** is the easiest to calculate owing to the low number of atoms, we evolved our simple model to another containing only one C_6F_5 group. In a first time, we still investigated the hydride exchange (*Figure 4.9*).

*Figure 4.9 (top) Ionic transition state TS-**50-I** of the exchange of hydrogen (in red and blue) and connected structures **51** after optimization. (bottom) Neutral transition state TS-**50-N** of the exchange of hydrogen (in red and blue) and connected structures **51** after optimization. Conditions: B3LYP, 6-31++G(d,p), no solvent. ΔG calculated in relation to **51**.*

First of all, we can see that the transition states and optimized structures are similar to these observed in absence of C_6F_5. In particular, regarding the ionic transition state TS-**50-I**, the borenium cation don't coordinate to the ortho-fluorine of C_6F_5 ring. Besides, we found that the presence of C_6F_5 importantly decreases the Gibbs free energy of the neutral transition state TS-**50-N** compared to ionic one TS-**50-I** (differences of 14.9 kcal/mol with B3LYP and 4.5 kcal/mol with LC-PW91 are noticed). *Finally, like in the previous case, we found that the TS-**50b** should not be involved in the transitions states of our reaction mechanism as it involves substituents beared by the phosphine-borane complex instead of the free borane*.

5.3.3. Using the model to seek for transition state of C_6F_5 migration.

Now that we have extensive description of the hydride exchange, we searched for a transition state for hydride and C_6F_5 exchange. To do so, we used TS-**50-I** as initial guess and we reversed the positions of C_6F_5 and one hydrogen (red or blue one). The obtained TS-**52** clearly show the exchange between H (red) and C_6F_5 (blue) as depicted in the *Figure 4.10*. We were delighted to show that TS-**52** connected to the hydride bridge **51** and to the mono-migration adduct + BH_3, **53** as expected. Interestingly, calculations showed that the barrier energy and Gibbs free energy of the transition state TS-**52** were higher than TS-**50-I**. It implies that the hydride exchange takes place faster than that of C_6F_5.

*Figure 4.10 Transition state of the hydride and C_6F_5 exchanges with **42a** and $H_2B(C_6F_5)$. Conditions: B3LYP, 6-31++G(d,p), solvent : C_6H_5F, PCM. ΔE are calculated in relation to TS-**52**.*

It must be noticed that the optimization of the Van der Walls adduct **53** did converge when using B3LYP. In that case, the use of LC-PW91 allowed the calculation to finish properly and highlights a higher Gibbs free energy of **53** than **51** by 17.9 kcal/mol*. This is in line with our previous conclusion that **53** will never be formed as the dimerization of BH_3 is expected to form the mono-migration adduct **47a** along with B_2H_6*.

We have now robust starting points to describe both the hydride and C_6F_5 exchanges occurring in the synthetic reactions.

5.4. Investigation in the experimental selectivity

5.4.1. Description of the observed reaction

Based on the previous structure of the transition state, we were able to calculate the reaction mechanism of the successive exchanges of the **three** C_6F_5 of the same borane with **one** of the hydride of **three** equivalent of phosphorous borane complex. This was examined for two different phosphorous borane complexes: H_3PBH_3 **42a** and $MeOPMe_2BH_3$ **42c**.

Regarding the starting point, which is used as zero in energy and Gibbs free energy, we have considered **42a** or **42c** and BY_3. The transition states were located for the three exchanges by analogy with TS-**52a,c** and are referred to TS-**52a,c-Y_3**, TS-**52a,c-Y_2** and TS-**52a,c-Y** (which

is equal to TS-**52a,c**). They are connected, in each case, to the hydride-bridged structures **51a,c-Y_3**, **51a,c-Y_2** and **51a,c-Y** on one side and to weak Van der Waals adducts **53a,c-Y_3**, **53a,c-Y_2** and **53a,c-Y** on the other side, which could not be fully optimized when using the functional B3LYP. As a consequence, we have used to discuss the energy of this connection to be the sum of the energy of the optimized separated fragments. Considering the separated intermediates for each step, the H_nBY_{3-n} structures (n = 1-3), are found to form stable dimers, which are thus considered to be altogether the final products of each subsequent migration and the starting material for the next step. The resulting reaction profiles for the three migrations computed with B3LYP are given in the *Figure 4.11*. The hydride bridged-structures are found to have higher Gibbs free energy than the starting fragments **42a,c** and H_nBY_{3-n} (monomeric for n = 0 and dimeric for n = 1-3) and are thus to be considered as unstable intermediates.

The structure of the transition state TS-**52a,c-Y_n** was strongly dependent on the number of Y groups on the borane precursor. However, as shown in the *Table 4.10*, the most notable changes on both the H-B and C-B bonds and the HBC angle occurred between the second and the third migration. While d(B-H) and d(C-B) are similar during the same migration process, it gradually decreases over the three migrations. In the meantime, the HBC angle increases.

*Table 4.10 Evolution of distances and angle of the transition states TS-**52c-Y_n** with $[MeOPMe_2BH_2]^+$ and $[HBX_3]^-$. X = H or Y (Y =C_6F_5).*

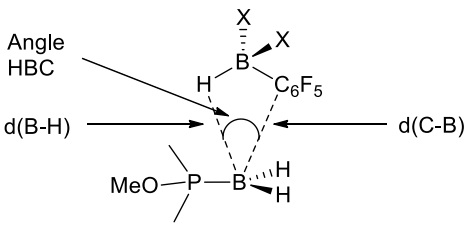

Distance or angle	TS-**52c-**Y_3	TS-**52c-**Y_2	TS-**52c-**Y_1
d(B-H) (Å)	2.797	2.614	2.452
d(C-B) (Å)	2.648	2.656	2.402
Angle (HBC) (°)	50.2	53.1	59.0

As highlighted in *Figure 4.11*, the activation energy for each step increases. This can be seen as the combination of two effects, on one side the stabilization of the starting intermediates through formation of more stable dimers, on the other side the smaller stabilization of the negative charge on the borohydride like fragment of the transition state as the number of Y substituents decreases.

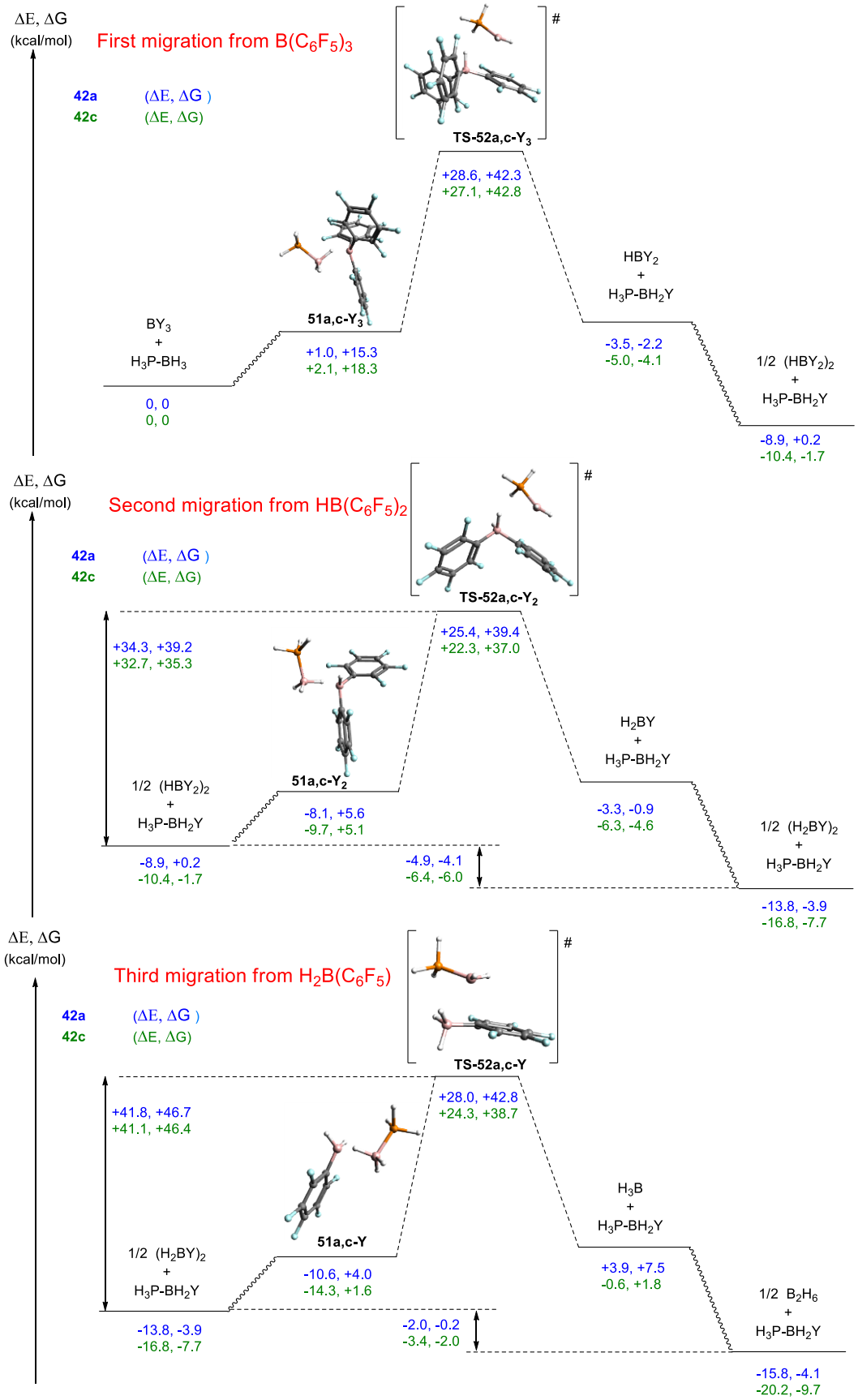

*Figure 4.11 Reaction profile of the migrations of Y (Y = C_6F_5) with **42a** (blue) and **42c** (green). Conditions: B3LYP, 6-31++G(d,p), solvent : C_6H_5F, PCM. Energies have been calculated with respect to R_3PBH_3 + BY_3 as zero energy. Dash lines shows connected structures and wavy lines show connection between minimums.*

In order to favour discussion, a simplified reaction profile of the three migrations of Y from BY_3 to both **42a** and **42c** with B3LYP or LC-PW91 have been drawn in the *Figure 4.12*. In this figure, unstable intermediates have not been drawn and the initial system R_3PBH_3 + BY_3 have been taken as the zero energy. In addition, both the reaction energy and the activation barriers of each migrations with B3LYP and LC-PW91 have been reported in the *Table 4.11* for H_3PBH_3 **42a** and in the *Table 4.12* for $MeOPMe_2BH_3$ **42c**.

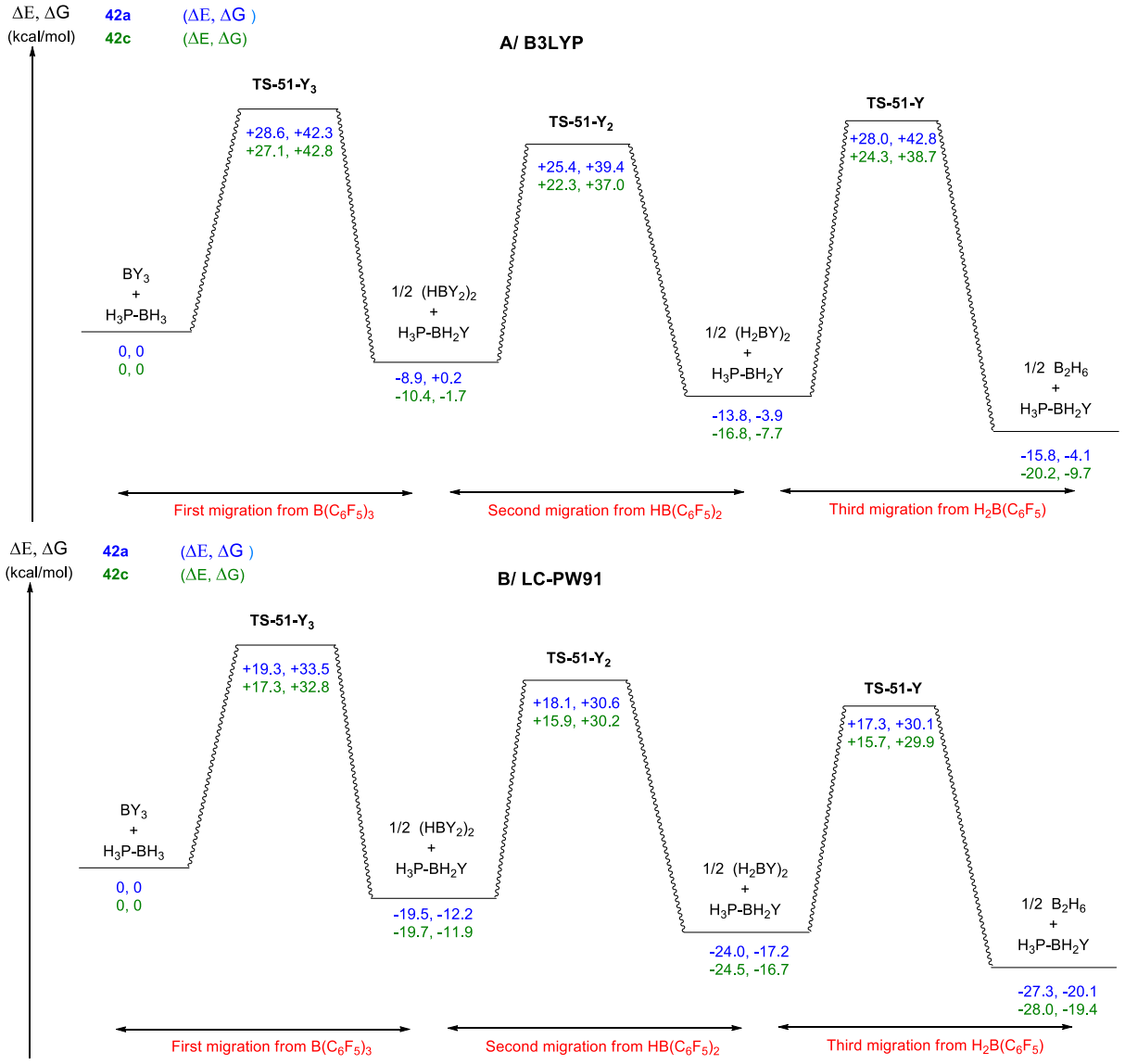

*Figure 4.12 Simplified reaction profile of the migrations of Y (Y = C_6F_5) with **42a** (blue) and **42c** (green). Conditions: B3LYP, 6-31++G(d,p), solvent : C_6H_5F, PCM. Energies have been calculated with respect to R_3PBH_3 + BY_3 as zero energy.*

We have already pointed out that the migrations become less and less exothermic as the reaction energies gradually increases with both functional and phosphines. On the contrary, the activation barriers, calculated between the transition state of each migration TS-**52a,c-Y_3**

and the two separated fragments, becomes higher. For the latest, a variation of almost 12 kcal/mol is observed between the first and the third transition state with B3LYP and almost 9 kcal/mol with LC-PW91. When comparing functionals, a significant difference (close to 10 kcal/mol) is observed between B3LYP and LC-PW91 for the first step, whereas smaller effects are observed for the remaining steps of the reaction path. This can once be associated to the formation of the H-bridge during this step, whereas all others are computed between reactants, TS and products which all exhibit an H-bridged structure.

*Table 4.11 Reaction energies and activation energies calculated with B3LYP and LC-PW91 for the three migrations with **42a**. Conditions: B3LYP, 6-31++G(d,p), solvent : C_6H_5F, PCM.*

E or G (kcal/mol)	Functional	First migration	Second migration	Third Migration
ΔE	B3LYP	-8.9	-4.9	-2.0
ΔE	LC-PW91	-19.5	-4.5	-3.3
ΔG	B3LYP	+0.2	-4.1	-0.1
ΔG	LC-PW91	-12.2	-5.0	-2.9
$\Delta E^{\#}$	B3LYP	+28.6	+34.3	+41.8
$\Delta E^{\#}$	LC-PW91	+19.3	+37.6	+41.3
$\Delta G^{\#}$	B3LYP	+42.3	+39.2	+46.7
$\Delta G^{\#}$	LC-PW91	+33.5	+42.8	+47.3

*Table 4.12 Reaction energies and activation energies calculated with B3LYP and LC-PW91 for the three migrations with **42c**. Conditions: B3LYP, 6-31++G(d,p), solvent : C_6H_5F, PCM.*

E or G (kcal/mol)	Functional	First migration	Second migration	Third Migration
ΔE	B3LYP	-10.4	-6.4	-3.4
ΔE	LC-PW91	-19.7	-4.8	-2.9
ΔG	B3LYP	-1.7	-6.0	-2.0
ΔG	LC-PW91	-11.9	-4.6	-2.9
$\Delta E^{\#}$	B3LYP	+27.1	+32.7	+41.1
$\Delta E^{\#}$	LC-PW91	+17.3	+35.6	+40.2
$\Delta G^{\#}$	B3LYP	+42.8	+38.7	+46.4
$\Delta G^{\#}$	LC-PW91	+32.8	+42.1	+46.4

A last important point is the influence of the substituents of the phosphine borane complex. *The reaction energies of the migrations are more favourable by 1.5 to 3.0 kcal/mol by*

substituting H_3P by $MeOPMe_2$ in the calculations. Similarly, the barrier activations are less elevated by 2.0 to 3.0 kcal/mol.

A close examination of the *Figure 4.11* showed that, considering the high barriers and the small exergonicity of the reaction, the overall reaction takes place under thermodynamic control. As a consequence, in spite of the increasing barrier, the reaction should proceed to completion without possibility to select a given intermediate.

5.4.2. Survey of the competition with a second migration

Our investigations in the migration of C_6F_5 from $BH_n(C_6F_5)_{3-n}$, $0 \leq n \leq 2$, highlighted both the kinetic and thermodynamic origins of the migration to form the mono-migration adducts **47a,c**. However, we questioned why we had never observed the formation of a second migration adduct. To verify the absence the latter competitive product, we calculated the energy profile of a second migration of C_6F_5 *from $H_2BC_6F_5$* with $H_3PBH_2C_6F_5$ **47a** and $MeOPMe_2BH_2C_6F_5$ **47c** by considering B3LYP and LC-PW91 as functional to yield $H_3PBH(C_6F_5)_2$ **48a** and $MeOPMe_2BH(C_6F_5)_3$ **48c** (*Figure 4.13*).

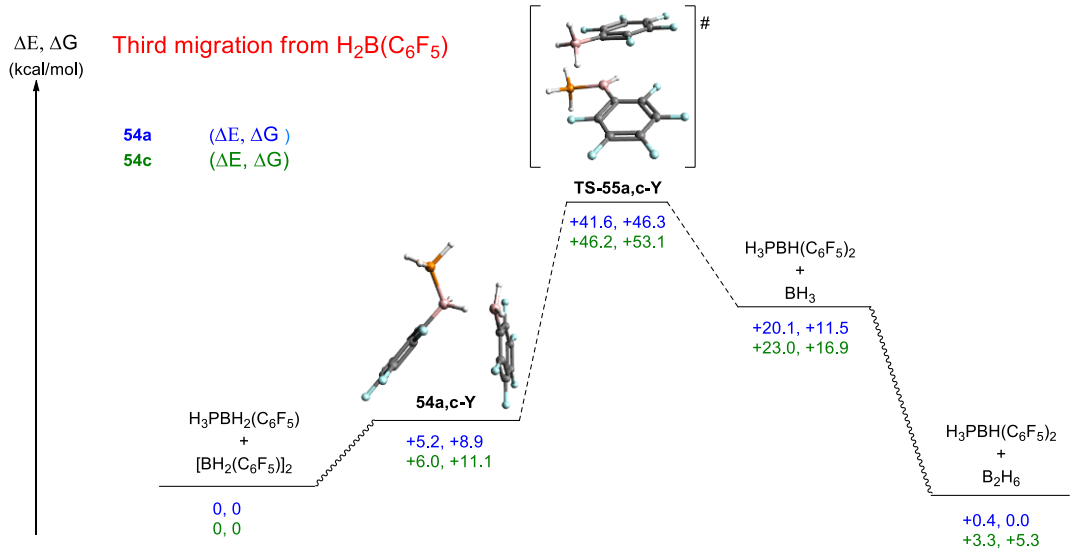

Figure 4.13 Calculations at the third migration of the mechanism of a second equivalent of C_6F_5 to yield the double adduct. Conditions: B3LYP, 6-31++G(d,p), solvent : C_6H_5F, PCM.

First of all, we have considered **47a,c** as well as the dimeric borane $[H_2BC_6F_5]_2$ as starting point of the reaction mechanism. Then hydride-bridges **54a,c-Y** have been shown to be unstable reaction intermediates connected to the transition state TS-**55a,c-Y**. Similarly to the previous reaction path, the latter TS-**55a,c-Y** is connected to the Van der Waals adduct, which correspond to the separated fragments: BH_3 + double migration adducts **56a,c**. After dimerization of BH_3, we get the final point of the reaction mechanism.

The *Table 4.13* shows the reaction energies and the activation energies associated to these transformations with the two phosphines, and by using the two functionals B3LYP and LC-PW91. Regarding the reactions energies, we find that the formation of **48a** is almost athermic while these of **48c** is endothermic and endergonic with the two functionals. These results are in marked contrast with these from the mono-migrations of C_6F_5 from $H_2B(C_6F_5)$ yielding **54a,c** as the reactions were both exothermic ad exergonic.

*Table 4.13 Reaction energies and activation energies calculated with B3LYP and LC-PW91 for the last migration of a second equivalent of C_6F_5 with **47a** and **47c**. Conditions: B3LYP, 6-31++G(d,p), solvent : C_6H_5F, PCM.*

E or G (kcal/mol)	Functional	$H_3PBH(C_6F_5)_2$ **48a** (product)	$MeOPMe_2BH(C_6F_5)_2$ **48c** (product)
ΔE	B3LYP	+0.4	+3.3
ΔE	LC-PW91	-1.1	0.0
ΔG	B3LYP	0.0	+5.3
ΔG	LC-PW91	-0.2	+2.1
$\Delta E^{\#}$	B3LYP	+41.6	+46.2
$\Delta E^{\#}$	LC-PW91	+44.5	+43.9
$\Delta G^{\#}$	B3LYP	+46.3	+53.1
$\Delta G^{\#}$	LC-PW91	+51.1	+51.9

In addition, by comparing the activation energies with these of the *Table 4.11* and *Table 4.12*, we can see that the second migration is more difficult than the first one. Indeed, with B3LYP and by considering the formation of **47c** with $H_2B(C_6F_5)$, the activation energy of the double migration leading to **48c** is 6.7 kcal/mol greater than the mono with B3LYP and 5.5 kcal/mol with LC-PW91. However, by considering **48a**, the barrier is less elevated by 0.4 kcal/mol with B3LYP and more elevated by 3.8 kcal/mol with LC-PW91 than for the mono migration forming **54a,c**.

To have a better view of the competition between the mono and the double migration of C_6F_5 from $H_2B(C_6F_5)$ yielding **47c** or **48c**, we drawn the *Figure 4.14*. On the left side is drawn the mono migration of C_6F_5 forming **47c**, and on the right side the double migration of C_6F_5 from **47c** and forming **48c**. It can be seen that the mono migration is more favourable by 7.3 kcal/mol than the double one and associated to an activation energy less elevated by 6.7 kacl/mol.

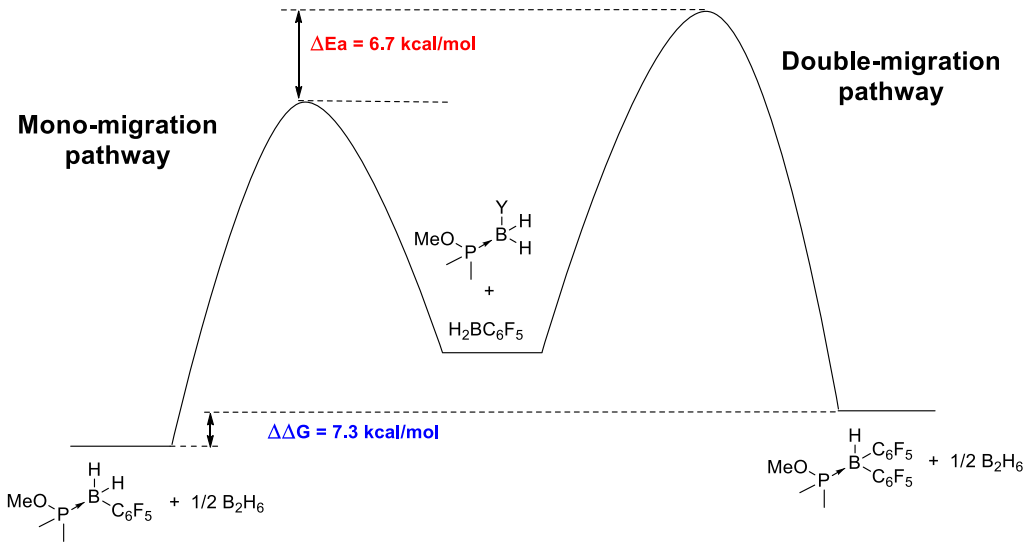

*Figure 4.14 Comparison of the reaction energy diagram of the migration of C_6F_5 with $H_2BC_6F_5$ and **47c** (Y = H or C_6F_5). B3LYP, 6-31++G(d,p), solvent : C_6H_5F, PCM.*

Even if we realized this study with $H_2BC_6F_5$ it provides a relevant trend of the selectivity as the migration from $H_2B(C_6F_5)$ are associated to the higher energy barriers. *As shown in Figure 4.14, and according to the Curtin-Hammet principle applied to the last migration, it seems fair to state that no double migration adduct should be formed*.

6. Conclusion and perspectives

6.1. Conclusion

To conclude this chapter, we investigated the use of phosphorous borane complexes in the presence of the Lewis acid $B(C_6F_5)_3$ to promote the intramolecular borylation reaction. However, the migration of C_6F_5 from the Lewis acid $B(C_6F_5)_3$ to phosphine and phosphinite borane complexes have been observed and studied in detail by the means of three methods: organic synthesis, physical-organic chemistry and computational chemistry.

Investigations of the reaction showed that 0.36 mol% of $B(C_6F_5)_3$ along with 1 equivalent of the phosphorous borane R_3PBH_3 adduct warmed at 140°C for 1h in C_6H_5F were necessary to promote the migration of C_6F_5 to yield $R_3PBH_2C_6F_5$ with excellent yield up to 93%. The methodology has been expanded and one of these new compounds have been shown to be able to reduce $B(C_6F_5)_3$ to allow a second migration of C_6F_5 to yield $R_3PBH(C_6F_5)_2$ in 75% yield in the same reaction conditions.

The reaction steps have been studied in detail and allowed us to propose the reaction mechanism showed in the *Figure 4.15*.

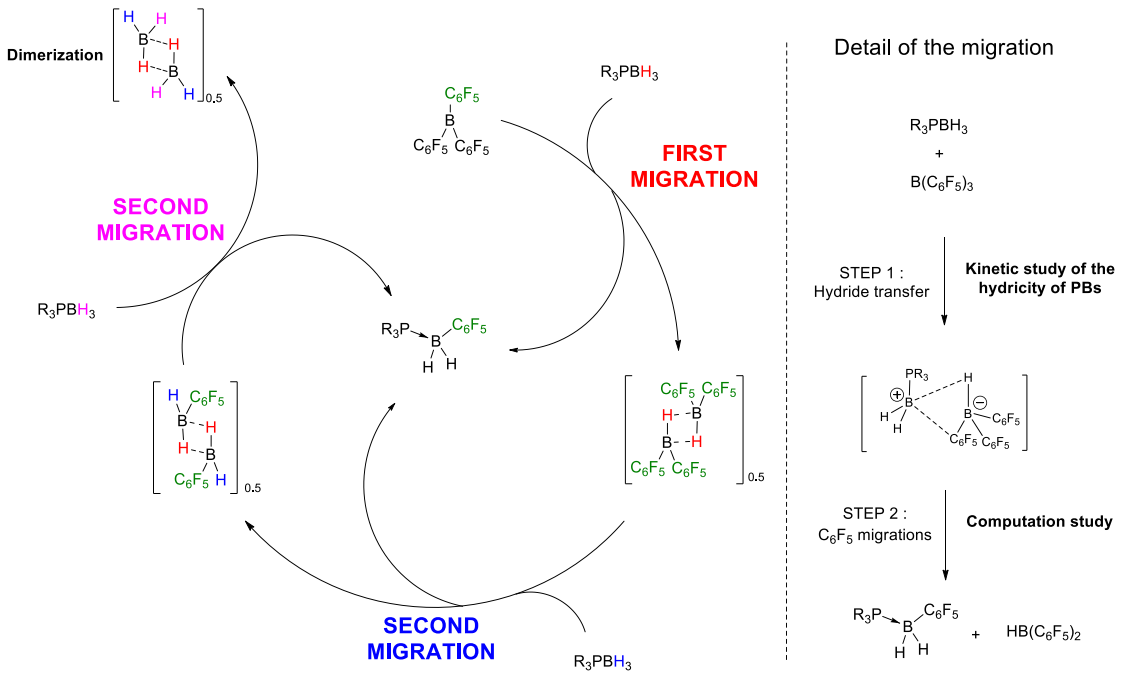

Figure 4.15 Proposed reaction mechanism for the three migrations of C_6F_5 from $B(C_6F_5)_3$ to phosphine and phosphinite borane complexes.

From one side, our kinetic study of the hydride transfer of phosphine borane complexes showed to PBs are able to provide an hydride to $B(C_6F_5)_3$. In addition, we also highlighted the effect of C_6F_5 on the decrease of the hydricity of PBs according to Mayr methodology. This was completed by a computational study of the three migrations with two phosphorous borane complexes. We were able to prove the formation of a transitions state involving a "borenium cation" like structure. In addition, the slightly negative reaction energies as well as the high energy barriers explained the occurrence of the three migrations at elevated temperatures under thermodynamic control. Finally, we investigated the non-occurrence of the formation of a second-migration adduct to show that its formation is less favourable and require high activation energies.

6.2. Perspectives

This part allowed us to synthesize new phosphine borane compounds bearing electron withdrawing groups, which is unusual in boron chemistry. Therefore, in the case of the double migrations adducts, the electron-deficient nature of the boron could be exploited to develop an original Umpolung reactivity at the boron center. Indeed, we wondered if the presence of the two C_6F_5 groups would confer acidic properties to the remaining hydrogen atom of $R_3PBH(C_6F_5)_2$. With this aim in mind, Bertand et al. reported the synthesis of a boryl anion under deprotonation of a carbene borane complex. The later anion has been shown to react as nucleophile with alkyl halides or gold(I) complex.[23] Despite this unique reactivity the

[23] Ruiz, D. A.; Ung, G.; Melaimi, M.; Bertrand, G. *Angew. Chem., Int. Ed.* **2013**, *52*, 7590.

synthesis of boryl anion suffers from important drawbacks. In this context, we believe that our system would be good candidate, exhibiting similar reactivity trend (*Scheme 4.24*).

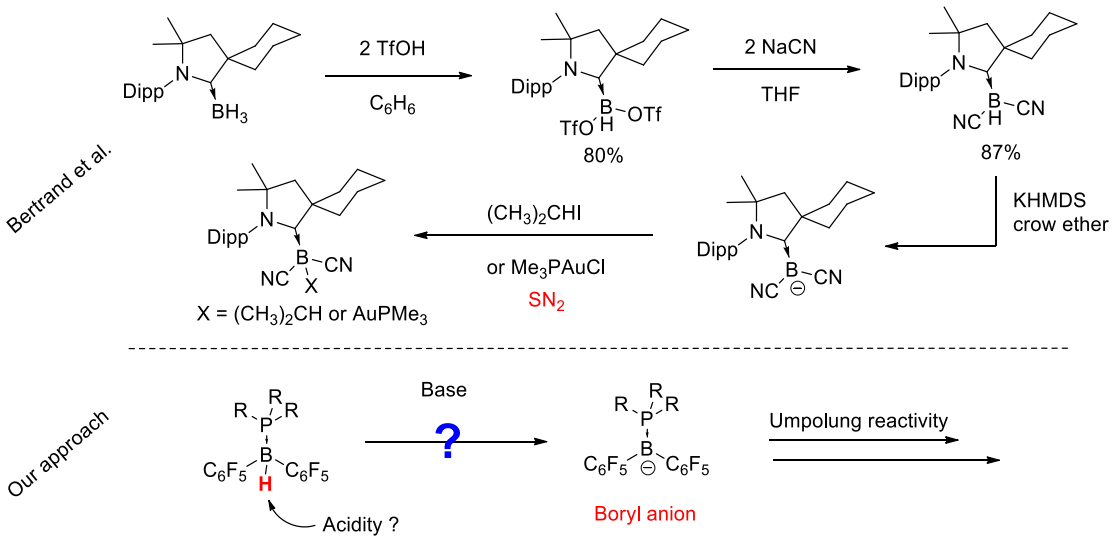

Scheme 4.24 Synthesis of boryl anion and nucleophilic substitution of alkyl halide or gold complex reported by Bertrand et al. (top) and our approach (bottom).

A last perspective of this study is in relation with the initial problematic of the intramolecular borylation of phosphine borane complexes. Now we understand that $B(C_6F_5)_3$ can't be used as catalyst because C_6F_5 groups are able to migrate, we can propose solutions to this drawback. First, this observed migration is mainly the consequence of the reactivity of the borohydride which are known to promote the migration of alkenyl or aryl groups. In our case, it is required to reduce the rate of the migration as we know that the intramolecular borylation can take place. To do so, one could build a covalent arm between the perfuorinated groups to limit their migration capabilities. Another alternative would be to decrease the number of fluorine on the aryl groups. In this case, a balance must be found between i) keeping a high Lewis acidity to allow the hydride abstraction and ii) prevent the migration of aryls.

5. Chapter V: Lewis acid catalyzed Regioselective Markovnikov hydrophosphination of styrene.

The addition of a P-H bond of primary or secondary phosphines across carbon-carbon double bonds continues to be a vibrant field of research for organic synthesis and catalysis. Because such a process is 100% atom economical, much efforts have focused during the last few decades not only to achieve high reaction yields but more importantly to fully control the selectivity outcomes of this reaction type.

As shown in Scheme 5.1, the addition of the P-H bond can lead to two regioisomers α and β, commonly known as Markovnikov and anti-Markovnikov adducts, respectively.[1] Traditionally, while anti-Markovnikov alkene hydrophosphination can be achieved either with basic[2] or radical[3] activation conditions, the Markovnikov version is better obtained under acidic conditions.[4]

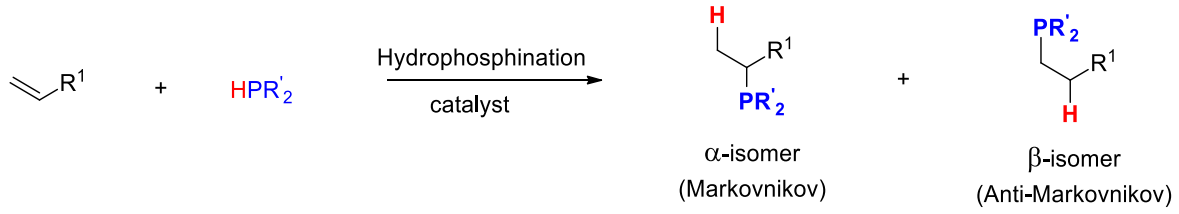

Scheme 5.1 Hydrophosphination of alkenes and formation of the two regioisomers α and β.

The remarkable progress of the field of catalysis, in particular transition-metal catalysis has strongly impacted the development of alkenes hydrophosphination and a full control of selectivity is now possible under catalytic conditions.[5] It should be mentioned, however, that most of these catalytic approaches enabled access to the anti-Markovnikov adducts whereas only a few methods allowed access to the other regioisomers.

In this chapter, we focused our attention on synthetic and mechanistic investigations of the first organocatalyzed Markovnikov alkene hydrophosphination. The following section summarizes most important contributions in this area including recent work from our laboratory.

1. Survey of the Markovnikov regioselective hydrophosphination in the literature

[1] a) Mimeau, D.; Delacroix, O.; Gaumont, A.-C. *Chem. Commun.* **2003**, 2928 b) Alonso, F.; Beletskaya, I. P.; Yus, M. *Chem. Rev.* **2004**, *104*, 3079 c) Delacroix, O.; Gaumont, A. C. *Curr. Org. Chem.* **2005**, *9*, 1851.
[2] a) Carlone, A.; Bartoli, G.; Bosco, M.; Sambri, L.; Melchiorre, P. *Chem. Commun.* **2007**, 722. b) Bunlaksananusorn, T.; Knochel, P. *J. Org. Chem.* **2004**, *69*, 4595.
[3] Cunningham, T. J.; Elsegood, M. R. J.; Kelly, P. F.; Smith, M. B.; Staniland, P. M. *Eur. J. Inorg. Chem.* **2008**, 2326.
[4] Hoff, M. C.; Hill, P. *J. Org. Chem.* **1958**, *24*, 356.
[5] For a review, see Koshti, V.; Gaikwad, S.; Chikkali, S. H. *Coordination Chemistry Reviews* **2014**, *265*, 52.

1.1. Metal free-mediated Markovnikov regioselective hydrophosphination of styrene

Markovnikov hydrophosphination of olefins catalysed by Bronsted acid has first been reported in 1958 by Hoff and Hill (Scheme 5.2).[4] In the presence of 0.5 or 1.0 equivalent of CH_3SO_3H and under 30 to 47 atm of PH_3, the hydrophosphination of terminal alkenes **1** takes place to yield the Markovnikov-adducts **2** in low to excellent yields (14-90%). A careful study of the reaction between PH_3 and propene showed that CH_3SO_3H afforded better yield (81%) than H_3PO_4, $PhSO_3H$, CF_3CO_2H or $BF_3.OEt_2$ (max 72%). The number of additions highlighted that, in the best cases, a ratio of 98:2 was noticed for the mono-phosphination **2** and the bis-phosphination **3**, respectively. This ratio increased to 90:10 in the worst case. Regarding the reaction mechanism, the authors proposed the protonation of the olefin to yield the internal carbocation which furnishes the phosphination adduct after addition of PH_3.

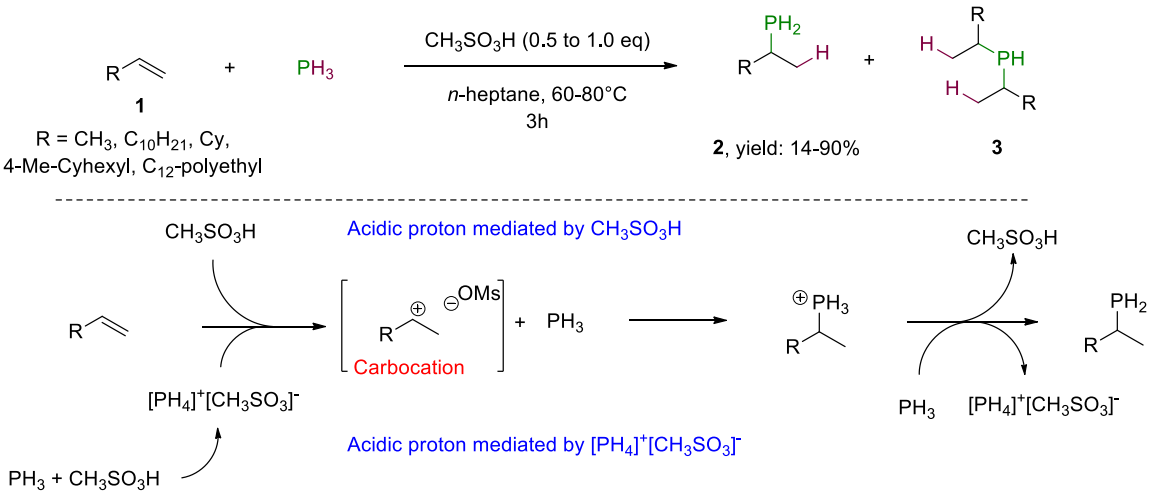

*Scheme 5.2 Bronsted acid catalysed Markovnikov hydrophosphination of olefins **1**.*

The same approach has been employed by Togni et al. in the synthesis of a chiral ferrocene-based amidine/amidinato ligand **4** used with $[Rh_2Cl_2(COD)_2]$ to form **5** (Scheme 5.3).[6] During the synthesis of the ligand **4**, the authors treated the vinyl ferrocene **6** by $HPPh_2$ in acetic acid at 60°C. Surprisingly, the hydrophosphination α-adduct **7** was obtained in good 83% yield and excellent diastereoisomeric ratio (d.r. > 100:1).

[6] Bertogg, A.; Togni, A. *Organometallics* **2006**, *25*, 622.

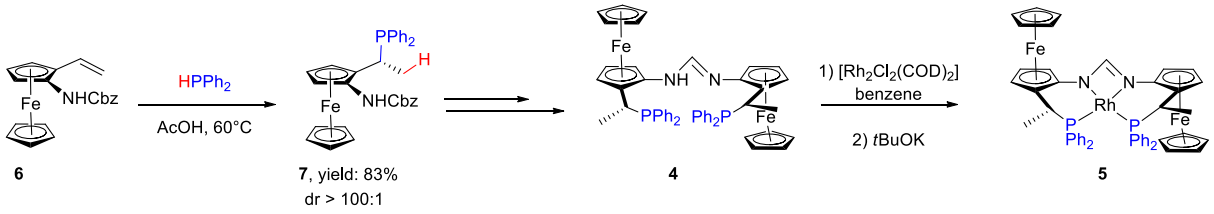

*Scheme 5.3 Markovnikov regioselective hydrophosphination of vinyl ferrocene **6** under acidic conditions.*

1.2. Transition metal-mediated Markovnikov hydrophosphination of styrenes

Due to the harsh conditions and substrate dependant methods mentioned in the above section, transition-metal catalyzed approaches have emerged in order to find versatile and smooth reactions conditions to realize the regioselective hydrophosphination. Over the past decades, Markovnikov regioselective hydrophosphination of alkenes has been mainly achieved by the group of Marks et al. using rare-earth metals such as Lanthanum, Samarium and Ytterbium.[7] In spite of the efficiency of the reported methods in term of catalyst loading (< 5 mol%), these conditions are limited to intramolecular hydrophosphination reactions.

Seeking for sustainable approaches using cheaper metals, a substrate dependent hydrophosphination method have been developed to promote the α-adduct. Indeed, in the presence of 2 mol% of $NiBr_2$, $HPPh_2$ adds regioselectively to vinylethers **8** in benzene for 2h at 80°C, to form the α-adducts **9** after oxidation in yield ranging from 40 to 85% (Scheme 5.4).[8] The authors proposed that the reaction mechanism involves the activation of the double bond with $[Ni]^{2+}$ to form a polarized π-complex **10** which is attacked by the phosphine to yield **11**. At the next step, the protonolysis of carbon-metal bond takes place instead of a β-hydrogen elimination, to furnish **9**.

[7] a) Douglass, M. R.; Marks, T. J. *J. Am. Chem. Soc.* **2000**, *122*, 1824 b) Douglass, M. R.; Ogasawara, M.; Hong, S.; Metz, M. V.; Marks, T. J. *Organometallics* **2002**, *21,* 283 c) Douglass, M. R.; Stern, C. L.; Marks, T. J. *J. Am. Chem. Soc.* **2001**, *123*, 10221 d) Motta, A.; Lanza, G.; Fragalà, I. L.; Marks, T. J. *Organometallics* **2004**, *23*, 4097 e) Kawaoka, A. M.; Douglass, M. R.; Marks, T. J. *Organometallics* **2003**, *22*, 4630.

[8] Kazankova, M. A.; Shulyupin, M. O.; Beletskaya, I. P. *Synlett* **2003**, *2*, 2155.

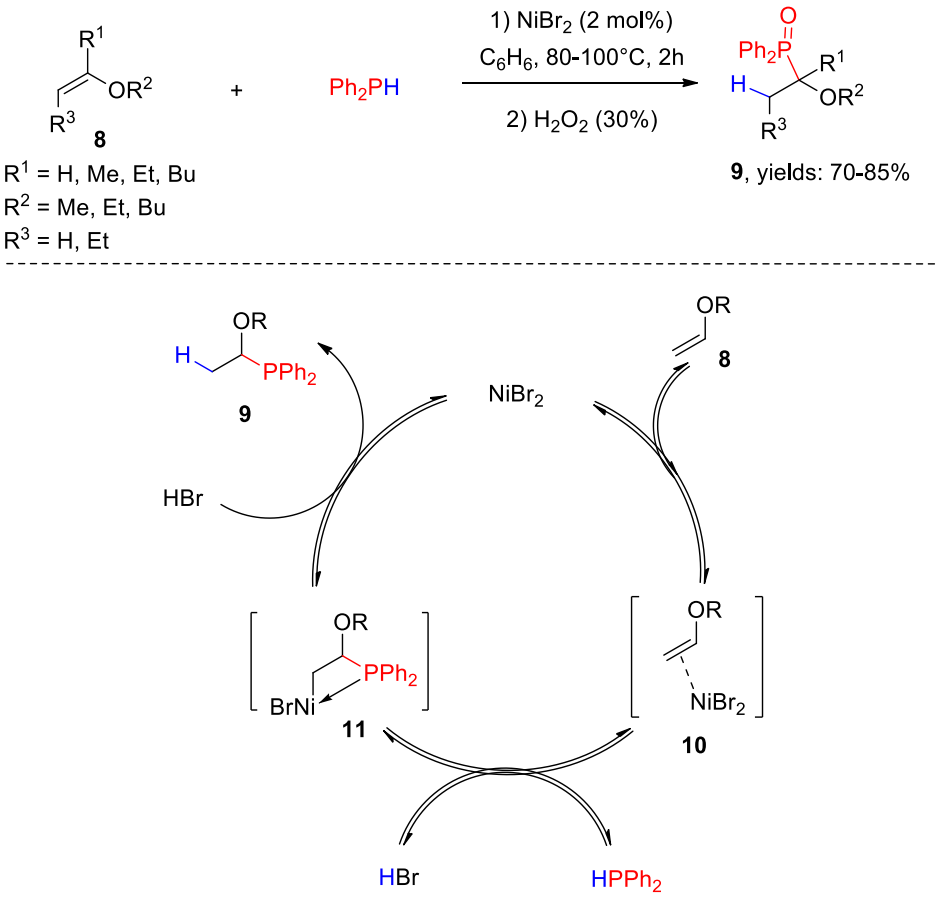

*Scheme 5.4 Nickel catalyzed hydrophosphination of vinylethers **8** by $HPPh_2$ and proposed reaction mechanism.*

In 2013, Gaumont et al. developed a method allowing to extend the scope of the electrophiles to a wide variety of aryl alkenes by using an iron-catalyst.[9] Remarkably, they were able to control the regioselectivity of the hydrophosphination by modifying the oxidation state of the iron catalyst. Indeed, they showed that the use of 30 mol% of $FeCl_2$ yields the β-regioisomer **12** while $FeCl_3$ promoted the formation of the α-regioisomer **13** (Scheme 5.5).

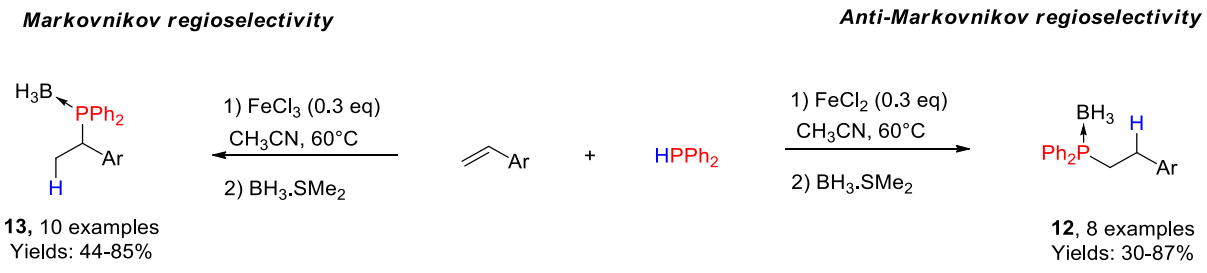

Scheme 5.5 Regioselective hydrophosphination of styrene derivatives controlled by the oxidation state of the iron catalyst.

[9] Routaboul, L.; Toulgoat, F.; Gatignol, J.; Lohier, J.-F.; Norah, B.; Delacroix, O.; Alayrac, C.; Taillefer, M.; Gaumont, A.-C. *Chem. - A Eur. J.* **2013**, *19*, 8760.

The authors proposed that the β-isomer **12** could resulted from a radical pathway probably initiated by the activation of traces of O_2. Indeed, addition of a radical inhibitor such as tert-butylcatechol or performing the reaction in the dark lowered the yield by 20 to 30%, but did not fully suppress the reaction. However, the reaction mechanism involved in the formation of the α-isomer must be completely different. Indeed, unlike in the case of the β-isomer, the authors showed that the reaction proceeded well with electron rich olefins while no reaction occurred with electron poor ones. Unfortunately, the paramagnetism of iron as well as the sensitivity of the reactive species made difficult the characterization of the intermediates.

2. Toward an organocatalyzed alkene Markovnikov regioselective hydrophosphination

2.1. Identification of the problem and proposed approach

Being a good ligand for iron, the high catalyst loading used by Gaumont et al. is perhaps due to a possible coordination of the Markovnikov adduct to the catalyst. Although this inhibition can, to some extent, by bypassed by the addition of one equivalent of BH_3, it can't obviously supress completely this Lewis acid Lewis base interaction.

In view of this problem, we reasoned that the use of a pure organic Lewis acid that weakly interact with the final phosphine might be a reasonable solution to overcome this problem. In this regard, we selected trityl cations ($[Ar_3C]^+$) as an organic catalyst for this specific reaction. Our choice of this organocatalysts was based on the following reasons:

1) The Markovnikov tertiary phosphine and the trityl cation can be seen as a Frustrated Lewis pair and their association, if it exists, should be shifted to the left side. This implies that the catalyst would not be inhibited.

2) As shown in the chapter 2, tertiary phosphonium salts resulting from the reaction of $[Ar_3C]^+$ with HPR_2 (R = aryl), exhibits a high Bronsted acidity ($2 < pK_a < 5$).

Based on these assumptions, we hypothesized that the association between the trityl cation **14a** and secondary phosphine **14b** should result in the formation of the adduct **14c** possessing an acidic proton. This adduct should protonate the olefin **14d** to generate the carbocation **14e**. This highly reactive electrophile would react at the diffusion limit with the phosphine $Ph_2P\text{-}CAr_3$ to form the adduct **14f**. The latter would finally release the tritylium catalyst and yield the final tertiary phosphine **14g** (Scheme 5.6).

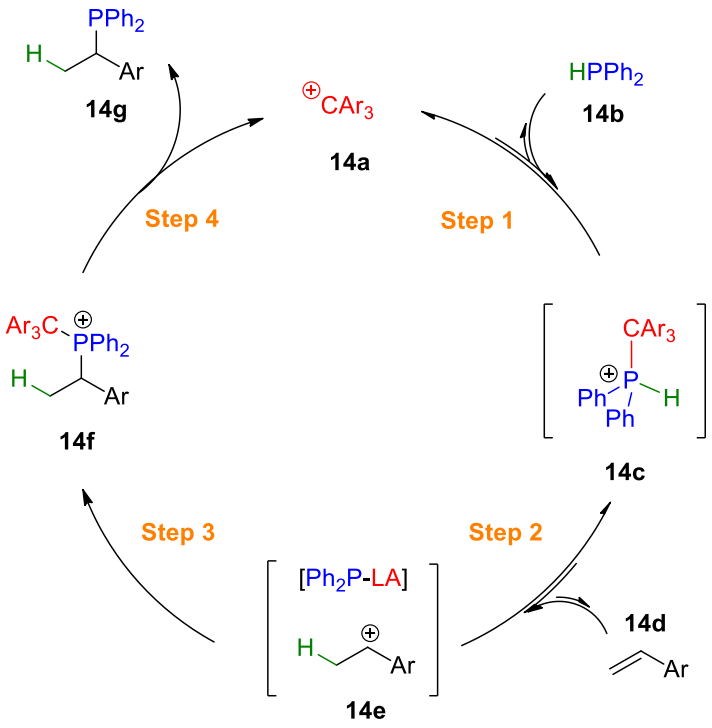

Scheme 5.6 Strategy for our Lewis acid catalyzed regioselective hydrophosphination of aryl alkenes.

According to this hypothesis, it is now required to find a suitable tritylium cation i) capable to reversibly interact with secondary phosphines to form an acidic phosphonium cation and ii) which is a good leaving groups to release the free tertiary phosphine.

2.2. Tritylium salts as organic Lewis acids

During our investigations, Stephan et al used these cations to catalyse the regioselective hydrothiolation of alkenes.[10] Indeed, they realized the synthesis of sulphide adduct **17** (20 examples) through a Markovnikov hydrothiolation of 1,1-disubstituted and trisubstituted olefins **15** with thiols **16** catalysed by the air-stable trityl-cation salt $[(MeOC_6H_4)CPh_2][BF_4]_3$ in yields ranging from 12 to 96% (Scheme 5.7). In particular, the authors showed that the hydrothiolation of terminal olefins as well as trisubstituted ones occurred with good conversions whereas the absence of a disubstituted carbon atom didn't furnish the expected adducts **17**. In addition, sterically hindered nucleophiles such as *i*PrSH yielded to low conversion. It was assumed that a carbocation **19** was formed upon protonation of **15** by the Lewis-acid Lewis-base complex **18**. Then the sulphide intermediate **20** adds on the later electrophile **19** to yield the desired products **17**.

[10] Mosaferi, E.; Ripsman, D.; Stephan, D. W. *Chem. Commun.* **2016,** *52*, 8291.

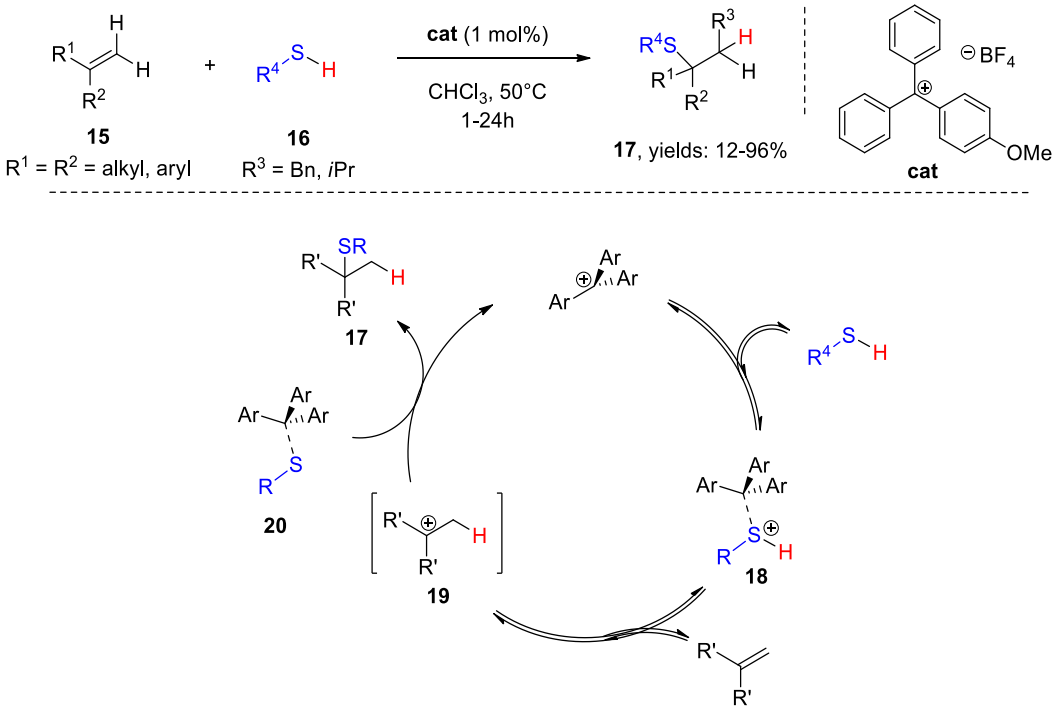

Scheme 5.7 Markovnikov regioselective organocatalyzed hydrothiolation of alkenes.

By applying this concept to our case, it can be assumed that $HPPh_2$ would behave similarly. Indeed, the formation of a Bronsted acid resulting from the association between $HPPh_2$ and the tritylium salt is possible as the coordination of the phosphorous lone electron pair should lead to the acidification of the P-H bond. Nevertheless, a careful survey of the nature of the Lewis acid must be done to induce the expected reactivity.

2.3. Characterization of tritylium salts and use in organocatalysis

In the next part, we will briefly describe the properties of tritylium salts as Lewis acids and survey their use in organic synthesis in order to find a suitable Lewis acid capable to promote the regioselective α-hydrophosphination.

2.3.1. Properties of tritylium salts

Tritylium salts correspond to triarylmethylium carbocation possessing a low-lying empty p orbital on the carbon atom. This electron deficiency makes them capable of accepting electrons and therefore activating an electrophile through electrostatic or orbital interactions towards nucleophilic attack.[11] The stability or Lewis acidity of relatively stable carbocations can be described by their pK_R^+ values. This unit value was introduced in 1955 by Schriesheim et al. and constitute a reference system for comparing carbocation stabilities in solution and it is defined as shown in equation 1 (Scheme 5.8).[12] By analogy with pK_a constants, pK_R^+ (equation 1) can be seen as the thermodynamic constants governing the equilibrium of the reaction the

[11] Bah, J.; Naidu, V. R.; Teske, J.; Franzén, J. *Adv. Synth. Catal.* **2014**, *357*, 148.
[12] N. C. Deno, J. J. Jaruzelski, A. Schriesheim, *J. Am. Chem. Soc.* **1955**, *77*, 3044.

Lewis acid with water and thus, it provides a quantitative scale of the reversibility of this equilibrium (Scheme 5.8).

More recently, Mayr et al. characterized various triarylmethylium cations through photometric determination of the rate constants *k* for their reactions with an excess of $HSiPh_3$ (reference nucleophile).[13] With these rate constants and based on the equation 2, largely discussed in the course of this PhD, they were able to quantify the electrophilicity of these electrophiles.

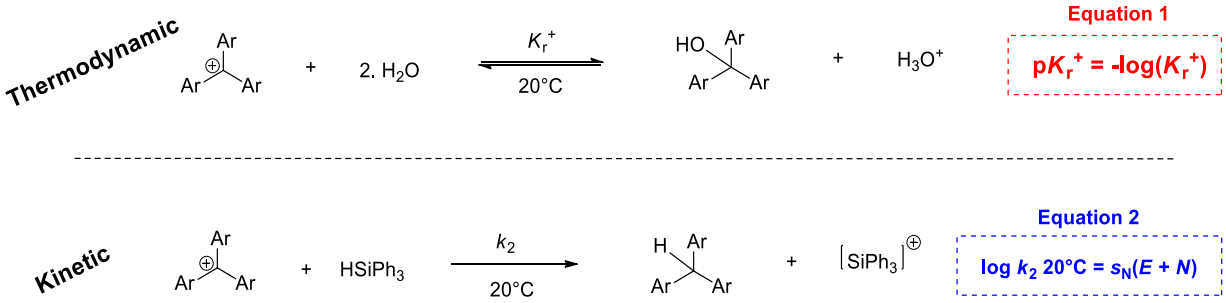

Scheme 5.8 Kinetic and thermodynamic tools to describe triarylcarbenium cations.

On the basis of these thermodynamic and kinetic descriptions, several tritylium cations have been studied to determine their pK_R^+ and (s_N, *N*) parameters (Table 5.1).

Table 5.1 pK_r^+ and *E* values for selected tritylums salts $[Ar_3C]^+[BF_4]^-$. pK_r^+ were measured in H_2SO_4 (80-95%) and *N* in CH_2Cl_2.

Tritylium salts $[Ar_3C]^+[BF_4]^-$ R^1, R^2, R^3	pK_r^+	*E*
22a, Ph, Ph, Ph	-6.63	0.51
22b, 4-MePh, Ph, Ph	-5.41	-0.13
22c, 4-MePh, 4-MePh, Ph	-4.71	-0.7
22d, 4-MeOPh, Ph, Ph	-3.4	-1.59
22e, 4-MeOPh, 4-MeOPh, Ph	-1.24	-3.04
22f, 4-MeOPh, 4-MeOPh, 4-MeOPh	0.82	-4.35
22g, 4-NMe_2Ph, Ph, Ph	3.88	-7.93
22h, 4-NMe_2Ph, 4-NMe_2Ph, 4-NMe_2Ph	9.36	-11.26

[13] Horn, M.; Mayr, H. European *J. Org. Chem*. **2011**, *87*, 6470

First, it can be seen that these catalysts have a reactivity range towards water spanning over a magnitude of 10^{16}. It highlights i) the strong influence of the substituents on the equilibrium constant and ii) their broad range of applications as organocatalysts. For instance, the addition of water is expected to be less reversible with $[Ph_3C]^+$ than $[(4\text{-MeOPh})Ph_2C]^+$ by roughly a factor of 1700. On the other hand, the addition of the hydride to $[Ph_3C]^+$ takes place 16 times faster than that to $[(4\text{-MeOPh})Ph_2C]^+$.

On the basis of these physical data, we can assume that carbocations should be ideal candidates to carry out Lewis acid catalyzed reactions. Indeed, as the nucleophilicity parameter of phosphines can be roughly estimated to 14 and having in mind that, according to Mayr rule of thumb, a reaction takes place at 20°C if $E + N > -5$, a reaction between phosphines and tritylium salts can be expected.[14] In addition, regarding the range of the pK_R^+ values, we anticipate that the reversibility of the formation of the phosphine-tritylium complex will be easily controlled by adjusting the substituents of the cation phenyl rings.

2.3.2. Uses of tritylium salts in Organic synthesis

Surprisingly, triarylcarbenium cations have been neglected as a class of Lewis acids in the field of organocatalysiss. It must be noticed the pioneering works of Mukaiyama and co-workers who employed tritylium salts and N-acyliminium ions as catalysts for Mukaiyama aldol reactions,[15] Sakurai allylations,[16] and Michael additions of silyl enol ethers to α,β-unsaturated ketones.[17] Recently, Franzén et al. have significantly explored the use of tritylium salts as organocatalyst.[11] In particular, they found that 0.1 mol% of $[Ph_3C]^+[BF_4]^-$ or $[(4\text{-MeOPh})Ph_2C]^+[BF_4]^-$ catalyzed the Diels-Alder cycloaddition of several diene and acrolein with full conversions depending on the nature of the organocatalysts (Scheme 5.9). Moreover, the aza-Diels-Alder version was also successfully achieved with 0.2 mol% of $[Ph_3C]^+[BF_4]^-$ in CH_2Cl_2 at r.t. within one hour to yield the exo-bicyclic adducts with full conversions.

[14] In must be noticed that this is an extrapolation as the *E* parameters of trityliums cations have been determined with non-sterically hindered nucleophiles.
[15] a) T. Mukaiyama, S. Kobayashi, M. Murakami, *Chem. Lett.* **1984**, *13*, 1759; b) S. Kobayashi, S. Murakami, T. A. Mukaiyama, *Chem. Lett.* **1985**, *14*, 447 c) S.-D. Chao, K.-C. Yen, C.-T. Chen, *Synlett* **1998**, 924; d) S.-D. Chao, K.-C. Yen, C.-H. Chen, I.-C. Chou, S.-W. Hon, C.-T. Chen, *J. Am. Chem. Soc*. **1997***, 119*, 11341
[16] T. Mukaiyama, H. Nagaoka, M. Murakami, M. Ohshi- ma, *Chem. Lett.* **1985**, 997
[17] S. Kobayashi, M. Murakami, T. Mukaiyama, *Chem. Lett.* **1985**, 953

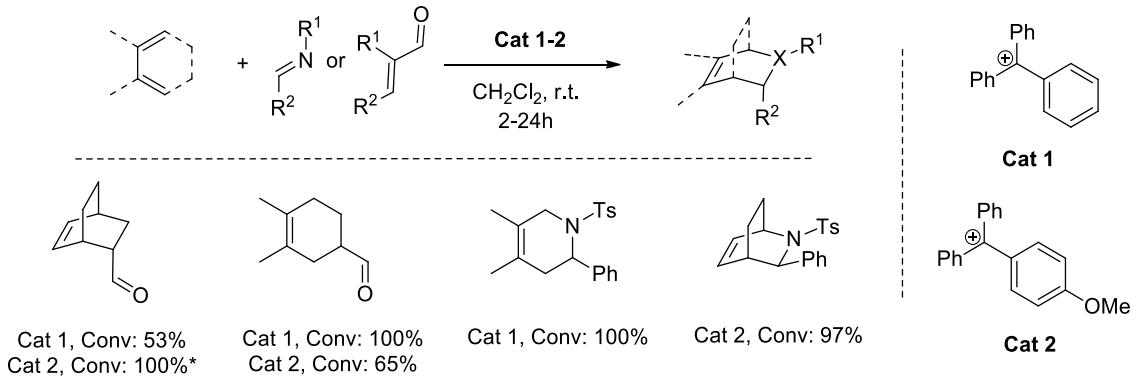

*Scheme 5.9 Organocatalyzed Diels Alder and aza-Diels Alder reactions of enone and imines with dienes. The counter ion of **cat-1,2** is $[BF_4]^-$ and have been omitted for the sake of clarity.*

In another type of reactions, Guo at al. found that triphenylmethylium cation catalyzes Povarov reactions with excellent yields in 1 h with a low loading of 0.5 mol% (Scheme 5.10).[18] In their methodology, 2,3-dihydrofuran was reacted with a serie of benzylidene aniline derivatives in THF at r.t. to yield the tricyclic adducts in yields ranging from 79 to 94%.

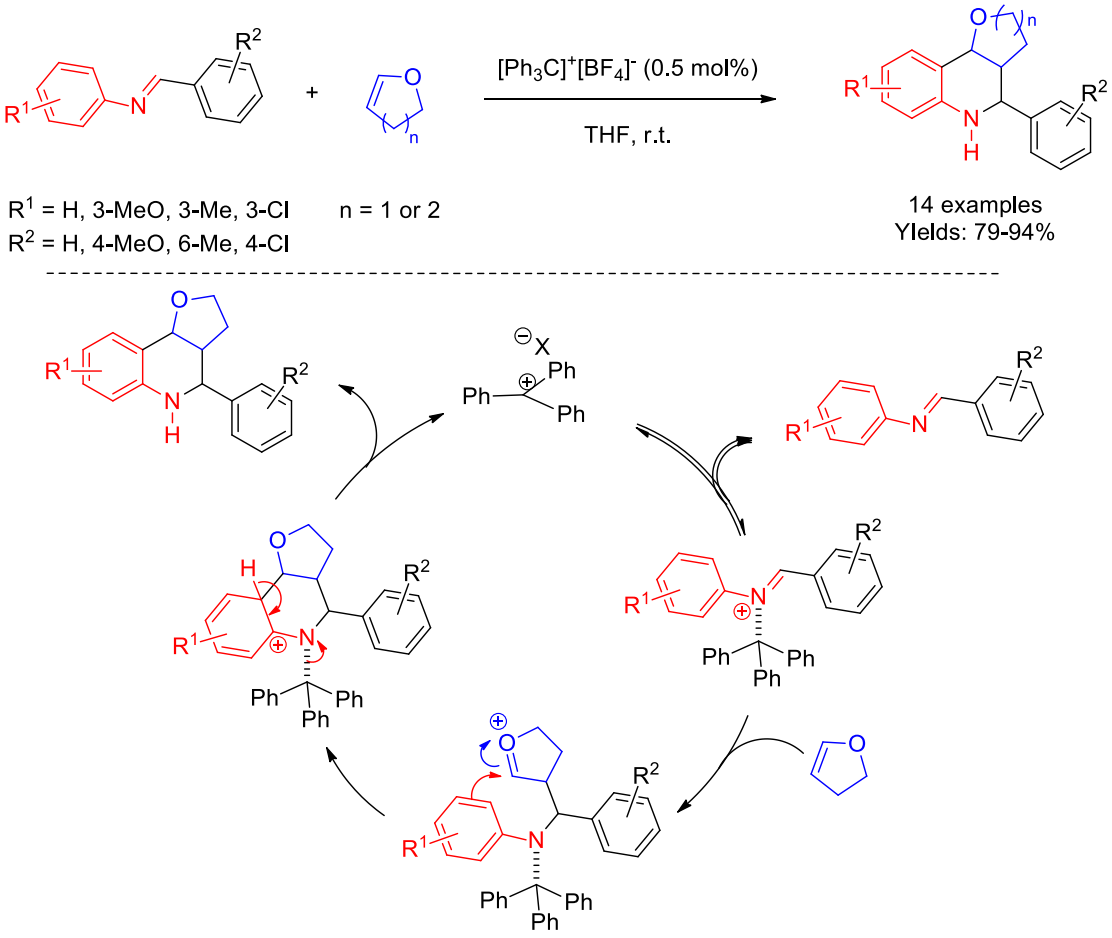

Scheme 5.10 Scope and proposed mechanism for the tritylium-catalyzed Povarov reaction.

[18] Huang, Y.; Qiu, C.; Li, Z.; Feng, W.; Gan, H.; Liu, J.; Guo, K. *ACS Sustain. Chem. Eng*. **2016**, *4*, 47

In the proposed reaction mechanism, the authors evoked the activation of the aniline though coordination of the electron lone pair of the nitrogen to yield an electrophilic iminium cation. The latter is attacked by the furan to yield a reactive intermediate which, after cyclization and tautomerization, generates the products.

3. Organocatalyzed Markovnikov hydrophosphination of alkenes.
   3.1. Development of the reaction conditions for the organo-catalyzed Markovnikov hydrophosphination of aryl alkenes.
      3.1.1. Proof of concept

We tested our previous hypothesis by performing the α-hydrophosphination as a proof of concept. To reach this goal, we selected the conditions developed by Stephan and we applied some minor modifications.

Because we expected the formation of a carbocation intermediate, we selected the 1,1-diphenylethylene **21** as model substrate. Indeed, the carbocation resulting from the protonation is known to be stabilized. Regarding now the nature of the phosphine, our experience of the chapter 2 allowed us to anticipate that dialkylphosphine would have higher pK_a values than diaryl ones and therefore, we chose the phosphine $HPPh_2$. Under these conditions, we expected the formation of an acidic phosphonium salt upon coordination of $HPPh_2$ and the tritylium salt $[Ph_3C][BF_4]$ **22a**, capable to protonate the olefin. Aware that thiols are much more acidic than phosphines, we also thought to warm the reaction mixture at higher temperature than 50°C and use polar solvents, such as CH_3CN, to stabilize the carbocation as much as possible (Scheme 5.11).

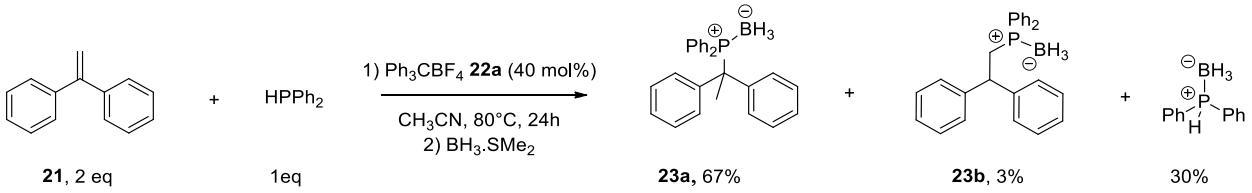

Scheme 5.11 Proof of the concept of the tritylium-catalyzed α-hydrophosphination of aryl olefins.

Under our conditions, we were delighted to observe the selective formation of the Markovnikov adduct **23a** in 67% conversion along with 30% of unreactive $HPPh_2$ according to ^{31}P NMR spectroscopy of the crude mixture. Only 3% of the anti-Markovnikov **23b** adduct were detected showing the excellent regioselectivity of the method. After purification on silica gel column chromatography, **23a** was isolated in 62% yield.

This first example is very important as it supports i) the expected reaction mechanism and ii) that the phosphine is the source of an acidic proton responsible for the formation of a carbocation.

3.1.2. Optimization of the reaction conditions

In the light of these encouraging results, we investigated in more details the influence of the reaction conditions on both the regioselectivity of the reaction and the yields. Several parameters were tested except the amount of the olefin which have been fixed to 2 equivalents according to our experience in hydrophosphination reactions.

3.1.2.1. Influence of the nature of the catalyst

In this singular reactivity, the nature of the organocatalyst plays the main role. As we obtained promising conversion with $[Ph_3C][BF_4]$ **22a**, we decided to investigate the influence of the electron demanding character of the catalyst. Indeed, as shown in the Scheme 5.12, electron demanding catalysts would form phosphonium salts possessing high Bronsted acidities, while electron deficient phosphines will give rise to the reverse effect. As a consequence, a subtle balance must be found between these two parameters.

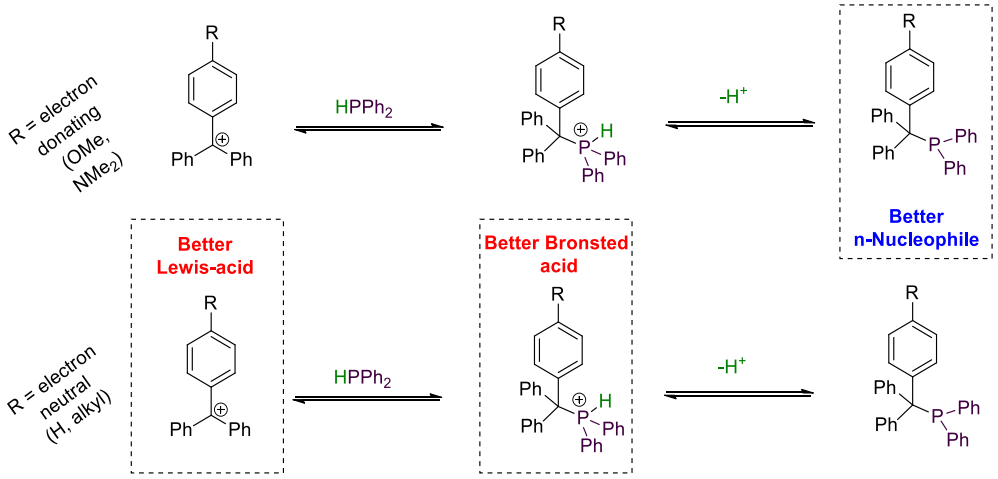

Scheme 5.12 Comparison of the effects of the Lewis acidity of tritylium salts on both the acidity of phosphoniums salts and the nucelophilicity of phosphines.

According to Mayr electrophilicity scale of trityl cations, the nature of the substituents strongly influences the reactive centre.[19] As it can be expected, the tritylium cation **22d** which was used by Stephan et al.[10], should have a lower Lewis acidity than **22a**. As a consequence, we thought to test several tritylium cations with electrophilicities comparable to that of **22d**. Based on this, we tested the above-mentioned catalysts **22a,d,g** and evaluated the effect of the counter ion as well as the catalyst loading (Table 5.2).

[19] Minegishi, S.; Mayr, H. *J. Am. Chem. Soc.* **2003**, *125*, 286.

*Table 5.2 Influence of the nature of the catalyst on the outcomes of the α-hydrophosphination of **21**. Y corresponds to the counter ion, W corresponds to $B(C_6F_5)_4$.*

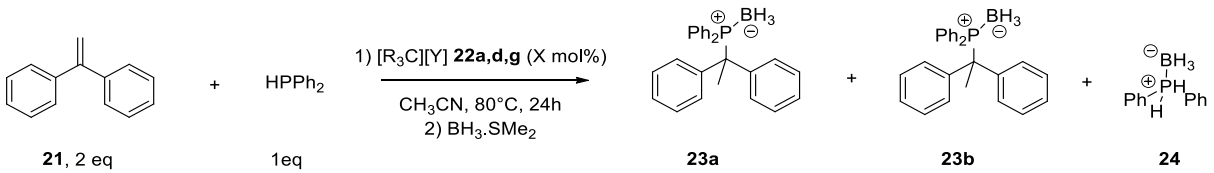

Entry	Catalyst	*E*	Loading X (mol%)	**23a** (%)	**23b** (%)	**24** (%)
1	$[Ph_3C][BF_4]$ **22a**	0.51	40	67	3	30
2	$[Ph_3C][B(C_6F_5)_4]$ **22a-W**	-	40	62	5	33
3	$[4\text{-}(MeOPh)CPh_2][BF_4]$ **22d**	-1.59	40	85	0	15
4	$[4\text{-}(NMe_2Ph)CPh_2][BF_4]$ **22g**	-7.93	40	0	10	90
5	$[4\text{-}(MeOPh)CPh_2][BF_4]$ **22d**	-1.59	20	83	0	17

We can see that the best Lewis acid of our series is $[4\text{-}(MeOPh)CPh_2][BF_4]$ **22d**. Decreasing further the electrophilicity of the catalyst such as **22g** led to no reaction with the phosphine as only the starting material we recovered. Besides, we can see that the nature of the counter anion doesn't influence the reaction. We could even decrease the catalyst loading to 20 mol% without any loss of regioselectivity. Diminishing further the catalyst loading to 10 mol% resulted in to a significant decrease of the α-adduct.

3.1.2.2. Influence of the solvent

Another important parameter to take into account is the nature of the solvent as we assume the formation of a carbocation. Polar solvents are known to stabilize the formation of charges intermediates, that's why we started our study with acetonitrile. Because the reaction mixture must be warmed to 80°C, solvents with low boiling point such as CH_2Cl_2 or Et_2O and

nucleophilic solvent such as ethanol were excluded. Consequently, we tested CH_3CN, $CHCl_3$, C_6H_5F, toluene, DMSO, DMF and $(CH_2Cl)_2$. Our screening showed that, under the reaction conditions described in the Table 5.2, CH_3CN and CH_3Cl yielded to the best ratios (**α**:**β**) which were (83:0) and (79:8) respectively. In order to keep a perfect regioselectivity, we extended our study by using CH_3CN. The use of the others solvent leaded to either important decrease of conversion or the formation of unidentified side-products.

3.1.2.3. Influence of the temperature, the concentration and the reaction time.

A last set of parameters are the temperature, the concentration and the reaction time. By using our last conditions, we evaluated the effects of these three parameters (Table 5.3).

*Table 5.3 Optimization of the temperature, the reaction time and the concentration of $HPPh_2$ in the reaction outcomes. * Several unidentified side-products were formed.*

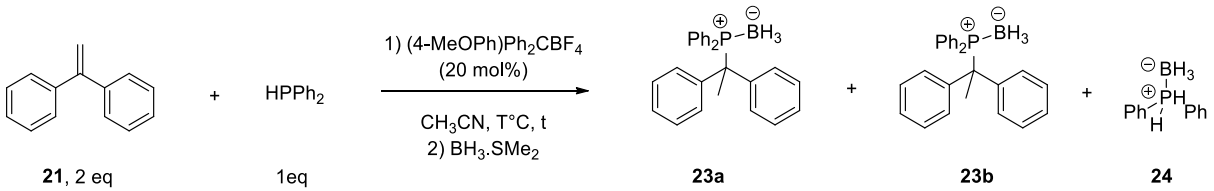

21, 2 eq 1eq **23a** **23b** **24**

Entry	[$HPPh_2$] (mol/L)	Temperature (°C)	Reaction time (h)	**23a** (%)	**23b** (%)	**24** (%)
1	0.5	20	24	2	0	90
2	0.5	60	24	18	5	77
3	0.5	90	24	90	6	4
4*	0.8	90	24	77*	2**	1*
5	0.2	90	24	63	34	3
6	0.4	90	16	95	3	2

After the optimization of the reaction conditions, we found that the α-hydrophosphination of **21** can be realized by employing 20 mol% of [4-(MeOPh)CPh_2][BF_4] **22d** in CH_3CN at 90°C for 16h to reach 95% conversion. After purification, **23a** was isolated in 81% yield.

3.1.3. Derivatization of the Markovnikov hydrophosphination

With the aim to evaluate the range of application of the method, we investigated the hydrophosphination of several aromatic alkenes **25a-p** diversely substituted (Scheme 5.13).

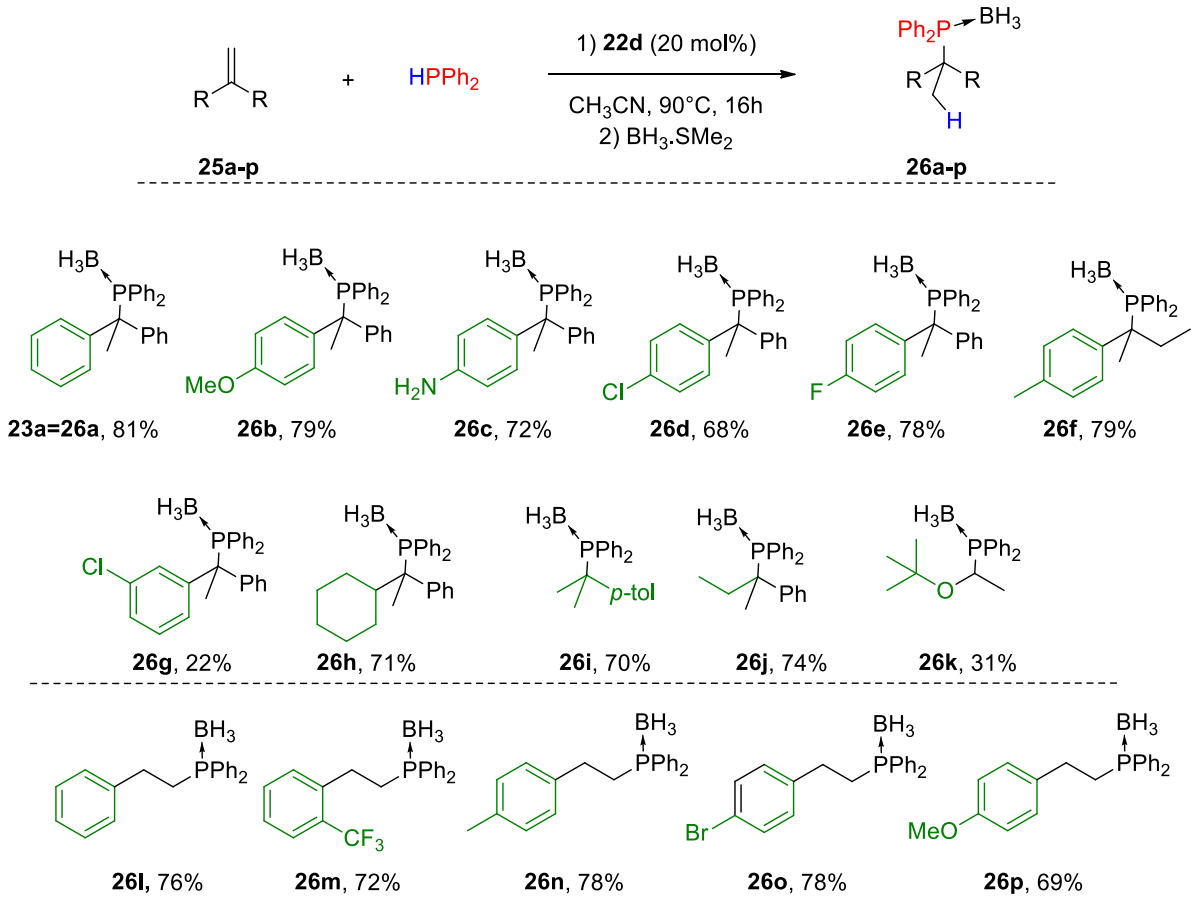

*Scheme 5.13 Scope of the tritylium salts catalysed hydrophosphination of aryl olefins. **25a-p** (2eq, 1.14 mmol), $HPPh_2$ (1eq, 0.57 mmol), **22d** (0.2 eq, 0.11 mmol), CH_3CN (1.4 mL, c = 0.4 mol/L).*

As shown in Scheme 5.13, 1,1-disubstituted olefins **25b,c,e,f** possessing electron donating groups or alkyl groups provide the α-adducts **26b,c,e,f** with good to excellent yields ranging from 81 to 68%. Interestingly, in **25g**, bearing a chloro substituent at the 3-position of the ring significantly decreased the yield to 22% compared to **25a** and **25d**. The hydrophosphination of the vinyl *tert*-butylether yielded the Markovnikov adduct **26k** in 31% yield. It also supports the mechanism involving a carbocation as carbocations possessing α-alkoxy groups are known to be stabilized. The structure of **26e** was confirmed using X-ray spectroscopy of **26e** obtained by slow evaporation of a solution in dichloromethane at r.t. for 2 days (Figure 5.1).

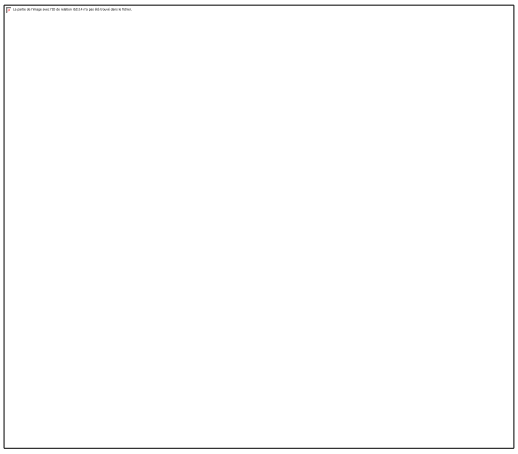

*Figure 5.1 X-ray structure of **26e** obtained by slow evaporation of a solution of **26e** in dichloromethane at r.t. in 2 days*

Regarding the reactivity of monosubstituted olefins **25l-p**, the anti-Markovnikov adducts **26l-p** have exclusively been isolated in good to excellent yields. It also supports the crucial requirement to have a stable sterically encumbered internal carbon.

In this part, we found an active organocatalysts and suitable conditions to perform the challenging α-hydrophosphination of olefins. While the scope showed that a broad range of olefins can be used, it is restricted to 1,1-disusbtituted olefins. The driving force of this reaction is the stability of the generated carbocation.

3.2. Insights in the reactions mechanisms of the organocatalyzed hydrophosphination.

Even if we have now strong proof of a reaction mechanism involving the protonation of the olefin by the phosphoniums salts and the formation of a carbocation, we wanted to confirm this hypothesis and gain further insights in the reaction mechanism.

3.2.1. Identification of the key parameters and catalytic species.

On the basis of our works on both $FeCl_3$ and tritylium salts catalyzed hydrophosphination of olefins, we can propose the following reaction mechanism (Figure 5.2). The proposed mechanism suggested that at least three parameters are relevant for the hydrophosphination.[20] i) The formation of the Lewis acid-Lewis base complex **27a**, ii) the pK_a of **27a** and thus the nature of HPR_2, and iii) the P-nucleophilicity of **27b**. As one might notice, these three parameters are dependent on both the phosphine and the tritylium cation. Because, we have already highlighted that only **22d** allow the formation of the α-adduct, we restricted the study to the investigation of the role of the phosphine.

[20] At this stage, we know that the alkene must be tuned to stabilize a carbocation intermediate and thus, we will not consider the influence of the olefin.

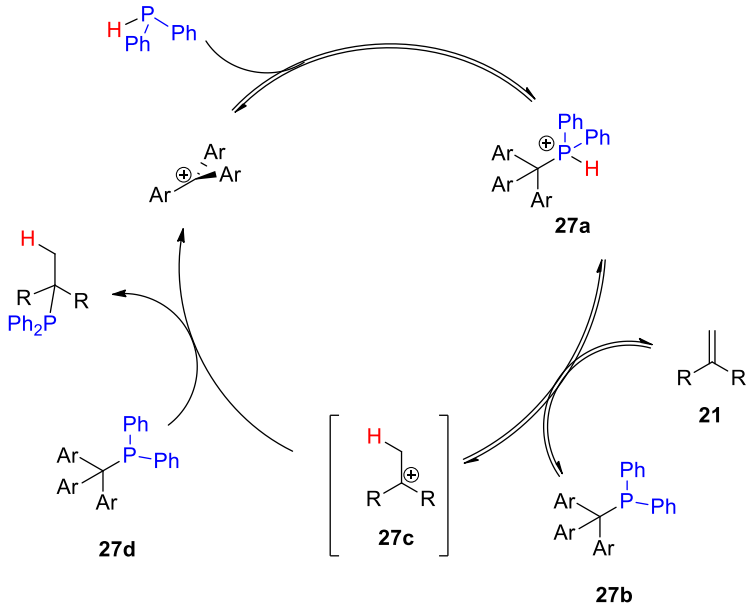

Figure 5.2 Expected reaction mechanism of the regioselective Markovnikov hydrophosphination of olefins catalysed by tritylium salts.

To do so, we considered two commercially available phosphines: $HPPh_2$ and $HPCy_2$. First of all, we studied the formation of **28a,b** by mixing 1 eq of $HPPh_2$ or $HPCy_2$ and 1 eq of **22d** in CH_3CN, respectively (Scheme 5.14). While the solution of **22d** in CH_3CN was red coloured, the addition of both $HPPh_2$ and $HPCy_2$ led to a deep decoloration to yield slightly yellow solutions. ^{31}P and ^{1}H NMR spectra of each solutions were recorded and are displayed in the Figure 5.3.

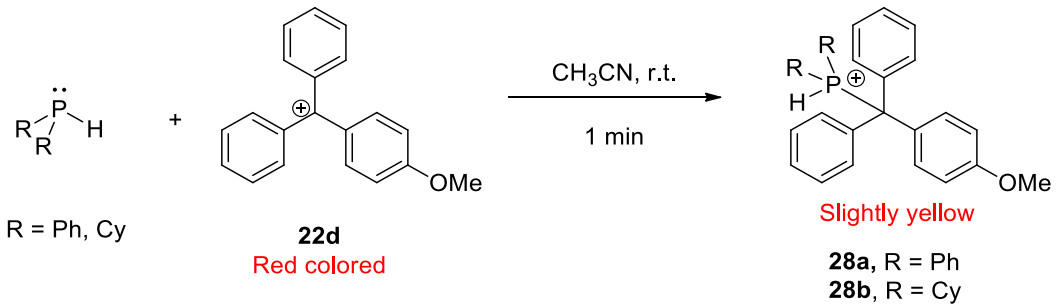

*Scheme 5.14 Synthesis of the intermediates **28a,b** resulting from the reaction of HPR_2 and **22d**. The counter-anion is $[BF_4]^-$, omitted for the sake of clarity.*

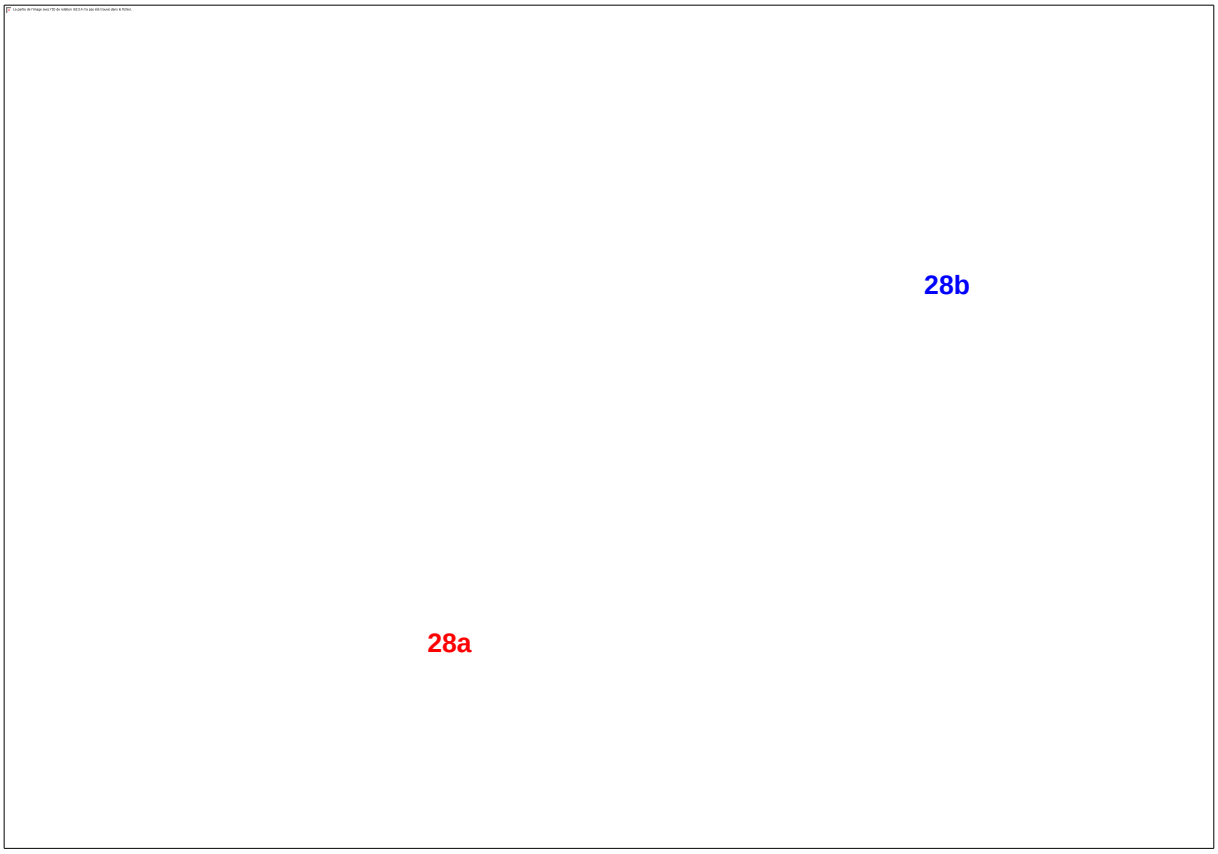

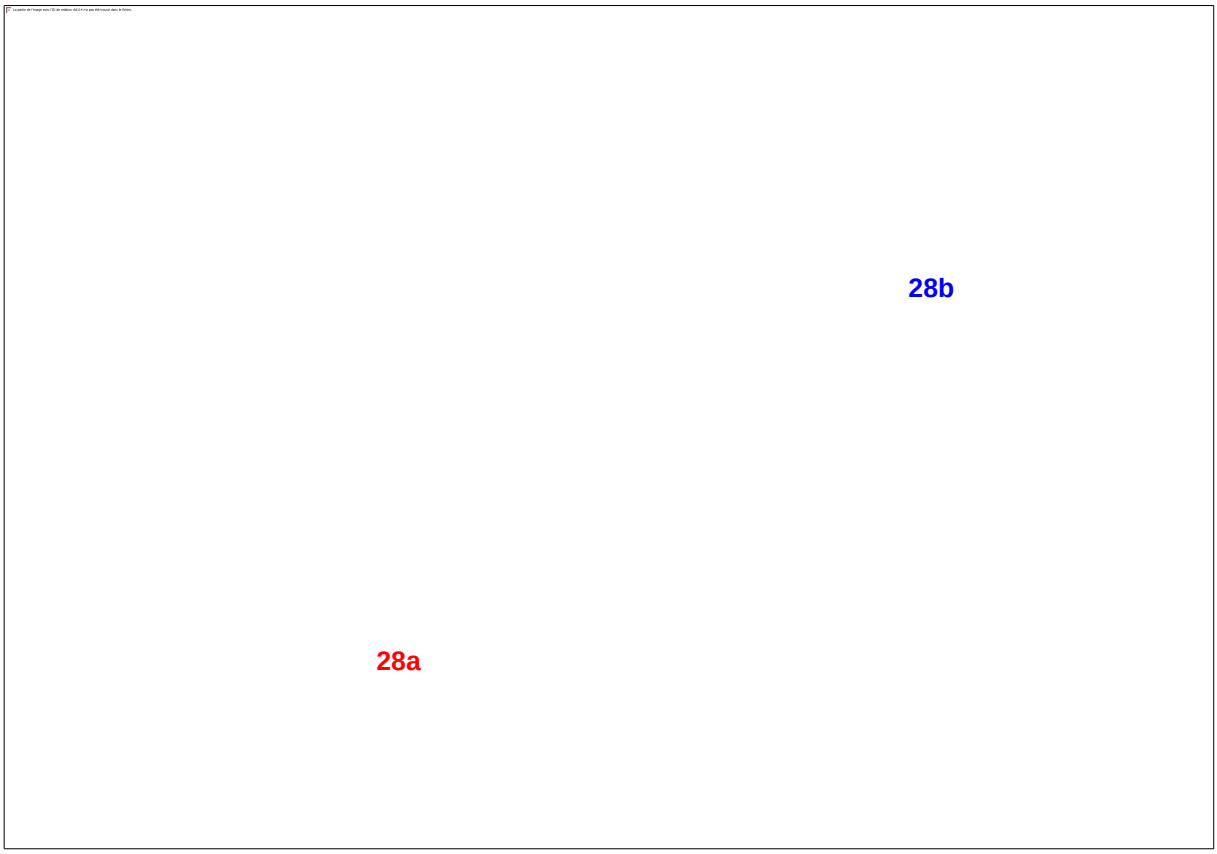

*Figure 5.3 ^{1}H NMR spectra of **28a,b** in CD_3CN at 20°C (top) and ^{31}P NMR spectra of **28a,b** in CD_3CN at 20°C (bottom)*

The Lewis-acid Lewis-base complexes **28a,b** are formed as both the ^{31}P and ^{1}H NMR spectra of $HPPh_2$ and $HPCy_2$ are strongly impacted. Regarding, **28a**, the hydrogen atom tethered to the phosphorous is still present and appears as a doublet with a coupling constant of 492 Hz as highlighted in both the ^{1}H and ^{31}P NMR spectra. Regarding the shift, the P-H bond of $HPPh_2$ alone is described at a doublet at δ = 5.21 ppm in ^{1}H NMR with a coupling constant of J = 220 Hz; and δ = -39.5 ppm in ^{31}P NMR.

As we can see, an important downfield shift occurs at both the H and P atoms of $HPPh_2$ showing a decrease of the electron density on P and an acidification of the proton in both **28a,b**. It is supported by the increasing values of the coupling constant from J = 220 Hz for to 450 Hz and 492 Hz for **28a** and **28b**, respectively, showing a weakening of the P-H bond. The same effect is observed with $HPCy_2$ but the shift of the proton is less pronounced.

3.2.2. Evaluation of the pK_a of the intermediates

Now we shed light on the formation of the Lewis-acid Lewis-base complexes **28a,b**, we targeted to investigate the pK_a of each phosphonium salts. We envisaged to use a method developed by Leito et al. successfully applied to the determination of the pK_a of phosphines in FLP chemistry.[21] Unfortunately, we were not able to extract relevant data from these methods. This is mainly due to the sensitivity of our compounds which slowly decomposes in air. Only a qualitative determination of the pK_a using bases with known pK_a was possible in CH_3CN at r.t. (even if we noticed the formation of some unidentified side-products along with the vanishes of **28a,b**). In the Table 5.4 are gathered the nature of the base and ratio between **28a,b** and its corresponding deprotonated form **29a,b**. Due to a lack of data about pKa in CH_3CN, reported values corresponds to pKa in water.[22]

*Table 5.4 Brief estimation of the pKa of **87a,b**. The ratio have been determined by NMR by excluding the presence of side products.*

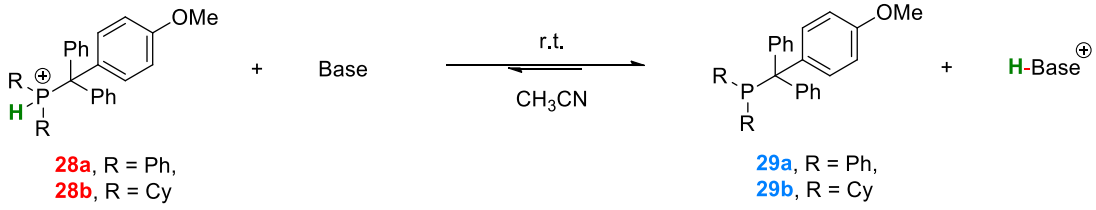

28a, R = Ph,
28b, R = Cy

29a, R = Ph,
29b, R = Cy

Acid	Base	pKa (base)	28a or 28b	29a or 29b
28a	Et_3N	11	0	100

[21] Greb, L.; Tussing, S.; Schirmer, B.; Oña-Burgos, P.; Kaupmees, K.; Lõkov, M.; Leito, I.; Grimme, S.; Paradies, J. *Chem. Sci.* **2013**, *4*, 2788.
[22] http://www.chem.wisc.edu/areas/reich/pkatable/

28a	imidazole	6	0	100
28a	$[CF_3CO_2][HPy]$	-0.3	0	100
28b	KHMDS	26	0	100
28b	*t*BuOK	17	20	80
28b	Et_3N	11	100	0

Even if the method is not accurate, we can postulate that the pK_a of **28a** < 0 while the pK_a of **28b** ≈ 20. This make a great difference in term of reactivity as the crucial step of our proposed mechanism is the formation of the carbocation.

3.2.3. Influence of the phosphine

To verify this effect of the pKa, the hydrophosphination of 1,1-diphenylethylene **21** have been performed with both **28a,b** under our previously optimized conditions as shown in the Scheme 5.15. The equation A shows that, in line with our hypothesis, the hydrophosphination does not take place with $HPCy_2$ presumably owing to the high pKa of the complex **28b**, unable to protonate **21**.

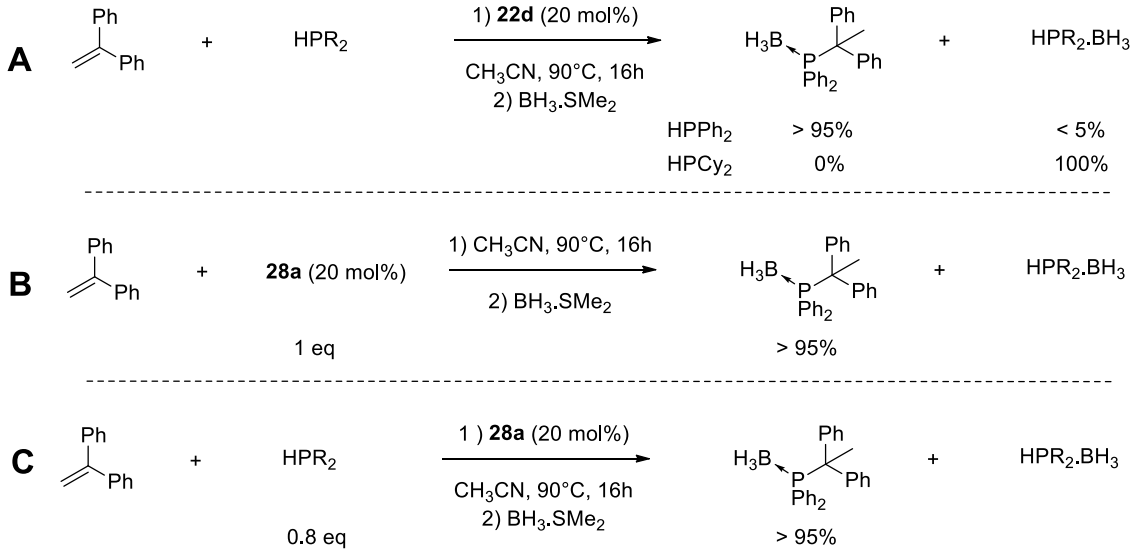

Scheme 5.15 Complementary hydrophosphination experiments to investigate A/ the effect of the phosphine and the pKa of the phosphonium salt, B/ and C/ the nature of the active species.

We also verified the involvement of **28a** in the reaction mechanism by reacting it with **21** under our previously optimized conditions (equation B). We were delighted to isolate the Markovnikov adduct in 79% yield after purification. Finally, the same experiment was conducted with only

20 mol% of **28a** and $HPPh_2$ to yield 80% of the desired adduct after purification, showing that **22d** successfully behave as a nucleofuge.

This last part provides further insights into the reaction mechanism of the regioselective Markovnikov hydrophosphination. It is now reasonable to postulate the involvement of a carbocation formed upon protonation of the olefin, confirming the proposed reaction mechanism (Figure 5.2). The nature of the phosphine as well as the fugacity of the tritylium salts are crucial parameters of this reactivity.

4. Conclusion and perspectives

4.1. Conclusion

This chapter has been dedicated to the development of an organic Lewis acid catalyzed Markovnikov regioselective hydrophosphination of alkenes. Traditionally, the selectivity for the Markovnikov adduct is achieved under acidic conditions or transition metal catalysis.

Based on this study and with the aim to develop an organocatalyzed approach, we employed tritylium cation as they were expected to reversibly bind secondary phosphines. Furthemore, we emphasized that the key step of the reaction mechanism was the formation of a Lewis-acid Lewis-base complex possessing an acidic proton. The pK_a of this proton have been shown to be crucial for the reactivity (Scheme 5.16).

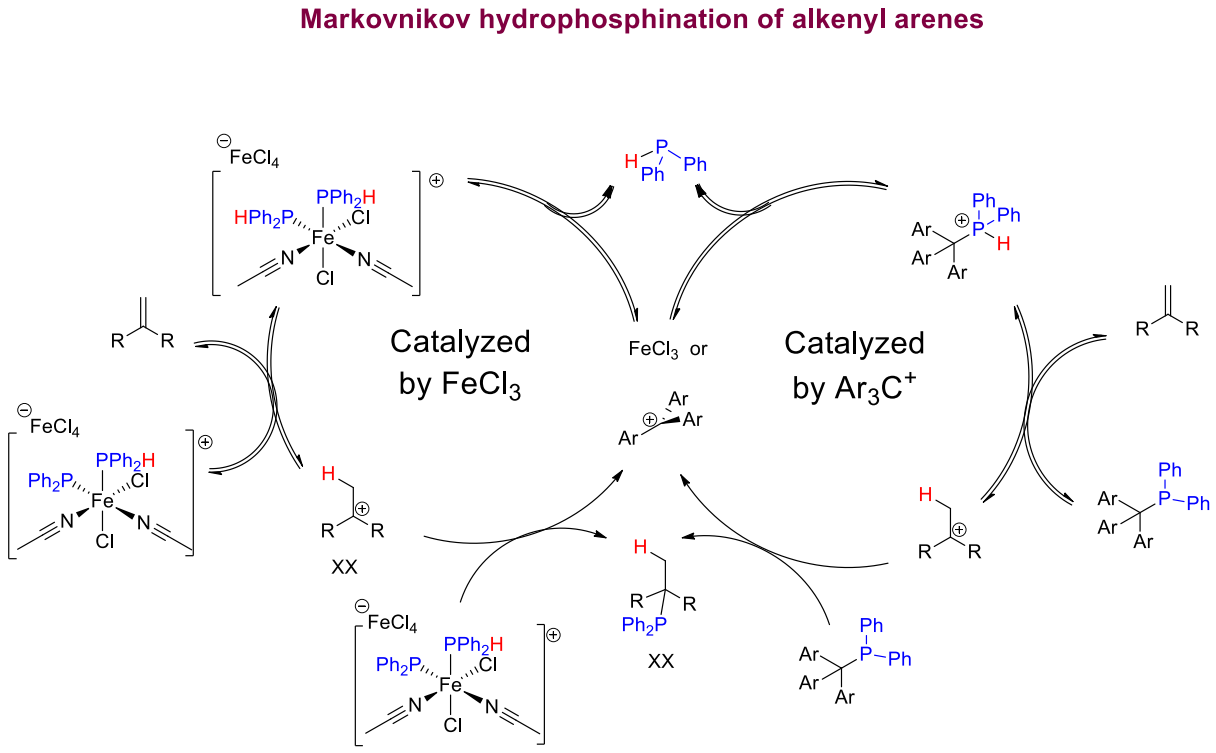

Scheme 5.16 Comparison of the Markovnikov catalysed hydrophosphination of alkenes with $HPPh_2$ catalysed by $FeCl_3$ or $[Ar_3C][BF_4]$. Acetonitrile have been added as it is the solvent.

Consequently, we hypothesized that the Markovnikov hydrophosphination would also proceed through the formation of a carbocation. Indeed, we found that 20 mol% of a tritylium salt catalyse the α-hydrophosphination of 1,1-disubstituted olefins with $HPPh_2$. The results provided useful mechanistic information to understand the puzzling $FeCl_3$-mediated hydrophosphination of styrenes previously reported in the group.

4.2. Perspectives

One of the main limitation in Markovnikov hydrophosphination of alkenes is the control of the enantioselectivity. Regarding an organometallic method, it would be fruitful to exploit the iron(III) catalyzed Markovnikov-hydrophosphination of alkenes, previously developed in our group. Assuming the same reaction mechanism than in the organocatalyzed version, a first method would be to take advantage of the formation of the carbocation by introducing a non-nucleophilic chiral anion (Scheme 5.17). Because the bond resulting from ion pair association are known to be strong, it might be anticipated that a "face" of the carbocation will be preferred during the attack of the phosphine. Based on this method, a solution would be to use a chiral phosphate anion.[23]

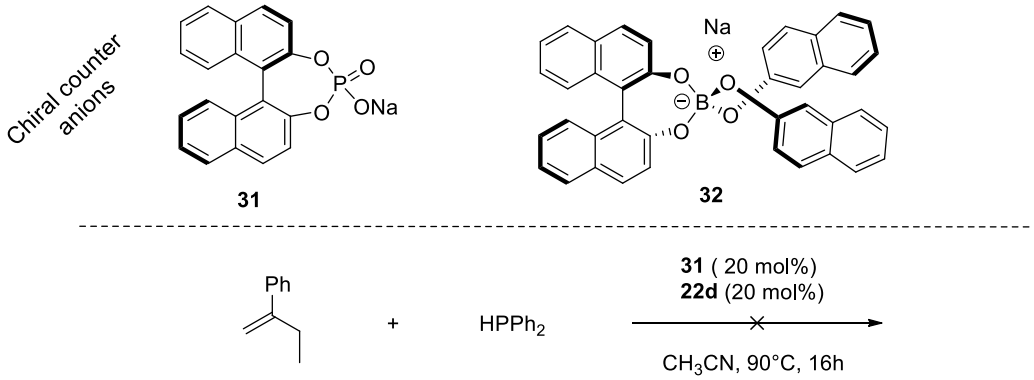

*Scheme 5.17 Structure of chiral anions and test of the enantioselective hydrophosphination of alkene catalyzed by **22d** and in the presence of the chiral phosphate anion **31**.*

We employed this strategy by using 20 mol% of the tritylum salt **22d** and 20 mol% of **31** (anion phosphate chirale) along with $HPPh_2$ and 1-phenyl-1-ethylethylene in CH_3CN at 90°C for 16h as shown in Scheme 5.17. Unfortunately, we didn't detect the formation of the Markovnikov adduct but the protonation of the phosphate anion to form the phosphoric acid (pK_a of diphenylphosphoric acid = 3.88 in dry DMSO). Another solution would be to use a chiral borate complexes **32**.[24] Because i) their synthesis is not straightforward and ii) a PhD last only three years, we did not investigate the potential of this way.

[23] Hamilton, G. L.; Kang, E. J.; Mba, M.; Toste, F. D. *Science* **2007**, *317*, 496.
[24] Llewellyn, D. B.; Adamson, D.; Arndtsen, B. A. *Org. Lett.* **2000**, *2*, 4165.

General Conclusion

This thesis presented the results of our research on the study of the interactions between organophosphorus and organoborane compounds, going from frustration of the P-B bond to organophosphorus borane complexes possessing strong P-B bond. The exploration of these modes of interaction combined with deep mechanistic studies allowed us design new types of reactions.

Figure 1 Summary of the fields explored during this PhD

In the first chapter, the activation of H_2 using two sterically hindered triarylphosphines in the presence of $B(C_6F_5)_3$ P/B FLPs was investigated. It was found that the encounter complex resulting from the heterolytic cleavage of H_2, already known to be an active catalyst in the hydrogenation of electron rich olefins, heterocycles and imines reacts differently with Michael acceptors. Indeed, a competition between the expected hydrogenation adducts and 1,4-hydrophosphination adduct, resulting from the addition of the triarylphosphine takes place. The competition has been investigated by kinetic and thermodynamic studies and the results were discussed along with Mayr linear free energy relationships. It led us to demonstrate that both the nucleophilicity and the Lewis basicity of triarylphosphines are the key parameters governing the competition between hydrogenation and hydrophosphination during the FLP catalyzed reduction of Michael acceptors. Besides, by exploiting the observed hydrophosphination occurring between phosphonium salts $[H\text{-}PR_3]^+[X]^-$ and several Michael acceptors, we developed a procedure to realize the intramolecular cross-coupling metathesis of diallyl phosphonium salts.

In a second chapter, the utilization of phosphine borane complexes as hydride donors was studied. Therefore, the hydricity of a representative array of primary, secondary and tertiary

phosphine boranes complexes was measured, showing that the nucleophilicity parameters are similar to that of trialkyl- or triarylamine borane complexes and silanes. Furthermore, we highlighted that both the geometry and the electronic structure of phosphines influence the hydricity of PBs. In fact, we found a correlation between the stability of the borenium cation resulting from the hydride abstraction of PBs and its hydricity. On the basis of these data, we were able to build a scale predicting the feasibility of the reduction of electrophiles with PBs.

In a third chapter, a migration reaction of the perfluorinated group C_6F_5 has been noticed during the reaction of phosphinite borane complexes and $B(C_6F_5)_3$ at elevated temperature, while an intramolecular borylation of the phosphinite borane complex was expected. Mechanistic investigations were conducted in order to rationalize the formation of the migration adduct. A combination of NMR and kinetics studies demonstrated that $B(C_6F_5)_3$ is able to abstract a hydride from the phosphorous borane precursor. Due to the assumption of the involvement of non-isolable intermediates, a detailed DFT-study was done to explain the origin of the migration, the requirement of elevated temperatures as well as the involvement of a “pseudo-borenium cation” in the transitions state.

In a fourth chapter, the regioselective Markovnikov hydrophosphination of styrene derivatives with $HPPh_2$ was investigated. In a first place, an iron(III) catalyzed reaction, already developed in our lab was studied to understand the origin of the regioselectivity. This study led us to design an organic Lewis acid catalyzed approach. Indeed, the use of 20 mol% of a tritylium salt catalyses the Markovnikov hydrophosphination of $HPPh_2$ to 1,1-disubstituted olefins. Mechanistic insights highlighted the probable involvement of a carbocation resulting from the protonation of the olefin which rationalizes the origin of the limited scope of olefins.

Experimental part

1. Materials and Analytics

1.1 Chemicals

All solvents were reagent grade. Toluene, THF, diethyl ether, acetonitrile and dichloromethane were purified by an Innovative Technology PURESOLV® purification system. Other chemicals were purchased from Acros Organics, Sigma aldricht or Fischer and used as received except PCl_3 and $B(C_6F_5)_3$ which were distilled or sublimated prior to use. Benzhydrylium ions were kindly offered by the group of Prof. Dr. Herbert Mayr (University of Munich). The solvents for the kinetic measurements were dried over CaH_2 and stored with 3Å MS under an argon atmosphere.

1.2 Analytics

^{1}H, ^{31}P, ^{11}B, ^{19}F and ^{13}C NMR spectra were recorded on a Bruker 400 MHz or 500 MHz spectrometers in $CDCl_3$, CD_2Cl_2 and CD_3CN. Chemical shifts are reported in ppm relative to the residual signals of the deuterated solvents as the internal standard ($CDCl_3$: δ_H = 7.26, δ_C = 77.2; CD_3CN: δ_H = 1.94, δ_C = 1.3; CD_2Cl_2: δ_H = 5.32, δ_C = 53.8). ^{13}C NMR spectra were recorded using an internal reference, ^{31}P NMR spectra were recorded using 85% H_3PO_4 as external reference, ^{11}B NMR spectra were recorded using $BF_3{\bullet}Et_2O$ as external reference and ^{19}F NMR spectra were recorded using $CFCl_3$ as external reference. Multiplicities are indicated by s (singlet), d (doublet), t (triplet), q (quartet), m (multiplet), and br (broad). Coupling constants, *J*, are reported in Hertz. Infrared spectra were recorded on a Spectrum One FT-IR Perkin Elmer spectrophotometer. High-resolution mass-spectra were obtained on a Waters Qtof Micro spectrometer. Melting points were recorded on a Gallenkamp Melting Point Apparatus.

1.3 Kinetics

The kinetics of the reactions of nucleophiles with the benzhydrylium ions were followed by UV/vis spectroscopy in CH_2Cl_2 or CH_3CN by using an Applied Photophysics SX20 Stopped Flow Spectrophotometer system. The kinetic measurements were performed with freshly prepared solutions of the phosphines in dichloromethane or acetonitrile. Kinetic runs were initiated by mixing equal volumes of solutions of the phosphines with the benzhydrylium tetrafluoroborates. The temperature of the solutions during the kinetic studies was maintained to (20 ± 0.2) °C by using circulating bath cryostats. Kinetic investigations of all reactions were performed with a high excess of over the electrophiles resulting in first-order kinetics. As a consequence, mono-exponential decays of the absorbance of the benzhydrylium ions were observed. The rate constants k_{obs} (s^{-1}) were obtained by least-squares fitting of the function $A(t) = A(0)\exp(-k_2.t) + C.t(0)$. According to the following equation $k_{obs} = k_2.[Nu]$, the first-

order rate constants k_{obs} were linearly dependent on the nucleophile concentrations, whereby the slopes corresponded to the second-order rate constants k_2 ($M^{-1}s^{-1}$).

1.4 Equilibrium constants

The equilibrium constants K for the reactions of Lewis bases with benzhydrylium ions were determined photometrically by monitoring the decays of the Lewis acids at λ_{max}. The measurements were carried out using a SX20 Stopped Flow spectrometer, which was controlled by Pro-Data SX software and connected to a Hellma 661.502-QX quartz Suprasil immersion probe (light path d = 2 mm) via fiber optic cables and standard SMA connectors. When the Lewis base was added to a solution of the stable benzhydrylium tetrafluoroborate, the absorbance gradually decreased from a constant value (A0). After a few seconds, when the equilibrium was reached (absorbances became constant (A)) leading to the maximum amount of the adduct (Ad). This procedure was repeated several times for each benzhydrylium salt solution. Assuming the validity of the Lambert-Beer law for the linear correlation between the absorbances and the concentrations of the benzhydrylium ions, the equilibrium constants K were determined according to the equations:

$$LA + LB \rightleftharpoons Ad \qquad\qquad K = \frac{[Ad]}{[LA]\times[LB]}$$

Finally, the K constants were determined using the following equation:

$$K = \frac{(A0 - A)}{A([LB]_0 - \frac{(A0 - A)}{\varepsilon \times d}}$$

Where the absorbance of the benzhydrylium ion (LB) before the addition is (A0) and after is (A), the concentration of the Lewis bases (LB) is written [LB], Ɛ is the molar extinction coefficient reported by Mayr and d the pathlenght of the spectrophotometer. [1] The temperature of the solutions during all equilibrium studies was kept constant at (20.0 ± 0.1) °C using a circulating bath thermostat. Note: for some carbocations, a plateau was not observed (the final absorbance was not constant). Consequently, the value of the final absorbance was taken from the tail of the exponential curve fitting.

[1] H. Mayr, J. Ammer, M. Baidya, B. Maji, T. A. Nigst, A. R. Ofial, T. Singer, *J. Am. Chem. Soc.* **2015**, *137*, 2580–2599.

Chapter 2: Metal-free Hydrogenation of electron-poor olefins catalysed by P/B Frustrated Lewis Pairs.

1. Synthetic part
   1.1 Preparation of phosphines **33,34** and **47**.

Tri(1-naphthyl)phosphine 33

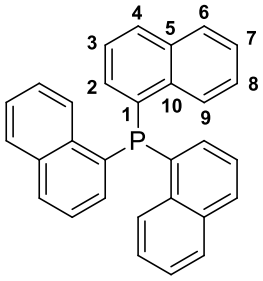

Formula : $C_{30}H_{21}P$
MW : 412.46 g/mol

The synthesis of **33** was performed following a modified procedure by Dabbawala *et al*.[1] A dried Schlenk flask was charged with 1-bromonaphthalene (5.2 mL, 37.7 mmol, 3.3 eq) in THF (30 mL) under an argon atmosphere. The mixture was cooled at -78°C and a solution of *n*-BuLi (25 mL of a 1.5 M solution in hexane, 37.7 mmol, 3.3 eq) was added dropwise under stirring. The reaction mixture was stirred for 1 h and a THF solution of phosphorous trichloride (1 mL, 11.42 mmol, 1 eq) was slowly added at -78°C over 10 min and stirred for 5 additional hours at 0°C. The brown mixture was then allowed to warm to room temperature; precipitated out inorganic salt was filtered off and washed with dry THF (2 × 10 mL). The precipitate was solubilized in dichloromethane (50 mL), and the organic phase was washed with saturated solutions of NH_4Cl (2 × 20 mL) and $NaHCO_3$ (20 mL) before drying over $MgSO_4$. The solvent was removed in vacuo to furnish **33** as a white solid (2.61 g, 6.33 mmol, 55%).

^{1}H-NMR (400.1 MHz, $CDCl_3$): δ 8.55 (dd, $^3J_{HH}$ = 8.3 Hz, $^4J_{HH}$ = 4.5 Hz, 3H, 4-H), 7.91 (d, $^3J_{HH}$ = 8.0 Hz, 3H, 9-H), 7.86 (d, $^3J_{HH}$ = 8.3 Hz, 3H, 6-H), 7.51 (d, $^3J_{HH}$ = 7.4 Hz, 3H, 3-H), 7.44 (d, $^3J_{HH}$ = 8.3 Hz, 3H, 8-H), 7.26 (d, $^3J_{HH}$ = 7.7 Hz, 3H, 7-H), 6.98 (d, $^3J_{HH}$ = 5.8 Hz, 3H, 2-H). **^{13}C-NMR** (100.6 MHz, $CDCl_3$): δ 135.8 (d, $^1J_{PC}$ = 23.0 Hz, Ar-C), 133.7 (d, $^2J_{PC}$ = 4.2 Hz, Ar-C), 133.6 (s, Ar-C), 133.0 (d, $^2J_{PC}$ = 10.7 Hz, Ar-C), 129.8 (s, Ar-C), 128.9 (d, $^2J_{PC}$ = 2.1 Hz, Ar-C), 126.8 (s, Ar-C), 126.6 (s, Ar-C), 126.2 (s, Ar-C), 126.1 (s, Ar-C). **^{31}P-NMR** (162.0 MHz, $CDCl_3$): δ -33.1 (s, P). **Mp** = 260-261°C. **IR** (neat, ATR probe, cm^{-1}): v 3046, 1499, 1383, 1331, 1256, 1205, 1163, 1139, 1022, 976, 951, 861, 822, 799, 774. **HRMS** (ESI positive) = [$C_{30}H_{22}P^+$] Calculated mass: 413.1459 g/mol, found mass: 413.1452 g/mol.

Tri(*o*-tolyl)phosphine 34

[1] Dabbawala, A. A.; Bajaj, H. C.; Rao, G. V. S.; Abdi, S. H. R. *Appl. Catal., A.* **2012,** *419–420,* 185.

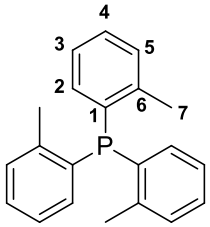

Formula : $C_{21}H_{21}P$
MW : 304.37 g/mol

The synthesis of **34** was done following a modified procedure reported by Goel *et al*.[2] A solution of 2-bromotoluene (5.00 mL, 41.6 mmol, 3.05 eq), in degassed THF (40 mL) was added dropwise to magnesium turnings (1.026 g, 42.2 mmol, 3.1 eq) under stirring at r.t. The addition rate was adjusted to maintain the reflux which corresponds to 40 min. The yellowish solution was then stirred at reflux for 1h before cooling down to r.t. A solution of phosphorus trichloride (1.20 mL, 13.6 mmol, 1 eq) in degassed THF (40 mL) was added dropwise to the Grignard solution in 30 minutes, leading to a yellowish solution, which was stirred for an additional hour at r.t. The crude mixture was quenched with an aqueous solution of saturated NH_4Cl (60 mL). The aqueous phase was extracted with degassed diethyl ether (2 × 40 mL) and the combined organic phases were dried over $MgSO_4$. The solvent was evaporated and the yellowish residue was recrystallized from hot ethanol two times to yield **34** as transparent crystalline needles (3.49 g, 11.5 mmol, 85%).

^{1}H-NMR (400.1 MHz, $CDCl_3$): δ 7.30-7.23 (m, 6H, 4,5-H), 7.11-7.07 (m, 3H, 3-H), 6.76-6.73 (m, 3H, 2-H), 2.41 (s, 9H, 7-H). **^{13}C-NMR** (100.6 MHz, $CDCl_3$): δ 142.8 (d, $^2J_{PC}$ = 25.9 Hz, Ar-C), 134.5 (d, $^1J_{PC}$ = 11.2 Hz, Ar-C), 133.2 (s, Ar-C), 130.2 (d, $^4J_{PC}$ = 5.2 Hz, Ar-C), 128.8 (s, Ar-C), 126.3 (s, Ar-C), 21.3 (d, $^3J_{PC}$ = 21.6 Hz, 7-C). **^{31}P-NMR** (162.0 MHz, $CDCl_3$): δ –29.6 (s, P). **Mp** = 126-127 °C. **IR** (neat, ATR probe, cm^{-1}): v 3056, 3002, 2969, 1587, 1466, 1450, 1377, 1270, 1201, 1160, 1129, 1068, 1030, 985, 800, 746, 716. **HRMS** (ESI) = [$C_{21}H_{22}P^+$] Calculated mass: 305.1459 g/mol, found mass: 305.1462 g/mol.

Ethyldiphenylphosphine 47

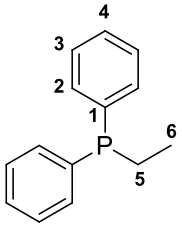

Formula : $C_{14}H_{15}P$
MW : 214.24 g/mol

A solution of ethylbromide (1.15 mL, 15.5 mmol, 1.1 eq), in degazed Diethyl ether (20 mL) was added dropwise to magnesium turnings (394 mg, 16.2 mmol, 1.1 eq) under stirring at r.t. The addition rate was adjusted to maintain the reflux which corresponds to 30 min. The brownish solution was stirred at reflux for 1h before cooling down to r.t. A solution of chlorodiphenylphosphine (2.64 mL, 14.7 mmol, 1.0 eq) in degazed diethyl ether (20 mL) was then added dropwise to the Grignard solution in 30 minutes leading to a yellowish solution which was stirred for an additional hour at r.t. The crude mixture was quenched with an aqueous solution of saturated NH_4Cl (15 mL) followed by water (10 mL) to dissolve the precipitates. The crude mixture was extracted with Diethyl ether (1 ×

[2] Allman, T.; Goel, R. G. *Can. J. Chem.* **1982**, *60*, 716.

20 mL) using a cannula and the solvent of the combined organic phases removed in vaccuo leading to **47** as a colourless oil (1.82 g, 8.5 mmol, 58%).

^{1}H-NMR (400.1 MHz, $CDCl_3$): δ 7.52-7.48 (m, 4H, H-3), 7.39-7.37 (m, 6H, H-2,4), 2.12 (q, $^{3}J_{HH}$ = 7.5 Hz, 2H, H-5), 1.16 (dt, $^{3}J_{HP}$ = 17.1 Hz, $^{3}J_{HH}$ = 7.5 Hz, 3H, H-6). **^{13}C-NMR** (100.6 MHz, $CDCl_3$): δ 138.9 (d, $^{4}J_{PC}$ = 8.7 Hz, C-1), 132.8 (d, $^{2}J_{PC}$ = 13.7 Hz, C-2), 128.6 (s, C-4), 128.5 (d, $^{3}J_{PC}$ = 12.1 Hz, C-3) 20.8 (d, $^{1}J_{PC}$ = 8.7 Hz, C-5), 10.2 (d, $^{2}J_{PC}$ = 15.8 Hz, C-6). **^{31}P-NMR** (162.0 MHz, $CDCl_3$): δ – 11.5 (s, P). **IR** (neat, ATR probe, cm^{-1}): Not determined due to the sensivity of the product toward air. **bp** = 291-292 °C / litt. 293°C. **MS/MS**(ESI) = $[C_{14}H_{16}P^{+}]$ Calculated mass: 215.1 g/mol, found mass: 215.1 g/mol.

1.2 Preparation of the phosphonium trifluoromethanesulfonate or tetrafuoroborate salts **33c, 34c, 43-47[OTf/BF_4]** and **84**.

General procedure

A 100 mL two necked round bottomed flask equipped with a stirrer was flamed two times in vacuo (10^{-2} mbar), backfilled with argon, and charged with the phosphine (3.81 mmol, 1 eq). Degassed diethyl ether (20 mL) was then added and the mixture was stirred for 5 min at r.t. until the phosphine was completely dissolved. The solution was subsequently cooled down to 0°C using an ice-bath. The dropwise addition of triflic acid (0.4 mL, 4.60 mmol, 1.2 eq) or $HBF_4.OEt_2$ (560 µL, 4.57 mmol, 1.2 eq) to this solution resulted in the formation of a white precipitate. The mixture was warmed at r.t. and stirred for additional 30 minutes. The resulting white precipitate was then filtrated and washed with cold diethyl ether (2 × 15 mL).

Tri(1-naphtyl) phosphonium trifluoromethanesulfonate salt 33c

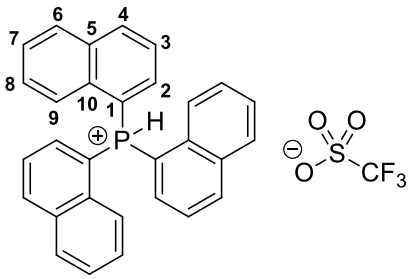

Formula : $C_{31}H_{22}F_3O_3PS$
MW : 562.54 g/mol

33c (1.865 g, 3.32 mmol, 87%).

33 (1.571 g, 3.81 mmol, 1 eq).

^{1}H-NMR (400.1 MHz, CD_3CN): δ 10.16 (d, $^{1}J_{HP}$ = 504.0 Hz, 1H, HP^{+}), 8.49-8.47 (m, 3H, Ar-H), 8.23-8.21 (m, 3H, Ar-H), 7.99-7.97 (m, 3H, Ar-H), 7.78-7.74 (m, 3H, Ar-H), 7.68-7.61 (m, 9H, Ar-H). **^{13}C-NMR** (100.6 MHz, CD_3CN): 139.4 (d, J_{PC} = 7.0 Hz, Ar-C), 138.3 (s, Ar-C), 134.9 (d, J_{PC} = 5.5 Hz, Ar-C), 133.8 (d, J_{PC} = 5.4 Hz, Ar-C), 131.1 (s, Ar-C), 130.4 (s, Ar-C), 129.1 (s, Ar-C), 127.0 (d, J_{PC} = 15.3 Hz, Ar-C), 125.4 (d, J_{PC} = 6.0 Hz, Ar-C), 110.7 (d, J_{PC} = 93.0 Hz, Ar-C), CF_3 was not detected. **^{31}P-NMR** (162.0 MHz, $CDCl_3$): δ –14.4 (d, $^{1}J_{HP}$ = 504.0 Hz, PH). **^{19}F-NMR** (376.5 MHz, $CDCl_3$): δ –79.4 (s, CF_3). **Mp =** 145-146 °C (decomposition). **IR** (neat, ATR probe, cm^{-1}): ν 2376, 2109, 1593, 1569, 1475, 1455, 1393, 1276, 1240, 1221, 1151, 1085, 1030, 927, 805, 768, 756, 708, 696. **HRMS**

(ESI positive) = [$C_{30}H_{22}P^+$] Calculated mass: 413.1459 g/mol, found mass: 413.1458 g/mol. (ESI negative) = [$CF_3O_3S^-$] Calculated mass: 148.9523 g/mol, found mass: 148.9520 g/mol.

Tri(o-tolyl) phosphonium trifluoromethanesulfonate salt 34c

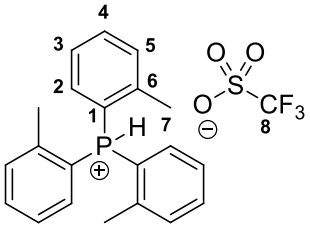

Formula : $C_{22}H_{22}F_3O_3PS$
MW : 454.44 g/mol

34c (1.632 g, 3.59 mmol, 94%).

34 (1.200 g, 3.81 mmol, 1 eq).

^{1}H-NMR (400.1 MHz, $CDCl_3$): δ 9.98 (d, $^1J_{HP}$ = 532.0 Hz, 1H, HP^+), 7.71 (d, $^3J_{HH}$ = 7.6 Hz, 3H, 5-H), 7.52 (d, $^3J_{HH}$ = 7.5 Hz, 3H, 4-H), 7.39 (d, $^3J_{HH}$ = 7.5 Hz, 3H, 3-H), 7.13 (dd, $^3J_{HP}$ = 15.8 Hz, $^3J_{HH}$ = 7.5 Hz, 3H, 2-H), 2.53 (s, 9H, 7-H). **^{13}C-NMR** (100.6 MHz, $CDCl_3$): 144.9 (d, $^2J_{PC}$ = 9.0 Hz, Ar-C), 135.8 (d, $^4J_{PC}$ = 3.3 Hz, Ar-C), 134.5 (d, $^2J_{PC}$ = 12.1 Hz, Ar-C), 133.0 (d, $^3J_{PC}$ = 10.0 Hz, Ar-C), 127.9 (d, $^3J_{PC}$ = 13.0 Hz, Ar-C), 120.9 (q, $^1J_{CF}$ = 320 Hz, CF_3, 8-C), 113.7 (d, $^1J_{PC}$ = 86.0 Hz, Ar-C), 21.4 (d, $^2J_{PC}$ = 6.1 Hz, 7-C). **^{31}P-NMR** (162.0 MHz, $CDCl_3$): δ –13.8 (d, $^1J_{HP}$ = 421.0 Hz, 1H, PH). **^{19}F-NMR** (376.5 MHz, $CDCl_3$): δ –78.2 (s, CF_3). **Mp =** 176-177 °C (decomposition). **IR** (neat, ATR probe, cm^{-1}): v 2376, 2109, 1593, 1569, 1475, 1455, 1393, 1276, 1240, 1221, 1151, 1085, 1030, 927, 805, 768, 756, 708, 696. **HRMS** (ESI positive) = [$C_{21}H_{22}P^+$] Calculated mass: 305.1459 g/mol, found mass: 305.1457 g/mol. (ESI negative) = [$CF_3O_3S^-$] Calculated mass: 148.9520 g/mol, found mass: 148.9520 g/mol.

Triphenylphosphonium tetrafluoroborate salt 43b[BF_4]

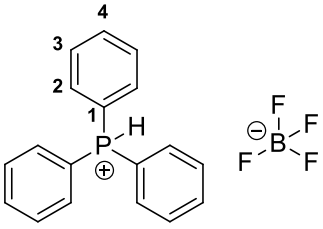

Formula : $C_{18}H_{16}BF_4P$
MW : 350.10 g/mol

43b[BF_4] (1.215 g, 3.47 mmol, 91%)

43 (1.00 g, 3.81 mmol, 1 eq).

^{1}H-NMR (400.1 MHz, $CDCl_3$): δ 9.12 (d, $^1J_{HP}$ = 536.0 Hz, 1H, PH), 7.80-7.74 (m, 9H, H-2,4), 7.67-7.63 (m, 6H, H-3). **^{13}C-NMR** (100.6 MHz, $CDCl_3$): δ 135.6 (s, C-4), 134.2 (d, $^2J_{PC}$ = 10.3 Hz, C-2), 130.7 (d, $^3J_{PC}$ = 11.3 Hz, C-3), C-1 not observed. **^{31}P-NMR** (162.0 MHz, $CDCl_3$): δ 3.8 (d, $^1J_{HP}$ = 536.0 Hz, 1H, P^+). **^{11}B-NMR** (128.4 MHz, $CDCl_3$): δ - 0.8 (s, BF_4). **^{19}F-NMR** (376.5 MHz, $CDCl_3$): δ – 150.2 (s, BF_4). **Mp** = 158-159°C (decomposition). **IR** (neat, ATR probe, cm^{-1}): v 3072 (C=C), 2421, 2112, 1585, 1483, 1439, 1333, 1288, 1167, 1076, 1024 (HP^+), 998, 912, 884, 770, 737, 698, 683. **HRMS** (ESI positive) = [$C_{18}H_{16}P^+$] Calculated mass: 263.0990 g/mol, found mass: 263.0978 g/mol. (ESI negative) = [BF_4^-] Calculated mass: 87.0 g/mol, found mass: 87.0 g/mol.

Triphenylphosphonium trifluoromethanesulfonate salt 43b[OTf]

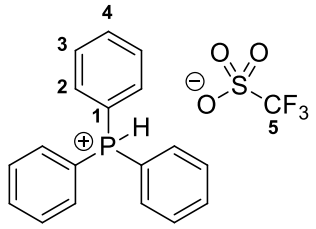

Formula : $C_{19}H_{16}F_3O_3PS$
MW : 412.36 g/mol

43b[OTf] (1.541 g, 3.74 mmol, 98%).

43 (1.00 g, 3.81 mmol, 1 eq).

^{1}H-NMR (400.1 MHz, $CDCl_3$): δ 9.69 (d, $^{1}J_{HP}$ = 540.0 Hz, 1H, PH), 7.81-7.76 (m, 9H, H-2,4), 7.68-7.63 (m, 6H, H-3). **^{13}C-NMR** (100.6 MHz, $CDCl_3$): δ 135.4 (d, $^{4}J_{PC}$ = 6.2 Hz, C-4), 134.1 (d, $^{2}J_{PC}$ = 10.1 Hz, C-2), 130.6 (d, $^{3}J_{PC}$ = 12.3 Hz, C-3), 120.7 (q (partial), $^{1}J_{CF}$ = 320 Hz, CF_3, C-7), 116.0 (d, $^{1}J_{PC}$ = 90.4 Hz, C-1). **^{31}P-NMR** (162.0 MHz, $CDCl_3$): δ 2.0 (d, $^{1}J_{HP}$ = 540.0 Hz, 1H, PH). **^{19}F-NMR** (376.5 MHz, $CDCl_3$): δ 6 78.3 (s, CF_3). **Mp =** 106-107 °C (decomposition). **IR** (neat, ATR probe, cm^{-1}): v 3064 (C=C), 2405, 2160, 1979, 1586, 1480, 1441, 1274, 1251, 1225, 1194, 1151, 1114, 1029 (HP^+), 906, 747, 722 and 689. **HRMS** (ESI positive) = [$C_{18}H_{16}P^+$] Calculated mass: 263.0990 g/mol, found mass: 263.0999 g/mol. (ESI negative) = [$CF_3O_3S^-$] Calculated mass: 149.0 g/mol, found mass: 149.0 g/mol.

D-triphenylphosphonium trifluoromethanesulfonate salt D-43b[OTf]

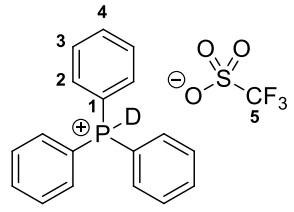

Formula : $C_{19}H_{15}DF_3O_3PS$
MW : 413.37 g/mol

D-43b[OTf] (1.558 g, 3.77 mmol, 99%).

Triphenylphosphine (1.000 g, 3.81 mmol, 1 eq).

^{1}H-NMR (400.1 MHz, $CDCl_3$): δ 7.81-7.76 (m, 9H, H-2,3), 7.68-7.63 (m, 6H, H-3).

Methyldiphenylphosphonium trifluoromethanesulfonate salt 44b[OTf]

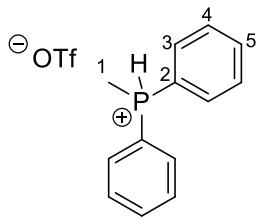

Chemical Formula: $C_{14}H_{14}F_3O_3PS$
Molecular Weight: 350.29

44b[OTf] (1.295 g, 3.70 mmol, 97%).

44 (763 mg, 3.81 mmol, 1 eq).

^{1}H-NMR (400.1 MHz, $CDCl_3$): δ 7.84-7.76 (m, 6H, H-3,5), 7.68-7.63 (m, 2H, H-4), 2.54 (d, *J* = 16.2 Hz, 3H, H-1), PH was not observed. **^{13}C-NMR** (100.6 MHz, $CDCl_3$): δ 135.5 (d, *J* = 5.8 Hz, C-Ar), 133.2 (d, *J* = 11.0 Hz, C-Ar), 130.7 (d, *J* = 15.2 Hz, C-Ar), 116.8 (d, $^{1}J_{PC}$ = 86.0 Hz, C-2), 6.7 (d, *J* = 51.2 Hz, C-1), CF_3 was not observed. **^{31}P-NMR** (162.0 MHz, $CDCl_3$): δ 1.2 (br, PH). **^{19}F-NMR** (376.5 MHz, $CDCl_3$): δ – 78.4 (s, CF_3). **Mp =** 88-89°C (decomposition). **IR** (neat, ATR probe, cm^{-1}): v 2922, 2330, 2089, 1441, 1407, 1300, 1260, 1223, 1151, 1115, 1028, 980, 939, 922, 813, 744, 686. **HRMS** (ESI positive) = [$C_{13}H_{14}P^+$] Calculated mass: 201.0833 g/mol, found mass: 201.0835 g/mol.

Dimethylphenylphosphonium trifluoromethanesulfonate salt 45b[OTf]

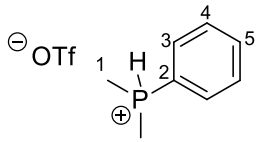

Chemical Formula: $C_9H_{12}F_3O_3PS$
Molecular Weight: 288.22

45b[OTf] (1.043 g, 3.62 mmol, 95%).

45 (526 mg, 3.81 mmol, 1 eq).

^{1}H-NMR (400.1 MHz, $CDCl_3$): δ 7.89-7.83 (m, 2H, H-3), 7.75-7.72 (m, 1H, H-5), 7.64-7.61 (m, 2H, H-4), 7.36 (d, *J* = 501.0 Hz, 1H, PH), 2.27 (d, *J* = 16.3 Hz, 6H, H-1). **^{13}C-NMR** (100.6 MHz, $CDCl_3$): δ 135.2 (d, *J* = 5.7 Hz, C-Ar), 132.2 (d, *J* = 13.1 Hz, C-Ar), 130.4 (d, *J* = 16.0 Hz, C-Ar), 118.7 (d, $^1J_{PC}$ = 88.7 Hz, C-2), 6.5 (d, *J* = 58.0 Hz, C-1), CF_3 was not observed. **^{31}P-NMR** (162.0 MHz, $CDCl_3$): δ 0.5 (d, *J* = 501 Hz, PH). **^{19}F-NMR** (376.5 MHz, $CDCl_3$): δ – 78.4 (s, CF_3). **Mp =** 65-66°C (decomposition). **IR** (neat, ATR probe, cm^{-1}): ν 2922, 2087, 1442, 1300, 1266, 1223, 1151, 1117, 1027, 981, 967, 742, 686. **HRMS** (ESI positive) = [$C_8H_{12}P^+$] Calculated mass: 139.0677 g/mol, found mass: 139.0706 g/mol.

Tributylphosphonium trifluoromethanesulfonate salt 46b[OTf]

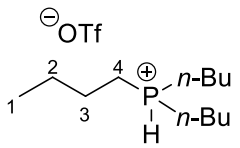

Chemical Formula: $C_{13}H_{28}F_3O_3PS$
Molecular Weight: 352.39

46b[OTf] (1.142 g, 3.24 mmol, 85%).

46 (777 mg, 3.81 mmol, 1 eq).

^{1}H-NMR (400.1 MHz, $CDCl_3$): δ 5.98 (d, *J* = 480.0 Hz, 1H, PH), 2.26-2.23 (m, 6H, H-4), 1.60-1.44 (m, 12H, H-2,3), 0.94-0.90 (m, 9H, H-1). **^{13}C-NMR** (100.6 MHz, $CDCl_3$): δ 24.7 (d, *J* = 4.8 Hz, C-2), 23.6 (d, *J* = 15.8 Hz, C-3), 16.4 (d, *J* = 47.2 Hz, C-4), 13.3 (s, C-1), CF_3 was not observed. **^{31}P-NMR** (162.0 MHz, $CDCl_3$): δ 13.8 (d, *J* = 480 Hz, PH). **^{19}F-NMR** (376.5 MHz, $CDCl_3$): δ – 78.4 (s, CF_3). **Mp =** 122-123°C (decomposition). **IR** (neat, ATR probe, cm^{-1}): ν 2963, 2937, 2876, 1467, 1384, 1284, 1044, 1031, 968, 943, 913, 855, 812, 730. **HRMS** (ESI positive) = [$C_{12}H_{28}P^+$] Calculated mass: 203.1929 g/mol, found mass: 203.1932 g/mol.

Ethyldiphenylphosphonium tetrafluoromethanesulfonate salt 47b[OTf].

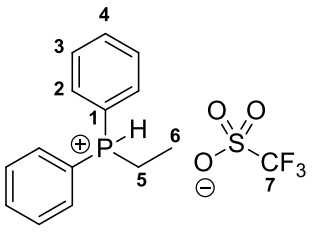

Formula : $C_{15}H_{16}F_3O_3PS$
MW : 364.32 g/mol

47b[OTf]. (981 mg, 2.62 mmol, 71%).

47 (815 mg, 3.81 mmol, 1 eq).

^{1}H-NMR (400.1 MHz, $CDCl_3$): δ 8.20 (d, $^1J_{HP}$ = 508 Hz, 1H, HP^+), 7.89-7.83 (m, 4H, H-2), 7.74-7.70 (m, 2H, H-4), 7.63-7.58 (m, 4H, H-3), 2.92-2.91 (m, 2H, H-5), 1.30 (dt, $^3J_{HP}$ = 20.2 Hz, $^3J_{HH}$ = 7.8 Hz, 3H, H-6). **^{13}C-NMR** (100.6 MHz, $CDCl_3$): δ 135.5 (d, $^4J_{PC}$ = 6.0 Hz, C-4), 133.5 (d, $^2J_{PC}$ = 10.3 Hz, C-2), 130.7 (d, $^3J_{PC}$ = 11.9 Hz, C-3), 120.9 (q, $^1J_{CF}$ = 320 Hz, CF_3, C-7), 115.7 (d, $^1J_{PC}$ = 92.0 Hz, C-1), 14.7 (d, $^2J_{PC}$ = 51.0 Hz, C-5), 7.2 (d, $^3J_{PC}$ = 7.3 Hz, C-6). **^{31}P-NMR** (162.0 MHz, $CDCl_3$): δ 11.2 (d, $^1J_{HP}$ = 508.0 Hz, 1H, PH). **^{19}F-NMR** (376.5 MHz, $CDCl_3$): δ – 78.3 (s, CF_3). **Mp =** 84-85°C (decomposition).

IR (neat, ATR probe, cm^{-1}): v 2963 (CH sp_3), 2424, 2160, 2024, 1794, 1589, 1441, 1251, 1223, 1158, 1113, 1028 (PH^+), 998, 918, 870, 733 and 690.
HRMS (ESI) = [$C_{14}H_{16}P^+$] Calculated mass: 215.0990 g/mol, found mass: 215.0999 g/mol. (ESI negative) = [$CF_3O_3S^-$] Calculated mass: 149.0 g/mol, found mass: 149.0 g/mol.

Diallylphenylphosphonium tetrafluoroborate salt 49

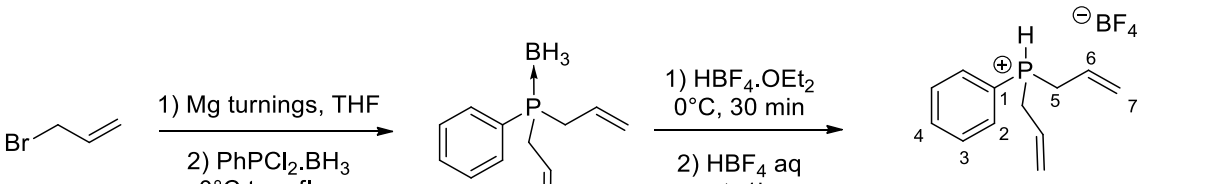

Chemical Formula: $C_{12}H_{16}BF_4P$
Molecular Weight: 278.03

The synthesis was done in two steps. The synthesis of diallylphenylphosphine borane complex was done following a procedure reported by Gouverneur.[3] The synthesis of diallylphenylphosphonium tetrafluoroborate salt **49** was done following a procedure by Denmark.[4]

49 (2.632 g, 9.47 mmol, 78% over two steps).
^{1}H{^{31}P}-NMR (400.1 MHz, $CDCl_3$): δ 7.84-7.82 (m, 2H, H-2), 7.79-7.74 (m, 1H, H-4), 7.67-7.63 (m, 2H, H-3), 6.93 (br, 1H, PH), 5.74-5.63 (m, 2H, H-6), 5.43-5.36 (m, 4H, H-7), 3.58-3.52 (m, 2H, H-5), 3.47-3.42 (m, 2H, H-5). **^{13}C-NMR** (100.6 MHz, $CDCl_3$): 135.4 (d, *J* = 3.0 Hz, C-Ar), 133.6 (d, *J* = 9.2 Hz, C-Ar), 130.5 (d, *J* = 13.0 Hz, C-Ar), 125.5 (d, *J* = 12.6 Hz, C-6), 123.5 (d, *J* = 10.6 Hz, C-7), 114.1 (d, *J* = 82.2 Hz, C-Ar), 24.6 (d, *J* = 44.5 Hz, C-5). **^{31}P-NMR** (162.0 MHz, $CDCl_3$): δ 12.6 (d, *J* = 499.0 Hz, PH). **^{19}F-NMR** (376.5 MHz, $CDCl_3$): δ – 149.5 (s, BF_4). **IR** (neat, ATR probe, cm^{-1}): v 2925, 1637, 1590, 1442, 1422, 1397, 1346, 1194, 1092, 990, 934, 895, 839, 796, 740.

1.3 Synthesis of Frustrated Lewis pairs **33b** and **34b**.

General procedure

The synthesis was performed following a procedure reported by Berionni.[5] In a flamed schlenk were placed **33c or 34c** (0.267 mmol, 1 eq), $B(C_6F_5)_3$ (0.267 mmol, 1 eq) and CH_2Cl_2 (c = 0.1 M, 2.6 mL) at 20°C under Ar. Triethylsilane Et_3SiH (47 µL, 0.293 mmol, 1.1 eq) was then added dropwise in the reaction mixture under stirring. After 10 min, the mixture was concentrated in vacuo to remove ¾ of the solvent and *n*-pentane (≈ 5 mL) was added to the resulting

[3] Slinn, C. a; Redgrave, A. J.; Hind, S. L.; Edlin, C.; Nolan, S. P.; Gouverneur, V. *Org. Biomol. Chem.* **2003**, *1*, 3820.
[4] Denmark, S. E.; Werner, N. S. *Org. Lett.* **2011**, *13*, 4596.
[5] Morozova, V.; Mayer, P.; Berionni, G. *Angew. Chem., Int. Ed.* **2015**, *54*, 14058.

suspension. It resulted, after sonication and strong stirring, in a clear suspension with a white precipitate. The solid was filtrated and washed two times with *n*-pentane (≈ 5 mL) under Ar. The resulting white solid was dried under high vacuum (10^{-2} mbar) overnight.

Tri(1-naphtyl)phosphonium tris(pentafluorophenyl)borohydride 33b

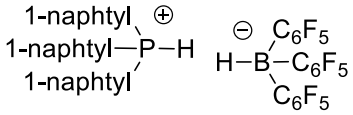

Formula : $C_{48}H_{23}BF_{15}P$
MW : 926.46 g/mol

33b (207 mg, 0.224 mmol, 84%).

33c (150 mg, 0.267 mmol, 1 eq).

^{1}H-NMR (400.1 MHz, CD_3CN): δ 10.11 (d, $^{1}J_{HP}$ = 432.0 Hz, 1H, HP^+), 8.46-8.45 (m, 3H, Ar-H), 8.22-8.20 (m, 3H, Ar-H), 8.01-7.98 (m, 3H, Ar-H), 7.77-7.73 (m, 3H, Ar-H), 7.67-7.59 (m, 9H, Ar-H), 3.62 (q (1:1:1:1), $^{1}J_{HB}$ = 95.0 Hz, 1H, HB^-). **^{13}C-NMR** (100.6 MHz, CD_3CN): δ 147.4 (s, Ar-C), 138.7 (s, Ar-C), 137.5 (s, Ar-C), 134.5 (d, *J* = 23.2 Hz, Ar-C), 133.6 (s, Ar-C), 130.6 (s, Ar-C), 129.8 (s, Ar-C), 128.6 (s, Ar-C), 126.5 (d, *J* = 12.5 Hz, Ar-C), 125.1 (d, *J* = 6.7 Hz, Ar-C), C_6F_5 was not observed. **^{31}P-NMR** (162.0 MHz, CD_3CN): δ –17.0 (br, HP^+). **^{11}B-NMR** (128.4 MHz, CD_3CN): δ –25.5 (d, $^{1}J_{HB}$ = 95.0 Hz, 1H, HB^-). **^{19}F-NMR** (376.5 MHz, CD_3CN): δ –133.7 (d, *J* = 21.7 Hz, ortho-CF), -164.5 (t, *J* = 19.8 Hz, para-CF), -167.6 (td, *J* = 7.6 Hz, *J* = 23.7 Hz, meta-CF). **Mp** = 135°C (decomposition). **IR** (neat, ATR probe, cm^{-1}): v 3062, 2995 (CH sp^3), 1508, 1465, 1370, 1274, 1096, 1060, 961, 801, 769, 738. **HRMS** (ESI positive) = [$C_{30}H_{22}P^+$] Calculated mass: 413.1459 g/mol, found mass: 413.1458 g/mol. (ESI negative) = [$C_{18}HBF_{15}^-$] Calculated mass: 512.9932 g/mol, found mass: 512.9937 g/mol.

Tri(*o*-tolyl)phosphonium tris(pentafluorophenyl)borohydride 34b

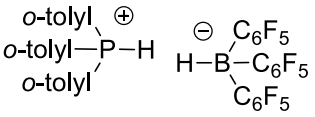

Chemical Formula: $C_{39}H_{23}BF_{15}P$
Molecular Weight: 818.36

34b (174 mg, 0.213 mmol, 80%).

34c (121 mg, 0.267 mmol, 1 eq).

^{1}H-NMR (400.1 MHz, CD_3CN): δ 8.93 (d, $^{1}J_{HP}$ = 502.0 Hz, 1H, HP^+), 7.86-7.82 (m, 3H, Ar-H), 7.66-7.63 (m, 3H, Ar-H), 7.53-7.48 (m, 3H, Ar-H), 7.28-7.23 (m, 3H, Ar-H), 3.64 (q (1:1:1:1), $^{1}J_{HB}$ = 96.0 Hz, 1H, HB^-), 2.24 (s, 9H, CH_3). **^{13}C-NMR** (100.6 MHz, CD_3CN): δ 151.1 (s, Ar-C), 145.5 (s, Ar-C), 137.4 (s, Ar-C), 136.3 (d, *J* = 23.2 Hz, Ar-C), 134.1 (s, Ar-C), 129.4 (d, *J* = 26.7 Hz, Ar-C), 21.6 (d, *J* = 14.9 Hz, CH_3-tolyl), C_6F_5 not observed. **^{31}P-NMR** (162.0 MHz, CD_3CN): δ –13.4 (d, *J* = 502.0 Hz, HP^+). **^{11}B-NMR** (128.4 MHz, CD_3CN): δ –25.5 (d, $^{1}J_{HB}$ = 96.0 Hz, 1H, HB^-). **^{19}F-NMR** (376.5 MHz, CD_3CN): δ –133.5 (d, *J* = 21.4 Hz, ortho-CF), -164.2 (t, *J* = 19.9 Hz, para-CF), -167.6 (td, *J* = 7.9 Hz, *J* = 21.9 Hz, meta-CF). **Mp** = 152°C (decomposition). **IR** (neat, ATR probe, cm^{-1}): v 3068, 2985 (CH sp^3), 2319, 1507, 1469, 1371, 1207, 1098, 1063, 962, 920, 754, 707. **HRMS** (ESI positive) = [$C_{21}H_{22}P^+$] Calculated mass: 305.1459 g/mol, found

mass: 305.1460 g/mol. (ESI negative) = [$C_{18}HBF_{15}^-$] Calculated mass: 512.9932 g/mol, found mass: 512.9938 g/mol.

1.4 Hydrophosphination of **35a** with phosphonium salts **33c** or **34c**

General procedure

A schlenk tube, equipped with a stirrer and flamed two times under vacuum and backfilled with argon was charged with the phosphonium salt **33c or 34c** (0.36 mmol, 1eq) followed by freshly distilled and degassed acetonitrile (2 mL, c = 0.2M). The mixture was stirred 5 min at r.t. until complete dissolution of the phosphonium salt, then **35a** (31 µL, 0.38 mmol, 1.05 eq) was added dropwise under stirring for 5 min. The reaction was allowed to proceed at r.t for 1 hour, then solvent was removed under vacuum and the residue was solidified upon trituration in diethyl ether (5mL) to yield a white precipitate.

(3-oxo)butyl tri(1-napthyl)phosphonium trifluoromethanesulfonate salt 37[OTf]

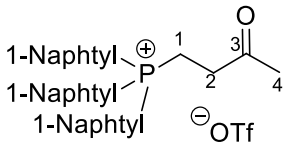

Formula : $C_{35}H_{28}F_3O_4PS$
MW : 632.63 g/mol

37[OTf] obtained as an orange solid (130 mg, 0.21 mmol, 57%).
33c (200 mg, 0.36 mmol, 1.1 eq),
^{1}H-NMR (400.1 MHz, CD_3CN): δ 8.44-8.42 (m, 3H, Ar-H), 8.16-8.14 (m, 3H, Ar-H), 8.10-8.04 (m, 3H, 2-H), 7.84-7.82 (m, 3H, Ar-H), 7.68-7.63 (m, 6H, Ar-H), 7.49-7.45 (m, 3H, Ar-H), 3.98 (br, 2H, 1-H), 2.67 (br, 2H, 2-H), 1.86 (s, 3H, 4-H). **^{13}C-NMR** (100.6 MHz, CD_3CN): δ 204.7 (s, 3-C), 139.2 (s, Ar-C), 137.9 (s, Ar-C), 135.4 (s, Ar-C), 133.7 (s, Ar-C), 131.7 (s, Ar-C), 129.9 (s, Ar-C), 128.7 (s, Ar-C), 126.9 (s, Ar-C), 126.7 (s, Ar-C), 115.4 (s, Ar-C), $CF_3SO_3^-$ is not observed, 37.9 (s, 2-C), 29.6 (s, 4-C), 20.6 (d, $^2J_{HP}$ = 58.4 Hz, 1-C). **^{31}P {^{1}H} -NMR** (162.0 MHz, CD_3CN): δ 33.8 (s, P^+). **^{19}F-NMR** (376.5 MHz, CD_3CN): δ –74.0 (s, CF_3). **Mp =** 104-105 °C (decomposition). **IR** (neat, ATR probe, cm^{-1}): v 2932, 1512, 1489, 1477, 1463, 1423, 1329, 1316, 1241, 1078, 1013, 884, 762, 742, 710. **HRMS** (ESI positive) = [$C_{34}H_{28}OP^+$] Calculated mass: 483.1878 g/mol, found mass: 483.1877 g/mol. (ESI negative) = [$CF_3O_3S^-$] Calculated mass: 148.9520 g/mol, found mass: 148.9522 g/mol.

(3-oxo)butyl tri(*o*-tolyl)phosphonium trifluoromethanesulfonate salt 38[OTf]

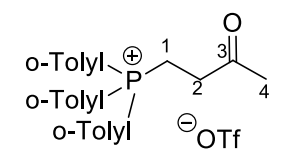

Formula : $C_{26}H_{28}F_3O_4PS$
MW : 524.53 g/mol

38[OTf] obtained as a white solid (130 mg, 0.26 mmol, 76%).
34c (150 mg, 0.34 mmol, 1.1 eq),
^{1}H-NMR (400.1 MHz, CD_3CN): δ 7.79-7.76 (m, 3H, Ar-H), 7.57-7.49 (m, 9H, Ar-H), 3.54-3.48 (m, 2H, 1-H), 2.68-2.61 (m, 2H, 2-H), 2.17 (s, 9H, CH_3-tolyl), 2.04 (s, 3H, 4-H). **^{13}C-NMR** (100.6 MHz, CD_3CN):

δ 204.7 (s, 3-C), 144.7 (s, Ar-C), 136.2 (s, Ar-C), 136.0 (s, Ar-C), 134.9 (s, Ar-C), 128.6 (s, Ar-C), 122.0 (q partial, $^{1}J_{CF}$ = 320.0 Hz, CF_3), 117.0 (d, $^{1}J_{CP}$ = 78.4 Hz, Ar-C), 37.7 (s, 2-C), 29.8 (s, 4-C), 22.9 (d, $^{3}J_{CP}$ = 5.4 Hz, CH_3-tolyl), 18.9 (d, $^{3}J_{CP}$ = 43.4 Hz, 1-C). **^{31}P {^{1}H} -NMR** (162.0 MHz, CD_3CN): δ 27.8 (s, P^+). **^{19}F-NMR** (376.5 MHz, CD_3CN): δ –79.3 (s, CF_3).
Mp = 142-143 °C (decomposition). **IR** (neat, ATR probe, cm^{-1}): v 3063, 2901 (CH sp^3), 1608 (C=O), 1522, 1439, 1485, 1363, 1277, 1256, 1224, 1159, 1103, 1055, 1027 (C-P^+), 996, 809, 755, 734, 719, 690. **HRMS** (ESI positive) = [$C_{25}H_{28}OP^+$] Calculated mass: 375.1875 g/mol, found mass: 375.1878 g/mol. (ESI negative) = [$CF_3O_3S^-$] Calculated mass: 148.9520 g/mol, found mass: 148.9516 g/mol.

1.5 Reactions of **33b** and **34b** with Michael acceptors **35a-e**

General procedure
In the glovebox, **33b or 34b** (22 µmol, 1 eq), olefin **35a-e** (1 eq) and CD_2Cl_2 (0.7 mL) were charged in an NMR tube. The tube was sealed, taken out of the glovebox, shaken for 15 min and left for 12h before NMR measurement. When both hydrogenation **(HH)** and hydrophosphination **(HP)** products were detected, a second NMR spectrum was recorded after 24h to control the evolution of the system.

Method for the determination of the ratio (HH):(HP)

The amount of both products was calculated using ^{1}H NMR of the mixture and based on the integration of protons from (HH) adduct and (HP) adduct. When an overlap was observed, a double comparison was performed and the ratio corresponding to the non-overlapped signals was reported. Example with the reaction of **34b** and **35a** (see NMR spectra below).

Using **Ha** and **Hc**: $(\mathbf{40}\boldsymbol{f}) = \frac{Int(Hc)}{Int(Hc)+Int(Ha)} = \frac{0.85}{0.85+0.68} = 55\%$ and $(\mathbf{39}\boldsymbol{a}) = 45\%$ (The values were not reported due to the OVERLAP)

Using **Hb** and **Hc**: $(\mathbf{40}\boldsymbol{f}) = \frac{Int(Hc)\times(\frac{1}{2})}{Int(Hc)\times(\frac{1}{2})+Int(Hb)\times(\frac{1}{3})} = \frac{0.427}{0.425+0.373} = 53\%$ and $(\mathbf{39}\boldsymbol{a}) = 47\%$ (The values were REPORTED)

Example: reaction of **33b** with **35a**

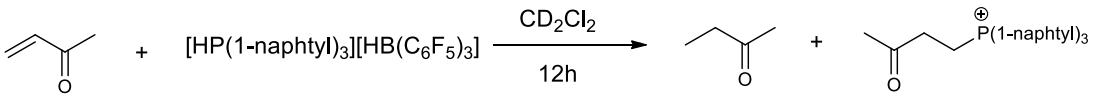

35a **33b** **39a** **40a**

According to the method, (**39a**) = 39% and (**40a**) = 61%.

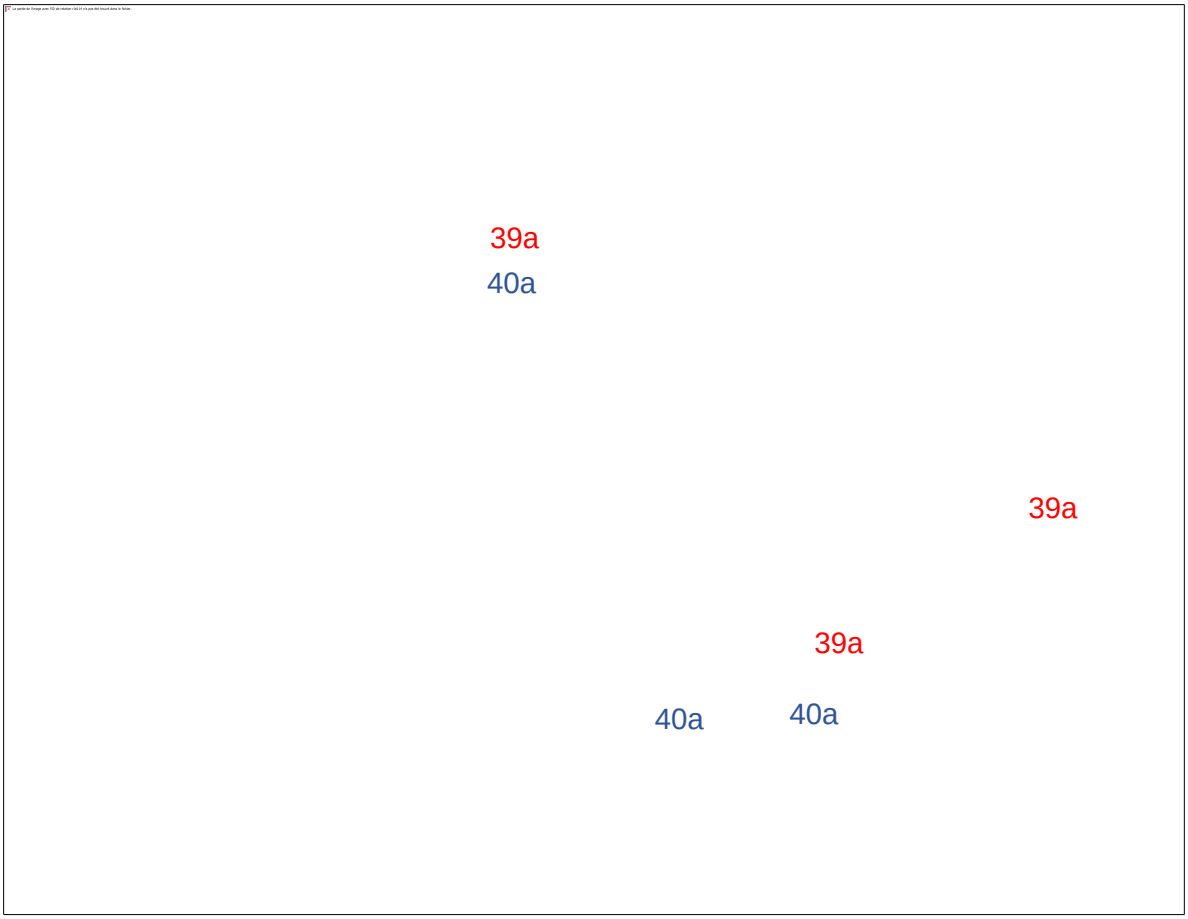
39a
40a
39a
39a
40a
40a

1.6 Products of the hydrophosphination of **35f** and **43b-45b**

General procedure

A 10 mL two-necked round bottomed flask, equipped with a stirrer and flamed two times under vaccuo and backfilled with argon was charged with the desired phosphonium salt **43b-47b** (1.20 mmol, 1eq), distilled and degassed acetonitrile (2 mL) and **35a-r** (126 µL, 1.26 mmol, 1.05 eq). The reaction was allowed to proceed at r.t under strong stirring. Every hour, an aliquot of the mixture was taken out and analysed by ^{31}P NMR spectroscopy to determine the conversion. At the end of the reaction, the solvent was removed under vaccuo to furnish the desired compound as a colourless oil. This residue solidifies upon trituration in ethyl acetate or diethyl ether (5mL) to yield a white precipitate.

(3-oxo)pentyl triphenylphosphonium trifluoromethanesulfonate salt 48a

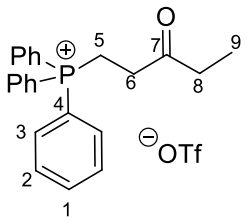

Chemical Formula: $C_{24}H_{24}F_3O_4PS$
Molecular Weight: 496.48

48a as a white solid (495 mg, 0.99 mmol, 83%). **43b** (495 mg, 1.20 mmol, 1.0 eq), **35f** (120 µL, 1.44 mmol, 1.2 eq). Precipitation in ethyl acetate.

^{1}H-NMR (400.1 MHz, $CDCl_3$): δ 7.83-7.78 (m, 3H, H-Ar), 7.71-7.68 (m, 12H, H-Ar), 3.68-3.58 (m, 2H, H-6), 3.04-2.97 (m, 2H, H-5), 2.38 (q, *J* = 7.2 Hz, 2H, H-8), 0.89 (t, *J* = 7.2 Hz, 3H, H-9). **^{13}C-NMR** (100.6 MHz, $CDCl_3$): δ 207.3 (d, *J* = 8.4 Hz, C-7), 135.5 (d, *J* = 7.5 Hz, C-Ar), 133.8 (d, *J* = 10.0 Hz, C-Ar), 130.8 (d, *J* = 13.5 Hz, C-Ar), 118.2 (d, *J* = 91.2 Hz, C-Ar), 35.8 (s, C-8), 34.5 (d, *J* = 8.2 Hz, C-6), 16.3 (d, *J* = 45.9 Hz, C-5), 7.7 (s, C-9), CF_3 was not observed. **^{31}P-NMR** (162.0 MHz, $CDCl_3$): δ 25.5 (s, P^+). **^{19}F-NMR** (376.5 MHz, $CDCl_3$): δ – 78.2 (s, CF_3). **Mp =** 178-179 °C. **IR** (neat, ATR probe, cm^{-1}): v 2978, 2947, 1716 (C=O), 1442, 1279, 1242, 1224, 1140, 1112, 1031, 997, 978, 752, 723. **HRMS** (ESI positive) = [$C_{23}H_{24}OP^+$] Calculated mass: 347.1565 g/mol, found mass: 347.1566 g/mol. (ESI negative) = [$CF_3O_3S^-$] Calculated mass: 148.9520 g/mol, found mass: 148.9525 g/mol.

(3-oxo)pentyl methyldiphenylphosphonium trifluoromethanesulfonate salt 48b

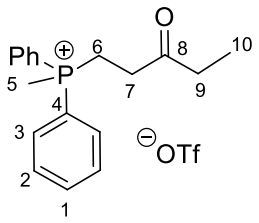

Chemical Formula: $C_{19}H_{22}F_3O_4PS$
Molecular Weight: 434.41

48b as a white solid (454 mg, 1.04 mmol, 83%). **44b** (420 mg, 1.20 mmol, 1.0 eq), **35f** (120 µL, 1.44 mmol, 1.2 eq). Precipitation in diethyl ether.

^{1}H-NMR (400.1 MHz, $CDCl_3$): δ 7.79-7.74 (m, 6H, H-Ar), 7.69-7.66 (m, 4H, H-Ar), 3.21-3.15 (m, 2H, H-7), 2.95-2.88 (m, 2H, H-6), 2.60 (d, *J* = 16.8 Hz, 3H, H-5), 2.41 (q, *J* = 7.1 Hz, 2H, H-9), 0.93 (t, 3H, H-10). **^{13}C-NMR** (100.6 MHz, $CDCl_3$): δ 207.9 (d, *J* = 6.9 Hz, C-8), 135.2 (d, *J* = 7.5 Hz, C-Ar), 132.5 (d, *J* = 9.8 Hz, C-Ar), 130.6 (d, *J* = 13.1 Hz, C-Ar), 119.4 (d, *J* = 89.0 Hz, C-Ar), 35.8 (s, C-9), 34.1 (d, *J* = 8.9 Hz, C-7), 17.2 (d, *J* = 25.2 Hz, C-6), 8.1 (d *J* = 61.2 Hz, C-5), 7.7 (s, C-10), CF_3 was not observed. **^{31}P-NMR** (162.0 MHz, $CDCl_3$): δ 25.2 (s, P^+). **^{19}F-NMR** (376.5 MHz, $CDCl_3$): δ – 78.3 (s, CF_3). **Mp =** 78-79 °C (decomposition). **IR** (neat, ATR probe, cm^{-1}): v 2989, 1716 (C=O), 1440, 1241, 1224, 1152, 1113, 1029, 908, 728, 689. **HRMS** (ESI positive) = [$C_{18}H_{22}OP^+$] Calculated mass: 285.1408 g/mol, found mass: 285.1411 g/mol. (ESI negative) = [$CF_3O_3S^-$] Calculated mass: 148.9520 g/mol, found mass: 148.9525 g/mol.

(3-oxo)pentyl dimethylphenylphosphonium trifluoromethanesulfonate salt 48c

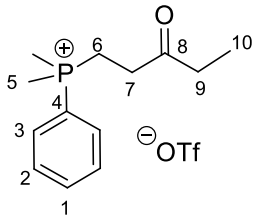

Chemical Formula: $C_{14}H_{20}F_3O_4PS$
Molecular Weight: 372.34

48c as a white solid (416 mg, 1.12 mmol, 93%). **45b** (350 mg, 1.20 mmol, 1.0 eq), **35f** (120 µL, 1.44 mmol, 1.2 eq). colourless oil.

^{1}H-NMR (400.1 MHz, $CDCl_3$): δ 7.84-7.79 (m, 2H, H-Ar), 7.73-7.70 (m, 1H, H-Ar), 7.66-7.62 (m, 2H, H-Ar), 2.89-2.75 (m, 4H, H-6,7), 2.41 (q, *J* = 7.0 Hz, 2H, H-9), 2.28 (d, *J* = 45.9 Hz, 6H, H-5), 0.94 (t, 3H, H-10). **^{13}C-NMR** (100.6 MHz, $CDCl_3$): δ 208.5 (d, *J* = 7.9 Hz, C-8), 134.5 (d, *J* = 8.9 Hz, C-Ar), 131.2 (d, *J* = 11.0 Hz, C-Ar), 130.1 (d, *J* = 10.5 Hz, C-Ar), 119.9 (d, *J* = 87.9 Hz, C-Ar), 35.2 (s, C-9), 34.2 (d, *J* = 5.0 Hz, C-7), 18.8 (d, *J* = 46.5 Hz, C-6), 8.2 (d, *J* = 56.0 Hz, C-5), 7.5 (s, C-10), CF_3 was not observed. **^{31}P-NMR** (162.0 MHz, $CDCl_3$): δ 26.0 (s, P^+). **^{19}F-NMR** (376.5 MHz, $CDCl_3$): δ – 78.4 (s, CF_3). **IR** (neat, ATR probe, cm^{-1}): v 2995, 2922, 1716 (C=O), 1440, 1252, 1223, 1153, 1116, 1031, 959, 746, 691. **HRMS** (ESI positive) = [$C_{13}H_{20}OP^+$] Calculated mass: 223.1252 g/mol, found mass: 223.1255 g/mol. (ESI negative) = [$CF_3O_3S^-$] Calculated mass: 148.9520 g/mol, found mass: 148.9522 g/mol.

1.7 Scope of the reaction of **43b** with various Michael acceptors **35a-r**

General procedure

A schlenk tube, equipped with a stirrer and flamed two times under vaccuo and backfilled with argon was charged with **43b** (150 mg, 0.36 mmol, 1eq) followed by freshly distilled and degassed acetonitrile (2 mL, [phosphonium] = 0.2M). The mixture was stirred 5 min at r.t. until complete dissolution of **43b**, then **35a-r** (0.38 mmol, 1.05 eq) was added dropwise under stirring for 5 min. The reaction was allowed to proceed at r.t for (t) hours, then solvent was removed under vaccuo to furnish the desired compound as a colourless oil. This residue solidifies upon trituration in ethyl acetate or diethyl ether (5mL) to yield a white precipitate.

(3-oxo)butyl triphenylphosphonium trifluoromethanesulfonate salt 36a

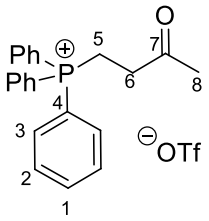

Formula : $C_{23}H_{22}F_3O_4PS$
MW : 482.45 g/mol

36a as a white solid (150 mg, 0.31 mmol, 87%), **35a** (31 µL, 0.38 mmol, 1.05 eq), reaction time (t) : 15 min. Precipitation in ethyl acetate.

^{1}H-NMR (400.1 MHz, $CDCl_3$): δ 7.82-7.79 (m, 3H, H-1), 7.71-7.66 (m, 12H, H-2,3), 3.57 (dt, $^{3}J_{HP}$ = 14.3 Hz, $^{3}J_{HH}$ = 7.5 Hz, 2H, H-6), 3.02 (dt, $^{2}J_{HP}$ = 16.3 Hz, $^{3}J_{HH}$ = 7.5 Hz, 2H, H-5), 2.09 (s, 3H, H-8). **^{13}C-NMR** (100.6 MHz, $CDCl_3$): δ 204.4 (d, $^{5}J_{CP}$ = 10.4 Hz, C-7), 135.6 (s, C-1), 133.8 (d, $^{2}J_{CP}$ = 10.0 Hz, C-3), 131.9 (d, $^{3}J_{CP}$ = 12.5 Hz, C-2), 121.1 (q, $^{1}J_{CF}$ = 320.3 Hz, CF_3), 118.1 (d, $^{2}J_{CP}$ = 86.9 Hz, C-4), 35.6 (d, $^{2}J_{CP}$ = 3.4 Hz, C-6), 29.5 (s, C-8), 16.5 (d, $^{2}J_{CP}$ = 56.1 Hz, C-5). **^{31}P-NMR** (162.0 MHz, $CDCl_3$): δ 25.4 (s, P^+). **^{19}F-NMR** (376.5 MHz, $CDCl_3$): δ – 78.2 (s, CF_3). **Mp =** 138-139 °C. **IR** (neat, ATR probe, cm^{-1}): v 2914 (CH sp^3), 2160, 2023, 1718 (C=O), 1442, 1411, 1282, 1259, 1224, 1138, 1113, 1031, 997, 874, 785, 751, 734, 724, 691. **HRMS** (ESI positive) = [$C_{22}H_{22}OP^+$] Calculated mass: 333.1408 g/mol, found mass: 333.1416 g/mol. (ESI negative) = [$CF_3O_3S^-$] Calculated mass: 149.0 g/mol, found mass: 149.0 g/mol.

(3-carbamoylpropyl)triphenylphosphonium trifluoromethanesulfonate salt 36b

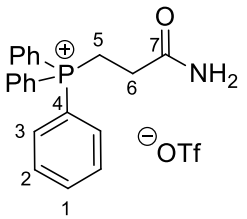

Formula : $C_{22}H_{21}F_3NO_4PS$
MW : 483.44 g/mol

36b as a white solid (148 mg, 0.24 mmol, 85%), **35b** (25.6 mg, 0.38 mmol 1.05 eq), reaction time (t) : 15h. Precipitation in ethyl acetate.

^{1}H-NMR (400.1 MHz, CD_3CN): δ 7.89-7.84 (m, 3H, H-1), 7.74-7.70 (m, 12H, H-2,3), 6.26 (s, 1H, NH_2), 5.78 (s, 1H, NH_2), 3.51-3.44 (m, 2H, H-6), 2.61-2.54 (m, 2H, H-5). **^{13}C-NMR** (100.6 MHz, CD_3CN): δ 171.6 (d, $^{3}J_{CP}$ = 8.7 Hz, C-7), 136.2 (d, $^{4}J_{CP}$ = 4.2 Hz, C-1), 134.7

(d, $^{2}J_{CP}$ = 8.9 Hz, C-3), 131.3 (d, $^{3}J_{CP}$ = 14.3 Hz, C-2), 122.1 (q partial, $^{1}J_{CF}$ = 320.0 Hz, CF_3), 119.1 (d, $^{1}J_{CP}$ = 76.4 Hz, C-4), 28.1 (d, $^{2}J_{CP}$ = 13.9 Hz, C-6), 18.6 (d, $^{1}J_{CP}$ = 41.8 Hz, C-5). **^{31}P-NMR** (162.0 MHz, CD_3CN): δ 24.6 (s, P^+). **^{19}F-NMR** (376.5 MHz, CD_3CN): δ – 79.3 (s, CF_3). **Mp =** 151-152 °C (decomposition). **IR** (neat, ATR probe, cm^{-1}): v 3374 (N-H), 3183, 2964 (CH sp^3), 2923, 2160, 2024, 1685 (C=O), 1435, 1302, 1258, 1224, 1153, 1115, 1029 (C-P^+), 998, 891, 799, 747, 728, 687. **HRMS** (ESI positive) = [$C_{21}H_{21}NOP^+$] Calculated mass: 334.1361 g/mol, found mass: 334.1364 g/mol. (ESI negative) = [$CF_3O_3S^-$] Calculated mass: 148.9518 g/mol, found mass: 148.9520 g/mol.

(3-methoxy-3-oxopropyl) triphenylphosphonium trifluoromethanesulfonate salt 36c

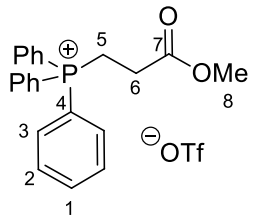

Formula : $C_{23}H_{22}F_3O_5PS$
MW : 498.45 g/mol

36c as a white solid (151 mg, 0.12 mmol, 84%), **35c** (33 mg, 0.38 mmol 1.05 eq), reaction time (t) : 2h. Precipitation in diethyl ether and filtration at 0°C.

^{1}H-NMR (400.1 MHz, CD_3CN): δ 7.88-7.84 (m, 3H, H-1), 7.72-7.68 (m, 12H, H-2,3), 3.55 (s, 3H, H-8), 3.47 (dt, $^{3}J_{HP}$ = 12.9 Hz, $^{3}J_{HH}$ = 7.2 Hz, 2H, H-6), 2.67 (dt, $^{2}J_{HP}$ = 16.1 Hz, $^{3}J_{HH}$ = 7.2 Hz, 2H, H-5). **^{13}C-NMR** (100.6 MHz, CD_3CN): δ 171.6 (d, $^{3}J_{CP}$ = 4.7 Hz, C-7), 136.3 (s, C-1), 134.7 (d, $^{2}J_{CP}$ = 9.2 Hz, C-3), 131.4 (d, $^{3}J_{CP}$ = 15.1 Hz, C-2), 122.0 (q partial, $^{1}J_{CF}$ = 320.0 Hz, CF_3), 118.7 (d, $^{1}J_{CP}$ = 75.9 Hz, C-4), 53.0 (s, C-8), 27.4 (d, $^{2}J_{CP}$ = 15.9 Hz, C-6), 18.7 (d, $^{1}J_{CP}$ = 45.9 Hz, C-5). **^{31}P-NMR** (162.0 MHz, CD_3CN): δ 23.9 (s, P^+). **^{19}F-NMR** (376.5 MHz, CD_3CN): δ – 79.3 (s, CF_3). **Mp =** 129-130 °C (decomposition). **IR** (neat, ATR probe, cm^{-1}): v 3069, 2948 (CH sp^3), 2915, 2161, 2011, 1733 (C=O), 1589, 1442, 1436, 1261, 1245, 1225, 1152, 1136, 1113, 1031(C-P^+), 997, 804, 743, 726, 690.

HRMS (ESI positive) = [$C_{22}H_{22}O_2P^+$] Calculated mass: 349.1357 g/mol, found mass: 349.1364 g/mol. (ESI negative) = [$CF_3O_3S^-$] Calculated mass: 149.0 g/mol, found mass: 149.0 g/mol.

(3-carboxypropyl)triphenyl phosphonium trifluoromethanesulfonate salt 36g

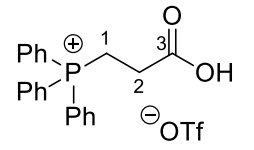

Formula : $C_{22}H_{20}F_3O_5PS$
MW : 484.43 g/mol

36g as a white solid (159 mg, 0.33 mmol, 91%), **35g** (30 µL, 0.38 mmol, 1.05 eq), reaction time (t): 2h. Precipitation in diethyl ether.

^{1}H-NMR (400.1 MHz, $CDCl_3$): δ 10.5 (sl, 1H, COOH), 7.79-7.76 (m, 3H, H-Ar), 7.66-7.64 (m, 12H, H-Ar), 3.53-3.50 (m, 2H, H-2), 2.80-2.77 (m, 2H, H-1). **^{13}C-NMR** (100.6 MHz, $CDCl_3$): δ 171.8 (d, $^{3}J_{CP}$ = 3.2 Hz, C-3), 135.6 (s, C-Ar), 133.6 (s, C-Ar), 130.9 (s, C-Ar), 120.1 (q partial, $^{1}J_{CF}$ = 320.0 Hz, CF_3), 117.5 (d, $^{1}J_{CP}$ = 77.6 Hz, C-Ar), 27.1 (s, C-2), 18.4 (d, $^{1}J_{CP}$ = 53.5 Hz, C-1). **^{31}P {^{1}H} -**

NMR (162.0 MHz, $CDCl_3$): δ 24.4 (s, P^+). **^{19}F-NMR** (376.5 MHz, $CDCl_3$): δ – 78.4 (s, CF_3). **Mp =** 82-83 °C (decomposition). **IR** (neat, ATR probe, cm^{-1}): v 3330 (OH), 3066, 2920 (CH sp^3), 2110, 1736 (C=O), 1589, 1486, 1440, 1412, 1264, 1223, 1146, 1113, 1031 (C-P^+), 997, 054, 899, 875, 797, 743, 727, 690. **HRMS** (ESI positive) = [$C_{21}H_{20}O_2P^+$] Calculated mass: 335.1201 g/mol, found mass: 335.1200 g/mol. (ESI negative) = [$CF_3O_3S^-$] Calculated mass: 149.0 g/mol, found mass: 149.0 g/mol.

(2-aza-2-methylpropyl)triphenylphosphonium trifluoromethanesulfonate salt 36i

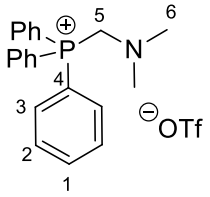

Formula : $C_{22}H_{23}F_3NO_3PS$
MW : 469.46 g/mol

36i as a white solid (119 mg, 0.24 mmol, 67%), **35i** (35 mg, 0.38 mmol 1.05 eq), reaction time (t) : 2h. Precipitation in ethyl acetate.

^{1}H-NMR (400.1 MHz, CD_3CN): δ 7.93-7.87 (m, 9H, H-1,3), 7.77-7.73 (m, 6H, H-2), 5.23 (s, 2H, H-5), 2.84 (s, 6H, H-6). **^{13}C-NMR** (100.6 MHz, CD_3CN): δ 136.8 (s, C-1), 135.5 (d, $^2J_{CP}$ = 48.0 Hz, C-3), 131.5 (d, $^3J_{CP}$ = 32.1 Hz, C-2), 122.0 (q partial, $^1J_{CF}$ = 320.0 Hz, CF_3), C-5 is not observed, 48.3 (s, C-6). **^{31}P-NMR** (162.0 MHz, CD_3CN): δ 15.1 (s, P^+). **^{19}F-NMR** (376.5 MHz, CD_3CN): δ – 79.3 (s, CF_3) **Mp =** 153-154 °C. **IR** (neat, ATR probe, cm^{-1}): v 3384, 2959 (CH sp^3), 2927, 2704, 2160, 2023, 1587, 1475, 1441, 1306, 1253, 1219, 1177, 1158, 1140, 1112, 1030 (C-P^+), 996, 872, 824, 747, 718, 689. **HRMS** (ESI positive) = [$C_{21}H_{23}NP^+$] Calculated mass: 320.1568 g/mol, found mass: 320.1557 g/mol. (ESI negative) = [$CF_3O_3S^-$] Calculated mass: 149.0 g/mol, found mass: 149.0 g/mol.

(1-methyl-3-oxo)pentyl triphenylphosphonium trifluoromethanesulfonate salt 36j

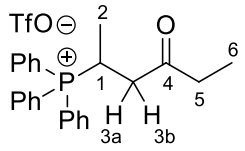

Formula : $C_{25}H_{26}F_3O_4PS$
MW : 510.51 g/mol

36j as an off-white solid (146 mg, 0.29 mmol, 79%), **35j** (42 µL, 0.38 mmol 1.05 eq), reaction time (t): 15 min. Precipitation in diethyl ether.

^{1}H-NMR (400.1 MHz, CD_3CN): δ 7.89-7.85 (m, 3H, H-Ar), 7.81-7.70 (m, 12H, H-Ar), 4.32-4.24 (m, 1H, H-1), 2.92 (dd, $^3J_{HP}$ = 17.7 Hz, $^3J_{HH}$ = 13.7 Hz, 1H, H-3a), 2.54 (ddd, $^3J_{HP}$ = 17.8 Hz, $^2J_{HH}$ = 13.7 Hz, $^3J_{HH}$ = 3.4 Hz, 1H, H-3b), 2.46-2.33 (m, 2H, H-5), 1.28 (dd, $^3J_{HP}$ = 18.9 Hz, $^3J_{HH}$ = 7.4 Hz, 3H, H-2), 0.97 (t, $^3J_{HH}$ = 7.4 Hz, H-6). **^{13}C-NMR** (100.6 MHz, CD_3CN): δ 207.0 (d, $^3J_{CP}$ = 15.4 Hz, C-4), 136.1 (s, C-Ar), 134.8 (d, $^2J_{CP}$ = 9.9 Hz, C-Ar), 131.4 (d, $^3J_{CP}$ = 12.4 Hz, C-Ar), CF_3 is not clearly observed, 42.9 (s, C-3), 36.8 (s, C-5), 23.0 (d, $^1J_{CP}$ = 52.5 Hz, C-1), 15.0 (s, C-2), 7.7 (s, C-6). **^{31}P-NMR** (162.0 MHz, CD_3CN): δ 30.3 (s, P^+). **^{19}F-NMR** (376.5 MHz, CD_3CN): δ – 79.3 (s, CF_3). **Mp =** 112-113 °C (decomposition). **IR** (neat, ATR probe, cm^{-1}): v 3064, 2978 (CH sp^3), 2915, 2160, 2024, 1715 (C=O), 1440, 1258, 1223, 1140, 1107, 1028 (C-P^+), 996, 909, 754,

737, 722, 693. **HRMS** (ESI positive) = [$C_{24}H_{26}OP^+$] Calculated mass: 361.1721 g/mol, found mass: 361.1710 g/mol. (ESI negative) = [$CF_3O_3S^-$] Calculated mass: 149.0 g/mol, found mass: 149.0 g/mol.

(N-(*p*-toluenesulforamide)-1-phenyl)methyl triphenylphosphonium trifluoromethane-sulfonate salt 36k

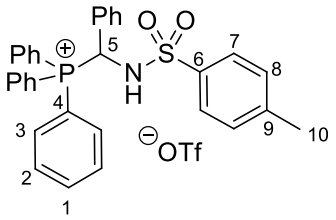

Chemical Formula: $C_{33}H_{29}F_3NO_5PS_2$
Molecular Weight: 671.69

36k as an off-white solid (169 mg, 0.26 mmol, 72%), **35k** (93 mg, 0.36 mmol 1.05 eq), reaction time (t): 2 min. Precipitation in diethyl ether.

^{1}H-NMR (400.1 MHz, CD_3CN): δ 7.91-7.88 (m, 3H, H-Ar), 7.73-7.59 (m, 12H, H-Ar), 7.43 (d, *J* = 11.0 Hz, 3H, H-Ar), 7.22 (t, *J* = 4.0 Hz, 1H, H-Ar), 7.03-6.98 (m, 3H, H-Ar), 6.76-6.75 (d, *J* = 4.2 Hz, 2H, H-6), 6.45 (dd, $^3J_{HP}$ = 16.3 Hz, $^4J_{HH}$ = 11.3 Hz, 2H, H-5), 5.58 (ls, 1H, NH), 2.21 (s, 3H, H-10). **^{13}C-NMR** (100.6 MHz, CD_3CN): δ 145.5 (s, C-Ar), 136.6 (d, J_{CP} = 3.0 Hz, C-Ar), 136.1 (d, J_{CP} = 9.2 Hz, C-Ar), 135.9 (d, J_{CP} = 8.9 Hz, C-Ar), 135.2 (d, J_{CP} = 11.9 Hz, C-Ar), 131.1 (d, J_{CP} = 11.9 Hz, C-Ar), 130.7 (d, J_{CP} = 3.7 Hz, C-Ar), 130.4 (s, C-Ar), 129.6 (s, C-Ar), 128.2 (s, C-Ar), 127.0 (s, C-Ar), 116.4 (d, *J* = 83.0 Hz, C-Ar), 56.5 (d, $^1J_{CP}$ = 61.4 Hz, C-5), 21.4 (s, C-10). **^{31}P{^{1}H}-NMR** (162.0 MHz, CD_3CN): δ 21.5 (s, P^+). **^{19}F-NMR** (376.5 MHz, CD_3CN): δ – 79.3 (s, CF_3). **Mp =** 71-72 °C (decomposition). **IR** (neat, ATR probe, cm^{-1}): ν 3183 (NH), 3066, 2922 (CH sp^3), 2160, 1977, 1439, 1277, 1249, 1157, 1107, 1028, 791, 751, 687. **HRMS** (ESI positive, product unstable) = [$C_{32}H_{29}NO_2PS^+$] Calculated mass: 522.1657 g/mol, found mass: 522.1656 g/mol. (ESI negative) = [$CF_3O_3S^-$] Calculated mass: 149.0 g/mol, found mass: 149.0 g/mol.

3-triphenylphosphonium 2(3H)-furanone trifluoromethanesulfonate salt 36l

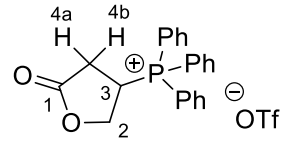

Formula : $C_{23}H_{20}F_3O_5PS$
MW : 496.44 g/mol

36l as a white solid (132 mg, 0.29 mmol, 79%), **35l** (25 µL, 0.38 mmol 1.05 eq), reaction time (t): 5 days. Precipitation in ethyl acetate.

^{1}H-NMR (400.1 MHz, CD_3CN): δ 7.94-7.90 (m, 3H, H-Ar), 7.81-7.72 (m, 12H, H-Ar), 4.95-4.81 (m, 2H, H-2), 4.55-4.48 (m, 1H, H-3), 3.45-3.33 (m, 1H, H-4a), 2.80-2.69 (m, 1H, H-4b). **^{13}C-NMR** (100.6 MHz, CD_3CN): δ 173.6 (d, $^3J_{CP}$ = 7.0 Hz, C-1), 136.8 (s, C-Ar), 134.9 (d, $^2J_{CP}$ = 9.9 Hz, C-Ar), 131.7 (d, $^3J_{CP}$ = 12.5 Hz, C-Ar), CF_3 is not clearly observed, 117.2 (d, $^1J_{CP}$ = 87.7 Hz, C-Ar), 66.6 (s, C-2), 29.8 (d, $^2J_{CP}$ = 2.0 Hz, C-4), 29.2 (d, $^1J_{CP}$ = 56.8 Hz, C-3). **^{31}P {^{1}H} -NMR** (162.0 MHz, CD_3CN): δ 32.0 (s, P^+). **^{19}F-NMR** (376.5 MHz, CD_3CN): δ – 74.0 (s, CF_3). **Mp =** 201-202 °C (decomposition). **IR** (neat, ATR probe, cm^{-1}): ν 2971 (CH sp^3), 2160, 2112, 1794 (C=O), 1587,

1439, 1285, 1255, 1223, 1166, 1145, 1028 (C-P$^+$), 996, 951, 839, 728, 692. **HRMS** (ESI positive) = [$C_{22}H_{20}O_2P^+$] Calculated mass: 347.1201 g/mol, found mass: 347.1197 g/mol. (ESI negative) = [$CF_3O_3S^-$] Calculated mass: 149.0 g/mol, found mass: 149.0 g/mol.

(3-oxo-1,3-diphenyl)propyl triphenylphosphonium trifluoromethanesulfonate salt 36m

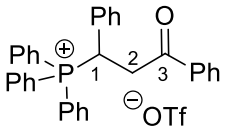

Formula : $C_{34}H_{28}F_3O_4PS$
MW : 620.62 g/mol

36m as an off-white solid (210 mg, 0.34 mmol, 94%), **35m** (78 µL, 0.38 mmol 1.05 eq), reaction time (t): 12h. Precipitation in diethyl ether.

^{1}H-NMR (400.1 MHz, $CDCl_3$): δ 8.10-8.08 (m, 2H, H-Ar), 7.85-7.81 (m, 4H, H-Ar), 7.71-7.67 (m, 8H, H-Ar), 7.52-7.45 (m, 10H, H-Ar), 7.32-7.20 (m, 4H, H-Ar), 7.08-7.06 (m, 2H, H-Ar), 5.41 (dd, $^1J_{HP}$ = 15.2 Hz, $^3J_{HH}$ = 9.4 Hz, 1H, H-1), 4.45-4.37 (m, 1H, H-2a), 3.87 (t, $^3J_{HP}$ = 16.0 Hz, 1H, H-2b). **^{13}C-NMR** (100.6 MHz, $CDCl_3$): δ 195.0 (d, $^3J_{CP}$ = 12.7 Hz, C-3), 135.9 (d, J_{CP} = 3.5 Hz, C-Ar), 135.2 (s, C-Ar), 134.6 (d, J_{CP} = 9.6 Hz, C-Ar), 134.5 (s, C-Ar), 134.2 (d, J_{CP} = 14.2 Hz, C-Ar), 131.6 (d, J_{CP} = 5.3 Hz, C-Ar), 131.1 (d, J_{CP} = 6.0 Hz, C-Ar), 130.9 (d, J_{CP} = 12.8 Hz, C-Ar), 129.8 (d, J_{CP} = 3.2 Hz, C-Ar), 129.7 (d, J_{CP} = 2.5 Hz, C-Ar), 129.2 (d, J_{CP} = 3.5 Hz, C-Ar), 122.8 (q partial, $^1J_{CF}$ = 320.0 Hz, CF_3), 116.9 (d, J_{CP} = 86.0 Hz, C-Ar), 39.4 (d, $^1J_{CP}$ = 50.0 Hz, C-1), 40.6 (s, C-2). **^{31}P-NMR** (162.0 MHz, $CDCl_3$): δ 28.1 (s, P$^+$). **^{19}F-NMR** (376.5 MHz, $CDCl_3$): δ – 78.0 (s, CF_3). **Mp =** 112-113 °C (decomposition). **IR** (neat, ATR probe, cm^{-1}): ν 3067, 2932 (CH sp^3), 2160, 1717 (C=O), 1508, 1363, 1334, 1256, 1222, 1147, 1028 (C-P$^+$), 982, 801, 770. **HRMS** (ESI positive) = [$C_{33}H_{28}OP^+$] Calculated mass: 471.1878 g/mol, found mass: 471.1874 g/mol. (ESI negative) = [$CF_3O_3S^-$] Calculated mass: 149.0 g/mol, found mass: 149.0 g/mol.

(1-phenyl-1-triphenylphosphonium)methyl diethyl malonate salt 36n

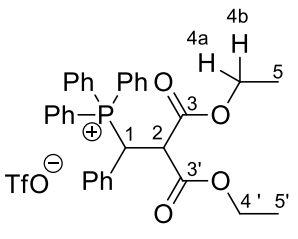

Formula : $C_{33}H_{32}F_3O_7PS$
MW : 660.64 g/mol

36n as transparent crystals (148 mg, 0.24 mmol, 82%), **35n** (80 µg, 0.38 mmol 1.05 eq), reaction time (t): 16 h. Precipitation in Ethyl acetate. Saturation of a solution of **36n** and acetonitrile with toluene provided crystals suitable for X-ray analysis in 2 days at – 35°C.

^{1}H-NMR (400.1 MHz, $CDCl_3$): δ 7.82-7.79 (m, 3H, H-Ar), 7.67-7.62 (m, 6H, H-Ar), 7.56-7.51 (m, 6H, H-Ar), 7.30-7.26 (m, 1H, H-Ar), 7.21-7.17 (m, 2H, H-Ar), 7.04-7.02 (m, 2H, H-Ar), 5.40 (dd, $^3J_{HP}$ = 13.4 Hz, $^3J_{HH}$ = 11.7 Hz, 1H, H-2), 4.57 (dd, $^2J_{HP}$ = 11.7 Hz, $^3J_{HH}$ = 8.5 Hz, 1H, H-1), 3.86 (q, $^3J_{HH}$ = 7.1 Hz, 2H, H-4'), 3.77-3.69 (m, 1H, H-4a), 3.58-3.50 (m, 1H, H-4b), 1.02 (t, $^3J_{HH}$ = 7.1

Hz, 3H, H-5), 0.87 (t, $^{3}J_{HH}$ = 7.2 Hz, H-5'). **^{13}C-NMR** (100.6 MHz, $CDCl_3$): δ 167.1 (d, $^{3}J_{CP}$ = 4.7 Hz, C-3'), 165.6 (d, $^{3}J_{CP}$ = 9.7 Hz, C-3), 135.6 (s, C-Ar), 135.2 (s, C-Ar), 131.2 (s, C-Ar), 130.5 (s, C-Ar), 130.1 (s, C-Ar), 129.8 (s, C-Ar), 129.7 (s, C-Ar), 121.2 (q partial, $^{1}J_{CF}$ = 320.0 Hz, CF_3), 116.8 (d, $^{1}J_{CP}$ = 79.4 Hz, C-Ar), 63.7 (s, C-4'), 63.3 (s, C-4), 54.4 (s, C-2), 44.5 (d, $^{1}J_{CP}$ = 39.4 Hz, C-1), 13.7 (s, C-9), 13.6 (s, C-5'). **^{31}P-NMR** (162.0 MHz, $CDCl_3$): δ 26.6 (s, P^+). **^{19}F-NMR** (376.5 MHz, $CDCl_3$): δ – 78.0 (s, CF_3). **Mp =** 166-167 °C (decomposition). **IR** (neat, ATR probe, cm^{-1}): v 3068, 2982 (CH sp^3), 2160, 2024, 1735 (C=O), 1695, 1438, 1372, 1264, 1225, 1162, 1145, 1107, 1028 (C-P^+), 997, 750, 725, 686. **HRMS** (ESI positive) = [$C_{32}H_{32}O_4P^+$] Calculated mass: 511.2038 g/mol, found mass: 511.2018 g/mol. (ESI negative) = [$CF_3O_3S^-$] Calculated mass: 149.0 g/mol, found mass: 149.0 g/mol.

1.8 Sequential hydrophosphination/ metathesis of phosphonium salts.

(3-oxo)pentyl diallylphenylphosphonium tetrafluoroborate salt 50

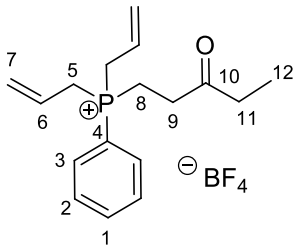

Chemical Formula: $C_{17}H_{24}BF_4OP$
Molecular Weight: 362.15

A 10 mL two-necked round bottomed flask, equipped with a stirrer and flamed two times under vaccuo and backfilled with argon was charged with **49** (334 mg, 1.20 mmol, 1.0 eq), distilled and degassed acetonitrile (6 mL) and **35f** (126 µL, 1.26 mmol, 1.05 eq). The reaction mixture was stirred overnight at 40°C. The crude mixture was then cooled to r.t., concentrated in vaccuo to remove volatiles and purified on a pad of silica gel column chromatography with acetone. The resulting brown solution was concentrated in vaccuo and dried overnight under reduced pressure (10^{-2} mbar) to yield a yellow oil (413 mg, 1.14 mmol, 95%).

^{1}H-NMR (400.1 MHz, $CDCl_3$): δ 7.82-7.77 (m, 2H, H-Ar), 7.75-7.71 (m, 1H, H-Ar), 7.68-7.63 (m, 2H, H-Ar), 5.64-5.54 (m, 2H, H-6), 5.48-5.37 (m, 4H, H-7), 3.48 (dd, *J* = 7.2 Hz, *J* = 8.7 Hz, 4H, H-5), 2.90 (dt, *J* = 7.0 Hz, *J* = 6.1 Hz, 2H, H-9), 2.72 (dt, *J* = 7.0 Hz, *J* = 5.5 Hz, 2H, H-8), 2.43 (q, *J* = 7.0 Hz, 2H, H-11), 0.94 (t, *J* = 7.0 Hz, 3H, H-12). **^{13}C-NMR** (100.6 MHz, $CDCl_3$): δ 209.2 (d, *J* = 4.2 Hz, C-10), 135.0 (d, *J* = 2.9 Hz, C-Ar), 132.3 (d, *J* = 8.5 Hz, C-Ar), 130.4 (d, *J* = 7.5 Hz, C-Ar), 125.6 (d, *J* = 12.7 Hz, C-6), 123.2 (d, *J* = 9.0 Hz, C-7), 116.5 (d, J = 82.3 Hz, C-Ar), 35.5 (s, C-11), 33.8 (d, *J* = 7.5 Hz, C-9), 25.7 (d, 35.4 Hz, C-5), 13.6 (d, *J* = 59.9 Hz, C-8), 7.7 (s, C-12). **^{31}P-NMR** (162.0 MHz, $CDCl_3$): δ 26.9 (s, P^+). **^{11}B-NMR** (128.4 MHz, $CDCl_3$): δ - 0.8 (s, BF_4). **^{19}F-NMR** (376.5 MHz, $CDCl_3$): δ -149.8 (s, BF_4). **IR** (neat, ATR probe, cm^{-1}): v 2992, 2925, 1714 (C=O), 1441, 1422, 1397, 1279, 1241, 1224, 1140, 1112, 1031, 997, 978, 753, 724. **HRMS** (ESI positive) = [$C_{17}H_{24}OP^+$] Calculated mass: 275.1565 g/mol, found mass:

275.1568 g/mol. (ESI negative) = [BF_4^-] Calculated mass: 87.0029 g/mol, found mass: 87.0031 g/mol.

1-(3-oxopentyl)-1-phenyl-2,5-dihydro-1H-phospholium tetrafluoroborate salt 51

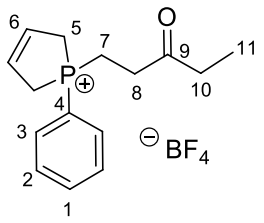

Chemical Formula: $C_{15}H_{20}BF_4OP$
Molecular Weight: 334.10

A 10 mL two-necked round bottomed flask, equipped with a stirrer and flamed two times under vaccuo and backfilled with argon was charged with **50** (200 mg, 0.552 mmol, 1.0 eq), distilled CH_2Cl_2 (2.5 mL) and Grubbs II catalyst (23 mg, 0.028 mmol, 0.05 eq). The reaction mixture was stirred overnight at reflux. The crude mixture was then cooled to r.t., concentrated in vaccuo to remove volatiles and purified on a pad of silica gel column chromatography with acetone. The resulting brown solution was concentrated in vaccuo and dried overnight under reduced pressure (10^{-2} mbar) to yield a yellow oil (168 mg, 0.502 mmol, 91%).

^{1}H-NMR (400.1 MHz, CD_3CN): δ 7.97-7.91 (m, 2H, H-Ar), 7.73-7.69 (m, 1H, H-Ar), 7.63-7.58 (m, 2H, H-Ar), 6.04 (d, *J* = 42.1 Hz, 2H, H-6), 5.51 (dd, *J* = 16.1 Hz, *J* = 4.2 Hz, 4H, H-5), 3.01-2.88 (m, 4H, H-7,8), 2.38-2.34 (m, 2H, H-10), 0.80 (t, *J* = 7.0, 3H, H-11). **^{13}C-NMR** (100.6 MHz, CD_3CN): δ 209.3 (d, *J* = 3.2 Hz, C-9), 135.1 (d, *J* = 2.9 Hz, C-Ar), 132.4 (d, *J* = 8.0 Hz, C-Ar), 130.4 (d, *J* = 7.2 Hz, C-Ar), 127.6 (d, *J* = 12.7 Hz, C-6), 119.3 (d, J = 79.3 Hz, C-Ar), 35.3 (s, C-10), 34.8 (d, *J* = 6.9 Hz, C-8), 29.4 (d, *J* = 51.0 Hz, C-5), 16.1 (d, *J* = 31.9 Hz, C-7), 7.4 (s, C-11). **^{31}P-NMR** (162.0 MHz, CD_3CN): δ 49.1 (s, P^+). **^{11}B-NMR** (128.4 MHz, CD_3CN): δ - 0.8 (s, BF_4). **^{19}F-NMR** (376.5 MHz, CD_3CN): δ -151.8 (s, BF_4). **IR** (neat, ATR probe, cm^{-1}): ν 2992, 2925, 1714 (C=O), 1441, 1422, 1397, 1279, 1241, 1224, 1140, 1112, 1031, 997, 978, 753, 724. **HRMS** (ESI positive) = [$C_{17}H_{24}OP^+$] Calculated mass: 275.1565 g/mol, found mass: 275.1568 g/mol. (ESI negative) = [BF_4^-] Calculated mass: 87.0029 g/mol, found mass: 87.0031 g/mol.

1.9 Reaction of phosphines and phosphonium salts with diarylcarbenium cations **[43-41d]** and **[43b-41d]**

Bis(4-dimethylaminophenyl)methyl-triphenyl-phosphonium tetrafluoroborate [43-41d]

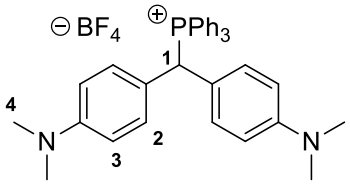

Formula : $C_{35}H_{36}BF_4N_2P$
MW : 602.45 g/mol

A round bottomed flask, equipped with a stirrer filled with argon was charged with **43** (262 mg, 1.0 mmol, 11.4 eq), **41d** (30 mg, 88 µmol, 1 eq) and dichloromethane (2 mL). The blue mixture was stirred at r.t. for 2h until it decolorizes to a light blue homogeneous solution. The solvent was removed and the crude was immediately washed with diethyl ether (5 mL). A green solid was isolated (38.4 mg, 64 µmol, 72%). Due to the important equilibrium constant between the free phosphine and the phosphonium salt, it was difficult to remove diethyl ether trapped in the solid. In addition, it is necessary to use an excess of phosphine to drive the equilibrium.

^{1}H-NMR (400.1 MHz, CD_3CN): δ 7.86-7.82 (m, 3H, H-Ar), 7.64-7.60 (m, 6H, H-Ar), 7.50-7.45 (m, 6H, H-Ar), 6.97-6.95 (m, 2H, H-2), 6.62-6.60 (m, 2H, H-3), 6.03 (d, $^{3}J_{HP}$ = 17.7 Hz, 1H, H-1), 2.89 (s, 12H, H-4). **^{13}C-NMR** (100.6 MHz, CD_3CN): δ 151.5 (s, C-Ar), 135.9 (s, C-Ar), 134.7 (s, C-Ar), 132.0 (s, C-Ar), 131.4 (s, C-Ar), 131.0 (s, C-Ar), 129.7 (s, C-Ar), 119.7 (d, $^{2}J_{HP}$ = 81.0, C-Ar), 113.3 (s, C-Ar), 48.3 (d, $^{2}J_{HP}$ = 41.0 Hz, C-1), 40.4 (s, C-4). **^{31}P {^{1}H} -NMR** (162.0 MHz, CD_3CN): δ 19.6 (s, P^+), - 5.9 (PPh_3). **^{11}B-NMR** (128.4 MHz, CD_3CN): - 1.2 (s, BF_4^-). **^{19}F-NMR** (376.5 MHz, CD_3CN): δ – 151.8 (s, BF_4^-). **Mp =** 94-95 °C (decomposition). **IR** (neat, ATR probe, cm^{-1}): v 2891 (CH sp^3), 1739, 1607, 1520, 1484, 1438, 1359, 1259, 1162, 1052, 1029 (C-P^+), 996, 946, 805, 732, 719, 690. **HRMS** (ESI positive) = Unstable

Bis(4-dimethylamoniumphenyl)methyl-triphenyl-phosphonium tetrafluoroborate di(trifluoromethanesulafonate) salt [43b-41d]

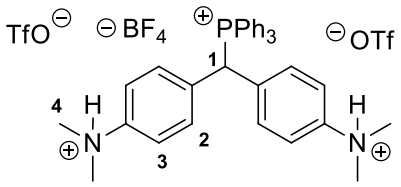

Formula : $C_{36}H_{37}BF_7N_2O_3PS$
MW : 752.53 g/mol

A round bottomed flask, equipped with a stirrer and filled with argon was charged with **43b[OTf]** (36 mg, 88 µmol, 1 eq), **41d** (30 mg, 88 µmol, 1 eq) and dichloromethane (2 mL). The blue mixture was stirred at r.t. for 2h until it decolorizes to a green blue homogeneous solution. The solvent was removed and the crude was washed with diethyl ether (2 × 5 mL) to afford a green solid (38.1 mg, 51 µmol, 58%).

^{1}H-NMR (400.1 MHz, CD_3CN): δ 7.89-7.86 (m, 3H, H-Ar), 7.68-7.63 (m, 6H, H-Ar), 7.55-7.50 (m, 6H, H-Ar), 7.21-7.19 (m, 2H, H-2), 7.09-7.07 (m, 2H, H-3), 6.30 (d, $^{3}J_{HP}$ = 17.7 Hz, 1H, H-1), 3.06 (s, 12H, H-4). **^{13}C-NMR** (100.6 MHz, CD_3CN): δ 147.6 (s, C-Ar), 136.3 (s, C-Ar), 135.9 (d, *J* = 12.2 Hz, C-Ar), 134.5 (d, *J* = 15.2 Hz, C-Ar), 132.7 (d, *J* = 7.0 Hz, C-Ar), 131.1 (d, *J* = 16.2 Hz, C-Ar), 130.0 (s, C-Ar), 129.6 (d, *J* = 5.1 Hz, C-Ar), 129.7 (s, C-Ar), 122.0 (q partial, $^{1}J_{CF}$ = 320.0 Hz, CF_3), 119.1 (s, C-Ar), 47.8 (d, $^{2}J_{HP}$ = 41.3 Hz, C-1), 44.2 (s, C-4). **^{31}P{^{1}H}-**

NMR (162.0 MHz, CD_3CN): δ 21.1 (s, P^+). **^{11}B-NMR** (128.4 MHz, CD_3CN): 4.2 (s, BF_4^-). **^{19}F-NMR** (376.5 MHz, CD_3CN): δ –79.3 (s, CF_3), - 151.4 (s, BF_4^-). **Mp =** 94-95 °C (decomposition). **IR** (neat, ATR probe, cm^{-1}): v 3062 ,2916 (CH sp^3), 1608, 1522, 1485, 1439, 1363, 1278, 1255, 1224, 1159, 1103, 1057, 1032 (C-P^+), 996, 947, 899, 811, 753, 734, 720, 691.**HRMS** (ESI positive) = unstable

2. Crystallographic data

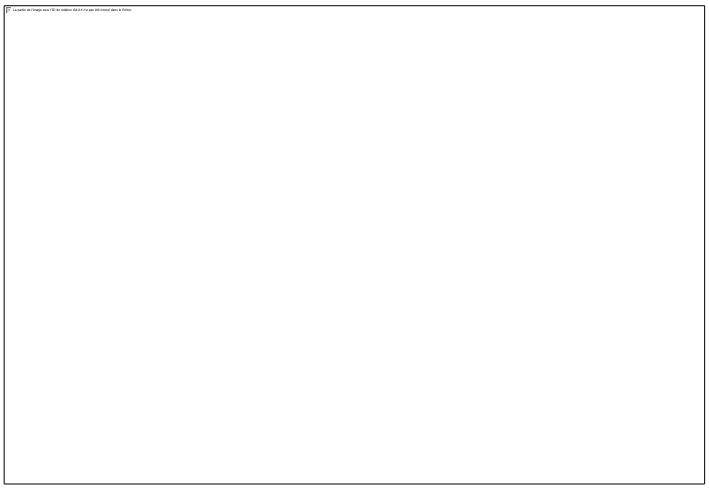

Single crystals of **[43b][BF_4]** suitable for X-ray crystallographic analysis were obtained from a solution of **[43b][BF_4]** in ethanol at – 35°C. X-ray diffraction experiments for monocrystal of **[43b][BF_4]** were performed at 294 K with graphite–monochromatized Mo K_α radiation (λ = 0.71073 Å) on a Bruker–Nonius Kappa CCD area detector diffractometer. Formula $C_{18}H_{16}BF_4P$, formula weight 350.09, crystal system orthorhombic, space group *P*nma, *a* = 10.7442(6) Å, *b* = 12.9153(6) Å, *c* = 12.4044(6) Å, α = β = γ = 90°, V = 1721.29(15) $Å^3$, Z = 4, calculated density = 1.351 g/cm^3, □ = 0.195 mm^{-1}, R_{int} = 0.0283, R[F^2>2σ(F^2)] = 0.0657, wR(F^2) = 0.2173. GOF = 1.038. Selected bond lengths (Å) : P1-C1 1.778(3), P1-C7 1.784(4), P1-H1 1.33(3). Program(s) used to solve structure: SHELXS–97. Program(s) used to refine structure: SHELXL–2014. Software used to prepare material for publication: SHELXL–2014.

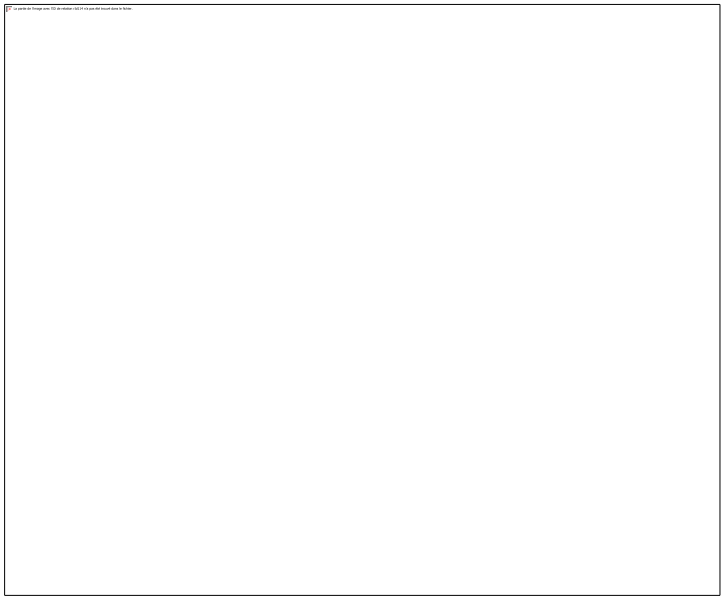

Single crystals of **36n** suitable for X-ray crystallographic analysis were obtained from a mixture of acetonitrile/toluene solution of **36n** at -35°C. X-ray diffraction experiments for monocrystal of **36n** were performed at 150 K with graphite–monochromatized Mo K_α radiation (λ = 0.71073 Å) on a Bruker–Nonius Kappa CCD area detector diffractometer. Formula $C_{33}H_{32}F_3O_7PS$, formula weight 660.61, crystal system monoclinic, space group *P*2(1)/n, *a* = 10.6040(4) Å, *b* = 17.8537(7) Å, *c* = 17.1939(7) Å, α = β = 90°, γ = 103.741(2)°, V = 3162.0(2) $Å^3$, Z = 4, calculated density = 1.388 g/cm^3, □ = 0.218 mm^{-1}, R_{int} = 0.0306, R[F^2>2σ(F^2)] = 0.0781, wR(F^2) = 0.1947. GOF = 1.065. Selected bond lengths (Å): P1-C21 1.794(3), P1-C15 1.797(3), P1-C27 1.804(3), P1-C7 1.844(3). Program(s) used to solve structure: SHELXS–97. Program(s) used to refine structure: SHELXL–2014. Program(s) used to refine structure: SHELXL–2014.

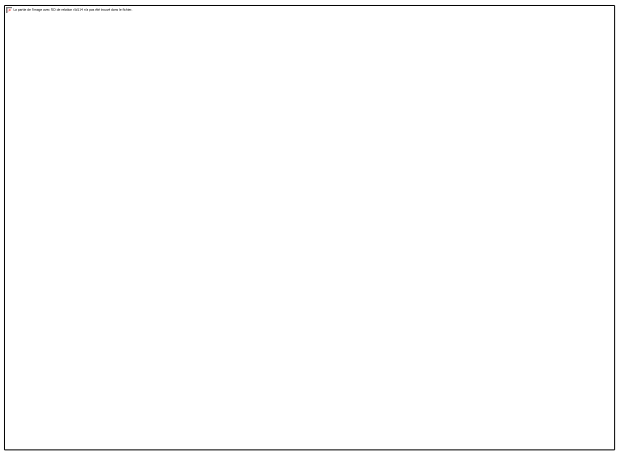

Single crystals of **[43b][41d]**suitable for X-ray crystallographic analysis were obtained by saturating a solution of **[43b][41d]** in acetonitrile with diethylether at r.t. for 2 days. X-ray diffraction experiments for monocrystal of **[43b][41d]** were performed at 150 K with graphite–monochromatized Mo K_α radiation (λ = 0.71073 Å) on a Bruker–Nonius Kappa CCD area detector diffractometer. Formula $C_{37}H_{38}BF_{10}N_2O_6PS_2$, formula weight 902.59, crystal system orthorhombic, space group *P*nma, *a* = 18.0131(4) Å, *b* = 26.2521(6) Å, *c* = 8.4802(2) Å, α = β =γ = 90°, V = 4010.13(16) $Å^3$, Z = 4, calculated density = 1.495 g/cm^3, □ = 0.267 mm^{-1}, R_{int} = 0.0303, R[F^2>2σ(F^2)] = 0.0601, wR(F^2) = 0.1760. GOF = 1.053. Selected bond lengths (Å) : P1-C10 1.799(2), P1-C16 1.801(4), P1-C1 1.847(4). Program(s) used to solve structure: SHELXS–97. Program(s) used to refine structure: SHELXL–2014. Software used to prepare material for publication: SHELXL–2014.

3. Kinetics

3.1 Determination of the second order rate constants

Table S1. Kinetics of the reaction of **43** with **41d** (CH_3CN, 20°C, stopped-flow, detection at 612 nm).

41d	**43**	**[43]/[41d]**	k_{obs}
2.50×10^{-5}	2.59×10^{-3}	104	70.0
2.50×10^{-5}	4.08×10^{-3}	163	125.5
2.50×10^{-5}	1.02×10^{-2}	409	305.5
2.50×10^{-5}	2.99×10^{-2}	1200	858.1
$k_2 = 2.86 \times 10^4$ M^{-1} s^{-1}			

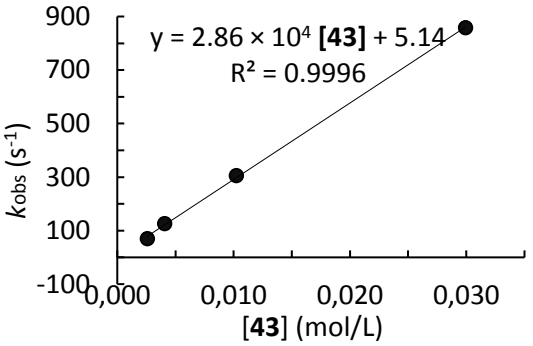

Table S2. Kinetics of the reaction of **43** with **41e** (CH_3CN, 20°C, stopped-flow, detection at 616 nm).

41e	**43**	**[43]/[41e]**	k_{obs}
2.47×10^{-5}	3.66×10^{-3}	148	11.6
2.47×10^{-5}	7.34×10^{-3}	297	20.0
2.47×10^{-5}	1.23×10^{-2}	498	36.0
2.47×10^{-5}	1.60×10^{-2}	646	46.6
k_2(20°C) = 2.87×10^3 M^{-1} s^{-1}			

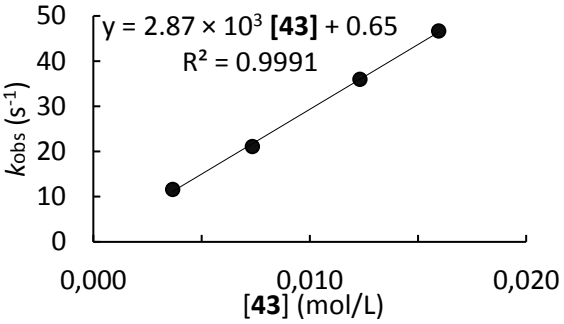

Table S3. Kinetics of the reaction of **43** with **41f** (CH_3CN, 20°C, stopped-flow, detection at 642 nm).

41f	**43**	**[43]/[41f]**	k_{obs}
2.03×10^{-5}	2.59×10^{-3}	128	23.6
2.03×10^{-5}	4.08×10^{-3}	201	25.2
2.03×10^{-5}	1.02×10^{-2}	502	38.1
2.03×10^{-5}	2.99×10^{-2}	1473	68.2
k_2(20°C) = 1.64×10^3 M^{-1} s^{-1}			

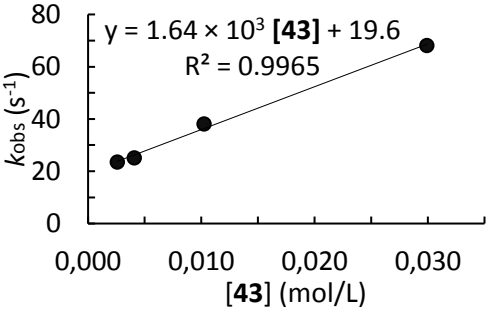

Table S4. Kinetics of the reaction of **43[BF_4]** with **41d** (CH_3CN 20°C, stopped-flow, detection at 612 nm)

41d	**43[BF_4]**	**[43[BF_4]]/[41d]**	k_{obs}
2.50×10^{-5}	1.10×10^{-3}	44	15.4
2.50×10^{-5}	2.04×10^{-3}	82	24.9
2.50×10^{-5}	4.96×10^{-3}	198	54.2
2.50×10^{-5}	1.00×10^{-2}	400	106.8
$k_2 = 1.03 \times 10^4$ M^{-1} s^{-1}			

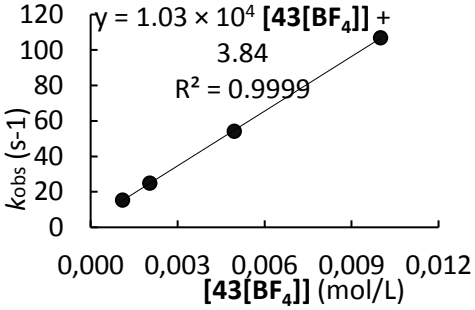

Table S5. Kinetics of the reaction of **43[BF_4]** with **41e** (CH_3CN 20°C, stopped-flow, detection at 616 nm)

41e	**43[BF_4]**	**[43[BF_4]]/[41e]**	k_{obs}
2.47×10^{-5}	3.68×10^{-3}	149	4.3
2.47×10^{-5}	5.71×10^{-3}	231	6.8
2.47×10^{-5}	1.20×10^{-2}	485	14.4
2.47×10^{-5}	1.94×10^{-2}	785	21.8
k_2(20°C) = 1.12×10^3 M^{-1} s^{-1}			

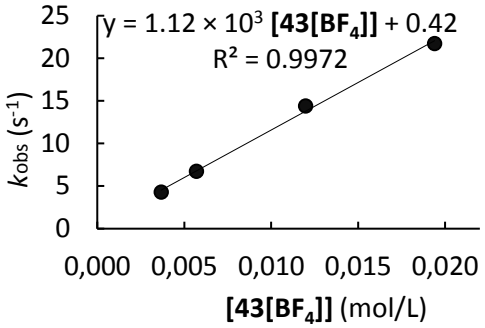

Table S6. Kinetics of the reaction of **43[BF_4]** with **41f** (CH_3CN, 20°C, stopped-flow, detection at 642 nm)

41f	**43[BF_4]**	**[43[BF_4]]/[41f]**	k_{obs}
2.50×10^{-5}	2.59×10^{-3}	104	70.0
2.50×10^{-5}	4.08×10^{-3}	163	125.5
2.50×10^{-5}	1.02×10^{-2}	409	305.5
2.50×10^{-5}	2.99×10^{-2}	1200	858.1
k_2(20°C) = 6.13×10^2 M^{-1} s^{-1}			

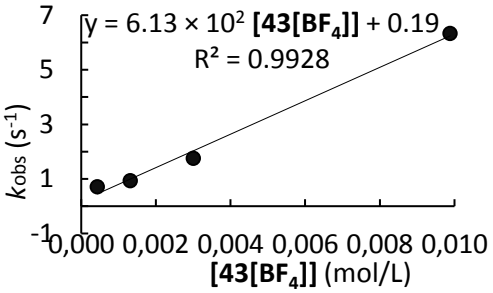

Table S7. Kinetics of the reaction of **43[OTf]** with **41d** (CH_3CN 20°C, stopped-flow, detection at 612 nm)

41d	**43[OTf]**	**[43[OTf]]/[41d]**	k_{obs}
2.64×10^{-5}	4.24×10^{-4}	16	8.0
2.64×10^{-5}	7.40×10^{-4}	28	11.1
2.64×10^{-5}	2.40×10^{-3}	91	30.4
2.64×10^{-5}	4.04×10^{-3}	153	48.4
k_2 = 1.13×10^4 M^{-1} s^{-1}			

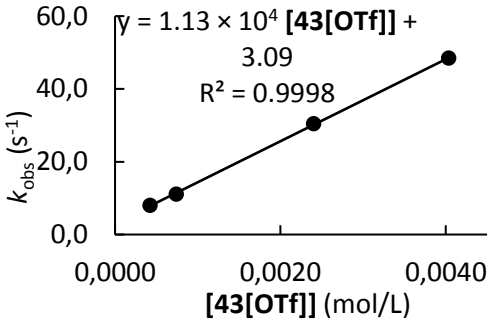

Table S8. Kinetics of the reaction of **43[OTf]** with **41e** (CH_3CN 20°C, stopped-flow, detection at 616 nm)

41e	**43[OTf]**	**[43[OTf]]/[41e]**	k_{obs}
2.47×10^{-5}	4.24×10^{-4}	17	0.66
2.47×10^{-5}	7.40×10^{-4}	30	0.95
2.47×10^{-5}	2.40×10^{-3}	97	3.4
2.47×10^{-5}	4.04×10^{-3}	163	5.5
k_2(20°C) = 1.37×10^3 M^{-1} s^{-1}			

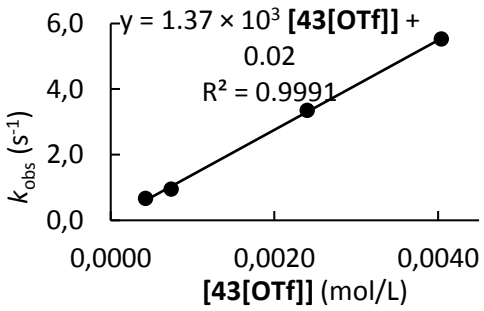

Table S9. Kinetics of the reaction of **43[OTf]** with **41f** (CH_3CN, 20°C, stopped-flow, detection at 642 nm)

41f	**43[OTf]**	**[43[OTf]]/[41f]**	k_{obs}
2.48×10^{-5}	4.24×10^{-4}	17	0.58
2.48×10^{-5}	5.46×10^{-4}	22	0.59
2.48×10^{-5}	1.79×10^{-3}	73	1.3
2.48×10^{-5}	4.09×10^{-3}	165	2.9
k_2(20°C) = 6.49×10^{2} M^{-1} s^{-1}			

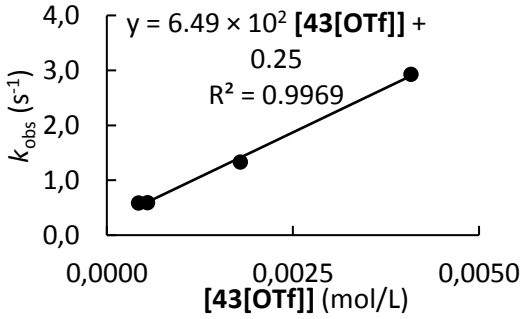

Table S10. Kinetics of the reaction of **D-43b[OTf]** with **41d** (CH_3CN, 20°C, stopped-flow, detection at 612 nm)

41d	**D-43b[OTf]**	**[D-43b[OTf]]/[41d]**	k_{obs}
2.64×10^{-5}	3.99×10^{-4}	15	8.4
2.64×10^{-5}	1.06×10^{-3}	40	15.4
2.64×10^{-5}	2.12×10^{-3}	80	27.4
2.64×10^{-5}	4.29×10^{-3}	163	55.6
k_2(20°C) = 1.22×10^{4} M^{-1} s^{-1}			

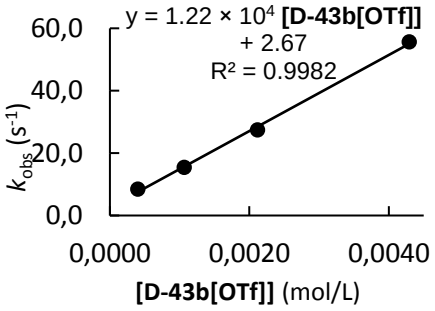

Table S11. Kinetics of the reaction of **D-43b[OTf]** with **41e** (CH_3CN, 20°C, stopped-flow, detection at 616 nm)

41e	**D-43b[OTf]**	**[D-43b[OTf]]/[41e]**	k_{obs}
2.47×10^{-5}	3.99×10^{-4}	16	0.54
2.47×10^{-5}	8.83×10^{-4}	36	0.86
2.47×10^{-5}	2.15×10^{-3}	87	1.48
2.47×10^{-5}	5.41×10^{-3}	219	3.07
k_2(20°C) = 1.48×10^{3} M^{-1} s^{-1}			

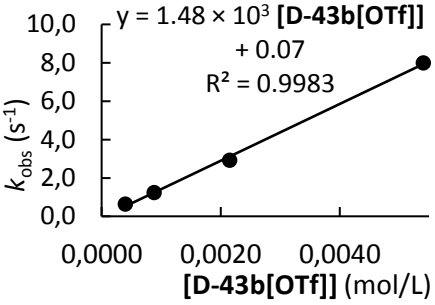

Table S12. Kinetics of the reaction of **D-43b[OTf]** with **41f** (CH_3CN, 20°C, stopped-flow, detection 642 nm)

41f	**D-43b[OTf]**	**[D-43b[OTf]]/[41f]**	k_{obs}
2.48×10^{-5}	4.23×10^{-4}	17	0.54
2.48×10^{-5}	1.06×10^{-3}	43	0.86
2.48×10^{-5}	2.12×10^{-3}	86	1.48
2.48×10^{-5}	4.30×10^{-3}	173	3.07
k_2(20°C) = 6.62×10^{2} M^{-1} s^{-1}			

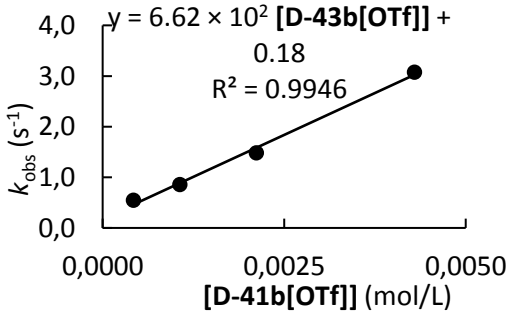

Table S13. Kinetics of the reaction of **43[OTf]** with **41d** (CH_2Cl_2 20°C, stopped-flow detection at 612nm)

41d	**43[OTf]**	**[43[OTf]]/[41d]**	k_{obs}
2.64×10^{-5}	1.21×10^{-3}	49	22.2
2.64×10^{-5}	2.17×10^{-3}	88	39.9
2.64×10^{-5}	3.84×10^{-3}	155	74.5
2.64×10^{-5}	8.13×10^{-3}	328	175.3
$k_2 = 2.22 \times 10^4$ M^{-1} s^{-1}			

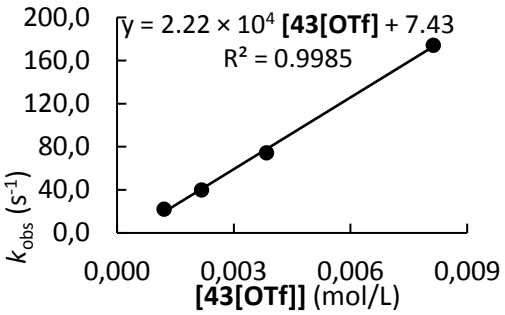

Table S14. Kinetics of the reaction of **43[OTf]** with **41e** (CH_2Cl_2 20°C, stopped-flow detection at 616 nm)

41e	**43[OTf]**	**[43[OTf]]/[41e]**	k_{obs}
2.47×10^{-5}	1.21×10^{-3}	49	1.4
2.47×10^{-5}	2.17×10^{-3}	88	2.6
2.47×10^{-5}	3.84×10^{-3}	155	5.1
2.47×10^{-5}	8.13×10^{-3}	328	12.9
k_2(20°C) = 1.68×10^3 M^{-1} s^{-1}			

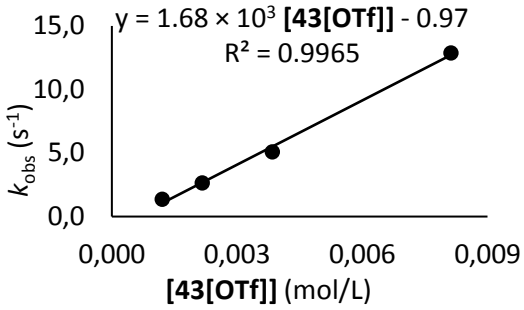

Table S15. Kinetics of the reaction of **43[OTf]** with **41f** (CH_2Cl_2 20°C, stopped-flow, detection at 642 nm)

41f	**43[OTf]**	**[43[OTf]]/[41f]**	k_{obs}
2.48×10^{-5}	1.21×10^{-3}	49	0.82
2.48×10^{-5}	2.17×10^{-3}	88	1.5
2.48×10^{-5}	3.84×10^{-3}	155	3.0
2.48×10^{-5}	8.13×10^{-3}	328	6.7
k_2(20°C) = 8.66×10^2 M^{-1} s^{-1}			

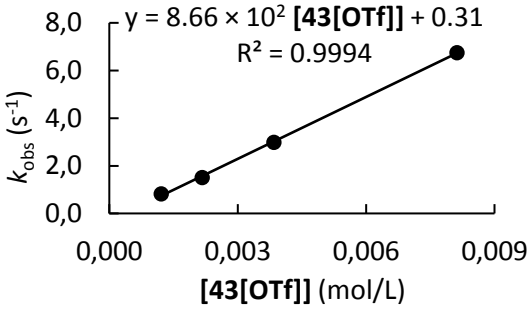

Table S16. Kinetics of the reaction of **47** with **41d** (CH_3CN, 20°C, stopped-flow, detection at 612 nm)

41d	**47**	**[47]/[41d]**	k_{obs}
2.64×10^{-5}	2.36×10^{-3}	95	304.0
2.64×10^{-5}	4.69×10^{-3}	189	509.1
2.64×10^{-5}	7.42×10^{-3}	300	712.5
2.64×10^{-5}	1.02×10^{-2}	413	923.6
k_2(20°C) = 7.74×10^4 M^{-1} s^{-1}			

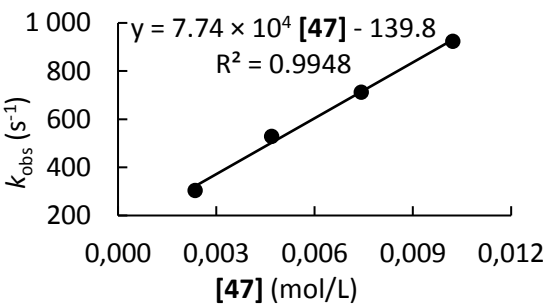

Table S17. Kinetics of the reaction of **47** with **41e** (CH_3CN, 20°C, stopped-flow, detection at 616 nm)

41e	**47**	**[47]/[41e]**	k_{obs}
2.47×10^{-5}	2.36×10^{-3}	95	23.4
2.47×10^{-5}	4.69×10^{-3}	189	46.5
2.47×10^{-5}	7.42×10^{-3}	300	76.0
2.47×10^{-5}	1.02×10^{-2}	413	107.4
k_2(20°C) = 1.07×10^{4} M^{-1} s^{-1}			

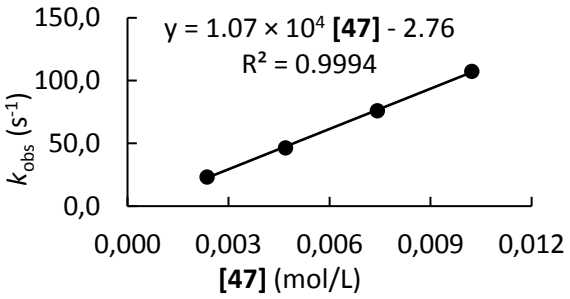

Table S18. Kinetics of the reaction of **47** with **41f** (CH_3CN, 20°C, stopped-flow, detection at 642 nm)

41f	**47**	**[47]/[41f]**	k_{obs}
2.48×10^{-5}	2.36×10^{-3}	95	17.1
2.48×10^{-5}	4.69×10^{-3}	189	32.6
2.48×10^{-5}	7.42×10^{-3}	300	50.2
2.48×10^{-5}	1.02×10^{-2}	413	69.9
k_2(20°C) = 6.69×10^{3} M^{-1} s^{-1}			

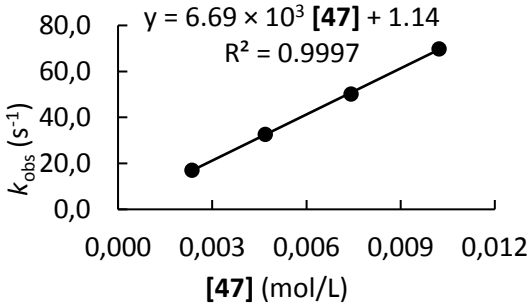

Table S19. Kinetics of the reaction of **47b[OTf]** with **41d** (CH_3CN, 20°C, stopped-flow, detection at 612 nm)

41d	**47b[OTf]**	**[47b[OTf]]/[41d]**	k_{obs}
2.64×10^{-5}	1.96×10^{-3}	79	4.11
2.64×10^{-5}	2.70×10^{-3}	109	4.43
2.64×10^{-5}	3.79×10^{-2}	153	5.15
k_2(20°C) = 5.74×10^{2} M^{-1} s^{-1}			

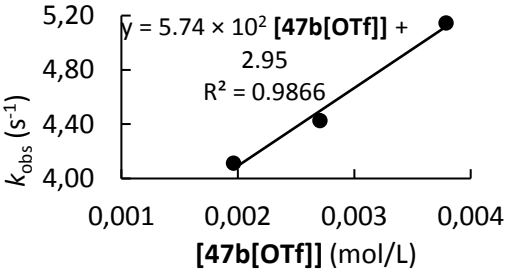

Table S20. Kinetics of the reaction of **47b[OTf]** with **41e** (CH_3CN, 20°C, stopped-flow, detection at 616 nm)

41e	**47b[OTf]**	**[47b[OTf]]/[41e]**	k_{obs}
2.47×10^{-5}	1.19×10^{-3}	48	0.203
2.47×10^{-5}	1.96×10^{-3}	79	0.246
2.47×10^{-5}	2.70×10^{-3}	109	0.291
2.47×10^{-5}	3.79×10^{-2}	153	0.358
k_2(20°C) = 5.98×10^{1} M^{-1} s^{-1}			

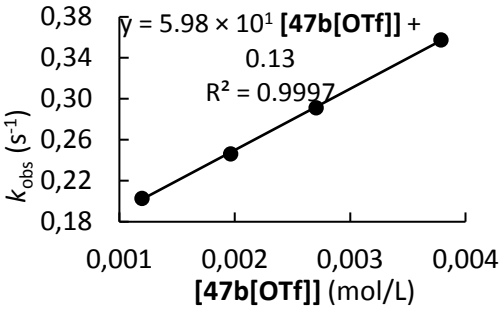

Table S21. Kinetics of the reaction of **47b[OTf]** with **41f** (CH_3CN, 20°C, stopped-flow, detection at 642 nm)

41f	**47b[OTf]**	**[47b[OTf]]/[41f]**	k_{obs}
2.48×10^{-5}	1.19×10^{-3}	48	0.145
2.48×10^{-5}	1.96×10^{-3}	79	0.162
2.48×10^{-5}	2.70×10^{-3}	109	0.180
2.48×10^{-5}	3.79×10^{-2}	153	0.209
$k_2 = 2.48 \times 10^{1}$ M^{-1} s^{-1}			

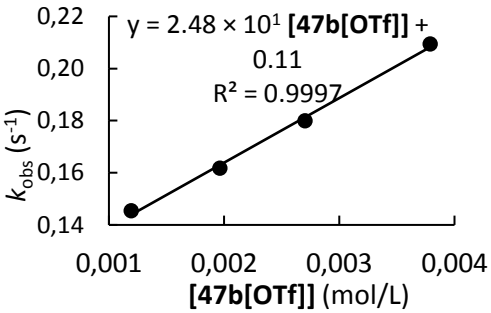

Table S22. Kinetics of the reaction of **33** with **41a** (CH_2Cl_2, 20°C, stopped-flow, detection at 586 nm)

[41a]	**[33]**	**[33]/[41a]**	k_{obs}
1.35×10^{-4}	7.52×10^{-3}	56	31.70
1.35×10^{-4}	9.46×10^{-3}	70	52.50
1.35×10^{-4}	1.21×10^{-2}	90	83.90
1.35×10^{-4}	1.52×10^{-2}	113	117.0
$k_2 = 1.11 \times 10^{4}$ M^{-1} s^{-1}			

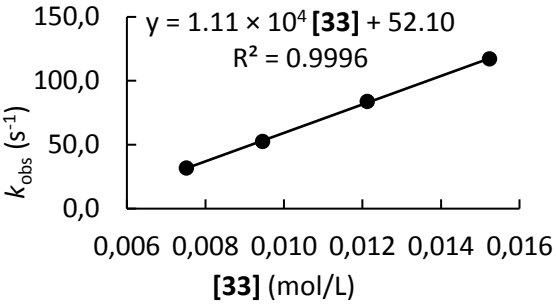

Table S23. Kinetics of the reaction of **33** with **41b** (CH_2Cl_2, 20°C, stopped-flow, detection at 671 nm)

41b	**33**	**[33]/[41b]**	k_{obs}
6.80×10^{-5}	7.52×10^{-3}	111	18.48
6.80×10^{-5}	9.46×10^{-3}	139	30.52
6.80×10^{-5}	1.21×10^{-2}	178	45.19
6.80×10^{-5}	1.52×10^{-2}	224	58.92
k_2(20°C) $= 5.23 \times 10^{3}$ M^{-1} s^{-1}			

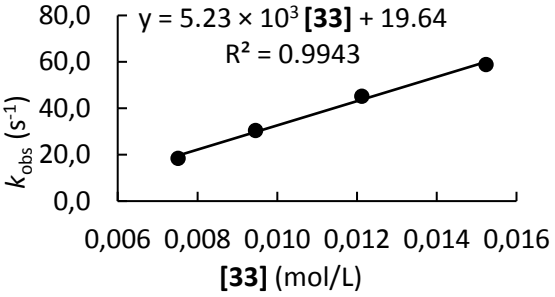

Note : Due to low solubility of the phosphine in acetonnitrile, we change the solvent for dichloromethane.

Table S24. Kinetics of the reaction of **33** with **41c** (CH_2Cl_2, 20°C, stopped-flow, detection at 611 nm)

41c	**33**	**[33]/[41c]**	k_{obs}
7.78×10^{-5}	7.52×10^{-3}	97	11.21
7.78×10^{-5}	9.46×10^{-3}	121	15.55
7.78×10^{-5}	1.21×10^{-2}	156	21.87
7.78×10^{-5}	1.52×10^{-2}	196	26.91
$k_2 = 2.05 \times 10^{3}$ M^{-1} s^{-1}			

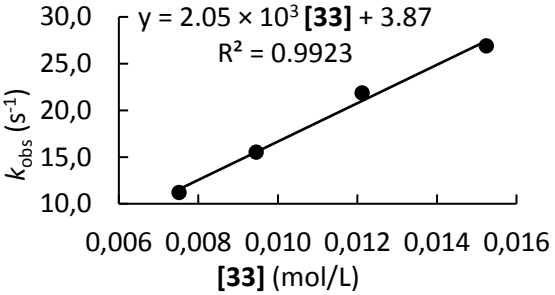

Note : Due to low solubility of the phosphine in acetonnitrile, we change the solvent for dichloromethane.

Table S25. Kinetics of the reaction of **34** with **41a** (CH_2Cl_2, 20°C, stopped-flow, detection at 586 nm)

41a	**34**	**[34]/[41a]**	k_{obs}
2.94×10^{-5}	6.74×10^{-4}	29	6.89
2.94×10^{-5}	1.03×10^{-3}	35	7.27
2.94×10^{-5}	1.40×10^{-3}	48	7.78
2.94×10^{-5}	1.69×10^{-3}	58	8.21
k_2(20°C) = 1.31×10^{3} M^{-1} s^{-1}			

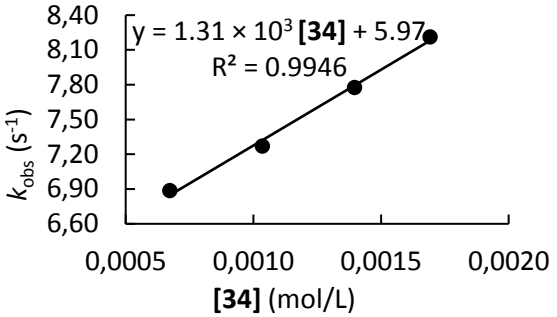

Note : Due to low solubility of the phosphine in acetonitrile, we change the solvent for dichloromethane.

Table S26. Kinetics of the reaction of **34** with **41b** (CH_2Cl_2, 20°C, stopped-flow, detection at 671 nm)

41b	**34**	**[34]/[41b]**	k_{obs}
2.79×10^{-5}	7.54×10^{-4}	27	3.90
2.79×10^{-5}	1.12×10^{-3}	40	4.02
2.79×10^{-5}	1.46×10^{-3}	52	4.11
2.79×10^{-5}	2.05×10^{-3}	74	4.28
k_2(20°C) = 2.87×10^{2} M^{-1} s^{-1}			

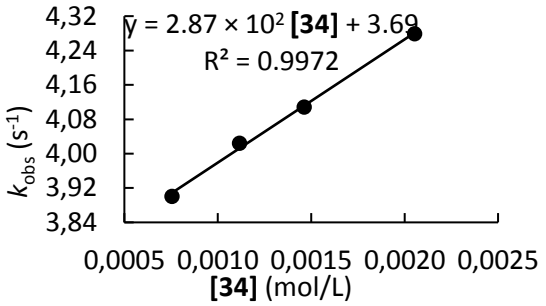

Note :Due to low solubility of the phosphine in acetonitrile, we change the solvent for dichloromethane.

Table S27. Kinetics of the reaction of **34** with **41c** (CH_2Cl_2, 20°C, stopped-flow, detection at 611 nm)

41c	**34**	**[34]/[41c]**	k_{obs}
4.15×10^{-5}	6.54×10^{-4}	16	0.78
4.15×10^{-5}	1.10×10^{-3}	27	0.83
4.15×10^{-5}	1.61×10^{-3}	39	0.88
4.15×10^{-5}	2.12×10^{-3}	51	0.93
k_2(20°C) = 9.48×10^{1} M^{-1} s^{-1}			

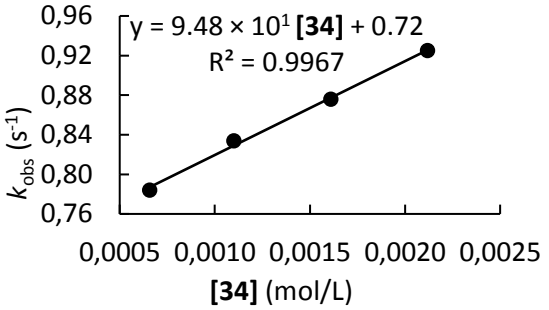

Note : Due to low solubility of the phosphine in acetonitrile, we change the solvent for dichloromethane.

3.2 Determination of the reactivity parameters *N* and s_N for the nucleophiles.

Table S28. Calculation of the reactivity parameters *N* and s_N for **33** using **41a-c** in CH_3CN, 20°C.

Electrophile	*E*	k_2 (M^{-1} s^{-1})	*Log* (k_2)
41a	-3.85	1.11×10^{4}	4.05
41b	-4.72	5.23×10^{3}	3.72
41c	-5.53	2.05×10^{3}	3.31
N = 13.17, s_N = 0.44			

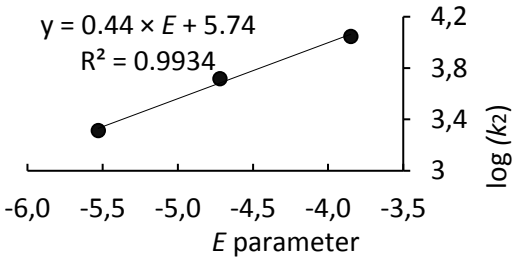

Table S29. Calculation of the reactivity parameters *N* and s_N for **34** using **41a-c** in CH_2Cl_2, 20°C.

Electrophile	*E*	k_2 ($M^{-1} s^{-1}$)	*Log* (k_2)
41a	-3.85	1.31×10^3	3.12
41b	-4.72	2.87×10^2	2.46
41c	-5.53	9.48×10^1	1.97
N = 8.40, s_N = 0.68			

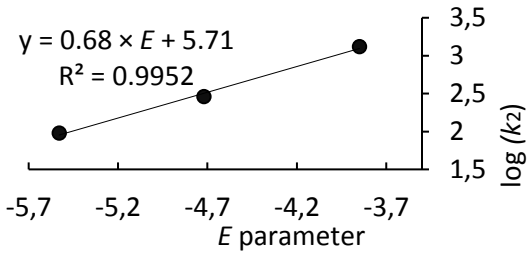

Table S30. Calculation of the reactivity parameters *N* and s_N for **43** using **41d-f** in CH_3CN, 20°C.

Electrophile	*E*	k_2 ($M^{-1} s^{-1}$)	Log (k_2)
41d	-7.02	2.86×10^4	4.46
41e	-8.76	2.87×10^3	3.46
41f	-9.45	1.64×10^3	3.21
N = 15.50, s_N = 0.52.			

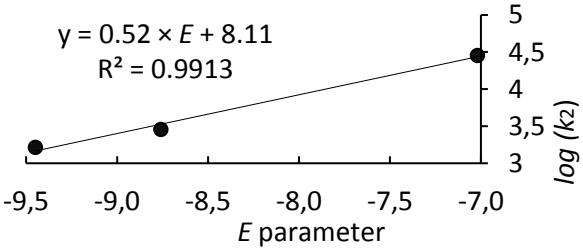

Table S31. Calculation of the reactivity parameters *N* and s_N for **43b[BF_4]** using **41d-f** in CH_3CN.

Electrophile	*E*	k_2 ($M^{-1} s^{-1}$)	Log (k_2)
41d	-7.02	1.03×10^4	4.01
41e	-8.76	1.12×10^3	3.05
41f	-9.45	6.13×10^2	2.79
N = 14.80, s_N = 0.51			

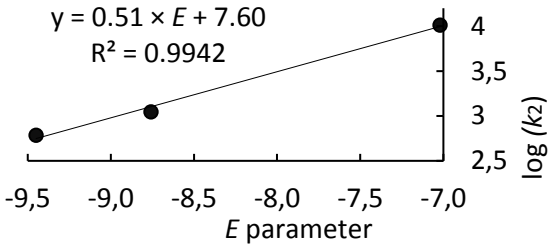

Table S32. Calculation of the reactivity parameters *N* and s_N for **43b[OTf]** using **41d-f** in CH_3CN.

Electrophile	*E*	k_2 ($M^{-1} s^{-1}$)	*Log* (k_2)
41d	-7.02	1.13×10^4	4.05
41e	-8.76	1.37×10^3	3.14
41f	-9.45	6.49×10^2	2.81
N = 14.91, s_N = 0.51			

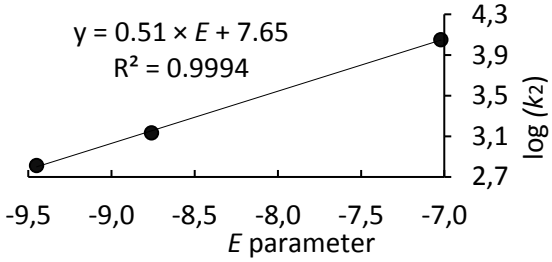

Table S33. Calculation of the reactivity parameters *N* and s_N for **D-43b[OTf]** using **41d-f** in CH_3CN.

Electrophile	*E*	k_2 ($M^{-1} s^{-1}$)	*Log* (k_2)
41d	-7.02	1.22×10^4	4.09
41e	-8.76	1.48×10^3	3.17
41f	-9.45	6.62×10^2	2.82
N = 14.80, s_N = 0.51			

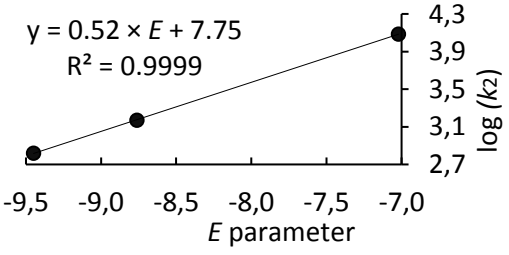

Table S34. Calculation of the reactivity parameters *N* and s_N for **43b[OTf]** using **41d-f** in CH_2Cl_2, 20°C.

Electrophile	*E*	k_2 ($M^{-1}\,s^{-1}$)	*Log* (k_2)
41d	-7.02	2.22×10^4	4.05
41e	-8.76	1.68×10^3	3.23
41f	-9.45	8.66×10^2	2.81
N = 14.32, s_N = 0.58			

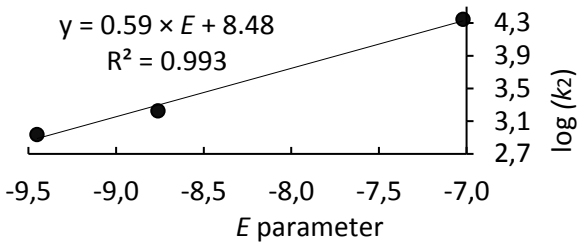

Table S35. Calculation of the reactivity parameters *N* and s_N for **47** using **41d-f** in CH_3CN, 20°C.

Electrophile	*E*	k_2 ($M^{-1}\,s^{-1}$)	*Log* (k_2)
41d	-7.02	7.74×10^4	4.89
41e	-8.76	1.07×10^4	4.03
41f	-9.45	6.69×10^3	3.83
N = 17.88, s_N = 0.45			

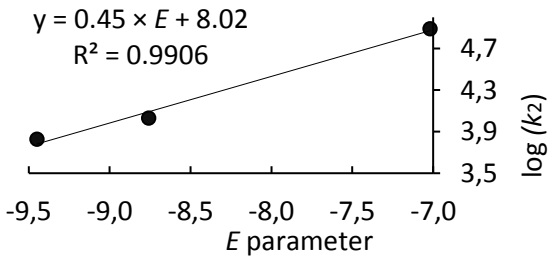

Table S36. Calculation of the reactivity parameters *N* and s_N for **47b[OTf]** using **41d-f** in CH_3CN, 20°C.

Electrophile	*E*	k_2 ($M^{-1}\,s^{-1}$)	*Log* (k_2)
41d	-7.02	5.74×10^2	2.76
41e	-8.76	5.98×10^1	1.78
41f	-9.45	2.48×10^1	1.39
N = 11.93, s_N = 0.56			

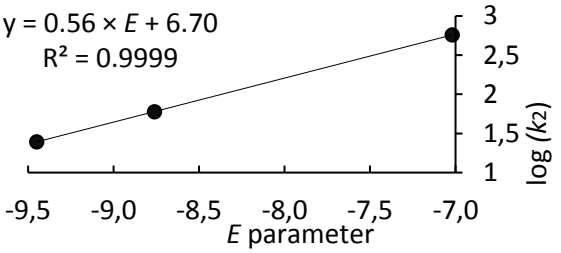

3.3 Equilibrium constants (K) for the reactions of phosphines and phosphonium salts with benzhydrilium cations.

Table 37. Determination of the equilibrium constant for the reaction of **33** and **41a** in CH_3CN. Ɛ(**33**) = 1.38×10^5 $M^{-1}.cm^{-1}$, T = 20 ± 0.1°C, detection at λ = 586 nm, d = 0.2 cm, [**33**]° = 6.16×10^{-5} M.

Entry	A_0	A	$[LB]_0$ (M)	*K* (M^{-1})
1	1.7015	0.0440	1.52×10^{-2}	2.48×10^3
2	1.7015	0.0584	1.21×10^{-2}	2.33×10^3
3	1.7015	0.1071	9.46×10^{-3}	1.59×10^3
4	1.7015	0.1616	7.52×10^{-3}	1.28×10^3
				K(average) = 1.92×10^3 M^{-1}

Table 38. Determination of the equilibrium constant for the reaction of **33** and **41b** in CH_2Cl_2. Ɛ(**33**) = 9.55×10^4 $M^{-1}.cm^{-1}$, T = 20 ± 0.1°C, detection at λ = 671 nm, d = 0.2 cm, [**33**]° = 4.38×10^{-5} M.

Entry	A_0	A	$[LB]_0$ (M)	*K* (M^{-1})
1	0.8360	0.0694	1.52×10^{-2}	7.27×10^2
2	0.8360	0.0917	1.21×10^{-2}	6.72×10^2

3	0.8360	0.1506	9.46×10^{-3}	4.83×10^{2}
4	0.8360	0.1972	7.52×10^{-3}	4.33×10^{2}

K(average) = 5.79×10^{2} M^{-1}

Table 39. Determination of the equilibrium constant for the reaction of **33** with **41c** in CH_2Cl_2. Ɛ(**33**) = 1.45×10^{5} $M^{-1}.cm^{-1}$, T = 20 ± 0.1°C, detection at λ = 611 nm, d = 0.2 cm, [**33**]° = 4.01×10^{-5} M.

Entry	A_0	A	$[LB]_0$ (M)	K (M^{-1})
1	1.2966	0.6655	3.63×10^{-2}	2.62×10^{1}
2	1.2784	0.4160	5.10×10^{-2}	4.15×10^{1}
3	1.2694	0.2581	6.27×10^{-2}	6.42×10^{1}
4	1.2275	0.1219	7.84×10^{-2}	1.23×10^{2}
5	1.2147	0.0812	9.61×10^{-2}	1.56×10^{2}

K(average) = 8.21×10^{1} M^{-1}

Table 40. Determination of the equilibrium constant for the reaction of **34** and **41a** in CH_2Cl_2. Ɛ(**34**) = 1.38×10^{5} $M^{-1}.cm^{-1}$, T = 20 ± 0.1°C, detection at λ = 586 nm, d = 0.2 cm, [**34**]° = 6.16×10^{-5} M.

Entry	A_0	A	$[LB]_0$ (M)	K (M^{-1})
1	2.4452	1.2818	5.49×10^{-3}	1.67×10^{2}
2	2.4335	0.9536	8.82×10^{-3}	1.77×10^{2}
3	2.4532	0.7593	1.18×10^{-2}	1.91×10^{2}
4	2.3774	0.5672	1.57×10^{-2}	2.04×10^{2}
5	2.3572	0.4968	1.82×10^{-2}	2.06×10^{2}

K(average) = 1.89×10^{2} M^{-1}

Table 41. Determination of the equilibrium constant for the reaction of **34** with **41b** in CH_2Cl_2. Ɛ(**34**) = 9.55×10^{4} $M^{-1}.cm^{-1}$, T = 20 ± 0.1°C, detection at λ = 671 nm, d = 0.2 cm, [**34**]° = 2.75×10^{-5} M.

Entry	A_0	A	$[LB]_0$ (M)	K (M^{-1})
1	0.5238	0.3694	5.49×10^{-3}	7.62×10^{1}
2	0.5241	0.3072	8.82×10^{-3}	8.01×10^{1}
3	0.5298	0.2535	1.18×10^{-2}	9.28×10^{1}
4	0.5228	0.2096	1.57×10^{-2}	9.54×10^{1}
5	0.5351	0.1993	1.82×10^{-2}	9.25×10^{1}

K(average) = 8.74×10^{1} M^{-1}

Table 42. Determination of the equilibrium constant for the reaction of **34** with **41c** in CH_2Cl_2. Ɛ(**34**) = 1.45×10^{5} $M^{-1}.cm^{-1}$, T = 20 ± 0.1°C, detection at λ = 611 nm, d = 0.2 cm, [**34**]° = 4.01×10^{-5} M.

Entry	A_0	A	$[LB]_0$ (M)	K (M^{-1})
1	1.3139	1.2576	5.49×10^{-3}	8.16
2	1.3042	1.1698	8.82×10^{-3}	1.30×10^{1}
3	1.2989	1.0889	1.18×10^{-2}	1.64×10^{1}
4	1.2996	0.9979	1.57×10^{-2}	1.93×10^{1}
5	1.3182	0.9711	1.82×10^{-2}	1.96×10^{1}

K(average) = 1.53×10^{1} M^{-1}

3.1 Determination of the *LB* parameters of phosphines 33 and 34

Table 43. Determination of the LB value for **33** and **34**. The LA values are taken literature. [1]

Nucleophile Solvent	Electrophile	LA	K(average) (M^{-1})	log($K_{average}$)	LB
33	**41a**	-5.39	1.92×10^{3}	3.28	8.67

CH_3CN	**41b**	-5.72	5.79×10^2	2.76	8.48
	41c	-6.82	8.21×10^1	1.91	8.72
					$LB_{average}$ = 8.62
34	**41a**	-5.39	1.89×10^2	2.28	7.67
CH_2Cl_2	**41b**	-5.72	8.74×10^1	1.94	7.66
	41c	-6.82	1.53×10^1	1.18	8.00
					$LB_{average}$ = 7.77

Chapter 3: Quantification of the Hydride Donor Ability of Phosphine Borane Complexes.

1. Synthetic part

1.1 Preparation of phosphine borane complexes 29a-j.

Ethyldiphenylphosphine borane complex 29b.

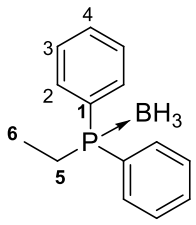

Chemical Formula: $C_{14}H_{18}BP$
Molecular Weight: 228.08

A solution of ethylbromide (2.25 mL, 30.1 mmol, 1.1 eq), in degazed THF (25 mL) was added dropwise to magnesium turning (0.73 g, 30.1 mmol, 1.1 eq) under stirring at r.t. The addition rate was adjusted so that the reflux was maintained which corresponds to 30 min. The brownish solution was then stirred at reflux for 1h before cooling down to r.t. A solution of chlorodiphenylphosphine (5.0 mL, 27.1 mmol, 1 eq) in degazed THF (25 mL) was added dropwise to the Grignard solution in 30 minutes leading to a yellowish solution which was stirred for an additional hour at r.t. The crude mixture was quenched with an aqueous solution of saturated NH_4Cl (15 mL) followed by water (10 mL) to dissolve the precipitates. The organic phase was cannulated and the aqueous phase was extracted with degazed THF (2 × 20 mL). Under argon, $BH_3.SMe_2$ (5.7 mL, 60.0 mmol, 2 eq) was added dropwise to the organic phase at 0°C in 30 min and the mixture was stirred for 2h at r.t. An aqueous solution of saturated NH_4Cl (15 mL) was added and the mixture was stirred for 1h at r.t. and extracted with CH_2Cl_2 (2 × 15 mL). The combined organic phase was washed with a saturated solution of $NaHCO_3$ (15 mL), dried over $MgSO_4$, filtered and concentrated. The crude oil was purified by silica gel column chromatography with the eluent: CH_2Cl_2/pentane (3:7) to afford a colourless oil (4.56 g, 19.9 mmol, 74%).

Rf (CH_2Cl_2/pentane) = 0.35 **^{1}H-NMR** (400.1 MHz, $CDCl_3$): δ 7.70-7.66 (m, 4H, H-Ar), 7.49-7.42 (m, 6H, H-Ar), 2.25 (dq, *J* = 10.9, 7.6 Hz, 2H, H-5), 1.15 (dt, *J* = 17.5, 7.6 Hz, 3H, H-6), 1.01 (q, *J* = 91.0 Hz, 3H, BH_3). **^{13}C-NMR** (100.6 MHz, $CDCl_3$): δ 132.3 (d, *J* = 11.1 Hz, C-Ar), 131.3 (d, *J* = 3.8 Hz, C-Ar), 129.5 (d, *J* = 55.1 Hz, C-Ar), 128.9 (d, *J* = 9.9 Hz, C-Ar), 19.0 (d, *J* = 39.8 Hz, C-5), 7.4 (s, C-6). **^{31}P{^{1}H}-NMR** (162.0 MHz, $CDCl_3$): δ 18.3 (q, *J* = 58.3 Hz, P). **^{11}B{^{1}H}-NMR** (128.4 MHz, $CDCl_3$): δ -40.1 (d, *J* = 58.3 Hz, BH_3). **HRMS** (ESI positive) = [$C_{14}H_{18}BNaP^+$] Calculated mass: 251.1137 g/mol, found mass: 251.1136 g/mol.

Diethylphenylphosphine borane complex 29c.

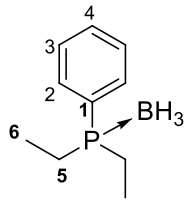

Chemical Formula: $C_{10}H_{18}BP$
Molecular Weight: 180.03

A solution of ethylbromide (8.2 mL, 110 mmol, 2.2 eq), in degazed THF (100 mL) was added dropwise to magnesium turnings (2.80 g, 115 mmol, 2.3 eq) under stirring at r.t. After the completion of the addition, the brownish solution was stirred at reflux for 1h before cooling down to r.t. A solution of dichlorophenylphosphine (6.8 mL, 50 mmol, 1 eq) in degazed THF (50 mL) was added dropwise to the Grignard solution in 30 minutes and the resulting mixture was stirred for an additional hour at r.t. The solution was quenched with an aqueous solution of saturated NH_4Cl (25 mL) followed by water (20 mL) to dissolve the precipitates. The organic phase was cannulated and the aqueous phase was extracted with degazed THF (2 × 40 mL). Under argon, $BH_3.SMe_2$ (5.7 mL, 60.0 mmol, 1.2 eq) was added dropwise to the organic phase at 0°C in 30 min and the mixture was stirred for 2h at r.t. An aqueous solution of saturated NH_4Cl (40 mL) was added and the mixture was stirred for 1h at r.t. and extracted with CH_2Cl_2 (2 × 30 mL). The combined organic phases were washed with an aqueous solution of saturated $NaHCO_3$ (15 mL), dried over $MgSO_4$, filtered and concentrated. The crude was purified by distillation to afford a colourless oil (6.66 g, 37 mmol, 74%). Spectroscopic data are in agreement with the literature. [201]

Bp (0.1 mbar): 154°C. **^{1}H-NMR** (400.1 MHz, $CDCl_3$): δ 7.72-7.68 (m, 2H, H-Ar), 7.50-7.44 (m, 3H, H-Ar), 1.92-1.83 (m, 4H, H-5), 1.06 (dt, *J* = 16.6 Hz, *J* = 7.6 Hz, 6H, H-6), 0.67 (q, *J* = 95.0 Hz, 3H, BH_3). **^{13}C-NMR** (100.6 MHz, $CDCl_3$): δ 132.1 (d, *J* = 8.3 Hz, C-Ar), 131.3 (d, *J* = 2.5 Hz, C-Ar), 128.8 (d, *J* = 9.2 Hz, C-Ar), 127.9 (d, *J* = 51.1 Hz, C-Ar), 18.4 (d, *J* = 38.9 Hz, C-5), 7.1 (d, *J* = 1.9 Hz, C-6). **^{31}P{^{1}H}-NMR** (162.0 MHz, $CDCl_3$): δ 19.7(q, *J* = 58.2 Hz, P). **^{11}B{^{1}H}-NMR** (128.4 MHz, $CDCl_3$): δ -41.9 (d, *J* = 58.2 Hz, BH_3). **HRMS** (ESI positive) = [$C_{10}H_{18}BNaP^+$] Calculated mass: 203.1137 g/mol, found mass: 203.1138 g/mol.

General procedure for the boration of phosphines (GP1)

All steps of the following procedure were achieved under inert atmosphere. To a 100 mL three necked round bottomed flask equipped with a stirrer, an additional funnel and a condenser containing a solution of the phosphine in degazed THF (c = 0.5M), was added dropwise $BH_3.SMe_2$. After stirring for 12 hours at ambient temperature, a saturated NH_4Cl solution, was gently added at 0°C. The mixture was left for 1h then poured into water and extracted with CH_2Cl_2. The combined organic phase was washed with a saturated solution of $NaHCO_3$, dried over $MgSO_4$, filtered and concentrated. Depending on the phosphine, filtration over silica gel

[201] Dunne, K. S.; Lee, S. E.; Gouverneur, V. *J. Organomet. Chem.* **2006**, *691*, 5246.

yielded the borane adducts in nearly quantitative yields after evaporation and high vacuum removal of the solvents.

Triphenylphosphine borane complex 29a.

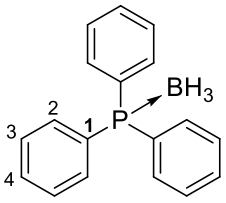

Chemical Formula: $C_{18}H_{18}BP$
Molecular Weight: 276.12

29a, off-white solid (2.05 g, 7.44 mmol, 93%), PPh_3 (2.10 g, 8.0 mmol, 1 eq), $BH_3.SMe_2$ (1.00 mL, 10.0 mmol, 1.3 eq), following (GP1). Spectroscopic data are in agreement with the literature.[202] **^{1}H-NMR** (400.1 MHz, $CDCl_3$): δ 7.60-7.56 (m, 6H, H-2), 7.53-7.49 (m, 3H, H-4), 7.46-7.42 (m, 6H, H-3), 1.28 (q, *J* = 81.4 Hz, 3H, BH_3). **^{13}C-NMR** (100.6 MHz, $CDCl_3$): δ 133.4 (d, *J* = 9.7 Hz, C-2), 131.5 (d, *J* = 2.4 Hz, C-4), 129.4 (d, *J* = 58.0 Hz, C-1), 129.0 (d, *J* = 10.2 Hz, C-3). **^{31}P-NMR** (162.0 MHz, $CDCl_3$): δ 20.6 (d, *J* = 56.2 Hz, P). **^{11}B-NMR** (128.4 MHz, $CDCl_3$): δ – 37.9 (m, BH_3). **Mp** = 183-184°C.

Tri(*n*-butyl)phosphine borane complex 29d.

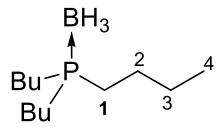

Chemical Formula: $C_{12}H_{30}BP$
Molecular Weight: 216.15

29d, colourless oil (1.68 g, 7.76 mmol, 97%), PBu_3 (2.00 mL, 8.0 mmol, 1 eq), $BH_3.SMe_2$ (1.00 mL, 10.0 mmol, 1.3 eq), following (GP1).
Eluent: CH_2Cl_2/pentane (3:7), **Rf** = 0.65. **^{1}H-NMR** (400.1 MHz, $CDCl_3$): δ 1.55-1.50 (m, 6H, H-1), 1.45-1.35 (m, 12H, H-2,3), 0.89 (t, *J* = 7.0 Hz, 9H, H-4), 0.34 (q, *J* = 88.7 Hz, 3H, BH_3). **^{13}C-NMR** (100.6 MHz, $CDCl_3$): δ 24.8 (d, *J* = 2.1 Hz, C-3), 24.5 (d, *J* = 12.6 Hz, C-2), 23.0 (d, *J* = 34.5 Hz, C-1), 13.7 (s, C-4). **^{31}P{^{1}H}-NMR** (162.0 MHz, $CDCl_3$): δ 14.4 (d, *J* = 62.7 Hz, P). **^{11}B{^{1}H}-NMR** (128.4 MHz, $CDCl_3$): δ -41.0 (d, *J* = 62.7 Hz, BH_3). **HRMS** (ESI positive) = [$C_{12}H_{30}BNaP^+$] Calculated mass: 239.2076 g/mol, found mass: 239.2082 g/mol.

Dicyclohexylphosphine borane complex 29e.

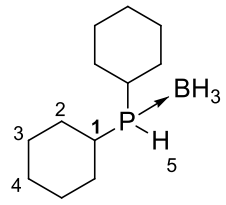

Chemical Formula: $C_{12}H_{26}BP$
Molecular Weight: 212.12

29e, transparent needles (2.76 g, 13.0 mmol, 87%), Cy_2PH (3.00 mL, 15.0 mmol, 1 eq), $BH_3.SMe_2$ (1.60 mL, 16.5 mmol, 1.1 eq), following (GP1). Spectroscopic data are in agreement with the literature.[203] Recrystallization from ethanol/dichloromethane. Eluent: CH_2Cl_2/pentane (5:5), **Rf** = 0.70. **^{1}H-NMR** (400.1 MHz, $CDCl_3$): δ 4.12 (d, *J* = 351.2 Hz, 1H, H-5), 1.87-1.72 (m, 12H, H-3,4), 1.40-1.22 (m, 10H, H-1,2), 0.40 (q, *J* = 92.2 Hz, 3H, BH_3).

[202] CAS : 2049-55-0.
[203] CAS : 108756-88-3

^{13}C-NMR (100.6 MHz, $CDCl_3$): δ 29.5 (d, *J* = 3.1 Hz, C-2), 29.1 (d, *J* = 33.5 Hz, C-3), 26.7 (dd, *J* = 19.8 Hz, 11.2 Hz, C-1), 26.0 (d, *J* = 1.2 Hz, C-4). **^{31}P{^{1}H}-NMR** (162.0 MHz, $CDCl_3$): δ 17.3 (m, P). **^{11}B{^{1}H}-NMR** (128.4 MHz, $CDCl_3$): δ -44.5 (d, *J* = 51.2 Hz, BH_3) **Mp** = 78-79°C.

Diphenylphosphine borane complex 29f

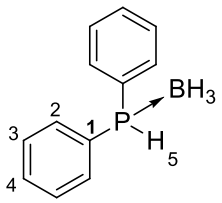

Chemical Formula: $C_{12}H_{14}BP$
Molecular Weight: 200.02

29f, transparent crystals (2.76 g, 21.9 mmol, 95%), Ph_2PH (4.00 mL, 23.0 mmol, 1 eq), $BH_3.SMe_2$ (8.7 mL, 92.0 mmol, 4.0 eq), following (GP1). Spectroscopic data are in agreement with the literature.[204]

^{1}H-NMR (400.1 MHz, $CDCl_3$): δ 7.70-7.65 (m, 4H, H-2), 7.52-7.44 (m, 6H, H-3,4), 6.31 (dq, *J* = 378.8, 6.9 Hz, 1H, H-5), 1.08 (q, *J* = 89.9 Hz, 3H, BH_3). **^{13}C-NMR** (100.6 MHz, $CDCl_3$): δ 133.1 (d, *J* = 9.4 Hz, C-2), 131.8 (d, *J* = 2.4 Hz, C-4), 129.2 (d, *J* = 10.3 Hz, C-3), 126.3 (d, *J* = 57.3 Hz, C-1). **^{31}P{^{1}H}-NMR** (162.0 MHz, $CDCl_3$): δ 1.3 (m, P). **^{11}B-NMR** (128.4 MHz, $CDCl_3$): δ -40.2 (d, *J* = 45.1 Hz, BH_3). **Mp** = 49-50°C.

Phenylphosphine borane complex 29g

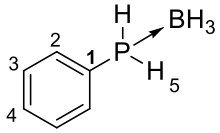

Chemical Formula: $C_6H_{10}BP$
Molecular Weight: 123.93

29g, transparent crystals (0.99 g, 8.0 mmol, 89%), $PhPH_2$ (10 mL of a solution at 10% in hexane, 9.0 mmol, 1 eq), $BH_3.SMe_2$ (3.4 mL, 36 mmol, 4 eq), following (GP1).

^{1}H-NMR (400.1 MHz, $CDCl_3$): δ 7.73-7.69 (m, 2H, H-2), 7.57-7.54 (m, 1H, H-4), 7.50-7.46 (m, 2H, H-3), 5.53 (dq, *J* = 371.6, 7.8 Hz, 2H, H-5), 0.88 (q, *J* = 96.1 Hz, 3H, BH_3). **^{13}C-NMR** (100.6 MHz, $CDCl_3$): δ 134.0 (d, *J* = 9.1 Hz, C-2), 132.3 (s, C-4), 129.5 (d, *J* = 10.7 Hz, C-3), C-1 is not observed. **^{31}P{^{1}H}-NMR** (162.0 MHz, $CDCl_3$): δ -47.4 (t, *J* = 371.6 Hz, P). **^{11}B{^{1}H}-NMR** (128.4 MHz, $CDCl_3$): δ -42.3 (qd, *J* = 101.3, 36.6 Hz, BH_3).

(Biphenyl)diphenylphosphine borane complexe 29h

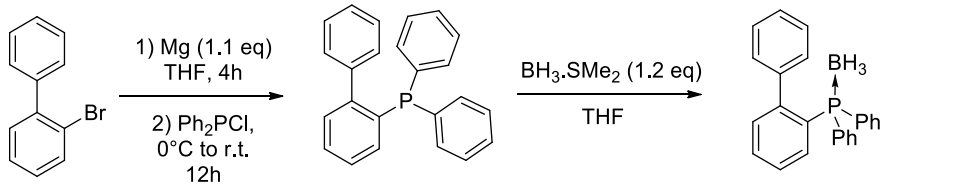

75%

Chemical Formula: $C_{24}H_{22}BP$
Molecular Weight: 352.22

93%

[204] CAS : 41593-58-2

The synthesis was done in two steps following a procedure described by Xu.[205] The last step was done following (GP1) in toluene. (Biphenyl)diphenylphosphine (1.0 g, 3.0 mmol, 1 eq), $BH_3.SMe_2$ (300 µL, 3.11 mmol, 1.05 eq), **29h** (968 mg, 2.75 mmol, 93%).

^{1}H-NMR (400.1 MHz, $CDCl_3$): δ 7.52-7.48 (m, 6H, H-Ar), 7.44-7.41 (m, 3H, H-Ar), 7.36-7.34 (m, 5H, H-Ar), 7.16-7.13 (m, 1H, H-Ar), 7.04-7.00 (m, 2H, H-Ar), 6.88-6.87 (m, 2H, H-Ar), 0.96 (q, *J* = 70.4 Hz, 3H, BH_3). **^{13}C-NMR** (100.6 MHz, $CDCl_3$): δ 148.3 (d, *J* = 9.5 Hz, C-Ar), 140.7 (d, *J* = 3.5 Hz, C-Ar), 135.2 (d, *J* = 9.4 Hz, C-Ar), 133.4 (d, *J* = 9.4 Hz, C-Ar), 132.5 (d, *J* = 8.0 Hz, C-Ar), 131.1 (d, *J* = 2.3 Hz, C-Ar), 131.0 (d, *J* = 2.3 Hz, C-Ar), 130.8 (s, C-Ar), 130.2 (s, C-Ar), 130.0 (s, C-Ar), 128.7 (d, *J* = 10.2 Hz, C-Ar), 128.4 (s, C-Ar), 127.8 (s, C-Ar), 127.6 (s, C-Ar), 127.6 (s, C-Ar), 127.3 (d, *J* = 9.6 Hz, C-Ar), quaternary carbons are not observed. **^{31}P{^{1}H}-NMR** (162.0 MHz, $CDCl_3$): δ 21.5 (br, P). **^{11}B{^{1}H}-NMR** (128.4 MHz, $CDCl_3$): δ -35.9 (br, BH_3). **Mp** = 193-194°C (decomposition). **HRMS** (ESI positive) = [$C_{24}H_{22}BNaP^+$] Calculated mass: 375.1450 g/mol, found mass: 375.1442 g/mol.

Phenyl diphenylphosphinite borane 29i

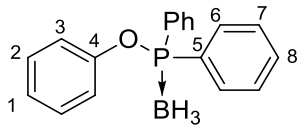

Chemical Formula: $C_{18}H_{18}BOP$
Molecular Weight: 292.12

The synthesis was done according to a procedure reported by Vedejs et al.[206] To a stirred solution of phenol (214 mg, 2.27 mmol, 1.2 eq) in degassed toluene (4 mL) was added chlorodiphenylphosphine (350 µL, 1.89 mmol, 1 eq) and triethylamine (390 µL, 2.8 mmol, 1.5 eq) under argon. The mixture was warmed at reflux for 12h under stirring in a sealed schlenck. After cooling to room temperature, the mixture was filtered, washed with toluene (3 x 10 mL) and concentrated to a half of the original volume in vacuo. To the resulting solution were added $BH_3.Me_2S$ (320 µL, 3.4 mmol, 1.8 eq) dropwise at 0°C. After stirring 2h, the solution was filtered through a plug of silica gel, flushing with dichloromethane (15 mL). The filtrate was concentrated under reduced pressure. The crude was purified by flash chromatrography on silica gel affording **29i** as an off-white solid (431 mg, 1.48 mmol, 78 %).

Eluent: Cyclohexane/diethylether (8:2), **Rf** = 0.50. **^{1}H-NMR** (400.1 MHz, $CDCl_3$): δ 7.87-7.83 (m, 4H, H-Ar), 7.58-7.48 (m, 6H, H-Ar), 7.24-7.22 (m, 2H, H-Ar), 7.13-7.09 (m, 1H, H-Ar), 7.02-7.00 (m, 2H, H-Ar), 1.04 (q, *J* = 89.7 Hz, 3H, BH_3). **^{13}C-NMR** (100.6 MHz, $CDCl_3$): δ 152.4 (d, *J* = 4.8 Hz, C-Ar), 132.3 (d, *J* = 2.3 Hz, C-Ar), 131.8 (s, C-Ar), 131.7 (d, *J* = 60.5 Hz, C-Ar), 129.6 (s, C-Ar), 128.9 (d, *J* = 10.6 Hz, C-Ar), 124.9 (s, C-Ar), 121.4 (d, *J* = 4.2 Hz, C-Ar). **^{31}P{^{1}H}-NMR** (162.0 MHz, $CDCl_3$): δ 109.3 (m, P). **^{11}B{^{1}H}-NMR** (128.4 MHz, $CDCl_3$): δ -39.4

[205] Wang, W.; Hammond, G. B.; Xu, B. J. Am. Chem. Soc., 2012, 134, 5697.
[206] C. Cazorla, T. S. De Vries, E. Vedejs, *Org. Lett.* **2013**, *15*, 984–987.

(d, J = 60.2 Hz, BH_3). **Mp** = 99-100 °C. **IR** (neat, ATR probe, cm^{-1}): v 2401, 1589, 1488, 1437, 1193, 1169, 1061 (C-P), 998, 910, 893. **HRMS** (ESI positive) = [$C_{18}H_{18}BONaP^+$] Calculated mass: 315.1086 g/mol, found mass: 315.1090 g/mol.

Boron, trihydro(5-phenyl-5*H*-benzo[*b*]phosphindole) 29j

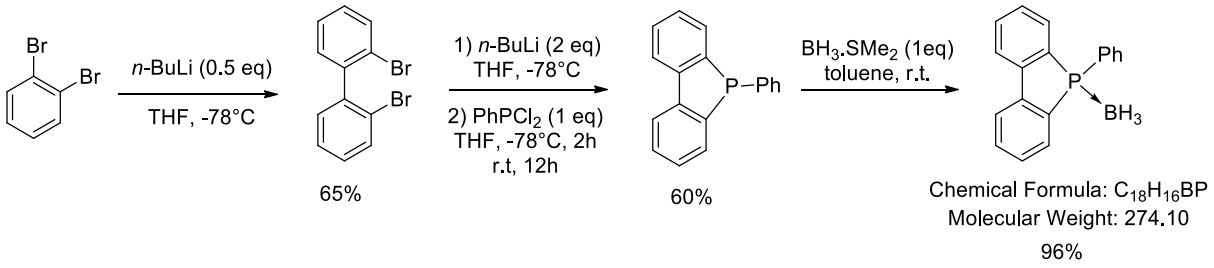

The synthesis was done in three steps following a procedure described by Van Delft. [207] The last step was done following (GP1) in toluene. 5-phenyl-5*H*-benzo[*b*]phosphindole (180 mg, 0.69 mmol, 1 eq), $BH_3.SMe_2$ (70 µL, 0.73 mmol, 1.1 eq), **29j** (182 mg, 0.66 mmol, 96%). **^{1}H-NMR** (400.1 MHz, $CDCl_3$): δ 7.95-7.93 (m, 1H, H-Ar), 7.73-7.69 (m, 1H, H-Ar), 7.63-7.64 (m, 2H, H-Ar), 7.45-7.40 (m, 2H, H-Ar), 7.3-7.33 (m, 1H, H-Ar), 1.14 (q, J = 66.3 Hz, 3H, BH_3). **^{13}C-NMR** (100.6 MHz, $CDCl_3$): δ 132.5 (s, C-Ar), 132.3 (d, J = 10.9 Hz, C-Ar), 132.0 (s, C-Ar), 131.7 (s, C-Ar), 130.5 (d, J = 10.8 Hz, C-Ar), 129.1 (d, J = 10.4 Hz, C-Ar), 128.9 (d, J = 10.4 Hz, C-Ar), 121.7 (d, J = 6.4 Hz, C-Ar), quaternary carbons are not observed. **^{31}P{^{1}H}-NMR** (162.0 MHz, $CDCl_3$): δ 24.8 (br, P). **^{11}B{^{1}H}-NMR** (128.4 MHz, $CDCl_3$): δ -39.1 (br, BH_3). **Mp** = 149-150°C (decomposition). **HRMS** (ESI positive) = [$C_{18}H_{16}BNaP^+$] Calculated mass: 297.0980 g/mol, found mass: 297.0984 g/mol.

1.3 Reactions of **29a** with **28b**, **28d** and **28e**.

General procedure (GP2)

In a 5 mL round bottomed flask equipped with a stirrer were placed $Ar_2.BF_4$ (11 µmol, 1 eq), **29a** (3.0 mg, 11 µmol, 1 eq) and 0.6 mL of CD_3CN. The solution was stirred for 48h at r.t. and the crude mixture was analysed by NMR spectroscopy.

[207] Van Kalkeren, H. A.; Leenders, S. H. A. M.; Hommersom, C. R. A.; Rutjes, F. P. J. T.; Van Delft, F. L. *Chem. - A Eur. J.* **2011**, *17*, 11290.

Reaction of **28a** and **29a**

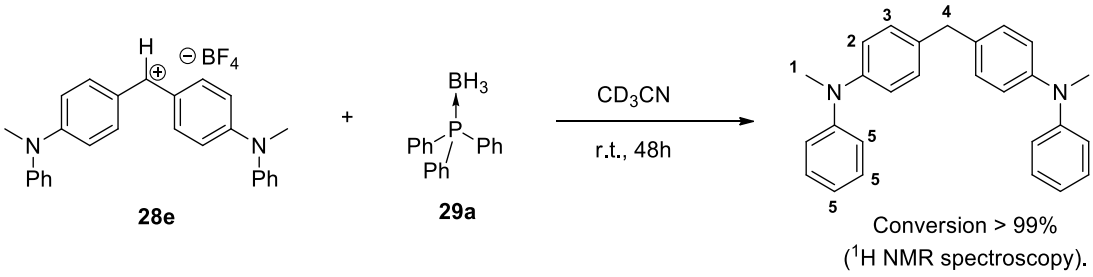

Conversion > 99%
(^{1}H NMR spectroscopy).

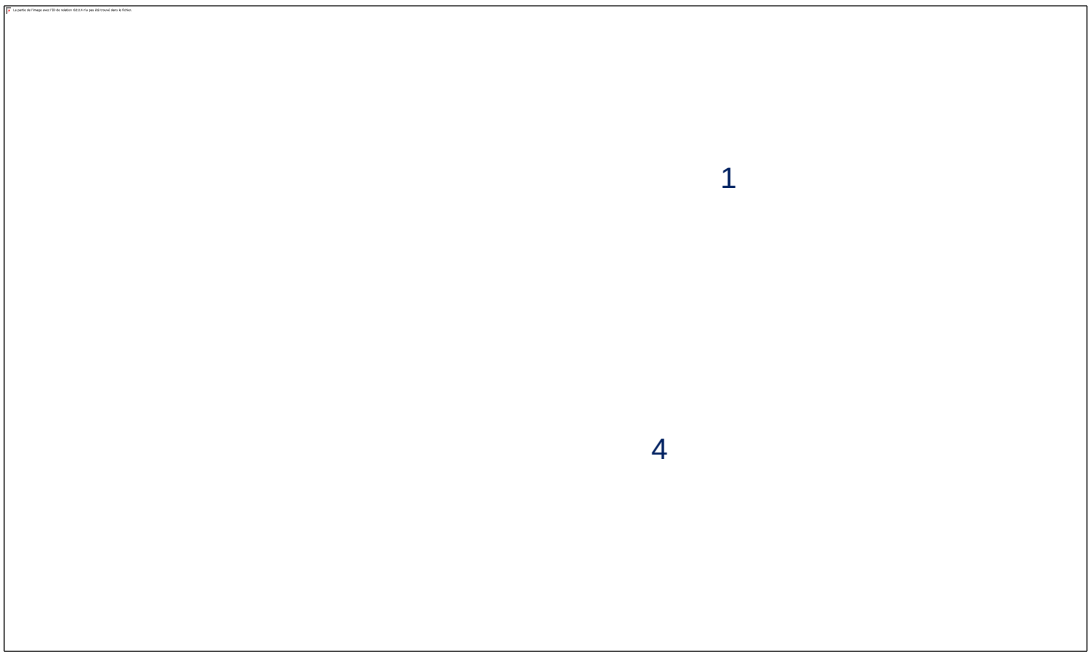

Reactions of **28d** and **29a**

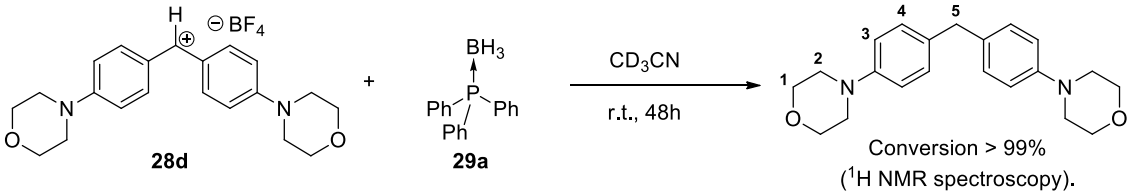

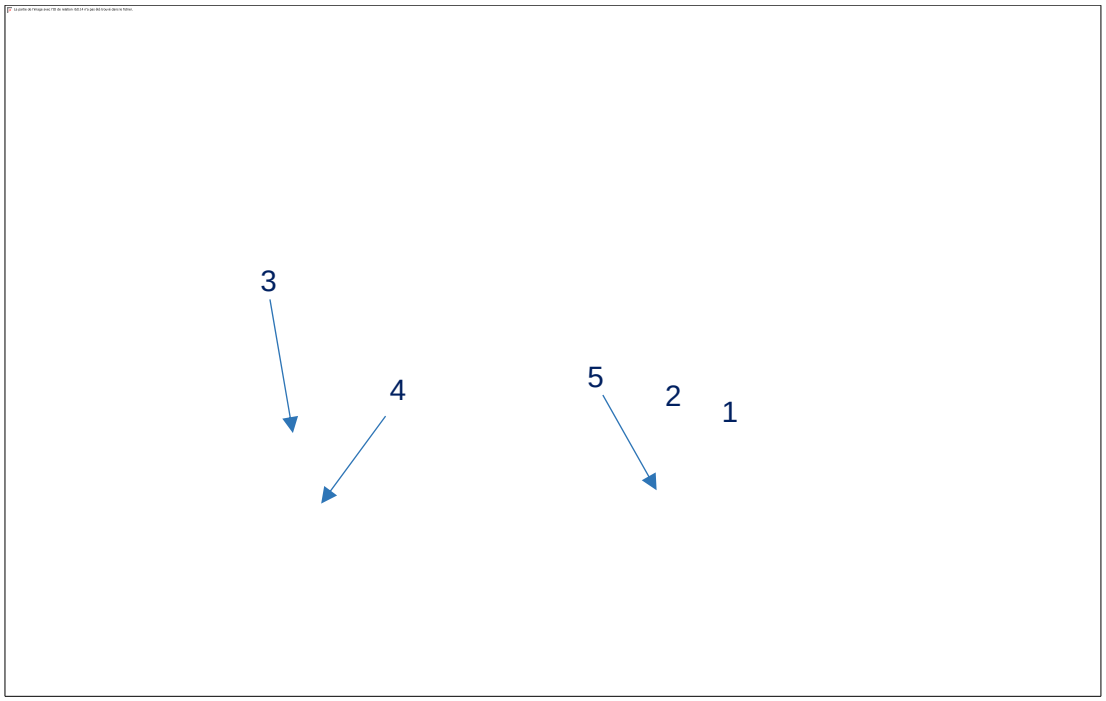

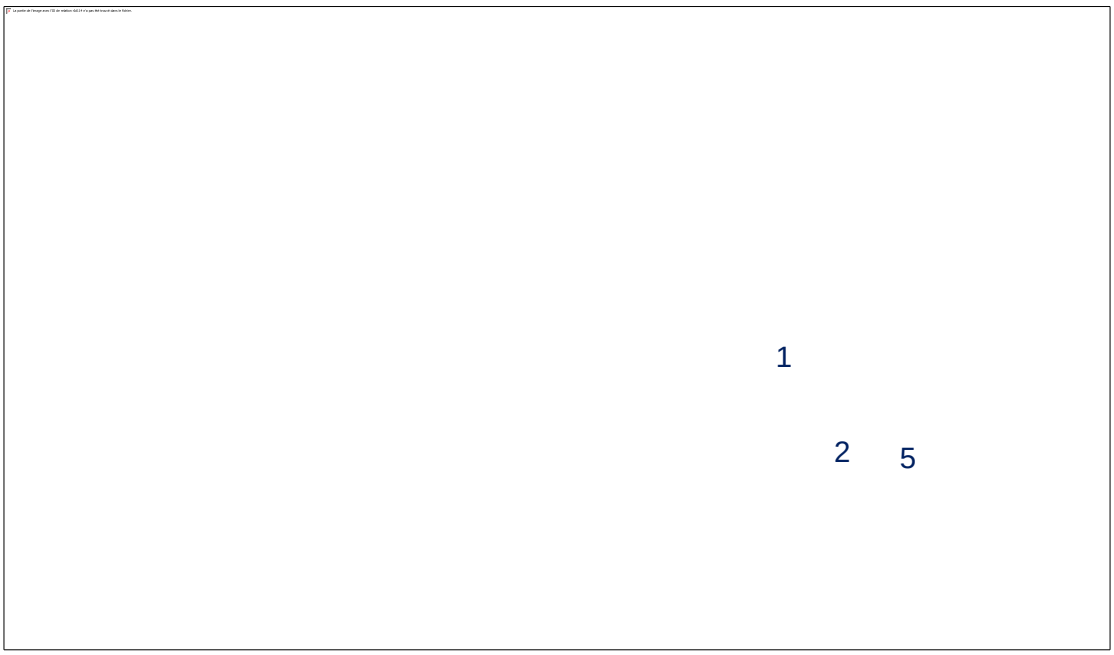

Reaction of **28b** and **29a**

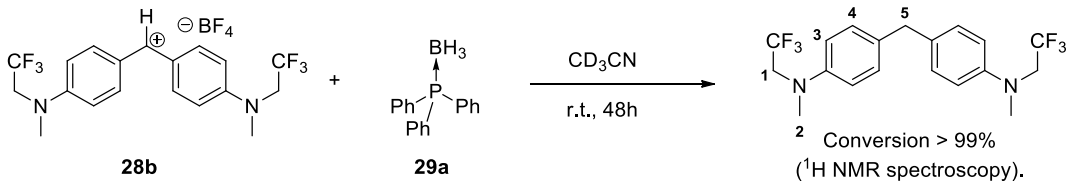

28b **29a**

Conversion > 99%
(^{1}H NMR spectroscopy).

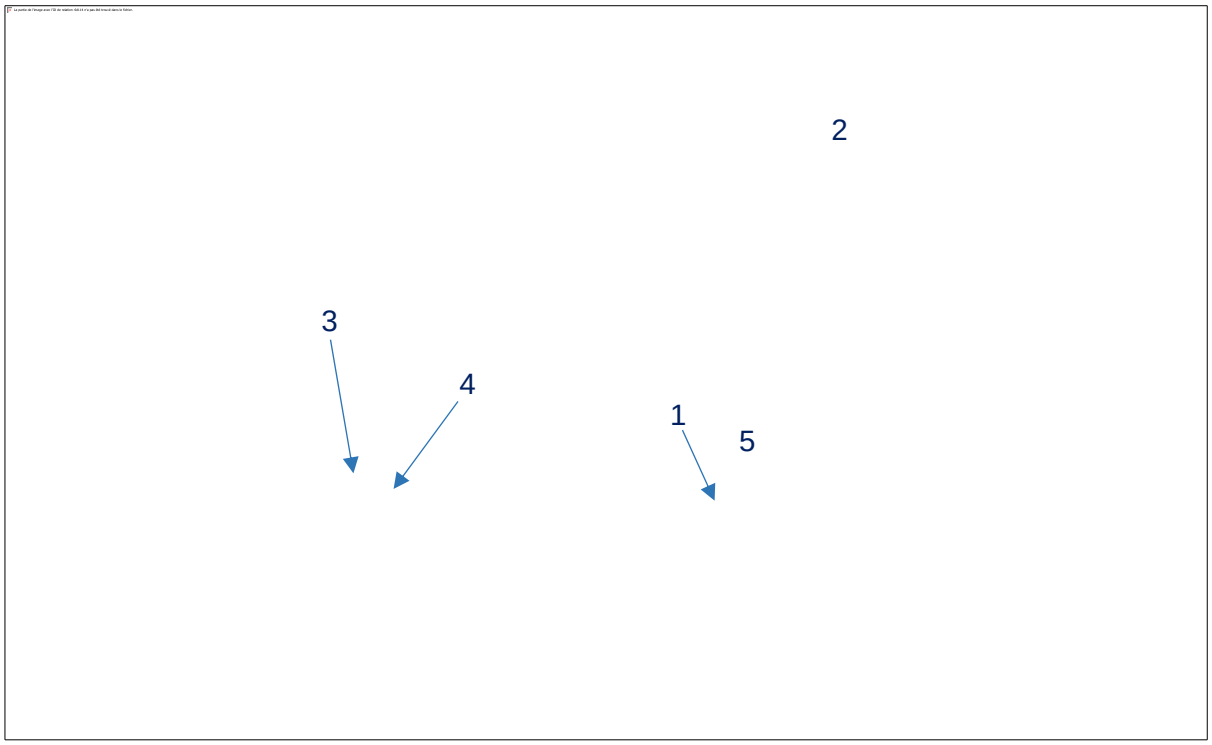

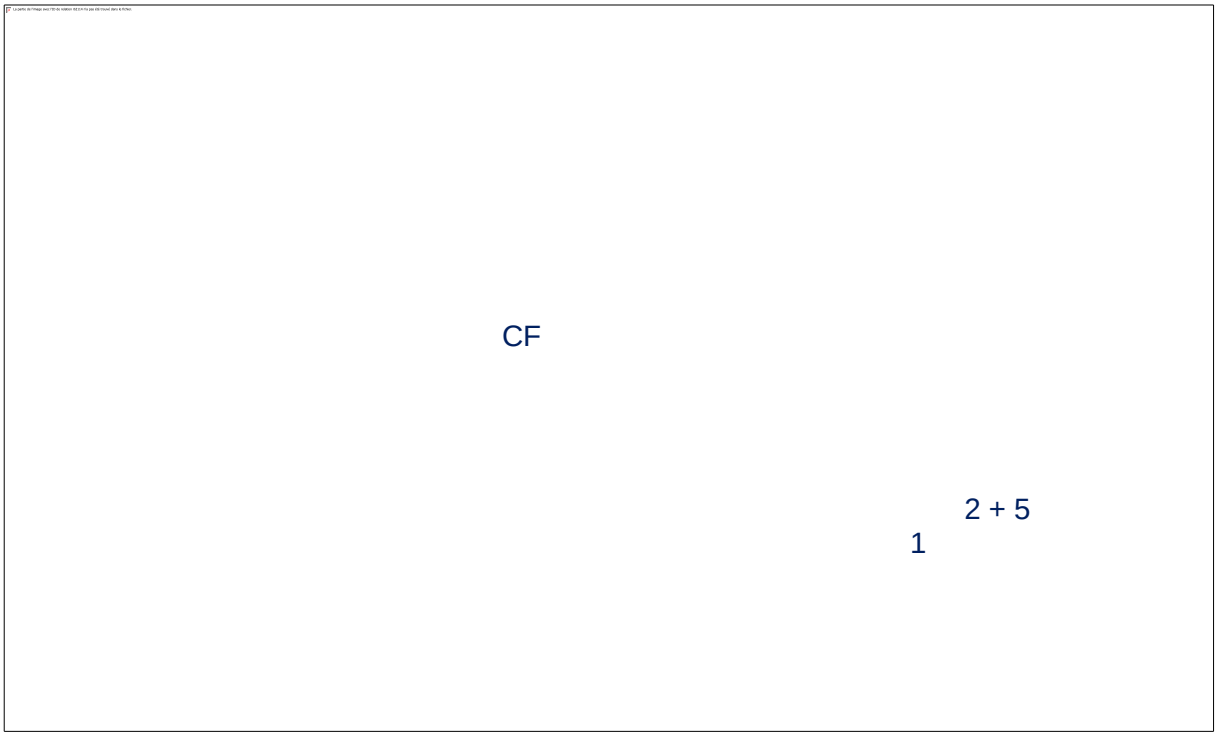

1.4 Reduction of **32** with **31a,c**

General procedure (GP3)

In a 5 mL round bottomed flask equipped with a stirrer were placed **32** (130 µL, 1.0 mmol, 1 eq), **31a** (152 µL, 1.05 mmol, 1.05 eq) or **31b** (120 µL, 1.05 mmol, 1.05 eq) or **31c** (100 µL, 1.05 mmol, 1.05 eq) and 2.5 mL of CH_2Cl_2. If required, $EtPPh_2$ (18 µL, 0.10 mmol, 0.1 eq) or (180 µL, 1.0 mmol, 1.0 eq) was added. The solution was stirred for 24h at r.t. before cooling the mixture to 0°C in a ice-bath. Then the solution was quenched with 1.0 mL of a solution of HCl (1.0 mol/L), and the aqueous phase was extracted with 3 × 10 mL of CH_2Cl_2 and dried over $MgSO_4$.

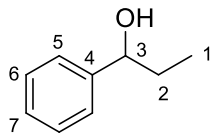

Chemical Formula: $C_9H_{12}O$
Molecular Weight: 136.19

^{1}H-NMR (400.1 MHz, $CDCl_3$): δ 7.39-7.36 (m, 3H, H-Ar), 7.34-7.32 (m, 2H, H-Ar), 4.41 (t, *J* = 7.2 Hz, 1H, H-3), 3.65 (s, 1H, OH), 1.81 (dq, *J* = 7.2 Hz, *J* = 6.9 Hz, 2H, H-2), 0.90 (t, *J* = 6.9 Hz, 3H, H-1). **^{13}C-NMR** (100.6 MHz, $CDCl_3$): δ 144.4 (d, *J* = 4.4 Hz, C-4), 128.8 (m, C-6), 127.2 (m, C-5), 127.0 (m, C-7), 76.5 (s, C-3), 31.7 (m, C-2), 10.0 (m, C-1). **CAS**: 93-54-9

2. Crystallographic data

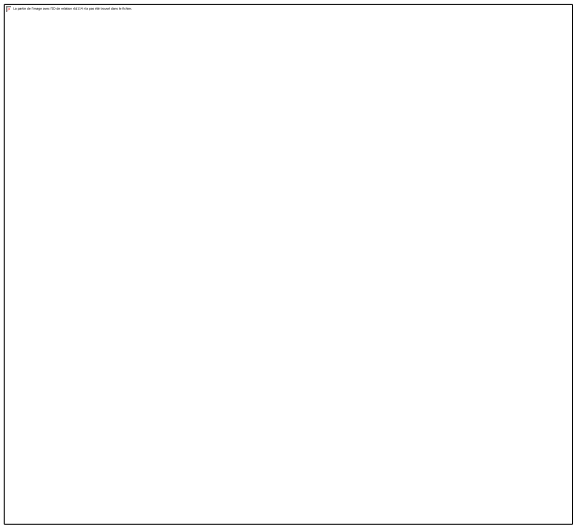

Single crystals of **29h** suitable for X-ray crystallographic analysis were obtained from a mixture of 58h, dichloromethane and ethanol at -20°C. X-ray diffraction experiments for monocrystal of **58h** were performed at 294 K with graphite–monochromatized Mo K□ radiation (λ = 0.71073 Å) on a Bruker–Nonius Kappa CCD area detector diffractometer. Formula $C_{24}H_{22}BP$, formula weight 352.22, space group *P 2₁*/n, *a* = 10.9701(5) Å, *b* = 12.7385(6) Å, *c* = 14.1571(7) Å, α = γ = 90°, β = 94.173(3) V = 1973.11 Å^3. Program(s) used to solve structure: SHELXS–97. Program(s) used to refine structure: SHELXL–2014. Software used to prepare material for publication: SHELXL–2014.

3. Kinetics

3.1 Determination of the second order rate constants

Table S1. Kinetics of the reaction of **29a** with **28d** (CH_2Cl_2, 20°C, stopped-flow, detection at 611 nm)

[28d]	**[29a]**	**[29a]/[28d]**	k_{obs}
4.01×10^{-5}	1.74×10^{-2}	433	2.57×10^{-2}
4.01×10^{-5}	2.17×10^{-2}	542	3.45×10^{-2}
4.01×10^{-5}	3.08×10^{-2}	768	5.13×10^{-2}
4.01×10^{-5}	3.55×10^{-2}	885	6.29×10^{-2}
k_2(20°C) = 2.01 L mol^{-1} s^{-1}			

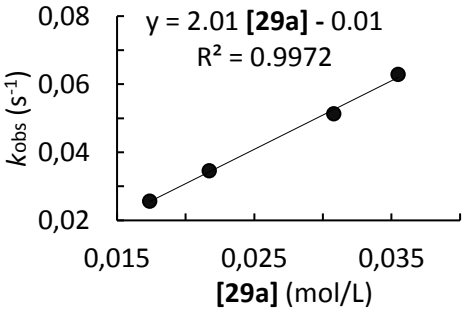

Table S2. Kinetics of the reaction of **29a** with **28c** (CH_2Cl_2, 20°C, stopped-flow, detection at 671 nm)

[28c]	**[29a]**	**[29a]/[28c]**	k_{obs}
3.74×10^{-5}	1.74×10^{-2}	465	2.93×10^{-1}
3.74×10^{-5}	2.17×10^{-2}	581	3.72×10^{-1}
3.74×10^{-5}	3.08×10^{-2}	823	5.05×10^{-1}
3.74×10^{-5}	3.55×10^{-2}	949	5.61×10^{-1}
k_2(20°C) = 1.48×10^{1} L mol^{-1} s^{-1}			

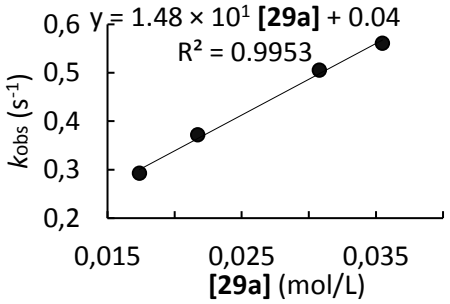

Table S3. Kinetics of the reaction of **29a** with **28b** (CH_2Cl_2, 20°C, stopped-flow, detection at 586 nm)

[28b]	**[29a]**	**[29a]/[28b]**	k_{obs}
3.36×10^{-5}	1.74×10^{-2}	517	8.19×10^{-1}
3.36×10^{-5}	2.17×10^{-2}	646	1.21
3.36×10^{-5}	3.08×10^{-2}	915	1.84
3.36×10^{-5}	3.55×10^{-2}	1055	2.11
k_2(20°C) = 7.08×10^{1} L mol^{-1} s^{-1}			

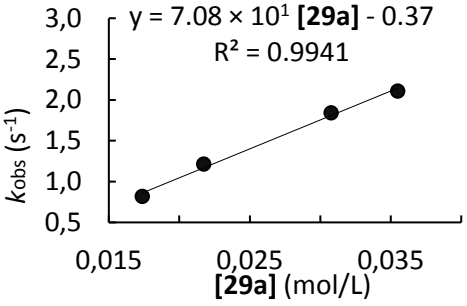

Table S10. Kinetics of the reaction of **29b** with **28e** (CH_2Cl_2, 20°C, stopped-flow, detection at 615 nm)

[28e]	**[29b]**	**[29b]/[28e]**	k_{obs}
1.10×10^{-4}	4.48×10^{-2}	408	2.60×10^{-1}
1.10×10^{-4}	5.26×10^{-2}	479	3.63×10^{-1}
1.10×10^{-4}	5.78×10^{-2}	526	4.49×10^{-1}
1.10×10^{-4}	6.46×10^{-2}	588	5.51×10^{-1}
k_2(20°C) = 1.48×10^{1} L mol^{-1} s^{-1}			

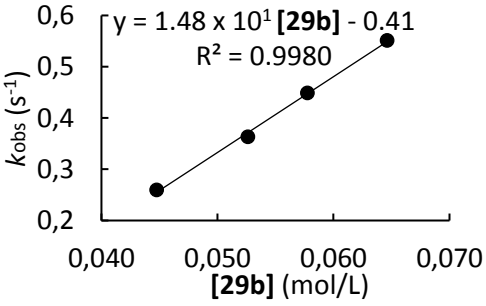

Table S4. Kinetics of the reaction of **29b** with **28d** (CH_2Cl_2, 20°C, stopped-flow, detection at 611 nm).

[28d]	**[29b]**	**[29b]/[28d]**	k_{obs}
7.55×10^{-5}	4.48×10^{-2}	593	9.26×10^{-1}
7.55×10^{-5}	5.26×10^{-2}	697	1.21
7.55×10^{-5}	5.78×10^{-2}	765	1.36
7.55×10^{-5}	6.46×10^{-2}	856	1.62
k_2(20°C) = 3.45×10^{1} L mol^{-1} s^{-1}			

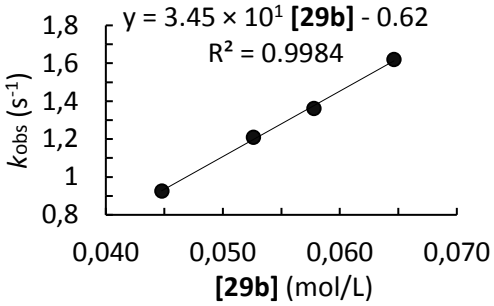

Table S5. Kinetics of the reaction of **29b** with **28c** (CH_2Cl_2, 20°C, stopped-flow, detection at 671 nm).

[28c]	**[29b]**	**[29b]/[28c]**	k_{obs}
7.14×10^{-5}	4.48×10^{-2}	627	3.18
7.14×10^{-5}	5.26×10^{-2}	737	5.12
7.14×10^{-5}	5.78×10^{-2}	809	6.08
7.14×10^{-5}	6.46×10^{-2}	905	6.99
k_2(20°C) = 1.92 x 10^{2} L mol^{-1} s^{-1}			

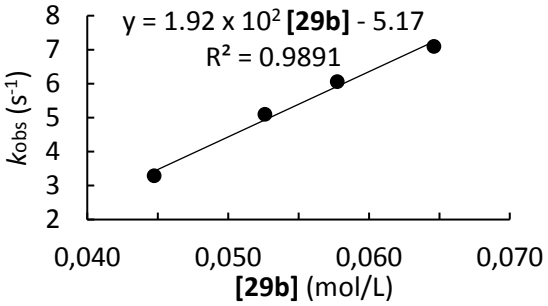

Table S6. Kinetics of the reaction of **29b** with **28b** (CH_2Cl_2, 20°C, stopped-flow, detection at 586 nm)

[28b]	**[29b]**	**[29b]/[28b]**	k_{obs}
8.83×10^{-5}	4.48×10^{-2}	507	1.19×10^{1}
8.83×10^{-5}	5.26×10^{-2}	596	1.80×10^{1}
8.83×10^{-5}	5.78×10^{-2}	654	2.19×10^{1}
8.83×10^{-5}	6.46×10^{-2}	732	2.64×10^{1}
k_2(20°C) = 7.32×10^{2} L mol^{-1} s^{-1}			

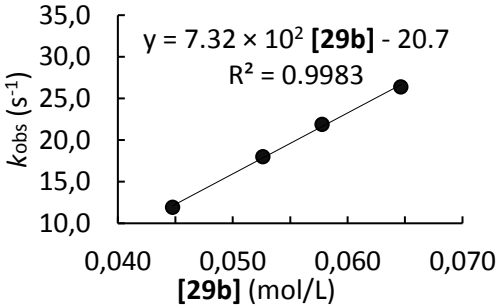

Table S7. Kinetics of the reaction of **29c** with **28d** (CH_2Cl_2, 20°C, stopped-flow, detection at 611 nm)

[28d]	**[29c]**	**[29c]/[28d]**	k_{obs}
7.55×10^{-5}	4.58×10^{-2}	607	2.10×10^{-1}
7.55×10^{-5}	5.50×10^{-2}	728	2.58×10^{-1}
7.55×10^{-5}	6.89×10^{-2}	912	3.18×10^{-1}
7.55×10^{-5}	8.08×10^{-2}	1071	3.78×10^{-1}
7.55×10^{-5}	8.72×10^{-2}	1155	4.08×10^{-1}
k_2(20°C) = 4.74 L mol^{-1} s^{-1}			

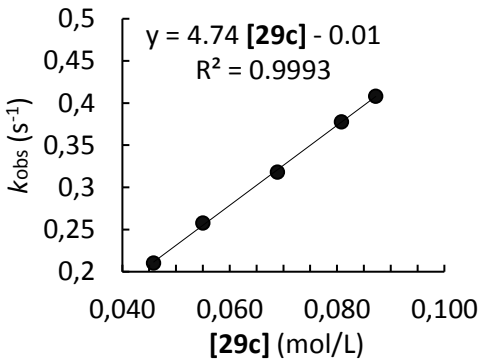

Table S8. Kinetics of the reaction of **29c** with **28c** (CH_2Cl_2, 20°C, stopped-flow, detection at 671 nm)

[28c]	[29c]	[29c]/[28c]	k_{obs}
7.14×10^{-5}	4.58×10^{-2}	642	1.26
7.14×10^{-5}	5.50×10^{-2}	770	1.41
7.14×10^{-5}	6.89×10^{-2}	965	1.82
7.14×10^{-5}	8.08×10^{-2}	1132	2.24
7.14×10^{-5}	8.72×10^{-2}	1222	2.40
k_2(20°C) = 2.89×10^{1} L mol^{-1} s^{-1}			

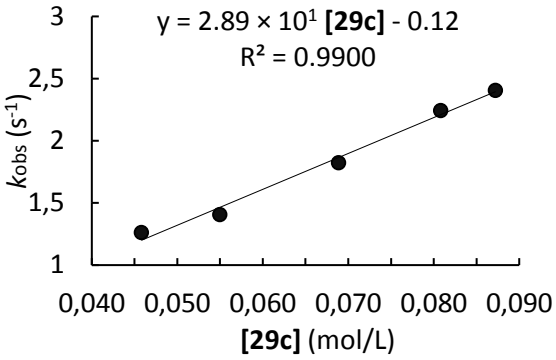

Table S9. Kinetics of the reaction of **29c** with **28b** (CH_2Cl_2, 20°C, stopped-flow, detection at 586 nm)

[28b]	[29c]	[29c]/[28b]	k_{obs}
6.31×10^{-5}	4.58×10^{-2}	727	4.73
6.31×10^{-5}	5.50×10^{-2}	872	6.01
6.31×10^{-5}	6.89×10^{-2}	1092	8.14
6.31×10^{-5}	8.08×10^{-2}	1282	9.86
6.31×10^{-5}	8.72×10^{-2}	1383	1.15×10^{1}
k_2(20°C) = 1.59×10^{2} L mol^{-1} s^{-1}			

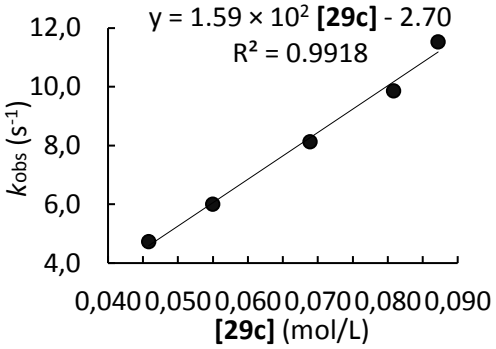

Table S10. Kinetics of the reaction of **29d** with **28e** (CH_2Cl_2, 20°C, stopped-flow, detection at 615 nm)

[28e]	[29d]	[29d]/[28e]	k_{obs}
9.91×10^{-5}	2.07×10^{-2}	209	1.50×10^{-1}
9.91×10^{-5}	2.24×10^{-2}	226	1.63×10^{-1}
9.91×10^{-5}	2.83×10^{-2}	287	2.30×10^{-1}
9.91×10^{-5}	3.11×10^{-2}	314	2.66×10^{-1}
9.91×10^{-5}	3.94×10^{-2}	398	3.71×10^{-1²}
k_2(20°C) = 1.19×10^{1} L mol^{-1} s^{-1}			

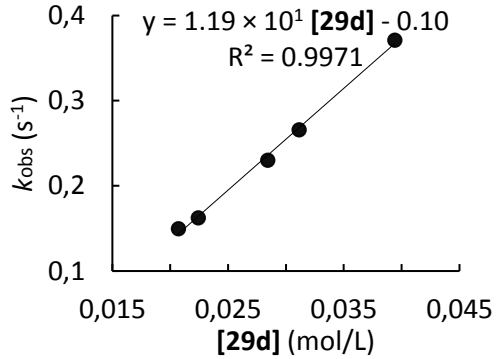

Table S11. Kinetics of the reaction of **29d** with **28d** (CH_2Cl_2, 20°C, stopped-flow, detection at 611 nm)

[28d]	[29d]	[29d]/[28d]	k_{obs}
7.55×10^{-5}	2.07×10^{-2}	274	5.77×10^{-1}
7.55×10^{-5}	2.24×10^{-2}	297	5.95×10^{-1}
7.55×10^{-5}	2.84×10^{-2}	377	7.94×10^{-1}
7.55×10^{-5}	3.11×10^{-2}	413	8.76×10^{-1}
7.55×10^{-5}	3.94×10^{-2}	522	1.11
k_2(20°C) = 2.94×10^{1} L mol^{-1} s^{-1}			

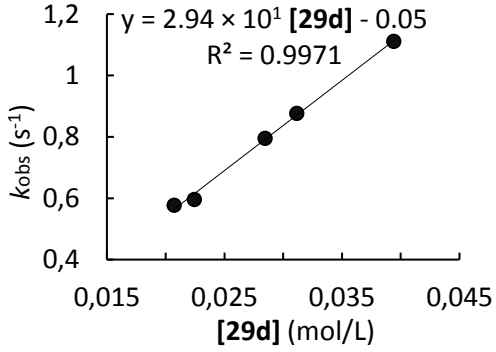

Table S12. Kinetics of the reaction of **29d** with **28c** (CH_2Cl_2, 20°C, stopped-flow, detection at 671 nm)

[28c]	[29d]	[29d]/[28c]	k_{obs}
7.14×10^{-5}	2.07×10^{-2}	290	3.19
7.14×10^{-5}	2.24×10^{-2}	314	3.44
7.14×10^{-5}	2.83×10^{-2}	398	4.29
7.14×10^{-5}	3.11×10^{-2}	436	4.77
7.14×10^{-5}	3.94×10^{-2}	552	5.81
k_2(20°C) = 1.42×10^2 L mol^{-1} s^{-1}			

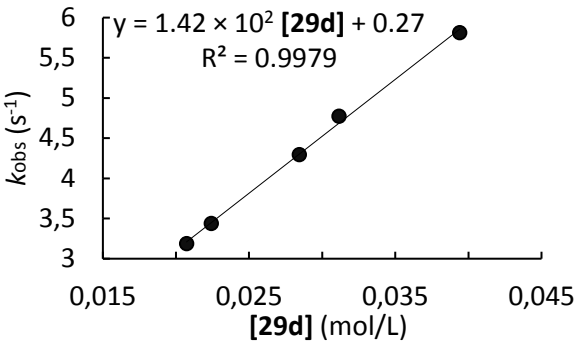

Table S13. Kinetics of the reaction of **29d** with **28b** (CH_2Cl_2, 20°C, stopped-flow, detection at 586 nm)

[28b]	[29d]	[29d]/[28b]	k_{obs}
6.31×10^{-5}	2.07×10^{-2}	329	1.63×10^1
6.31×10^{-5}	2.24×10^{-2}	356	1.73×10^1
6.31×10^{-5}	2.83×10^{-2}	451	2.22×10^1
6.31×10^{-5}	3.11×10^{-2}	494	2.43×10^1
6.31×10^{-5}	3.94×10^{-2}	625	2.98×10^1
k_2(20°C) = 7.38×10^2 L mol^{-1} s^{-1}			

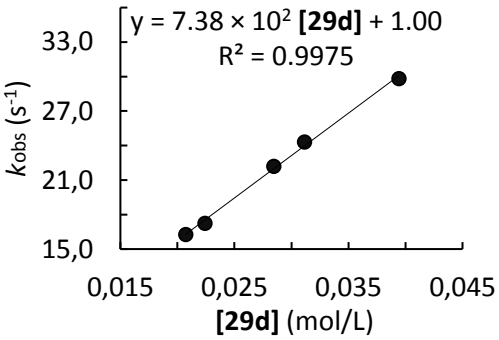

Table S14. Kinetics of the reaction of **29e** with **28d** (CH_2Cl_2, 20°C, stopped-flow, detection at 611 nm)

[28d]	[29e]	[29e]/[28d]	k_{obs}
3.54×10^{-5}	3.80×10^{-3}	107	4.87×10^{-2}
3.54×10^{-5}	7.59×10^{-3}	214	8.07×10^{-2}
3.54×10^{-5}	1.08×10^{-2}	306	1.15×10^{-1}
3.54×10^{-5}	1.49×10^{-2}	420	1.53×10^{-1}
3.54×10^{-5}	1.94×10^{-2}	550	1.91×10^{-1}
k_2(20°C) = 9.24 L mol^{-1} s^{-1}			

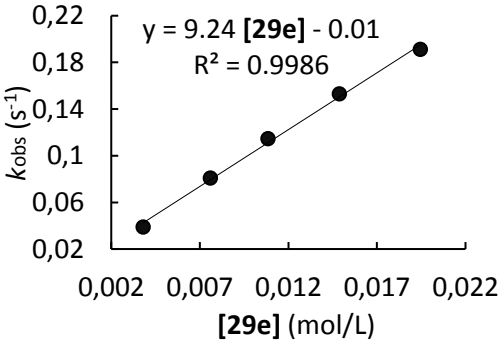

Table S15. Kinetics of the reaction of **29e** with **28c** (CH_2Cl_2, 20°C, stopped-flow, detection at 671 nm)

[28c]	[29e]	[29e]/[28c]	k_{obs}
1.36×10^{-5}	3.80×10^{-3}	279	1.99×10^{-1}
1.36×10^{-5}	7.59×10^{-3}	558	3.95×10^{-1}
1.36×10^{-5}	1.08×10^{-2}	797	5.81×10^{-1}
1.36×10^{-5}	1.49×10^{-2}	1094	7.56×10^{-1}
1.36×10^{-5}	1.94×10^{-2}	1430	9.32×10^{-1}
k_2(20°C) = 4.71×10^1 L mol^{-1} s^{-1}			

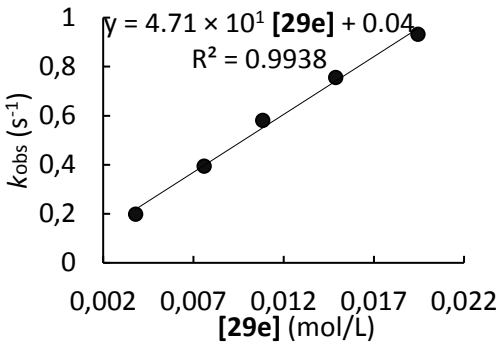

Table S16. Kinetics of the reaction of **29e** with **28b** (CH_2Cl_2, 20°C, stopped-flow, detection at 586 nm)

[28b]	[29e]	[29e]/[28b]	k_{obs}
2.73×10^{-5}	3.80×10^{-3}	139	1.99×10^{-1}
2.73×10^{-5}	7.59×10^{-3}	278	3.05×10^{-1}
2.73×10^{-5}	1.08×10^{-2}	397	5.81×10^{-1}
2.73×10^{-5}	1.49×10^{-2}	544	7.56×10^{-1}
2.73×10^{-5}	1.94×10^{-2}	712	9.32×10^{-1}
k_2(20°C) = 2.18×10^{2} L mol^{-1} s^{-1}			

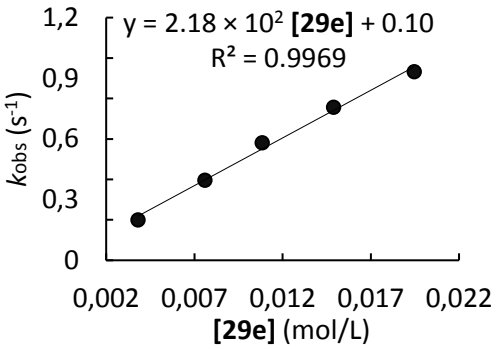

Table S17. Kinetics of the reaction of **29f** with **28d** (CH_2Cl_2, 20°C, stopped-flow, detection at 611 nm).

[28d]	[29f]	[29f]/[28d]	k_{obs}
3.30×10^{-5}	3.75×10^{-3}	114	3.04×10^{-3}
3.30×10^{-5}	6.75×10^{-3}	204	5.10×10^{-3}
3.30×10^{-5}	9.75×10^{-3}	295	7.01×10^{-3}
3.30×10^{-5}	1.45×10^{-2}	439	1.06×10^{-2}
3.30×10^{-5}	2.30×10^{-2}	696	1.83×10^{-2}
k_2(20°C) = 7.92×10^{-1} L mol^{-1} s^{-1}			

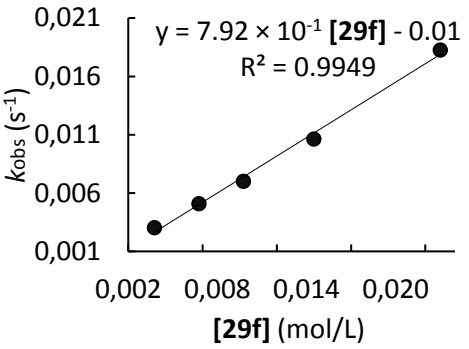

Table S18. Kinetics of the reaction of **29f** with **28c** (CH_2Cl_2, 20°C, stopped-flow, detection at 671 nm).

[28c]	[29f]	[29f]/[28c]	k_{obs}
2.04×10^{-5}	3.75×10^{-3}	184	2.20×10^{-2}
2.04×10^{-5}	6.75×10^{-3}	331	2.97×10^{-2}
2.04×10^{-5}	9.75×10^{-3}	478	4.45×10^{-2}
2.04×10^{-5}	1.45×10^{-2}	711	5.96×10^{-2}
2.04×10^{-5}	2.30×10^{-2}	1128	9.71×10^{-2}
k_2(20°C) = 3.94 L mol^{-1} s^{-1}			

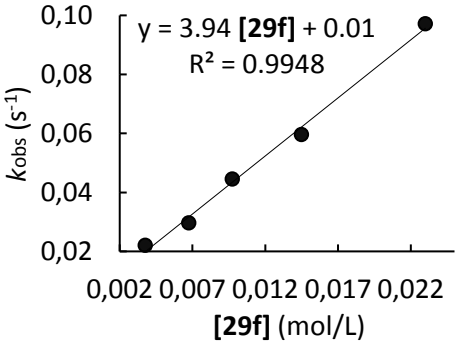

Table S19. Kinetics of the reaction of **29f** with **28b** (CH_2Cl_2, 20°C, stopped-flow, detection at 586 nm).

[28b]	[29f]	[29f]/[28b]	k_{obs}
3.36×10^{-5}	3.32×10^{-3}	99	6.19×10^{-2}
3.36×10^{-5}	6.30×10^{-3}	187	1.18×10^{-1}
3.36×10^{-5}	9.07×10^{-3}	270	1.66×10^{-1}
3.36×10^{-5}	1.11×10^{-2}	332	2.05×10^{-1}
3.36×10^{-5}	1.41×10^{-2}	421	2.82×10^{-1}
k_2(20°C) = 1.99×10^{1} L mol^{-1} s^{-1}			

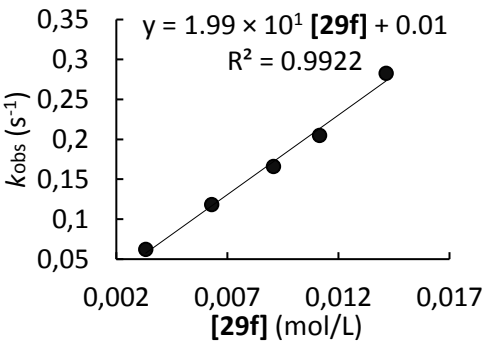

Tale S27. Kinetics of the reaction of **29g** with **28d** (CH_2Cl_2, 20°C, stopped-flow, detection at 611 nm)

[28d]	[29g]	[29g]/[28d]	k_{obs}
3.54×10^{-5}	6.82×10^{-3}	193	8.94×10^{-2}
3.54×10^{-5}	1.03×10^{-2}	292	1.56×10^{-1}
3.54×10^{-5}	1.21×10^{-2}	343	2.01×10^{-1}
3.54×10^{-5}	1.63×10^{-2}	462	2.91×10^{-1}
k_2(20°C) = 2.14×10^{1} L mol^{-1} s^{-1}			

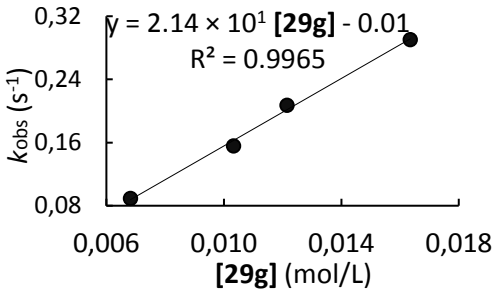

Table S28. Kinetics of the reaction of **29g** with **28c** (CH_2Cl_2, 20°C, stopped-flow, detection at 671 nm)

[28c]	[29g]	[29g]/[28c]	k_{obs}
1.87×10^{-5}	4.16×10^{-3}	222	9.22×10^{-2}
1.87×10^{-5}	8.15×10^{-3}	436	3.11×10^{-1}
1.87×10^{-5}	1.11×10^{-2}	594	5.11×10^{-1}
1.87×10^{-5}	1.38×10^{-2}	738	7.29×10^{-1}
k_2(20°C) = 6.56×10^{1} L mol^{-1} s^{-1}			

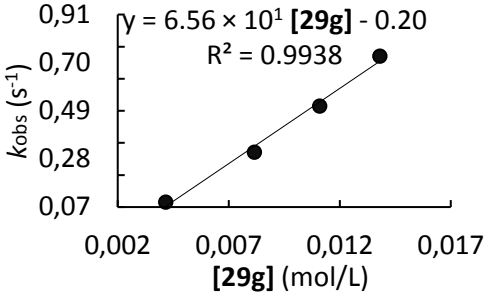

Table S29. Kinetics of the reaction of **29g** with **28b** (CH_2Cl_2, 20°C, stopped-flow, detection at 586 nm)

[28b]	[29g]	[29g]/[28b]	k_{obs}
2.73×10^{-5}	6.82×10^{-3}	250	5.28×10^{-1}
2.73×10^{-5}	1.03×10^{-2}	378	1.32
2.73×10^{-5}	1.21×10^{-2}	445	2.04
2.73×10^{-5}	1.63×10^{-2}	598	3.07
k_2(20°C) = 2.72×10^{2} L mol^{-1} s^{-1}			

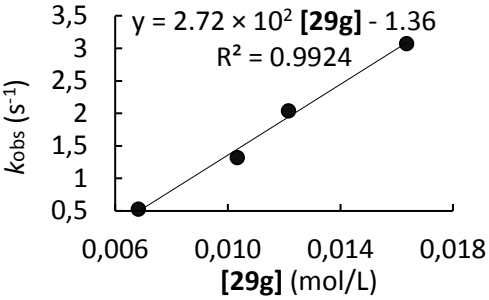

Table S20. Kinetics of the reaction of **29h** with **28f** (CH_2Cl_2, 20°C, stopped-flow, detection at 615 nm)

[28f]	[29h]	[29h]/[28f]	k_{obs}
2.95×10^{-5}	3.65×10^{-3}	124	5.13×10^{-3}
2.95×10^{-5}	5.18×10^{-3}	176	7.09×10^{-3}
2.95×10^{-5}	6.80×10^{-3}	231	9.17×10^{-3}
2.95×10^{-5}	8.72×10^{-3}	296	1.20×10^{-2}
k_2(20°C) = 1.34 L mol^{-1} s^{-1}			

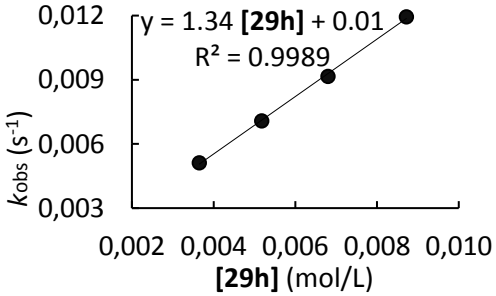

Table S21. Kinetics of the reaction of **29h** with **28d** (CH_2Cl_2, 20°C, stopped-flow, detection at 611 nm)

[28d]	[29h]	[29h]/[28d]	k_{obs}
2.36×10^{-5}	3.65×10^{-3}	155	1.41×10^{-1}
2.36×10^{-5}	5.18×10^{-3}	220	1.85×10^{-1}
2.36×10^{-5}	6.80×10^{-3}	288	2.38×10^{-1}
2.36×10^{-5}	8.72×10^{-3}	369	3.01×10^{-1}
2.36×10^{-5}	1.08×10^{-2}	459	3.58×10^{-1}
k_2(20°C) = 3.07×10^{1} L mol $^{-1}$ s^{-1}			

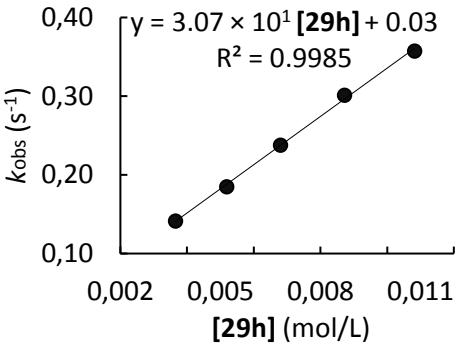

Table S22. Kinetics of the reaction of **29h** with **28b** (CH_2Cl_2, 20°C, stopped-flow, detection at 586 nm)

[28b]	[29h]	[29h]/[28b]	k_{obs}
4.20×10^{-5}	3.65×10^{-3}	87	6.23
4.20×10^{-5}	5.18×10^{-3}	123	8.23
4.20×10^{-5}	6.80×10^{-3}	162	1.14×10^{1}
4.20×10^{-5}	8.72×10^{-3}	2017	1.47×10^{1}
4.20×10^{-5}	1.08×10^{-2}	257	1.81×10^{1}
k_2(20°C) = 1.70×10^{3} L mol $^{-1}$ s^{-1}			

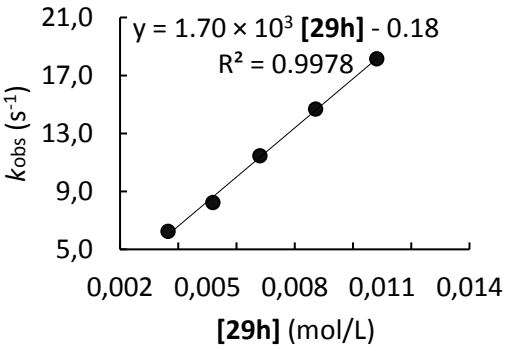

Table S23. Kinetics of the reaction of **29h** with **28a** (CH_2Cl_2, 20°C, stopped-flow, detection at 601 nm)

[28a]	[29h]	[29h]/[28a]	k_{obs}
3.83×10^{-5}	3.65×10^{-3}	95	2.30×10^{1}
3.83×10^{-5}	5.18×10^{-3}	135	3.23×10^{1}
3.83×10^{-5}	6.80×10^{-3}	177	4.06×10^{1}
3.83×10^{-5}	8.72×10^{-3}	227	4.82×10^{1}
3.83×10^{-5}	1.08×10^{-2}	282	5.73×10^{1}
k_2(20°C) = 4.70×10^{3} L mol $^{-1}$ s^{-1}			

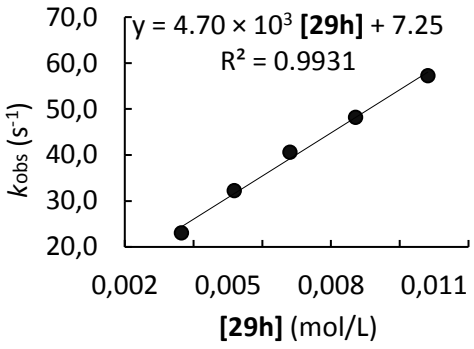

Table S23. Kinetics of the reaction of **29i** with **28e** (CH_2Cl_2, 20°C, stopped-flow, detection at 615 nm)

[28e]	[29i]	[29i]/[28e]	k_{obs}
1.10×10^{-4}	3.52×10^{-2}	320	2.60×10^{-1}
1.10×10^{-4}	4.14×10^{-2}	377	3.63×10^{-1}
1.10×10^{-4}	4.54×10^{-2}	413	4.49×10^{-1}
1.10×10^{-4}	5.08×10^{-2}	462	5.51×10^{-1}
k_2(20°C) = 1.88×10^{1} L mol $^{-1}$ s^{-1}			

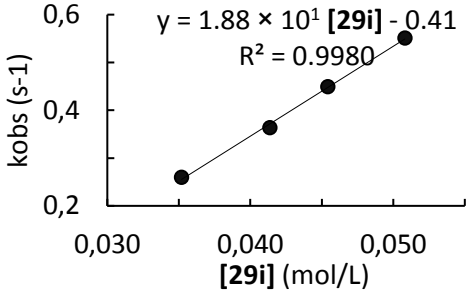

Table S23. Kinetics of the reaction of **29i** with **28d** (CH_2Cl_2, 20°C, stopped-flow, detection at 619 nm)

[28d]	**[29i]**	**[29i]/[28d]**	k_{obs}
7.55×10^{-5}	3.52×10^{-3}	466	9.26×10^{-1}
7.55×10^{-5}	4.14×10^{-3}	548	1.21
7.55×10^{-5}	4.54×10^{-3}	602	1.36
7.55×10^{-5}	5.08×10^{-3}	673	1.61
k_2(20°C) = 4.39×10^{1} L mol $^{-1}$ s^{-1}			

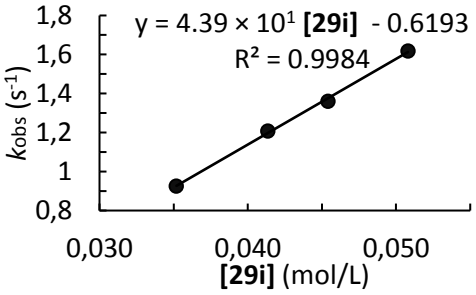

Table S23. Kinetics of the reaction of **29i** with **28c** (CH_2Cl_2, 20°C, stopped-flow, detection at 667 nm)

[28c]	**[29i]**	**[29i]/[28c]**	k_{obs}
7.14×10^{-5}	3.52×10^{-3}	493	3.18
7.14×10^{-5}	4.14×10^{-3}	579	5.12
7.14×10^{-5}	4.54×10^{-3}	636	6.08
7.14×10^{-5}	5.08×10^{-3}	712	6.99
k_2(20°C) = 2.45×10^{2} L mol $^{-1}$ s^{-1}			

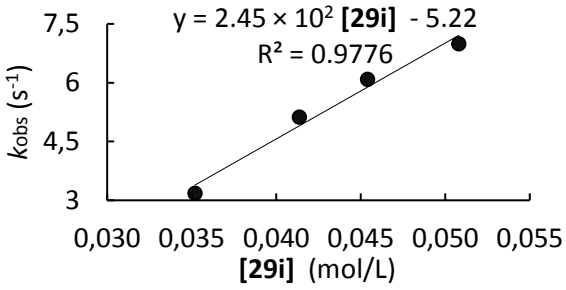

Table S23. Kinetics of the reaction of **29i** with **28b** (CH_2Cl_2, 20°C, stopped-flow, detection at 586 nm)

[28b]	**[29i]**	**[29i]/[28b]**	k_{obs}
8.83×10^{-5}	3.52×10^{-3}	399	1.19×10^{1}
8.83×10^{-5}	4.14×10^{-3}	469	1.80×10^{1}
8.83×10^{-5}	4.54×10^{-3}	514	2.19×10^{1}
8.83×10^{-5}	5.08×10^{-3}	576	2.64×10^{1}
k_2(20°C) = 9.31×10^{2} L mol $^{-1}$ s^{-1}			

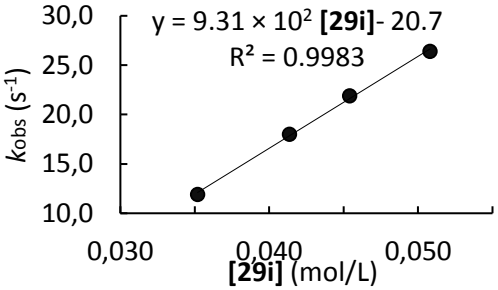

Table S24. Kinetics of the reaction of **29j** with **28d** (CH_2Cl_2, 20°C, stopped-flow, detection at 611 nm)

[28d]	**[29j]**	**[29j]/[28d]**	k_{obs}
2.36×10^{-5}	1.86×10^{-3}	79	1.80×10^{-3}
2.36×10^{-5}	2.83×10^{-3}	120	2.67×10^{-3}
2.36×10^{-5}	3.72×10^{-3}	158	3.40×10^{-3}
2.36×10^{-5}	4.69×10^{-3}	199	4.08×10^{-3}
2.36×10^{-5}	5.71×10^{-3}	242	4.73×10^{-3}
k_2(20°C) = 7.61×10^{-1} L mol $^{-1}$ s^{-1}			

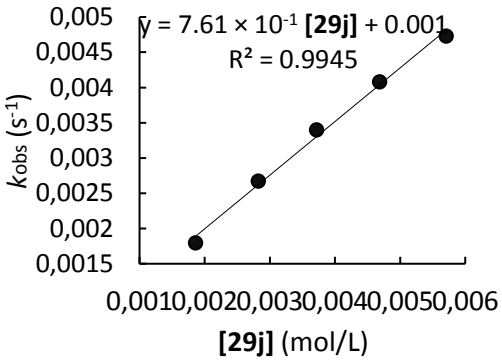

Table S25. Kinetics of the reaction of **29j** with **28b** (CH_2Cl_2, 20°C, stopped-flow, detection at 586 nm)

[28b]	**[29j]**	**[29j]/[28b]**	k_{obs}
4.20×10^{-5}	1.86×10^{-3}	44	1.14×10^{-1}
4.20×10^{-5}	2.83×10^{-3}	67	1.37×10^{-1}
4.20×10^{-5}	3.72×10^{-3}	89	1.51×10^{-1}
4.20×10^{-5}	4.69×10^{-3}	112	1.76×10^{-1}
4.20×10^{-5}	5.71×10^{-3}	136	2.03×10^{-1}
k_2(20°C) = 2.27×10^{1} L mol^{-1} s^{-1}			

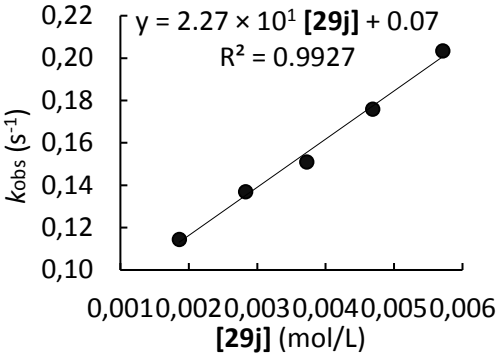

Table S26. Kinetics of the reaction of **29j** with **28a** (CH_2Cl_2, 20°C, stopped-flow, detection at 601 nm)

[28a]	**[29j]**	**[29j]/[28a]**	k_{obs}
3.83×10^{-5}	1.86×10^{-3}	49	6.96×10^{-1}
3.83×10^{-5}	2.83×10^{-3}	74	8.89×10^{-1}
3.83×10^{-5}	3.72×10^{-3}	97	1.04
3.83×10^{-5}	4.69×10^{-3}	122	1.18
3.83×10^{-5}	5.71×10^{-3}	149	1.32
k_2(20°C) = 1.62×10^{2} L mol^{-1} s^{-1}			

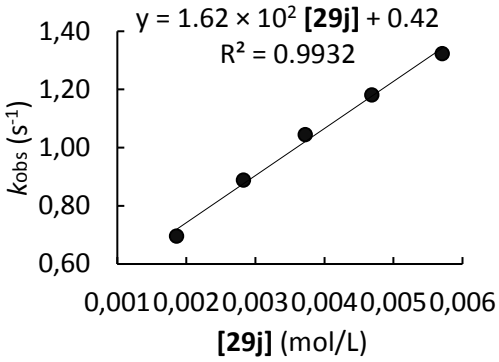

3.2 Determination of the kinetic parameters *N* and s_N

Table S30. Calculation of the reactivity parameters *N* and s_N for **29a** using **28b-d** in CH_2Cl_2.

Electrophile	*E*	Log (k_2)
28d	-5.53	0.30
28c	-4.72	1.17
28b	-3.85	1.85
N = 5.91, s_N = 0.92.		

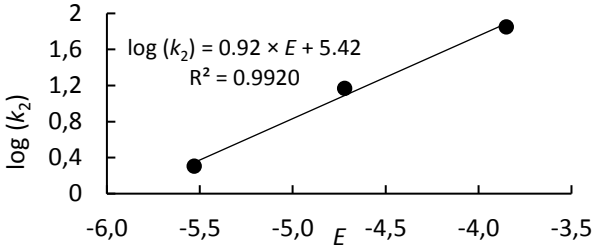

Table S31. Calculation of the reactivity parameters *N* and s_N for **29b** using **28b-e** in CH_2Cl_2.

Electrophile	*E*	Log (k_2)
28e	-5.89	1.17
28d	-5.53	1.54
28c	-4.72	2.28
28b	-3.85	2.86
N = 7.36, s_N = 0.83.		

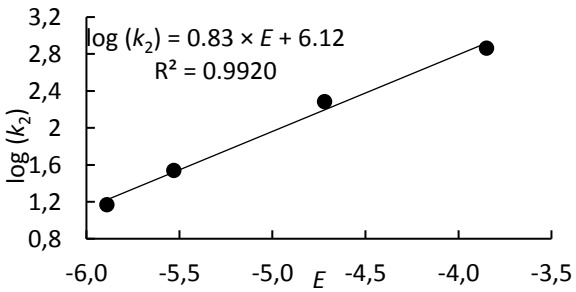

Table S32. Calculation of the reactivity parameters *N* and s_N for **29c** using **28b-d** in CH_2Cl_2.

Electrophile	*E*	Log (k_2)
28d	-5.53	0.68
28c	-4.72	1.46
28b	-3.85	2.20
N = 6.29, s_N = 0.91.		

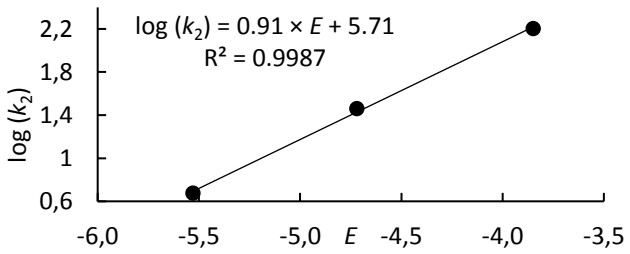

Table S33. Calculation of the reactivity parameters *N* and s_N for **29d** using **28b-e** in CH_2Cl_2.

Electrophile	*E*	Log (k_2)
28e	-5.89	1.08
28d	-5.53	1.47
28c	-4.72	2.15
28b	-3.85	2.87
N = 7.18, s_N = 0.87.		

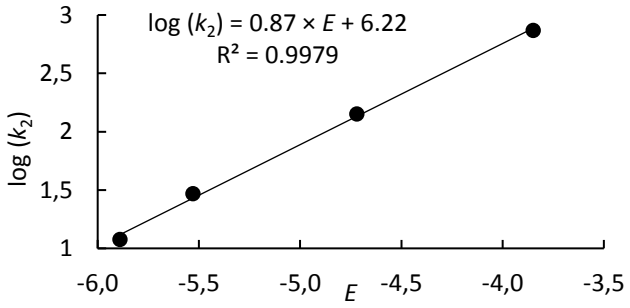

Table S34. Calculation of the reactivity parameters *N* and s_N for **29e** using **28b-d** in CH_2Cl_2.

Electrophile	*E*	Log (k_2)
28d	-5.53	0.97
28c	-4.72	1.67
28b	-3.85	2.34
N = 6.73, s_N = 0.82.		

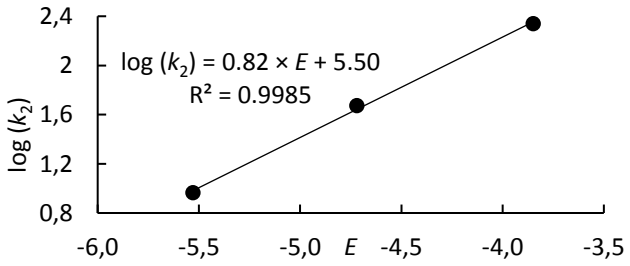

Table S35. Calculation of the reactivity parameters *N* and s_N for **29f** using **28b-d** in CH_2Cl_2.

Electrophile	*E*	Log (k_2)
28d	-5.53	-0.10
28c	-4.72	0.60
28b	-3.85	1.30
N = 5.42, s_N = 0.83.		

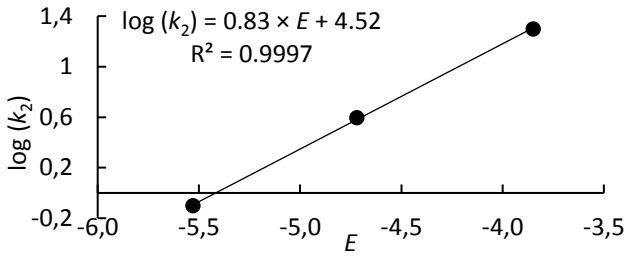

Table S36. Calculation of the reactivity parameters *N* and s_N for **29h** using **28a,b,d,f** in CH_2Cl_2.

Electrophile	*E*	Log (k_2)
28f	-7.02	0.13
28d	-5.53	1.49
28b	-3.85	3.23
28a	-3.14	3.67
N = 7.16, s_N = 0.94.		

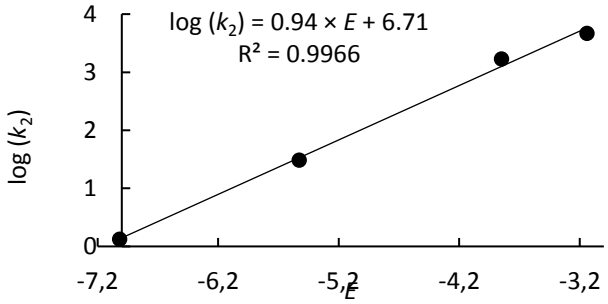

Table S37. Calculation of the reactivity parameters *N* and s_N for **29j** using **28a,b,d** in CH_2Cl_2.

Electrophile	*E*	Log (k_2)
28c	-5.53	-0.12
28b	-3.85	1.36
28a	-3.14	2.21
N = 5.37, s_N = 0.96.		

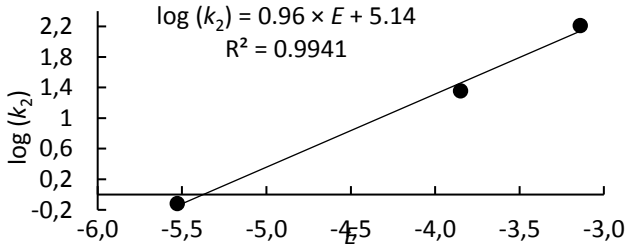

Table S38. Calculation of the reactivity parameters *N* and s_N for **29g** using **28b-d** in CH_2Cl_2.

Electrophile	*E*	Log (k_2)
28d	-5.53	1.33
28c	-4.72	1.82
28b	-3.85	2.43
N = 7.53, s_N = 0.66.		

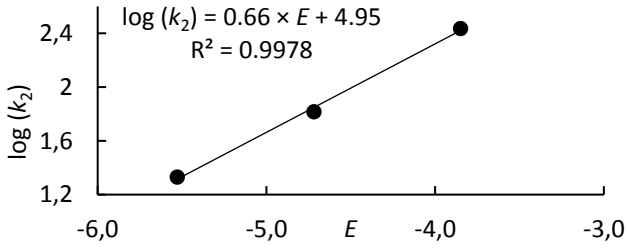

Table S38. Calculation of the reactivity parameters *N* and s_N for **29i** using **28b-e** in CH_2Cl_2.

Electrophile	*E*	Log (k_2)
28e	-5.89	1.27
28d	-5.53	1.64
28c	-4.72	2.39
28b	-3.85	2.97
N = 7.48, s_N = 0.83.		

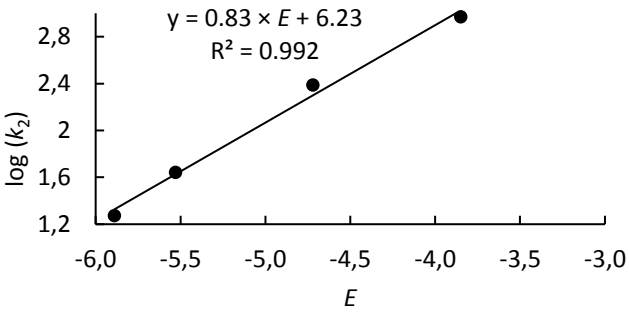

Chapter 4: Quantification of the Hydride Donor Ability of Phosphine Borane Complexes.

1. Synthetic part

1.1 Tests for the catalyzed intramolecular borylation of **27a**

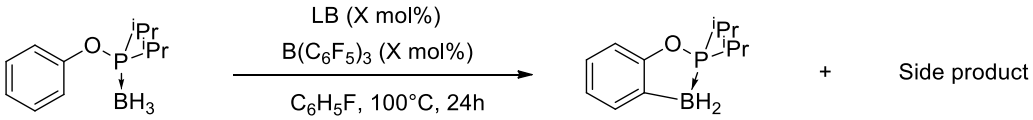

27a **28a** **31**

General procedure

In a schenlk tube equipped with a stirred and under argon atmosphere were added successively **27a** (40 mg, 0.18 mmol, 1 eq), the Lewis base (0.04 mmol, 0.2 eq), $B(C_6F_5)_3$ (20 mg, 0.04 mmol, 0.2 eq) and C_6H_5F (1.0 mL). The Schlenk was sealed and the mixture stirred for 5 min at r.t. before warming at 100°C or 140°C for 24h. At the end of the reaction, an aliquot of the crude mixture was taken and analysed by NMR spectroscopy.

1.2 Synthesis of phosphinite borane complexes **37a-p**

For the synthesis and characterization of **37l-o** and **37q-s**, see the experimental section in the chapter 3.

General procedure

The synthesis was done according to a procedure reported by Vedejs et al.[1] To a stirred solution of phenol derivative (2.3 mmol, 1.2 eq) in degassed toluene (4 mL) was added chloro-diisopropylphosphine or chloro-diphenylphosphine (1.9 mmol, 1.0 eq) and triethylamine (2.8 mmol, 1.5 eq) under argon. The mixture was warmed at reflux for 12h under stirring in a sealed schlenck. After cooling to room temperature, the mixture was filtered, washed with toluene (3 x 10 mL) and concentrated to a half of the original volume in vacuo. To the resulting solution were added $BH_3.Me_2S$ (320 µL, 3.4 mmol, 1.8 eq) dropwise at 0°C. After stirring 2h, the solution was filtered through a plug of silica gel, flushing with dichloromethane (15 mL). The filtrate was concentrated under reduced pressure. The crude was purified by flash chromatrography on silica gel affording the corresponding phosphinite-borane complex.

Phenyl diisopropylphosphinite borane 37a

[1] C. Cazorla, T. S. De Vries, E. Vedejs, *Org. Lett.* **2013**, *15*, 984–987.

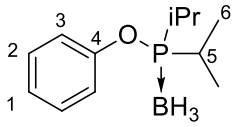

Chemical Formula: $C_{12}H_{22}BOP$
Molecular Weight: 224.09

37a as a colourless oil (372 mg, 1.66 mmol, 88%), phenol (214 mg, 2.27 mmol, 1.2 eq), Chlorodiisopropyl phosphine (300 µL, 1.89 mmol, 1 eq), triethylamine (395 µL, 2.84 mmol, 1.5 eq).

Eluent: Cyclohexane/diethylether (95:5), **Rf** = 0.19. **^{1}H-NMR** (400.1 MHz, $CDCl_3$): δ 7.31-7.27 (m, 2H, H-3), 7.14-7.09 (m, 3H, H-1,2), 2.28-2.19 (m, 2H, H-5), 1.28 (ddd, *J* = 23.3 Hz, 15.0 Hz, 7.2 Hz, 12H), 0.49 (q, *J* = 96.0 Hz, 3H, BH_3). **^{13}C-NMR** (100.6 MHz, $CDCl_3$): δ 153.8 (d, *J* = 6.2 Hz, C-Ar), 129.5 (s, C-Ar), 124.3 (s, C-Ar), 121.0 (d, *J* = 3.4 Hz, C-Ar), 26.5 (d, *J* = 36.6 Hz, C-5), 16.3 (dd, *J* = 55.7 Hz, 1.8 Hz, C-6). **^{31}P{^{1}H}-NMR** (162.0 MHz, $CDCl_3$): δ 143.8 (m, P). **^{11}B-NMR** (128.4 MHz, $CDCl_3$): δ -43.4 (qd, *J* = 96.2Hz, 61.0 Hz, BH_3). **IR** (neat, ATR probe, cm^{-1}): v 2967 (CH sp^3), 2936, 2369, 2355, 2319, 1591, 1489, 1464, 1205, 1164, 1067 (C-P), 1025, 894, 882. **HRMS** (ESI positive) = [$C_{12}H_{22}BONaP^+$] Calculated mass: 247.1399 g/mol, found mass: 247.1405 g/mol.

Phenyl diphenylphosphinite borane 37b

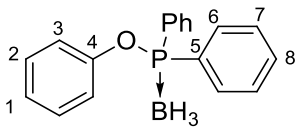

Chemical Formula: $C_{18}H_{18}BOP$
Molecular Weight: 292.12

37b as an off-white solid (431 mg, 1.48 mmol, 78 %), Phenol (214 mg, 2.27 mmol, 1.2 eq), Chlorodiphenyl phosphine (350 µL, 1.89 mmol, 1 eq), triethylamine (395 µL, 2.84 mmol, 1.5 eq).

Eluent: Cyclohexane/diethylether (8:2), **Rf** = 0.50. **^{1}H-NMR** (400.1 MHz, $CDCl_3$): δ 7.87-7.83 (m, 4H, H-Ar), 7.58-7.48 (m, 6H, H-Ar), 7.24-7.22 (m, 2H, H-Ar), 7.13-7.09 (m, 1H, H-Ar), 7.02-7.00 (m, 2H, H-Ar), 1.04 (q, *J* = 89.7 Hz, 3H, BH_3). **^{13}C-NMR** (100.6 MHz, $CDCl_3$): δ 152.4 (d, *J* = 4.8 Hz, C-Ar), 132.3 (d, *J* = 2.3 Hz, C-Ar), 131.8 (s, C-Ar), 131.7 (d, *J* = 60.5 Hz, C-Ar), 129.6 (s, C-Ar), 128.9 (d, *J* = 10.6 Hz, C-Ar), 124.9 (s, C-Ar), 121.4 (d, *J* = 4.2 Hz, C-Ar). **^{31}P{^{1}H}-NMR** (162.0 MHz, $CDCl_3$): δ 109.3 (m, P). **^{11}B{^{1}H}-NMR** (128.4 MHz, $CDCl_3$): δ -39.4 (d, *J* = 60.2 Hz, BH_3). **Mp** = 99-100 °C. **IR** (neat, ATR probe, cm^{-1}): v 2401, 1589, 1488, 1437, 1193, 1169, 1061 (C-P), 998, 910, 893. **HRMS** (ESI positive) = [$C_{18}H_{18}BONaP^+$] Calculated mass: 315.1086 g/mol, found mass: 315.1090 g/mol.

3-methylphenyl diisopropylphosphinite borane 37c

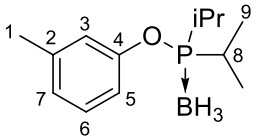

Chemical Formula: $C_{13}H_{24}BOP$
Molecular Weight: 238.11

37c as a colourless oil (290 mg, 1.22 mmol, 64%), m-cresol (240 µL, 2.29 mmol, 1.2 eq), Chlorodiisopropyl phosphine (300 µL, 1.89 mmol, 1 eq), triethylamine (395 µL, 2.84 mmol, 1.5 eq).

Eluent: Cyclohexane/diethylether (95:5), **Rf** = 0.63. **^{1}H-NMR** (400.1 MHz, $CDCl_3$): δ 7.18-7.14 (m, 1H, H-Ar), 6.95-6.91 (m, 3H, H-Ar), 2.33 (s, 3H, H-1), 2.27-2.18 (m, 2H, H-8), 1.33-1.22 (m, 12H, H-9), 0.48 (q, *J* = 94.5 Hz, 3H, BH_3). **^{13}C-NMR** (100.6 MHz, $CDCl_3$): δ 153.7 (d, *J* = 6.2 Hz, C-Ar), 139.6 (s, C-Ar), 129.1 (s, C-Ar), 125.1 (s, C-Ar), 121.6 (d, *J* = 3.4 Hz, C-Ar), 117.9 (d, *J* = 3.3 Hz, C-Ar), 26.5 (d, *J* = 36.6 Hz, C-8), 21.5 (s, C-1), 16.3 (dd, *J* = 54.1, 1.8 Hz, C-9). **^{31}P{^{1}H}-NMR** (162.0 MHz, $CDCl_3$): δ 143.1 (m, P) **^{11}B{^{1}H}-NMR** (128.4 MHz, $CDCl_3$): δ -43.4 (d, *J* = 60.5 Hz, BH_3). **IR** (neat, ATR probe, cm^{-1}): v 2868 (CH sp^3), 2935, 2380, 1607, 1585, 1488, 1464, 1246, 1148, 1029 (c-P), 985, 948, 884, 820, 781. **HRMS** (ESI positive) = [$C_{13}H_{24}BONaP^+$] Calculated mass: 261.1556 g/mol, found mass: 261.1563 g/mol.

3-methylphenyl diphenylphosphinite borane 37d

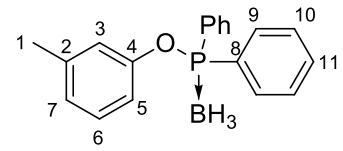

Chemical Formula: $C_{19}H_{20}BOP$
Molecular Weight: 306.15

37d as a colourless oil (353 mg, 1.15 mmol, 61 %), m-cresol (240 mg, 2.29 mmol, 1.2 eq), Chlorodiphenyl phosphine (350 µL, 1.89 mmol, 1 eq), triethylamine (395 µL, 2.84 mmol, 1.5 eq).

Eluent: Cyclohexane/diethylether (8:2), **Rf** = 0.70. **^{1}H-NMR** (400.1 MHz, $CDCl_3$): δ 7.86-7.82 (m, 4H, H-Ar), 7.58-7.47 (m, 6H, H-Ar), 7.12-7.09 (m, 1H, H-Ar), 6.93-6.78 (m, 3H, H-Ar), 2.27 (s, 3H, H-1), 1.06 (q, *J* = 87.4 Hz, 3H, BH_3). **^{13}C-NMR** (100.6 MHz, $CDCl_3$): δ 152.3 (d, *J* = 4.9 Hz, C-Ar), 139.8 (s, C-Ar), 132.3 (d, *J* = 2.2 Hz, C-Ar), 131.7 (d, *J* = 11.5 Hz, C-Ar), 129.2 (s, C-Ar), 128.9 (d, *J* = 10.6 Hz, C-Ar), 125.7 (s, C-Ar), 122.0 (d, *J* = 4.2 Hz, C-Ar), 118.2 (d, *J* = 4.2 Hz, C-Ar), 21.5 (s, C-1), quaternary carbon is not obsersevd. **^{31}P{^{1}H}-NMR** (162.0 MHz, $CDCl_3$): δ 108.8 (m, P). **^{11}B{^{1}H}-NMR** (128.4 MHz, $CDCl_3$): δ -39.4 (d, *J* = 58.9 Hz, BH_3). **IR** (neat, ATR probe, cm^{-1}): v 2922 (CH sp^3), 2375, 1607, 1585, 1437, 1245, 1143, 1110, 1057 (C-P), 944, 827, 782, 733. **HRMS** (ESI positive) = [$C_{19}H_{20}BONaP^+$] Calculated mass: 329.1243 g/mol, found mass: 329.1246 g/mol.

4-Methoxyphenyl diisopropylphosphinite borane 37e

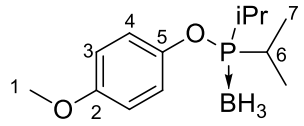

Chemical Formula: $C_{13}H_{24}BO_2P$
Molecular Weight: 254.11

37e as a colourless oil (320 mg, 1.26 mmol, 67%), 4-methoxyphenol (281 mg, 2.27 mmol, 1.2 eq), Chlorodiisopropyl phosphine (300 µL, 1.89 mmol, 1 eq), triethylamine (395 µL, 2.84 mmol, 1.5 eq).

Eluent: Cyclohexane/diethylether (8:2), **Rf** = 0.65. **^{1}H-NMR** (400.1 MHz, $CDCl_3$): δ 7.05-7.03 (m, 2H, H-Ar), 6.81-6.79 (m, 2H, H-Ar), 3.77 (s, 3H, H-1), 2.25-2.16 (m, 2H, H-6), 1.33-1.21 (m, 12H, H-7), 0.44 (q, *J* = 91.6 Hz, 3H, BH_3). **^{13}C-NMR** (100.6 MHz, $CDCl_3$): δ 156.3 (s, C-Ar),

147.4 (d, *J* = 6.1 Hz, C-Ar), 121.9 (d, *J* = 3.2 Hz, C-Ar), 114.5 (s, C-Ar), 55.8 (s, C-1), 26.4 (d, *J* = 36.5 Hz, C-6), 16.4 (d, *J* = 55.6 Hz, 1.8 Hz, C-7). **$^{31}P\{^{1}H\}$-NMR** (162.0 MHz, $CDCl_3$): δ 143.6 (m, P). **$^{11}B\{^{1}H\}$-NMR** (128.4 MHz, $CDCl_3$): δ -43.6 (d, *J* = 60.9 Hz, BH_3). **IR** (neat, ATR probe, cm^{-1}): v 2966 (CH sp^3), 2936, 2876, 2384, 1503, 1464, 1295, 1248, 1198, 1030 (C-P), 903, 831. **HRMS** (ESI positive) = [$C_{13}H_{24}BO_2NaP^+$] Calculated mass: 277.1505 g/mol, found mass: 277.1508 g/mol.

4-Methoxyphenyl diphenylphosphinite borane 37f

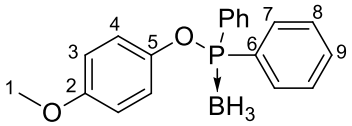

Chemical Formula: $C_{19}H_{20}BO_2P$
Molecular Weight: 322.15

37f as a colourless oil (543 mg, 1.69 mmol, 89 %), 4-methoxyphenol (282 mg, 2.27 mmol, 1.2 eq), Chlorodiphenyl phosphine (350 µL, 1.89 mmol, 1 eq), triethylamine (395 µL, 2.84 mmol, 1.5 eq).

Eluent: Cyclohexane/diethylether (8:2), **Rf** = 0.60. **^{1}H-NMR** (400.1 MHz, $CDCl_3$): δ 7.86-7.82 (m, 4H, H-Ar), 7.58-7.49 (m, 6H, H-Ar), 6.93-6.91 (m, 2H, H-Ar), 6.76-6.74 (m, 2H, H-Ar), 3.74 (s, 3H, H-1), 1.04 (q, *J* = 82.3 Hz, 3H, BH_3). **^{13}C-NMR** (100.6 MHz, $CDCl_3$): δ 156.6 (s, C-Ar), 145.9 (d, *J* = 5.0 Hz, C-Ar), 132.3 (d, *J* = 2.0 Hz, C-Ar), 131.8 (d, *J* = 62.5 Hz, C-Ar), 131.7 (d, *J* = 11.5 Hz, C-Ar), 128.8 (d, *J* = 10.6 Hz, C-Ar), 122.3 (d, *J* = 3.9 Hz, C-Ar), 114.5 (s, C-Ar), 55.6 (s, C-1). **$^{31}P\{^{1}H\}$-NMR** (162.0 MHz, $CDCl_3$): δ 109.5 (m, P). **$^{11}B\{^{1}H\}$-NMR** (128.4 MHz, $CDCl_3$): δ -39.5 (d, *J* = 57.0 Hz, BH_3). **IR** (neat, ATR probe, cm^{-1}): v 2955 (CH sp^3), 2836, 2373, 1501, 1437, 1296, 1249, 1193, 1111, 1057, 1031 (C-P), 896, 831, 733. **HRMS** (ESI positive) = [$C_{19}H_{20}BO_2NaP^+$] Calculated mass: 345.1192 g/mol, found mass: 345.1194 g/mol.

4-Chlorophenyl diisopropylphosphinite borane 37g

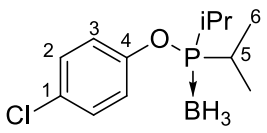

Chemical Formula: $C_{12}H_{21}BClOP$
Molecular Weight: 258.53

37g as a colourless oil (461 mg, 1.74 mmol, 94%), 4-chlorophenol (292 mg, 2.27 mmol, 1.2 eq), Chlorodiisopropyl phosphine (300 µL, 1.89 mmol, 1 eq), triethylamine (395 µL, 2.84 mmol, 1.5 eq).

Eluent: Cyclohexane/ethyl acetate (95:5), **Rf** = 0.37 **^{1}H-NMR** (400.1 MHz, $CDCl_3$): δ 7.25-7.23 (m, 2H, H-Ar), 7.08-7.06 (m, 2H, H-Ar), 2.27-2.18 (m, 2H, H-5), 1.32-1.21 (m, 12H, H-6), 0.44 (q, *J* = 96.6 Hz, 3H, BH_3). **^{13}C-NMR** (100.6 MHz, $CDCl_3$): δ 152.2 (d, *J* = 6.1 Hz, C-Ar), 129.6 (d, *J* = 30.5 Hz, C-Ar), 129.3 (s, C-Ar), 26.3 (d, *J* = 36.2 Hz, C-5), 16.1 (dd, *J* = 56.3 Hz, 1.9 Hz, C-6). **$^{31}P\{^{1}H\}$-NMR** (162.0 MHz, $CDCl_3$): δ 145.9 (m, P).

$^{11}B\{^1H\}$-NMR (128.4 MHz, $CDCl_3$): δ -43.5 (d, *J* = 58.3 Hz, BH_3). **IR** (neat, ATR probe, cm^{-1}): v 2968, 2937, 2383, 1486, 1465, 1213, 1164, 1090, 1012, 901, 882, 831. **HRMS** (ESI positive) **=** [$C_{12}H_{21}BONaPCl^+$] Calculated mass: 281.1009 g/mol, found mass: 281.1011 g/mol.

4-Chlorophenyl diphenylphosphinite borane 37h

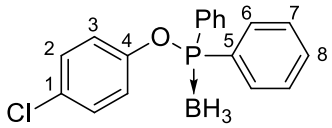

Chemical Formula: $C_{18}H_{17}BClOP$
Molecular Weight: 326.56

37h as a colourless oil (442 mg, 1.35 mmol, 72 %), 4-chlorophenol (292 mg, 2.27 mmol, 1.2 eq), Chlorodiphenyl phosphine (350 µL, 1.89 mmol, 1 eq), triethylamine (395 µL, 2.84 mmol, 1.5 eq).

Eluent: Cyclohexane/diethylether (8:2), **Rf** = 0.58. **^{1}H-NMR** (400.1 MHz, $CDCl_3$): δ 7.85-7.80 (m, 4H, H-Ar), 7.59-7.49 (m, 6H, H-Ar), 7.21-7.19 (m, 2H, H-Ar), 6.95-6.93 (m, 2H, H-Ar), 1.03 (q, *J* = 86.4 Hz, 3H, BH_3). **^{13}C-NMR** (100.6 MHz, $CDCl_3$): δ 150.9 (d, *J* = 4.8 Hz, C-Ar), 132.5 (d, *J* = 2.3 Hz, C-Ar), 131.7 (d, *J* = 11.5 Hz, C-Ar), 131.3 (d, *J* = 60.5 Hz, C-Ar), 130.3 (s, C-Ar), 129.6 (s, C-Ar), 129.0 (d, *J* = 10.7 Hz, C-Ar), 122.8 (d, *J* = 4.1 Hz, C-Ar). **$^{31}P\{^1H\}$-NMR** (162.0 MHz, $CDCl_3$): δ 111.2 (m, P). **$^{11}B\{^1H\}$-NMR** (128.4 MHz, $CDCl_3$): δ -39.5 (d, *J* = 58.2 Hz, BH_3). **IR** (neat, AiiTR probe, cm^{-1}): v 2375, 2305, 1489, 1485, 1437, 1204, 1112, 1090, 1057, 1028 (C-P), 1023, 999, 895, 831. **HRMS** (ESI positive) = [$C_{18}H_{17}BONaPCl^+$] Calculated mass: 349.0696 g/mol, found mass: 349.0700 g/mol.

2,6-dimethylphenyl diisopropylphosphinite borane 37i

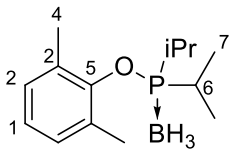

Chemical Formula: $C_{14}H_{26}BOP$
Molecular Weight: 252.14

37i as a colourless oil (424 mg, 1.68 mmol, 89%), 2,6-dimethylphenol (277 mg, 2.27 mmol, 1.2 eq), Chlorodiisopropyl phosphine (300 µL, 1.89 mmol, 1 eq), triethylamine (395 µL, 2.84 mmol, 1.5 eq).

Eluent: Cyclohexane/diethylether (95:5), **Rf** = 0.40. **^{1}H-NMR** (400.1 MHz, $CDCl_3$): δ 7.55-7.52 (m, 1H, H-Ar), 7.46-7.45 (m, 1H, H-Ar), 7.23-7.19 (m, 1H, H-Ar), 2.71-2.64 (m, 2H, H-6), 2.61 (s, 6H, H-4), 1.65-1.52 (m, 12H, H-7), 0.77 (q, *J* = 92.5 Hz, 3H, BH_3). **^{13}C-NMR** (100.6 MHz, $CDCl_3$): δ 130.3 (d, *J* = 2.1 Hz, C-Ar), 129.4 (d, *J* = 1.1 Hz, C-Ar), 129.2 (s, C-Ar), 128.4 (s, C-Ar), 125.4 (s, C-Ar), 124.5 (d, *J* = 1.3 Hz, C-Ar), 27.8 (d, *J* = 33.9 Hz, C-6), 18.5 (s, C-4), 17.0 (d, *J* = 57.5 Hz, C-7). **$^{31}P\{^1H\}$-NMR** (162.0 MHz, $CDCl_3$): δ 144.6 (m, P). **$^{11}B\{^1H\}$-NMR** (128.4 MHz, $CDCl_3$): δ -42.1 (d, *J* = 62.5 Hz, BH_3). **IR** (neat, ATR probe, cm^{-1}): v 2968 (CH sp^3), 2934, 2354, 1465, 1387, 1265, 1175, 1094, 1065, 1030 (C-P), 902, 885, 764. **HRMS** (ESI positive) = [$C_{14}H_{26}BONaP^+$] Calculated mass: 275.1712 g/mol, found mass: 275.1717 g/mol.

2,6-dimethylphenyl diphenylphosphinite borane 37j

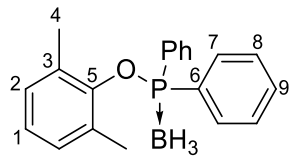

Chemical Formula: $C_{20}H_{22}BOP$
Molecular Weight: 320.17

37j as an off-white solid (392 mg, 1.22 mmol, 65 %), 2,6-dimethylphenol (277 mg, 2.27 mmol, 1.2 eq), Chlorodiphenyl phosphine (350 µL, 1.89 mmol, 1 eq), triethylamine (395 µL, 2.84 mmol, 1.5 eq).

Eluent: Cyclohexane/diethylether (9:1), **Rf** = 0.67. **^{1}H-NMR** (400.1 MHz, $CDCl_3$): δ 8.29-8.24 (m, 4H, H-Ar), 7.82-7.77 (m, 6H, H-Ar), 7.66-7.61 (m, 1H, H-Ar), 7.45-7.41 (m, 1H, H-Ar), 7.38-7.33 (m, 1H, H-Ar), 2.23 (s, 6H, H-4), 1.17 (q, *J* = 84.2 Hz, 3H, BH_3). **^{13}C-NMR** (100.6 MHz, $CDCl_3$): δ 151.5 (s, C-Ar), 133.6 (d, *J* = 64.5 Hz, C-Ar), 132.0 (d, *J* = 2.4 Hz, C-Ar), 131.1 (d, *J* = 11.6 Hz, C-Ar), 129.0 (d, *J* = 1.4 Hz, C-Ar), 128.8 (d, *J* = 10.8 Hz, C-Ar), 125.0 (s, C-Ar), 115.5 (d, *J* = 20.9 Hz, C-Ar), 18.7 (s, C-4). **^{31}P{^{1}H}-NMR** (162.0 MHz, $CDCl_3$): δ 104.7 (m, P). **^{11}B{^{1}H}-NMR** (128.4 MHz, $CDCl_3$): δ -41.3 (d, *J* = 56.7 Hz, BH_3). **Mp** = 160-161 °C. **IR** (neat, ATR probe, cm^{-1}): v 2955, 2918, 2387, 1472, 1438, 1161, 1110, 1089, 1059, 902, 788. **HRMS** (ESI positive) = [$C_{20}H_{22}BONaP^{+}$] Calculated mass: 343.1399 g/mol, found mass: 343.1398 g/mol.

1-Naphtyl diphenylphosphinite borane 37k

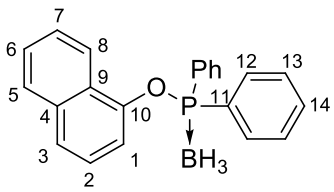

Chemical Formula: $C_{22}H_{20}BOP$
Molecular Weight: 342.18

37k as a white solid (543 mg, 1.59 mmol, 84%), 1-Naphtol (332 mg, 2.29 mmol, 1.2 eq), Chlorodiphenyl phosphine (350 µL, 1.89 mmol, 1 eq), triethylamine (395 µL, 2.84 mmol, 1.5 eq).

Eluent: Cyclohexane/diethylether (8:2), **Rf** = 0.45. **^{1}H-NMR** (400.1 MHz, $CDCl_3$): δ 8.03-8.01 (m, 1H, H-Ar), 7.96-7.92 (m, 4H, H-Ar), 7.83-7.81 (m, 1H, H-Ar), 7.61-7.57 (m, 3H, H-Ar), 7.55-7.43 (m, 6H, H-Ar), 7.29-7.26 (m, 1H H-Ar), 7.11-7.09 (m, 1H, H-Ar), 1.11 (q, *J* = 67.4 Hz, 3H, BH_3). **^{13}C-NMR** (100.6 MHz, $CDCl_3$): δ 148.7 (d, *J* = 5.2 Hz, C-Ar), 134.9 (s, C-Ar), 132.4 (d, *J* = 2.3 Hz, C-Ar), 131.8 (d, *J* = 62.7 Hz, C-Ar), 131.7 (d, *J* = 11.5 Hz, C-Ar), 129.0 (d, *J* = 10.6 Hz, C-Ar), 127.9 (s, C-Ar), 127.3 (d, *J* = 4.2 Hz, C-Ar), 126.7 (s, C-Ar), 126.2 (s, C-Ar), 125.4 (s, C-Ar), 124.5 (s, C-Ar), 122.1 (s, C-Ar), 115.4 (d, *J* = 5.2 Hz, C-Ar). **^{31}P{^{1}H}-NMR** (162.0 MHz, $CDCl_3$): δ 109.6 (m, P). **^{11}B-NMR** (128.4 MHz, $CDCl_3$): δ -39.4 (m, BH_3). **IR** (neat, ATR probe, cm^{-1}): v 3063, 2357, 1574, 1437, 1392, 1261, 1234, 1114, 1083, 1050, 910, 808. **Mp** = 164-165 °C (decomposition). **HRMS** (ESI positive) = [$C_{22}H_{20}BONaP^{+}$] Calculated mass: 365.1243 g/mol, found mass: 365.1244 g/mol.

1.4 Synthesis of the mono migration adduct **38a-p**

General procedure

In the glove box, to Schlenk equipped with a stirrer were added the phosphinite/phosphine borane complex (0.25 mmol, 1 eq), $B(C_6F_5)_3$ (46 mg, 0.09 mmol, 0.36 eq) and fluorobenzene (1 mL, [phosphinite borane] = 0.5 mol/L). The mixture was warmed at 140°C under stirring for 1h. After the completion of the reaction, the solvent was removed in vaccuo and the resulting crude mixture was purified by flash chromatography on silica gel affording the corresponding C_6F_5 mono-migration adduct.

Phenyl diphenylphosphinite pentafluorophenylborane 31 = **38a**

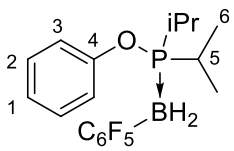

Chemical Formula: $C_{18}H_{21}BF_5OP$
Molecular Weight: 390.14

38a as a colourless oil (73 mg, 187 µmol, 75 %), Phenyl diphenylphosphinite borane (56 mg, 250 µmol, 1.0 eq) and $B(C_6F_5)_3$ (46 mg, 90 µmol, 0.36 eq).

Eluent: Cyclohexane, **Rf** = 0.35. **^{1}H-NMR** (400.1 MHz, $CDCl_3$): δ 7.29-7.25 (m, 2H, H-Ar), 7.15-7.11 (m, 1H, H-Ar), 7.08-7.06 (m, 2H, H-Ar), 2.46-2.37 (m, 2H, H-5), 2.28-1.81 (m, 2H, BH_2), 1.35-1.23 (m, 12H, H-6). **^{13}C-NMR** (100.6 MHz, $CDCl_3$): δ 152.8 (d, *J* = 8.2 Hz, C-Ar), 129.6 (s, C-Ar), 124.9 (s, C-Ar), 121.0 (d, *J* = 2.9 Hz, C-Ar), 26.8 (d, *J* = 33.9 Hz, C-5), 16.3 (d, *J* = 29.6 Hz, C-6). **^{31}P{^{1}H}-NMR** (162.0 MHz, $CDCl_3$): δ 127.1 (m, P). **^{11}B{^{1}H}-NMR** (128.4 MHz, $CDCl_3$): δ -35.7 (d, *J* = 65.5 Hz, BH_2). **^{19}F-NMR** (376.4 MHz, $CDCl_3$) δ -128.2 (d, *J* = 21.3 Hz, F_{ortho}), -159.8 (td, *J* = 20.2, 6.2 Hz, F_{para}), -164.5 (td, *J* = 24.2, 9.6 Hz, F_{meta}). **IR** (neat, ATR probe, cm^{-1}): v 2971 (CH sp^3), 2937, 2880, 2394, 1642, 1592, 1509, 1489, 1465, 1203, 1092, 1024 (C-P), 997, 889. **HRMS** (ESI positive) = [$C_{18}H_{21}BOF_5NaP^+$] Calculated mass: 413.1241 g/mol, found mass: 413.1248 g/mol.

Phenyl diphenylphosphinite pentafluorophenylborane 38b

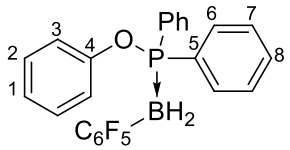

Chemical Formula: $C_{24}H_{17}BF_5OP$
Molecular Weight: 458.17

38b as a colourless oil (97 mg, 212 µmol, 85 %), Phenyl diphenylphosphinite borane (73 mg, 250 µmol, 1.0 eq) and $B(C_6F_5)_3$ (46 mg, 90 µmol, 0.36 eq).

Eluent: toluene/petroleum ether (1:1), **Rf** = 0.80. **^{1}H-NMR** (400.1 MHz, $CDCl_3$): δ 7.80-7.77 (m, 4H, H-Ar), 7.60-7.56 (m, 2H, H-Ar), 7.51-7.47 (m, 4H, H-Ar), 7.21-7.17 (m, 2H, H-Ar), 7.10-7.06 (m, 1H, H-Ar), 6.95-6.93 (m, 2H, H-Ar), 2.89-2.28 (m, 2H, BH_2). **^{13}C-NMR** (100.6 MHz, $CDCl_3$): δ 152.0 (d, *J* = 6.7 Hz, C-Ar), 132.7 (d, *J* = 2.4 Hz, C-Ar), 131.8 (d, *J* = 10.9 Hz, C-Ar), 129.5 (s, C-Ar), 129.4 (d, *J* = 63.4 Hz, C-Ar), 128.9 (d, *J* = 10.6 Hz, C-Ar), 124.8 (s, C-Ar), 120.5 (d, *J* = 4.5 Hz, C-Ar). **^{31}P{^{1}H}-NMR** (162.0 MHz, $CDCl_3$): δ 95.4 (d, *J* = 76.1 Hz, P). **^{11}B{^{1}H}-NMR** (128.4 MHz,

$CDCl_3$): δ -32.2 (d, *J* = 57.2 Hz, BH_2). **^{19}F NMR** (376.4 MHz, $CDCl_3$): δ -128.3 (d, *J* = 22.7 Hz, F_{ortho}), -159.5 (td, *J* = 20.3 Hz, 6.8 Hz, F_{meta}), -164.8 (td, *J* = 23.6 Hz, 9.7 Hz, F_{para}). **IR** (neat, ATR probe, cm^{-1}): v 3064, 2384, 1591, 1509, 1489, 1467, 1438, 1197, 1110, 1091, 995. **HRMS** (ESI positive) = [$C_{24}H_{17}BOF_5NaP^+$] Calculated mass: 481.0928 g/mol, found mass: 481.0929 g/mol.

3-methylphenyl diisopropylphosphinite pentafluorophenylborane 38c

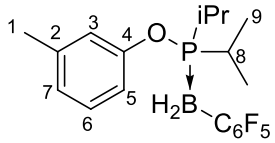

Chemical Formula: $C_{19}H_{23}BF_5OP$
Molecular Weight: 404.16

38c as a colourless oil (78 mg, 193 µmol, 77 %), 3-methylphenyl diphenylphosphinite borane (60 mg, 250 µmol, 1.0 eq) and $B(C_6F_5)_3$ (46 mg, 90 µmol, 0.36 eq).

Eluent: toluene/ petroleum ether (1:9), **Rf** = 0.35. **^{1}H-NMR** (400.1 MHz, $CDCl_3$): δ 7.69 (s, 1H, H-Ar), 7.57-7.53 (m, 1H, H-Ar), 7.36-7.34 (m, 1H, H-Ar), 7.30-7.28 (m, 1H, H-Ar), 2.89-2.78 (m, 2H, H-8), 2.73 (s, 3H, H-1), 2.48-2.05 (m, 2H, BH_2), 1.79-1.67 (m, 12H, H-9). **^{13}C-NMR** (100.6 MHz, $CDCl_3$): δ 152.7 (d, *J* = 8.2 Hz, C-Ar), 139.9 (s, C-Ar), 129.2 (s, C-Ar), 125.7 (s, C-Ar), 121.5 (d, *J* = 2.9 Hz, C-Ar), 117.8 (d, *J* = 2.9 Hz, C-Ar), 26.8 (d, *J* = 34.1 Hz, C-8), 21.4 (s, C-1), 16.3 (d, *J* = 21.4 Hz, C-9). **^{31}P{^{1}H}-NMR** (162.0 MHz, $CDCl_3$): δ 126.5 (m, P). **^{11}B{^{1}H}-NMR** (128.4 MHz, $CDCl_3$): δ -35.7 (d, *J* = 60.5 Hz, BH_2). **^{19}F-NMR** (376.4 MHz, $CDCl_3$) δ -128.2 (d, *J* = 17.7 Hz, F_{ortho}), -160.0 (td, *J* = 20.1, 5.0 Hz, F_{para}), [-164.6 – (-164.7)] (m, F_{meta}). **IR** (neat, ATR probe, cm^{-1}): v 2974, 2939, 2392, 1586, 1488, 1509, 1465, 1245, 1148, 1092 (C-P), 994, 952, 889, 829, 780. **HRMS** (ESI positive) = [$C_{19}H_{23}BOF_5NaP^+$] Calculated mass: 427.1397 g/mol, found mass: 427.1398 g/mol.

3-methylphenyl diphenylphosphinite pentafluorophenylborane 38d

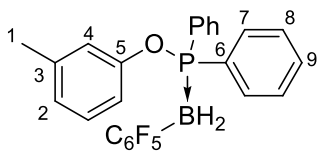

Chemical Formula: $C_{25}H_{19}BF_5OP$
Molecular Weight: 472.19

38d as a white solid (109 mg, 231 µmol, 93 %), 3-methylphenyl diphenylphosphinite borane (77 mg, 250 µmol, 1.0 eq) and $B(C_6F_5)_3$ (46 mg, 90 µmol, 0.36 eq).

Eluent: toluene/petroleum ether (3:7), **Rf** = 0.42. **^{1}H-NMR** (400.1 MHz, $CDCl_3$): δ 7.80-7.75 (m, 4H, H-Ar), 7.60-7.56 (m, 2H, H-Ar), 7.51-7.47 (m, 4H, H-Ar), 7.06-7.02 (m, 2H, H-Ar), 6.89-6.87 (m, 1H, H-Ar), 6.71-6.69 (m, 1H, H-Ar), 2.84-2.44 (m, 2H, BH_2), 2.23 (s, 3H, H-1). **^{13}C-NMR** (100.6 MHz, $CDCl_3$): δ 151.8 (s, C-Ar), 139.8 (s, C-Ar), 132.6 (d, *J* = 2.4 Hz, C-Ar), 131.8 (d, *J* = 10.8 Hz, C-Ar), 129.7 (d, *J* = 63.8 Hz, C-Ar), 129.1 (s, C-Ar), 128.8 (d, *J* = 10.6 Hz, C-Ar), 125.6 (s, C-Ar), 121.2 (s, C-Ar), 117.3 (d, *J* = 4.4 Hz, C-Ar), 21.2 (s, C-1). **^{31}P{^{1}H}-NMR** (162.0 MHz, $CDCl_3$): δ

95.0 (m, P). **$^{11}B\{^1H\}$-NMR** (128.4 MHz, $CDCl_3$): δ -32.3 (d, *J* = 61.3 Hz, BH_2). **^{19}F NMR** (376.4 MHz, $CDCl_3$): δ -128.2 (d, *J* = 22.5 Hz, F_{ortho}), -159.7 (td, *J* = 20.3 Hz, 6.8 Hz, F_{meta}), -164.9 (td, *J* = 23.6 Hz, 9.6 Hz, F_{para}). **Mp** = 82-83°C. **IR** (neat, ATR probe, cm^{-1}): v 3067, 2417, 1509, 1471, 1438, 1247, 1144, 1113, 1089, 996, 955, 916. **HRMS** (ESI positive) = $[C_{25}H_{19}BOF_5NaP^+]$ Calculated mass: 495.1084 g/mol, found mass: 495.1090 g/mol.

4-Methoxyphenyl diisopropylphosphinite pentafluorophenylborane 38e

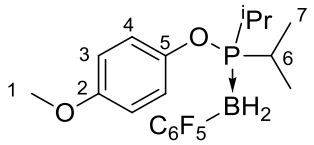

Chemical Formula: $C_{19}H_{23}BF_5O_2P$
Molecular Weight: 420.16

38e as a colourless oil (92 mg, 219 µmol, 88 %), 4-methoxyphenyl diphenylphosphinite borane (64 mg, 250 µmol, 1.0 eq) and $B(C_6F_5)_3$ (46 mg, 90 µmol, 0.36 eq).

Eluent: cyclohexane / toluene (8:2), **Rf** = 0.25. **^{1}H-NMR** (400.1 MHz, $CDCl_3$): δ 6.99-6.96 (m, 2H, H-Ar), 6.77-6.75 (m, 2H, H-Ar), 3.77 (s, 3H, H-1), 2.43-2.34 (m, 2H, H-6), 2.21-1.76 (m, 2H, BH_2), 1.35-1.22 (m, 12H, H-7). **^{13}C-NMR** (100.6 MHz, $CDCl_3$): δ 156.6 (s, C-Ar), 146.4 (d, *J* = 8.2 Hz, C-Ar), 121.8 (d, *J* = 2.8 Hz, C-Ar), 114.5 (s, C-Ar), 55.8 (s, C-1), 26.6 (d, *J* = 34.0 Hz, C-6), 16.4 (s, C-7), 16.1 (d, *J* = 2.1 Hz, C-7'). **$^{31}P\{^1H\}$-NMR** (162.0 MHz, $CDCl_3$): δ 126.8 (m, P). **$^{11}B\{^1H\}$-NMR** (128.4 MHz, $CDCl_3$): δ -35.9 (d, *J* = 62.7 Hz, BH_2). **^{19}F NMR** (376.4 MHz, $CDCl_3$): δ -128.1 (d, *J* = 22.3 Hz, F_{ortho}), -159.9 (td, *J* = 20.3, 6.4 Hz, F_{para}), -164.6 (td, *J* = 24.0, 9.7 Hz, F_{meta}). **IR** (neat, ATR probe, cm^{-1}): v 2971 (CH sp^3), 2940, 2391, 1642, 1511, 1464, 1250, 1197, 1091, 1034 (C-P), 996, 925, 887. **HRMS** (ESI positive) = $[C_{19}H_{23}BO_2F_5NaP^+]$ Calculated mass: 443.1347 g/mol, found mass: 443.1348 g/mol.

4-Methoxyphenyl diphenylphosphinite pentafluorophenylborane 38f

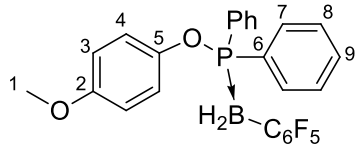

Chemical Formula: $C_{25}H_{19}BF_5O_2P$
Molecular Weight: 488.19

38f as a white solid (113 mg, 232 µmol, 93 %), 4-Methoxyphenyl diphenylphosphinite borane (81 mg, 250 µmol, 1.0 eq) and $B(C_6F_5)_3$ (46 mg, 90 µmol, 0.36 eq).

Eluent: toluene/petroleum ether (3:7), **Rf** = 0.39. **^{1}H-NMR** (400.1 MHz, $CDCl_3$): δ 7.78-7.74 (m, 4H, H-Ar), 7.60-7.56 (m, 2H, H-Ar), 7.51-7.47 (m, 4H, H-Ar), 6.85-6.83 (m, 2H, H-Ar), 6.69-6.67 (m, 2H, H-Ar), 3.73 (s, H-1), 2.72-2.31 (m, 2H, BH_2). **^{13}C-NMR** (100.6 MHz, $CDCl_3$): δ 156.5 (s, C-Ar), 145.5 (d, *J* = 6.8 Hz, C-Ar), 132.6 (d, *J* = 2.3 Hz, C-Ar), 131.9 (d, *J* = 10.8 Hz, C-Ar), 129.4 (d, *J* = 63.4 Hz, C-Ar), 128.8 (d, *J* = 10.6 Hz, C-Ar), 121.4 (d, *J* = 4.2 Hz, C-Ar), 114.4 (s, C-Ar), 55.6 (s, C-1). **$^{31}P\{^1H\}$-NMR** (162.0 MHz, $CDCl_3$): δ 96.1 (m, P). **$^{11}B\{^1H\}$-NMR** (128.4 MHz, $CDCl_3$): δ -32.0 (m, BH_2). **^{19}F NMR** (376.4 MHz, $CDCl_3$): δ -128.2 (d, *J* = 23.0 Hz, F_{ortho}), -159.7 (td, *J* =

20.3 Hz, 6.7 Hz, F_{meta}), -164.9 (td, *J* = 23.7 Hz, 9.6 Hz, F_{para}). **Mp** = 104-105°C. **IR** (neat, ATR probe, cm^{-1}): v 3064, 2955, 2402, 1503, 1469, 1438, 1194, 1182, 1094, 1029, 1009, 923. **HRMS** (ESI positive) = [$C_{25}H_{19}BO_2F_5NaP^+$] Calculated mass: 511.1034 g/mol, found mass: 511.1033 g/mol.

4-Chlorophenyl diisopropylphosphinite pentafluorophenylborane 38g

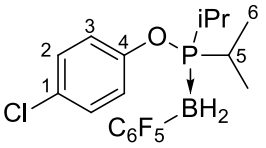

Chemical Formula: $C_{18}H_{20}BClF_5OP$
Molecular Weight: 424.58

38g as transparent crystals (93 mg, 218 µmol, 87 %), 4-chlorophenyl diphenylphosphinite borane (65 mg, 250 µmol, 1.0 eq) and $B(C_6F_5)_3$ (46 mg, 90 µmol, 0.36 eq). Recrystallized from hexane/CH_2Cl_2. **^{1}H-NMR** (400.1 MHz, $CDCl_3$): δ 7.25-7.23 (m, 2H, H-3), 7.05-7.03 (m, 2H, H-2), 2.43-2.34 (m, 2H, H-5), 2.06-1.52 (m, 2H, BH_2), 1.34-1.21 (m, 12H, H-6). **^{13}C-NMR** (100.6 MHz, $CDCl_3$): δ 151.4 (d, *J* = 8.1 Hz, C-Ar), 130.3 (s, C-Ar), 129.6 (s, C-Ar), 122.3 (d, *J* = 2.9 Hz, C-Ar), 26.7 (d, *J* = 33.6 Hz, C-5), 16.4 (s, C-6), 16.0 (d, *J* = 2.4 Hz, C-6). **^{31}P{^{1}H}-NMR** (162.0 MHz, $CDCl_3$): δ 129.3 (m, P). **^{11}B{^{1}H}-NMR** (128.4 MHz, $CDCl_3$): δ -35.7 (d, *J* = 61.7 Hz, BH_2). **^{19}F NMR** (376.4 MHz, $CDCl_3$): δ -128.2 (d, *J* = 22.3 Hz, F_{ortho}), -159.9 (td, *J* = 20.2 Hz, 6.4 Hz, F_{para}), -164.6 (td, *J* = 24.0, 9.6 Hz, F_{meta}). **Mp** = 91-92 °C. **IR** (neat, ATR probe, cm^{-1}): v 2977, 2420, 2378, 1510, 1485, 1421, 1402, 1391, 1211, 1089, 997, 907. **HRMS** (ESI positive) = [$C_{18}H_{20}BOF_5NaPCl^+$] Calculated mass: 447.0851 g/mol, found mass: 447.0850 g/mol.

4-Methoxyphenyl diphenylphosphinite pentafluorophenylborane 38h

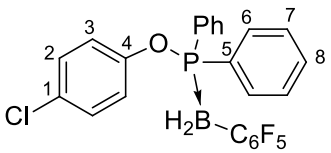

Chemical Formula: $C_{24}H_{16}BClF_5OP$
Molecular Weight: 492.61

38h as a white solid (111 mg, 225 µmol, 90 %), 4-Chlorophenyl diphenylphosphinite borane (82 mg, 250 µmol, 1.0 eq) and $B(C_6F_5)_3$ (46 mg, 90 µmol, 0.36 eq). Eluent: toluene/petroleum ether (3:7), **Rf** = 0.50. **^{1}H-NMR** (400.1 MHz, $CDCl_3$): δ 7.77-7.72 (m, 4H, H-Ar), 7.61-7.57 (m, 2H, H-Ar), 7.52-7.47 (m, 4H, H-Ar), 7.17-7.15 (m, 2H, H-Ar), 6.91-6.89 (m, 2H, H-Ar), 2.86-2.24 (m, 2H, BH_2). **^{13}C-NMR** (100.6 MHz, $CDCl_3$): δ 150.4 (d, *J* = 6.7 Hz, C-Ar), 132.9 (d, *J* = 2.3 Hz, C-Ar), 131.9 (d, *J* = 10.9 Hz, C-Ar), 130.2 (s, C-Ar), 129.5 (s, C-Ar), 129.0 (d, *J* = 10.7 Hz, C-Ar), 128.8 (d, *J* = 61.5 Hz, C-Ar), 121.9 (d, *J* = 4.4 Hz, C-Ar). **^{31}P{^{1}H}-NMR** (162.0 MHz, $CDCl_3$): δ 97.8 (m, P). **^{11}B{^{1}H}-NMR** (128.4 MHz, $CDCl_3$): δ -32.3 (d, *J* = 82.9 Hz, BH_2). **^{19}F NMR** (376.4 MHz, $CDCl_3$): δ -128.4 (d, *J* = 22.7 Hz, F_{ortho}), -159.1 (td, *J* = 20.3 Hz, 6.9 Hz, F_{meta}), -164.6 (td, *J* = 23.7 Hz, 9.6 Hz, F_{para}). **Mp** = 81-82°C. **IR** (neat, ATR probe, cm^{-1}): v 3059, 2923, 2386, 1511, 1489, 1467, 1434, 1207, 1109, 1089, 996, 921. **HRMS** (ESI positive) = [$C_{24}H_{16}BOF_5NaPCl^+$] Calculated mass: 515.0538 g/mol, found mass: 515.0544 g/mol.

2,6-dimethylphenyl diisopropylphosphinite pentafluorophenylborane 38i

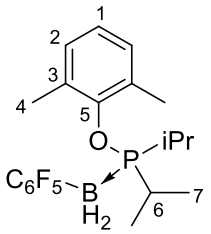

Chemical Formula: $C_{20}H_{25}BF_5OP$
Molecular Weight: 418.19

38i as an off-white solid (89 mg, 213 µmol, 85 %), 2,6-dimethylphenyl diphenylphosphinite borane (63 mg, 250 µmol, 1.0 eq) and $B(C_6F_5)_3$ (46 mg, 90 µmol, 0.36 eq).

Eluent: toluene/ petroleum ether (1:9), **Rf** = 0.35. **^{1}H-NMR** (400.1 MHz, $CDCl_3$): δ 6.89-6.86 (m, 3H, H-Ar), 2.81-2.71 (m, 2H, H-6), 2.19 (s, 3H, H-4), 2.08-1.57 (m, 2H, BH_2), 1.49-1.39 (m, 12H, H-7). **^{13}C-NMR** (100.6 MHz, $CDCl_3$): δ 151.2 (d, *J* = 8.6 Hz, C-Ar), 129.9 (d, *J* = 2.2 Hz, C-Ar), 129.3 (s, C-Ar), 125.0 (s, C-Ar), 29.7 (d, *J* = 32.6 Hz, C-6), 18.1 (s, C-4), 17.5 (s, C-4'), 17.1 (d, *J* = 4.5 Hz, C-7). **^{31}P{^{1}H}-NMR** (162.0 MHz, $CDCl_3$): δ 124.4 (m, P). **^{11}B{^{1}H}-NMR** (128.4 MHz, $CDCl_3$): δ -34.4 (d, *J* = 67.4 Hz, BH_2). **^{19}F NMR** (376.4 MHz, $CDCl_3$) δ -128.1 (d, *J* = 22.8 Hz, F_{ortho}), -160.4 (td, *J* = 20.3, 6.1 Hz, F_{para}), [-164.9 – (-165.0) (m, F_{meta}). **Mp** = 127-128°C. **IR** (neat, ATR probe, cm^{-1}): v 2920 (CH sp^3), 2510, 1466, 1375, 1277, 1166, 1090, 1063, 1042 (C-P), 995, 925, 905, 891. **HRMS** (ESI positive) = [$C_{20}H_{25}BOF_5NaP^+$] Calculated mass: 441.1554 g/mol, found mass: 441.1559 g/mol.

2,6-Dimethylphenyl diphenylphosphinite pentafluorophenylborane 38j

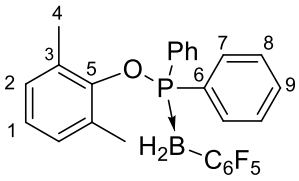

Chemical Formula: $C_{26}H_{21}BF_5OP$
Molecular Weight: 486.22

38j as a white solid (108 mg, 223 µmol, 89 %), 2,6-Dimethylphenyl diphenylphosphinite borane (80 mg, 250 µmol, 1.0 eq) and $B(C_6F_5)_3$ (46 mg, 90 µmol, 0.36 eq).

Recrystallized from a solution of **38j** in CH_2Cl_2/*n*-pentane. Eluent: toluene/petroleum ether (3:7), **Rf** = 0.54. **^{1}H-NMR** (400.1 MHz, $CDCl_3$): δ 7.96-7.92 (m, 4H, H-Ar), 7.54-7.47 (m, 6H, H-Ar), 6.92-6.89 (m, 1H, H-Ar), 6.83-6.82 (m, 2H, H-Ar), 2.79-2.32 (m, 2H, BH_2), 1.88 (s, H-4). **^{13}C-NMR** (100.6 MHz, $CDCl_3$): δ 151.1 (s, C-Ar), 132.5 (s, C-Ar), 132.1 (d, *J* = 2.4 Hz, C-Ar), 131.8 (s, C-Ar), 131.0 (d, *J* = 10.6 Hz, C-Ar), 130.2 (s, C-Ar), 128.9 (s, C-Ar), 128.7 (d, *J* = 10.7 Hz, C-Ar), 125.3 (s, C-Ar), 18.6 (s, C-4). **^{31}P{^{1}H}-NMR** (162.0 MHz, $CDCl_3$): δ 88.5 (m, P). **^{11}B{^{1}H}-NMR** (128.4 MHz, $CDCl_3$): δ -33.0 (d, *J* = 61.3 Hz, BH_2). **^{19}F NMR** (376.4 MHz, $CDCl_3$): δ -126.9 (d, *J* = 22.2 Hz, F_{ortho}), -159.9 (td, *J* = 20.3 Hz, 6.6 Hz, F_{meta}), -165.0 (td, *J* = 23.6 Hz, 9.5 Hz, F_{para}). **Mp** = 158-159°C. **IR** (neat, ATR probe, cm^{-1}): v 3058, 2924, 2373, 1511, 1468, 1438, 1377, 1160, 1095, 984, 921, 892. **HRMS** (ESI positive) = [$C_{26}H_{21}BOF_5NaP^+$] Calculated mass: 509.1241 g/mol, found mass: 509.1240 g/mol.

1-Naphtyl diphenylphosphinite pentafluorophenylborane 38k

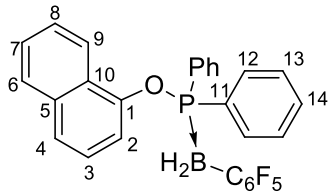

Chemical Formula: $C_{28}H_{19}BF_5OP$
Molecular Weight: 508.23

38k as a white solid (98 mg, 232 µmol, 77 %), 1-Naphtyl diphenylphosphinite borane (86 mg, 250 µmol, 1.0 eq) and $B(C_6F_5)_3$ (46 mg, 90 µmol, 0.36 eq).

Eluent: toluene/petroleum ether (3:7), **Rf** = 0.45. **^{1}H-NMR** (400.1 MHz, $CDCl_3$): δ 7.98-7.96 (m, 1H, H-Ar), 7.93-7.98 (m, 4H, H-Ar), 7.81-7.79 (m, 1H, H-Ar), 7.62-7.57 (m, 2H, H-Ar), 7.55-7.50 (m, 4H, H-Ar), 7.48-7.46 (m, 1H, H-Ar), 7.44-7.42 (m, 1H, H-Ar), 7.21-7.17 (m, 1H, H-Ar), 7.01-6.99 (m, 1H, H-Ar), 2.95-2.20 (m, 2H, BH_2). **^{13}C-NMR** (100.6 MHz, $CDCl_3$): δ 148.2 (d, *J* = 6.7 Hz, C-Ar), 134.6 (s, C-Ar), 132.7 (d, *J* = 2.4 Hz, C-Ar), 131.6 (d, *J* = 10.9 Hz, C-Ar), 130.00 (d, *J* = 63.0 Hz, C-Ar), 129.0 (d, *J* = 10.7 Hz, C-Ar), 127.8 (s, C-Ar), 126.8 (d, *J* = 4.6 Hz, C-Ar), 126.4 (d, *J* = 39.9 Hz, C-Ar), 124.9 (d, *J* = 21.5 Hz, C-Ar), 121.2 (s, C-Ar), 114.7 (d, *J* = 4.9 Hz, C-Ar). **^{31}P{^{1}H}-NMR** (162.0 MHz, $CDCl_3$): δ 95.4 (m, P). **^{11}B{^{1}H}-NMR** (128.4 MHz, $CDCl_3$): δ -32.1 (m, BH_2). **^{19}F NMR** (376.4 MHz, $CDCl_3$): δ -128.4 (d, *J* = 22.8 Hz, F_{ortho}), -159.7 (td, *J* = 20.3 Hz, 6.9 Hz, F_{meta}), -164.8 (td, *J* = 23.5 Hz, 9.6 Hz, F_{para}). **Mp** = 119-120°C. **IR** (neat, ATR probe, cm^{-1}): v 3059, 2923, 2386, 1511, 1489, 1467, 1434, 1207, 1109, 1089, 996, 921. **HRMS** (ESI positive) = $[C_{28}H_{19}BOF_5NaP^+]$ Calculated mass: 531.1084 g/mol, found mass: 531.1091 g/mol.

Triphenylphosphine pentafluorophenylborane 38l

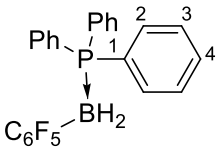

Chemical Formula: $C_{24}H_{17}BF_5P$
Molecular Weight: 442.17

38l as a white solid (95 mg, 215 µmol, 86 %), triphenylphosphine borane (69 mg, 250 µmol, 1.0 eq) and $B(C_6F_5)_3$ (46 mg, 90 µmol, 0.36 eq).

Eluent: toluene/petroleum ether (3:7), **Rf** = 0.52. **^{1}H-NMR** (400.1 MHz, $CDCl_3$): δ 7.54-7.50 (m, 9H, H-Ar), 7.46-7.41 (m, 6H, H-Ar), 3.07-2.33 (m, 2H, BH_2). **^{13}C-NMR** (100.6 MHz, $CDCl_3$): δ 133.4 (d, *J* = 9.1 Hz, C-Ar), 131.7 (d, *J* = 2.5 Hz, C-Ar), 128.9 (d, *J* = 10.3 Hz, C-Ar), 127.0 (d, *J* = 58.4 Hz, C-Ar). **^{31}P{^{1}H}-NMR** (162.0 MHz, $CDCl_3$): δ 13.0 (m, P). **^{11}B{^{1}H}-NMR** (128.4 MHz, $CDCl_3$): δ -31.2 (m, BH_2). **^{19}F NMR** (376.4 MHz, $CDCl_3$): δ -128.1(d, *J* = 22.3 Hz, F_{ortho}), -159.5 (td, *J* = 20.3 Hz, 6.9 Hz, F_{meta}), -164.7 (td, *J* = 23.7 Hz, 9.8 Hz, F_{para}). **Mp** = 111-112°C. **IR** (neat, ATR probe, cm^{-1}): v 3068, 2395, 1511, 1469, 1435, 1103, 1089, 1019, 998, 907, 889. **HRMS** (ESI positive) = $[C_{24}H_{17}BF_5NaP^+]$ Calculated mass: 465.0979 g/mol, found mass: 465.0984 g/mol.

Ethyldiphenylphosphine pentafluorophenylborane 38m

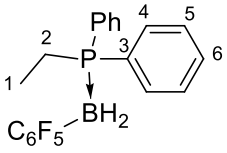

Chemical Formula: $C_{20}H_{17}BF_5P$
Molecular Weight: 394.13

38m as a white solid (82 mg, 207 µmol, 83 %), Ethyldiphenylphosphine borane (57 mg, 250 µmol, 1.0 eq) and $B(C_6F_5)_3$ (46 mg, 90 µmol, 0.36 eq). *Synthesis done on 2 mmol scale: yield = 92%.*

Eluent: toluene/petroleum ether (1:9), **Rf** = 0.28. **^{1}H-NMR** (400.1 MHz, $CDCl_3$): δ 7.54-7.50 (m, 6H, H-Ar), 7.44-7.43 (m, 4H, H-Ar), 2.68-2.15 (m, 2H, BH_2), 2.24 (td, *J* = 15.1 Hz, 7.5 Hz, 2H, H-2), 1.12 (dt, *J* = 16.9 Hz, 7.5 Hz, 3H, H-1). **^{13}C-NMR** (100.6 MHz, $CDCl_3$): 132.5 (d, *J* = 8.3 Hz, C-Ar), 131.6 (d, *J* = 2.5 Hz, C-Ar), 128.8 (d, *J* = 9.9 Hz, C-Ar), 126.9 (d, *J* = 56.5 Hz, C-Ar), 16.9 (d, *J* = 36.8 Hz, C-2), 6.7 (s, C-1). **^{31}P{^{1}H}-NMR** (162.0 MHz, $CDCl_3$): δ 12.6 (d, *J* = 81.3 Hz, P). **^{11}B{^{1}H}-NMR** (128.4 MHz, $CDCl_3$): δ -34.6 (d, *J* = 62.3 Hz, BH_2). **^{19}F NMR** (376.4 MHz, $CDCl_3$): δ -129.1 (d, *J* = 22.6 Hz, F_{ortho}), -159.7 (td, *J* = 20.2 Hz, 6.8 Hz, F_{meta}), -164.7 (td, *J* = 24.1 Hz, 9.8 Hz, F_{para}). **Mp** = 93-94°C. **IR** (neat, ATR probe, cm^{-1}): v 3065, 2925, 2359, 1640, 1509, 1469, 1436, 1090, 992, 965, 912. **HRMS** (ESI positive) = [$C_{20}H_{17}BF_5NaP^+$] Calculated mass: 417.0979 g/mol, found mass: 417.0985 g/mol.

Diethylphenylphosphine pentafluorophenylborane 38n

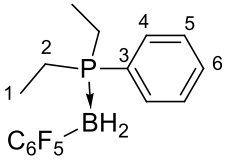

Chemical Formula: $C_{16}H_{17}BF_5P$
Molecular Weight: 346.08

38n as a colourless oil (67 mg, 193 µmol, 77 %), Diethylphenylphosphine borane (45 mg, 250 µmol, 1.0 eq) and $B(C_6F_5)_3$ (46 mg, 90 µmol, 0.36 eq). The product decomposes after 36h hours at r.t.

Eluent: toluene/petroleum ether (5:95), **Rf** = 0.32. **^{1}H-NMR** (400.1 MHz, $CDCl_3$): δ 7.65-7.61 (m, 2H, H-Ar), 7.53-7.46 (m, 3H, H-Ar), 2.45-1.80 (m, 2H, BH_2), 1.93-1.87 (m, 4H, H-2), 1.11-1.03 (m, 6H, H-1). **^{13}C-NMR** (100.6 MHz, $CDCl_3$): 131.8 (d, *J* = 7.6 Hz, C-Ar), 131.6 (d, *J* = 2.5 Hz, C-Ar), 129.0 (d, *J* = 9.6 Hz, C-Ar), 125.4 (d, *J* = 53.7 Hz, C-Ar), 15.8 (d, *J* = 36.4 Hz, C-2), 6.5 (d, *J* = 3.3 Hz, C-1). **^{31}P{^{1}H}-NMR** (162.0 MHz, $CDCl_3$): δ 12.0 (d, *J* = 85.2 Hz, P). **^{11}B{^{1}H}-NMR** (128.4 MHz, $CDCl_3$): δ -33.0 (d, *J* = 66.7 Hz, BH_2). **^{19}F NMR** (376.4 MHz, $CDCl_3$): δ -129.3 (d, *J* = 21.6 Hz, F_{ortho}), -159.8 (td, *J* = 20.2 Hz, 6.2 Hz, F_{meta}), -164.4 (td, *J* = 24.6 Hz, 9.8 Hz, F_{para}). **IR** (neat, ATR probe, cm^{-1}): v 2978, 2944, 2387, 1642, 1509, 1462, 1438, 1090, 990, 965, 887. **HRMS** (ESI positive): decomposition of the product.

Tri-*n*-butylphosphine pentafluorophenylborane 38o

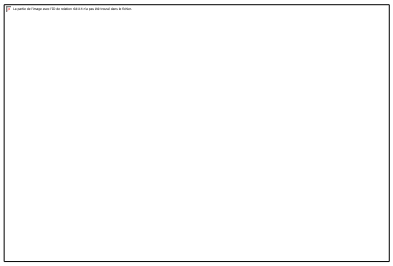

38o as a colourless oil (80 mg, 210 µmol, 84 %), tri-*n*-butylphosphine borane (54 mg, 250 µmol, 1.0 eq) and $B(C_6F_5)_3$ (46 mg, 90 µmol, 0.36 eq).

Eluent: toluene/petroleum ether (1:9), **Rf** = 0.65. **^{1}H-NMR** (400.1 MHz, $CDCl_3$): δ 1.92-1.61 (m, 2H, BH_2), 1.58-1.54 (m, 2H, H-4), 1.40-1.36 (m, 12H, H-2,3), 0.92 (t, *J* = 6.7 Hz, 9H, H-1). **^{13}C-NMR** (100.6 MHz, $CDCl_3$): 24.3 (d, *J* = 16.2 Hz, C-3), 24.3 (s, C-2), 20.7 (d, *J* = 34.3 Hz, C-4), 13.5 (s, C-1). **^{31}P{^{1}H}-NMR** (162.0 MHz, $CDCl_3$): δ 7.5 (d, *J* = 83.9 Hz, P). **^{11}B{^{1}H}-NMR** (128.4 MHz, $CDCl_3$): δ -34.5 (d, *J* = 62.4 Hz, BH_2). **^{19}F NMR** (376.4 MHz, $CDCl_3$): δ -129.9 (d, *J* = 23.5 Hz, F_{ortho}), -160.0 (td, *J* = 20.2 Hz, 6.5 Hz, F_{meta}), -164.4 (td, *J* = 24.6 Hz, 9.8 Hz, F_{para}). **IR** (neat, ATR probe, cm^{-1}): ν 2961, 2934, 2379, 1509, 1462, 1382, 1088, 994, 922, 887. **HRMS** (ESI positive) = [$C_{18}H_{29}BF_5NaP^+$] Calculated mass: 405.1918 g/mol, found mass: 405.1906 g/mol.

1.5 Synthesis of **39** via a double migration of the C_6F_5 moiety

Ethyldiphenylphosphine bis-pentafluorophenylborane 39

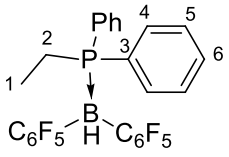

Chemical Formula: $C_{26}H_{16}BF_{10}P$
Molecular Weight: 560.17

In the glove box, to a schlenk equipped with a stirrer were placed **38m** (79 mg, 200 µmol, 1 eq), $B(C_6F_5)_3$ (37 mg, 72 µmol, 0.36 eq) and fluorobenzene (1 mL). The mixture was warmed at 140°C under stirring for 1h. After the completion of the reaction, the solvent was removed in vaccuo and the resulting crude mixture was purified by flash chromatrography on silica gel affording **39** as a white solid (84 mg, 150 µmol, 75%). Recrystallization from hexane/dichloromethane yielded colourless crystals suitable for X-rays diffraction.

Eluent: cyclohexane/ethyl acetate (95:5), **Rf** = 0.45. **^{1}H-NMR** (400.1 MHz, $CDCl_3$): δ 7.57-7.54 (m, H2, H-Ar), 7.45-7.40 (m, 8H, H-Ar), 4.09-3.60 (m, 1H, BH), 2.37-2.29 (m, 2H, H-2), 1.04-0.96 (m, 3H, H-1). **^{13}C-NMR** (100.6 MHz, $CDCl_3$): 132.8 (d, *J* = 7.8 Hz, C-Ar), 132.0 (s, C-Ar), 128.9 (d, *J* = 10.1 Hz, C-Ar), 125.0 (d, *J* = 58.6 Hz, C-Ar), 18.0 (d, *J* = 38.6 Hz, C-2), 7.19 (s, C-1). **^{31}P{^{1}H}-NMR** (162.0 MHz, $CDCl_3$): δ 10.4 (d, *J* = 54.9 Hz, P). **^{11}B{^{1}H}-NMR** (128.4 MHz, $CDCl_3$): δ -24.8 (s, BH_2). **^{19}F NMR** (376.4 MHz, $CDCl_3$): δ -128.5 (d, *J* = 20.7 Hz, F_{ortho}), -157.7 (t, *J* = 20.3 Hz, F_{meta}), -163.6 (td, *J* = 25.4 Hz, 9.8 Hz, F_{para}). **Mp** = 158-159°C. **IR** (neat, ATR probe, cm^{-1}): ν 2448, 1642, 1512, 1462, 1438, 1286, 1090, 1037, 963, 914. **HRMS** (ESI positive)**:** decomposition of the product

2. Crystallographic data

2,6-dimethylphenyl diisopropylphosphinite pentafluorophenylborane 38i

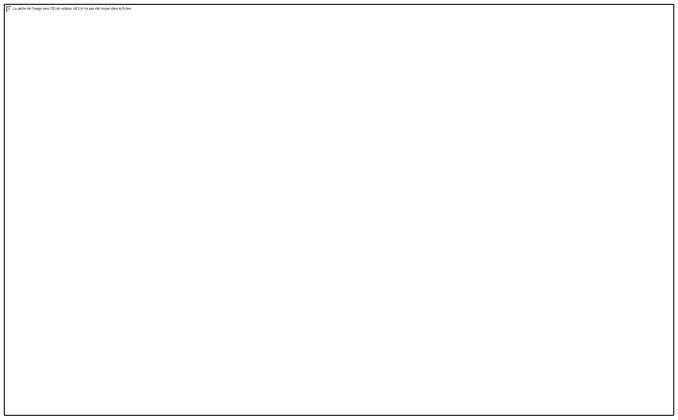

Single crystals of **38i** suitable for X-ray crystallographic analysis were obtained by recrystallization from a saturated solution of **38i** in *n*-pentane and diethyl ether. X-ray diffraction experiments for monocrystal of **38i** were performed at 294 K with graphite–monochromatized Mo K□ radiation (λ = 0.71073 Å) on a Bruker–Nonius Kappa CCD area detector diffractometer. Formula $C_{20}H_{25}BF_5OP$, formula weight 418.19, crystal system monoclinic, space group *P* 2_1, *a* = 10.6096(3) Å, *b* = 14.9685(4) Å, *c* = 13.5615(4) Å, α = γ = 90°, β = 109.7710(1)°, V = 2026.74 $Å^3$. Program(s) used to solve structure: SHELXS–97. Program(s) used to refine structure: SHELXL–2014. Software used to prepare material for publication: SHELXL–2014.

Ethyldiphenylphosphine bis-pentafluorophenylborane 39

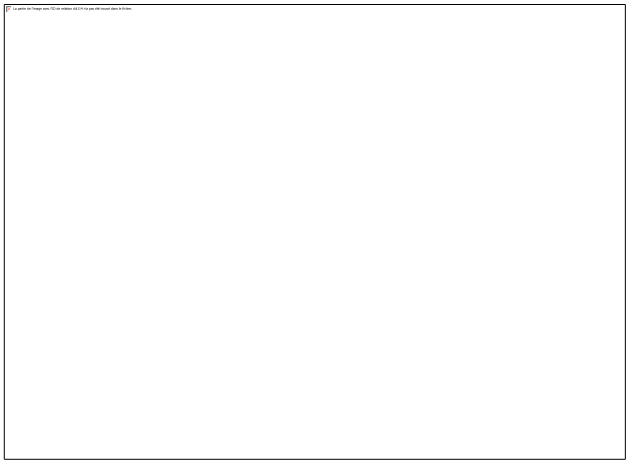

Single crystals of **39** suitable for X-ray crystallographic analysis were obtained by slow evaporation of a solution of **39** in a mixture CH_2Cl_2/heptane. X-ray diffraction experiments for monocrystal of **39** were performed at 294 K with graphite–monochromatized Mo K□ radiation (λ = 0.71073 Å) on a Bruker–Nonius Kappa CCD area detector diffractometer. Formula $C_{26}H_{16}BF_{10}P$, formula weight 560.16, crystal system orthorhombic, space group *P* -1, *a* = 8.7213(4) Å, *b* = 10.3460(5) Å, *c* = 14.3440(7) Å, α = 98.571(2)°, β = 101.045(2)°, γ = 111.937(2)°, V = 1143.2 $Å^3$. Program(s) used to solve structure: SHELXS–97. Program(s) used to refine structure: SHELXL–2014. Software used to prepare material for publication: SHELXL–2014.

3. Kinetic parameters

3.1 Determination of the second order rate constants of the reactions

Table S1. Kinetics of the reaction of **38m** with **41a** (CH_2Cl_2, 20°C, stopped-flow, detection at 586 nm)

[41a]	[38m]	[38m]/[41a]	k_{obs}
2.02×10^{-4}	5.07×10^{-3}	25	3.03×10^{-2}
2.02×10^{-4}	9.64×10^{-3}	48	7.05×10^{-2}
2.02×10^{-4}	1.60×10^{-2}	79	1.38×10^{-1}
2.02×10^{-4}	1.99×10^{-2}	99	1.80×10^{-1}
2.02×10^{-4}	2.54×10^{-2}	126	2.63×10^{-1}
k_2(20°C) = 1.02×10^{1} L mol^{-1} s^{-1}			

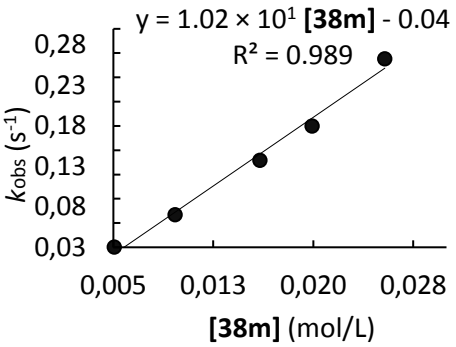

Table S2. Kinetics of the reaction of **38m** with **41b** (CH_2Cl_2, 20°C, stopped-flow, detection at 572 nm)

[41b]	[38m]	[38m]/[41b]	k_{obs}
8.00×10^{-5}	5.07×10^{-3}	64	3.12×10^{-2}
8.00×10^{-5}	9.64×10^{-3}	121	4.21×10^{-2}
8.00×10^{-5}	1.60×10^{-2}	200	5.68×10^{-2}
8.00×10^{-5}	1.99×10^{-2}	249	6.42×10^{-2}
8.00×10^{-5}	2.54×10^{-2}	317	7.91×10^{-2}
k_2(20°C) = 2.32 L mol^{-1} s^{-1}			

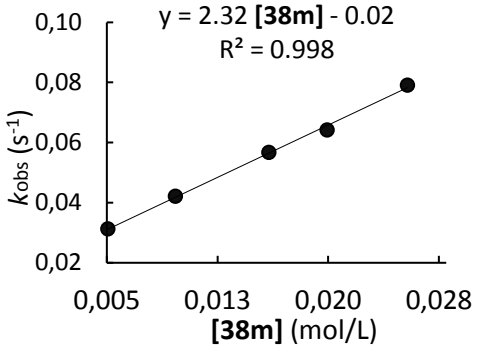

Table S3. Kinetics of the reaction of **38m** with **41c** (CH_2Cl_2, 20°C, stopped-flow, detection at 619 nm)

[41c]	[38m]	[38m]/[41c]	k_{obs}
8.49×10^{-5}	5.07×10^{-3}	60	1.19×10^{-3}
8.49×10^{-5}	9.64×10^{-3}	114	2.99×10^{-3}
8.49×10^{-5}	1.60×10^{-2}	188	7.06×10^{-3}
8.49×10^{-5}	1.99×10^{-2}	235	8.79×10^{-3}
8.49×10^{-5}	2.54×10^{-2}	299	1.09×10^{-2}
k_2(20°C) = 5.32×10^{-1} L mol^{-1} s^{-1}			

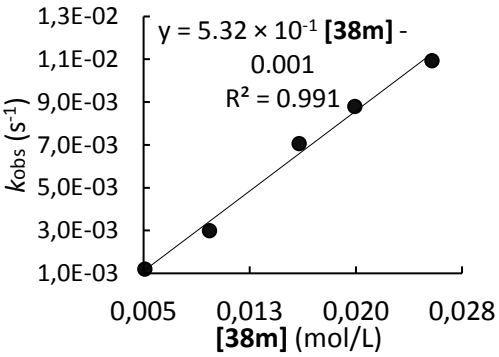

Table S10. Kinetics of the reaction of **38m** with **41d** (CH_2Cl_2, 20°C, stopped-flow, detection at 621 nm)

[41d]	[38m]	[38m]/[41d]	k_{obs}
5.38×10^{-5}	1.40×10^{-2}	259	2.09×10^{-3}
5.38×10^{-5}	1.60×10^{-2}	297	2.80×10^{-3}
5.38×10^{-5}	1.99×10^{-2}	370	4.60×10^{-3}
5.38×10^{-5}	2.54×10^{-2}	471	6.98×10^{-3}
5.38×10^{-5}	3.13×10^{-2}	582	9.01×10^{-3}

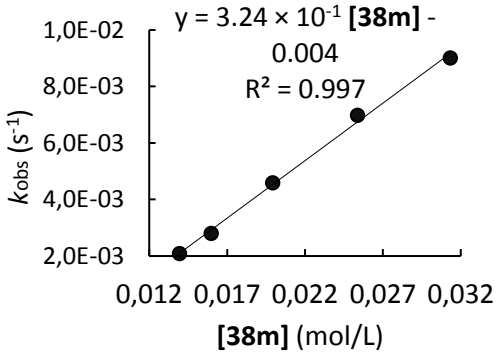

k_2(20°C) = 3.24 × 10^{-1} L mol^{-1} s^{-1}

Table S32. Calculation of the reactivity parameters *N* and s_N for **38m** using **41a-d** in CH_2Cl_2.

Electrophile	*E*	Log (k_2)
41a	-3.85	1.01
41b	-4.72	0.37
41c	-5.53	-0.27
41d	-5.89	-0.49
N = 5.20, s_N = 0.74.		

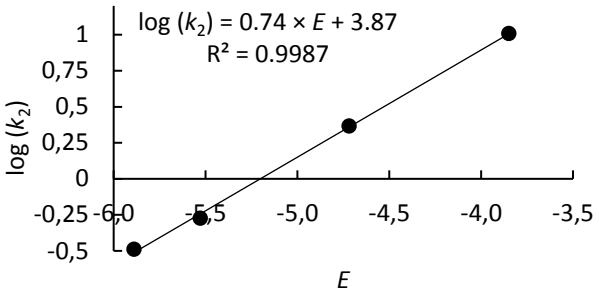

Table S10. Kinetics of the reaction of **39** with **41a** (CH_2Cl_2, 20°C, stopped-flow, detection at 586 nm)

[41a]	**[39]**	**[39]/[41a]**	k_{obs}
2.02 × 10^{-4}	2.86 × 10^{-3}	14	4.12 × 10^{-4}
2.02 × 10^{-4}	4.11 × 10^{-3}	20	1.23 × 10^{-3}
2.02 × 10^{-4}	5.89 × 10^{-3}	29	1.97 × 10^{-3}
2.02 × 10^{-4}	7.23 × 10^{-3}	36	2.88 × 10^{-3}
2.02 × 10^{-4}	9.21 × 10^{-3}	46	3.79 × 10^{-3}
k_2(20°C) = 5.42 × 10^{-1} L mol^{-1} s^{-1}			

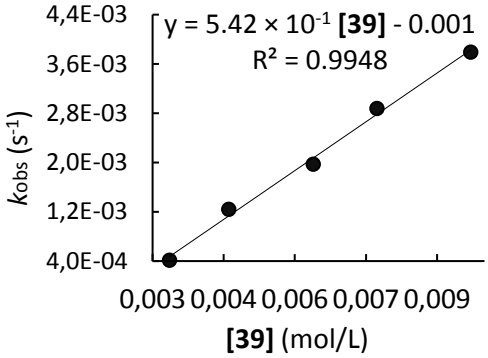

4. Details of the computational study

Calculations have been performed with Gaussian 16. First the geometries were optimized using DFT calculations with B3LYP, B3PW91, CAM-B3LYP, PW91 or LC-PW91 as functional and with 6-31++G(d,p) as basis set. The solvation was taken into account with the PCM model.

- Example of an optimization calculation of the hydride bridge H_3PBH_2-H-BH_3 **44**

```
%nprocshared=8
# opt SCRF=(PCM,solvent=fluorobenzene) freq LC-PW91PW91/6-31++g(d,p)

Title Card Required

0 1
 H    0.604409    1.164198    1.293457
 H   -1.223922   -0.037572    1.148797
 P   -0.790397    1.266961    1.428082
 H   -0.935437    1.337156    2.827303
 H   -1.186392    3.753549    0.922538
 B   -1.664722    2.740311    0.490009
 H   -2.847044    2.597634    0.605649
 H   -1.307573    2.739650   -0.718228
 B   -1.091437    1.736763   -1.706943
```

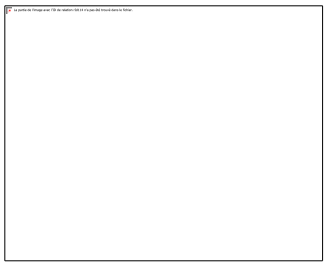

H	-1.819159	1.753486	-2.938743
H	-0.029480	1.636942	-2.246222
H	-1.269474	0.576978	-1.456033

- Example of a transition state calculation of **TS-52c-Y_2**

%nprocshared=8
%Mem=1000Mw
opt=(TS,noeigentest,calcFC,addredund) SCRF=(PCM,solvent=fluorobenzene) freq b3lyp/6-31++g(d,p)

Title Card Required

0 1

C	5.715320	-0.752073	2.874543
C	5.579480	-1.547514	1.752703
C	6.620989	-1.467780	0.846215
C	7.692576	-0.626276	1.006137
C	7.764127	0.169852	2.127844
C	6.770861	0.106095	3.074671
B	4.365000	-2.617701	1.643858
C	4.489646	-3.703458	2.817769
C	3.564242	-3.862271	3.823524
C	3.681105	-4.810457	4.815884
C	4.767488	-5.649670	4.826077
C	5.720147	-5.527476	3.842759
C	5.560900	-4.567329	2.872161
F	2.480171	-3.088613	3.879952
F	6.513038	-4.492262	1.941003
F	6.772930	-6.333632	3.840230
F	4.895423	-6.567941	5.770541
F	2.755960	-4.921123	5.759688
F	6.597192	-2.189214	-0.268879
F	8.657098	-0.568009	0.101072
F	8.787826	0.983775	2.294333
F	6.845032	0.858156	4.160734
F	4.783756	-0.789092	3.819037
B	3.876520	-0.257287	0.808853
P	2.869430	-1.077293	-0.600871
C	3.818551	-1.795201	-1.919686
C	1.554052	-2.188662	-0.167780
O	2.191142	0.254124	-1.192228
H	4.768747	0.400867	0.373471
H	3.231952	0.120003	1.730995
H	3.300973	-2.055800	1.794864
H	4.398420	-3.169205	0.568201
C	1.400089	0.116482	-2.339089
H	0.900627	-2.327095	-1.030911
H	1.965852	-3.151365	0.131495
H	0.983544	-1.770849	0.662385
H	3.153626	-2.087732	-2.733946
H	4.537413	-1.059400	-2.281775
H	4.357888	-2.671221	-1.560633
H	1.006643	1.090052	-2.627674
H	2.004407	-0.285926	-3.150747
H	0.573892	-0.561746	-2.130940

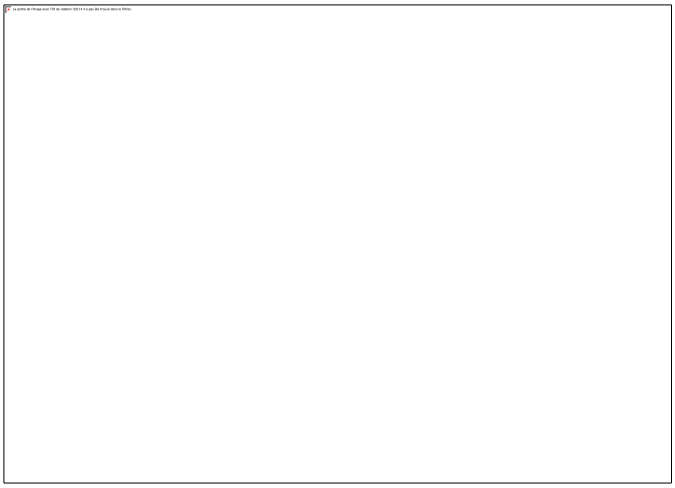

2 7 D

7 31 D
31 24 D
24 2 D

Chapter 5: Organic Lewis Acid-Catalyzed Regioselective Markovnikov Hydrophosphination of Styrene

1. Synthetic part

1.1. Synthesis of carbocations **22a,d,g**[1]

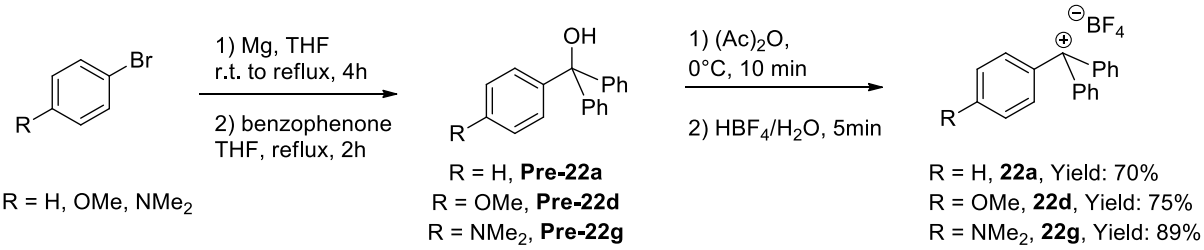

R = H, OMe, NMe_2

R = H, **Pre-22a**
R = OMe, **Pre-22d**
R = NMe_2, **Pre-22g**

R = H, **22a**, Yield: 70%
R = OMe, **22d**, Yield: 75%
R = NMe_2, **22g**, Yield: 89%

The synthesis of **Pre-22a,d,g** have been done following classical Grignard procedures.[2]

General procedure

The synthesis was done according to a procedure reported by Mayr et al. **Pre-22a,d,g** (3.5 mmol, 1 eq) was dissolved in acetic anhydride (5 mL) and the solution cooled to 0 °C. An ethereal solution of tetrafluoroboric acid (1.0 mL, 54 % w/v, 6.2 mmol) of was added dropwise and a red precipitate was immediately formed. After 5 minutes stirring at 0°C, 20 mL of CH_3CN were added and the azeotropic solvent-mixture was removed in vaccuo (reproduced 2 times). Then 20 mL of diethylether were added and the precipitate was filtered off, washed with diethyl ether, and dried in vacuum. **22a,d,g** were obtained as yellow to red solids which were not stable at room temperature and decomposed within several days (except for 86d which was stable even after months).

Triphenylmethylium tetrafluoroborate salt 22a

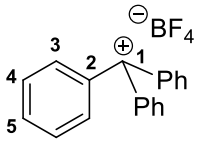

Chemical Formula: $C_{19}H_{15}BF_4$
Molecular Weight: 330.13

22a is obtained as a yellow solid (810 mg, 2.45 mmol, 70%). **^{1}H-NMR** (400.1 MHz, CD_3CN): δ 7.77-7.69 (m, 3H, H-5), 7.57-7.52 (m, 6H, H-3), 7.31-7.28 (m, 6H, H-4). **^{13}C-NMR** (100.6 MHz, CD_3CN): δ 203.9 (s, C-1), 152.8 (s, C-5), 140.5 (s, C-2), 137.9 (s, C-3), 131.9 (s, C-4).

[4-methoxyphenyl]-diphenylmethylium tetrafluoroborate salt 22d

[1] Carbocation **22a-[$B(C_6F_5)_4$]** is commercially available. CAS (**22a-[$B(C_6F_5)_4$]**) 136040-19-2

[2] M. Horn, H. Mayr, *Chem. Eur. J.* **2010**, *16*, 7469-7477.

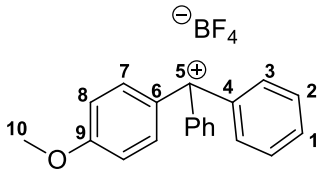

Chemical Formula: $C_{20}H_{17}BF_4O$
Molecular Weight: 360.15

22d is obtained as a red solid (948 mg, 2.63 mmol, 75%) **^{1}H-NMR** (400.1 MHz, CD_3CN): δ 7.77-7.68 (m, 2H, H-1), 7.61-7.57 (m, 4H, H-3), 7.42-7.36 (m, 4H, H-2), 7.31-7.26 (m, 2H, H-7), 6.98-6.81 (m, 2H, H-8), 3.81 (s, 3H, H-10). **^{13}C-NMR** (100.6 MHz, CD_3CN): δ 200.9 (s, C-5), 180.1 (s, C-9), 152.8 (s, C-Ar), 142.6 (s, C-Ar), 140.5 (s, C-Ar), 139.7 (s, C-Ar), 137.9 (s, C-Ar), 131.9 (s, C-Ar), 119.8 (s, C-Ar), 55.0 (s, C-10).

[4-*N,N*-dimethylamino]-diphenylmethylium tetrafluoroborate salt 22g

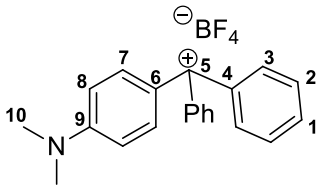

Chemical Formula: $C_{21}H_{21}BF_4N$
Molecular Weight: 374.20

22g is obtained as a dark-red solid (1.17 g, 3.11 mmol, 89%) **^{1}H-NMR** (400.1 MHz, CD_3CN): δ 7.72-7.65 (m, 2H, H-1), 7.61-7.56 (m, 4H, H-3), 7.40-7.32 (m, 4H, H-2), 7.24-7.19 (m, 2H, H-7), 6.95-6.89 (m, 2H, H-8), 2.68 (s, 6H, H-10). **^{13}C-NMR** (100.6 MHz, CD_3CN): δ 215.9 (s, C-5), 182.0 (s, C-9), 152.4 (s, C-Ar), 144.7 (s C-Ar), 141.5 (s, C-Ar), 138.6 (s, C-Ar), 137.9 (s, C-Ar), 131.8 (s, C-Ar), 121.0 (s, C-Ar), 29.5 (s, C-10).

1.2 Scope of the tritylium catalyzed Markovnikov hydrophosphination **26a-p**

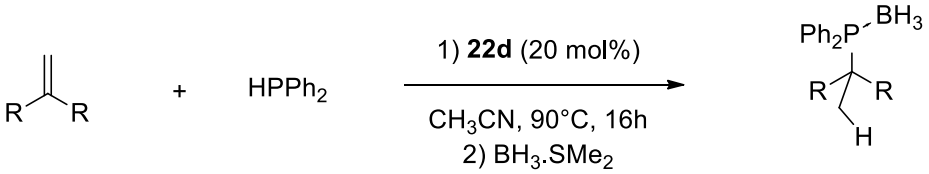

25a-p **26a-p**

General procedure

A flamed Schlenk equipped with a stirrer and containing **22d** (40 mg, 0.11 mmol, 0.2 eq) was stored under high vaccum (10^{-2} mbar) for 30 minutes. Then, the Schleck was backfilled with argon and $HPPh_2$ (100 µL, 0.57 mmol, 1 eq), **25a-p** (1.14 mmol, 2 eq) and CH_3CN (1.4 mL) were successively added. The Schlenk was sealed and the mixture warmed at 90°C for 16h under stirring. At the end of the reaction, the crude mixture was cooled to 0°C and connected at the Schlenk line before adding dropwise $BH_3.SMe_2$ (57 µL, 0.6 mmol, 1.2 eq) under stirring for 2h. Then 2 g of SiO_2 were added portionwise in the Schlenk under vigorous stirring resulting in an exothermic H_2 release. After removal of the solvent in vaccuo, the crude was purified by silica gel column chromatography to yield **26a-p**.

(1,1-diphenylethyl)diphenylphosphine borane complex 26a

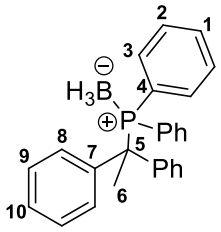

Chemical Formula: $C_{26}H_{26}BP$
Molecular Weight: 380.27

26a is obtained as a white solid (176 mg, 0.46 mol, 81%) **^{1}H-NMR** (400.1 MHz, $CDCl_3$): δ 7.43-739 (m, 2H, H-Ar), 7.38-7.34 (m, 4H, H-Ar), 7.28-7.17 (m, 14H, H-Ar), 2.06 (d, *J* = 15.1 Hz, 3H, H-6), 1.58-0.62 (m, 3H, BH_3). **^{13}C-NMR** (100.6 MHz, $CDCl_3$): δ 148.6 (d, *J* = 66.1 Hz, C-Ar), 142.5 (s, C-Ar), 134.6 (d, *J* = 8.0 Hz, C-Ar), 130.9 (d, *J* = 2.3 Hz, C-Ar), 129.8 (d, *J* = 4.9 Hz, C-Ar), 128.0 (s, C-Ar), 127.9 (s, C-Ar), 127.8 (s, C-Ar), 127.2 (d, *J* = 1.6 Hz, C-Ar), 49.8 (d, *J* = 23.2 Hz, C-5), 26.7 (s, C-6). **^{31}P{^{1}H}-NMR** (162.0 MHz, $CDCl_3$): δ 37.8 (m, P). **^{11}B-NMR** (128.4 MHz, $CDCl_3$): δ -34.8 (m, B). **Mp** = 95-96 °C. **HRMS** (ESI positive) = $[C_{26}H_{26}BPNa]^+$ Calculated mass: 403.1763 g/mol, found mass: 403.1768 g/mol.

[1-(4-Methoxyphenyl)-1-phenylethyl]diphenylphosphine borane 26b

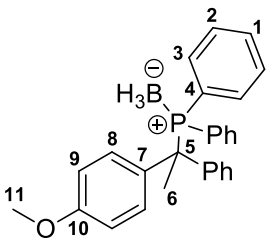

Chemical Formula: $C_{27}H_{28}BOP$
Molecular Weight: 410.30

26b is obtained as a colourless oil (185 mg, 0.45 mol, 79%) **^{1}H-NMR** (400.1 MHz, $CDCl_3$): δ 7.51-7.32 (m, 6H, H-Ar), 7.26-7.21 (m, 9H, H-Ar), 7.18 (d, *J* = 9.3 Hz, 2H, H-8), 6.75 (d, *J* = 8.5 Hz, 2H, H-9), 3.80 (s, 3H, H-11), 2.04 (d, *J* = 15.0 Hz, 3H, H-6), 1.60-0.91 (m, 3H, BH_3). **^{13}C-NMR** (100.6 MHz, $CDCl_3$): δ 161.6 (s, C-10), 145.8 (s, C-Ar), 137.9 (s, C-Ar), 134.6 (d, *J* = 7.8 Hz, C-Ar), 134.5 (s, C-Ar), 130.9 (s, C-Ar), 130.8 (s, C-Ar), 129.7 (d, *J* = 4.8 Hz, C-Ar), 127.9 (d, *J* = 8.2 Hz, C-Ar), 127.8 (s, C-Ar), 127.1 (s, C-Ar), 113.0 (s, C-Ar), 55.2 (s, C-11), 48.9 (d, *J* = 25.4 Hz, C-5), 26.8 (s, C-6). **^{31}P{^{1}H}-NMR** (162.0 MHz, $CDCl_3$): δ 37.6 (m, P). **^{11}B-NMR** (128.4 MHz, $CDCl_3$): δ -34.8 (m, B). **HRMS** (ESI positive) = $[C_{27}H_{28}BOPNa]^+$ Calculated mass: 433.1869 g/mol, found mass: 433.1874 g/mol.

[1-(4-amino)-1-phenylethyl]diphenylphosphine borane 26c

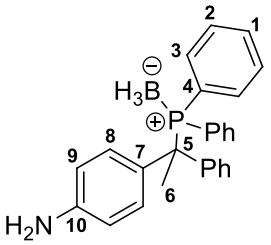

Chemical Formula: $C_{26}H_{27}BNP$
Molecular Weight: 395.28

26c is obtained as a colourless oil (162 mg, 0.41 mol, 72%) **^{1}H-NMR** (400.1 MHz, $CDCl_3$): δ 7.49-7.33 (m, 6H, H-Ar), 7.27-7.21 (m, 9H, H-Ar), 7.11 (d, *J* = 7.7 Hz, 2H, H-9), 6.76 (d, *J* = 7.4 Hz, 2H, H-8), 4.62 (ls, 2H, NH_2), 2.01 (d, *J* = 14.7 Hz, 3H, H-6), 1.49-0.71 (m, 3H, H-Ar). **^{13}C-NMR** (100.6 MHz, $CDCl_3$): δ 167.1 (s, C-10), 143.5 (s, C-Ar), 134.7 (s, C-Ar), 134.6 (s, C-Ar), 131.0 (s, C-Ar), 131.0 (s, C-Ar), 129.7 (s, C-Ar), 128.0 (s, C-Ar), 128.0 (s, C-Ar), 127.8 (s, C-Ar), 127.2 (s, C-Ar), 116.7 (s, C-Ar), 49.8 (d, *J* = 19.4 Hz,

C-5), 26.9 (s, C-6). **$^{31}P\{^{1}H\}$-NMR** (162.0 MHz, $CDCl_3$): δ 37.6 (m, P). **^{11}B-NMR** (128.4 MHz, $CDCl_3$): δ -35.4 (m, B). **HRMS** (ESI positive) = $[C_{26}H_{27}BNPNa]^+$ Calculated mass: 418.1872 g/mol, found mass: 418.1873 g/mol.

[1-(4-chloro)-1-phenylethyl]diphenylphosphine borane 26d

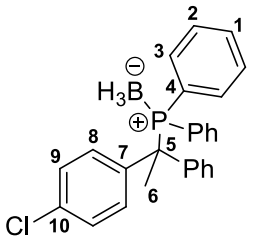

Chemical Formula: $C_{26}H_{25}BClP$
Molecular Weight: 414.71

26d is obtained as a colourless oil (161 mg, 0.39 mol, 68%) **^{1}H-NMR** (400.1 MHz, $CDCl_3$): δ 7.48 (dd, *J* = 18.2, 11.2 Hz, 2H, H-1), 7.45-7.37 (m, 4H, H-Ar), 7.31 (dd, *J* = 13.1, 5.0 Hz, 4H, H-Ar), 7.29-7.07 (m, 9H, H-Ar), 2.08 (d, ^{3}J = 14.8 Hz, 3H, H-6), 1.57-0.58 (m, 3H, BH_3). **^{13}C-NMR** (100.6 MHz, $CDCl_3$): δ 141.1 (s, C-Ar), 134.7 (d, *J* = 8.1 Hz, C-Ar), 134.5 (d, *J* = 8.1 Hz, C-Ar), 133.0 (d, *J* = 9.5 Hz, C-Ar), 131.2 (d, *J* = 4.8 Hz, C-Ar), 131.1 (s, C-Ar), 129.7 (d, *J* = 4.8 Hz, C-Ar), 128.2 (s, C-Ar), 128.1 (d, *J* = 3.4 Hz, C-Ar), 128.0 (s, C-Ar), 127.9 (d, *J* = 5.0 Hz, C-Ar), 127.4 (s, C-Ar), 49.4 (d, *J* = 23.0 Hz, C-5), 26.8 (d, *J* = 3.2 Hz, C-6). **$^{31}P\{^{1}H\}$-NMR** (162.0 MHz, $CDCl_3$): δ 37.8 (m, P). **^{11}B-NMR** (128.4 MHz, $CDCl_3$): δ -35.1 (m, B). **HRMS** (ESI positive) = $[C_{26}H_{25}BClPNa]^+$ Calculated mass: 437.1373 g/mol, found mass: 437.1375 g/mol.

[1-(4-fluorophenyl)-1-phenylethyl]diphenylphosphine borane 26e

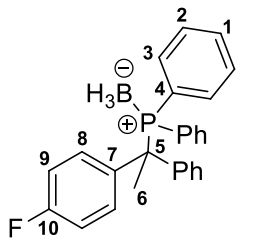

Chemical Formula: $C_{26}H_{25}BFP$
Molecular Weight: 398.26

26e is obtained as a white solid (177 mg, 0.44 mol, 78%) **^{1}H-NMR** (400.1 MHz, $CDCl_3$): δ 7.44 (t, *J* = 7.4 Hz, 2H, H-Ar), 7.38 (dd, *J* = 16.7, 8.3 Hz, 4H, H-Ar), 7.33-7.15 (m, 11H, H-Ar), 6.91 (t, *J* = 8.6 Hz, 2H, H-9), 2.06 (d, *J* = 14.8 Hz, 1H, H-6), 1.78-0.71 (m, 3H, BH_3). **^{13}C-NMR** (100.6 MHz, $CDCl_3$): δ 142.4 (s, C-Ar), 138.1 (d, *J* = 3.4 Hz, C-Ar), 134.7 (d, *J* = 8.1 Hz, C-Ar), 134.5 (d, *J* = 8.0 Hz, C-Ar), 131.5 (dd, *J* = 7.8, 4.8 Hz, C-Ar), 131.0 (d, *J* = 2.6 Hz, C-Ar), 129.6 (d, *J* = 4.9 Hz, C-Ar), 128.8 (d, *J* = 14.2 Hz, C-Ar), 128.1 (dd, *J* = 9.6, 6.4 Hz, C-Ar), 127.9 (s, C-Ar), 127.3 (s, C-Ar), 114.5 (d, *J* = 21.1 Hz, C-Ar), 49.2 (d, *J* = 23.3 Hz, C-5), 26.9 (s, C-6). **$^{31}P\{^{1}H\}$-NMR** (162.0 MHz, $CDCl_3$): δ 38.1 (m, P). **^{11}B-NMR** (128.4 MHz, $CDCl_3$): δ -34.9 (m, B). **^{19}F-NMR** (377.1 MHz, $CDCl_3$): δ -115.2 (m, F). **Mp** = 126-127°C. **HRMS** (ESI positive) = $[C_{26}H_{25}BFPNa]^+$ Calculated mass: 421.1669 g/mol, found mass: 421.1672 g/mol.

[2-(4-methylphenyl)-2-ethylmethyl]diphenylphosphine borane 26f

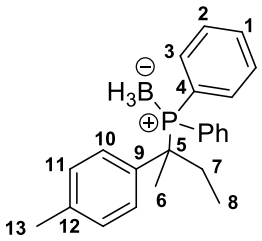

Chemical Formula: $C_{23}H_{28}BP$
Molecular Weight: 346.25

26f is obtained as a white solid (156 mg, 0.45 mol, 79%) **^{1}H-NMR** (400.1 MHz, $CDCl_3$): δ 7.62 (dd, *J* = 19.6, 10.9 Hz, 2H, H-1), 7.55-7.41 (m, 4H, H-3), 7.40-7.29 (m, 4H, H-2), 6.99 (d, *J* = 8.1 Hz, 2H, H-11), 6.71 (d, *J* = 7.0 Hz, 2H, H-10), 2.34 (s, 3H, H-13), 2.32-2.13 (m, 2H, H-7), 1.55 (d, *J* = 17.1 Hz, 3H, H-6), 1.49-0.71 (m, 3H, BH_3), 0.64 (t, *J* = 7.3 Hz, 3H, H-8). **^{13}C-NMR** (100.6 MHz, $CDCl_3$): δ 135.1 (d, *J* = 7.9 Hz, C-Ar), 134.4 (d, *J* = 8.0 Hz, C-Ar), 131.3 (d, *J* = 2.4 Hz, C-Ar), 130.9 (d, *J* = 2.5 Hz, C-Ar), 128.8 (d, *J* = 3.3 Hz, C-Ar), 128.4 (d, *J* = 1.8 Hz, C-Ar), 128.0 (d, *J* = 6.5 Hz, C-Ar), 127.9 (d, *J* = 6.5 Hz, C-Ar), 42.7 (d, *J* = 26.7 Hz, C-5), 29.2 (d, *J* = 6.1 Hz, C-7), 20.9 (s, C-13), 20.1 (d, *J* = 4.7 Hz, C-6), 7.4 (d, *J* = 12.0 Hz, C-8). **^{31}P{^{1}H}-NMR** (162.0 MHz, $CDCl_3$): δ 33.1 (m, P). **^{11}B-NMR** (128.4 MHz, $CDCl_3$): δ -38.6 (m, B). **Mp** = 88-89°C. **HRMS** (ESI positive) = $[C_{23}H_{28}BPNa]^+$ Calculated mass: 369.1919 g/mol, found mass: 369.1921 g/mol.

[1-(3-chlorophenyl)-1-phenylethyl]diphenylphosphine borane 26g

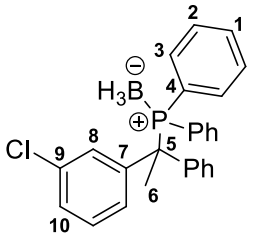

Chemical Formula: $C_{26}H_{25}BClP$
Molecular Weight: 414.71

26g is obtained as a colourless oil (52 mg, 0.13 mol, 22%) **^{1}H-NMR** (400.1 MHz, $CDCl_3$): δ 7.72-7.61 (m, 1H, C-8), 7.49-7.42 (m, 3H, H-Ar), 7.40-7.35 (m, 4H, H-Ar), 7.34-7.22 (m, 9H, H-Ar), 7.22-7.13 (m, 1H, H-Ar), 7.11 (d, *J* = 1.6 Hz, 1H, H-Ar), 2.06 (d, *J* = 16.9 Hz, 3H, H-6), 1.78-0.58 (m, 3H, BH_3). **^{13}C-NMR** (100.6 MHz, $CDCl_3$): δ 143.5 (s, C-Ar), 142.1 (m, C-Ar), 133.6 (t, *J* = 7.7 Hz, C-Ar), 132.8 (m, C-Ar), 132.2 (m, C-Ar), 130.1 (s, C-Ar), 128.7 (d, *J* = 4.8 Hz, C-Ar), 128.6 (d, *J* = 4.9 Hz, C-Ar), 128.1 (s, C-Ar), 127.8 (s, C-Ar), 127.2 (s, C-Ar), 127.1 (dd, *J* = 9.6, 4.5 Hz, C-Ar), 126.9 (s, C-Ar), 126.3 (d, *J* = 10.2 Hz, C-Ar), 48.5 (d, *J* = 22.1 Hz, C-5), 25.6 (s, C-6). **^{31}P{^{1}H}-NMR** (162.0 MHz, $CDCl_3$): δ 38.2 (m, P). **^{11}B-NMR** (128.4 MHz, $CDCl_3$): δ -35.0 (m, B). **HRMS** (ESI positive) = $[C_{26}H_{25}BClPNa]^+$ Calculated mass: 437.1373 g/mol, found mass: 437.1377 g/mol.

[1-cyclohexyl-1-phenylethyl]diphenylphosphine borane 26h

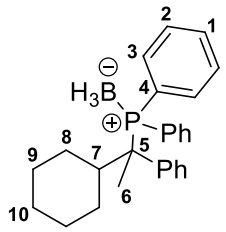

Chemical Formula: $C_{26}H_{32}BP$
Molecular Weight: 386.32

26h is obtained as a slightly yellow solid (156 mg, 0.40 mol, 71%) **^{1}H-NMR** (400.1 MHz, $CDCl_3$): δ 7.73 (t, *J* = 8.4 Hz, 2H, H-Ar), 7.54-7.39 (m, 3H, H-Ar), 7.39-7.28 (m, 3H, H-Ar), 7.21 (dd, *J* = 10.7, 4.7 Hz, 2H, H-Ar), 7.12-7.08 (m, 5H, H-Ar), 2.62 (dd, *J* = 19.2, 11.3 Hz, 1H, H-7), 1.69 (d, *J* = 11.6 Hz, 3H, H-6), 1.67-1.47 (m, 2H, H-8), 1.54-0.58 (m, 3H, BH_3), 1.36-1.25 (m, 2H, H-8), 1.21 (dt, *J* = 24.4, 11.8 Hz, 2H, H-9), 1.07 (td, *J* = 18.1, 11.5 Hz, 2H, H-9), 0.85 (dt, *J* = 12.3, 9.6 Hz, 1H, H-10). **^{13}C-NMR** (100.6 MHz, $CDCl_3$): δ 141.4 (s, C-Ar), 135.3 (d, *J* = 7.9 Hz, C-Ar), 133.5 (d, *J* = 7.6 Hz, C-Ar), 130.8 (s, C-Ar), 130.2 (s, C-Ar), 128.4 (d, *J* = 4.2 Hz, C-Ar), 128.1-127.7 (m, C-Ar), 127.6 (d, *J* = 1.9 Hz, C-Ar), 48.6 (d, *J* = 22.8 Hz, C-5), 45.1 (d, *J* = 5.0 Hz, C-7), 29.9 (s, C-9), 28.1 (d, *J* = 8.7 Hz, C-8), 26.6 (d, *J* = 17.4 Hz, C-6), 17.6 (s, C-10). **^{31}P{^{1}H}-NMR** (162.0 MHz, $CDCl_3$): δ 32.5 (m, P). **^{11}B-NMR** (128.4 MHz, $CDCl_3$): δ -36.9 (m, B). **Mp** = 64-65°C. **HRMS** (ESI positive) = $[C_{26}H_{32}BPNa]^+$ Calculated mass: 409.2232 g/mol, found mass: 409.2237 g/mol.

[1-methyl-1-*p*-tolylethyl]diphenylphosphine borane 26i

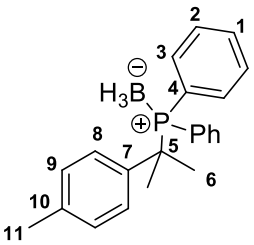

Chemical Formula: $C_{22}H_{26}BP$
Molecular Weight: 332.23

26i is obtained as a white solid (133 mg, 0.40 mol, 70%) **^{1}H-NMR** (400.1 MHz, $CDCl_3$): δ 7.47 (t, *J* = 8.5 Hz, 4H, H-3), 7.41 -7.30 (m, 2H, H-1), 7.26 (td, *J* = 7.7, 1.8 Hz, 4H, H-2), 6.89 (d, *J* = 8.0 Hz, 2H, H-8), 6.70 (t, *J* = 13.6 Hz, 2H, H-9), 2.24 (s, 3H, H-11), 1.56 (d, *J* = 15.9 Hz, 6H, H-6), 1.50-0.49 (m, 3H, BH_3). **^{13}C-NMR** (100.6 MHz, $CDCl_3$): δ 139.5 (d, *J* = 5.3 Hz, C-Ar), 136.7 (d, *J* = 2.1 Hz, C-Ar), 134.5 (d, *J* = 8.0 Hz, C-Ar), 131.1 (d, *J* = 2.4 Hz, C-Ar), 128.4 (d, *J* = 1.6 Hz, C-Ar), 128.0 (d, *J* = 9.8 Hz, C-Ar), 128.0 (s, C-Ar), 127.0 (d, *J* = 51.0 Hz, C-Ar), 38.8 (d, *J* = 26.5 Hz, C-5), 25.8 (d, *J* = 5.4 Hz, C-6), 21.0 (s, C-11). **^{31}P{^{1}H}-NMR** (162.0 MHz, $CDCl_3$): δ 32.7 (m, P). **^{11}B-NMR** (128.4 MHz, $CDCl_3$): δ -38.6 (m, B). **Mp** = 116-117°C. **HRMS** (ESI positive) = $[C_{22}H_{26}BPNa]^+$ Calculated mass: 355.1763 g/mol, found mass: 355.1763 g/mol.

[2-phenylbutyl]diphenylphosphine borane 26j

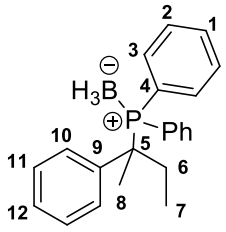

Chemical Formula: $C_{22}H_{26}BP$
Molecular Weight: 332.23

26j is obtained as a white solid (140 mg, 0.42 mol, 74%) **^{1}H-NMR** (400.1 MHz, $CDCl_3$): δ 7.48-7.33 (m, 2H, H-Ar), 7.33-7.21 (m, 4H, H-Ar), 7.20-7.09 (m, 3H, H-Ar), 7.08-7.01 (m, 1H, H-Ar), 6.98 (t, *J* = 7.4 Hz, 2H, H-Ar), 6.63 (d, *J* = 7.7 Hz, 2H, H-Ar), 2.09 (qq, *J* = 14.3, 7.3 Hz, 2H, H-6), 1.37 (d, *J* = 17.0 Hz, 3H, H-8), 1.29-0.53 (m, 3H, BH_3), 0.45 (t, *J* = 7.3 Hz, 3H, H-7). **^{13}C-NMR** (100.6 MHz, $CDCl_3$): δ 139.6 (d, *J* = 5.8 Hz, C-Ar), 135.1 (d, *J* = 8.0 Hz, C-Ar), 134.4 (d, *J* = 8.0 Hz, C-Ar), 131.1 (dd, *J* = 36.8, 2.4 Hz, C-Ar), 128.9 (d, *J* = 3.3 Hz, C-Ar), 128.0 (dd, *J* = 9.6, 7.1 Hz, C-Ar), 127.7 (d, *J* = 1.8 Hz, C-Ar), 126.9 (d, *J* = 2.1 Hz, C-Ar), 43.1 (d, *J* = 26.4 Hz, C-5), 29.3 (d, *J* = 5.9 Hz, C-6), 20.1 (d, *J* = 4.6 Hz, C-8), 7.4 (d, *J* = 11.9 Hz, C-7). **^{31}P{^{1}H}-NMR** (162.0 MHz, $CDCl_3$): δ 33.7 (m, P). **^{11}B-NMR** (128.4 MHz, $CDCl_3$): δ -38.6 (m, B). **Mp** = 95-96°C **HRMS** (ESI positive) = $[C_{22}H_{26}BPNa]^+$ Calculated mass: 355.1763 g/mol, found mass: 355.1765 g/mol.

(1-ethyl)diphenylphosphine borane *tert*-butyl ether 26k

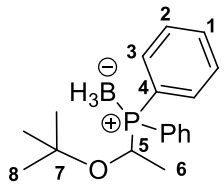

Chemical Formula: $C_{18}H_{26}BOP$
Molecular Weight: 300.18

26k is obtained as a white solid (53 mg, 0.18 mol, 31%) **^{1}H-NMR** (400.1 MHz, $CDCl_3$): δ 7.98-7.85 (m, 2H, H-Ar), 7.56-7.43 (m, 2H, H-Ar), 7.36-7.22 (m, 3H, H-Ar), 7.17 (dtd, *J* = 8.4, 6.9, 1.7 Hz, 3H, H-Ar), 4.11 (qd, *J* = 6.7, 2.1 Hz, 1H, H-5), 1.25 (dd, *J* = 16.6, 6.8 Hz, 3H, H-6), 1.08-0.68 (m, 3H, BH_3), 0.64 (s, 9H, H-8). **^{13}C-NMR** (100.6 MHz, $CDCl_3$): δ 134.9 (d, *J* = 8.3 Hz, C-3), 133.5 (d, *J* = 8.7 Hz, C-3), 131.5 (d, *J* = 2.4 Hz, C-1), 130.9 (d, *J* = 2.5 Hz, C-1), 128.9 (d, *J* = 55.7 Hz, C-4), 128.5 (d, *J* = 9.8 Hz, C-2), 128.2 (d, *J* = 10.0 Hz, C-2), 125.8 (d, *J* = 55.0 Hz, C-4), 76.0 (d, *J* = 4.8 Hz, C-7), 69.0 (d, *J* = 44.1 Hz, C-5), 27.83 (s, C-8), 19.5 (d, *J* = 7.3 Hz, C-6). **^{31}P{^{1}H}-NMR** (162.0 MHz, $CDCl_3$): δ 25.0 (m, P). **^{11}B-NMR** (128.4 MHz, $CDCl_3$): δ -40.0 (m, B). **Mp** = 78-79°C. **HRMS** (ESI positive) = $[C_{18}H_{26}BOPNa]^+$ Calculated mass: 323.1712 g/mol, found mass: 323.1715 g/mol.

(2-Phenylethyl)diphenylphosphine borane 26l

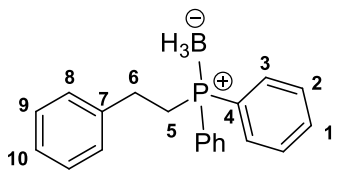

Chemical Formula: $C_{20}H_{22}BP$
Molecular Weight: 304.17

26l is obtained as a white solid (132 mg, 0.43 mol, 76%) **^{1}H-NMR** (400.1 MHz, $CDCl_3$): δ 7.75-7.69 (m, 4H, H-8), 7.53-7.49 (m, 2H, H-1), 7.49-7.44 (m, 4H, H-2), 7.30-7.26 (m, 2H, H-9), 7.22-7.18 (m, 1H, H-10), 7.18-7.15 (m, 2H, H-8), 2.86-2.80 (m, 2H, H-6), 2.57-2.49 (m, 2H, H-5), 1.38-0.68 (m, 3H, BH_3). **^{13}C-NMR** (100.6 MHz, $CDCl_3$): δ 141.4 (d, *J* = 14.9 Hz, C-7), 132.3 (d, *J* = 9.7 Hz, C-3), 131.4 (d, *J* = 2.4 Hz, C-1), 129.3 (d, *J* = 54.9 Hz, C-4), 129.0 (d, *J*

= 9.9 Hz, C-2), 128.7 (s, C-9), 128.2 (s, C-8), 126.5 (d, C-10), 29.3 (d, *J* = 1.1 Hz, C-6), 27.9 (d, *J* = 35.1 Hz, C-5). **^{31}P{^{1}H}-NMR** (162.0 MHz, $CDCl_3$): δ 17.0 (m, P). **^{11}B-NMR** (128.4 MHz, $CDCl_3$): δ -39.9 (m, B). **Mp** = 67-68°C. **HRMS** (ESI positive) = $[C_{20}H_{20}BPNa]^+$ Calculated mass: 327.1715 g/mol, found mass: 327.1719 g/mol.

[2-(2-Trifluoromethylphenyl)ethyl]diphenylphosphine borane 26m

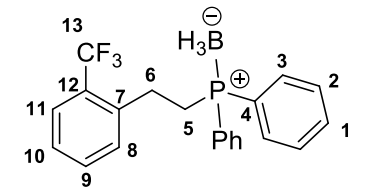

Chemical Formula: $C_{21}H_{21}BF_3P$
Molecular Weight: 372.17

26m is obtained as a white solid (153 mg, 0.41 mol, 72%) **^{1}H-NMR** (400.1 MHz, $CDCl_3$): δ 7.75-7.69 (m, 4H, H-Ar), 7.62-7.58 (m, 1H, H-Ar), 7.53-7.49 (m, 2H, H-Ar), 7.49-7.44 (m, 5H, H-Ar), 7.37-7.31 (m, 1H, H-Ar), 7.31-7.27 (m, 1H, H-Ar), 3.01-2.95 (m, 2H, H-6), 2.53-2.46 (m, 2H, H-5), 1.48-0.71 (m, 3H, BH_3). **^{13}C-NMR** (100.6 MHz, $CDCl_3$): δ 140.2 (dq, *J* = 15.5, 1.6 Hz, C-7), 132.3 (d, *J* = 9.2 Hz, C-Ar), 132.0 (q, *J* = 1.0 Hz, C-Ar), 131.5 (d, *J* = 2.7 Hz, C-Ar), 131.4 (s, C-Ar), 129.0 (d, *J* = 10.9 Hz, C-Ar), 128.9 (d, *J* = 55.1 Hz, C-4), 128.3 (q, *J* = 29.9 Hz, C-12), 126.7 (s, C-Ar), 126.2 (q, *J* = 5.7 Hz, C-11), 124.5 (q, *J* = 275.1 Hz, C-13), 28.5 (d, *J* = 31.1 Hz, C-5), 26.5 (d, *J* = 2.1 Hz, C-6). **^{31}P{^{1}H}-NMR** (162.0 MHz, $CDCl_3$): δ 15.1 (m, P). **^{11}B-NMR** (128.4 MHz, $CDCl_3$): δ -39.8 (m, B). **^{19}F-NMR** (377.0 MHz, $CDCl_3$): δ -59.6 (s, CF_3). **Mp** = 63-64°C. **HRMS** (ESI positive) = $[C_{21}H_{21}BF_3PNa]^+$ Calculated mass: 395.1619 g/mol, found mass: 395.1620 g/mol.

[2-(4-methylphenyl)ethyl]diphenylphosphine borane 26n

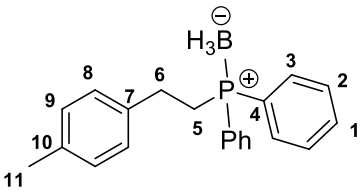

Chemical Formula: $C_{21}H_{24}BP$
Molecular Weight: 318.20

26n is obtained as a white solid (142 mg, 0.44 mol, 78%) **^{1}H-NMR** (400.1 MHz, $CDCl_3$): δ 7.78-7.67 (m, 4H, H-3), 7.56-7.42 (m, 6H, H-1,2), 7.14-7.03 (m, 4H, H-8,9), 2.86-2.74 (m, 2H, H-6), 2.58-2.44 (m, 2H, H-5), 2.32 (s, 3H, H-11), 1.88-0.41 (m, 3H, BH_3). **^{13}C-NMR** (100.6 MHz, $CDCl_3$): δ 138.3 (d, *J* = 15.1 Hz, C-7), 136.0 (s, C-10), 132.2 (d, *J* = 9.4 Hz, C-3), 131.3 (q, *J* = 2.3 Hz, C-1), 129.4 (s, C-9), 129.4 (d, *J* = 55.0 Hz, C-4), 129.0 (d, *J* = 9.9 Hz, C-2), 128.0 (s, C-8), 28.8 (d, *J* = 1.0 Hz, C-6), 27.5 (d, *J* = 35.2 Hz, C-5), 21.1 (s, C-11). **^{31}P{^{1}H}-NMR** (162.0 MHz, $CDCl_3$): δ 16.0 (m, P). **^{11}B-NMR** (128.4 MHz, $CDCl_3$): δ -36.7 (m, B). **Mp** = 77-78°C **HRMS** (ESI positive) = $[C_{21}H_{24}BPNa]^+$ Calculated mass: 341.1606 g/mol, found mass: 341.1615 g/mol.

[2-(4-Bromophenyl)ethyl]diphenylphosphine borane 26o

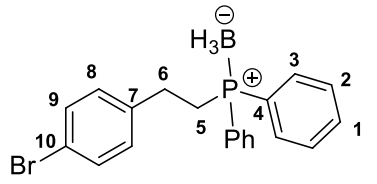

Chemical Formula: $C_{20}H_{21}BBrP$
Molecular Weight: 383.07

26o is obtained as a colourless oil (170 mg, 0.44 mol, 78%) **^{1}H-NMR** (400.1 MHz, $CDCl_3$): δ 7.80-7.77 (m, 4H, H-3), 7.76-7.51 (m, 8H, H-Ar), 6.80-6.75 (m, 2H, H-Ar), 2.83-2.75 (m, 2H, H-6), 2.55-2.44 (m, 2H, H-5), 1.88-0.41 (m, 3H, BH_3). **^{13}C-NMR** (100.6 MHz, $CDCl_3$): δ 140.3 (d, *J* = 14.4 Hz, C-7), 132.3 (d, *J* = 9.0 Hz, C-3), 131.8 (s, C9), 131.5 (d, *J* = 2.5 Hz, C-1), 130.0 (s, C-8), 129.1 (d, *J* = 55.4 Hz, C-4), 129.0 (d, *J* = 10.0 Hz, C-2), 120.3 (s, C-10), 28.8 (d, *J* = 1.7 Hz, C-6), 27.8 (d, *J* = 35.6 Hz, C-5). **^{31}P{^{1}H}-NMR** (162.0 MHz, $CDCl_3$): δ 16.0 (m, P). **^{11}B-NMR** (128.4 MHz, $CDCl_3$): δ -36.6 (m, B). **HRMS** (ESI positive) = $[C_{20}H_{21}BBrPNa]^+$ Calculated mass: 405.0555 g/mol, found mass: 405.0558 g/mol.

[2-(4-Methoxyphenyl)ethyl]diphenylphosphine borane 26p

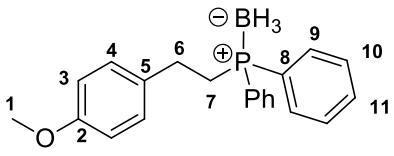

Chemical Formula: $C_{21}H_{24}BOP$
Molecular Weight: 334.20

26p is obtained as a colourless oil (131 mg, 0.39 mol, 69%) **^{1}H-NMR** (400.1 MHz, $CDCl_3$): δ 7.76-7.66 (m, 4H, H-9), 7.52-7.39 (m, 6H, H-10,11), 7.11-7.03 (m, 2H, H-4), 6.85-6.77 (m, 2H, H-3), 3.77 (s, 3H, H-1), 2.85-2.71 (m, 2H, H-6), 2.56-2.42 (m, 2H, H-7), 1.89-0.35 (m, 3H, H_3B). **^{13}C-NMR** (100.6 MHz, $CDCl_3$): δ 158.2 (s, C-2), 133.3 (s, C-Ar), 132.2 (s, C-Ar), 131.3 (s, C-Ar), 129.3 (d, ^{1}J = 55.4 Hz, C-8), 129.1 (s, C-Ar), 129.0 (s, C-Ar), 114.1 (s, C-Ar), 55.3 (s, C-1), 28.3 (d, ^{2}J = 1.6 Hz, C-6), 28.1 (d, ^{1}J = 34.6 Hz, C-7). **^{31}P{^{1}H}-NMR** (162.0 MHz, $CDCl_3$): δ 16.7 (m, P). **^{11}B-NMR** (128.4 MHz, $CDCl_3$): δ -36.7 (m, B). **HRMS** (ESI positive) = $[C_{21}H_{22}OP^+]$ (M – BH_3 + H]$^+$ Calculated mass: 321.1408 g/mol, found mass: 321.1399 g/mol.

2. Mechanistic study

2.1 Synthesis and characterization of **28a,b**

General procedure

In a flamed round-bottomed flask filled with argon and equipped with a stirrer was placed **22d** (1.0 g, 2.78, 1.0 eq) and CH_3CN (5.5 mL). HPR_2 (2.78 mmol, 1 eq) was added dropwise with a syringe at r.t. to the red mixture under stirring leading to a slightly yellow homogeneous solution. After 10 min, the solvent was removed in vaccuo to yield a yellow solid which was kept under high vaccum (10^{-2} mbar) for 2h at 0°C. Both **28a,b** must be stored at -35°C and under inert atmosphere.

(1-(4-methoxyphenyl)diphenylmethyl)diphenylphosphine borane 28a

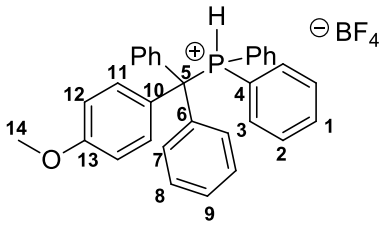

Chemical Formula: $C_{32}H_{28}BF_4OP$
Molecular Weight: 546.34

28a is obtained as a yellow solid (1.40 g, 2.56 mol, 92%). *Moisture sensitive*

^{1}H-NMR (400.1 MHz, CD_3CN): δ 8.84 (d, *J* = 492.0 Hz, 1H, HP^+), 7.81 (t, *J* = 8.5 Hz, 2H, H-Ar), 7.56-7.42 (m, 11H, H-Ar), 7.35-7.19 (m, 7H, H-Ar), 7.17-7.06 (m, 2H, H-Ar), 7.02 (t, *J* = 11.7 Hz, 2H, H-Ar), 3.86 (s, 3H, H-14). **^{13}C-NMR** (100.6 MHz, CD_3CN): δ 160.9 (d, *J* = 2.4 Hz, C-13), 138.1 (s, C-Ar), 136.0 (d, *J* = 3.0 Hz, C-Ar), 135.6 (d, *J* = 9.3 Hz, C-Ar), 134.4 (d, *J* = 16.4 Hz, C-3), 132.7 (d, *J* = 6.6 Hz, C-7), 130.9 (dd, *J* = 12.7, 9.9 Hz, C-2), 130.0 (d, *J* = 1.0 Hz, C-Ar), 129.4 (s, C-Ar), 128.30 (s, C-Ar), 117.1 (d, *J* = 77.4 Hz, C-4), 115.2 (d, *J* = 1.4 Hz, C-Ar), 62.4 (d, *J* = 42.4 Hz, C-5), 55.9 (s, C-14). **^{31}P{^{1}H}-NMR** (162.0 MHz, CD_3CN): δ 11.7 (d, *J* = 492.0 Hz, P^+). **{^{1}H}-^{11}B-NMR** (128.4 MHz, CD_3CN): δ -1.12 (m, F_4B^-). **^{19}F-NMR** (377.0 MHz, CD_3CN): δ -151.4 (s, F_4B^-). **Mp** = 55-56°C (decomposition). **HRMS** (ESI positive) = unstable

(1-(4-methoxyphenyl)diphenylmethyl)dicyclohexylphosphine borane 28b

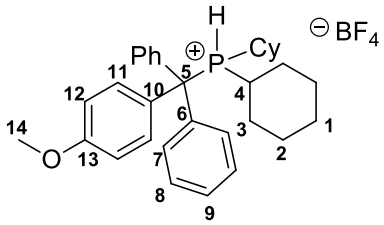

Chemical Formula: $C_{32}H_{40}BF_4OP$
Molecular Weight: 558.44

28b is obtained as a yellow solid (1.48 g, 2.64 mol, 95%). *Moisture sensitive*

^{1}H-NMR (400.1 MHz, CD_3CN): δ 7.54-7.47 (m, 4H, H-7), 7.47-7.38 (m, 6H, H-8,9), 7.33 (dt, *J* = 22.5, 11.2 Hz, 2H, H-11), 7.62-6.41 (dt, *J* = 450.0, 5.2 Hz, 1H, HP^+), 7.05 (d, *J* = 8.9 Hz, 2H, H-12), 3.84 (s, 3H, H-14), 2.48-2.22 (m, 2H, H-4), 1.86-1.60 (m, 6H, H-1,2,3), 1.57-1.34 (m, 4H, H-1,2,3), 1.34-1.09 (m, 6H, H-1,2,3), 1.01 (s, 2H, H-1,2,3). **^{13}C-NMR** (100.6 MHz, CD_3CN): δ 160.5 (s, C-13), 141.5-138.4 (m, C-10), 131.4 (s, C-Ar), 130.2 (s, C-Ar), 129.4 (s, C-Ar), 129.3 (s, C-Ar), 128.8 (d, *J* = 17.2 Hz, C-Ar), 115.4 (s, C-Ar), 59.8 (d, *J* = 38.0 Hz, C-5), 55.9 (s, C-14), 31.9 (d, *J* = 37.2 Hz, C-4), 30.9 (d, *J* = 4.7 Hz, C-2), 28.0 (d, *J* = 3.6 Hz, C-2), 27.1 (d, *J* = 12.6 Hz, C-3), 26.3 (d, *J* = 12.9 Hz, C-3), 25.3 (s, C-1). **^{31}P{^{1}H}-NMR** (162.0 MHz, CD_3CN): δ 22.67 (d, *J* = 450.0 Hz, P^+). **{^{1}H}-^{11}B-NMR** (128.4 MHz, CD_3CN): δ -1.13 (m, F_4B^-). **^{19}F-NMR** (377.0 MHz, CD_3CN): δ -151.4 (s, F_4B^-) **Mp** = 112-113°C (decomposition). **HRMS** (ESI positive) = unstable

2.2 Evaluation of the pK_a of **28a,b**

In a flamed round-bottomed flask filled with argon and equipped with a stirrer were placed **28a** or **28b** (0.10 mmol, 1.0 eq), the base (0.10 mmol, 1.0 eq) and CH_3CN (1.0 mL). The mixture

was stirred for 2h at r.t. Then, an aliquot was taken out, diluted with 0.5 mL of CD_3CN and placed in an NMR tube and analysed by ^{31}P NMR spectroscopy.

Example: Reaction of **28b** with *t*-BuOK

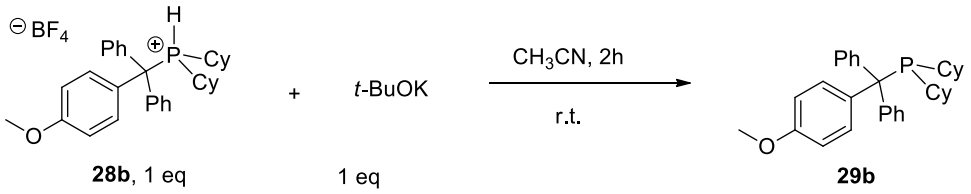

28b, 1 eq 1 eq **29b**

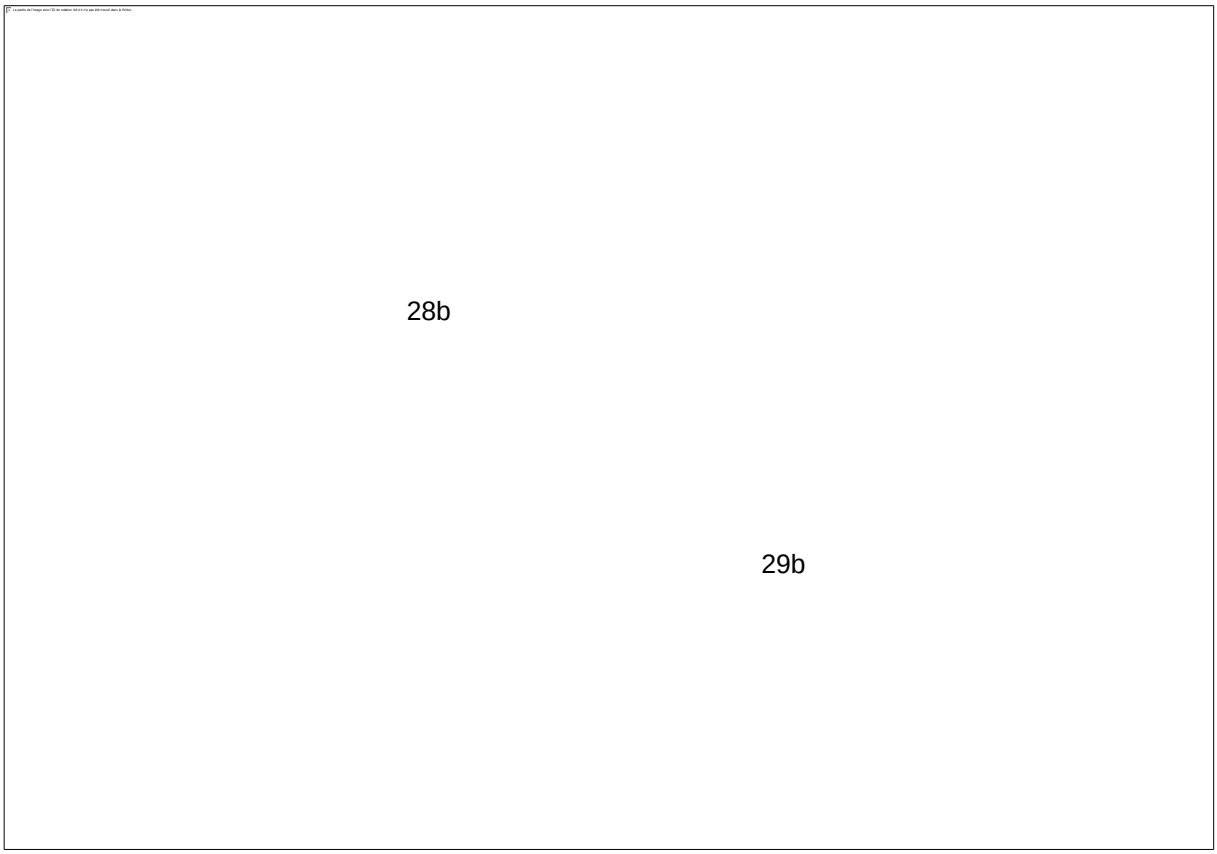

*Figure 1 ^{31}P NMR spectra of the reaction between **87b** and t-*BuOK

At the thermodynamic equilibrium, we get [**28b**] = 8.04 × 10^{-5} mol/L and [**29b**] = 1.96 × 10^{-5} mol/L.

Curriculum Vitae

Jonathan Dupré

✉ jonathan.dupre@ensicaen.fr
75 Avenue Georges Clémenceau
14000 Caen-France
☎ +33 (0)6.37.16.51.87

01/29/1990
Married without children
French
Driving licence

Skills and strengths

Organic chemistry	*Physical chemistry*	*Computational skills*	*skills*
✓ Synthesis and methodology	✓ Kinetics and thermodynamics (UV-vis stopped flow, IR and NMR in situ)	✓ Windows, Linus, Mac	✓ English (spoken and written).
✓ Purification, characterization	✓ DFT-calculations (Gaussian)	✓ Software: Chemdraw, Mestrenova, Topspin.	✓ Leadership and team builder
✓ Reaction mechanisms			✓ People management
✓ Bioactive compounds			✓ Teaching

Current status

Current position — PhD student in Physico-Organic Chemistry at the Université Normande de Chimie. Laboratoire de Chimie Moléculaire et Thio-organique (LCMT)–CNRS 6507, headed by Prof. Dr. Thierry Lequeux (lcmt.ensicaen.fr/).

Education and academic activities

2014-2017 — PhD student in the group of Prof. Dr. Annie-Claude Gaumont on “Mechanistic aspects of phosphines and phosphine-boranes complexes in hydrophosphination and hydride transfer reactions with olefins » Supervisor: Dr. Sami Lakhdar, Caen Univ., LCMT.

2011-2014 — Engineer diploma in chemistry and Master double diploma in molecular chemistry Ecole Nationale Supérieure de Chimie de Paris (chimie-paristech.fr) and University Pierre et Marie Curie (master.chimie.upmc.fr).

Publications

1) F. Meemken, A. Baiker, J. Dupré, K. Hungerbühler, *ACS Catal.* **2014**, *4*, 344–354.
2) J. dupré, A-. C. Gaumont, S. Lakhdar, *Org. Lett.* **2017**, 19, 694-697
3) J. dupré, A-. C. Gaumont, S. Lakhdar, Synthesis, in preparation

Conferences

1) J. Dupré, S. Lakhdar, A-. C. Gaumont. How the regioselectivity of the hydrophosphination of Alkenyl Arenes can be controlled through the oxidation state of the Iron Catalyst? JNOEJC, Rouen/FR, 9-12 June **2015**. Poster awarded by the first price
2) J. Dupré, S. Lakhdar, A-. C. Gaumont, Remote control of the regioselectivity in hydrophosphination of alkenes with diphenylphosphine: The how and why, 11th ICHAC, Caen, 14-19 of June **2015**. Poster

3) J. Dupré, S. Lakhdar, A-. C. Gaumont, Mayr Nucleophilicity and Lewis Basicity Parameters: A Key to Understand the Reactivity of Triarylphosphanes in Frustrated Lewis Pairs Chemistry, 13th ANORCQ, Rouen/FR, 24-27 Avril **2016**. Talk awarded by the first price.

4) J. Dupré, S. Lakhdar, A-. C. Gaumont. The pivotal role of the Lewis Base partner in Frustrated Lewis Pairs-Catalyzed Hydrogenation of Michael Acceptors: A Mechanistic Approach. EuCheMs, Séville, 11-15 Septembre **2016**. Talk

5) J. Dupré, S. Lakhdar, A-. C. Gaumont, Understanding the Reactivity of Phosphine–Boranes and Related Structures Through a Combination of Kinetic and Theoretical Approaches, JNOEJC, Caen, 8-9 Juin **2017**, Talk awarded by the first price.

Professional experiences

2016-2017	Molecular modelization training of phosphine-borane reactivity. Calculations computed with Gaussian and gaussview and treatment with Molden. Supervisor: Pr. Dr. Hélène Gérard, University Pierre et Marie Curie, LCT, Paris.
Jan-Aou 2014	PhD thesis internship: “Synthesis of new phosphorous-containing polymers for the recovery of precious metals”. 6-months internship at MagPie Polymers. MagPie Polymers - magpie-polymers.com. Dr. Steve Van Zutphen
Fev-sept 2013	Research project: “Heterogeneous Asymetric hydrogenation of α-diketone catalyzed by cinchona modified by Pt/Al_2O_3 catalysts”. ETH Zurich, Prof. Alfons Baiker, Prof. Konrad Hungerbühler, Dr. Fabian Meemken.

Activities and responsibilities

2016-2017	Teaching chemistry to undergraduate students 3h/week.
2016	Supervision of three bachelor students for a 2 months’ internship.
06/13/2016	Head member of the organizing committee of a Normand congress: 100 attendants, 40 posters, 12 talks and 2 invited speakers.
2015-2016	PhD representative at Normand doctoral school of chemistry.
2015-2016	Teaching chemistry at the University of Caen at bachelor degree level, 4h/week.

Interests

Horse-riding in competition for 14 years, running and swimming (twice a week).
Cinema (action and science-fiction), reading (science & philosophy) and music.

References

PhD director: Prof. Dr. Annie-Claude Gaumont, Université Normandie, LCMT, Caen, annie-claude.gaumont@ensicaen.fr and PhD supervisor Dr. Sami Lakhdar, Université Normandie, LCMT, Caen, sami.lakhdar@ensicaen.fr
Molecular modelization training : Prof. Dr. Hélène Gérard, University Pierre et Marie Curie, LCT, Paris, helene.gerard@upmc.fr
PhD thesis internship: Dr. Steve Van Zutphen, MagPie Polymers, Nemours (France), steve@magpie-polymers.com
Research project: Prof. Alfons Baiker, ETH Zürich, *alfons.baiker*@chem.ethz.ch

Résumé de la thèse

Les travaux décrits dans ce manuscrit de thèse concernent l'exploitation des interactions acide-base de Lewis entre deux partenaires organophosphorés et organoborés. Quatre types d'interactions ont été particulièrement au cœur de notre étude, allant de la frustration de la liaison P-B à la formation de complexes acide base de Lewis fortement liés. L'étude de ces interactions, couplée à des outils de physico-chimie organique et de chimie théorique, nous ont permis, non seulement de comprendre les paramètres clés de la réactivité mais également de mettre en avant de nouvelles voies de synthèse. Dans un premier temps, notre étude s'est portée sur l'hydrogénation de composés insaturés par les Paires de Lewis Frustrées (FLP). Ainsi, l'origine de l'incapacité des P/B à réduire les accepteurs de Michael a été expliquée par des mesures cinétiques de la nucléophilie et de la basicité de Lewis de phosphines encombrées. Dans une seconde partie, l'hydricité de complexes de phosphine borane (PBs) variées a été mesurée, nous permettant d'établir une échelle de prédiction de la réduction de divers électrophiles en présence de ces donneurs d'hydrure ioniques. Cette étude nous a conduit à considérer les PBs comme substrats dans des réaction de borylation intramoléculaire impliquant BH_3 comme source de bore. Cependant, des résultats inattendus ont mis en exergue une migration prépondérante à la borylation lors de la réaction entre les PBs et un acide de Lewis, donnant accès à une nouvelle familles de PBs possédant un atome de bore électro-déficitaire. Des études cinétiques couplées à une étude par DFT ont permis de rationaliser la réactivité observée. Enfin, l'exploitation des interactions réversibles entre une phosphine secondaire et un acide de Lewis organique ou métallique nous ont permis de contrôler la régiosélectivité lors de l'hydrophosphination d'alcènes 1,1-disubstitués par les diarylphosphines. Nos études mécanistiques soutiennent fortement l'implication d'un carbocation comme intermédiaire réactionnel.

1) Objectifs de la thèse

Les composés phosphorés sont très utilisés en synthèse organique car ils donnent accès à une réactivité très diversifiée grâce à la présence du doublet non liant de l'atome de phosphore et à sa polarisabilité. Ainsi, en présence d'un acide de Lewis, ce dernier peut donner lieu à la formation d'un complexe acide-base de Lewis, aux propriétés très intéressantes en synthèse.

Dans un premier temps, lorsque l'acide de Lewis et la phosphine sont trop encombrés, le précédent adduit ne se forme pas mais le doublet de la phosphine n'est pas complétement disponible. Cette interaction très faible donne lieu à la formation d'une paire de Lewis frustrée. Cette dernière est capable d'activer la molécule de dihydrogène pour permettre l'hydrogénation de doubles liaisons. Cependant, dans le cas de phosphines nucléophiles, nous avons montré l'existence d'une réaction compétitive donnant place à la formation de l'adduit d'hydrophosphination.

La suppression des répulsions stériques entre l'acide de Lewis et la base de Lewis donnent lieu à des interactions réversibles entre les deux précédents adduits. En effet, la réaction réversible entre un acide de Lewis et une base de Lewis nous a permis de développer une méthode d'hydrophosphination de doubles liaisons de types aryle-alcènes. Nous avons montré que la réaction peut être catalysée soit par un catalyseur organique comme un sel de tritylium ou métallique comme $FeCl_3$. L'étude du mécanisme réactionnel nous a permis de mettre en exergue la formation d'un sel de phosphonium comme intermédiaire clé permettant d'expliquer la sélectivité en faveur de l'adduit Markovnikov.

1) Paires de Lewis Frustrées

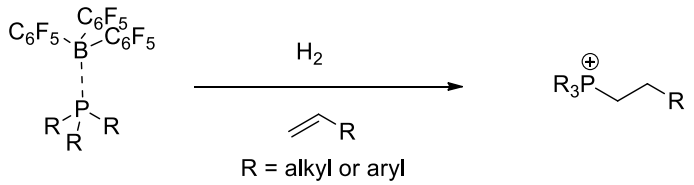

2) Hydrophosphination d'aryl alcènes

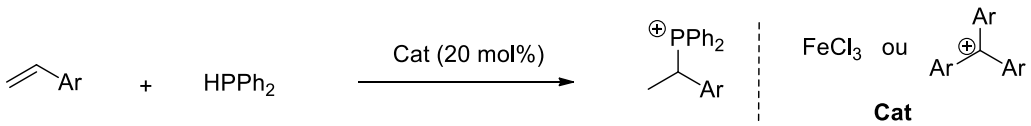

3) Hydricité des complexes de phosphines boranes

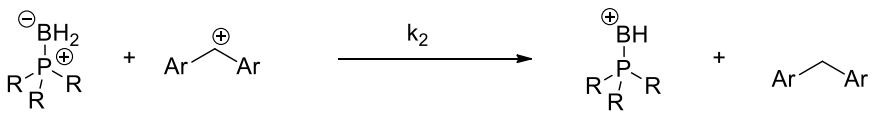

4) Migration de groupement perfluoré

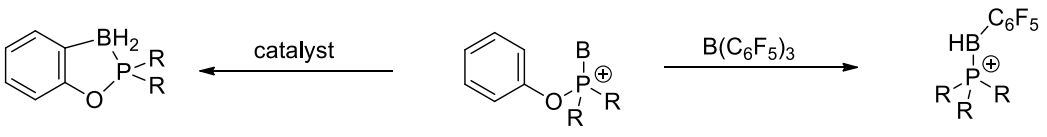

En revanche, lorsqu'une liaison forte est créée entre l'acide et la base de Lewis, comme dans le case des phosphines boranes, les hydrogènes portés par l'atome de bore deviennent nucléophiles. Nous avons donc montré que ces hydrures sont capables de réduire une large gamme d'électrophiles activés comme les iminiums ou les carbocations. L'hydricité des phosphines boranes a ainsi pu être mesurée à l'aide de la méthode dites des « cations Benzhydrilium » développée par le groupe du professeur Herbert Mayr. Nous avons ainsi pu comparer l'hydricité des complexes de phosphine borane avec celle des carbène et amine boranes, plus communément utilisés en synthèse organique.

Enfin, la réactivité des complexes de phosphine borane en présence d'un acide de Lewis a été envisagée afin de former des liaisons C-B au travers de réactions de borylation. Cependant, nous n'avons jamais observé la formation de l'adduit de borylation. En effet, en présence de $B(C_6F_5)_3$, nous avons montré que les phosphine et phosphinite boranes diversement fonctionnalisées donnent place une réaction de migration de C_6F_5 de $B(C_6F_5)_3$ pour conduire à des adduits de mono-migration. Afin d'élucider le mécanisme réactionnel, des études cinétiques et DFT ont été réalisées dans le laboratoire et en collaboration avec le laboratoire de chimie théorique de Paris. Ainsi, nous avons mesuré la nucléophilie des phosphines boranes et calculé le mécanisme réactionnel expliquant la mono-migration observée.

2) Positionnement par rapport à la concurrence nationale et internationale :

Concernant la partie Paire de Lewis frustrées, la rupture de la liaison H-H lors de l'activation de la molécule d'hydrogène a été très étudié par de nombreux groupes.[1]

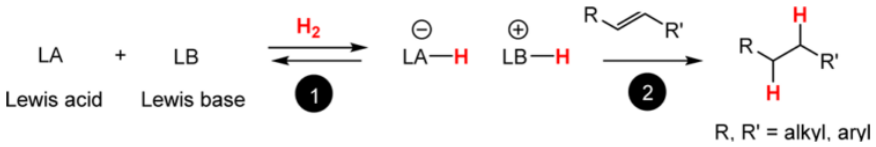

En revanche, l'étude du mécanisme de l'hydrogénation a été moins étudiée. A notre connaissance, seul deux publications font état de cette étude. Berionni et al. ont quantifié l'hydricité de borohydrure d'ammonium et de phosphonium à l'aide de l'équation d'énergie libre de Mayr (1).[2]

$$\log (k_2) = s_N (E + N) \qquad (1)$$

Ils ont ainsi démontré que l'hydricité dépend fortement des substituant porté par l'atome de bore. D'autres part, Paradies et al. ont isolé et caractérisé différentes FLP, comme la paire Fluorophosphine/$B(C_6F_5)_3$. Ils ont également montré que l'acidité du sel de phosphonium joue

un rôle important dans l'hydrogénation des doubles liaisons polarisées.[3] En effet, le proton acide du phosphonium est capable d'activer l'alcène pour former le carbocation correspondant qui peut ensuite être réduit par le borohydrure. Ainsi, la tri(1-naphtyl)phosphine ($(C_{10}H_7)_3P$) (pKa (C_2H4Cl_2) = 6.7) s'est révélée être une bonne base de Lewis pour la réduction d'oléfines riches sous H_2. A part cette étude mécanistique, les phosphines boranes ont largement été utilisée pour l'hydrogénation d'hétérocycles, d'imines, d'alcènes et d'éthers d'énol silylés. Malgré ces exemples, les doubles liaisons électro-déficitaires n'ont jamais été réduites par de tels systèmes.

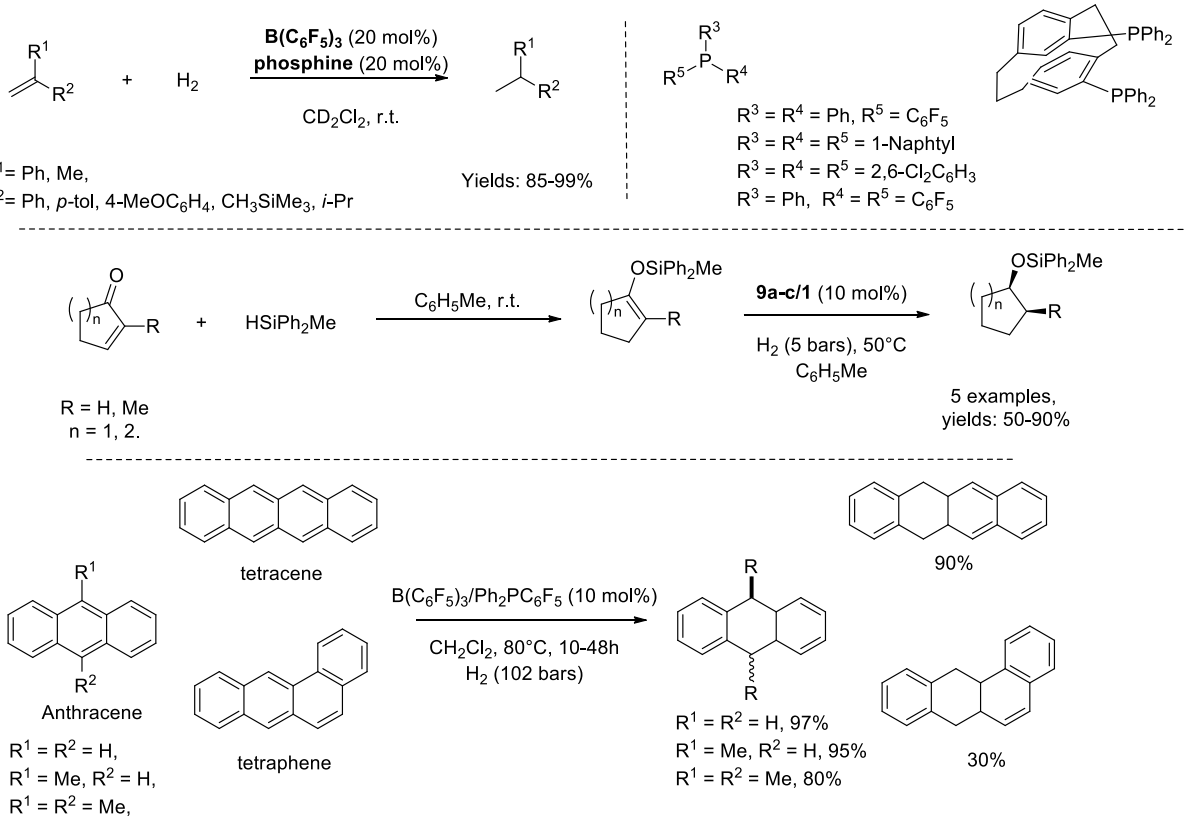

En ce qui concerne la dernière partie concerne l'hydrophosphination d'aryle alcènes par $HPPh_2$ organo- ou métallo-catalysée et fait suite aux travaux initié par notre groupe. En 2013, notre groupe à développer une méthode regioselective d'hydrophosphination de dérivés du styrène catalysée par un complexe de fer et conduisant sélectivement aux adduits α ou β.[6] Cette approche permet de former le régio-isomère désiré en modifiant simplement le degré d'oxydation du complexe de fer utilisé, comme indiqué sur le schéma.

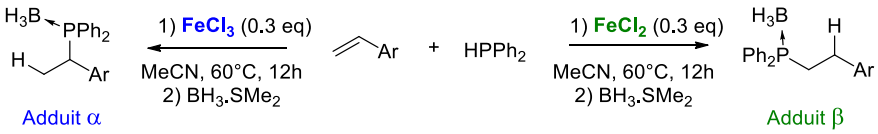

Ainsi, l'utilisation de $FeCl_2$ conduit à l'obtention de l'adduit β alors que la même réaction catalysée par $FeCl_3$ donne exclusivement accès au régioisomère α. D'un point de vue mécanistique, l'accès à l'adduit β implique la présence de radicaux, probablement initiés par une oxydation du fer(II) en fer(III). L'étude de cette voie réactionnelle ne sera pas détaillée dans ce rapport. En revanche, nous présenterons brièvement les premiers éléments de l 'étude portant sur l'étude du mécanisme conduisant à l'adduit α afin de comprendre pourquoi la réaction nécessite l'utilisation d'une quantité de catalyseur de l'ordre de 30%.

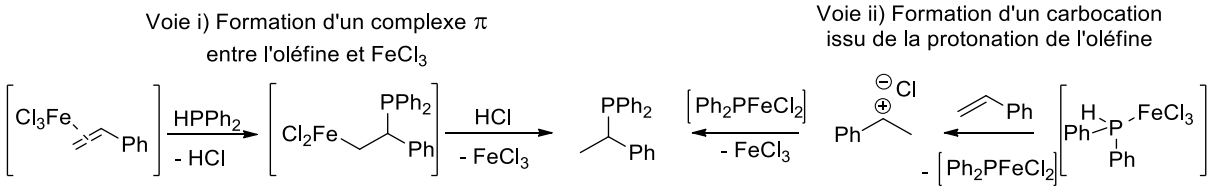

Deux mécanismes sont possibles, comme indiqués dans le schéma 8. Ces derniers impliquent i) soit une activation de la double liaison du dérivé styrénique conduisant à un complexe-π, activant ainsi l'oléfine vis-à-vis de l'addition de la phosphine ii) soit une coordination de la phosphine secondaire conduisant à une exaltation de l'acidité du proton permettant la protonation de l'oléfine pour conduire à un carbocation benzylique stable. Jusqu'à maintenant, le mécanisme n'a pu être prouvé de manière univoque. Cependant, une étude réalisée par le groupe du prof. Beletskaya concernant l'hydrophosphination de régiosélectivité Markovnikov à partir de vinyléthers donnent des arguments en faveur du mécanisme par formation d'un complexe-π, comme indiqué dans le schéma ci-contre. En effet, en recherchant une méthode nécessitant l'emploi de métaux peu couteux, une méthode dite « substrat dépendante » a été développée afin de promouvoir la formation de l'adduit α. En présence de 2 mol% d'un sel de nickel $NiBr_2$, $HPPh_2$ s'additionne régioselectivement sur les vinyléthers dans le benzène à 80°C en seulement 2 heures pour conduire à l'adduit Markovnikov avec de bons rendements après oxydation. Les auteurs proposent la formation d'un complexe π entre le centre métallique et l'oléfine conduisant à une espèce très électrophile. Le précédent adduit et ensuite attaqué par la phosphine pour conduire à une espèce organométallique qui, après protonolyse donne accès au régioisomère désiré et au catalyseur.

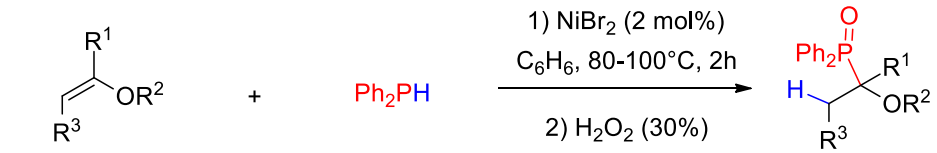

R^1 = H, Me, Et, Bu
R^2 = Me, Et, Bu
R^3 = H, Et

Yields: 70-85%

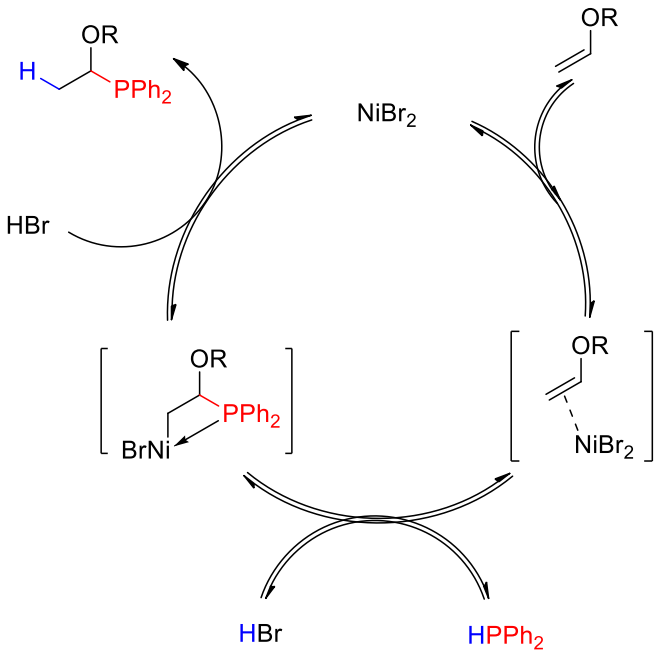

Toutefois, des travaux récents du prof. Stephan décrivent l'hydrothiolation d'alcènes substitués en utilisant les sels de tritylium. En effet, les auteurs ont réalisé la synthèse de sulfures (20 exemples) par une hydrothiolation de régioselectivité Markovnikov d'alcènes 1,1-disubstitués et tri substitués avec des thiols, catalysée par le sel de tritylium $(4\text{-MeOPh})CPh_2.BF_4$ avec des rendements de 12 à 96%. En particulier, les auteurs ont proposé la formation d'un carbocation résultant de la protonation de l'oléfine par le complexe issu de la complexation entre le thiol et l'acide de Lewis.

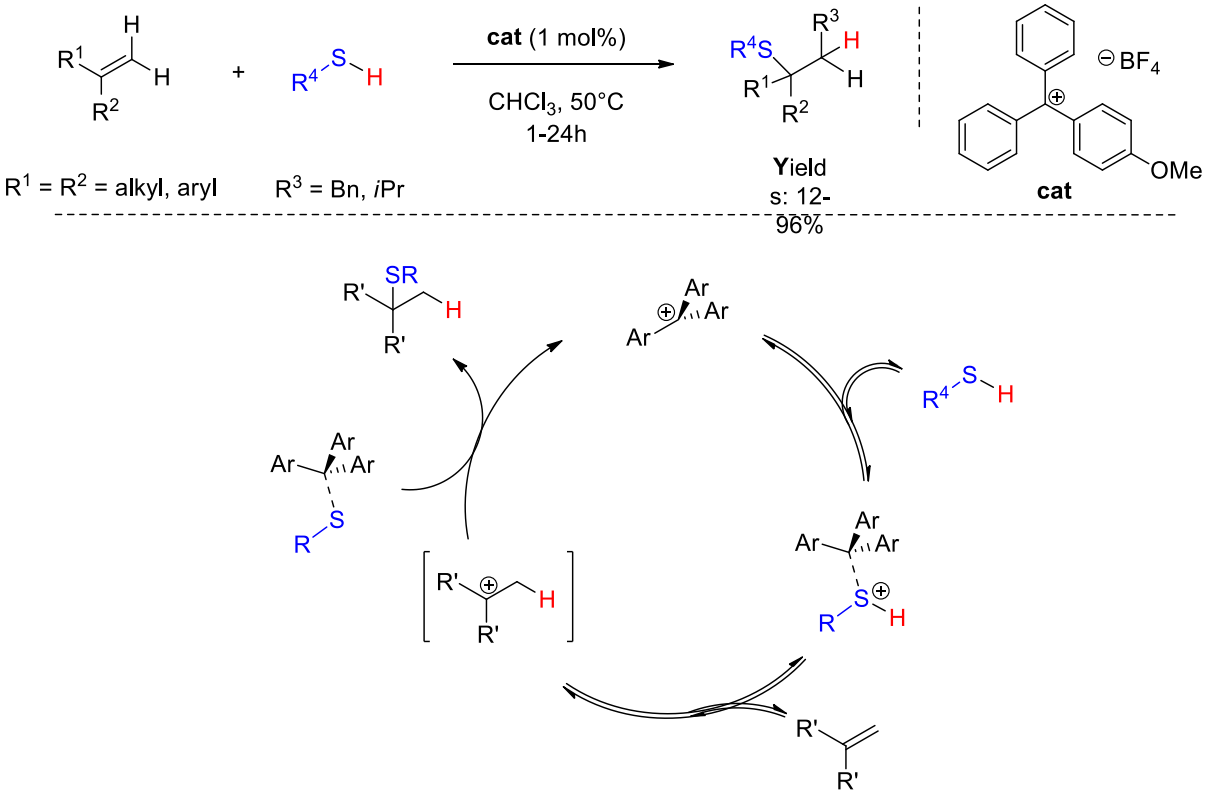

Le troisième partie, dédiée à la mesure de l'hydricité de complexes de phosphine borane, s'inscrit dans le cadre de la mise au point d'agents de réduction ioniques doux. En effet, les complexes d'amine, carbene et phosphine borane sont assez couramment utilisé en synthèse organique pour la réduction de composés électrophiles comme les cétones, les aryle triflates ou les dérivés halogénés.

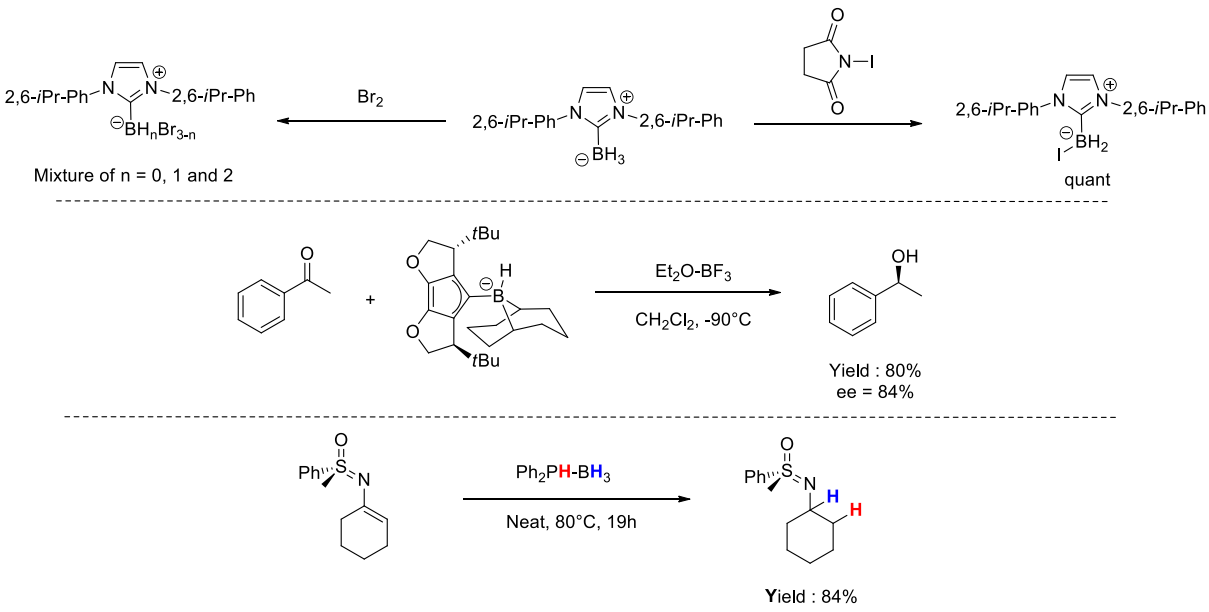

Le groupe du prof. Mayr a établi une échelle de l'hydricité de complexes de bases de Lewis-borane, permettant une comparaison directe de la nucléophilie des donneurs d'hydrure

commun. Cependant, les phosphines borane n'ont jamais été incluses à cette échelle, et il semble donc intéressant de mesurer leurs paramètres de nucléophilie. Cela s'avère d'autant plus intéressant que Curran et al. ont relevé des incohérences de réactivité entre les phosphines boranes diversement substituées. En effet, les auteurs ont étudié la réactivité d'une série de complexes base de lewis-BH_3 dans des réactions d'insertions de de B-H catalysée par un complexe de rhodium. Au cours de cette étude, les auteurs ont mesuré les vitesses de réactions au second ordre pour les différents donneurs d'hydrure. Alors que les carbène et amine borane présentes des vitesses de réactions bien différentes, l'analyse de celle des phosphines borane s'avère identique pour Ph_3PBH_3 et Bu_3PBH_3 alors qu'il est bien connu que ces deux phosphines ont des propriétés stériques et électroniques différentes. Il s'avère donc important de comprendre l'origine de ces déviations.

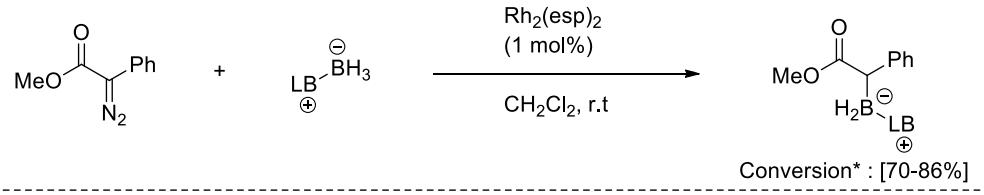

LB-BH_3					
				Bu_4N	R = Ph, or R = Bu
$k_{relative}$ (L/mol/s)	2.5	1	0.33	0.18	0.06

En ce qui concerne la migration de groupements perfluorés, cette transformation a été reportée seulement deux fois avec les complexes Me_2SBH_3 et Ph_3PBH_3. En 2010, Lancaster et al ont montré que H_3B-SMe_2 et $(C_6F_5)_3B_3OEt_2$ donnent accès à deux adduit d'échange de ligand selon qu'un ou deux groupements C_6F_5 ont été échangés.[4] Ainsi, dans l'éther de pétrole en présence d'un excès de SMe_2 l'adduit de double migration de C_6F_5 est obtenu alors que l'adduit de mono-migration est isolé en présence d'un excès de H_3B-SMe_2.

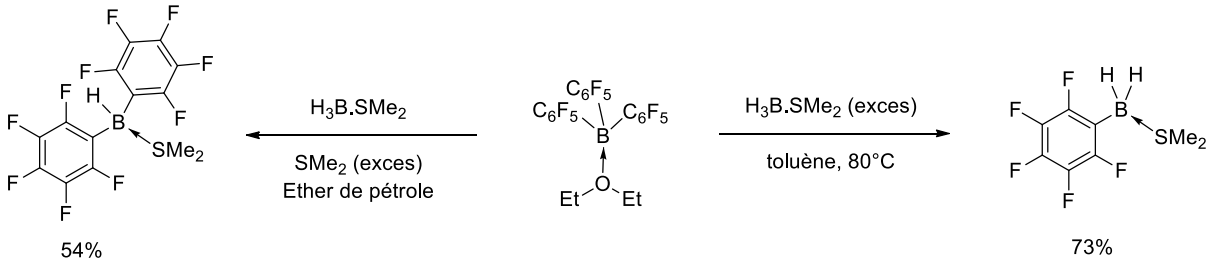

De plus, en 2013, Prokovfjevs a montré la migration de C_6F_5 lors d'une étude sur les dimère borenium. L'emploi de 0.36 eq de $(C_6F_5)_3B$ avec 1 équivalent de la phosphine borane Ph_3PBH_3

sous 50°C donne accès à l'adduit de mono-migration avec un rendement de 71%.[5] En dépit de ces deux exemples, aucune étude mécanistiques sur la migration du groupement C_6F_5 n'a été entreprise alors que les adduits formés présentent des propriétés électroniques intéressantes.

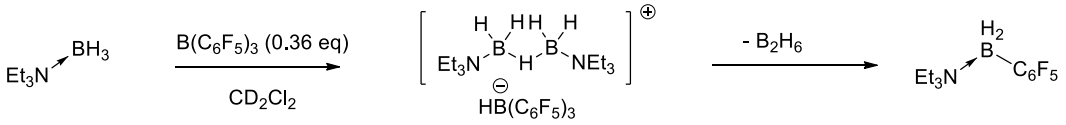

Entry	LB-BH_3	Solvent	Product	Rendement* (%)
1*	Et_3N-BH_3	C_6H_5F	Et_3N-$BH_2(C_6F_5)$	> 99
2	Me_3N-BH_3	CH_2Cl_2	Me_3N-$BH_2(C_6F_5)$	97
3	$BnMe_2N$-BH_3	C_6H_5F	$BnMe_2N$-$BH_2(C_6F_5)$	> 99
4	Ph_3P-BH_3	CH_2Cl_2	Ph_3P-$BH_2(C_6F_5)$	71

De façon plus large, cette étude s'inscrit dans la cadre des réactions de borylation dont la source de bore est apportée par le fragment BH_3. En effet, les complexes base de Lewis borane sont des réactifs qui ont suscité un fort attrait dans les réactions de borylation. Ces complexes présentes l'avantage de d'être stables à l'air et aux conditions aqueuses. De plus, ces composés sont des précurseurs de de borénium trivalent, largement utilisés en synthèse organiques.

Références :

1 (a) Stephan, D. W. *Acc. Chem. Res.* **2015**, *48*, 306. (b) Stephan, D.W. *J. Am. Chem. Soc.* **2015**, *137*, 10018. (c) Welch, G. C.; San Juan, R. R.; Masuda, J. D.; Stephan, D. W. *Science* **2006**, *314*, 1124

2 Morozova, V.; Mayer, P.; Berionni, G. *Angew. Chem., Int. Ed.* **2015**, *54*, 14508.

3 Greb, L.; Tussing, S.; Schirmer, B.; Oña-Burgos, P.; Kaupmees, K.; Lõkov, M.; Leito, I.; Grimme, S.; Paradies, J. *Chem. Sci.* **2013**, *4*, 2788

4 Fuller, A. M.; Hughes, D. L.; Lancaster, S. J.; White, C. M. *Organometallics* **2010,** *29*, 2194.

5 Prokofjevs, A. *Angew. Chem., Int. Ed.* **2015**, *54*, 13401.

6 Routaboul, L.; Toulgoat, F.; Gatignol, J.; Lohier, J.-F.; Norah, B.; Delacroix, O.; Alayrac, C.; Taillefer, M.; Gaumont, A.-C. *Chem. - A Eur. J.* **2013**, *19*, 8760.

3) Principaux résultats de la thèse

A/ Partie Paires de Lewis frustrées

L'étude du mécanisme de l'hydrogénation de doubles liaisons électro-déficitaires nous a permis de mettre en avant un réaction d'hydrophosphination de la double liaison.

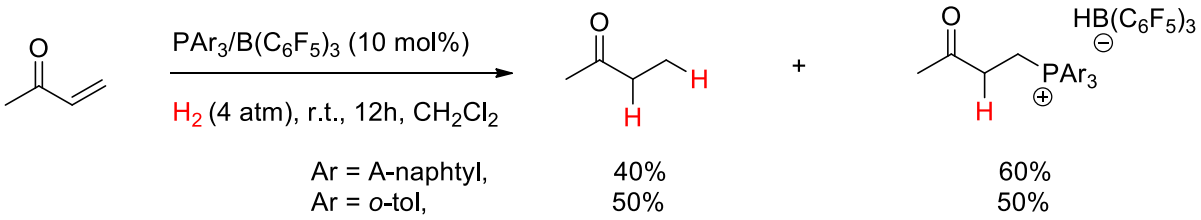

Nous avons par ailleurs montré que cette hydrophosphination compétitive n'est pas limitée au cas de la méthylvinyl cétone. En effet, divers électrophiles ont été utilisés, conduisant à des ratios différents selon la valeur de l'électrophile de l'accepteur de Michael.

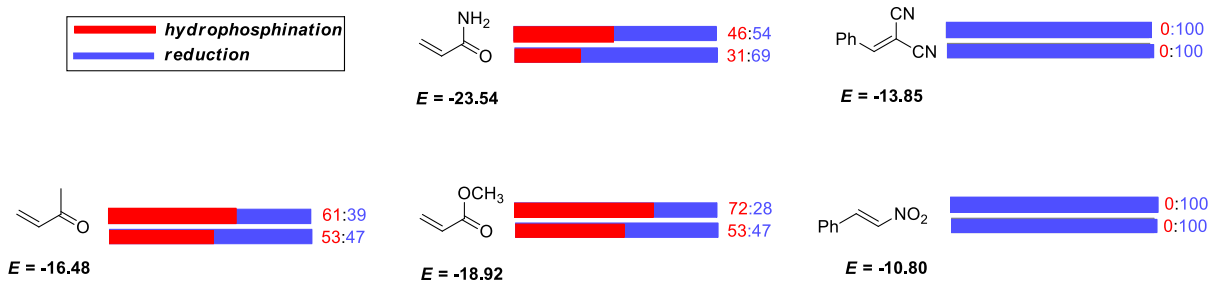

Afin de comprendre l'origine de ce sous-produit, nous avons quantifié la nucléophilie des phosphines encombrées par mesures cinétiques en utilisant la relation d'énergie libre de Mayr (1). Les deux phosphines différentes que nous avons étudiées, $P(o\text{-tol})_3$ et $P(1\text{-Naphtyl})_3$, ont respectivement conduites aux valeurs de nucléophilie suivantes : 8.40 et 13.17. Ces valeurs permettent d'expliquer la sélectivité de l'addition des phosphines ainsi que de proposer le mécanisme réactionnel suivant pour la compétition entre l'hydrogénation et l'hydrophosphination selon la nature de la phosphine.

- Dans le cas d'une trialkylphosphine, le pK_a du sel de phosphonium associé est élevé (pK_a ~ 8). Par conséquent, le transfert d'hydrure à lieu dans un premier temps, suivi de la protonation du carbanion. Ainsi, le produit d'hydrogénation est formé et le système catalytique acide de Lewis- base de Lewis frustré est libéré pouvant à nouveau activer H_2.

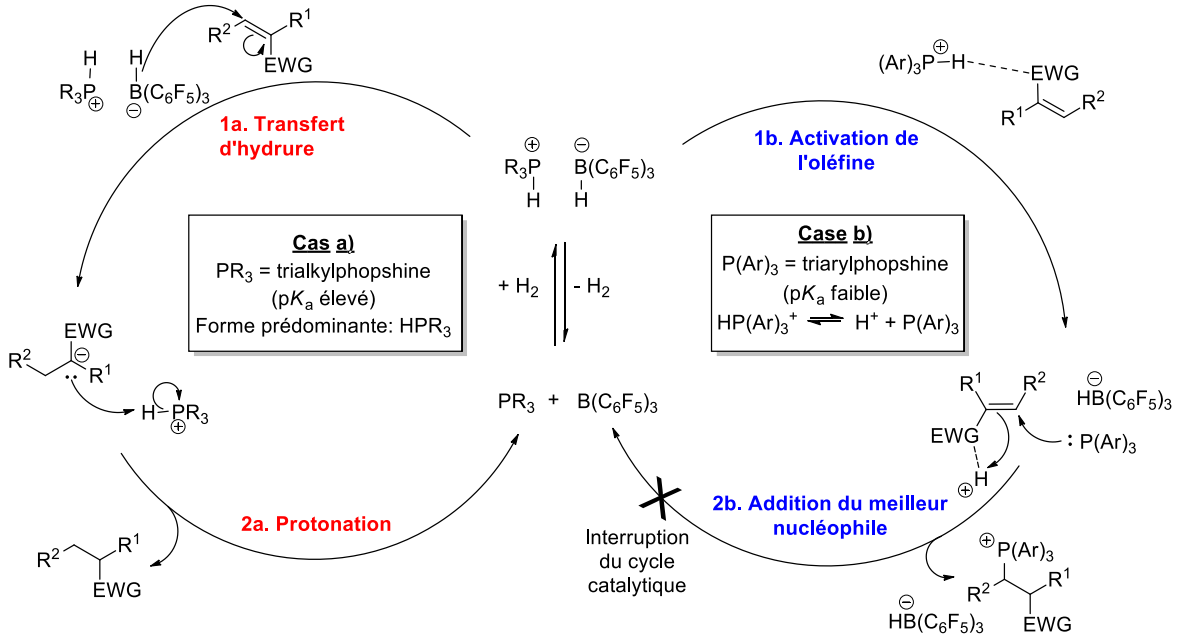

- Dans le cas d'une triarylphosphine, le pK_a du sel de phosphonium est bas, ce qui implique que la liaison P-H est plus labile. Une activation de l'accepteur de Michael est alors possible par les protons labiles, conduisant à une espèce possédant une électrophile exacerbée face à deux nucléophiles dans le milieu : la triarylphosphine et le borohydrure. Dans ce cas, le paramètre cinétique l'emporte et l'addition de la phosphine à lieu. L'irréversibilité de la réaction résulte du piégeage de l'intermédiaire par les protons en solution, conduisant au produit d'hydrophosphination contenant la base de Lewis de la FLP, ce qui tue le catalyseur et stoppe la réaction.

Cette étude montre que l'hydrogénation de doubles liaisons électro-déficitaires par les paires de Lewis frustrées est en compétition avec la réaction d'hydrophosphination. Dans le cas des triarylphosphines, cette dernière voie est privilégiée.

B/ Hydrophosphination Markovnikov d'aryle alcènes avec $HPPh_2$

Suite aux travaux de notre groupe sur l'hydrophosphination régiosélective de styrène avec $HPPh_2$ catalysée par $FeCl_3$ nous avons développé une méthode organo-catalysée de cette réaction avec un parfait maintien de la régiosélectivité. Ainsi, sur la base des travaux de Stephan et al. décrivant l'hydrothiolation d'alcènes catalysée par les sels de tritylium, nous avons utilisé ces mêmes catalyseurs pour l'hydrophosphination.[8]

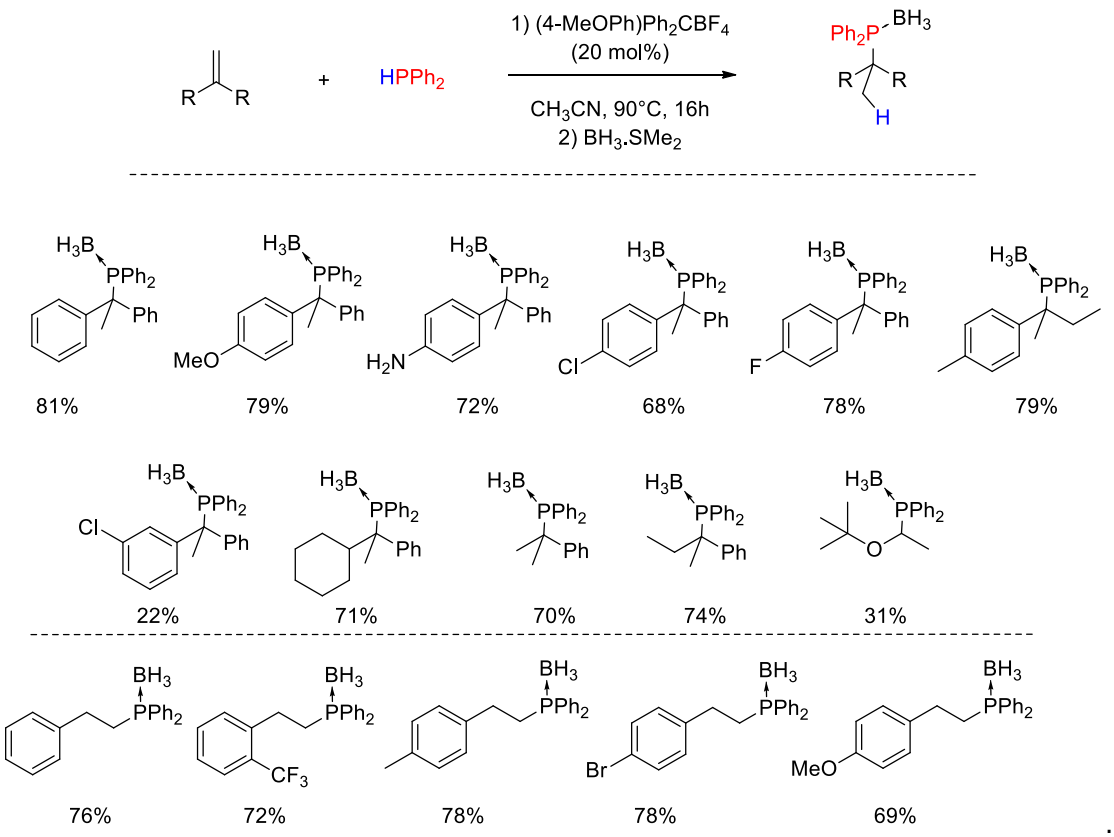

Ainsi, nous avons pu mettre en place une méthode nécessitant l'utilisation de 20 mol% de catalyseur, 2 équivalents d'alcène (pour éviter la dimérisation) à 90°C pur conduire à l'adduit Markovnikov avec des rendements de 22 à 81%. Nous avons pu montrer que la réactivité est grandement influencée par la nature électronique de l'oléfine. Ainsi, les oléfines enrichies conduisent à de meilleurs rendements que les oléfines appauvries.

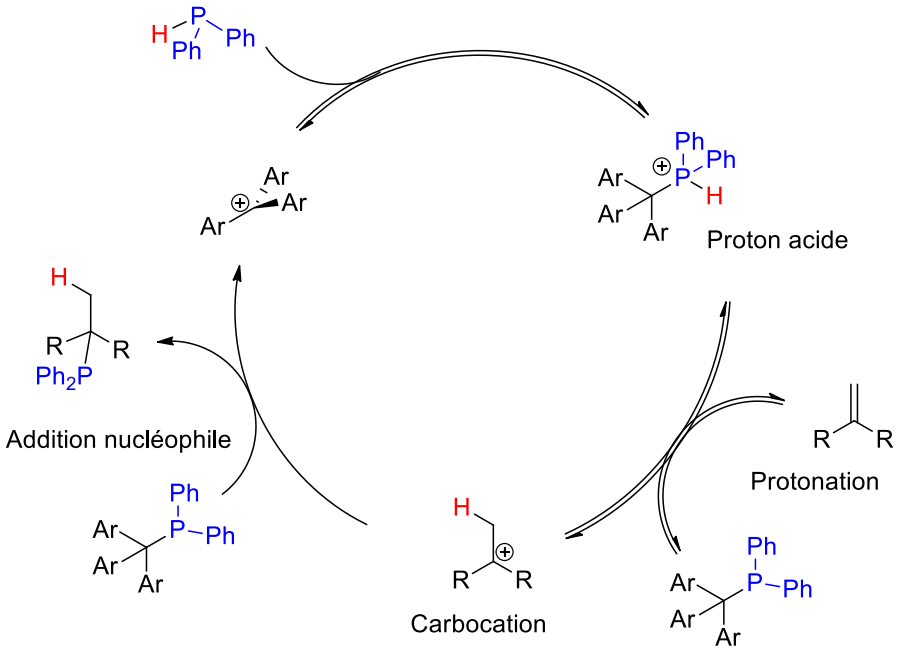

Ce phénomène a été expliqué par l'implication d'un carbocation comme intermédiaire réactionnel. Sur la base de ces résultats nous avons pu proposer le mécanisme réactionnel ci-dessous. Ce mécanisme réactionnel est appuyé par des mesurés du pKa de sels de phosphoniums par RMN. Nous avons sélectionné les complexes issus de 1) l'association entre $HPPh_2$ et le sel de tritylium ($4(MeOPh)CPh_2.BF_4$ et 2) l'association entre $HPCy_2$ et le sel de tritylium ($4(MeOPh)CPh_2.BF_4$. Alors que la mesure du pK_a du premier complexe a donné une valeur proche de zéro, celle du second complexe est, quant à elle, proche de 20. Cette impressionnante différence illustre bien l'importance électronique de la nature des substituent de la phosphine sur les propriétés électroniques du complexe final. Ainsi, le complexe $HPCy_2$ + $(4(MeOPh)CPh_2$ ayant un pKa élevé, la protonation de l'oléfine n'a pas lieu et le scope se limite ainsi aux phosphines les moins nucléophiles telles que les diarylphosphines. Par ailleurs, il est important de noter que l'emploi d'un contre ion chiral pourrait permettre la formation d'une paire d'ion chirale entre la carbocation et l'anion introduit. Cette perspective est très intéressante car la synthèse de phosphine encombrées optiquement actives n'a jamais été réalisée par hydrophosphination organocatalysée.

C/ Mesure de l'hydricité des complexes de phosphine borane

En 2013, Mayr et al. ont mesuré l'hydricité de donneurs d'hydrures tels que les carbène-, amine-borane, les esters de Hantzsch et les silanes. En utilisant l'échelle de nucléophilie, les auteurs ont pu caractériser chaque centre nucléophile par ses paramètres *N* et s_N issu de la relation d'énergie libre (1).

$$\log (k_2) = s_N (E + N) \qquad (1)$$

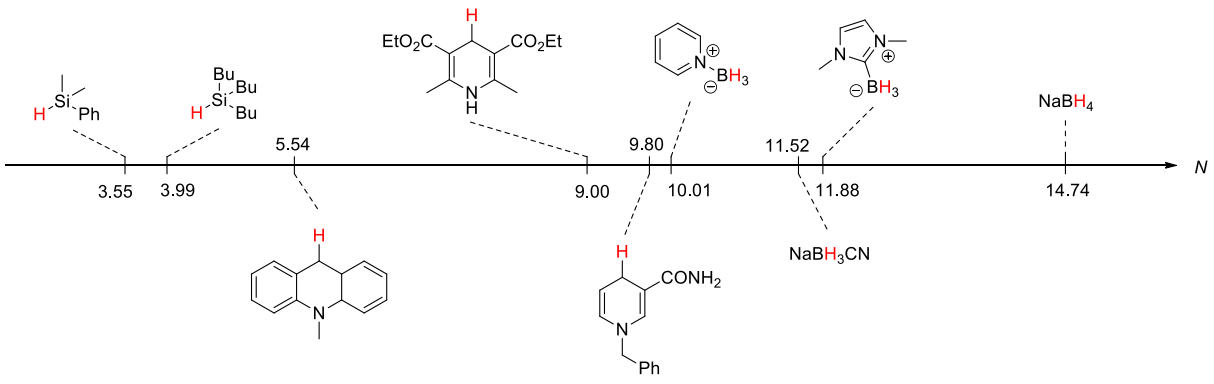

Nous avons donc complété cette étude en mesurant l'hydricité des phosphines boranes. Ces mesures ont été réalisées à l'aide de carbocation de références dont le paramètre d'électrophile est connu, ce sont les sels de diarylcarbénium. Le suivi par spectrophotométrie UV-Visible des réactions donne le profil suivant.

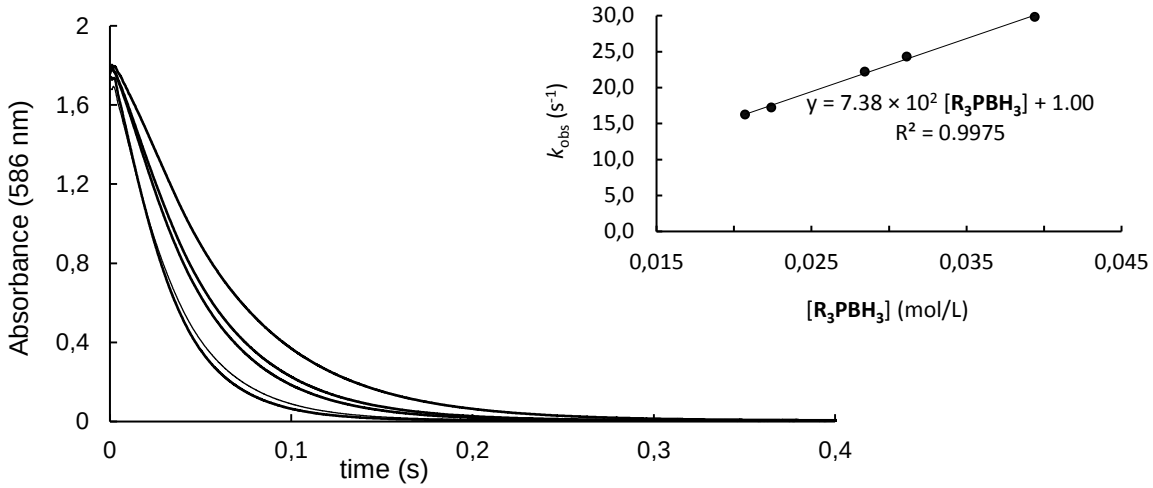

Ainsi, en déterminant la valeur de la constante de vitesse au second ordre, il est possible de calculer la valeur du paramètre de nucléophilie associé à la phosphine borane étudiée. Pour cela, il suffit de tracer log(k_2) en fonction des paramètres d'électrophile des carbocations étudiés. Nous avons ainsi pu déterminer la nucléophilie d'une série de 11 phosphine boranes diversement fonctionnalisées.

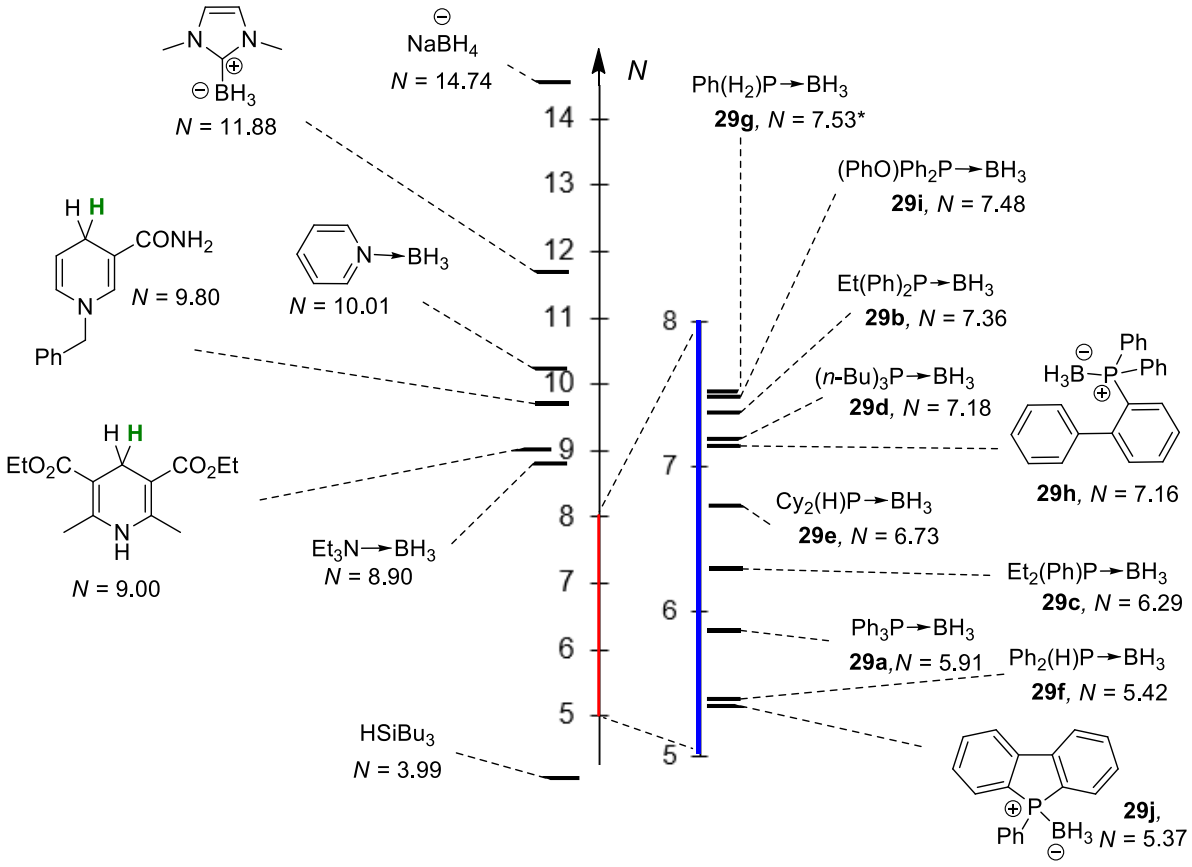

A la lumière de ces résultats, une échelle de prédiction de la faisabilité des réductions de divers électrophiles par les phosphines borane comparée à d'autres donneur d'hydrure a été construite.

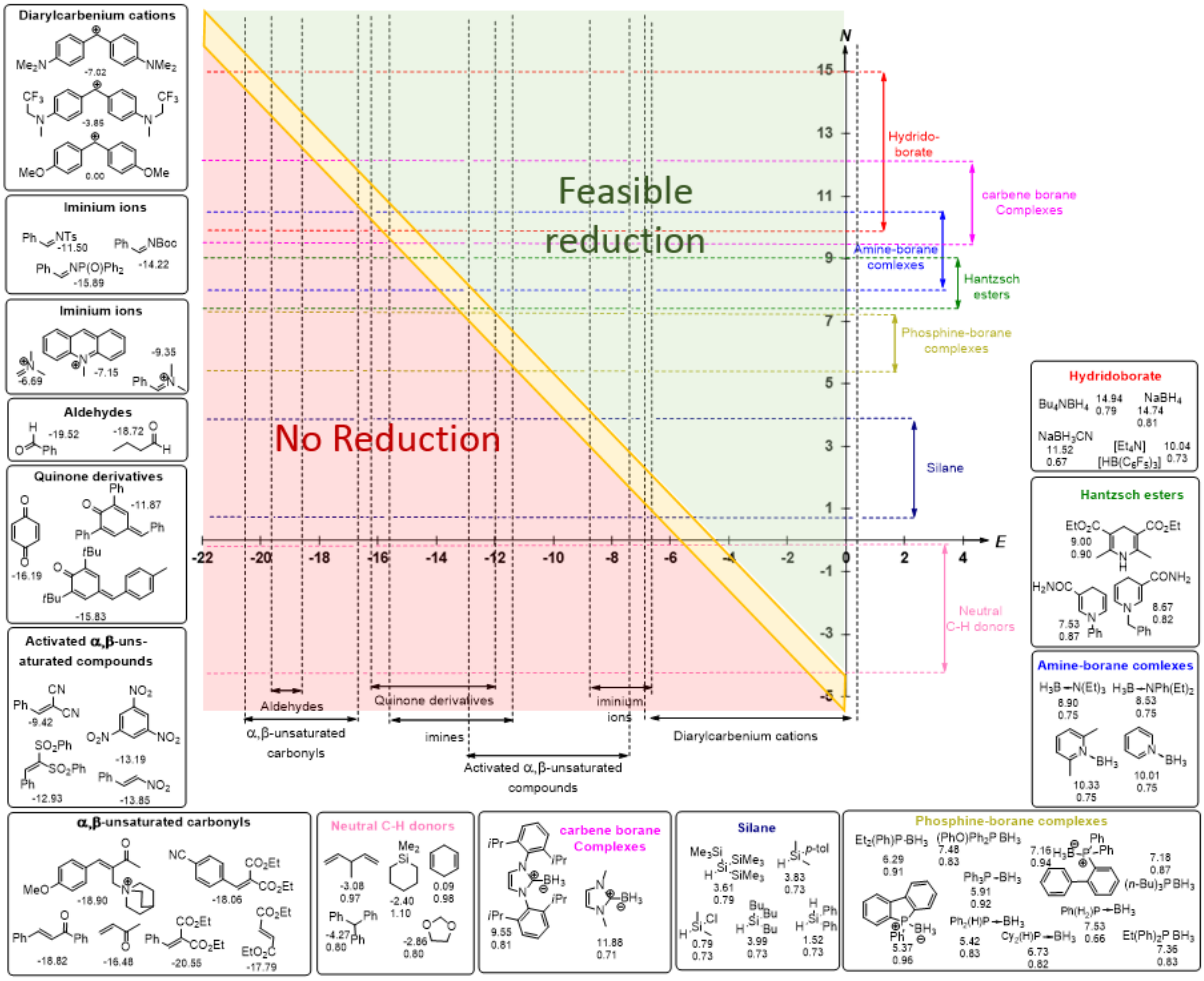

Enfin, au cours de notre étude, nous avons souhaité connaitre les paramètres clés permettant d'accroitre significativement la nucléophilie des phosphines boranes. Nous avons ainsi mis en lumière que la stabilité du cation borénium issu de l'abstraction de l'hydrure des phosphine borane est le critère clé pour comprendre l'évolution de l'hydricité des phosphine boranes.

D/ Migration de C_6F_5 de $B(C_6F_5)_3$ avec les phosphines boranes

En 2016, Hou et al. ont décrit l'hydrosilylation de dérivé d'aniline catalysée par $B(C_6F_5)_3$. Les auteurs ont montré que 1 mol% de l'acide de Lewis à 120°C dans le chlorobenzène permet de promouvoir l'hydrosilylation en position 4 d'une grande variété d'anilines avec des rendements de 60 à 84%. Le mécanisme postulé implique la formation d'un adduit acide-base de Lewis entre $B(C_6F_5)_3$ et $PhSiH_3$ très polarisé. Ce dernier adduit réagit avec l'aniline pour conduire au dérivé silylé et au borohydrure $HB(C_6F_5)_3$, capable de déprotoner l'intermédiaire de Whealand pour régénérer le catalyseur et libérer le produit plus H_2.[7]

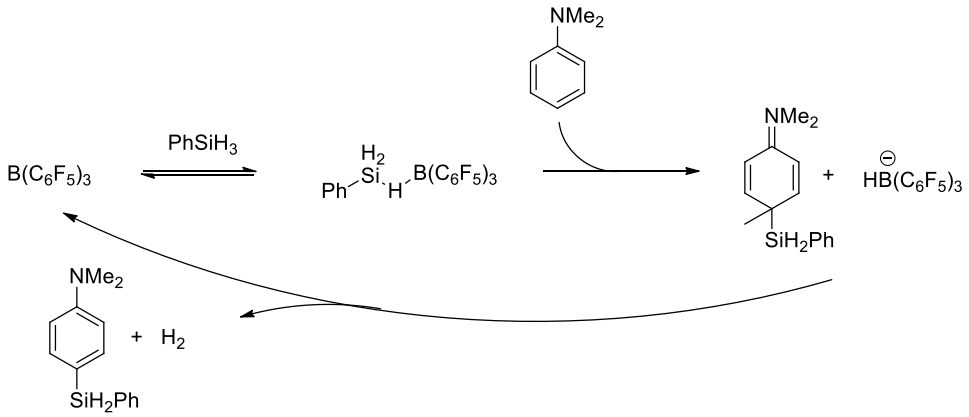

Sur la base de ce travail, nous avons souhaité réalisé la borylation intramoléculaire de phosphinite borane catalysée par $B(C_6F_5)_3$. Toutefois, la réaction entre $B(C_6F_5)_3$ et $PhOP(iPr)_2BH_3$ n'a pas conduit à l'adduit de borylation intramoléculaire mais au produit de mono-migration de C_6F_5.

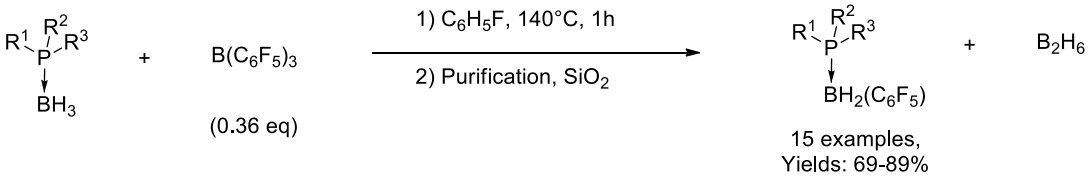

Le mécanisme de cette réaction a été étudié par deux méthodes. Premièrement, nous avons mesuré la nucléophilie d'une grande variété de phosphine boranes afin de savoir si ces dernières sont capables de réduire $B(C_6F_5)_3$. Les résultats nous ont indiqués des valeurs de nucléophilies *N* comprises entre 6 et 8, indiquant une nucléophilie inférieure à celle des amines boranes ou des esters de Hantzsch mais supérieure aux silanes. De plus, nous avons confirmé la capacité des phosphines boranes à former $[HB(C_6F_5)_3]^-$. Afin de comprendre plus en détail le mécanisme réactionnel, nous avons solliciter une collaboration avec le prof. Hélène Gérard (LCT, Jussieu) et calculer le mécanisme réactionnel par DFT.

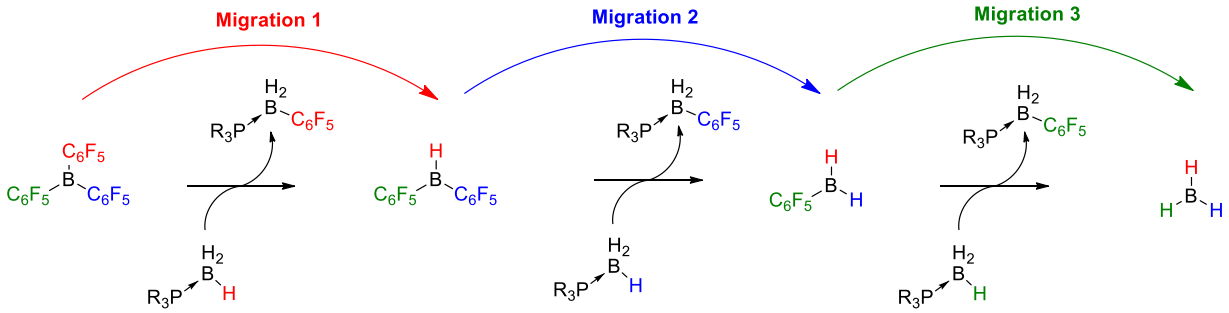

D'un point de vue thermodynamique, nous avons montré que la réaction globale de migration des trois fragments C_6F_5 est exergonique en considérant quatre phosphine boranes

différentes. Ainsi, cela rend compte de la réactivité observée et montre également que la substitution des phosphines accroit la stabilité des produits.

Sans dimerization de BH_3

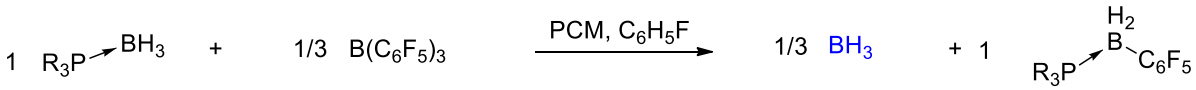

Dimerization de BH_3 en B_2H_6

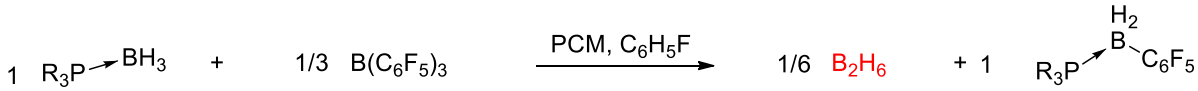

R_3PBH_3	Sans dimérisation de BH_3		Dimérisation de BH_3	
	ΔE (kcal/mol)	ΔG (kcal/mol)	ΔE (kcal/mol)	ΔG (kcal/mol)
H_3PBH_3	+1.3 (-0.2)	+2.5 (-0.6)	-5.3 (-9.1)	-1.3 (-6.7)
Ph_3PBH_3	+1.3	+2.6	-5.2	-1.3
Me_3PBH_3	-0.8	+0.5	-7.3	-3.4
$MeOPMe_2BH_3$	-0.2 (-0.4)	+0.6 (-0.3)	-6.7 (-9.3)	-3.2 (-6.5)

Le calcul des chacune des trois migrations montre également qu'elles sont favorables d'un point de vue thermodynamique. De plus, cette étude montre que la migration la plus difficile est la première puisqu'elle donne accès à une constante d'équilibre plus grande que les deux autres et ce, qu'elle que soit la nature de la phosphine borane impliquée.

R_3PBH_3	E or G (kcal/mol)	Première migration	Seconde migration	Troisième migration
H_3PBH_3	ΔE	-8.9 (-19.2)	-4.9 (-4.5)	-2.0 (-3.3)
	ΔG	+0.2 (-12.2)	-4.1 (-5.0)	-0.2 (-2.9)
$MeOPMe_2BH_3$	ΔE	-10.4 (-19.7)	-6.4 (-4.8)	-3.4 (-3.5)
	ΔG	-1.7 (-11.9)	-6.0 (-4.8)	-2.0 (-2.7)

Afin de décrire le mécanisme global, nous avons ensuite calculé les états de transition associé à chacune des étapes élémentaires du mécanisme. Une étude détaillée a montré que les états de transition impliquent un pseudo cation-borénium très électrophile et qui permet la migration d'un groupement C_6F_5 issu du sel de borohydrure résultant de l'abstraction d'un ion hydrure entre le tris-pentafluorophenylborane et la phosphinite borane de départ.

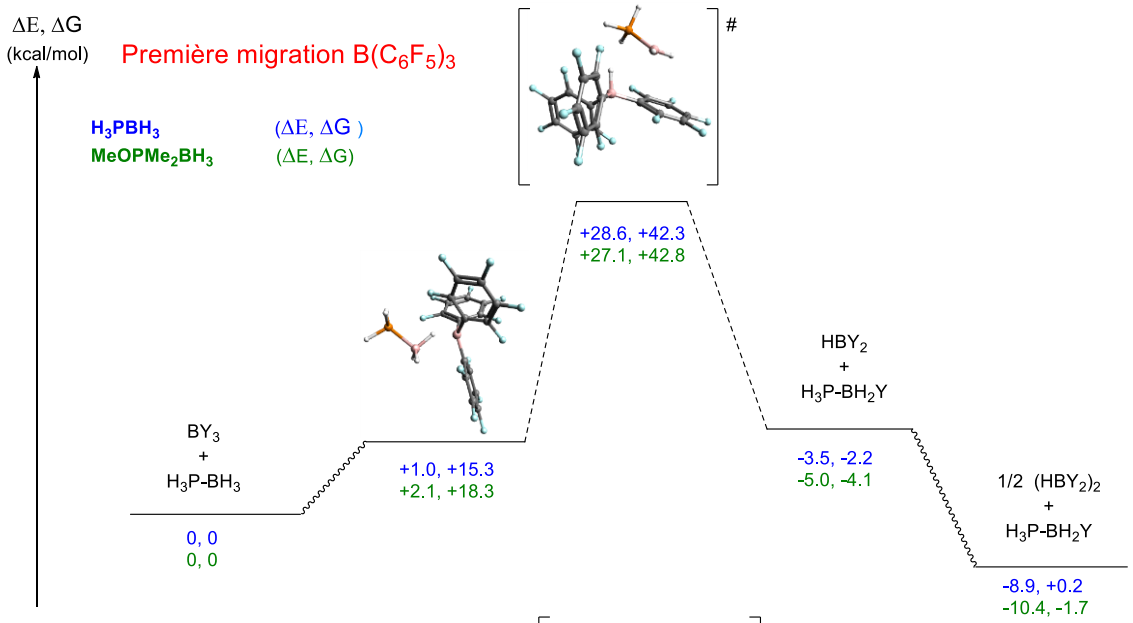
ΔE, ΔG
(kcal/mol)
Première migration B(C6F5)3
H3PBH3 (ΔE, ΔG)
MeOPMe2BH3 (ΔE, ΔG)
#
+28.6, +42.3
+27.1, +42.8
HBY2
+
H3P-BH2Y
BY3
+
H3P-BH3
+1.0, +15.3
+2.1, +18.3
-3.5, -2.2
-5.0, -4.1
1/2 (HBY2)2
+
H3P-BH2Y
0, 0
0, 0
-8.9, +0.2
-10.4, -1.7

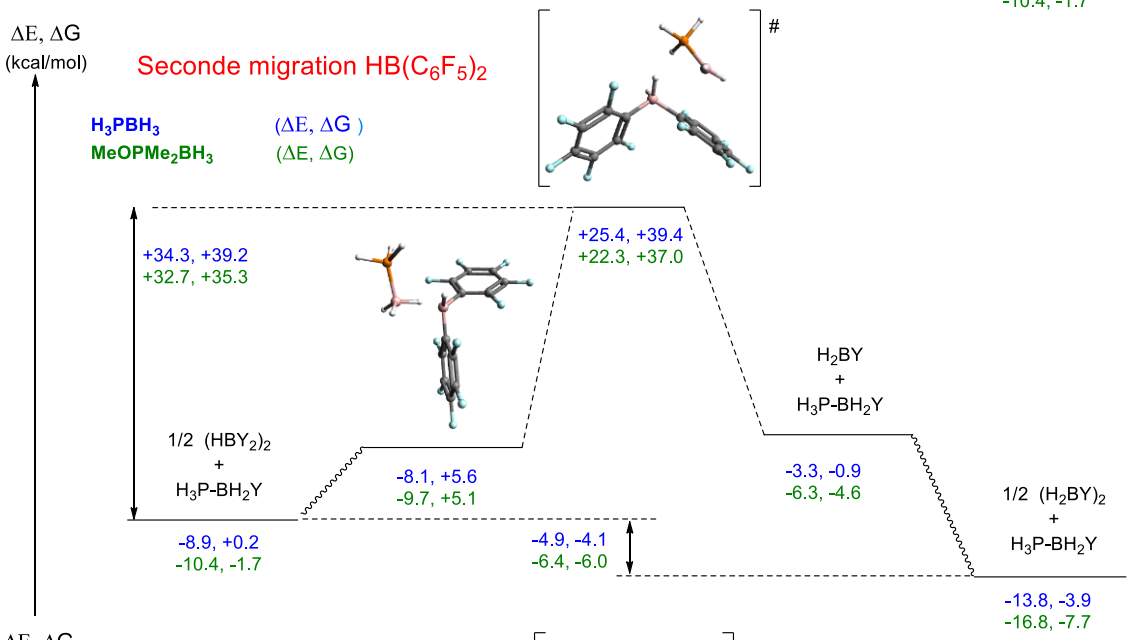
ΔE, ΔG
(kcal/mol)
Seconde migration HB(C6F5)2
H3PBH3 (ΔE, ΔG)
MeOPMe2BH3 (ΔE, ΔG)
#
+34.3, +39.2
+32.7, +35.3
+25.4, +39.4
+22.3, +37.0
H2BY
+
H3P-BH2Y
1/2 (HBY2)2
+
H3P-BH2Y
-8.1, +5.6
-9.7, +5.1
-3.3, -0.9
-6.3, -4.6
1/2 (H2BY)2
+
H3P-BH2Y
-8.9, +0.2
-10.4, -1.7
-4.9, -4.1
-6.4, -6.0
-13.8, -3.9
-16.8, -7.7

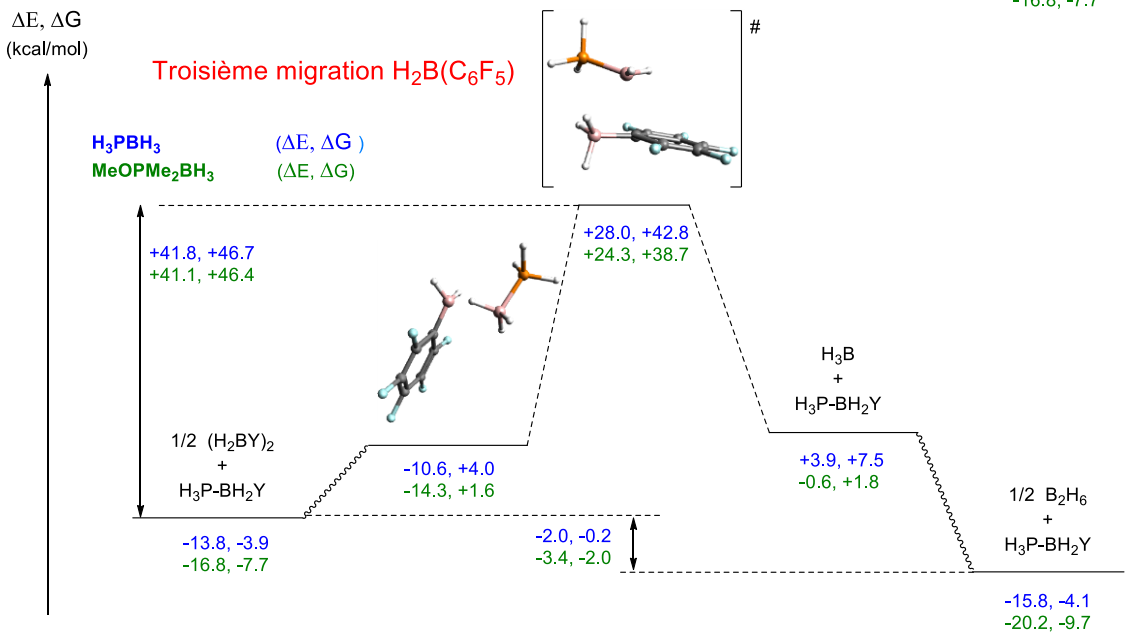
ΔE, ΔG
(kcal/mol)
Troisième migration H2B(C6F5)
H3PBH3 (ΔE, ΔG)
MeOPMe2BH3 (ΔE, ΔG)
#
+41.8, +46.7
+41.1, +46.4
+28.0, +42.8
+24.3, +38.7
H3B
+
H3P-BH2Y
1/2 (H2BY)2
+
H3P-BH2Y
-10.6, +4.0
-14.3, +1.6
+3.9, +7.5
-0.6, +1.8
1/2 B2H6
+
H3P-BH2Y
-13.8, -3.9
-16.8, -7.7
-2.0, -0.2
-3.4, -2.0
-15.8, -4.1
-20.2, -9.7

Ainsi, nous avons pu expliquer l'origine de la mono-migration de C_6F_5 ainsi que la nécessité d'imposer une température élevée au système. De plus, nous avons justifié la formation d'un état de transition impliquant un cation borénium.

4) Conclusion

En conclusion, cette thèse a présenté les résultats de notre recherche sur les interactions entre les composés organophosphorés et organoborés, allant de la frustration de la liaison P-B à l'établissement d'une liaison forte entre l'acide et la base de Lewis. L'exploration de ces modes d'interaction combinés à nos études mécanistiques nous ont permis de mettre au pont de nouvelles réaction chimiques permettant l'accès à des composés nouveaux ou déjà connus en synthèse organique.

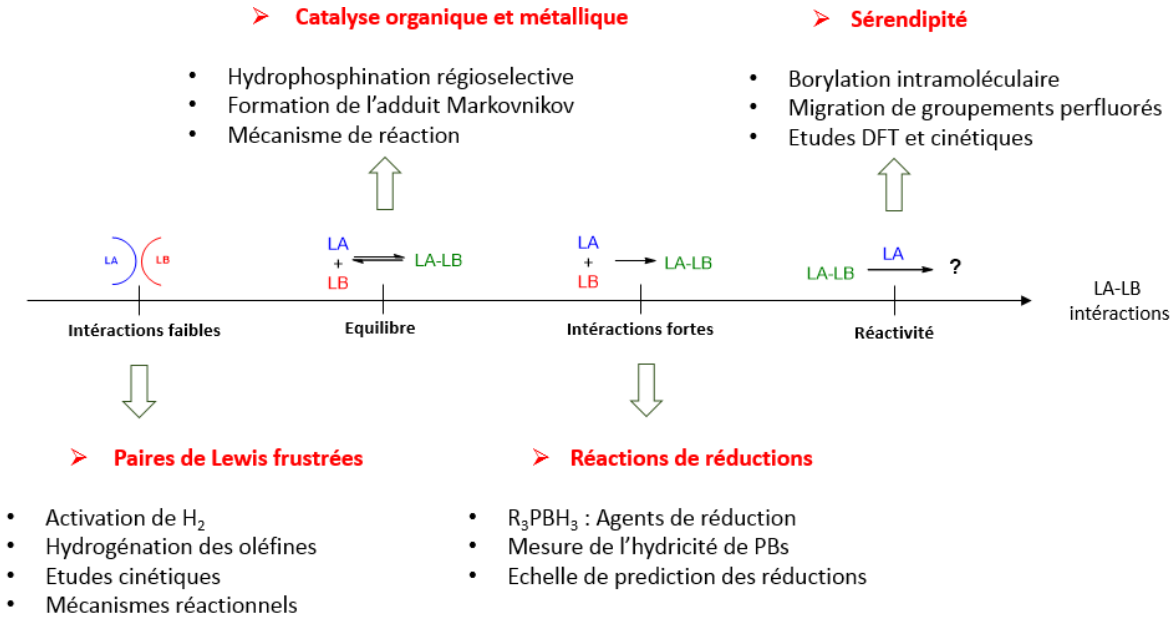

Résumé

Les travaux décrits dans ce manuscrit de thèse concernent l'exploitation des interactions acide-base de Lewis entre deux partenaires organophosphorés et organoborés. Quatre types d'interactions ont été particulièrement au cœur de notre étude, allant de la frustration de la liaison P-B à la formation de complexes acide base de Lewis fortement liés. L'étude de ces interactions, couplée à des outils de physico-chimie organique et de chimie théorique, nous ont permis, non seulement de comprendre les paramètres clés de la réactivité mais également de mettre en avant de nouvelles voies de synthèse. Dans un premier temps, notre étude s'est portée sur l'hydrogénation de composés insaturés par les Paires de Lewis Frustrées (FLP). Ainsi, l'origine de l'incapacité des P/B à réduire les accepteurs de Michael a été expliquée par des mesures cinétiques de la nucléophilie et de la basicité de Lewis de phosphines encombrées. Dans une seconde partie, l'hydricité de complexes de phosphine borane (PBs) variées a été mesurée, nous permettant d'établir une échelle de prédiction de la réduction de divers électrophiles en présence de ces donneurs d'hydrure ioniques. Cette étude nous a conduit à considérer les PBs comme substrats dans des réaction de borylation intramoléculaire impliquant BH_3 comme source de bore. Cependant, des résultats inattendus ont mis en exergue une migration prépondérante à la borylation lors de la réaction entre les PBs et un acide de Lewis, donnant accès à une nouvelle familles de PBs possédant un atome de bore électro-déficitaire. Des études cinétiques couplées à une étude par DFT ont permis de rationaliser la réactivité observée. Enfin, l'exploitation des interactions réversibles entre une phosphine secondaire et un acide de Lewis organique ou métallique nous ont permis de contrôler la régiosélectivité lors de l'hydrophosphination d'alcènes 1,1-disubstitués par les diarylphosphines. Nos études mécanistiques soutiennent fortement l'implication d'un carbocation comme intermédiaire réactionnel.

Abstract

The research in this thesis describes the exploration of the Lewis-acid Lewis-base interactions between organophopshine and organoborane compounds. We focused our attention on four types of interactions going from frustrating to stong P-B bonds. Our understanding of these interactions is based on detailed kinetics and computational calculations, allowing us to find a new reactivity of these species. In a first part, we studied the metal-free hydrogenation of unsaturated compounds using Frustrated Lewis Pairs (FLPs). Based on the measurement of the nucleophilicity and the Lewis basicity parameters of sterically hindered phosphines, we were able to explain reasons of the failure of P/B FLPs to catalyse the hydrogenation of Michael acceptors under H_2. In the second chapter, we employed the Mayr's linear-free energy relationship to measure the hydricity of various phosphine borane complexes (PBs) and compare their reactivity to commons hydride donors. Based on these kinetic parameters, we next turned our attention to investigate the effect of a strong Lewis acid, ($B(C_6F_5)_3$), to prevent the expected intramolecular borylation of PBs to take place. By combining kinetic and computational investigations, we have been able to understand factors controlling this reaction. In the last chapter, we reported on the regioselective organocatalytic Markovnikov hydrophosphination of aryl alkenes. Importantly, we highlighted that the reversible formation of a phosphine-Lewis acid complex is in the core of the catalytic process. Mechanistic investigations support the formation of a carbocation in the catalytic cycle.